INL/EXT-15-36742

RELAP5-3D Developmental Assessment: Comparison of Version 4.3.4i on Linux and Windows

Paul D. Bayless

October 2015

INL is a U.S. Department of Energy National Laboratory
operated by Battelle Energy Alliance

NOTICE

OBLIGATIONS OF EXPORT COMPLIANCE

Recipient is responsible for its own compliance with laws and regulations governing export controls including, for example, the Export Administration Regulations (EAR) (15 CFR Parts 730), the International Traffic in Arms Regulations (ITAR) (22 CFR Parts 120-130), and the Nuclear Regulatory Commission and Department of Energy export regulations (10 CFR Parts 110 and 810). Being provided this document or product, directly or indirectly, shall not be construed to constitute a governmental license or authorization.

INL/EXT-15-36742

RELAP5-3D Developmental Assessment: Comparison of Version 4.3.4i on Linux and Windows

Paul D. Bayless

October 2015

Idaho National Laboratory
Idaho Falls, Idaho 83415

http://www.inl.gov

Prepared for the
U. S. Department of Energy
Under DOE Idaho Operations Office
Contract DE-AC07-05ID14157

ABSTRACT

Figures have been generated comparing the parameters used in the developmental assessment of the RELAP5-3D code, version 4.3i, compiled on Linux and Windows platforms. The figures, which are the same as those used in Volume III of the RELAP5-3D code manual, compare calculations using the semi-implicit solution scheme with available experiment data. These figures provide a quick, visual indication of how the code predictions differ between the Linux and Windows versions.

CONTENTS

FIGURES

TABLES

RELAP5-3D Developmental Assessment: Comparison of Version 4.3.4i on Linux and Windows

1. INTRODUCTION

This document contains plots comparing the semi-implicit simulation results for the developmental assessment cases using RELAP5-3D version 4.3.4i compiled on Linux and Windows platforms. Its purpose is to provide a quick, visual comparison of how results differ between the Linux and Windows versions of the code, both of which were compiled using Version 13.1 of the Intel Fortran Compiler. The developmental assessment provided in Volume III of the RELAP5-3D code manual[1.1] is from the Linux version.

Most of the text in the assessment report has been removed in the creation of this report. All of the diagrams and early report chapters have been retained so that the figure numbers in this report match those in the assessment report. In the figure legends, "lnx" refers to calculations using the Linux version, and "win" refers to calculations using the Windows version.

Differences observed in the comparison figures are divided into two categories. Significant differences signify that the assessment judgment may be different. Noticeable differences signify that the two simulations are not identical, but a difference in the assessment finding is unlikely. Significant differences were observed in the cases listed below:

- ROSA-IV Test SB-CL-18
- LOFT L2-5 (1-D)
- LOFT L2-5 (3-D).

Noticeable differences were observed in the cases listed below:

- Water over steam (3-D)
- Bubbling steam through liquid
- FLECHT Test 31504
- FLECHT Test 31701
- UPTF Test 6
- LOFT Experiment L3-7
- ROSA-IV Test SB-CL-18

- Semiscale natural circulation Tests 1, 2, 3, and 10
- LOBI Test A1-04R
- LOFT Experiment L2-5 (1-D)
- LOFT Experiment L2-5 (3-D).

All of the differences were reviewed to determine their potential effect on the assessment findings; two changes in the assessment judgments for these cases would be expected. Further details are provided in Chapter 6.

1.1 Reference

1.1. P.D. Bayless, editor, *RELAP5-3D Code Manual Volume III: Developmental Assessment*, INL/MIS-15-36723, Rev. 4.3, Idaho National Laboratory, October 2015.

2. DEVELOPMENTAL ASSESSMENT MATRIX

Most of the text has been removed, although the first two sections have been maintained to preserve table numbering consistent with Volume III.

2.1 Methodology and Case Selection

2.2 Matrix Summary

Table 2.2-1 lists the phenomenological assessment cases and the principal phenomena or code models that each addresses.

Table 2.2-1. Phenomenological assessment cases.

Case Description	Models Validated
Bubbling steam through liquid	Entrainment, two-phase level
Cladding oxidation	Cladding oxidation
Conduction enclosure	Conduction enclosure
Conduction enclosure 1-D transient	Conduction enclosure
Conduction enclosure 2-D transient	Conduction enclosure
Core power	Point kinetics
Fill/drain	Level tracking
Gravity wave 1-D	Stratification, force term
Gravity wave 3-D	Stratification, force term
Manometer	Noncondensables, wall friction, liquid level, oscillations
Point kinetics ramp	Point kinetics
Pryor pressure comparison	Water packing
Pure radial symmetric flow (3-D)	3-D momentum equations
Rigid body rotation (3-D)	3-D momentum equations
R-theta symmetric flow (3-D)	3-D momentum equations
Water faucet	Hydro numerics, gravity, momentum equation
Water over steam (1-D)	Gravitational head, liquid level, gravity
Water over steam (3-D)	Gravitational head, liquid level, gravity

The separate effects cases and the phenomena they address are provided in Table 2.2-2.

Table 2.2-2. Separate effects assessment cases.

Case Description	Models Validated
Bennett Heated Tube Tests 5358, 5294 and 5394	Non-equilibrium heat transfer, CHF, subcooled boiling, steam cooling
Christensen Test 15	Subcooled boiling heat transfer, void profile
Dukler air-water flooding	CCFL
Edwards' Pipe	Vapor generation, flashing, critical flow, pressure wave propagation
FLECHT-SEASET Test 31504	Reflood model (low reflood rate), two-phase level, natural circulation, subcooled boiling, steam cooling, quench front, interphase evaporation, entrainment, CCFL, condensation heat transfer
FLECHT-SEASET Test 31701	Reflood model (high reflood rate), two-phase level, steam cooling, entrainment, CCFL, condensation heat transfer, quench front
Full-scale reactor coolant pump	Two-phase pump behavior
GE 1/6-scale jet pump	Jet pump
GE Level Swell, 1 ft. Test 1004-3	Vapor generation, interphase drag, two-phase level
GE Level Swell, 4 ft. Test 5801-15	Vapor generation, interphase drag, two-phase level
LOFT L3-1	Accumulator model
Marviken Test 22	Subcooled choking model, flashing, two-phase level
Marviken Test 24	Subcooled choking model, flashing, two-phase level
Marviken Test CFT 21	Subcooled critical flow, saturated liquid critical flow
Marviken Test JIT 11	Saturated vapor critical flow, interfacial drag in bubbly/slug, pool boiling, void profile
MB2 Test 1712	Steam generator behavior
MIT Pressurizer	Wall condensation, interfacial heat transfer, pressurizer level, thermal stratification
Moby Dick air-water	Critical flow
Neptunus	Pressurizer
ORNL THTF Tests 3.07.9B, 3.07.9N, 3.07.9W	CHF, film boiling, steam cooling

Table 2.2-2. Separate effects assessment cases.

Case Description	Models Validated
ORNL THTF Test 3.09.10	Void profile in rod bundles, radiation heat transfer
Royal Institute of Technology Tube Test 261	CHF
UPTF Downcomer Countercurrent Flow Test 6, Run 131	Downcomer CCFL, lower plenum refill, condensation, noncondensables, two-phase level, thermal stratification, interphase drag, entrainment

Table 2.2-3 presents the integral effects cases.

Table 2.2-3. Integral effects assessment cases.

Case Description	Experiment Type
LOBI Test A1-04R	Large break LOCA
LOFT L2-5 (1-D)	Large break LOCA
LOFT L2-5 (3-D)	Large break LOCA
LOFT L3-7	1-in. small break LOCA
ROSA-IV Test SB-CL-18	6-in. small break LOCA
Semiscale NC Tests 1, 2, 3, 10	Loop natural circulation

3. PHENOMENOLOGICAL CASES

This chapter presents the phenomenological assessment case results.

3.1 Water Faucet

Figures comparing simulations using Linux and Windows code versions are presented. Diagrams are included so that the figure numbering is the same as that in Volume III of the RELAP5-3D code manual. No differences were observed in the figures.

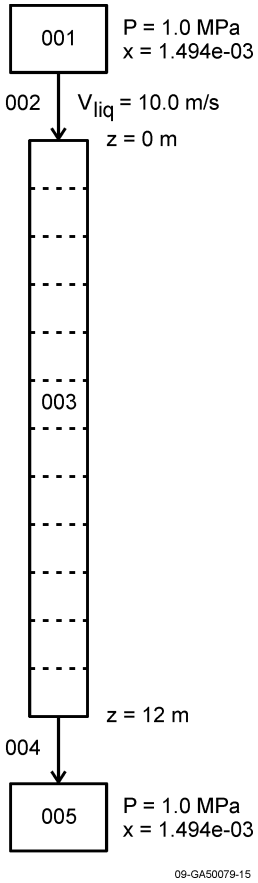

Figure 3.1-1. RELAP5-3D nodalization for the water faucet test case.

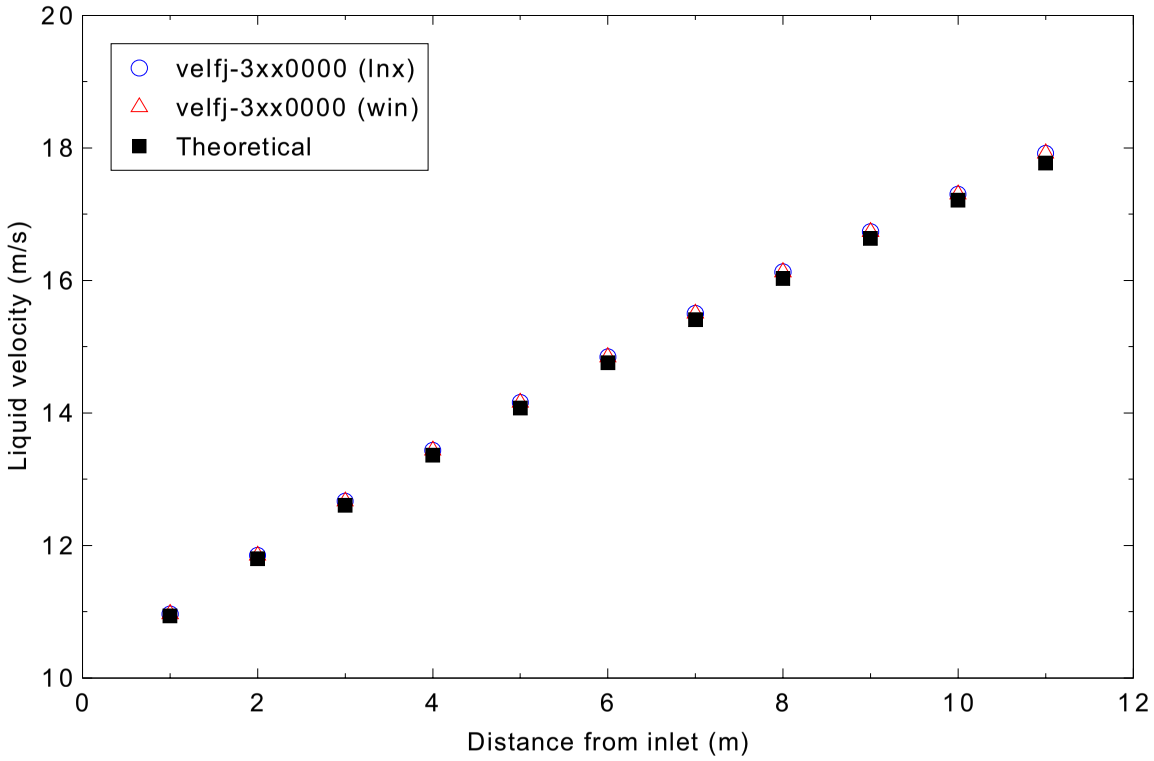

Figure 3.1-2. Comparison of RELAP5-3D calculated liquid velocity with the exact solution for the water faucet case.

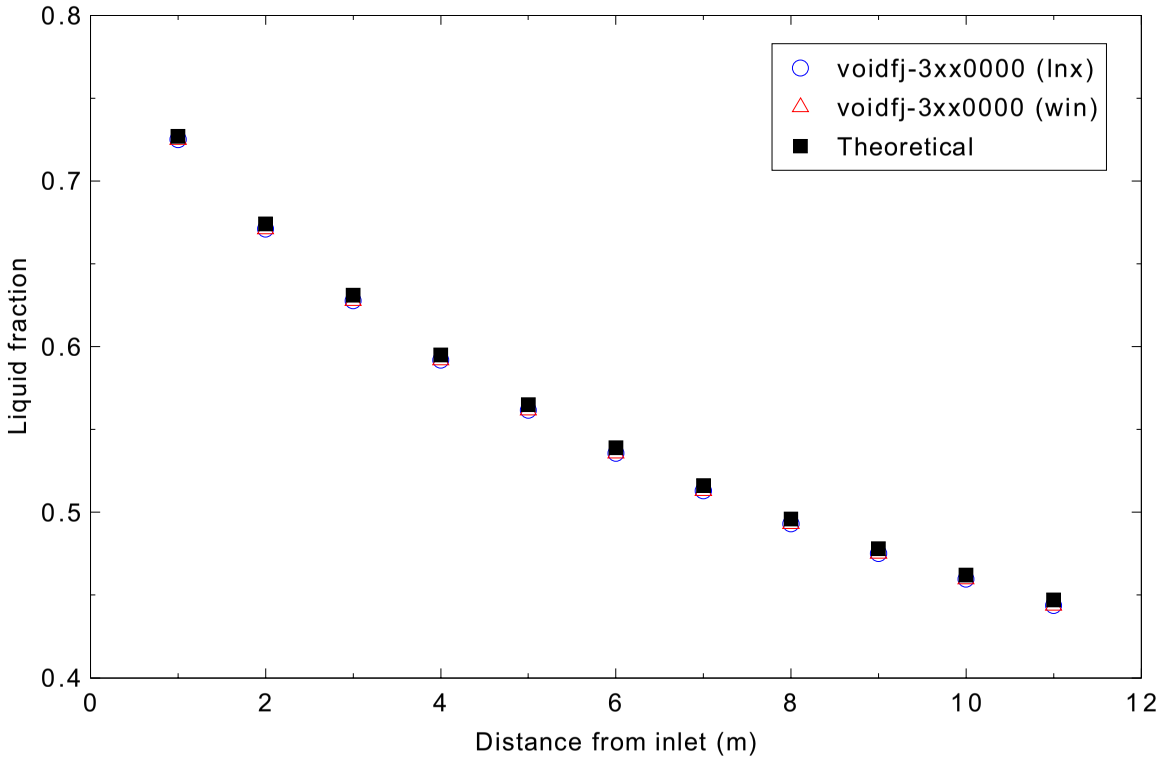

Figure 3.1-3. Comparison of RELAP5-3D calculated liquid fraction with the exact solution for the water faucet case.

3.2 Water over Steam (1-D)

Figures comparing simulations using Linux and Windows code versions are presented. Diagrams are included so that the figure numbering is the same as that in Volume III of the RELAP5-3D code manual. No differences were observed in the figures.

Figure 3.2-1. RELAP5-3D nodalization diagram for the 1-D water over steam problem.

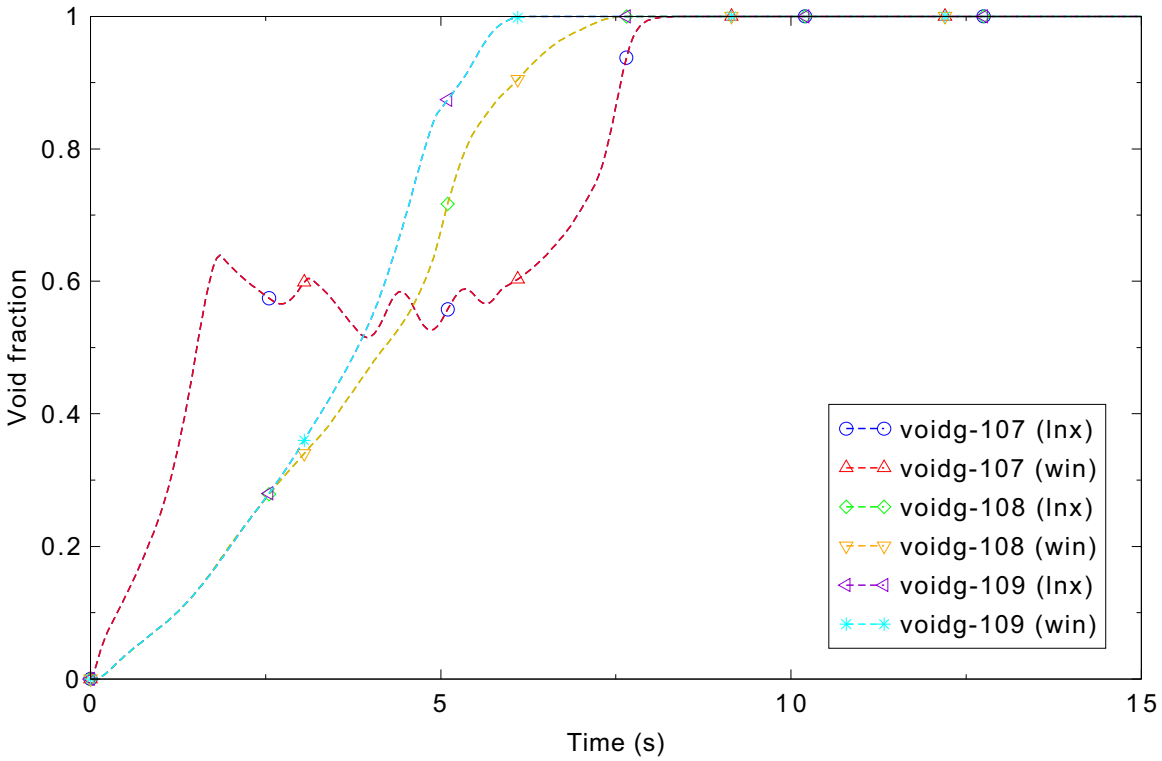

Figure 3.2-2. Void fraction in the top three volumes (7-9) for the 1-D water over steam problem.

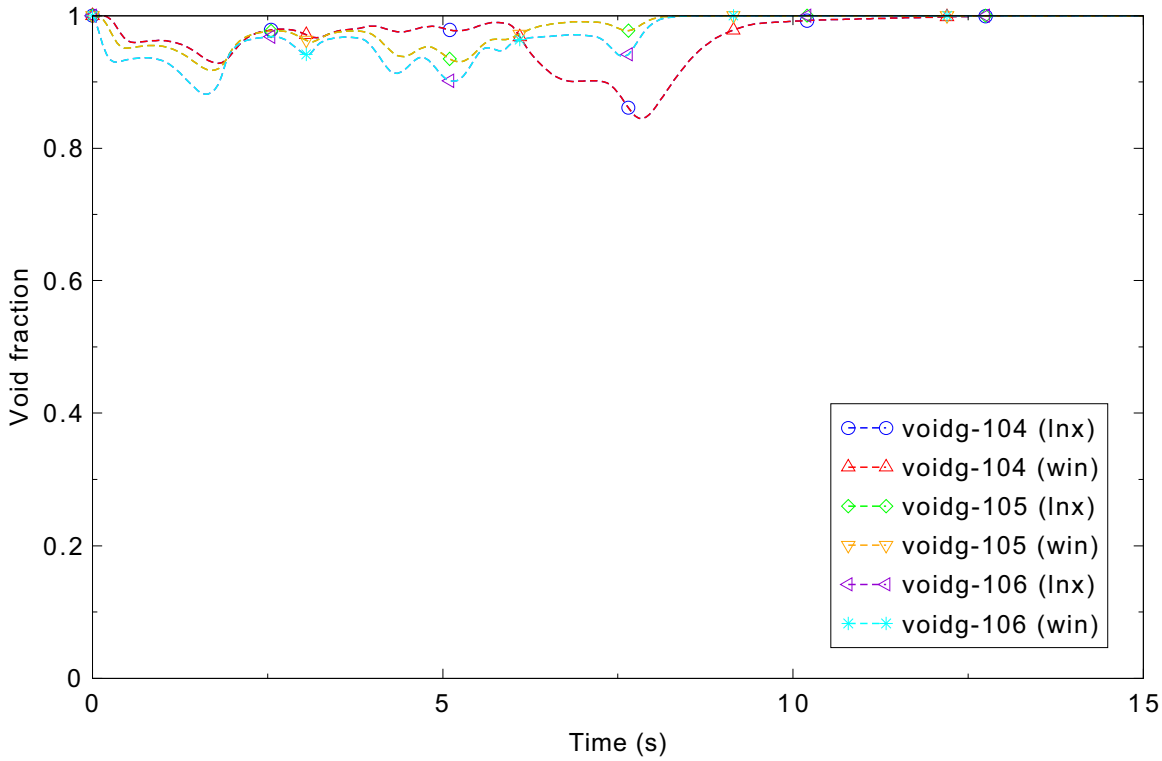

Figure 3.2-3. Void fraction in the middle three volumes (4-6) for the 1-D water over steam problem.

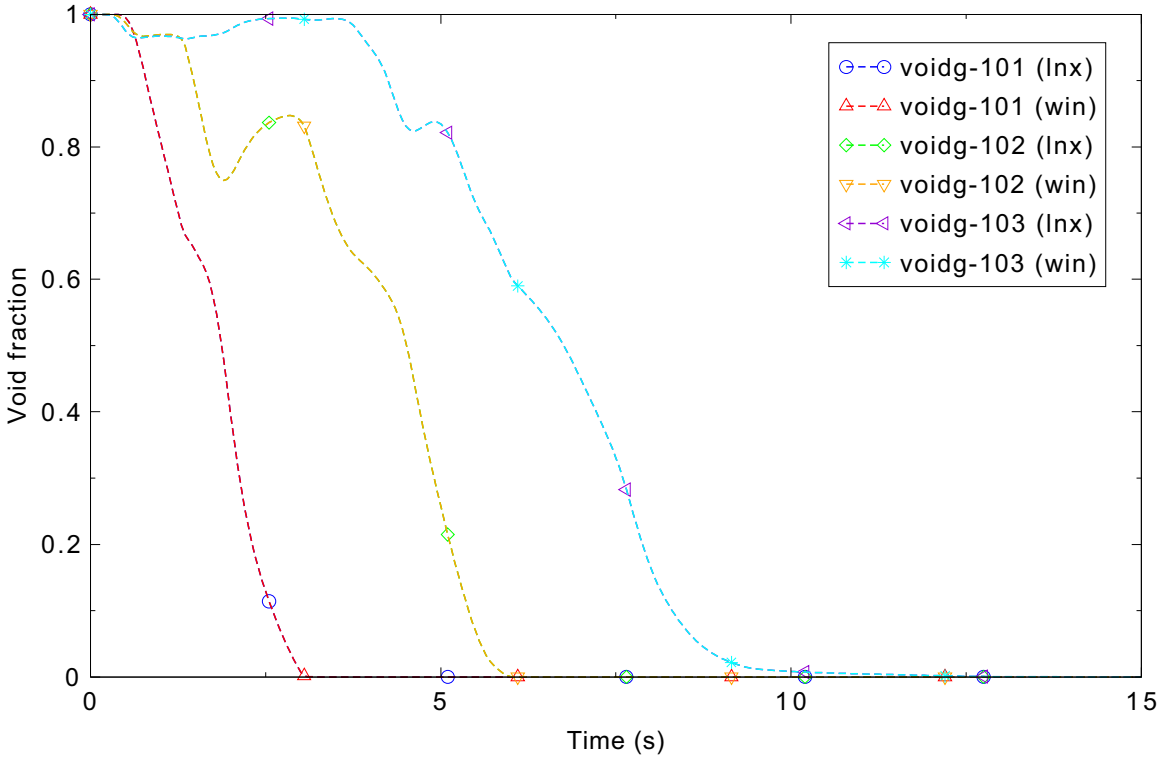

Figure 3.2-4. Void fraction in the bottom three volumes (1-3) for the 1-D water over steam problem.

3.3 Water over Steam (3-D)

Figures comparing simulations using Linux and Windows code versions are presented. Diagrams are included so that the figure numbering is the same as that in Volume III of the RELAP5-3D code manual. Noticeable differences were observed in Figures 3.3-2, 3, and 4.

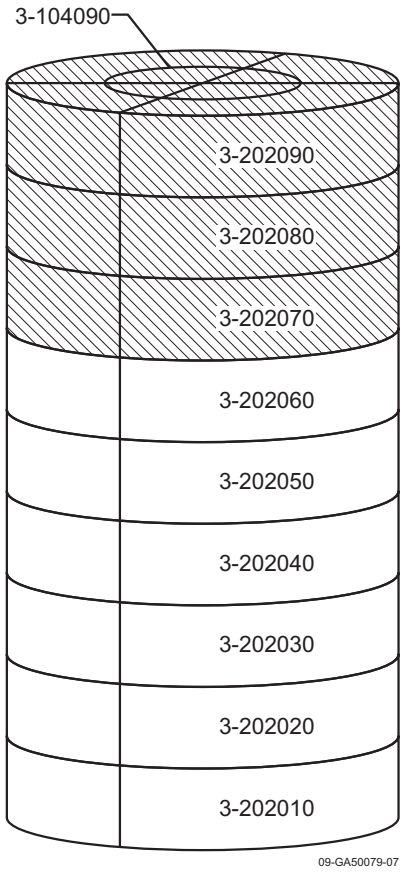

Figure 3.3-1. RELAP5-3D nodalization diagram for the 3-D water over steam problem.

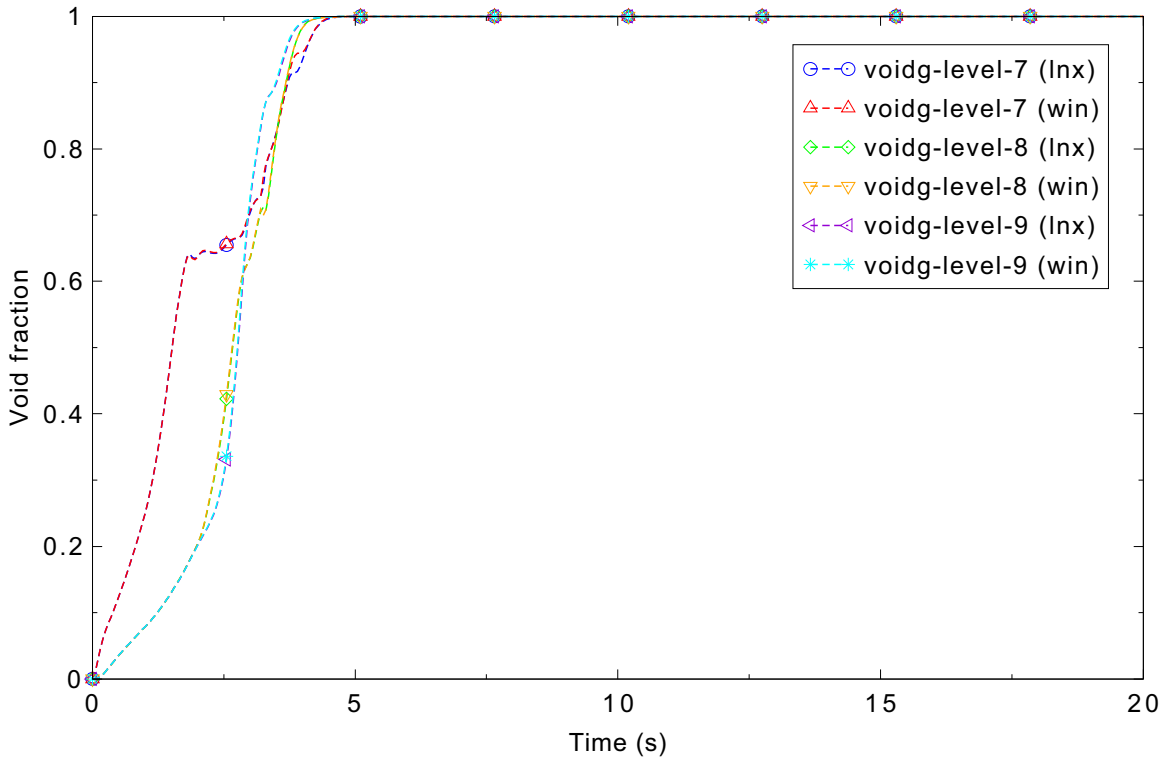

Figure 3.3-2. Void fraction in the top three axial levels (7-9) for the 3-D water over steam problem.

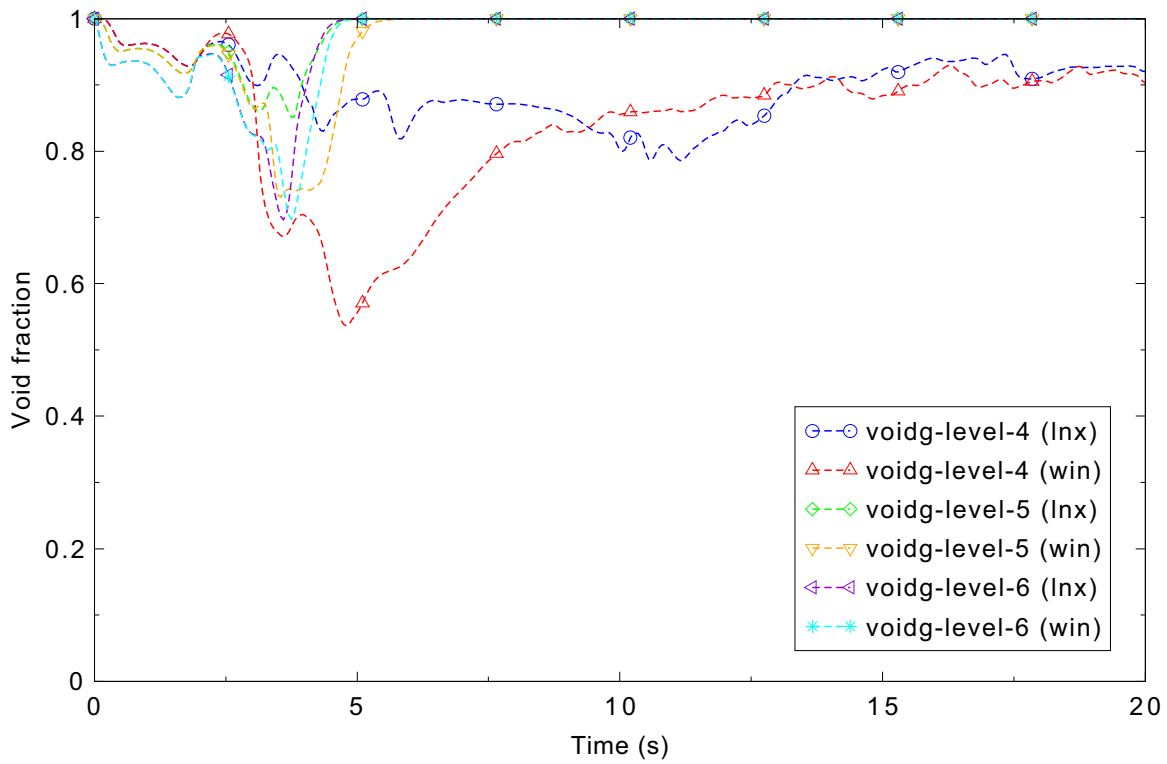

Figure 3.3-3. Void fraction in the middle three axial levels (4-6) for the 3-D water over steam problem.

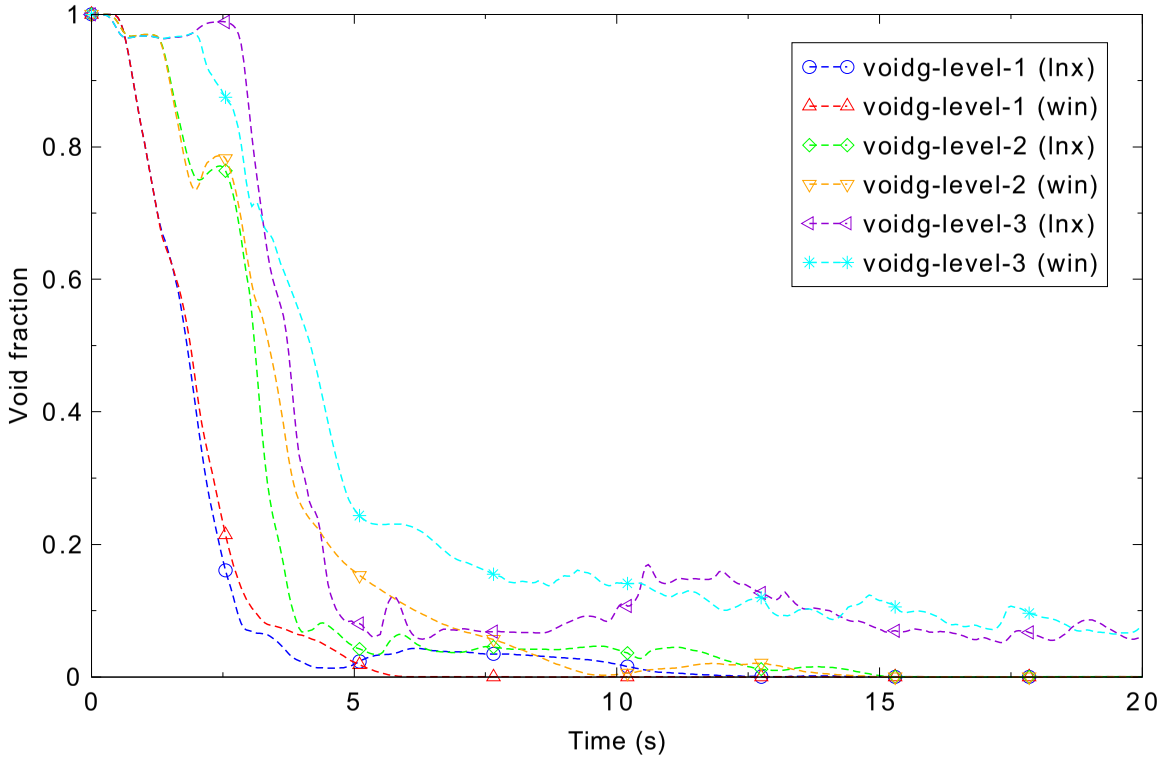

Figure 3.3-4. Void fraction in the bottom three axial levels (1-3) for the 3-D water over steam problem.

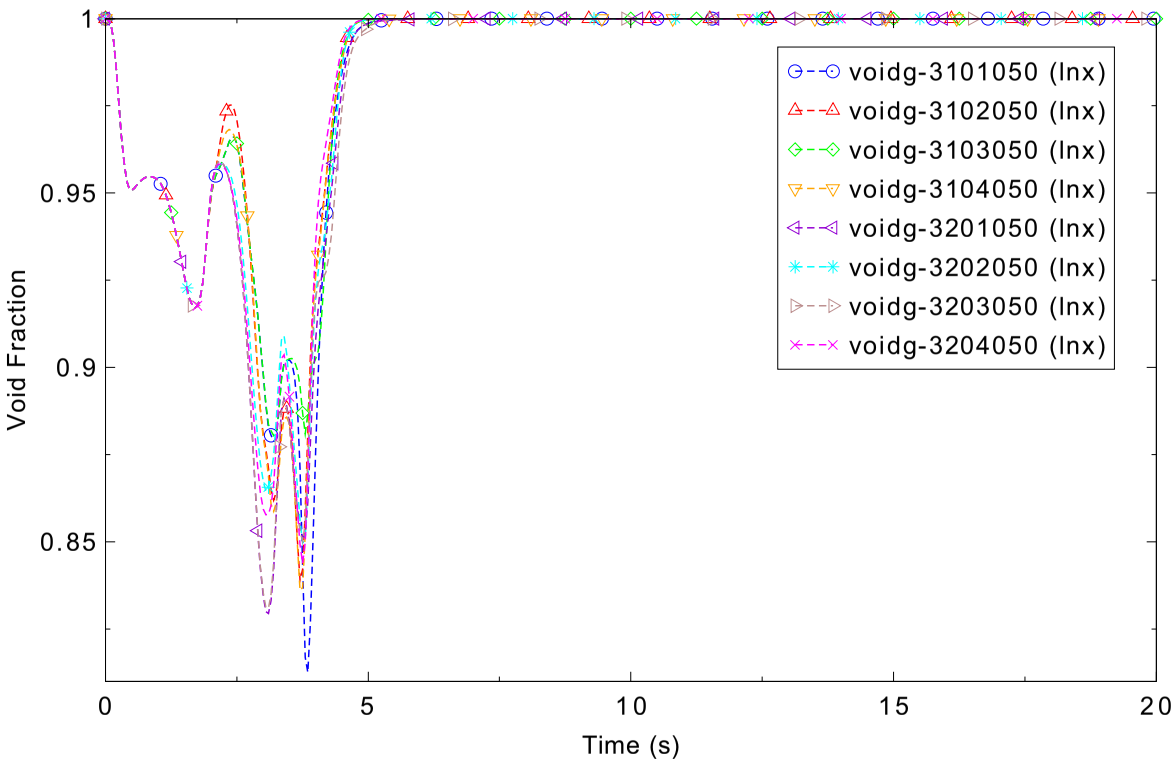

Figure 3.3-5. Void fraction in each of the eight segments of axial level 5 for the 3-D water over steam problem.

3.4 Fill-Drain

Figures comparing simulations using Linux and Windows code versions are presented. Diagrams are included so that the figure numbering is the same as that in Volume III of the RELAP5-3D code manual. No differences were observed in the figures.

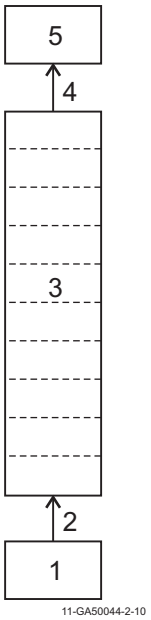

Figure 3.4-1. Nodalization diagram for Fill-Drain test.

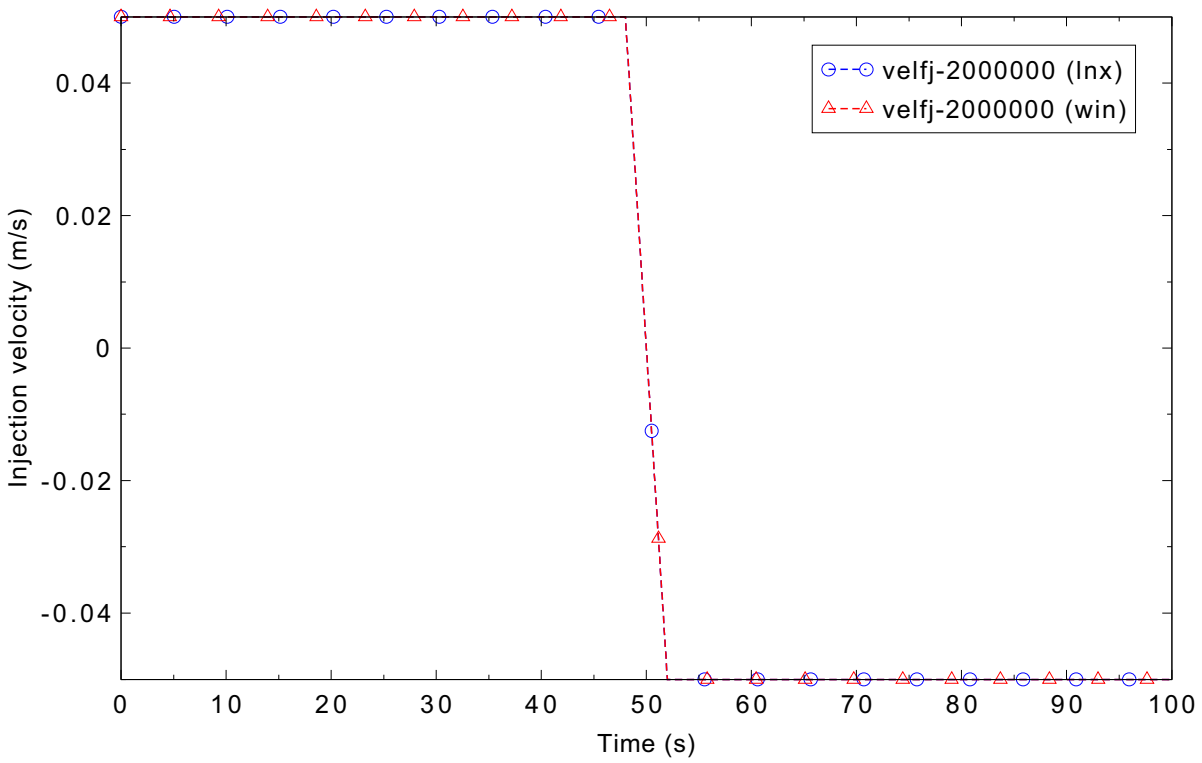

Figure 3.4-2. Injection flow liquid velocity comparison for the Fill-Drain test.

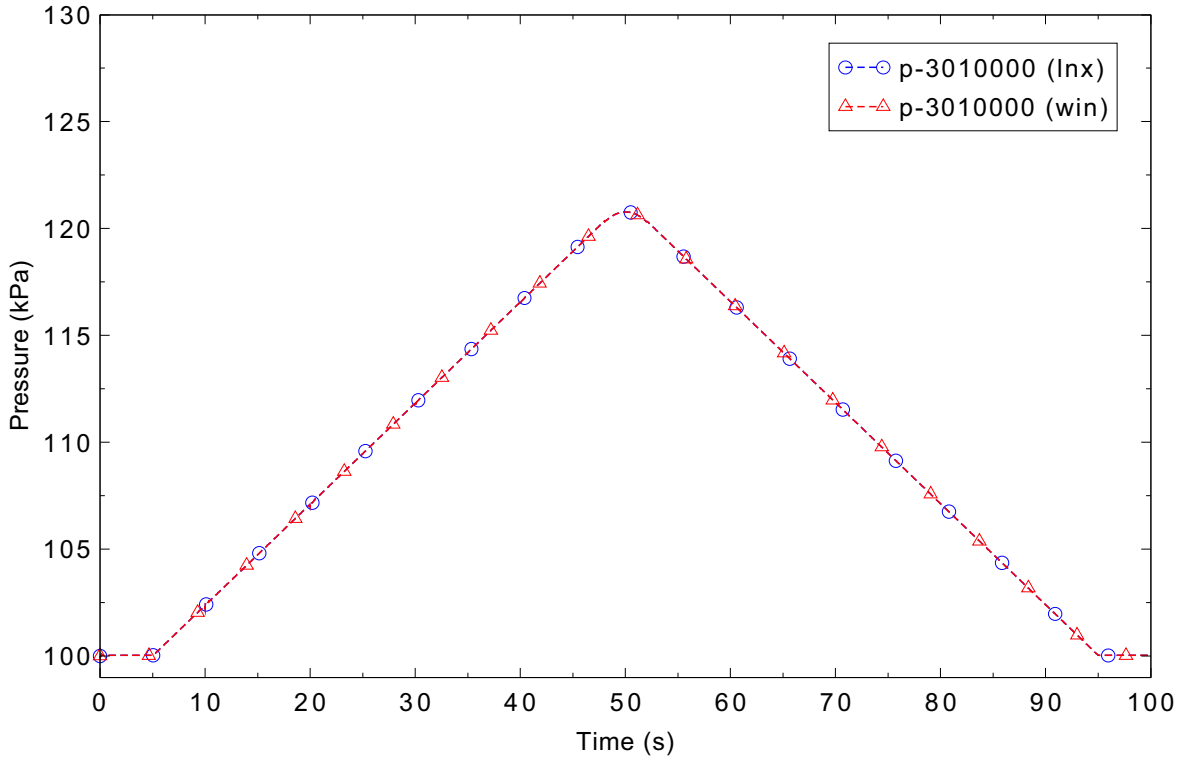

Figure 3.4-3. Bottom volume pressure comparison for the Fill-Drain test.

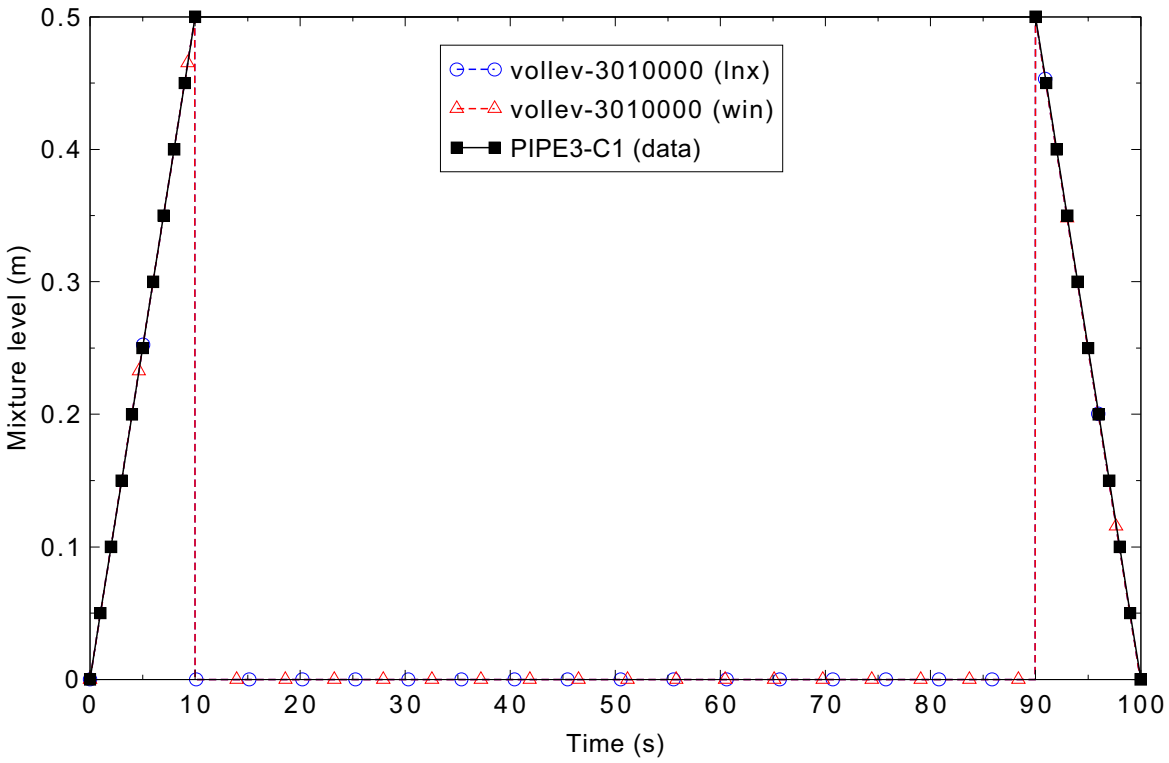

Figure 3.4-4. Mixture level comparison in volume 3-01 for the Fill-Drain test.

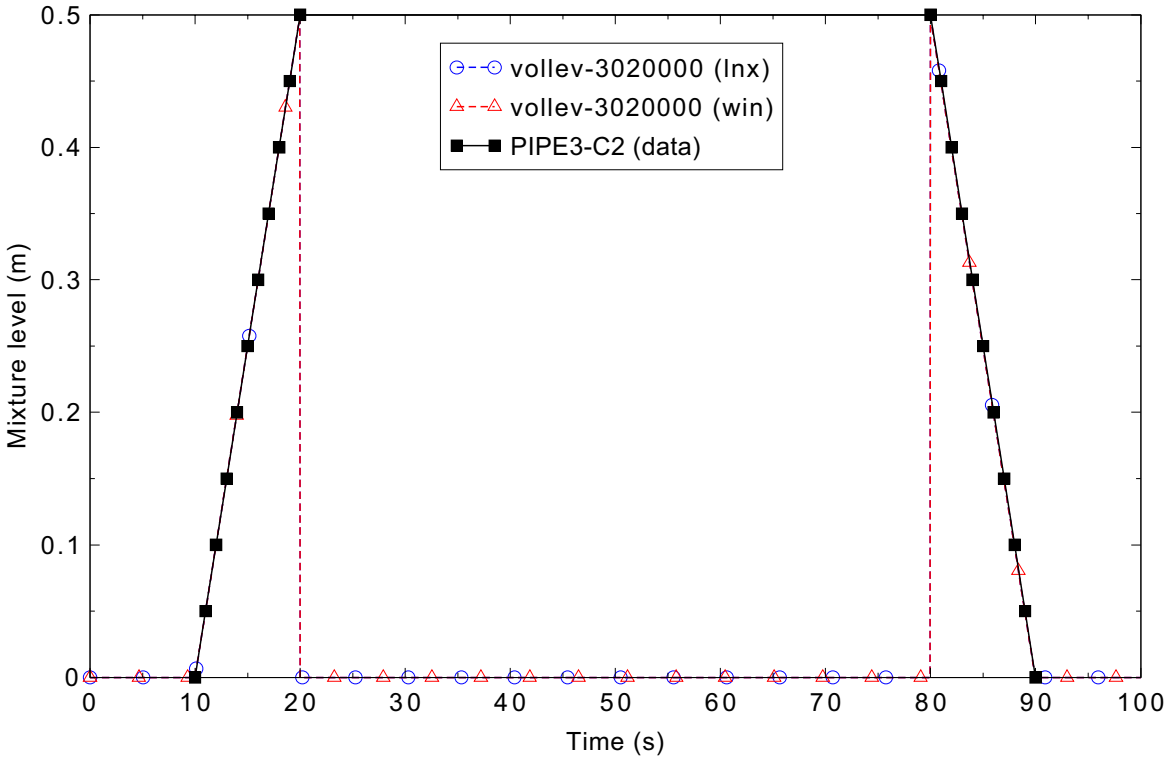

Figure 3.4-5. Mixture level comparison in volume 3-02 for the Fill-Drain test.

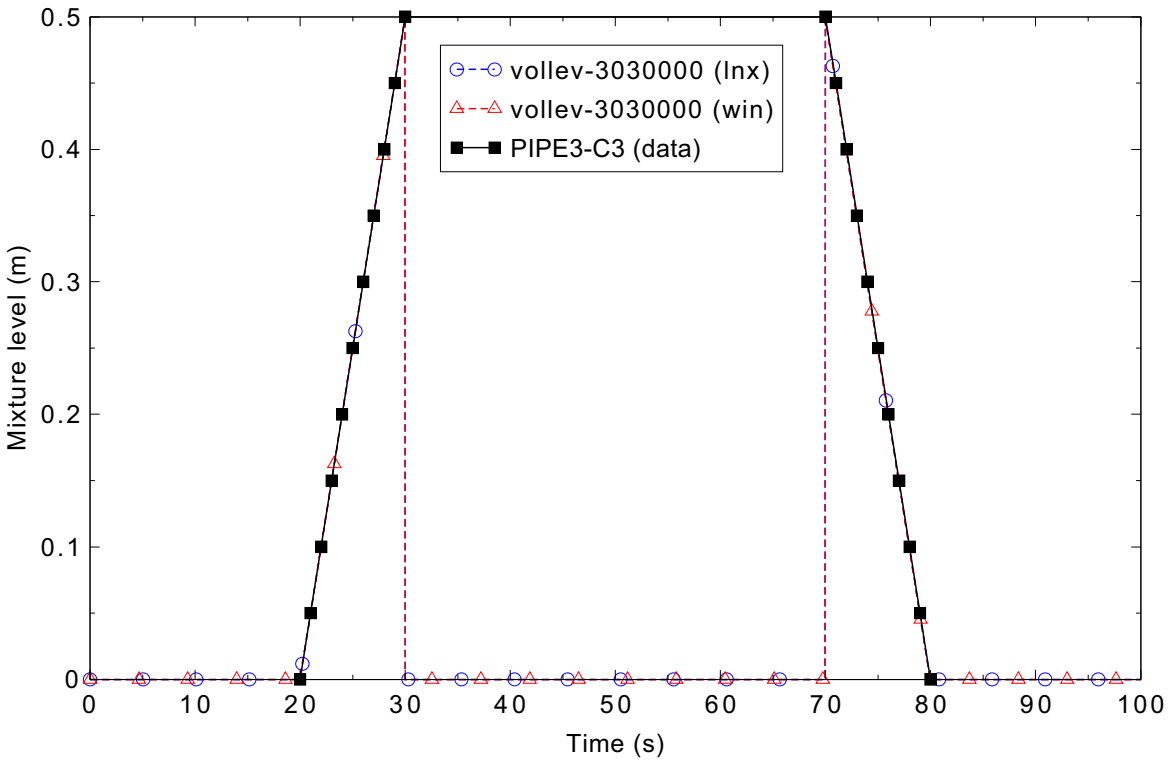

Figure 3.4-6. Mixture level comparison in volume 3-03 for the Fill-Drain test.

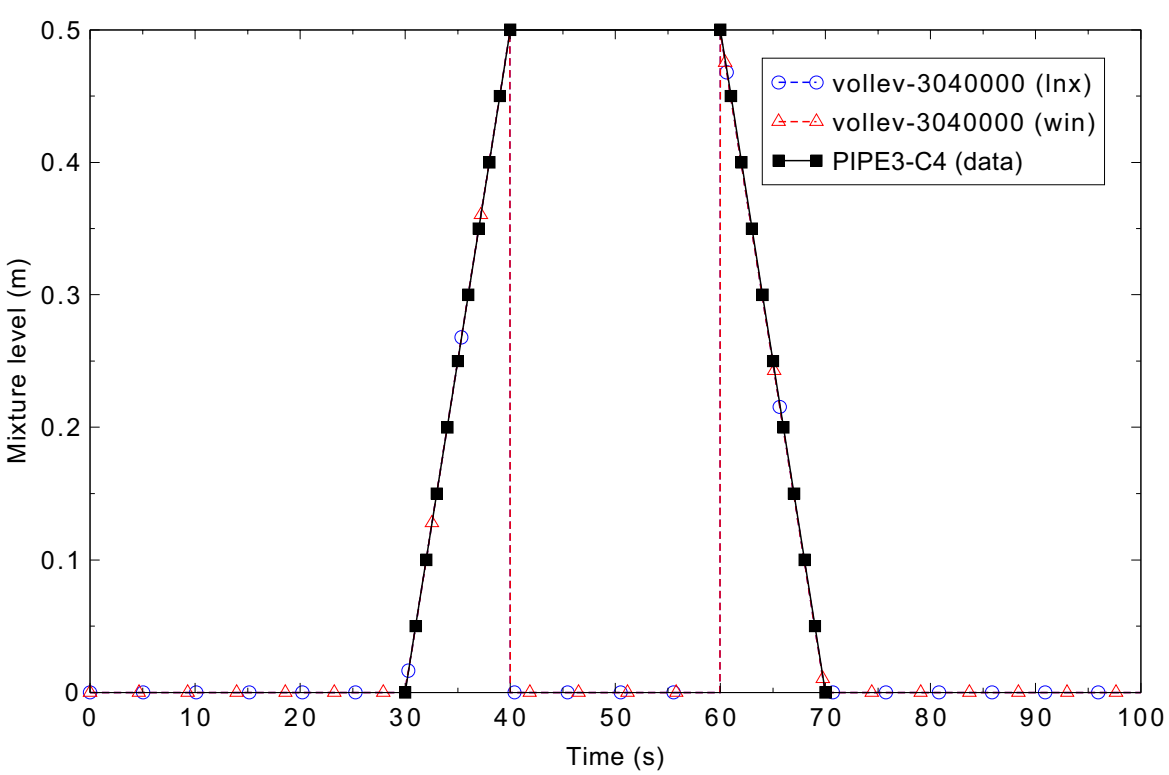

Figure 3.4-7. Mixture level comparison in volume 3-04 for the Fill-Drain test.

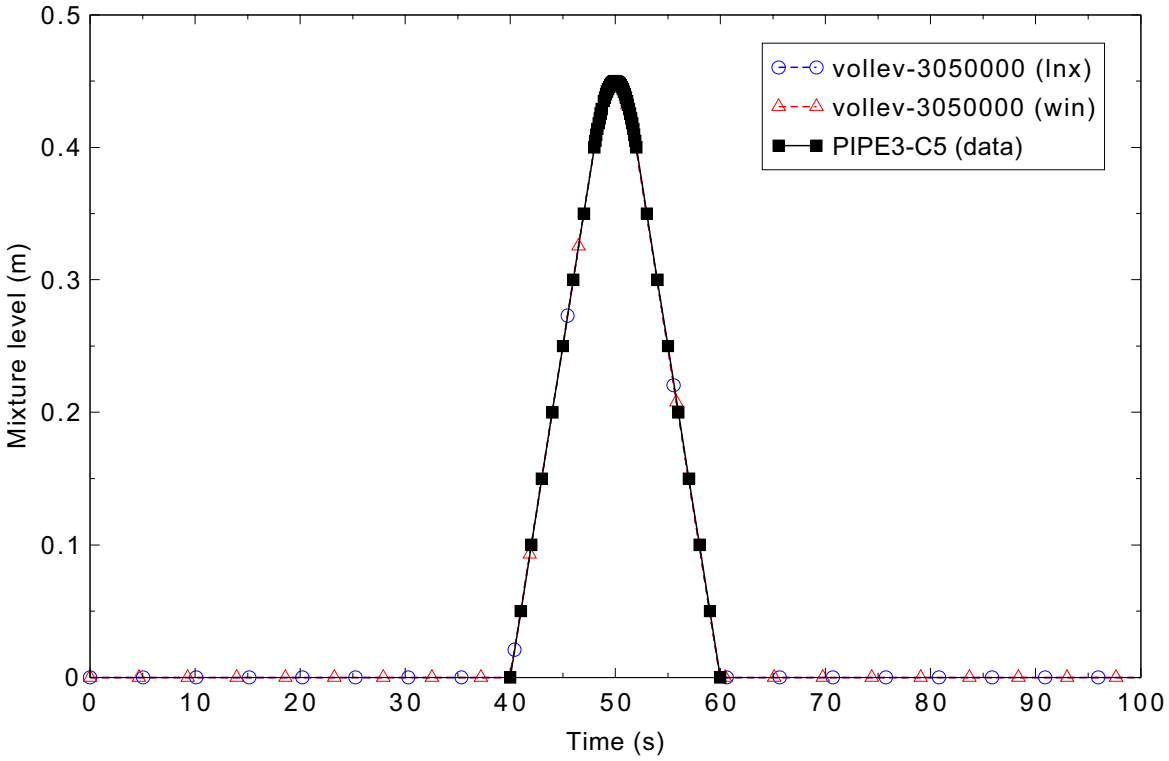

Figure 3.4-8. Mixture level comparison in volume 3-05 for the Fill-Drain test.

3.5 Bubbling Steam through Liquid

Figures comparing simulations using Linux and Windows code versions are presented. Diagrams are included so that the figure numbering is the same as that in Volume III of the RELAP5-3D code manual. Noticeable differences were observed in Figures 3.5-6, 7, and 8.

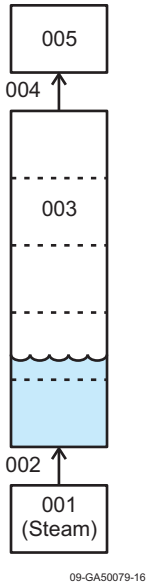

Figure 3.5-1. RELAP5-3D nodalization for the bubbling steam through liquid test case.

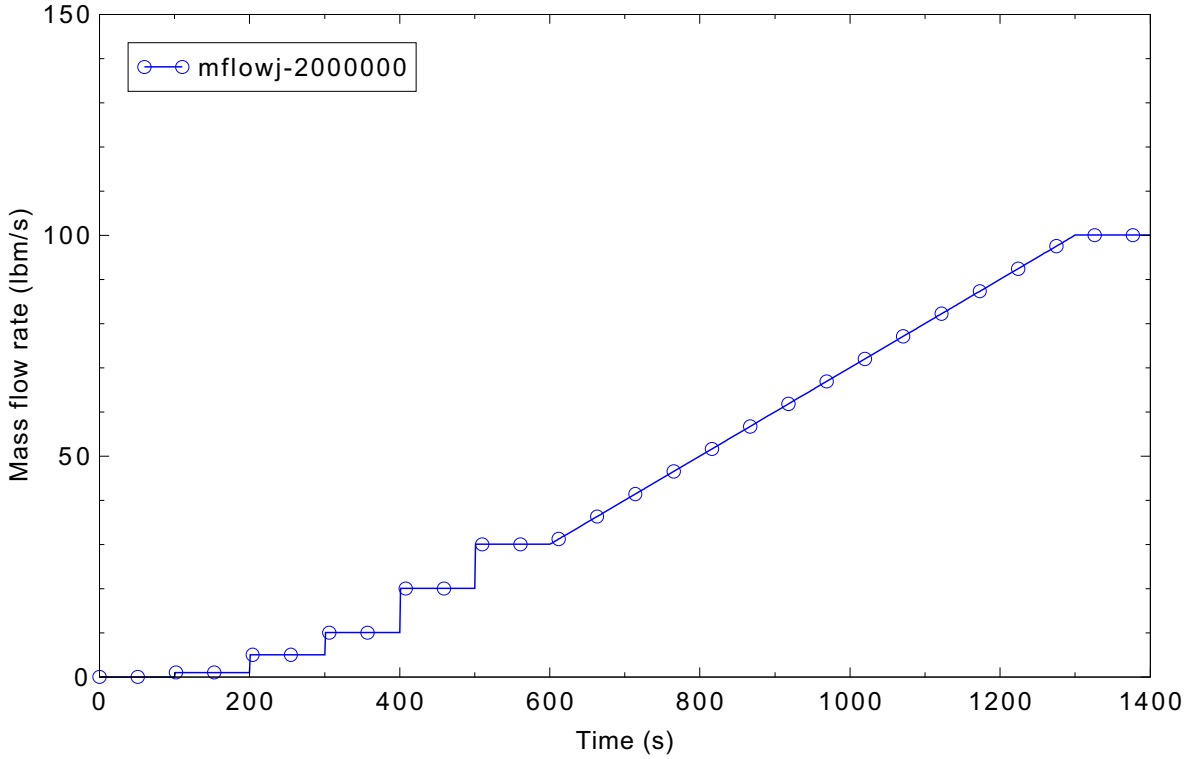

Figure 3.5-2. Mass flow rate of saturated steam at time-dependent junction 002 for the bubbling steam through liquid case.

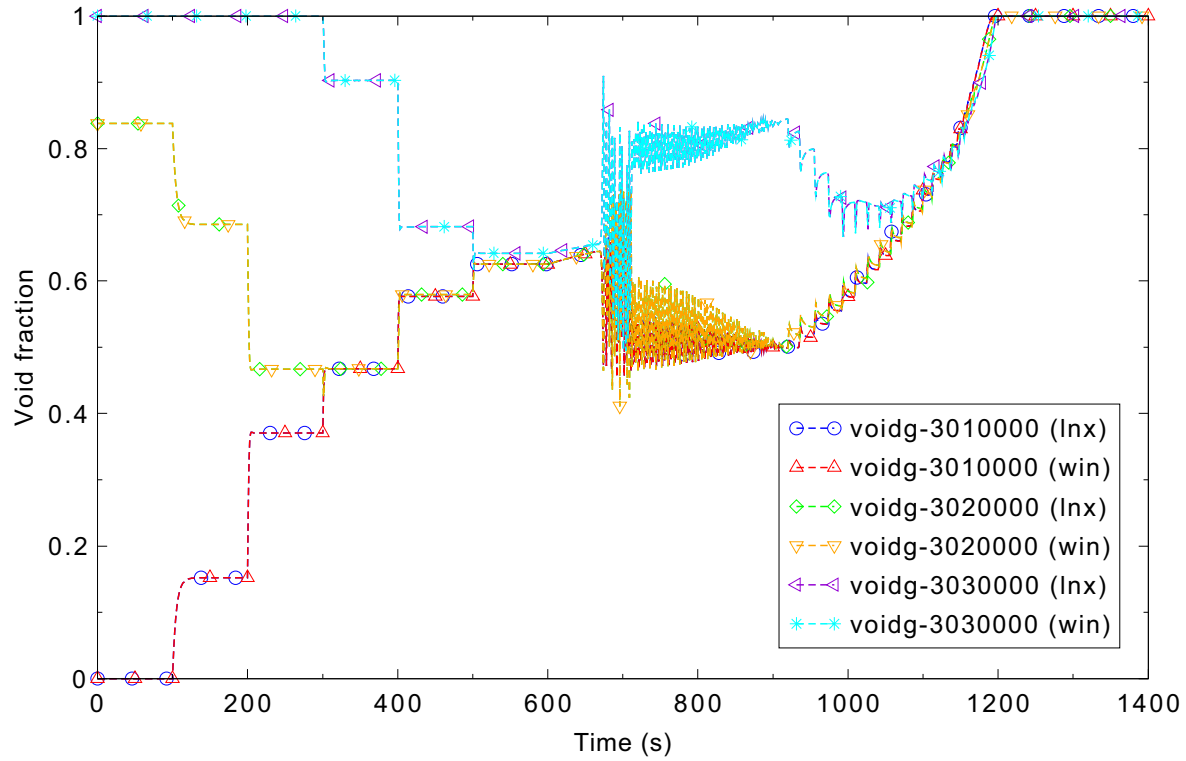

Figure 3.5-3. Void fractions in the pipe for the semi-implicit bubbling steam through liquid case.

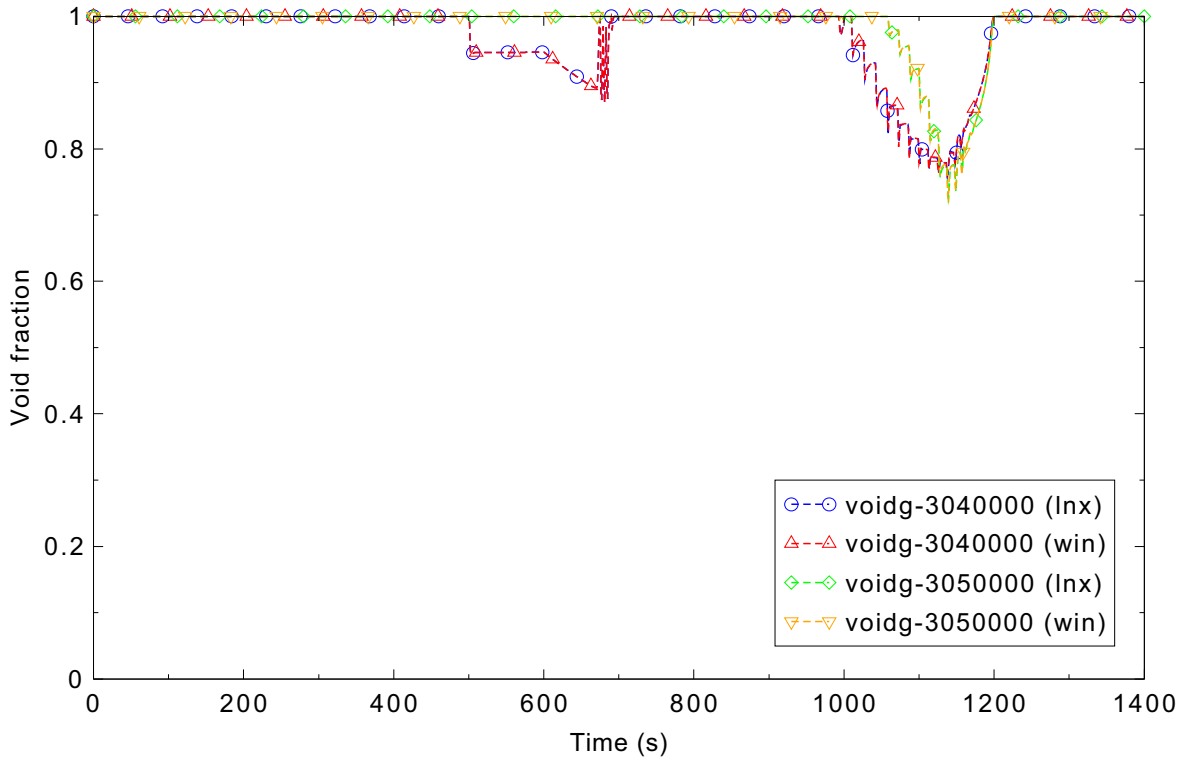

Figure 3.5-4. Void fractions in the pipe for the semi-implicit bubbling steam through liquid case.

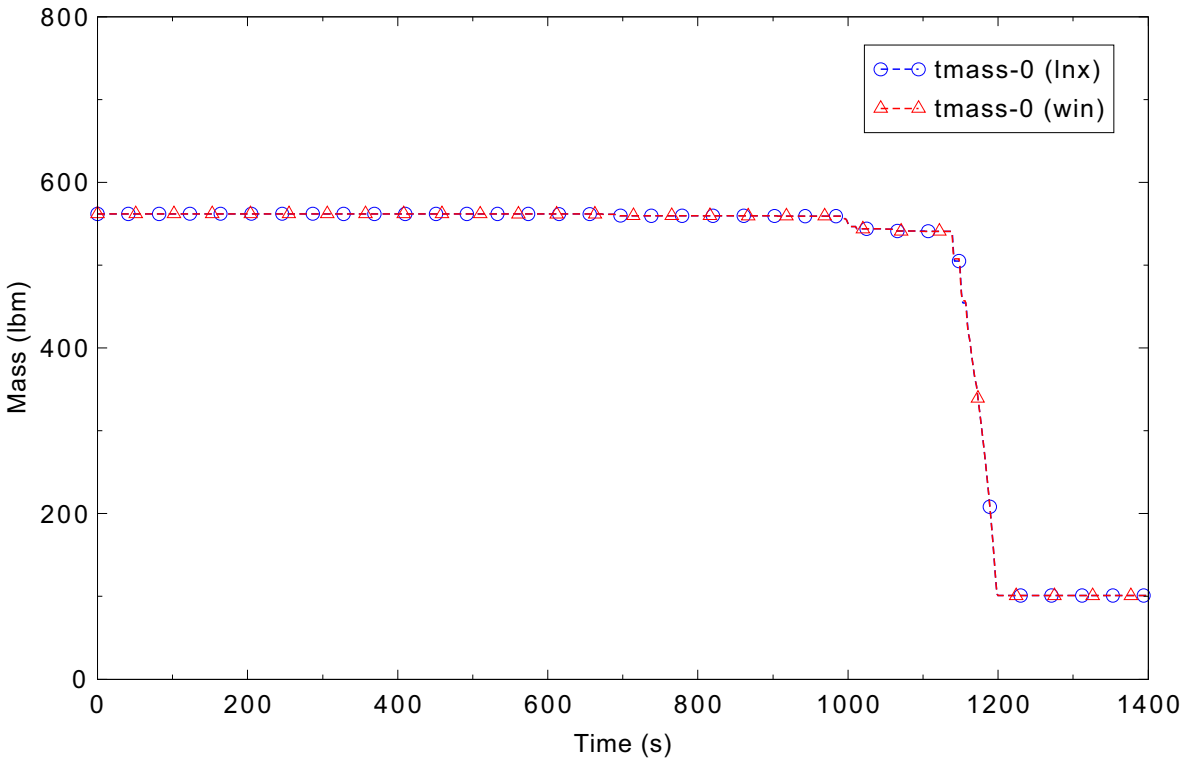

Figure 3.5-5. Total system mass for the bubbling steam through liquid case.

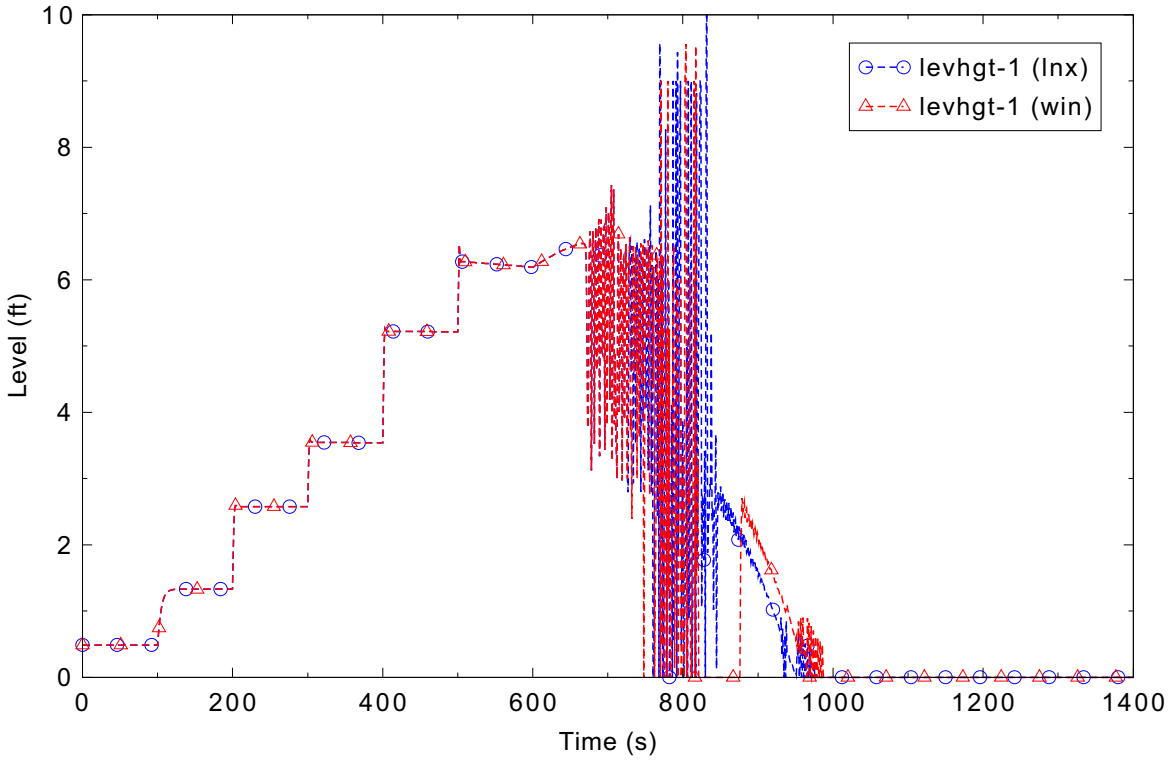

Figure 3.5-6. Mixture level in the pipe for the bubbling steam through liquid case with mixture level tracking.

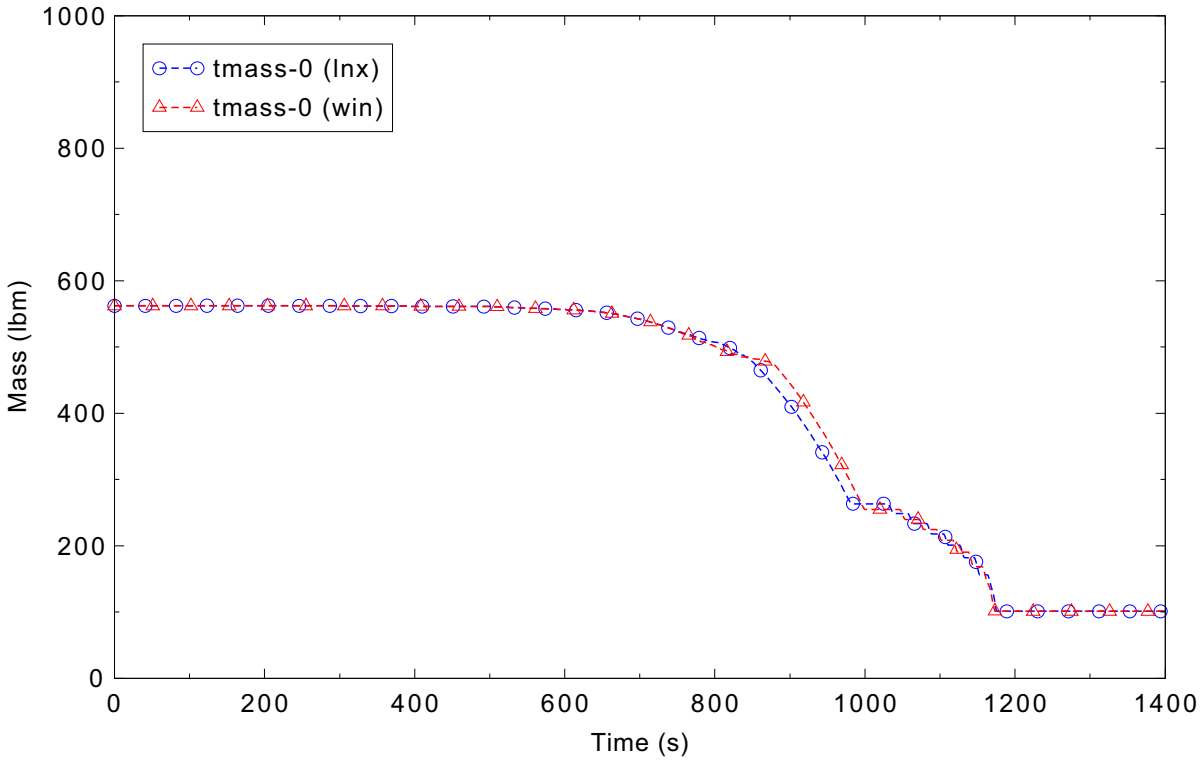

Figure 3.5-7. Total system mass for the bubbling steam through liquid case with mixture level tracking.

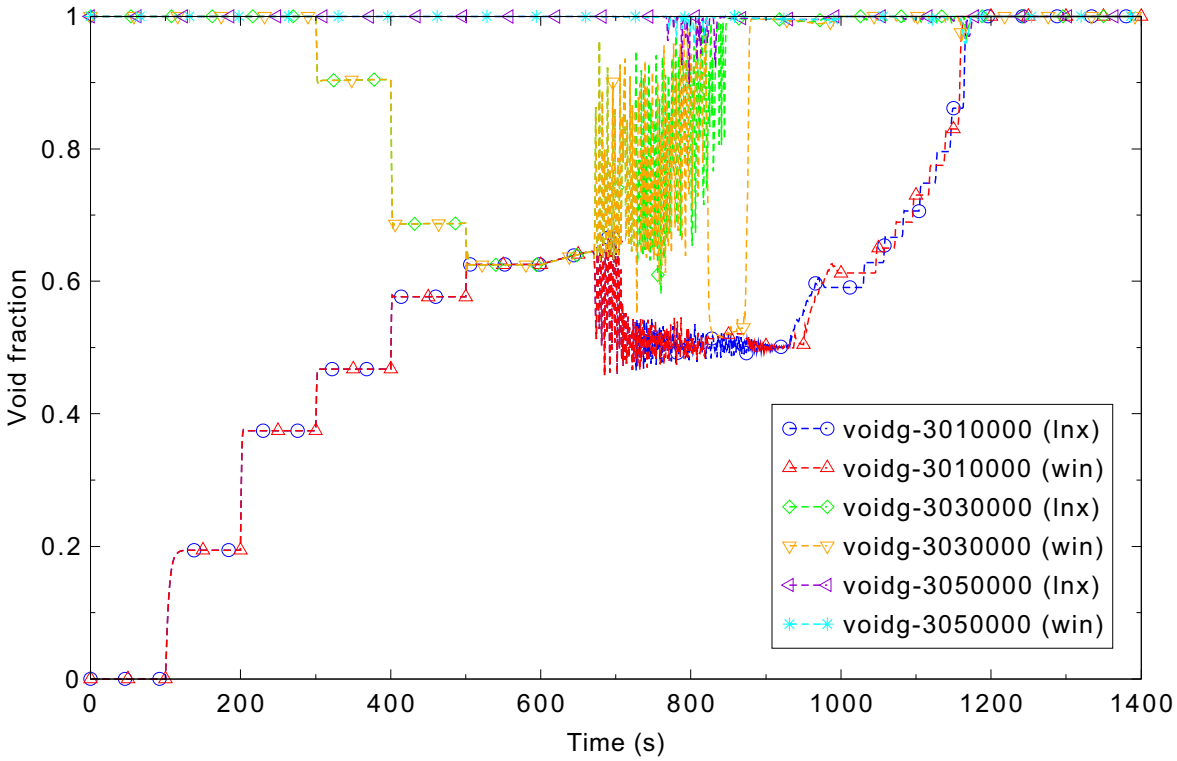

Figure 3.5-8. Void fractions in the pipe for the semi-implicit bubbling steam through liquid case with mixture level tracking.

3.6 Manometer

Figures comparing simulations using Linux and Windows code versions are presented. Diagrams are included so that the figure numbering is the same as that in Volume III of the RELAP5-3D code manual. No differences were observed in the figures.

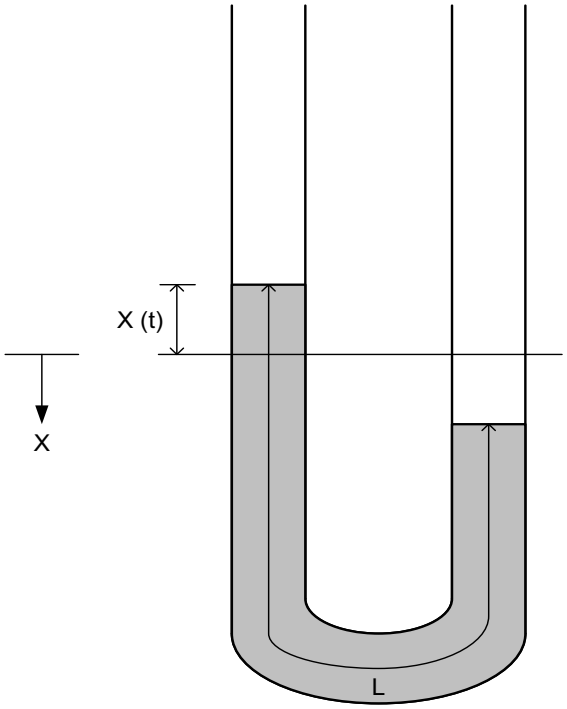

Figure 3.6-1. Schematic of oscillation manometer.

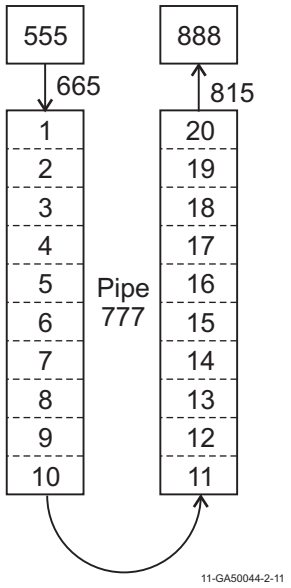

Figure 3.6-2. Nodalization diagram of nitrogen-water Manometer test input model.

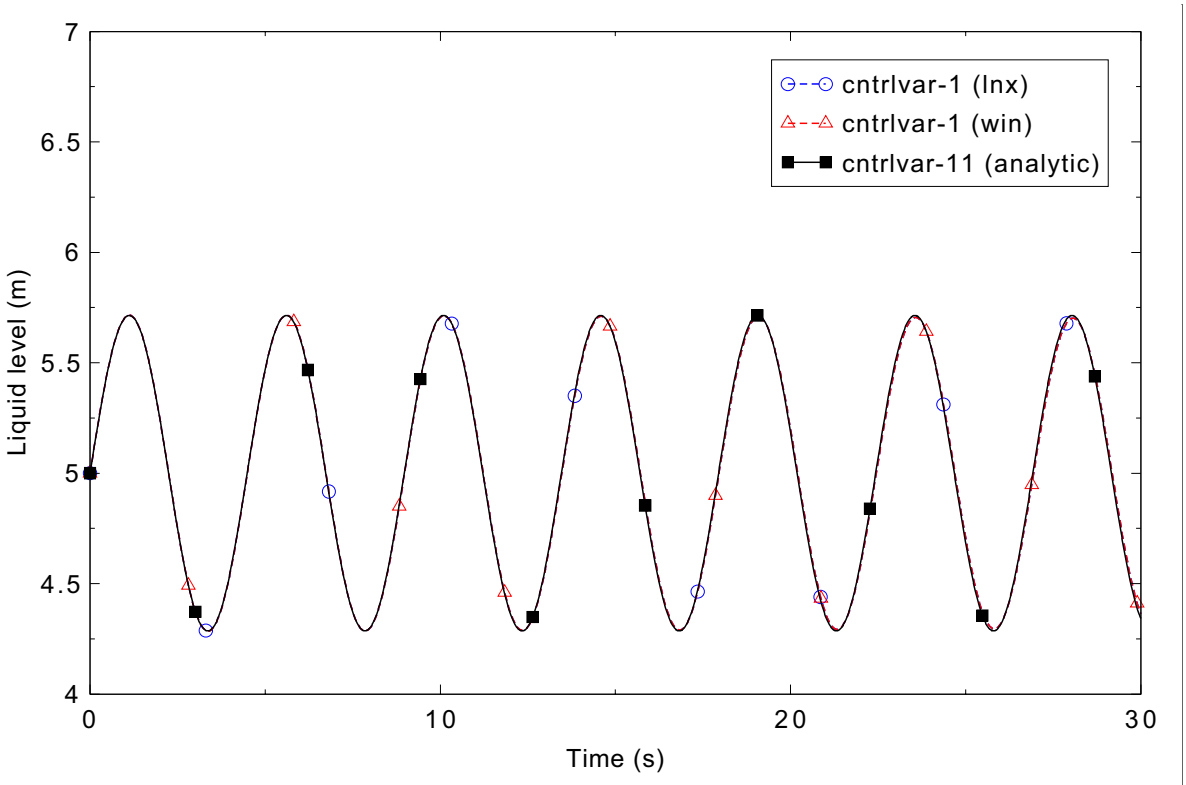

Figure 3.6-3. Comparison of water levels in the left leg for Manometer test.

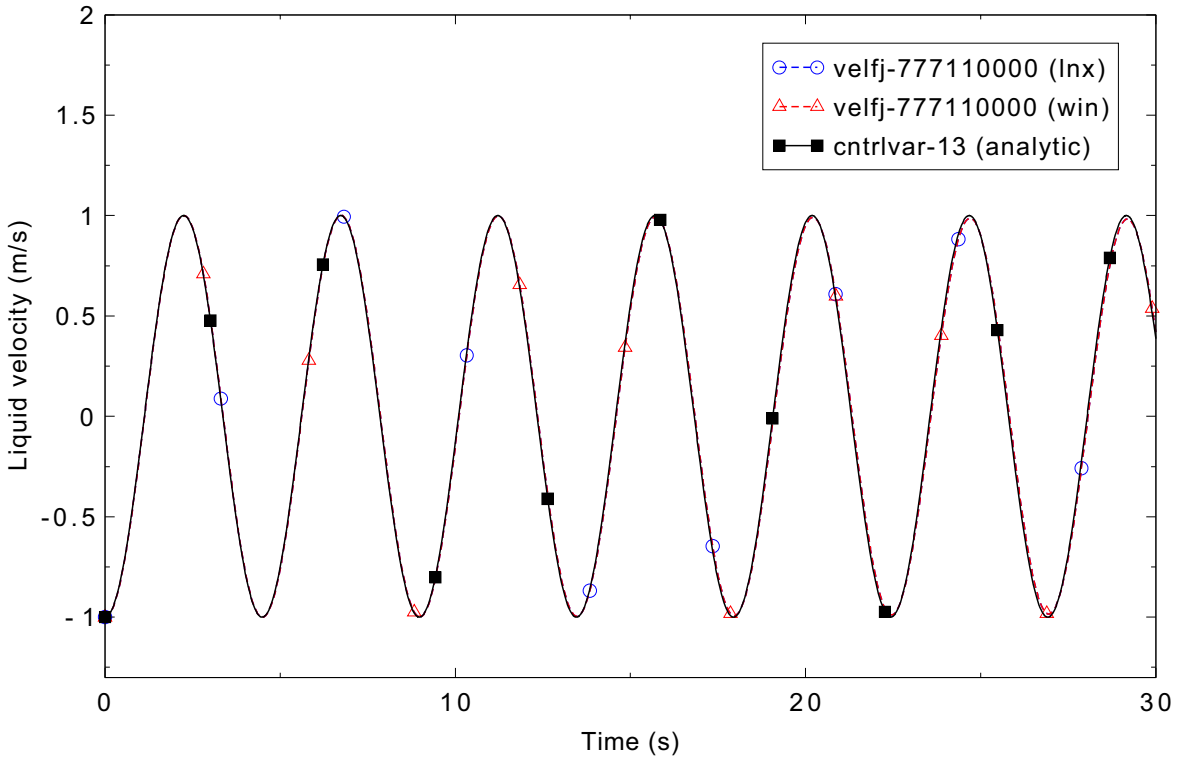

Figure 3.6-4. Comparison of liquid velocities for Manometer test.

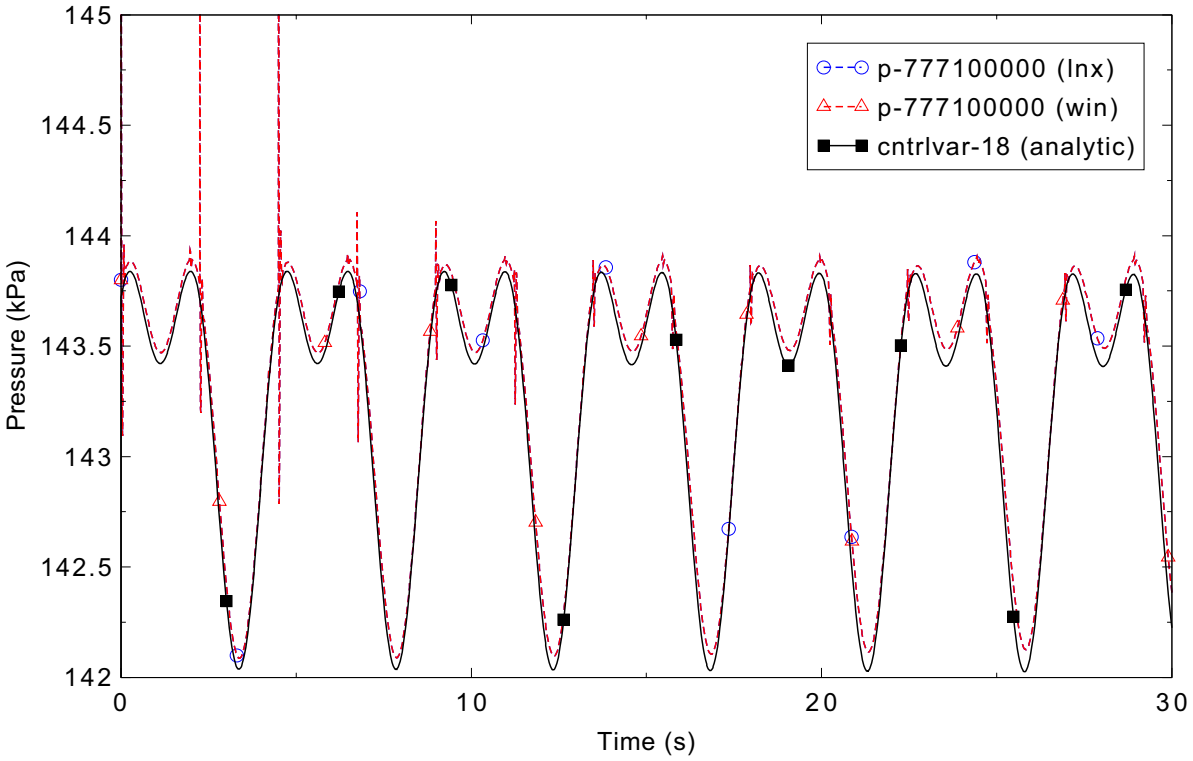

Figure 3.6-5. Comparison of bottom pressure for Manometer test.

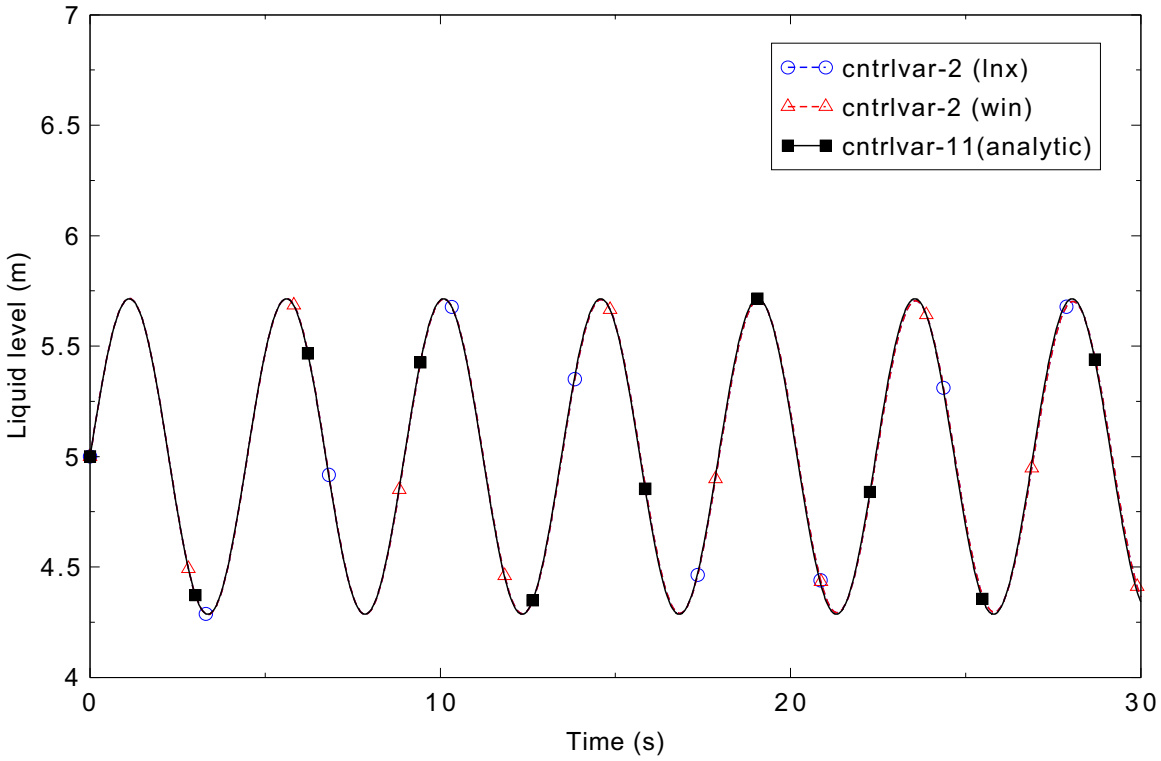

Figure 3.6-6. Comparison of water levels in the right leg for Manometer test.

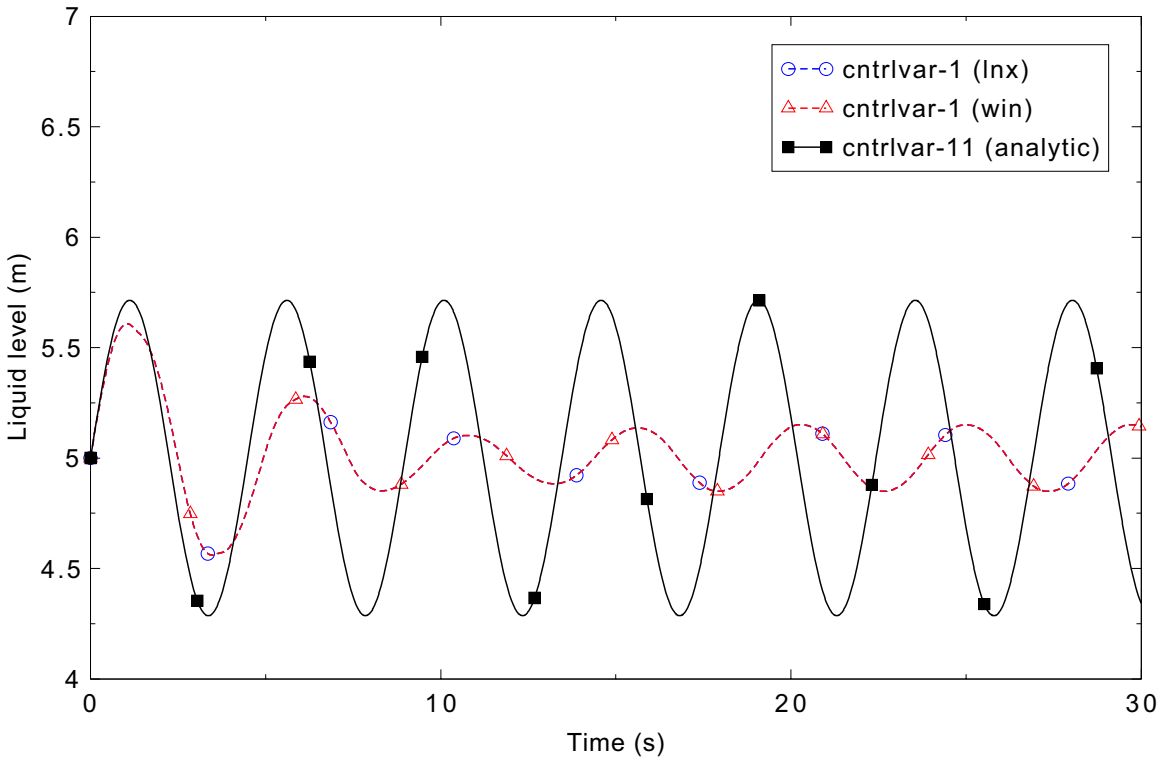

Figure 3.6-7. Comparison of water levels in the left leg for Manometer test without mixture level tracking.

3.7 Gravity Wave (1-D)

Figures comparing simulations using Linux and Windows code versions are presented. Diagrams are included so that the figure numbering is the same as that in Volume III of the RELAP5-3D code manual. No differences were observed in the figures.

.

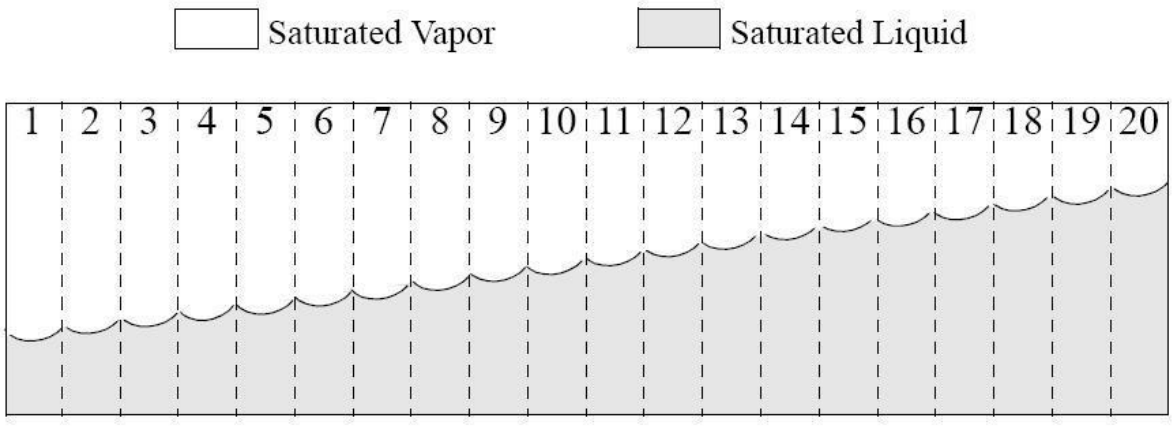

Figure 3.7-1. RELAP5-3D nodalization diagram for the 1-D gravity wave problem.

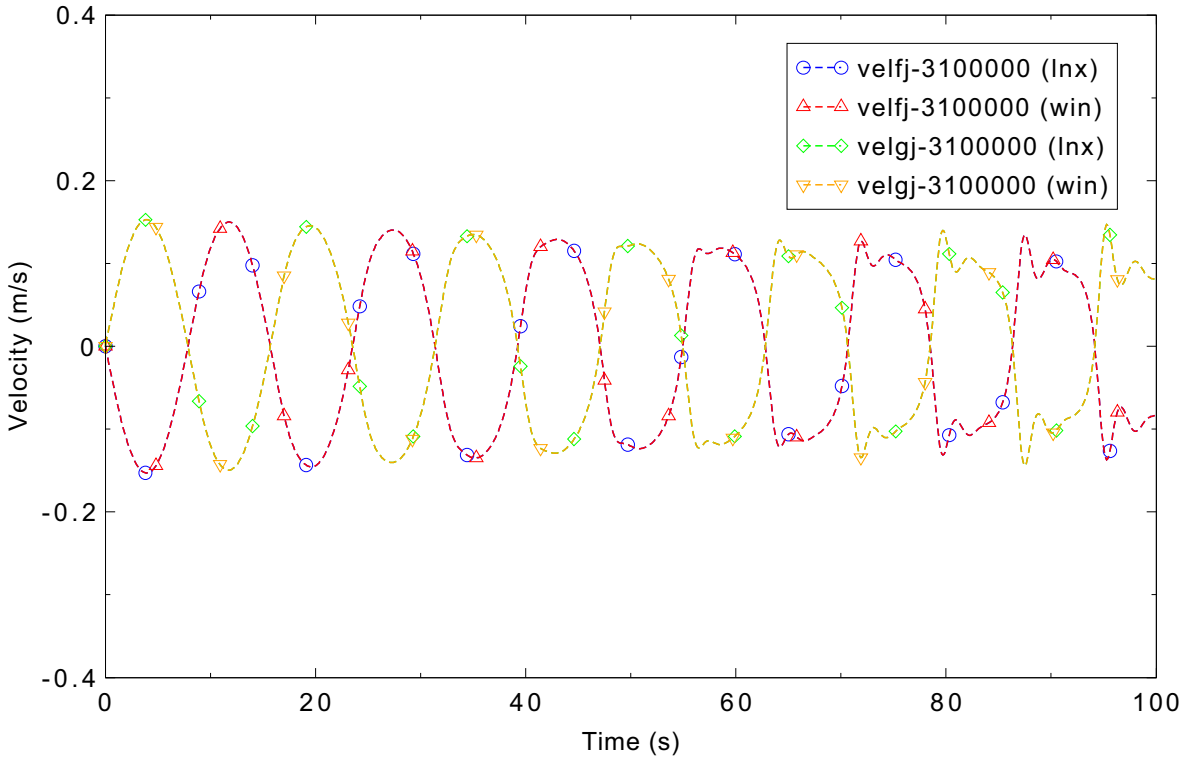

Figure 3.7-2. Calculated liquid and vapor velocities at mid-pipe, gravity wave 1-D, Card 1 Option 7 on.

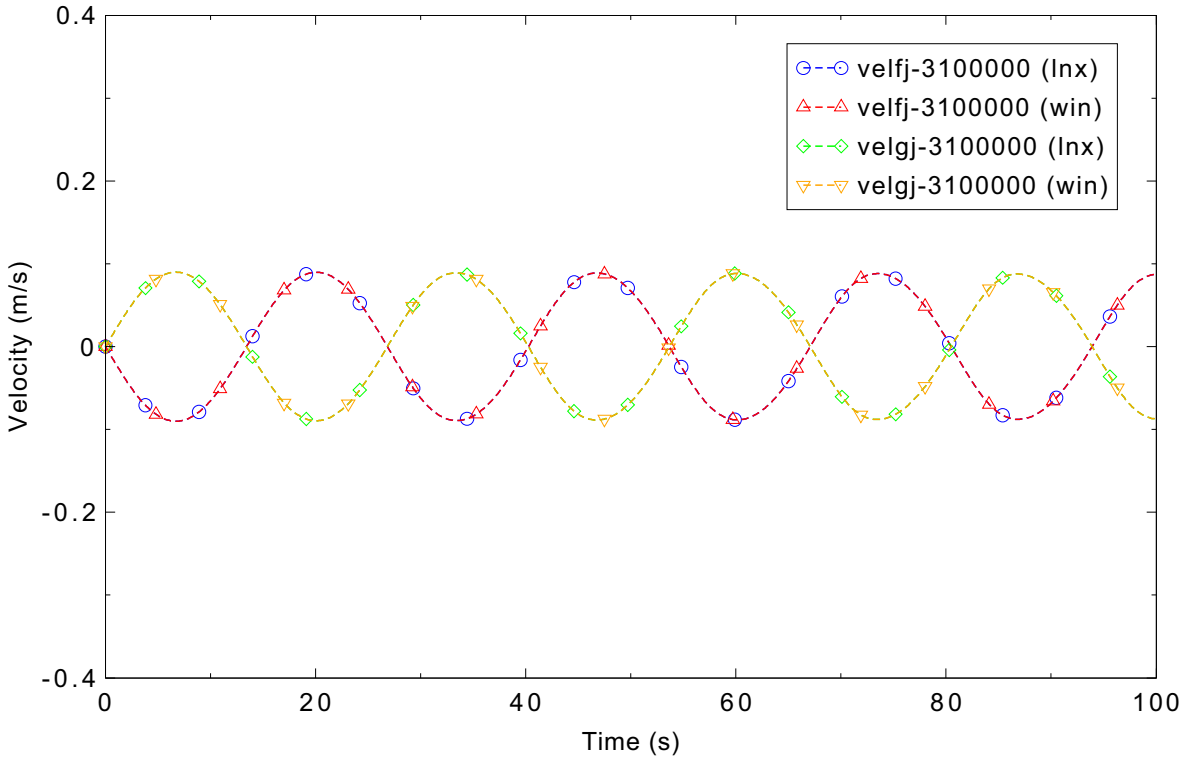

Figure 3.7-3. Calculated liquid and vapor velocities at mid-pipe, gravity wave 1-D, Card 1 Option 7 off.

3.8 Gravity Wave (3-D)

Figures comparing simulations using Linux and Windows code versions are presented. Diagrams are included so that the figure numbering is the same as that in Volume III of the RELAP5-3D code manual. No differences were observed in the figures.

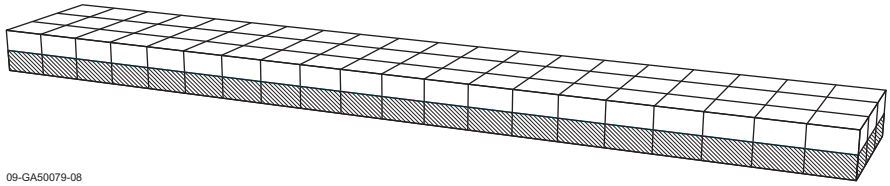

Figure 3.8-1. RELAP5-3D nodalization diagram for the 3-D gravity wave problem.

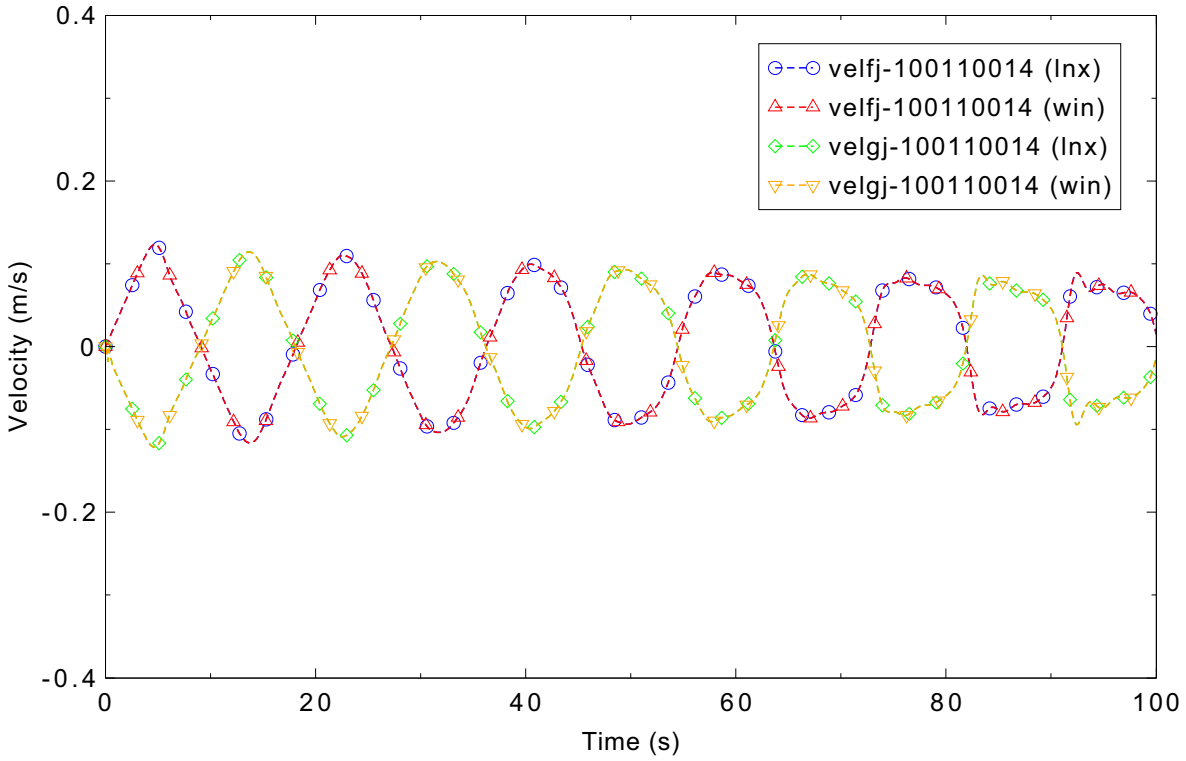

Figure 3.8-2. Calculated liquid and vapor velocities mid-duct, x-interval 1, gravity wave 3-D, Card 1 Option 7 on.

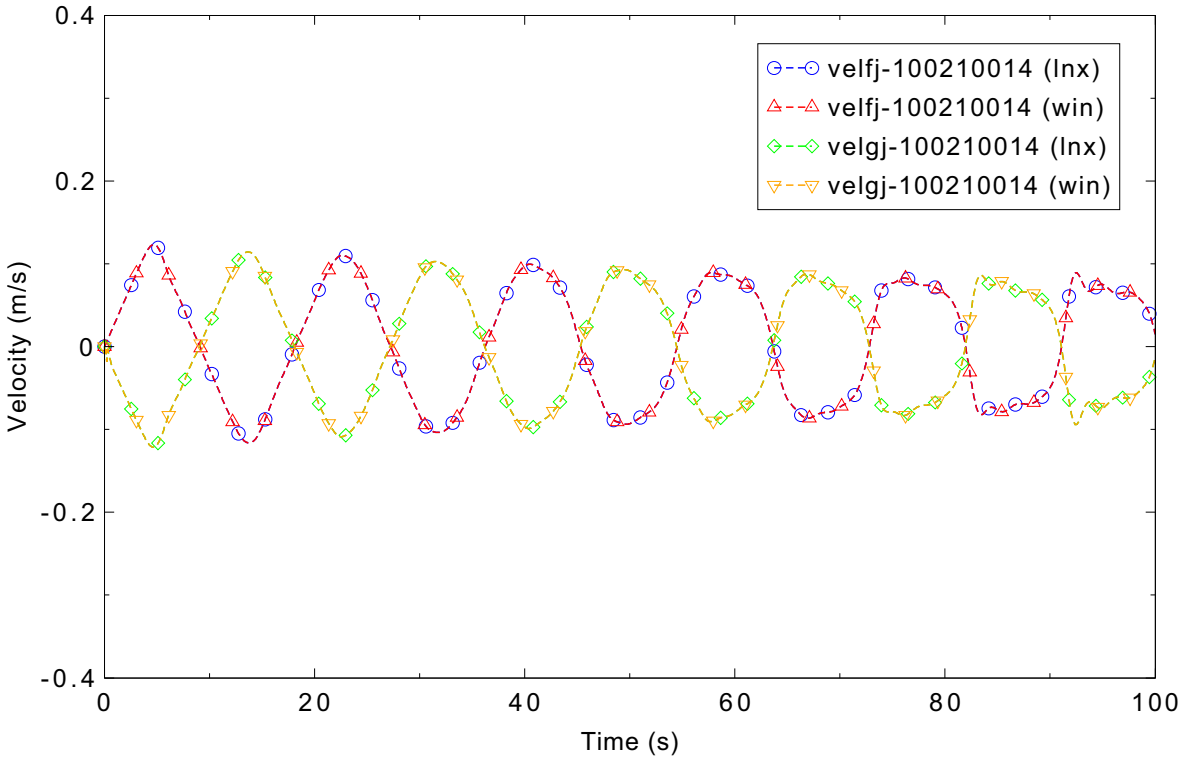

Figure 3.8-3. Calculated liquid and vapor velocities mid-duct, x-interval 2, gravity wave 3-D, Card 1 Option 7 on.

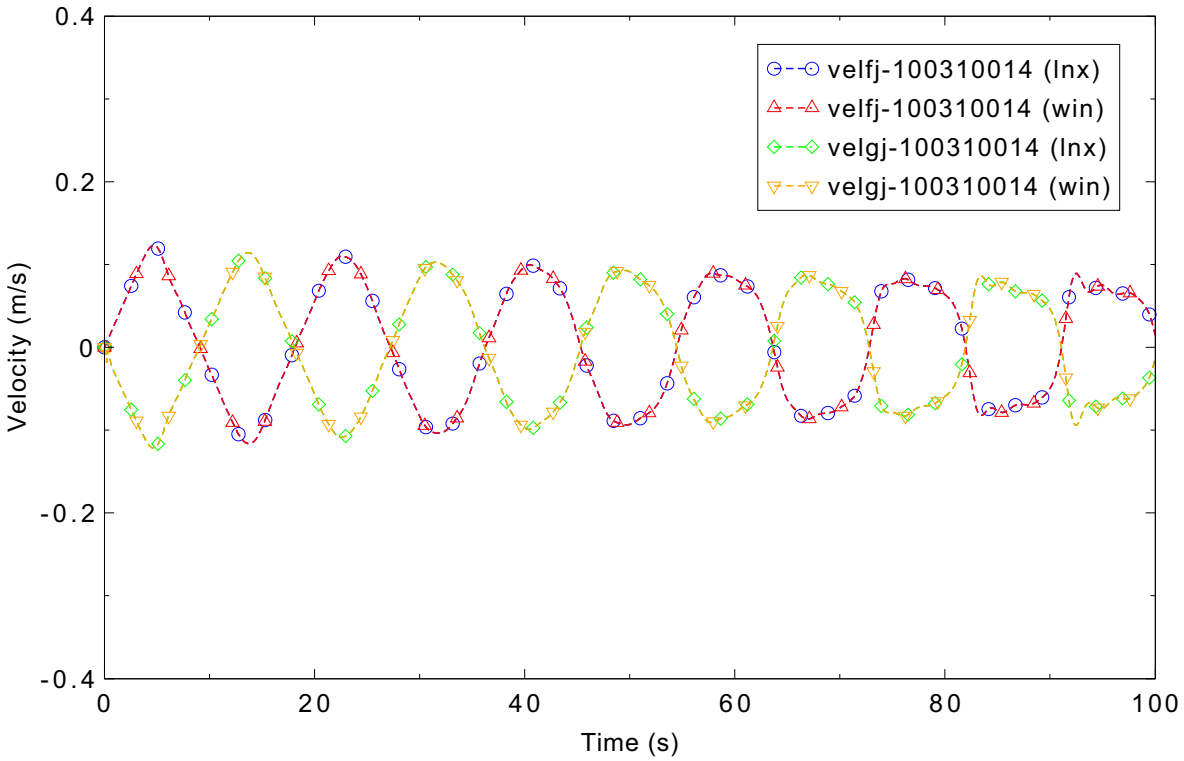

Figure 3.8-4. Calculated liquid and vapor velocities mid-duct, x-interval 3, gravity wave 3-D, Card 1 Option 7 on.

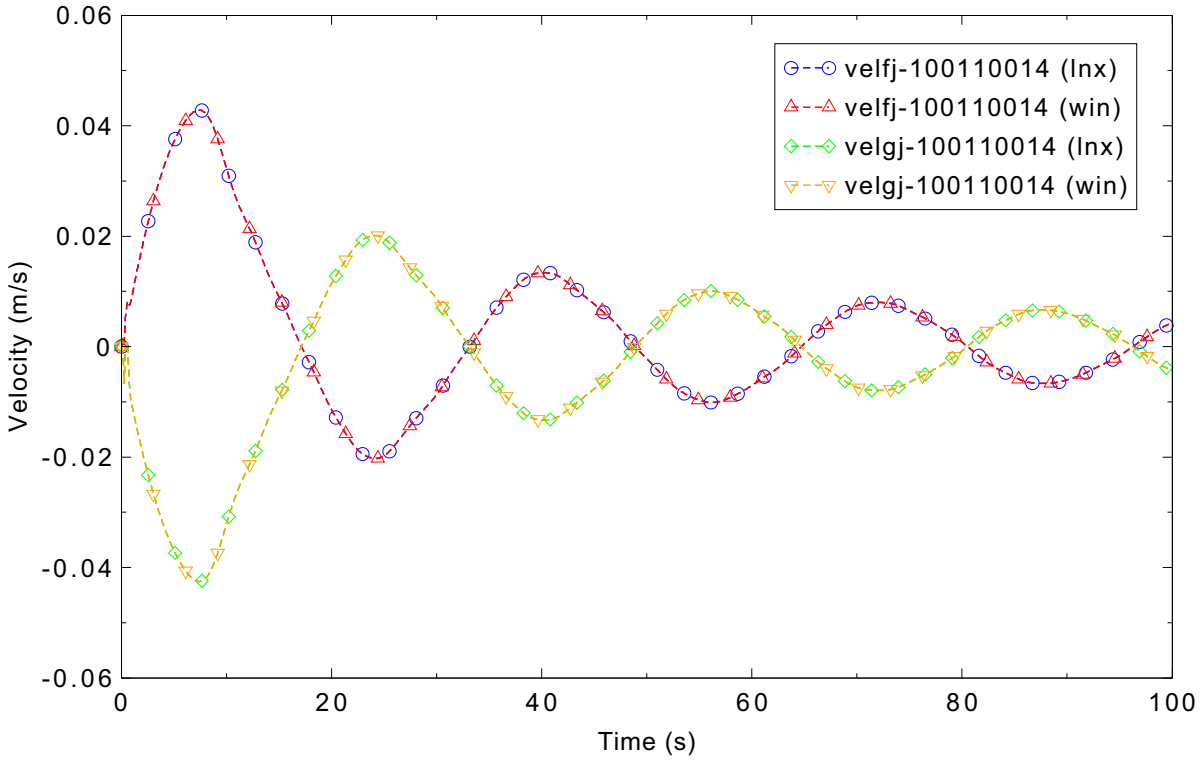

Figure 3.8-5. Calculated liquid and vapor velocities mid-duct, x-interval 1, gravity wave 3-D, Card 1 Option 7 off.

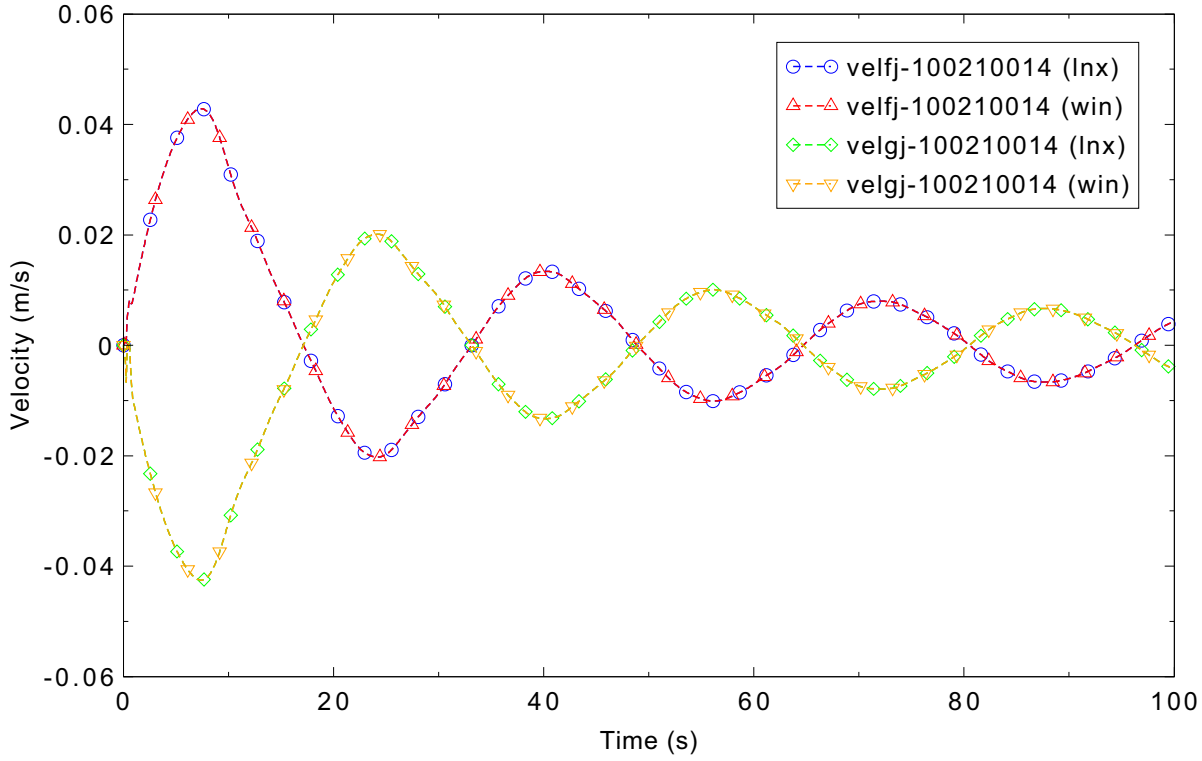

Figure 3.8-6. Calculated liquid and vapor velocities mid-duct, x-interval 2, gravity wave 3-D, Card 1 Option 7 off.

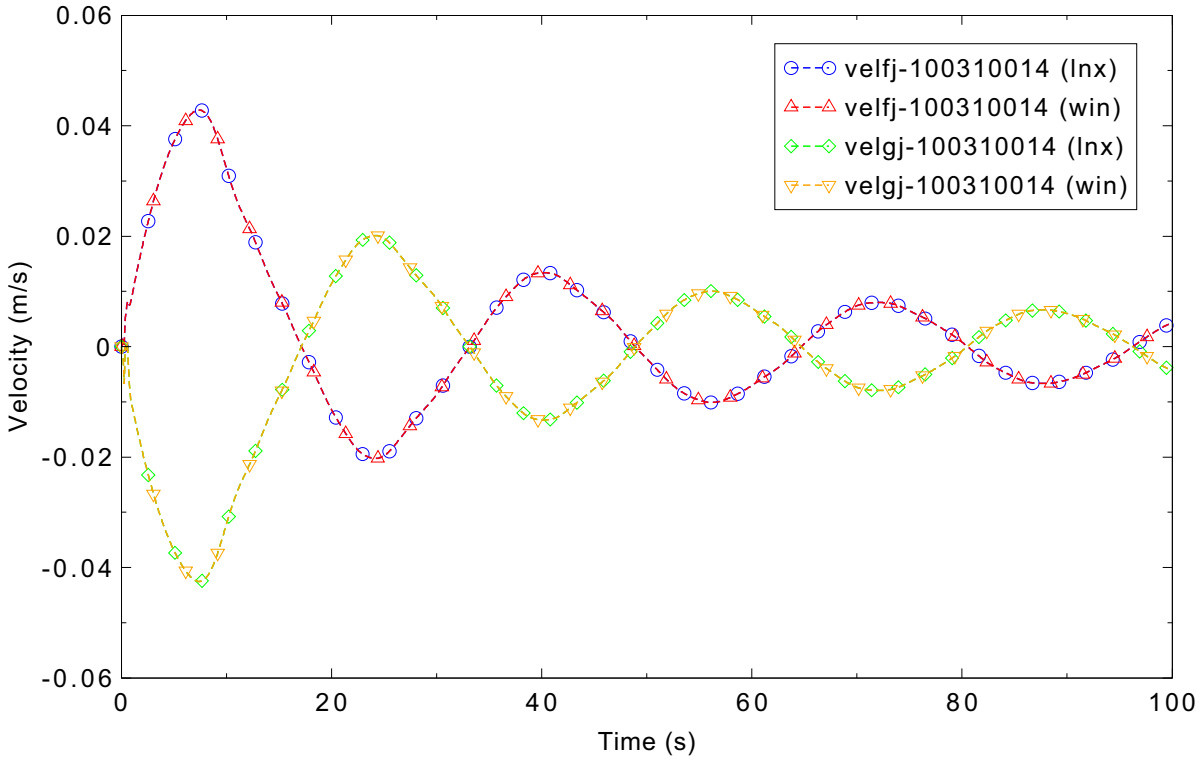

Figure 3.8-7. Calculated liquid and vapor velocities mid-duct, x-interval 3, gravity wave 3-D, Card 1 Option 7 off.

3.9 Pryor Pressure Comparison

Figures comparing simulations using Linux and Windows code versions are presented. Diagrams are included so that the figure numbering is the same as that in Volume III of the RELAP5-3D code manual. No differences were observed in the figures.

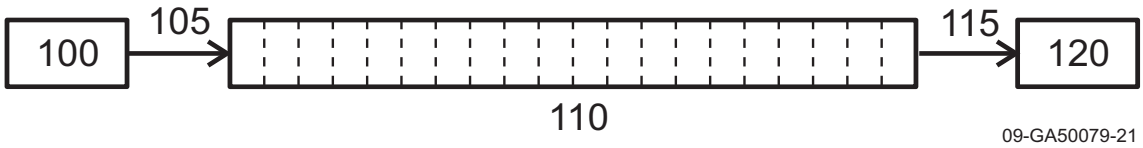

Figure 3.9-1. Nodalization diagram for the Pryor pressure test problem.

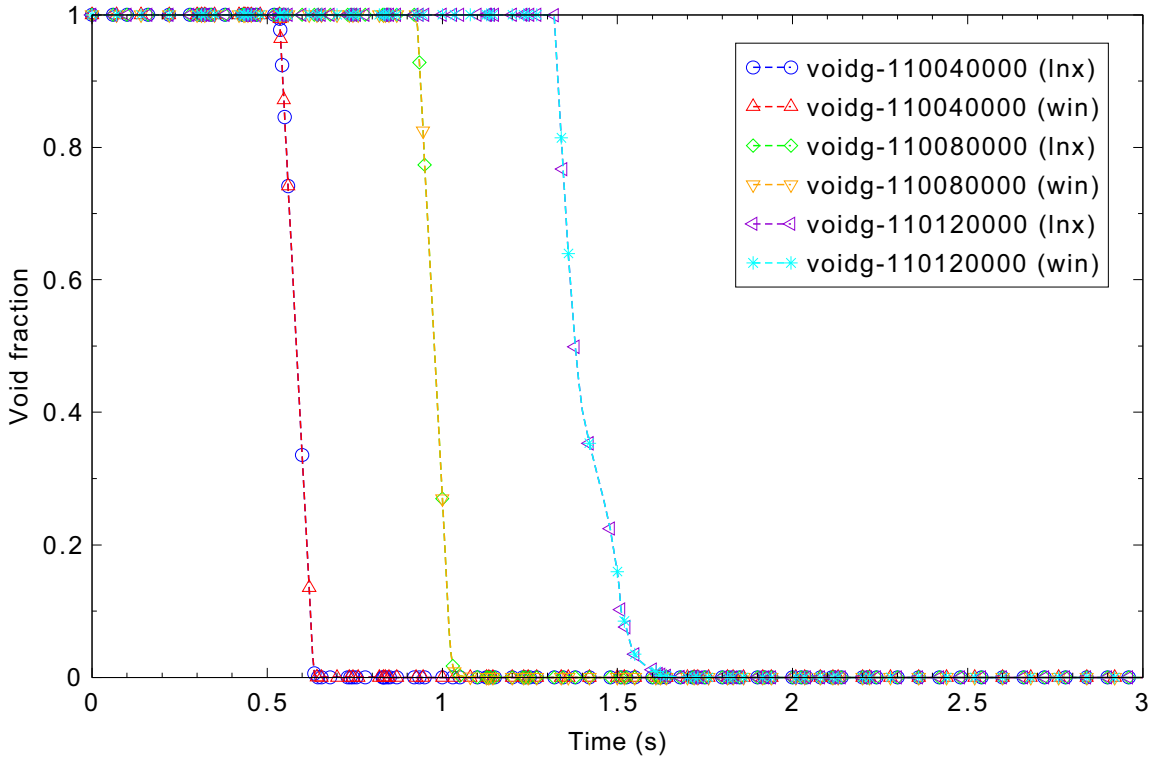

Figure 3.9-2. Void fraction for Pryor pressure test, semi-implicit case with maximum dt = 0.02 s.

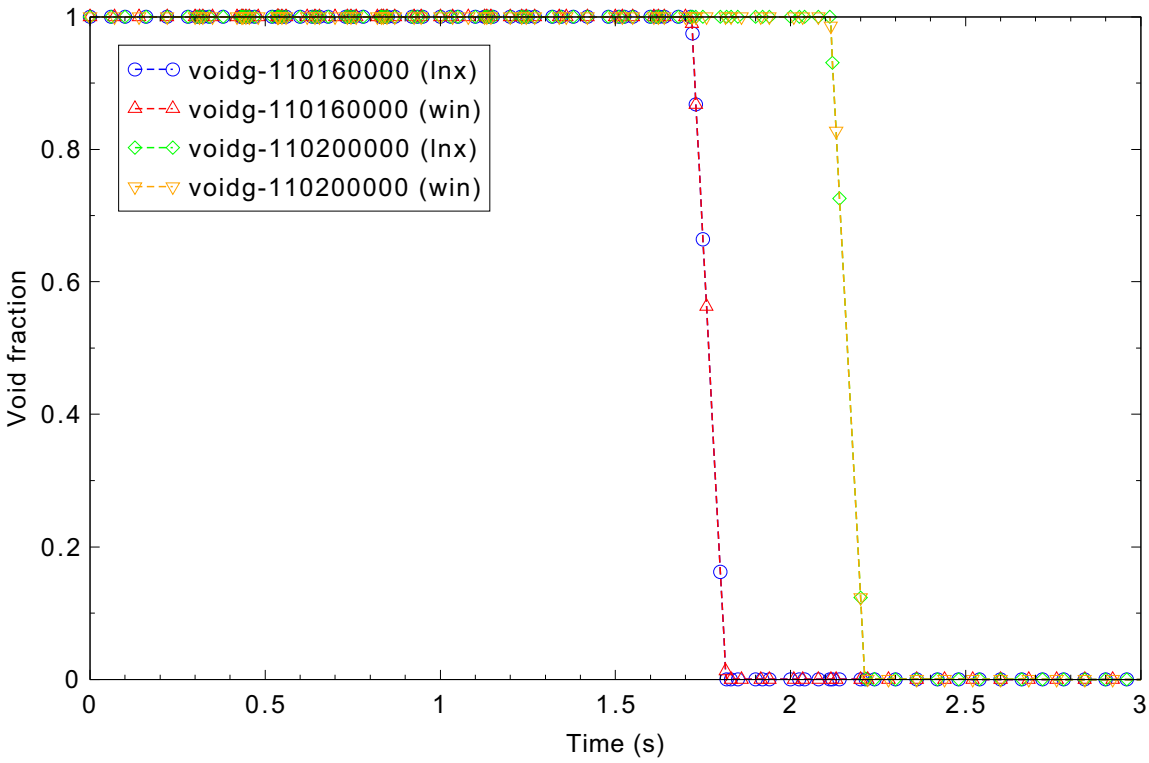

Figure 3.9-3. Void fraction for Pryor pressure test, semi-implicit case with maximum dt = 0.02 s.

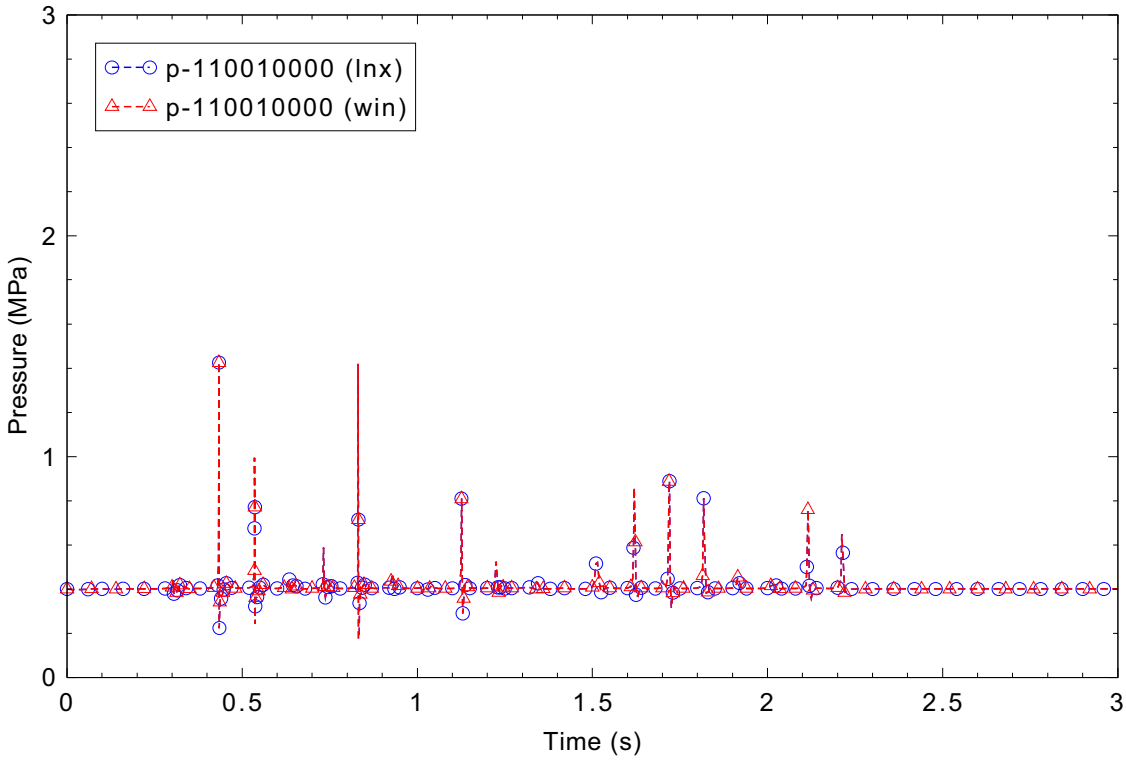

Figure 3.9-4. Volume 1 pressure for Pryor pressure test, semi-implicit case with maximum dt = 0.02 s.

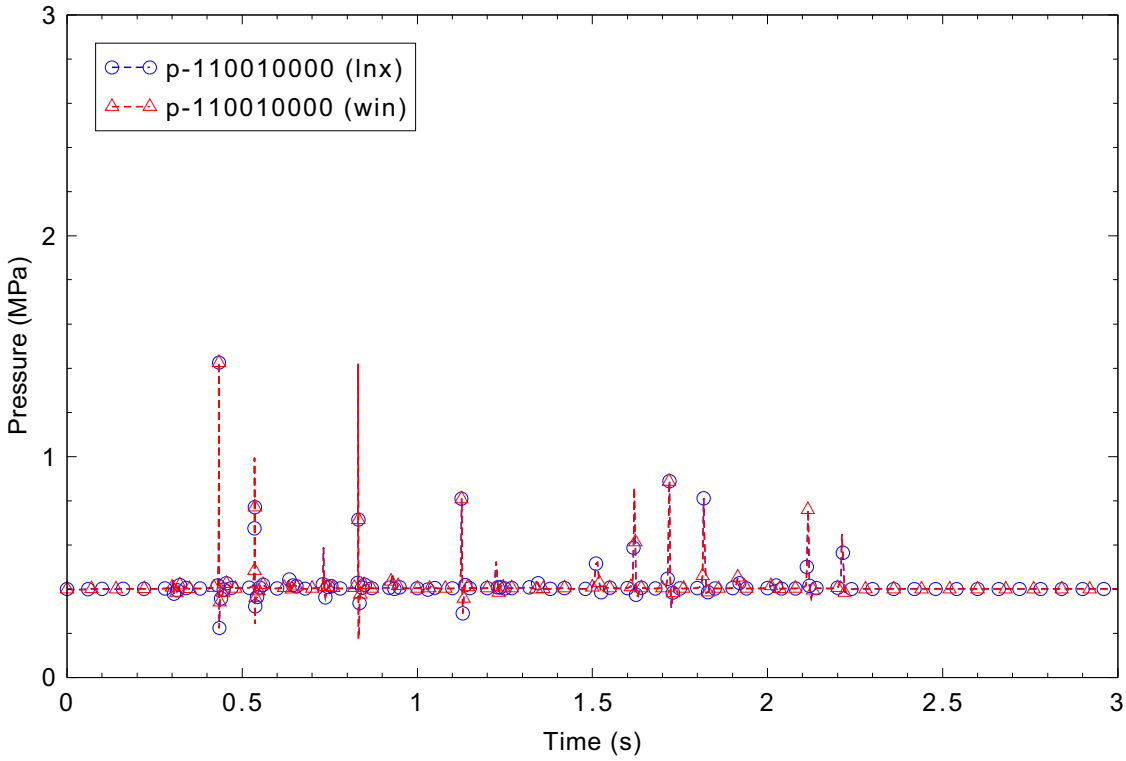

Figure 3.9-5. Volume 1 pressure for Pryor pressure test, semi-implicit case with maximum dt = 0.02 s.

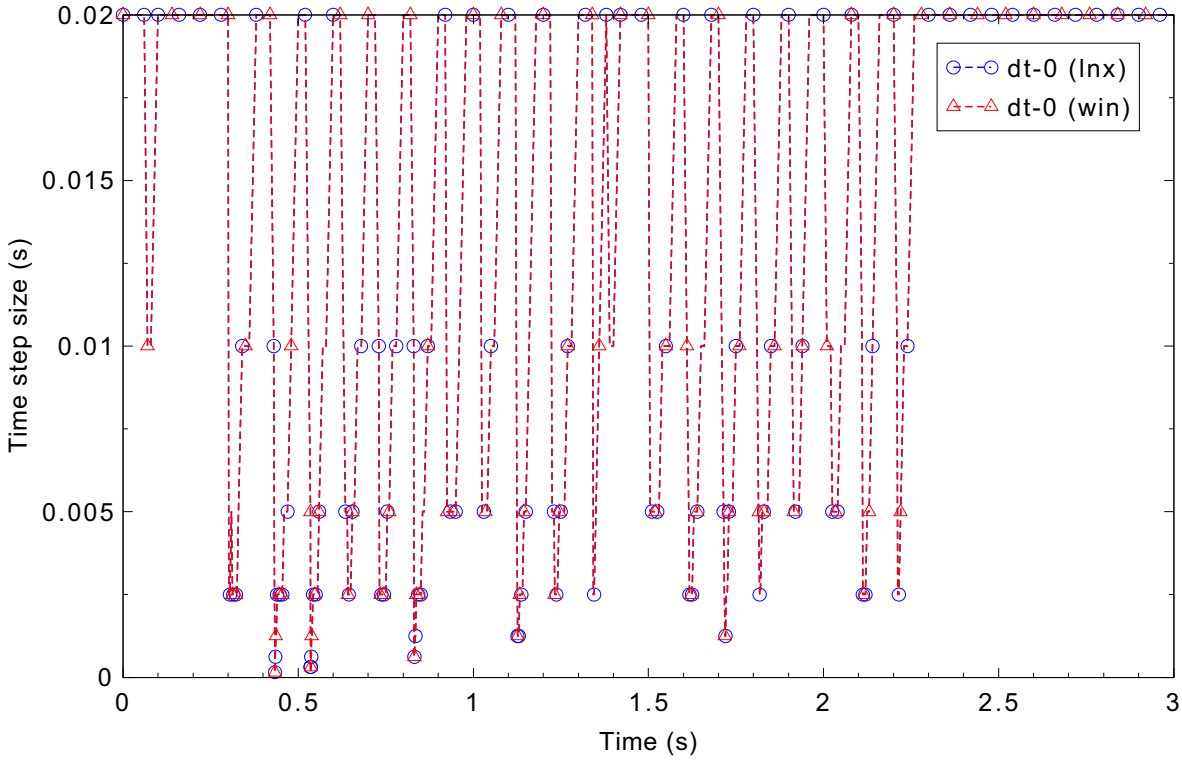

Figure 3.9-6. Time step size for Pryor pressure test, semi-implicit case with maximum dt = 0.02 s.

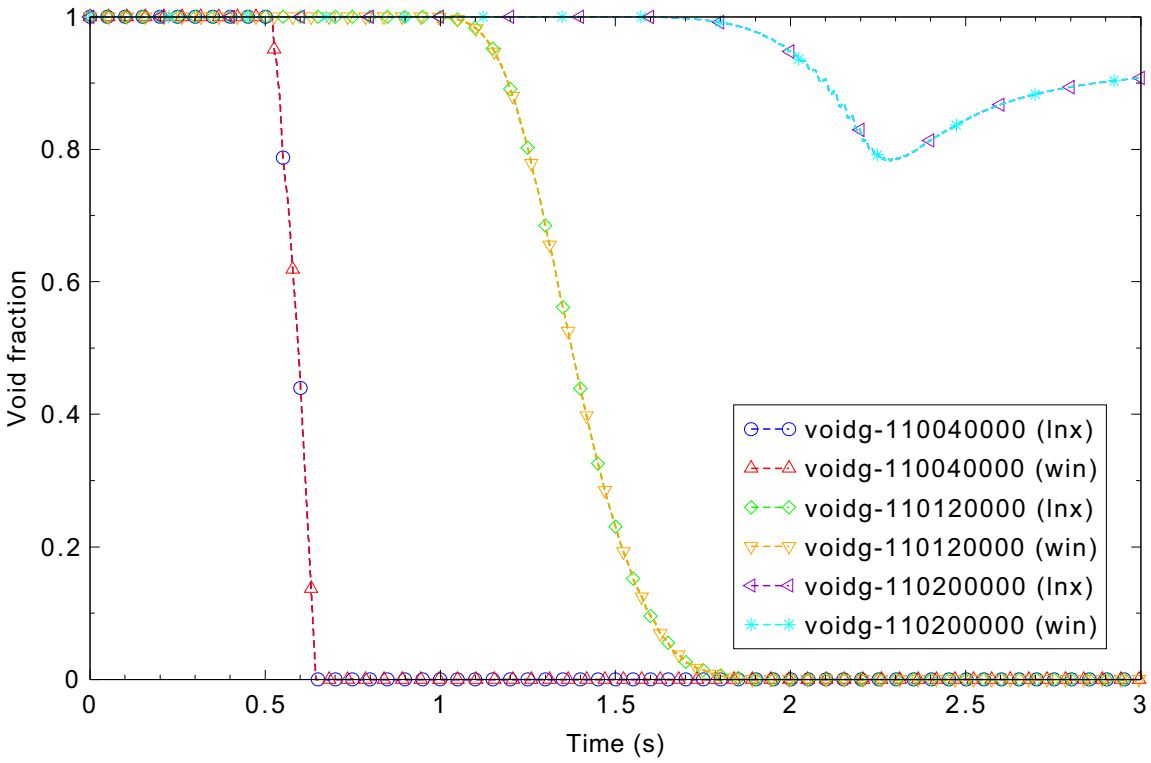

Figure 3.9-7. Void fraction for Pryor pressure test, semi-implicit case with maximum dt = 10^{-4} s.

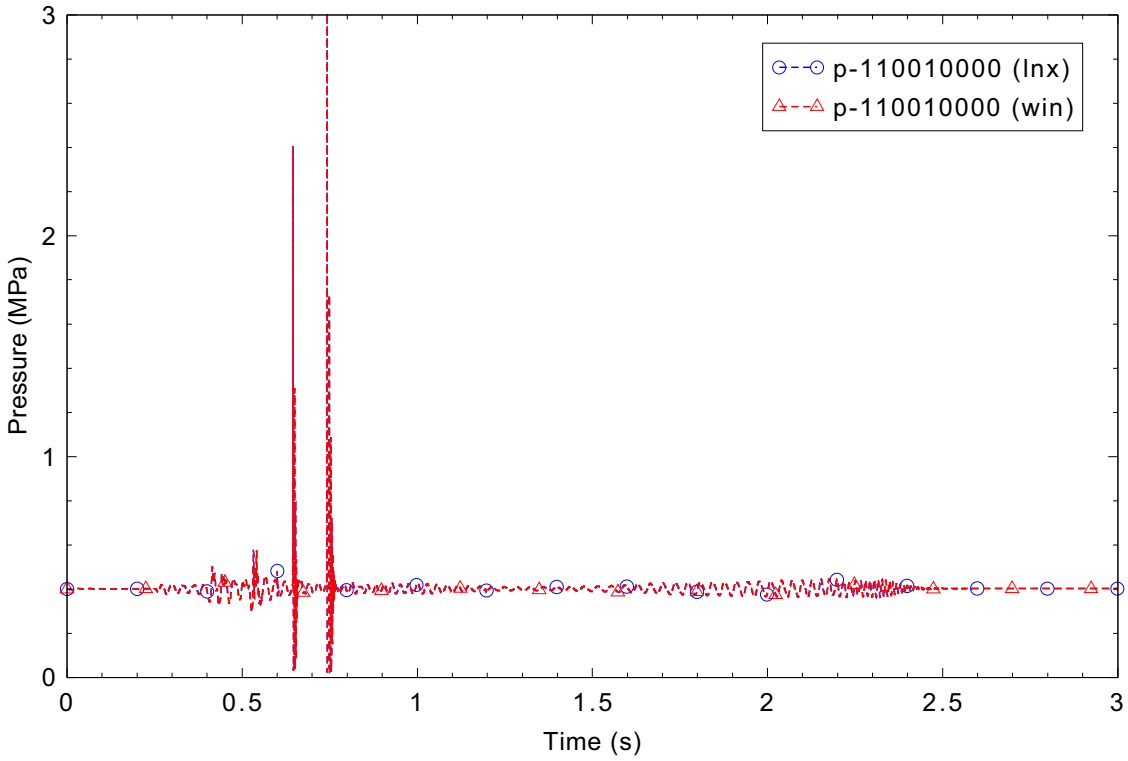

Figure 3.9-8. Volume 1 pressure for Pryor pressure test, semi-implicit case with maximum dt = 10^{-4} s.

3.10 Core Power

Figures comparing simulations using Linux and Windows code versions are presented. No differences were observed in the figures.

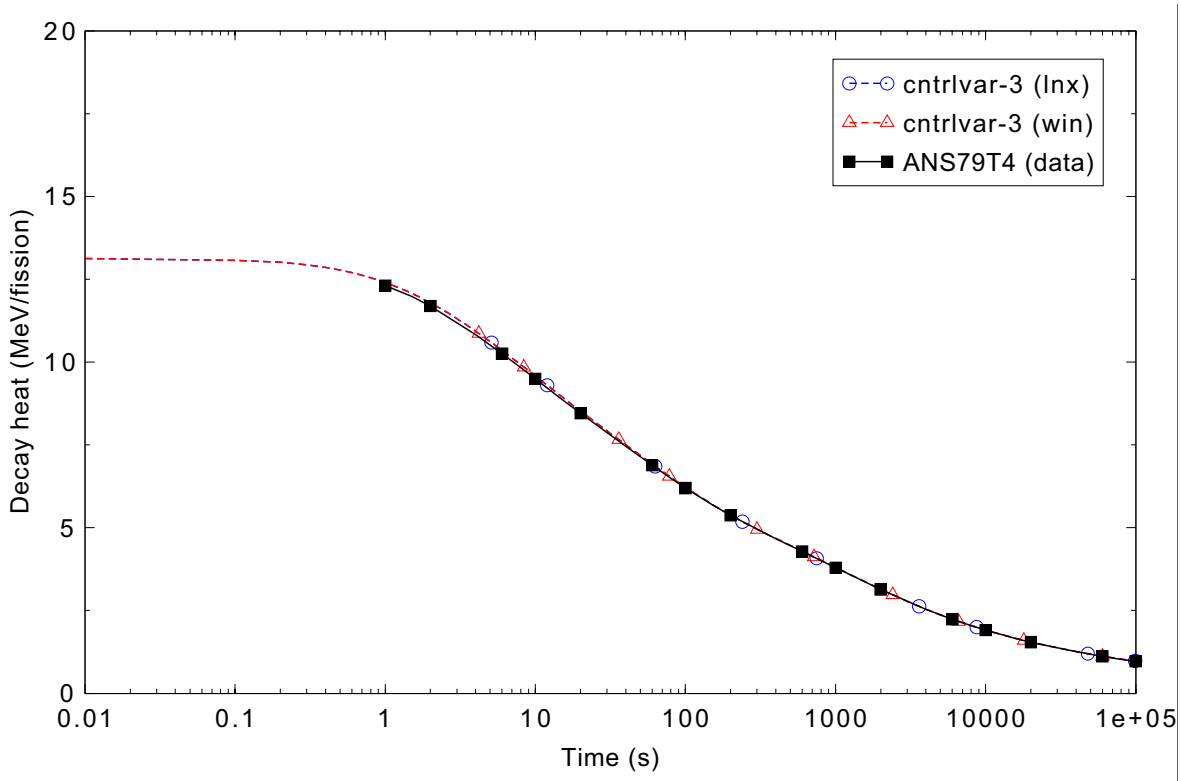

Figure 3.10-1. Decay heat comparison for the ans79.i test problem.

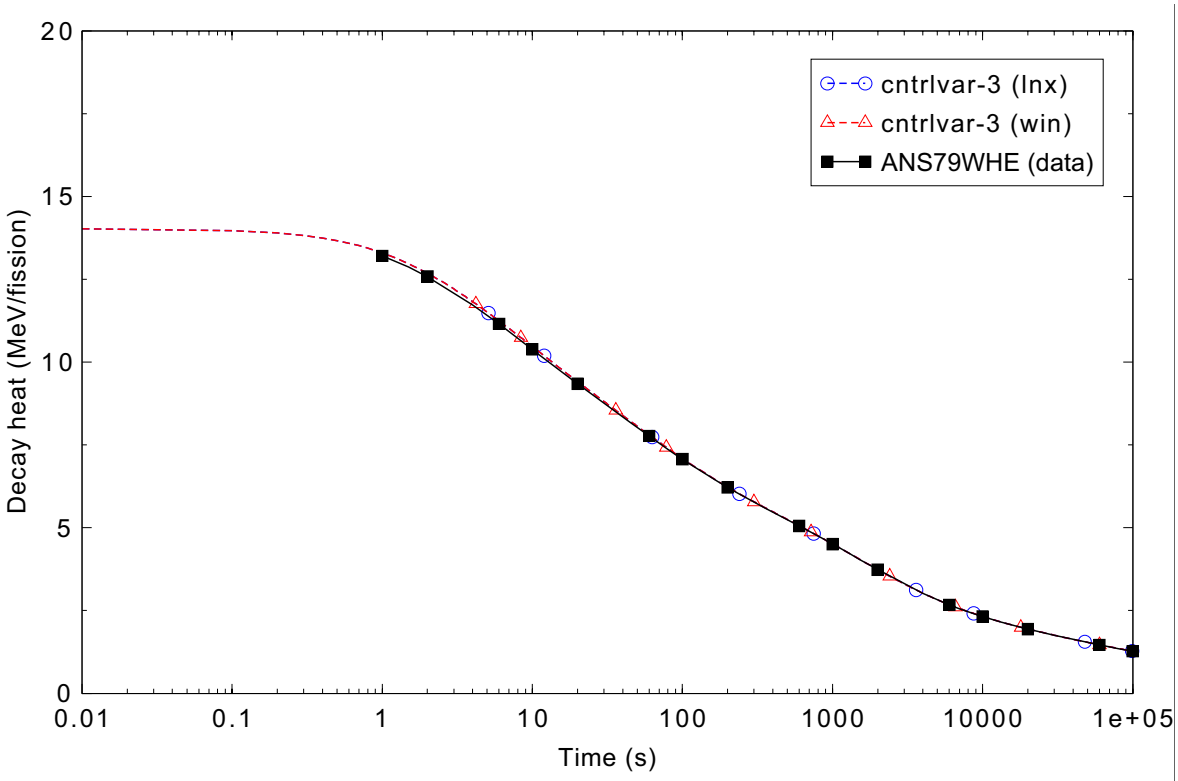

Figure 3.10-2. Decay heat comparison for the ans79ac.i test problem.

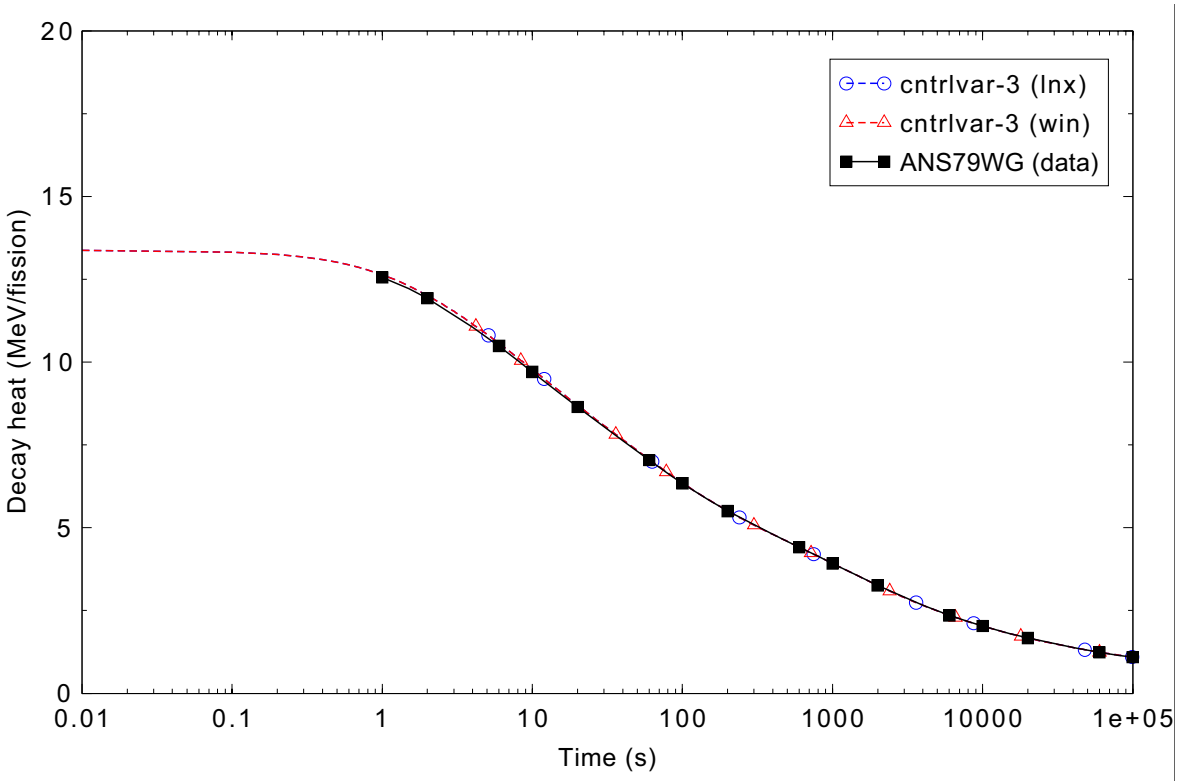

Figure 3.10-3. Decay heat comparison for the ans79G.i test problem.

3.11 Point Kinetics Ramp

Figures comparing simulations using Linux and Windows code versions are presented. No differences were observed in the figures.

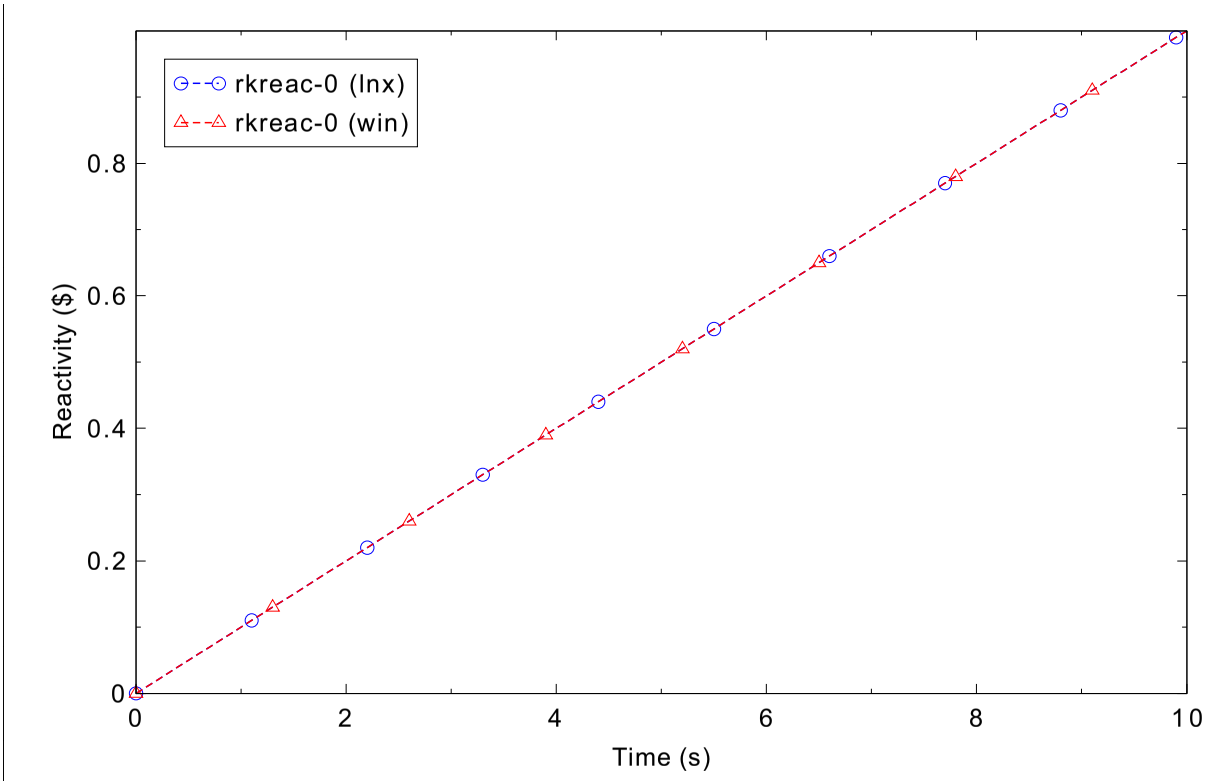

Figure 3.11-1. Reactivity comparison for the point kinetics ramp problem.

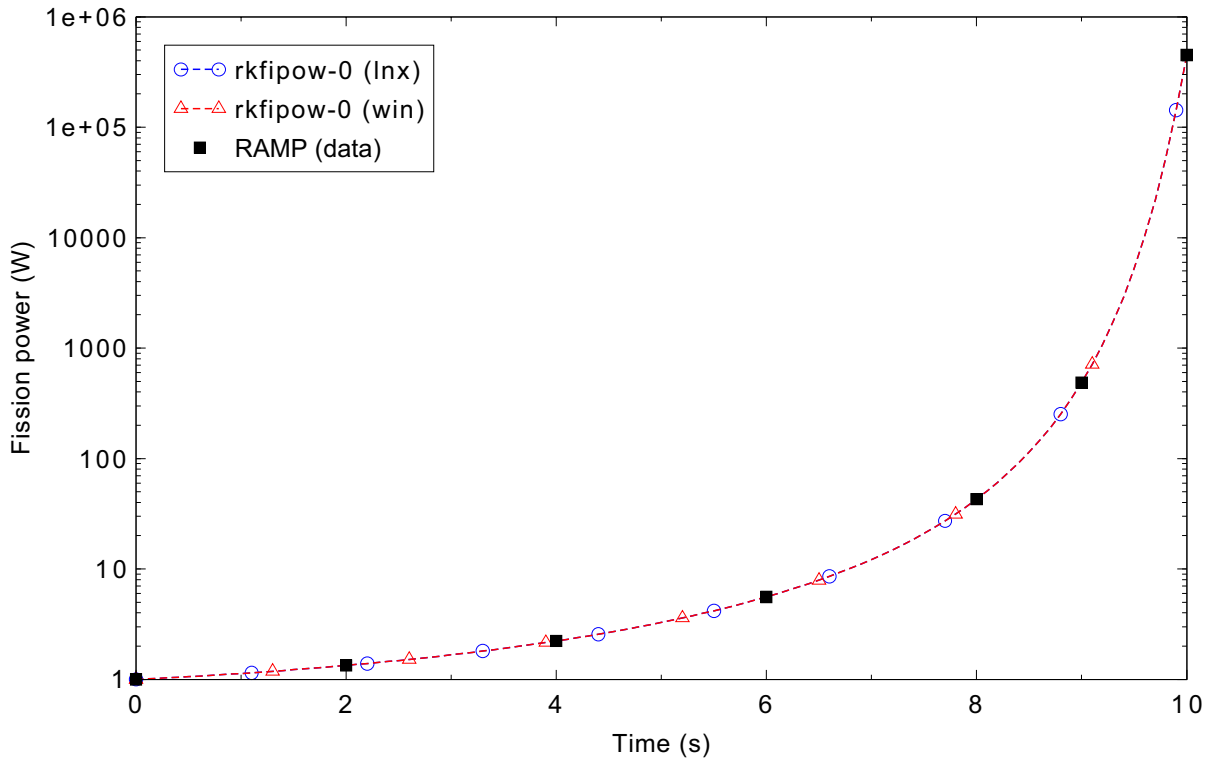

Figure 3.11-2. Fission power comparison for the point kinetics ramp problem with dt = 10^{-5} s.

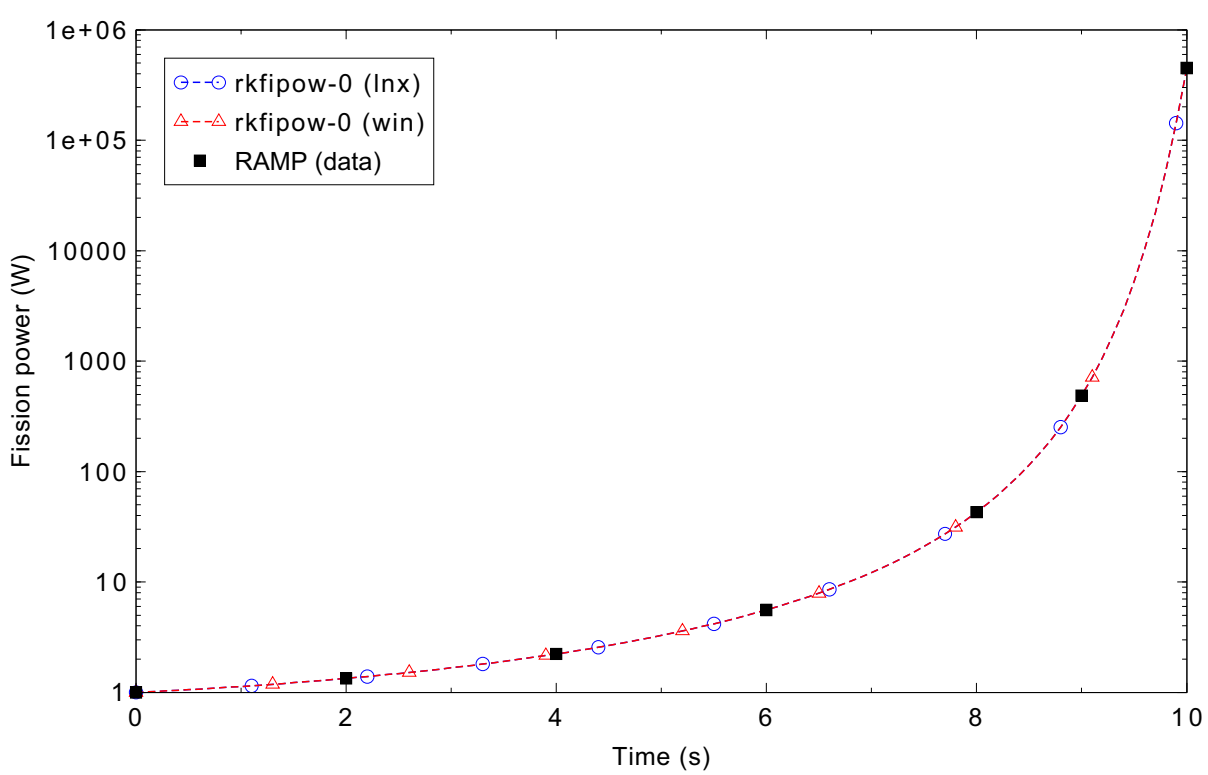

Figure 3.11-3. Fission power comparison for the point kinetics ramp problem with dt = 0.01 s.

3.12 Pure Radial Symmetric Flow (3-D)

Figures comparing simulations using Linux and Windows code versions are presented. Diagrams are included so that the figure numbering is the same as that in Volume III of the RELAP5-3D code manual. No differences were observed in the figures.

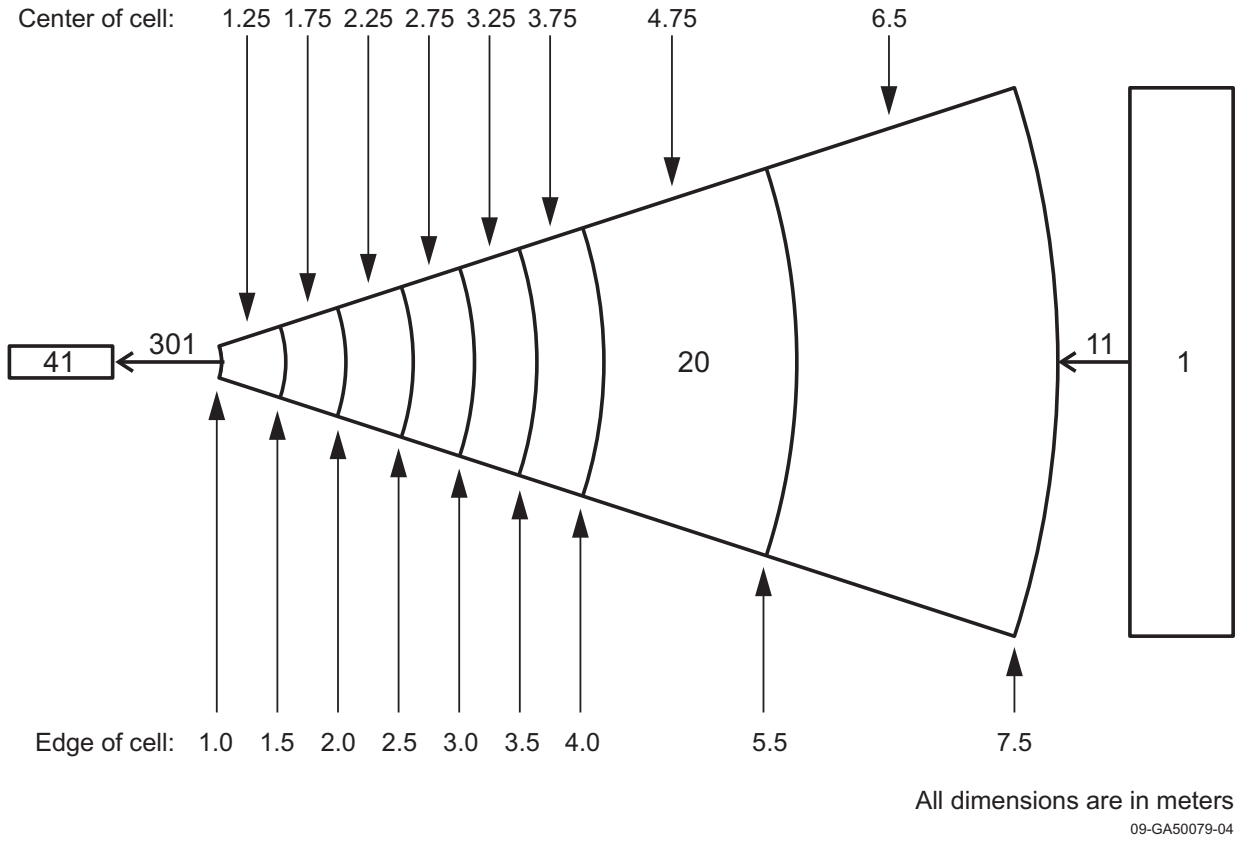

Figure 3.12-1. RELAP5-3D nodalization for the pure radial symmetric flow problem.

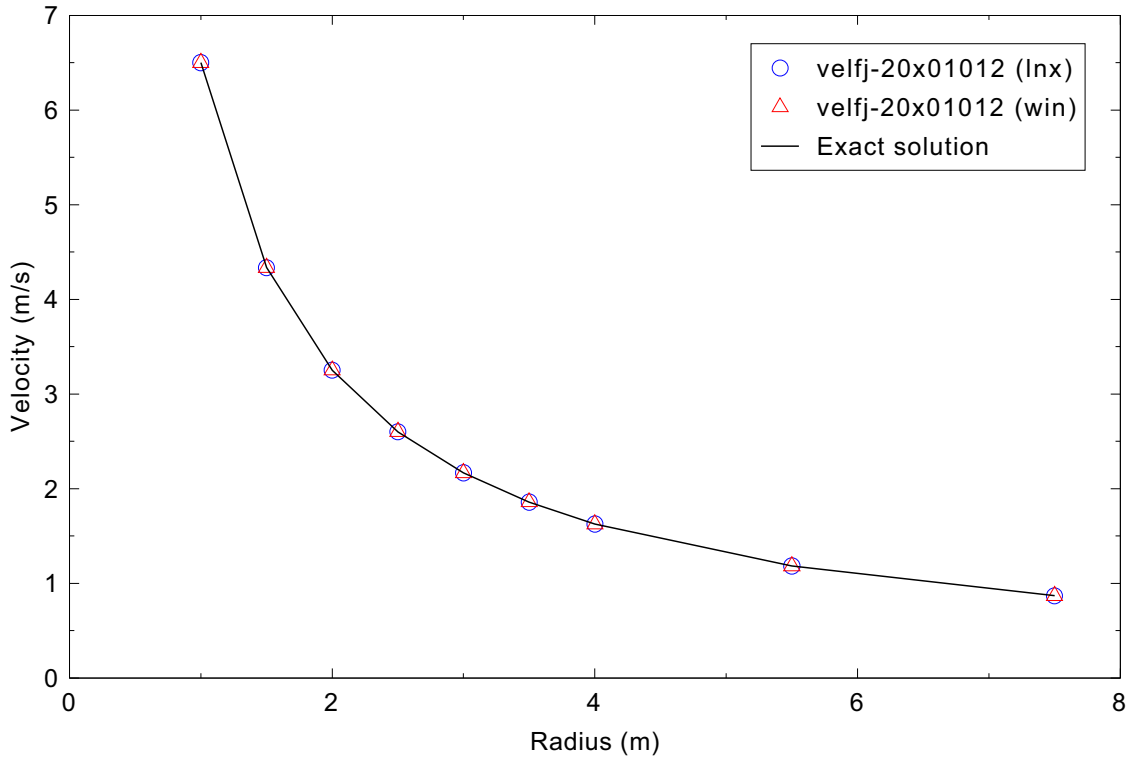

Figure 3.12-2. Radial velocity distribution for the pure radial symmetric flow problem.

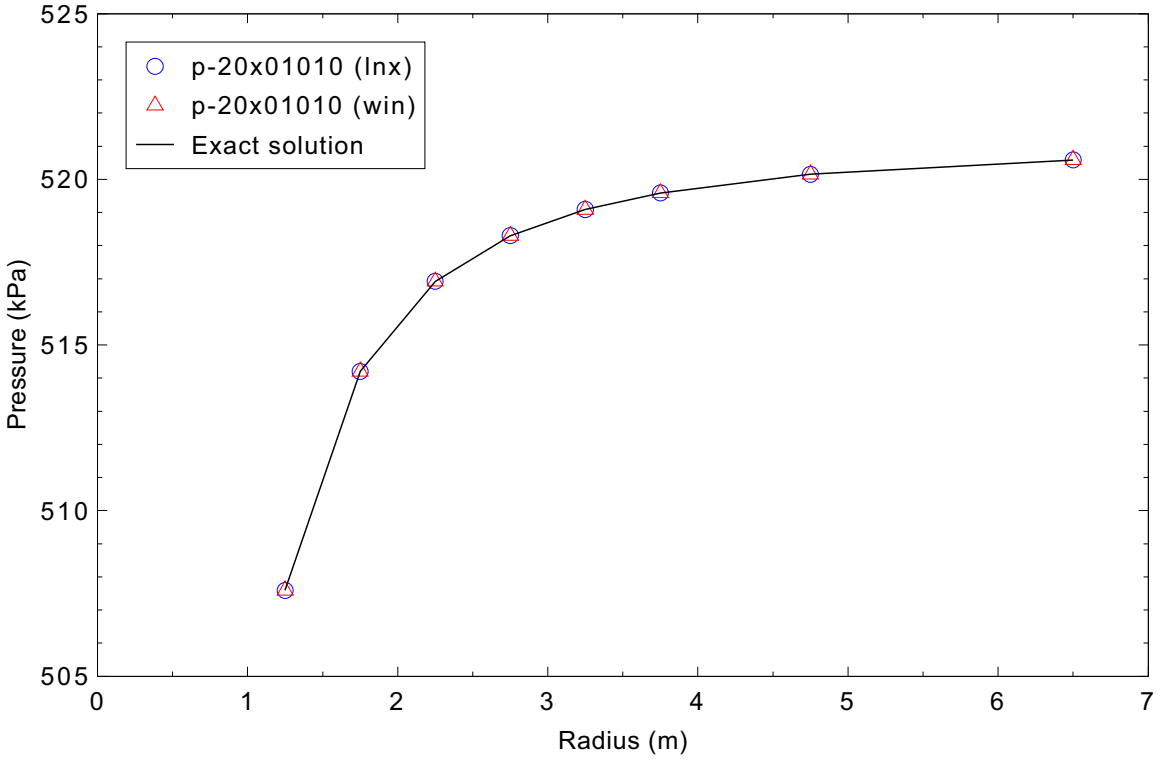

Figure 3.12-3. Radial pressure distribution for the pure radial symmetric flow problem.

3.13 Rigid Body Rotation (3-D)

Figures comparing simulations using Linux and Windows code versions are presented. Diagrams are included so that the figure numbering is the same as that in Volume III of the RELAP5-3D code manual. No differences were observed in the figures.

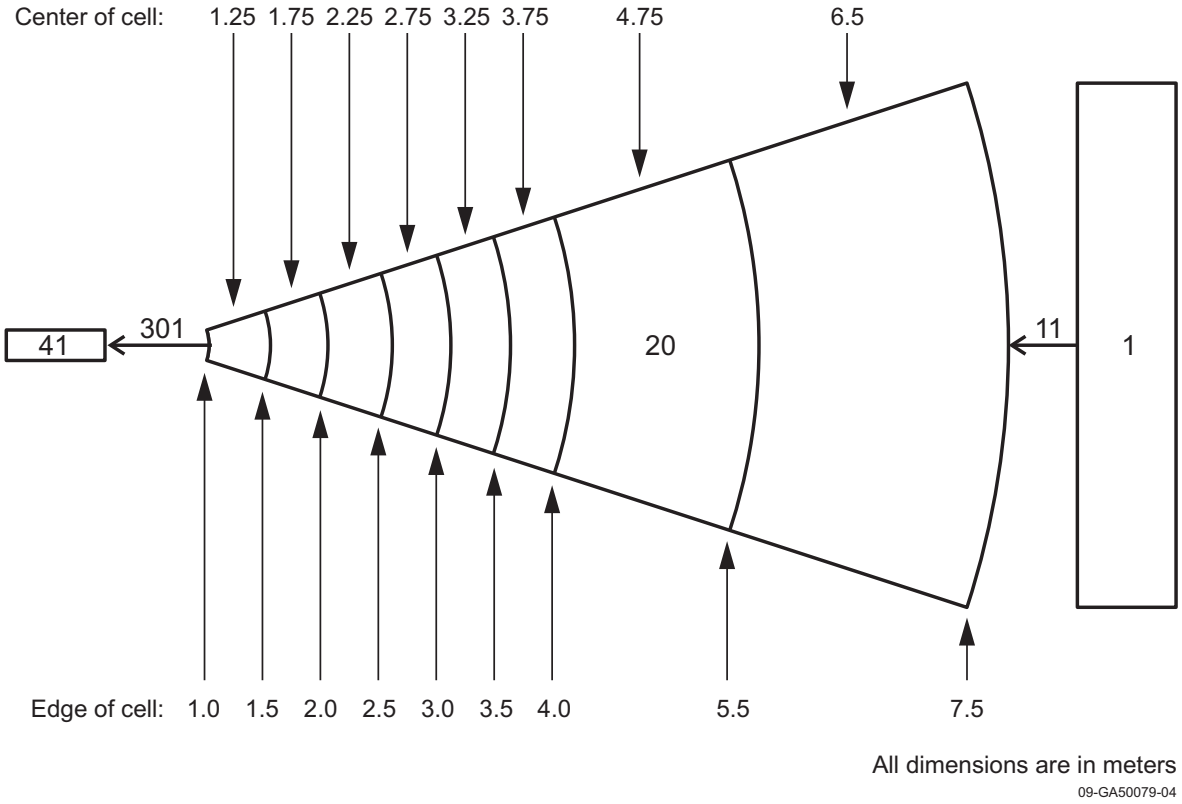

Figure 3.13-1. RELAP5-3D nodalization for the rigid body rotation problem.

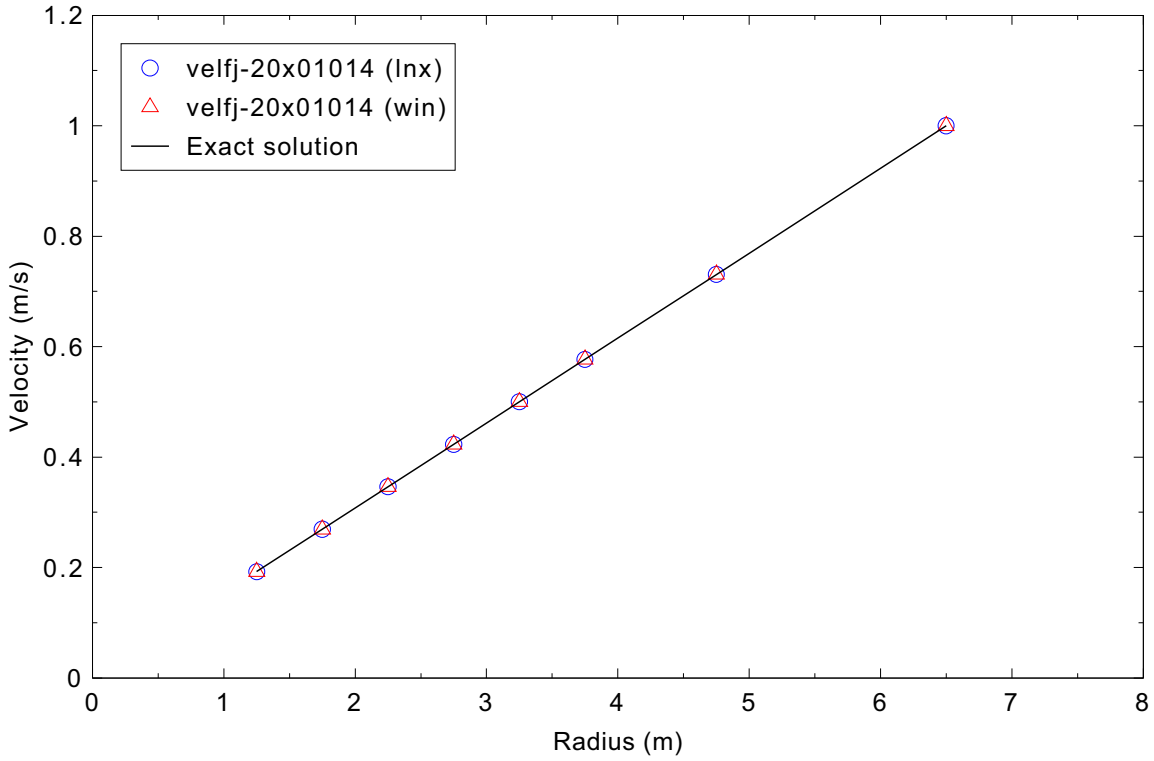

Figure 3.13-2. Azimuthal velocity distribution for the rigid body rotation problem.

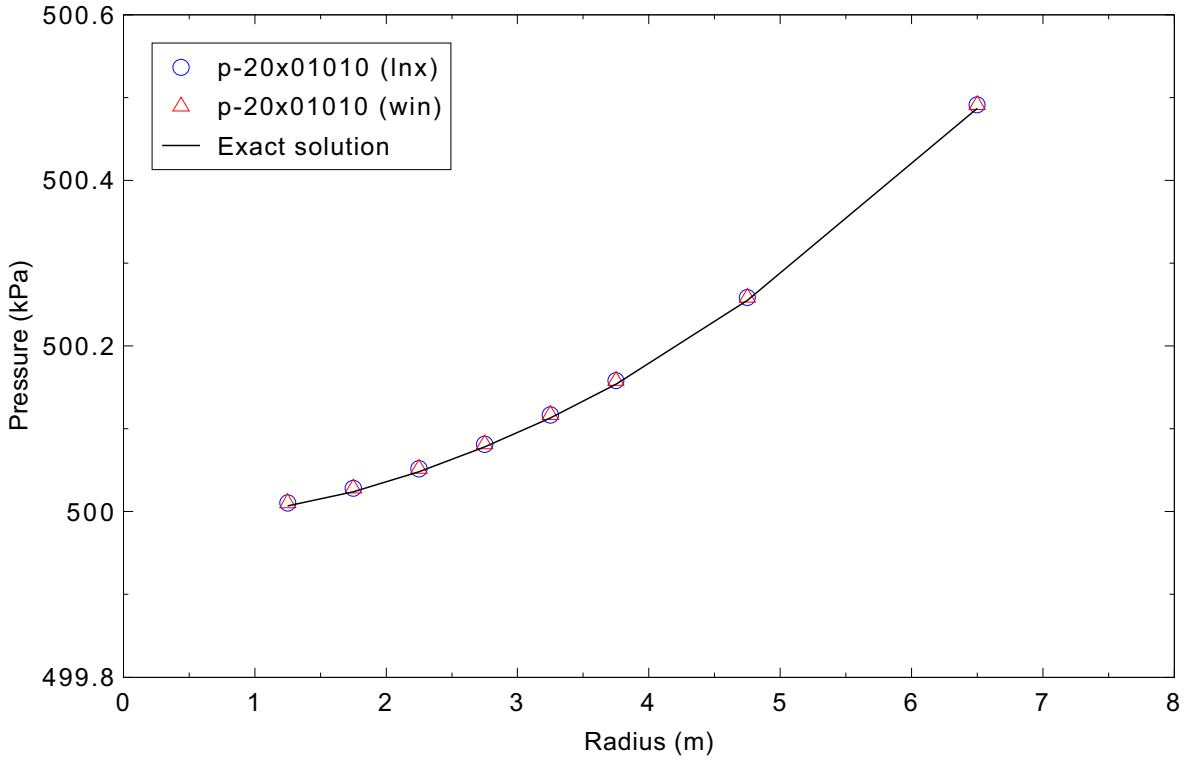

Figure 3.13-3. Radial pressure distribution for the rigid body rotation problem.

3.14 R-Theta Symmetric Flow (3-D)

Figures comparing simulations using Linux and Windows code versions are presented. Diagrams are included so that the figure numbering is the same as that in Volume III of the RELAP5-3D code manual. No differences were observed in the figures.

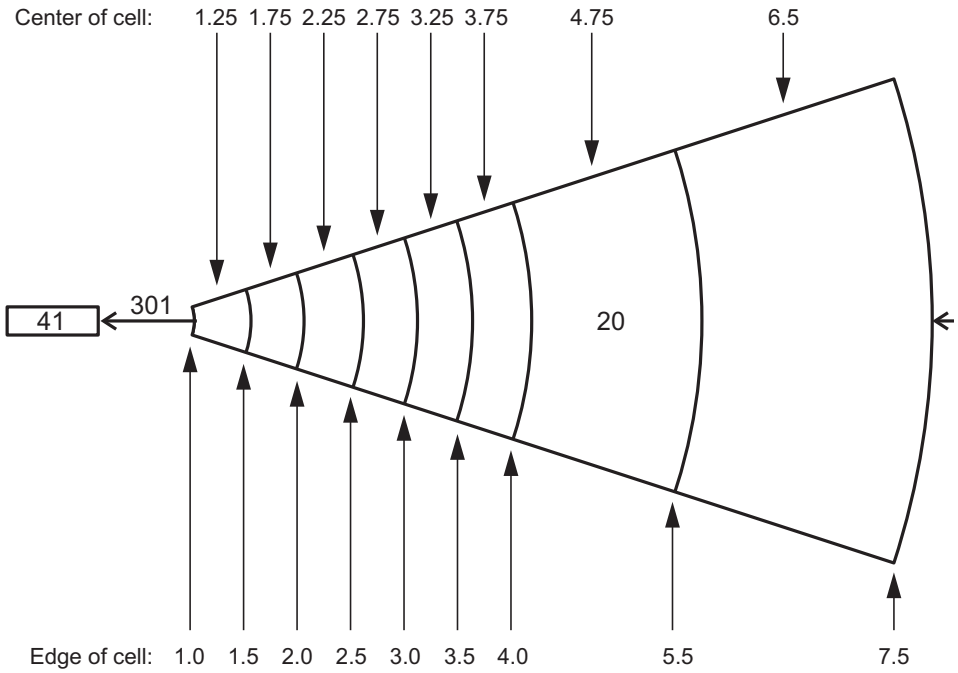

Figure 3.14-1. RELAP5-3D nodalization for the r-theta symmetric flow problem.

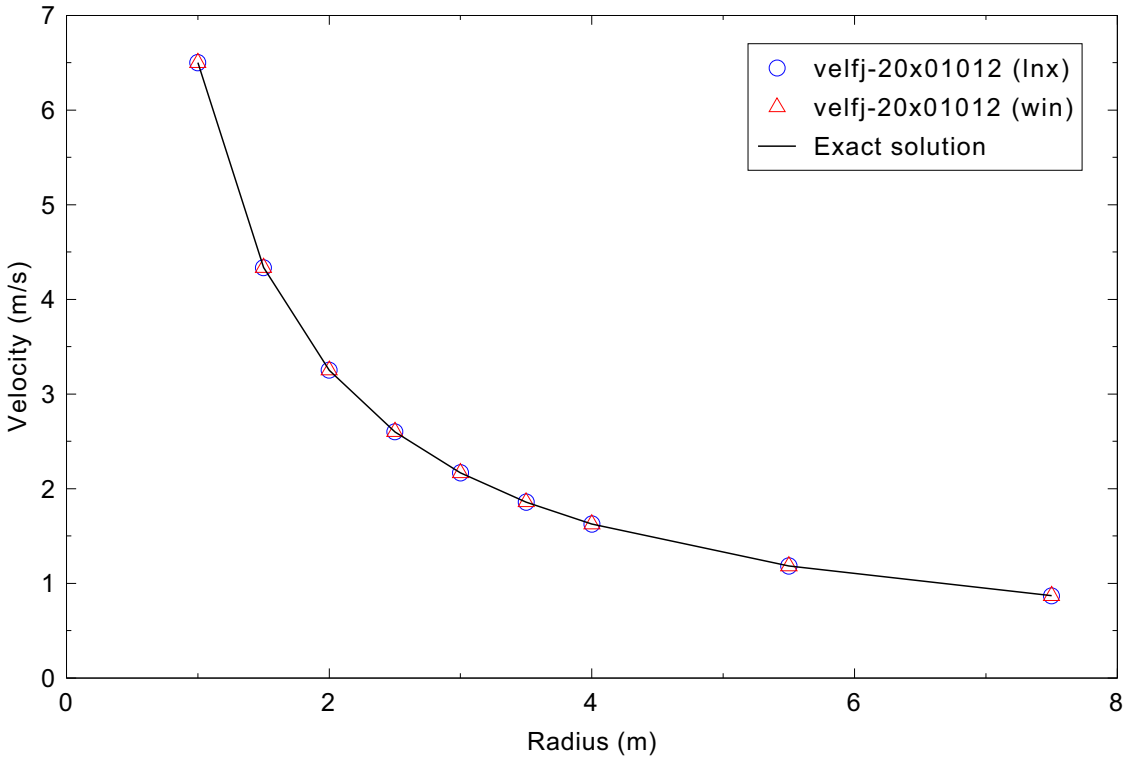

Figure 3.14-2. Radial velocity distribution for the r-theta symmetric flow problem.

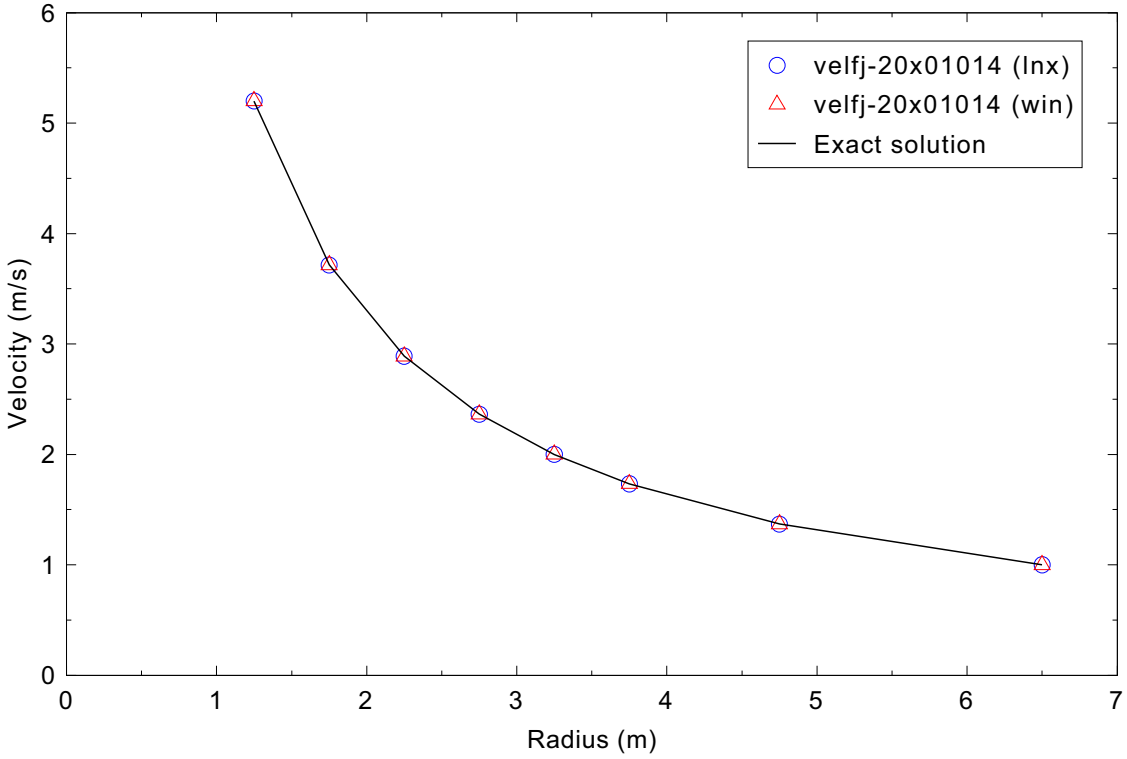

Figure 3.14-3. Azimuthal velocity distribution for the r-theta symmetric flow problem.

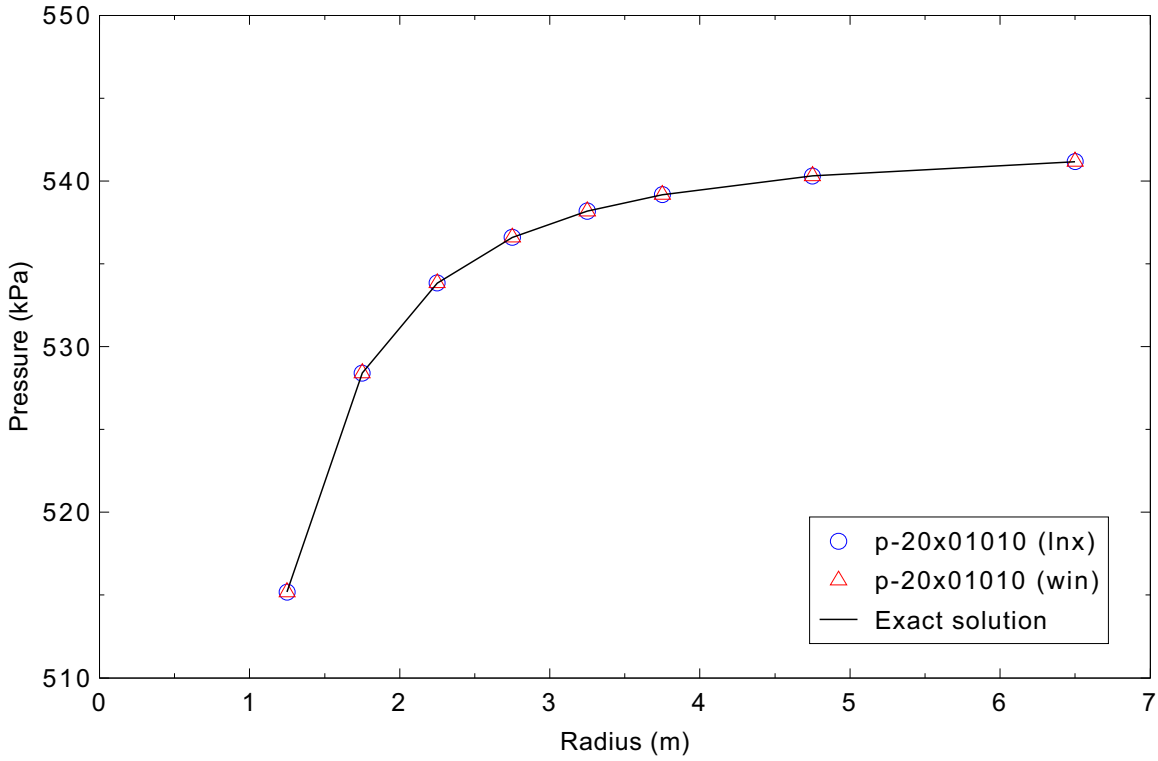

Figure 3.14-4. Radial pressure distribution for the r-theta symmetric flow problem.

3.15 Conduction Enclosure

Figures comparing simulations using Linux and Windows code versions are presented. Diagrams are included so that the figure numbering is the same as that in Volume III of the RELAP5-3D code manual. The 3-D figures should be ignored, as they may not reflect the current code version. No differences were observed in the figures.

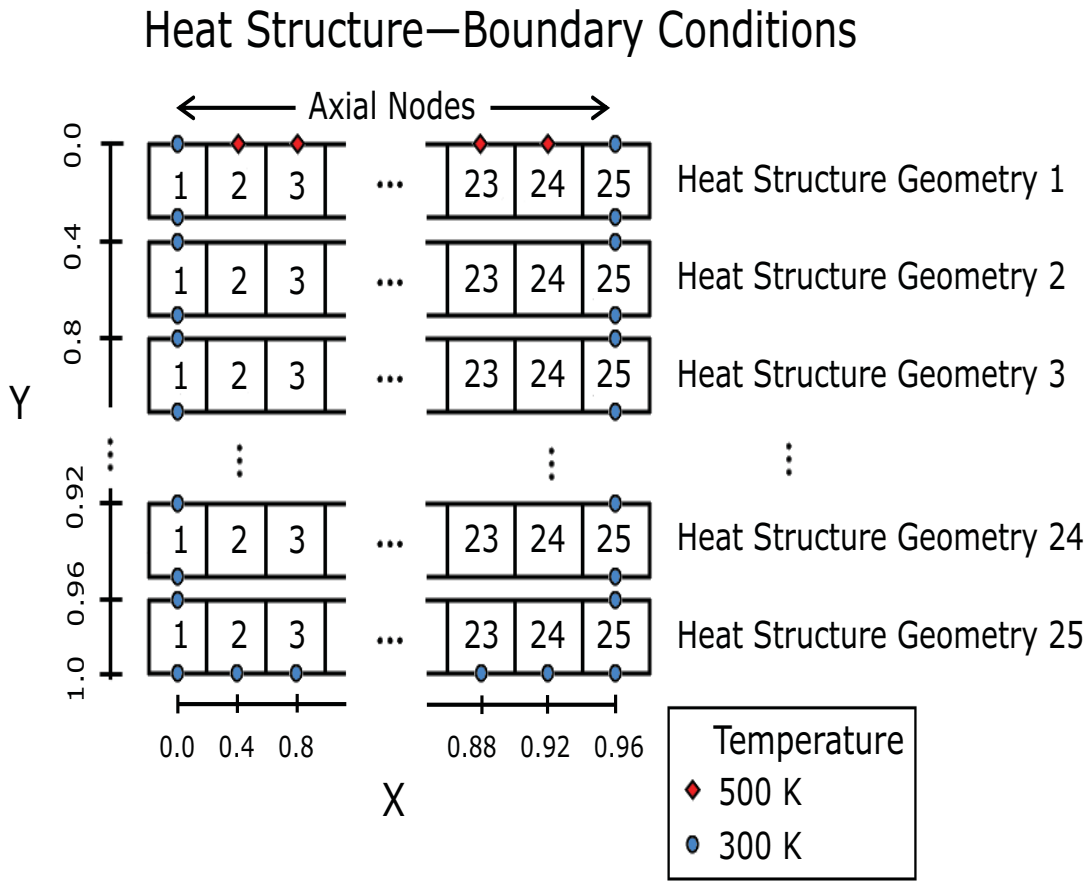

Figure 3.15-1. Heat structure layout with boundary conditions for the conduction enclosure problem.

. (3.15-1)

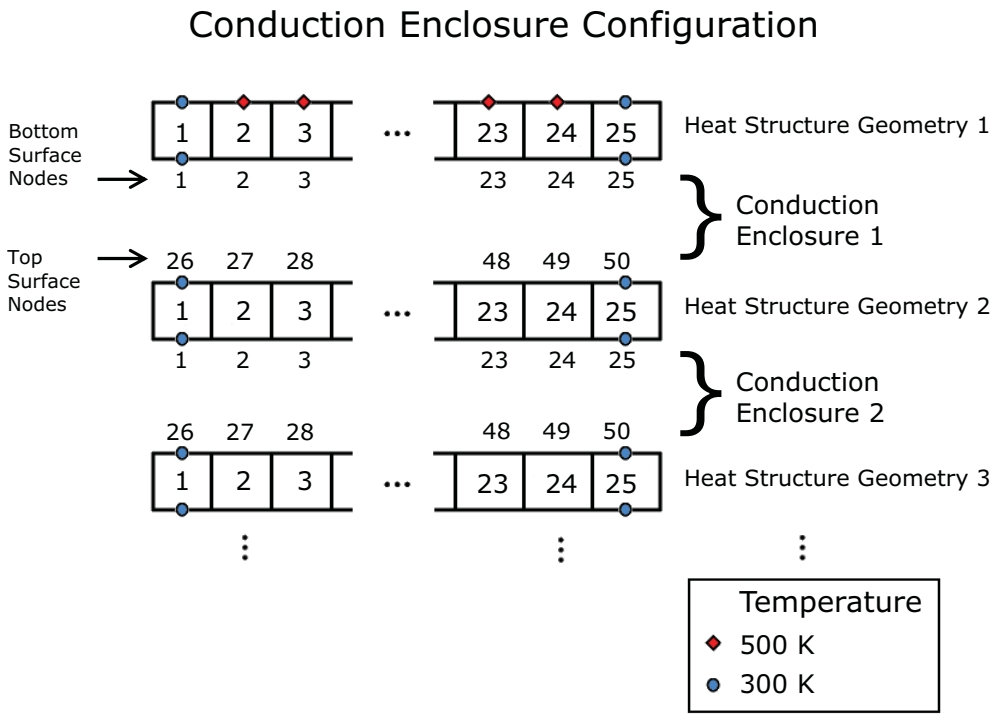

Figure 3.15-2. View of heat structure surfaces included in the conduction enclosures.

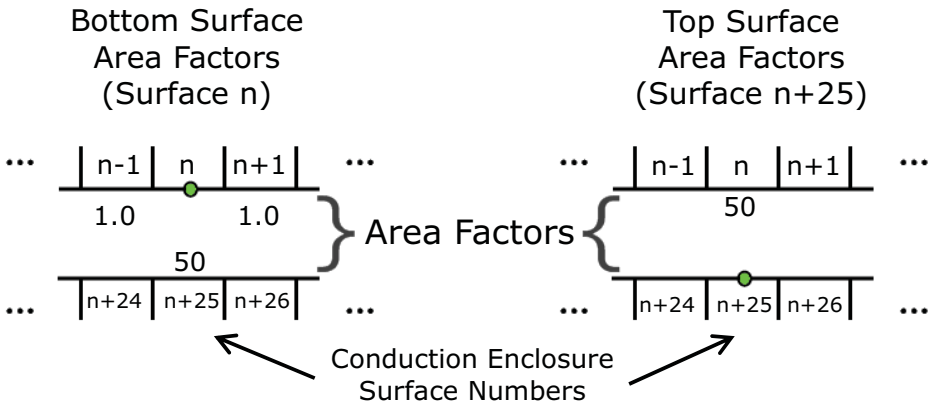

Figure 3.15-3. Area factors used to define axial contact of heat structure cells as well as contact between separate heat structure geometries.

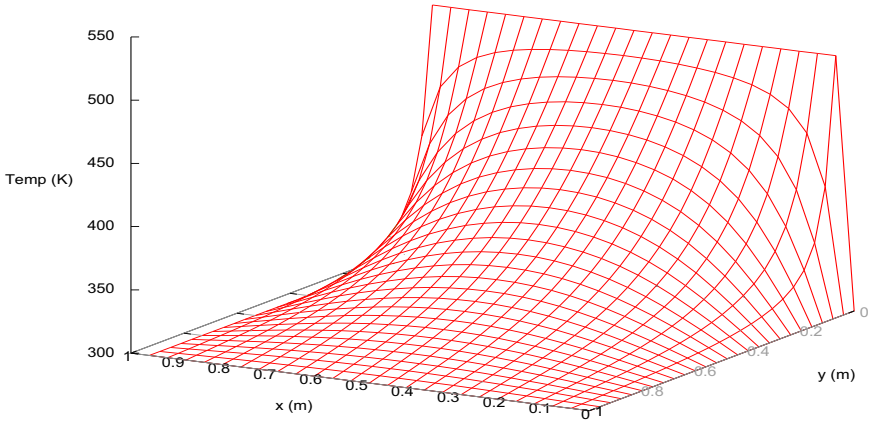

Figure 3.15-4. Steady state temperature for the heated plate problem based on a 3800-term expansion of the series solution.

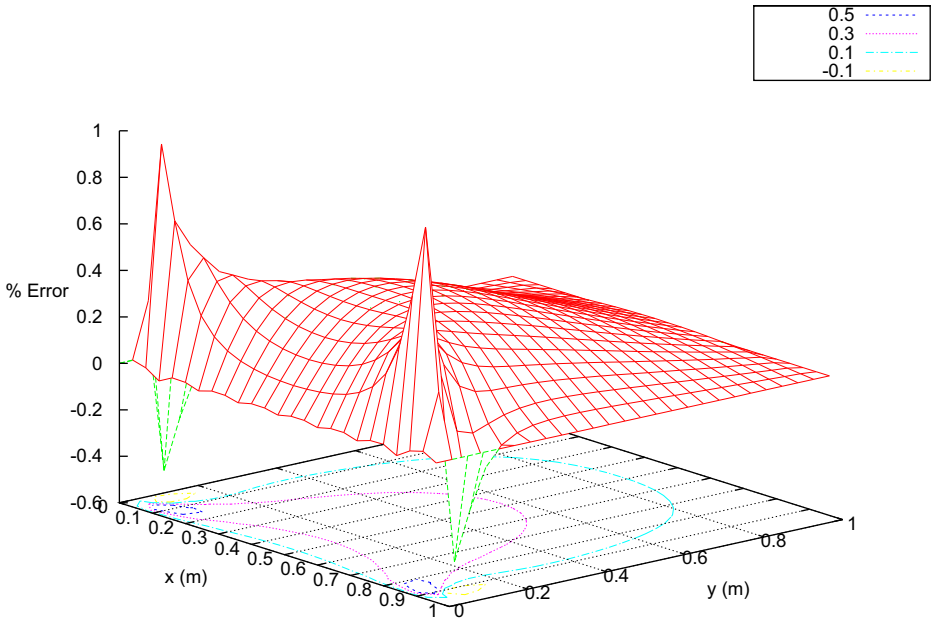

Figure 3.15-5. Local steady state temperature error for the RELAP5-3D solution vs. series solution.

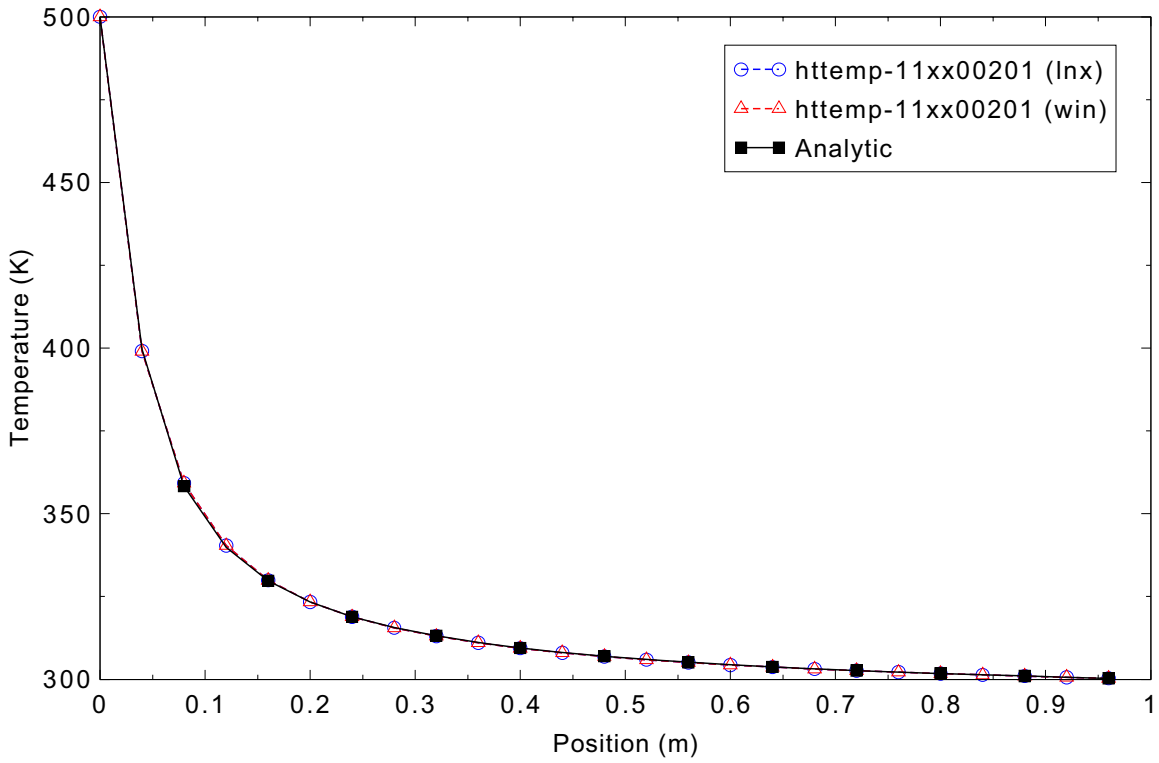

Figure 3.15-6. Heated plate steady state series solution and the RELAP5-3D solution along x equal to 0.04 m.

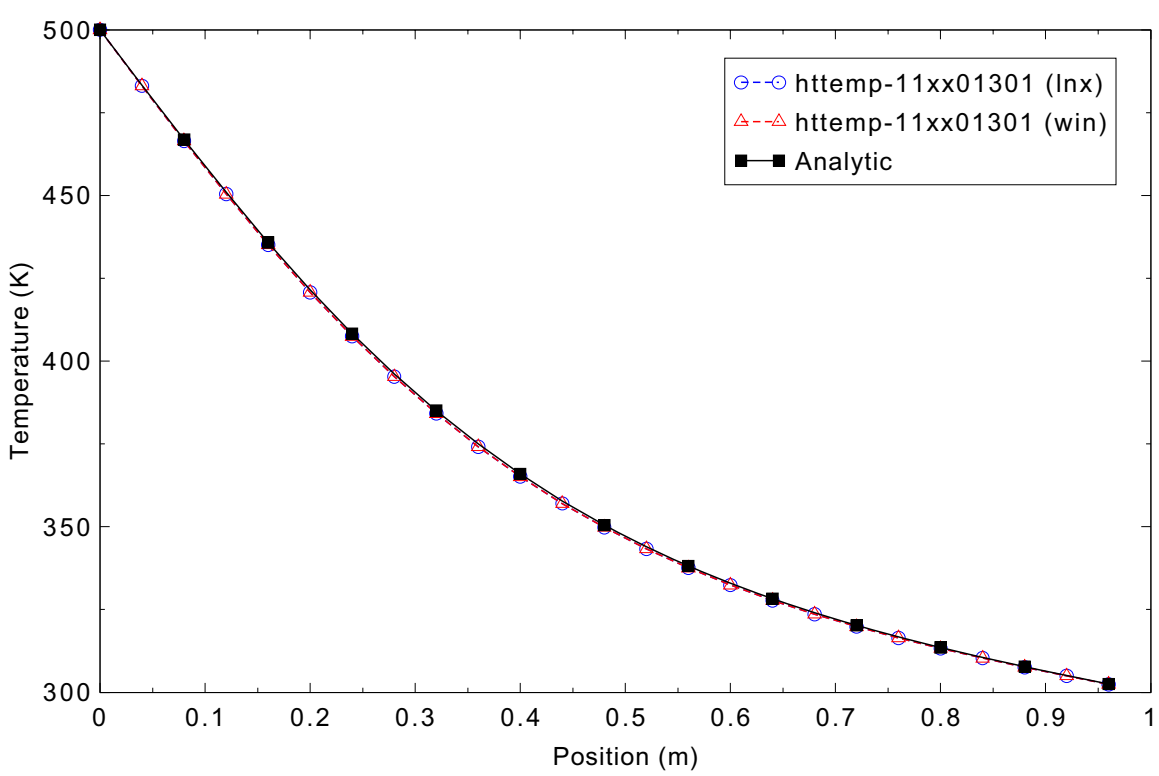

Figure 3.15-7. Heated plate steady state series solution and the RELAP5-3D solution along x equal to 0.48 m.

3.16 Conduction Enclosure: 1-D Transient Model

Figures comparing simulations using Linux and Windows code versions are presented. Diagrams are included so that the figure numbering is the same as that in Volume III of the RELAP5-3D code manual. The 3-D figures should be ignored, as they may not reflect the current code version. No differences were observed in the figure.

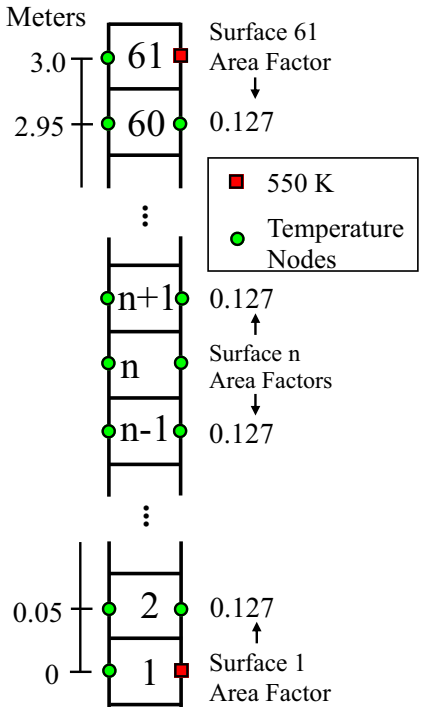

Figure 3.16-1. Rod area factors and end boundary conditions for 1-D conduction enclosure.

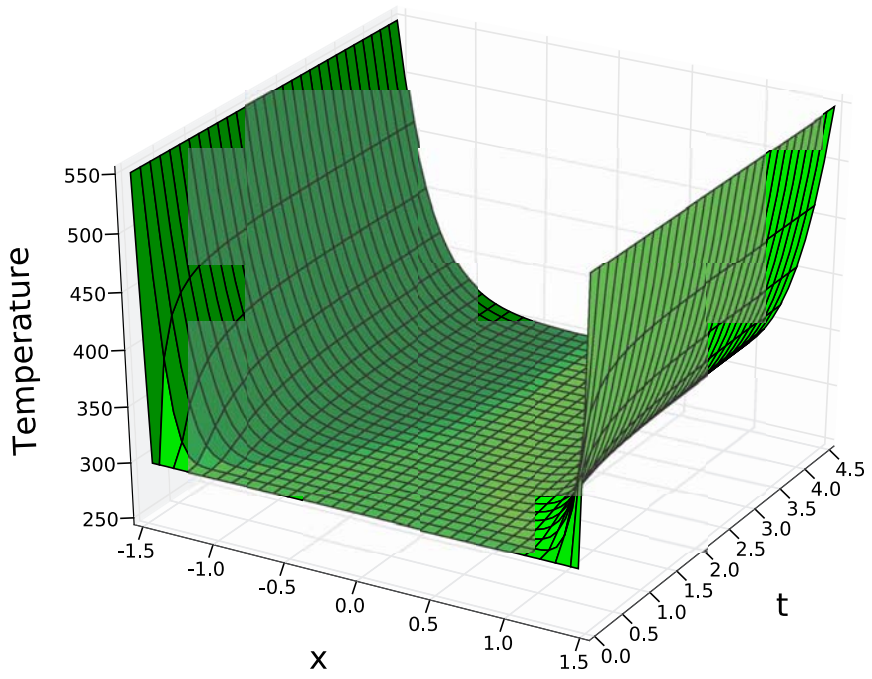

Figure 3.16-2. 1-D conduction enclosure axial temperature vs. time (in hours) based on a 10,000-term

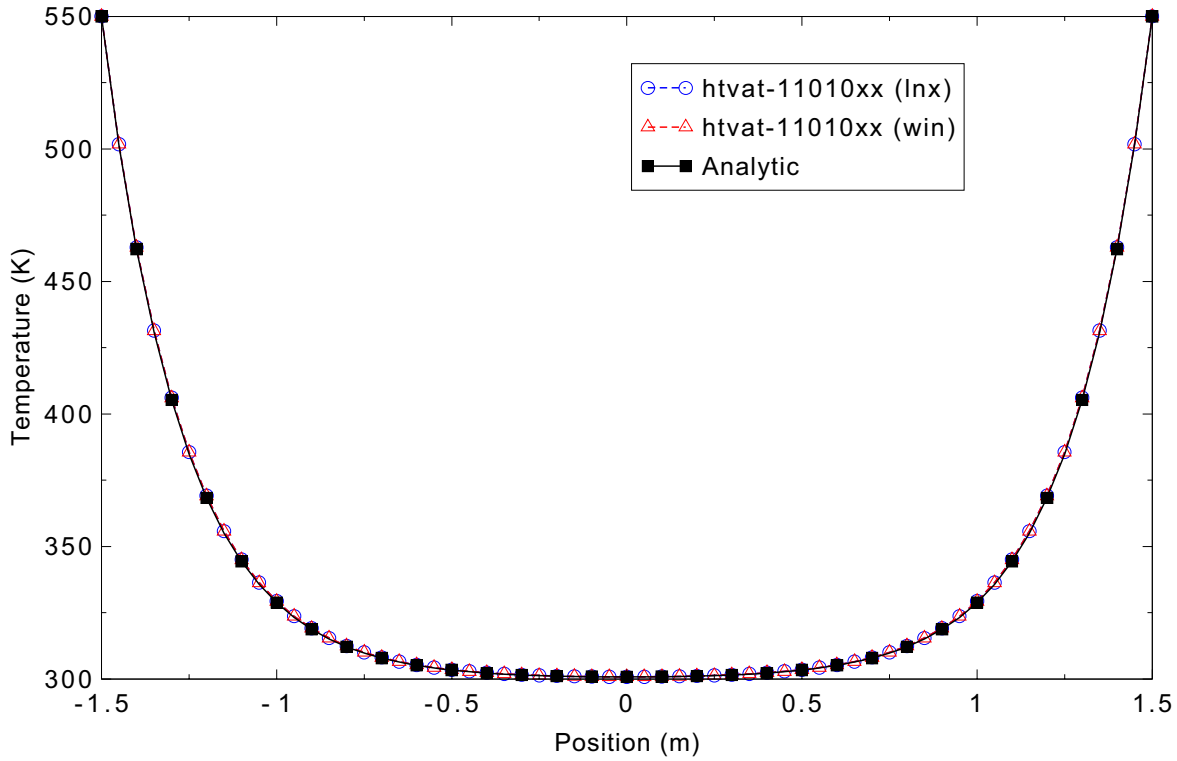

Figure 3.16-3. 1-D conduction enclosure temperature comparison with analytical solution at 10 h.

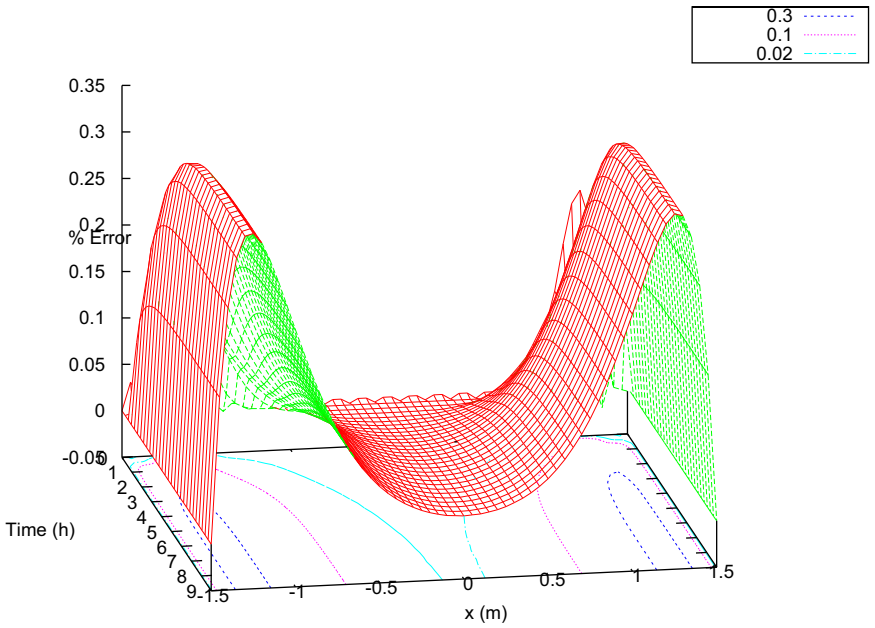

Figure 3.16-4. 1-D conduction enclosure local percent error for the rod with heated ends vs. position along the rod and time.

.

3.17 Conduction Enclosure: 2-D Transient Model

Figures comparing simulations using Linux and Windows code versions are presented. Diagrams are included so that the figure numbering is the same as that in Volume III of the RELAP5-3D code manual. The 3-D figures should be ignored, as they may not reflect the current code version. No differences were observed in the figure.

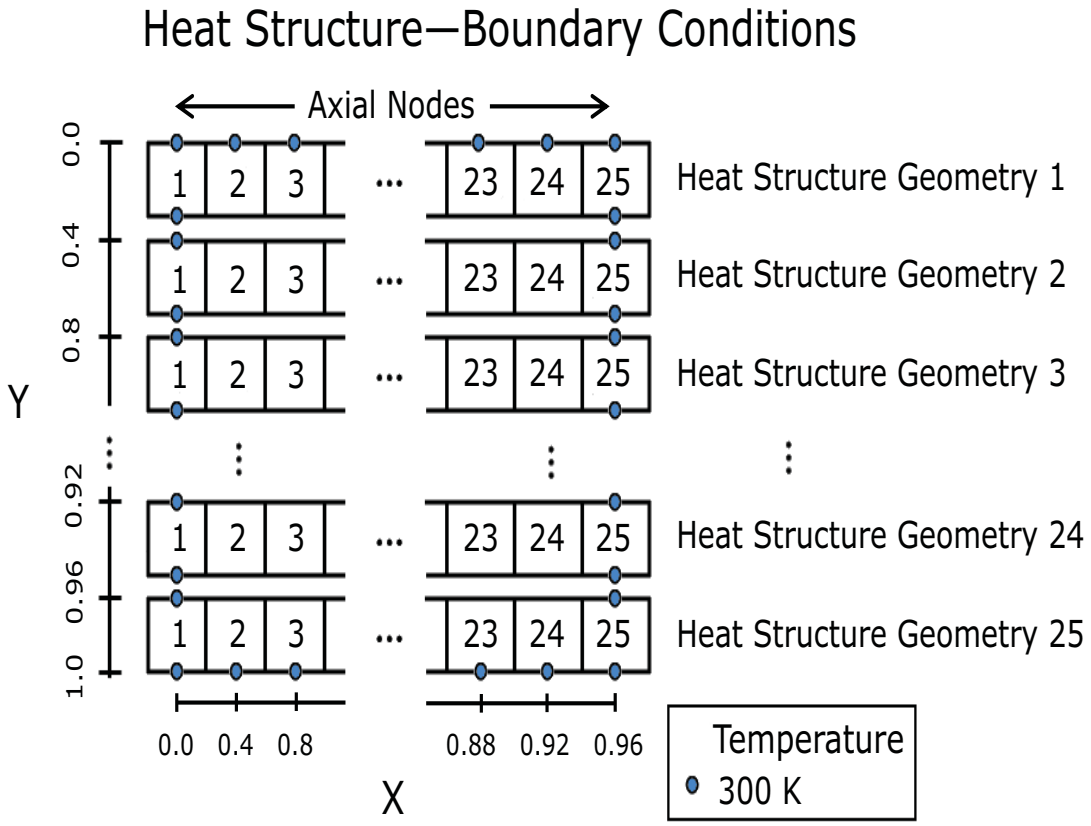

Figure 3.17-1. Boundary conditions for the transient heated plate model for 2-D conduction enclosure.

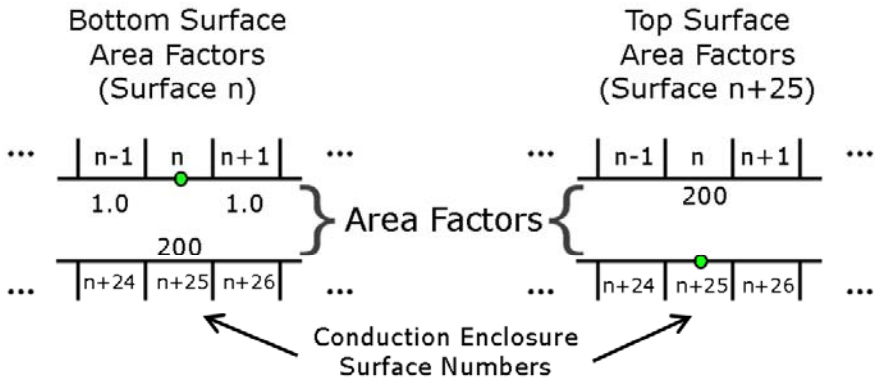

Figure 3.17-2. Area factors for the 2-D plate transient heat conduction model.

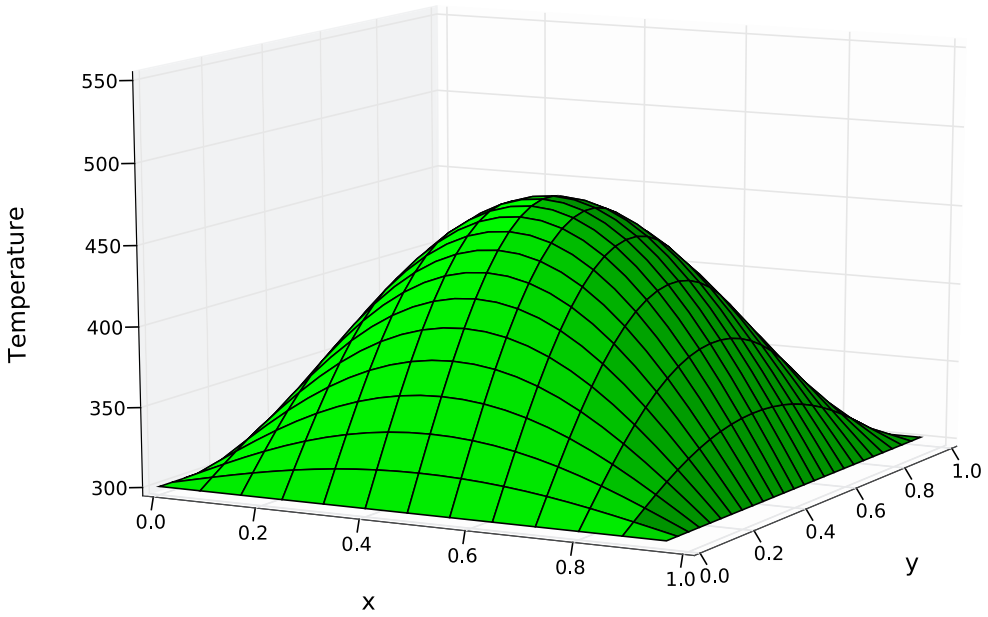

Figure 3.17-3. Plate temperature after one hour for 2-D conduction enclosure.

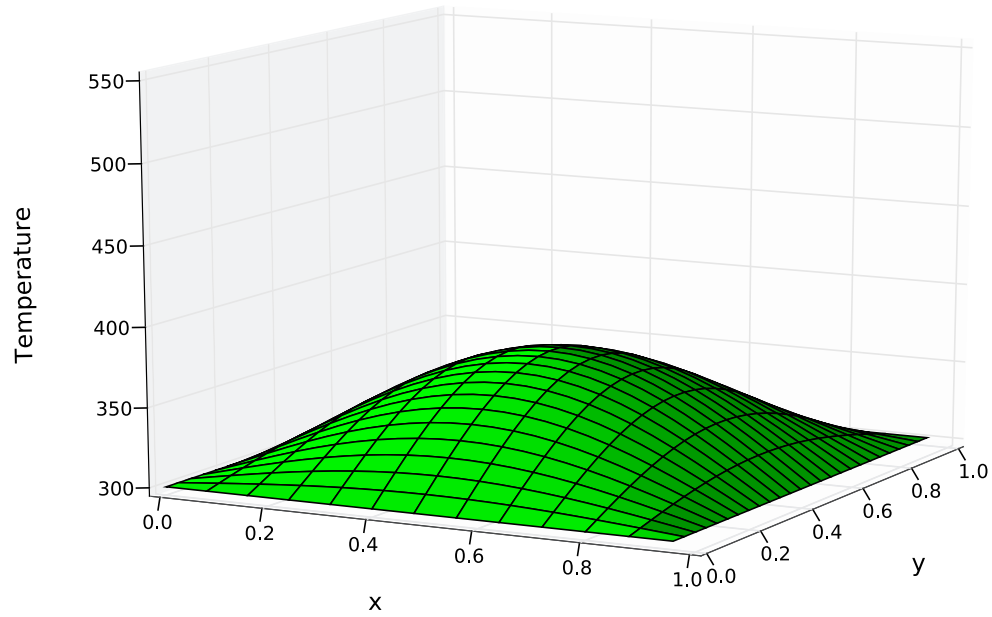

Figure 3.17-4. Plate temperature after two hours for 2-D conduction enclosure.

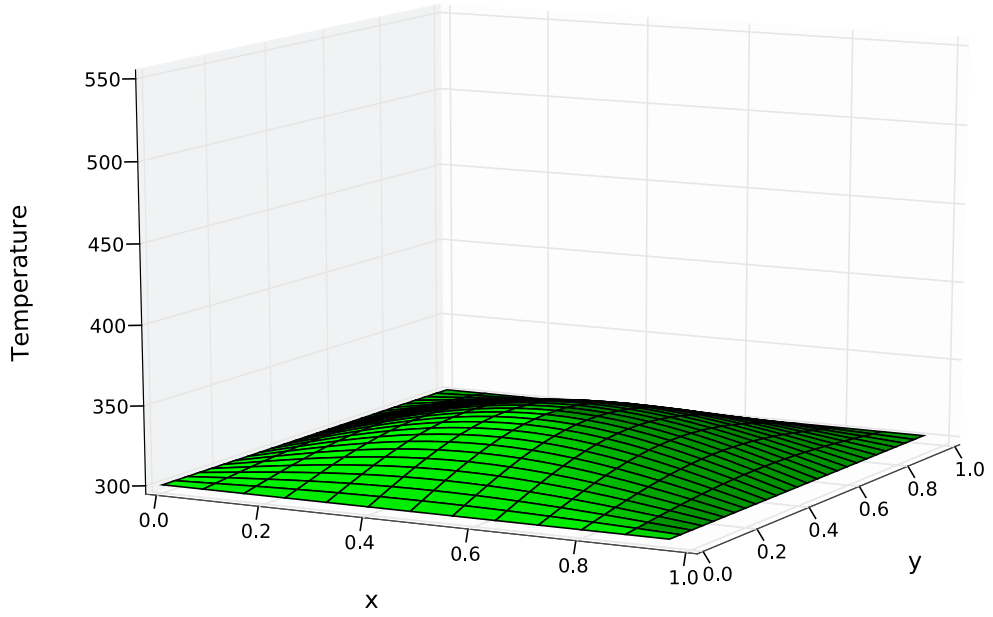

Figure 3.17-5. Plate temperature after three hours for 2-D conduction enclosure.

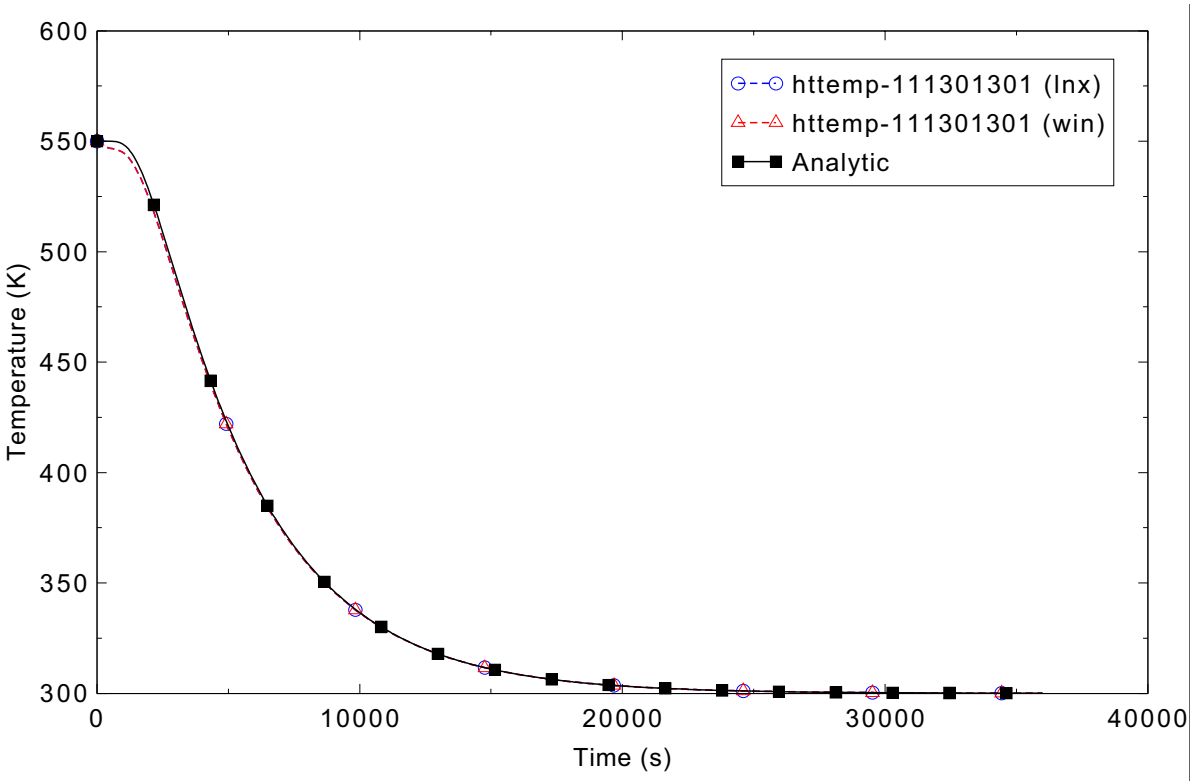

Figure 3.17-6. 2-D conduction enclosure temperature comparison with analytical solution. Temperature is taken at point x=0.2 m, y=0 m.

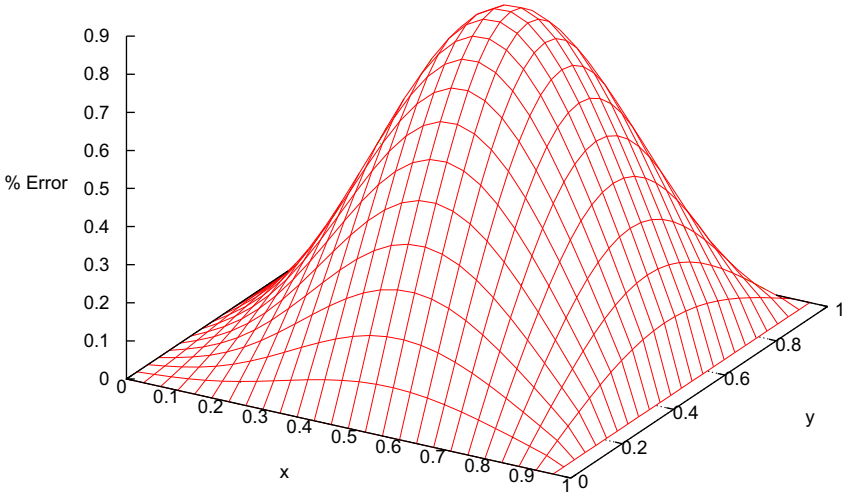

Figure 3.17-7. Local percent error of the transient temperature response for 2-D conduction enclosure at a time of one hour.

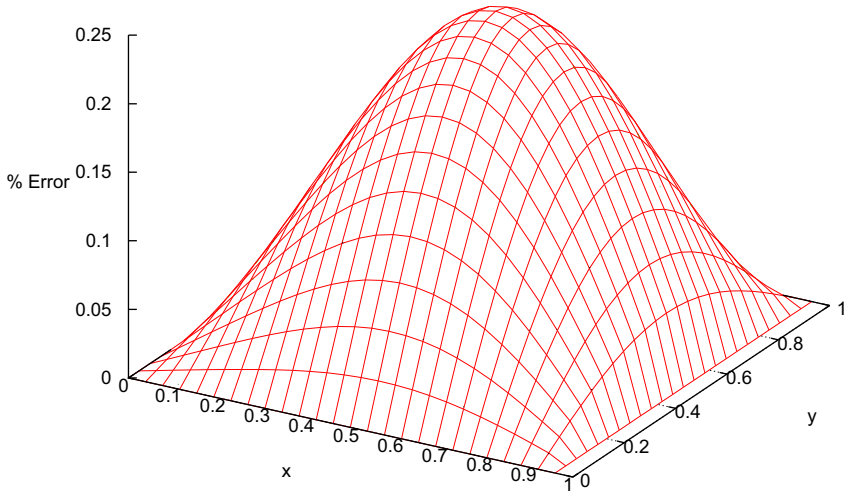

Figure 3.17-8. Local percent error of the transient temperature response for 2-D conduction enclosure at a time of two hours.

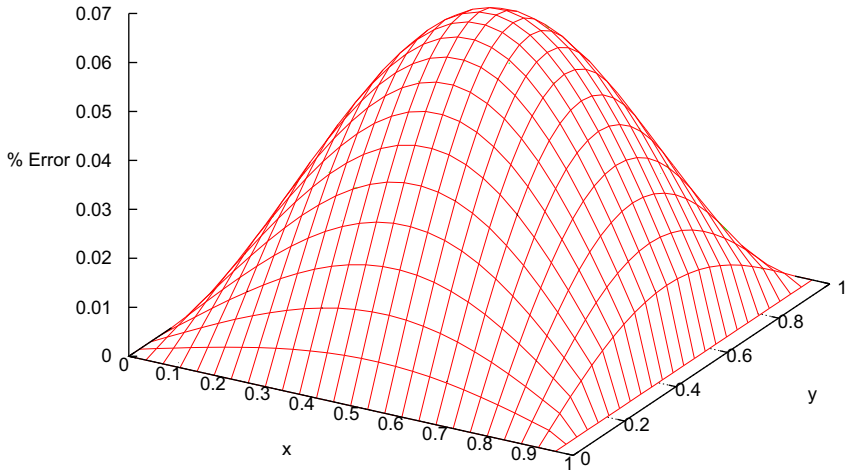

Figure 3.17-9. Local percent error of the transient temperature response for 2-D conduction enclosure at a time of three hours.

3.18 Cladding Oxidation

Figures comparing simulations using Linux and Windows code versions are presented. No differences were observed in the figures.

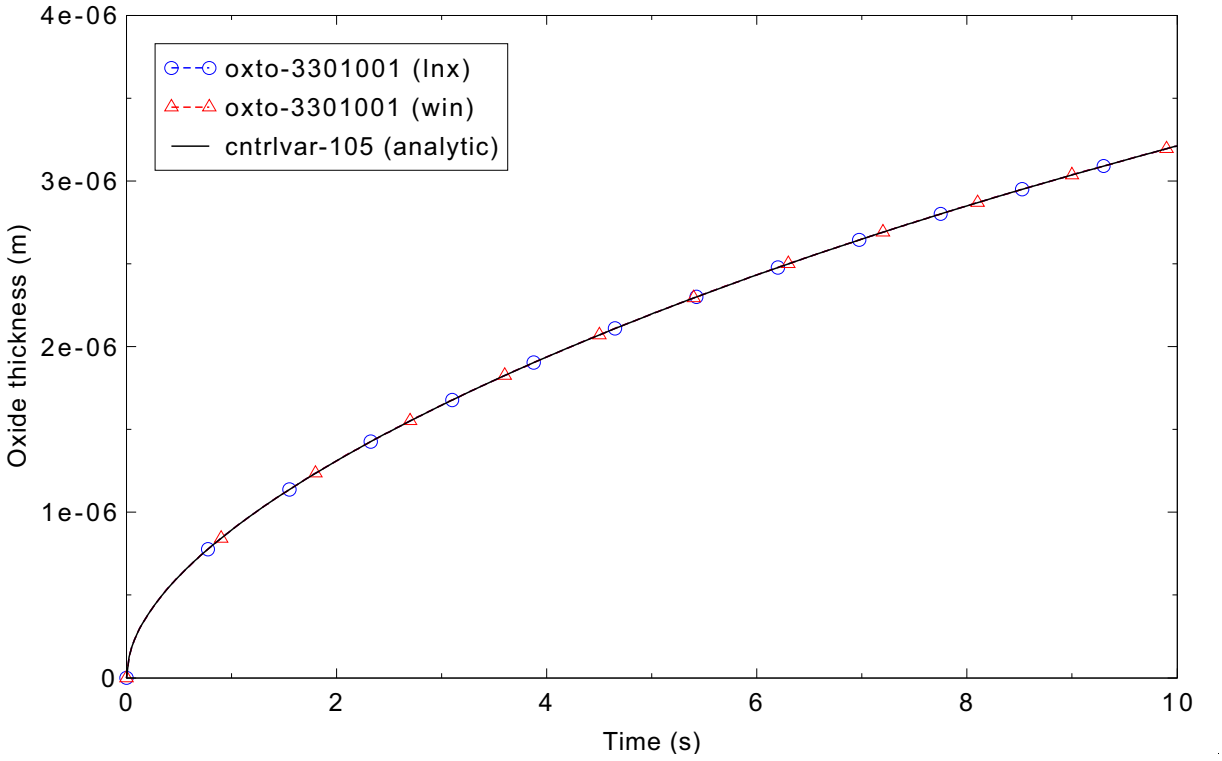

Figure 3.18-1. Oxide thickness for a cylindrical structure using the default metal-water reaction model.

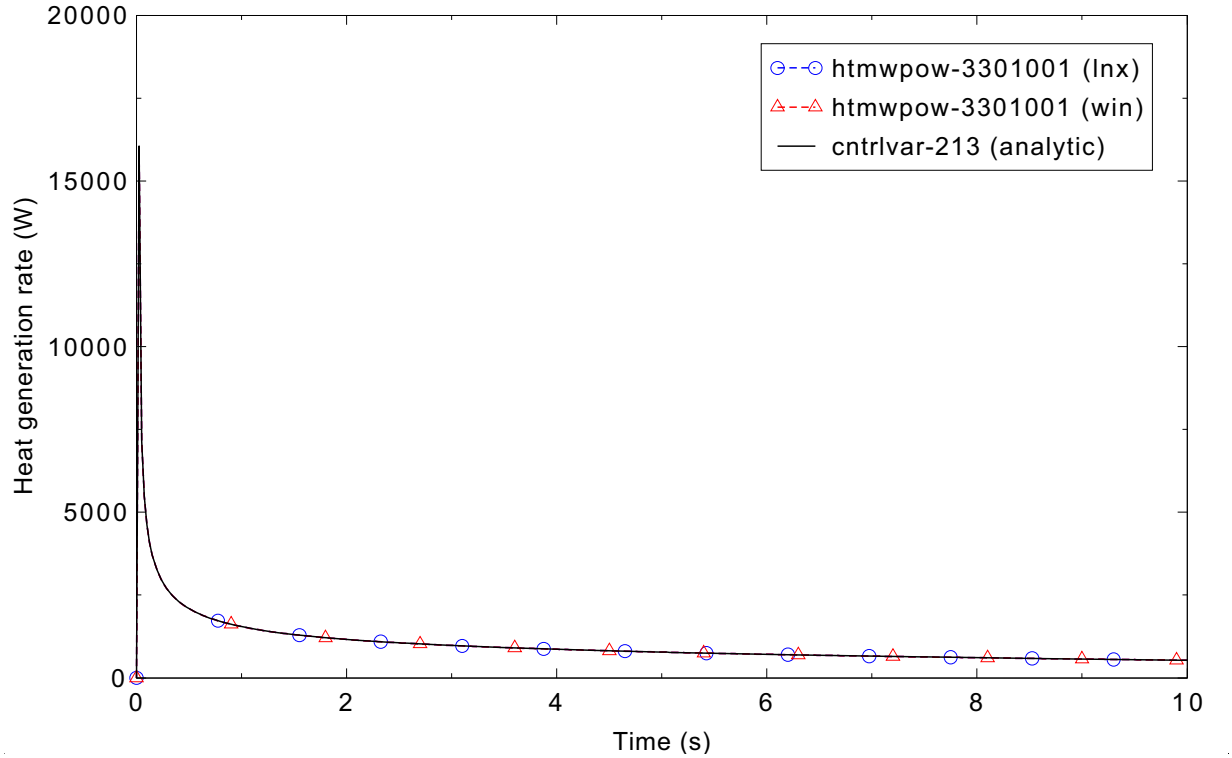

Figure 3.18-2. Oxidation heat generation for a cylindrical structure using the default metal-water reaction model.

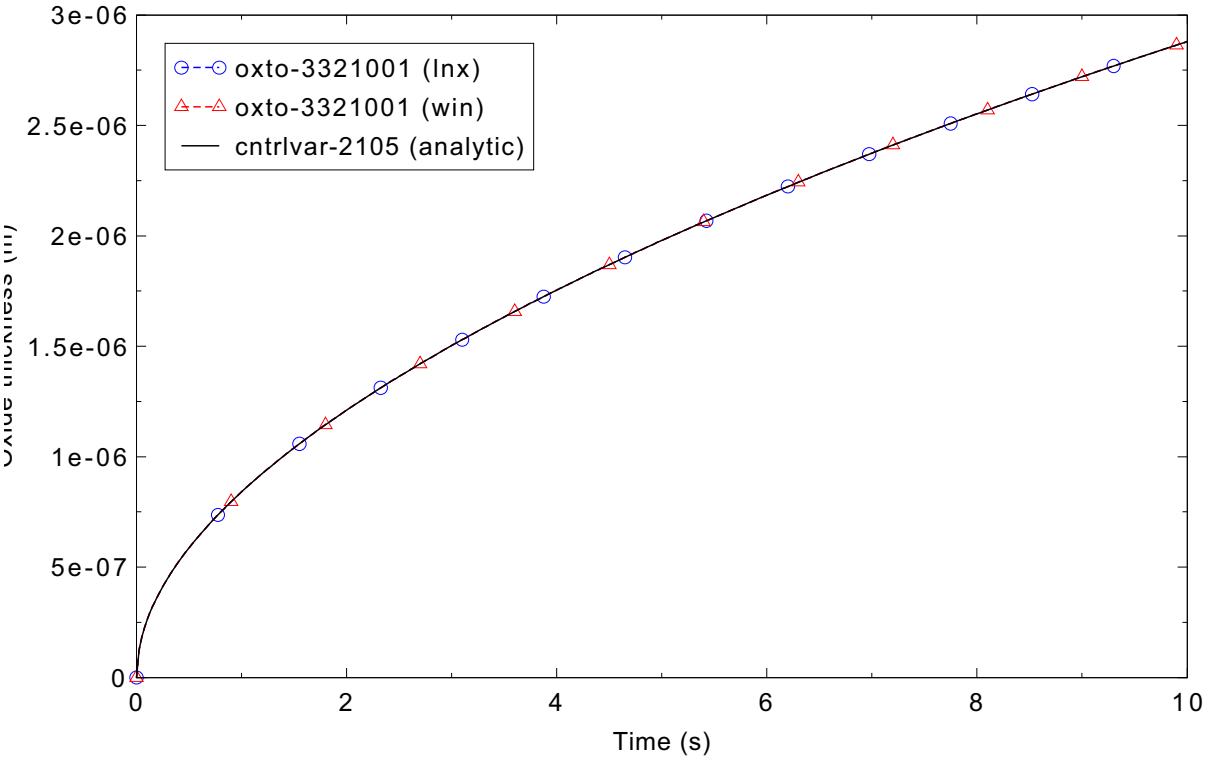

Figure 3.18-3. Oxide thickness for a rectangular structure with user-input rate constants.

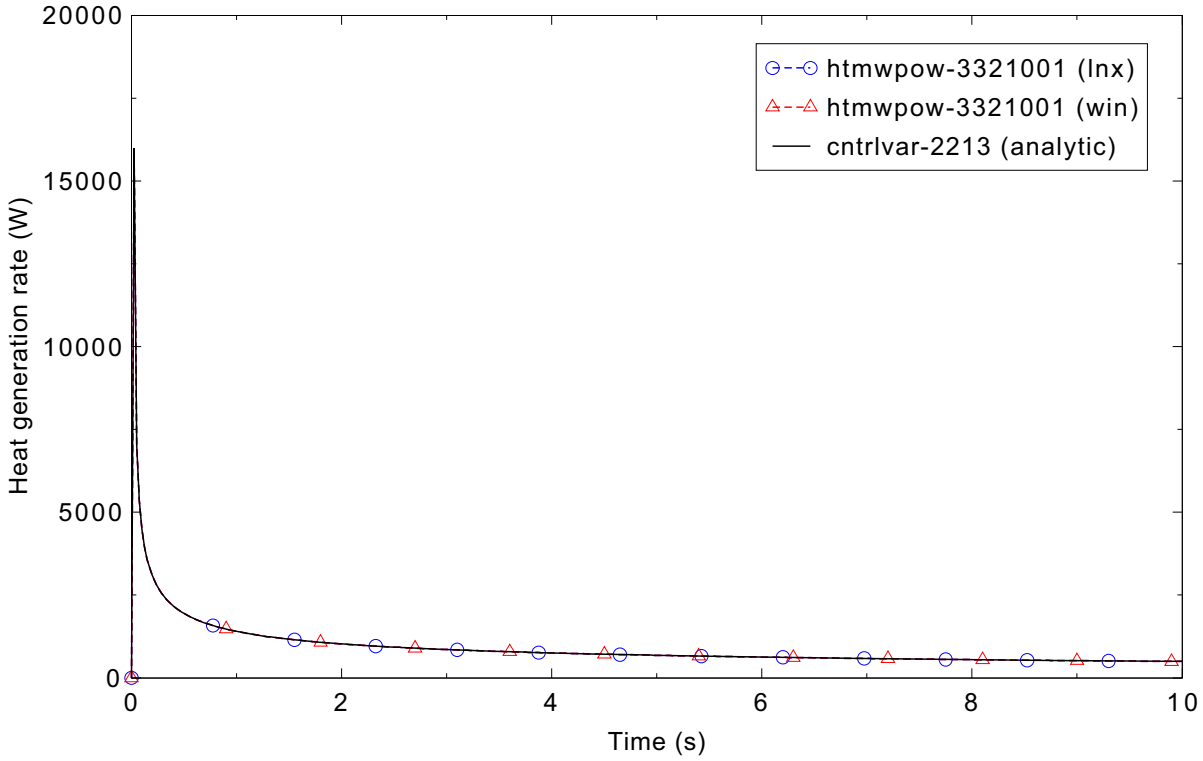

Figure 3.18-4. Oxidation heat generation for a rectangular structure with user-input rate constants.

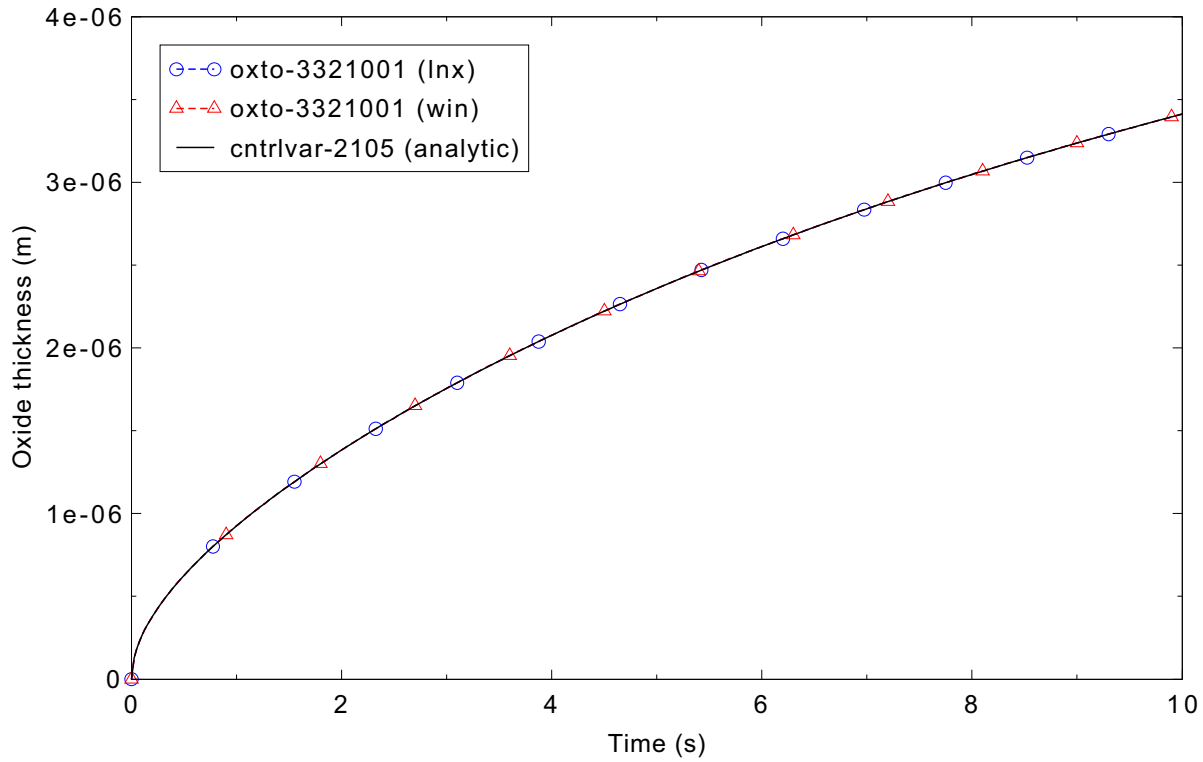

Figure 3.18-5. Oxide thickness for a spherical structure with user-input rate constants.

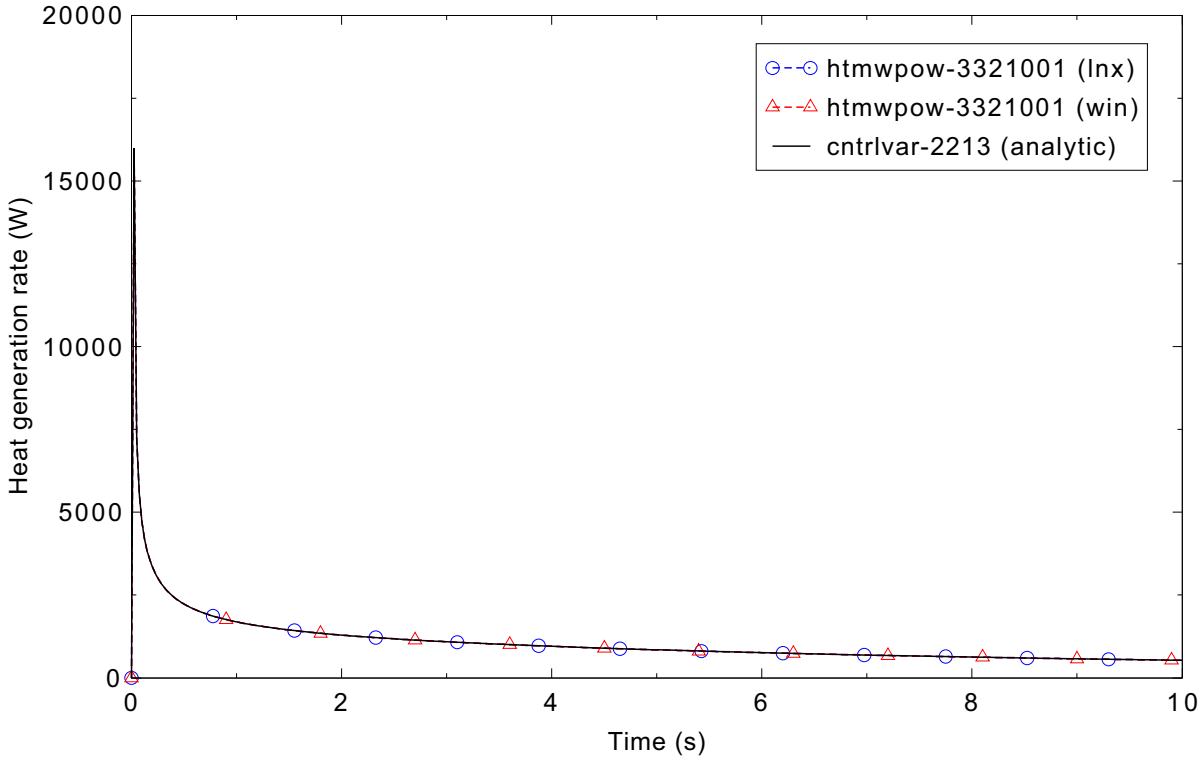

Figure 3.18-6. Oxidation heat generation for a spherical structure with user-input rate constants.

4. SEPARATE EFFECTS CASES

The chapter presents the separate effects assessment case results.

4.1 Edwards-O'Brien Blowdown Test

Figures comparing simulations using Linux and Windows code versions are presented. Diagrams are included so that the figure numbering is the same as that in Volume III of the RELAP5-3D code manual. No differences were observed in the figures.

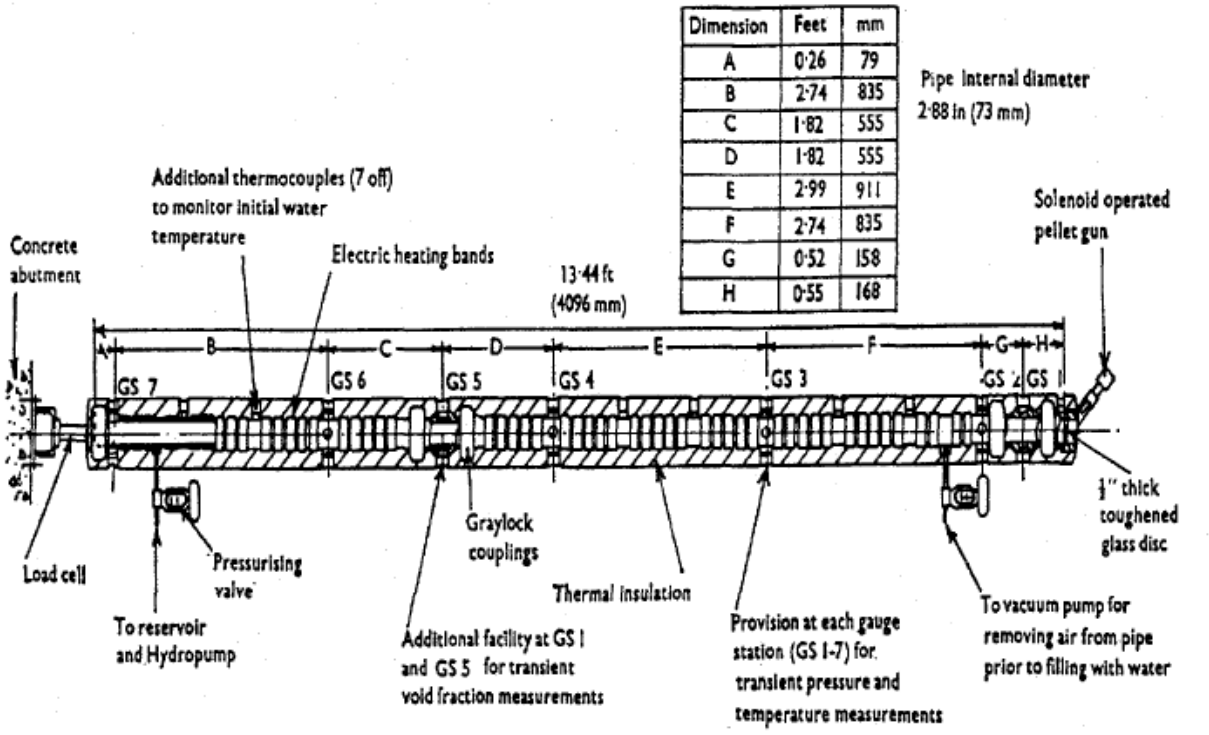

Figure 4.1-1. Edwards-O'Brien test facility.

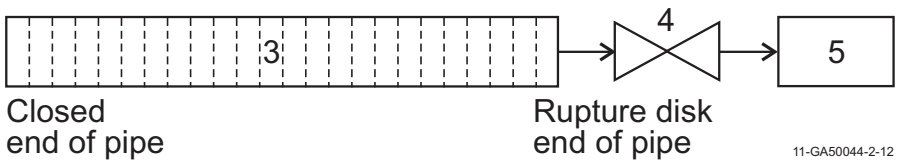

Figure 4.1-2. Diagram of the RELAP5-3D Edwards-O'Brien model.

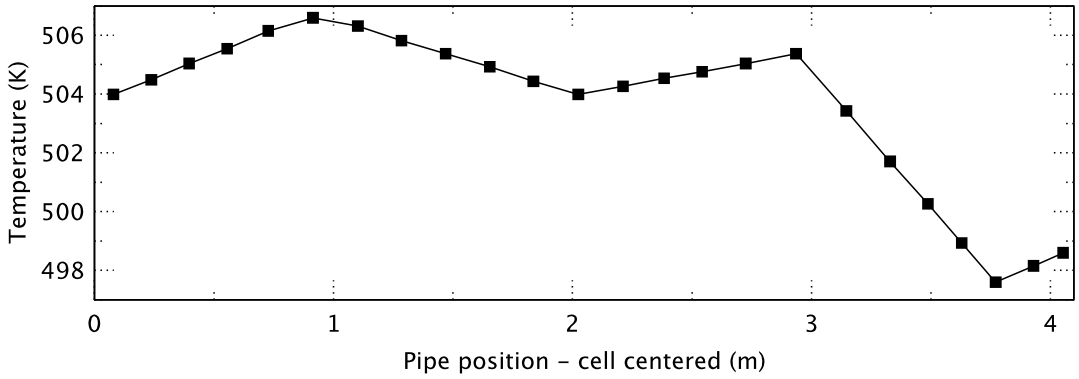

Figure 4.1-3. Non-uniform temperature distribution for Edwards-O'Brien model.

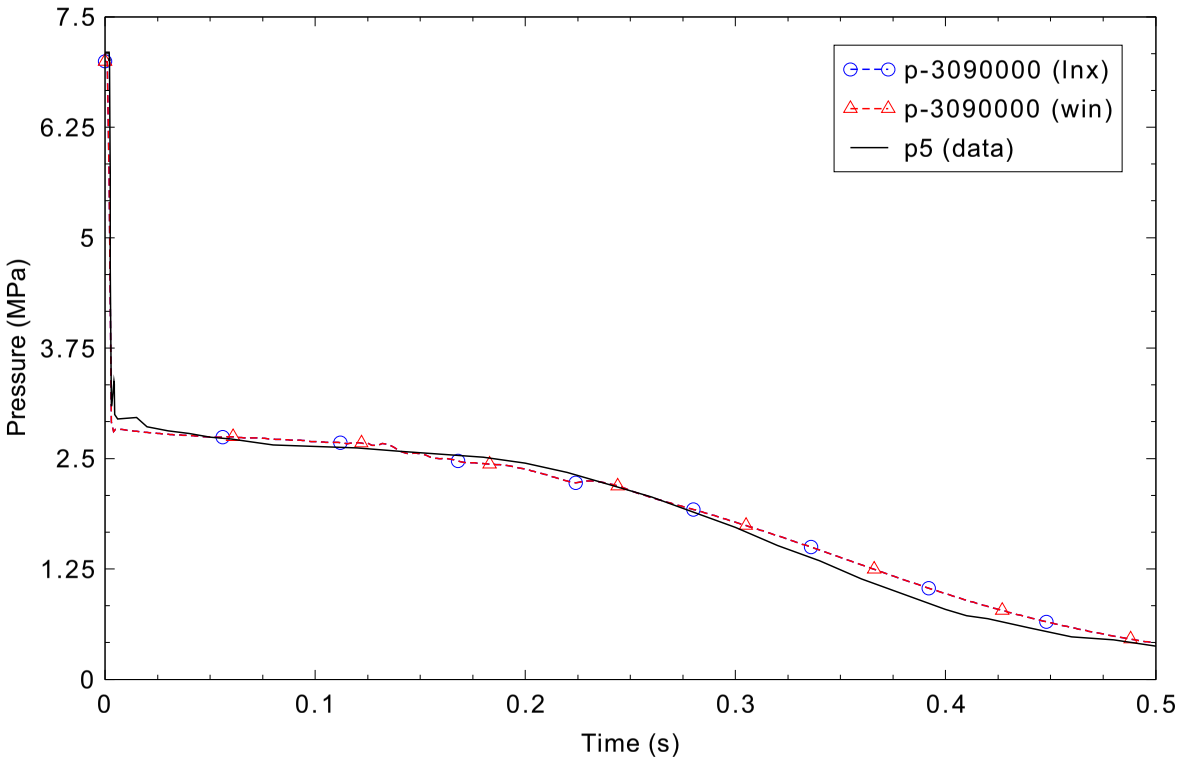

Figure 4.1-4. Measured and calculated pressures for the Edwards-O'Brien blowdown test.

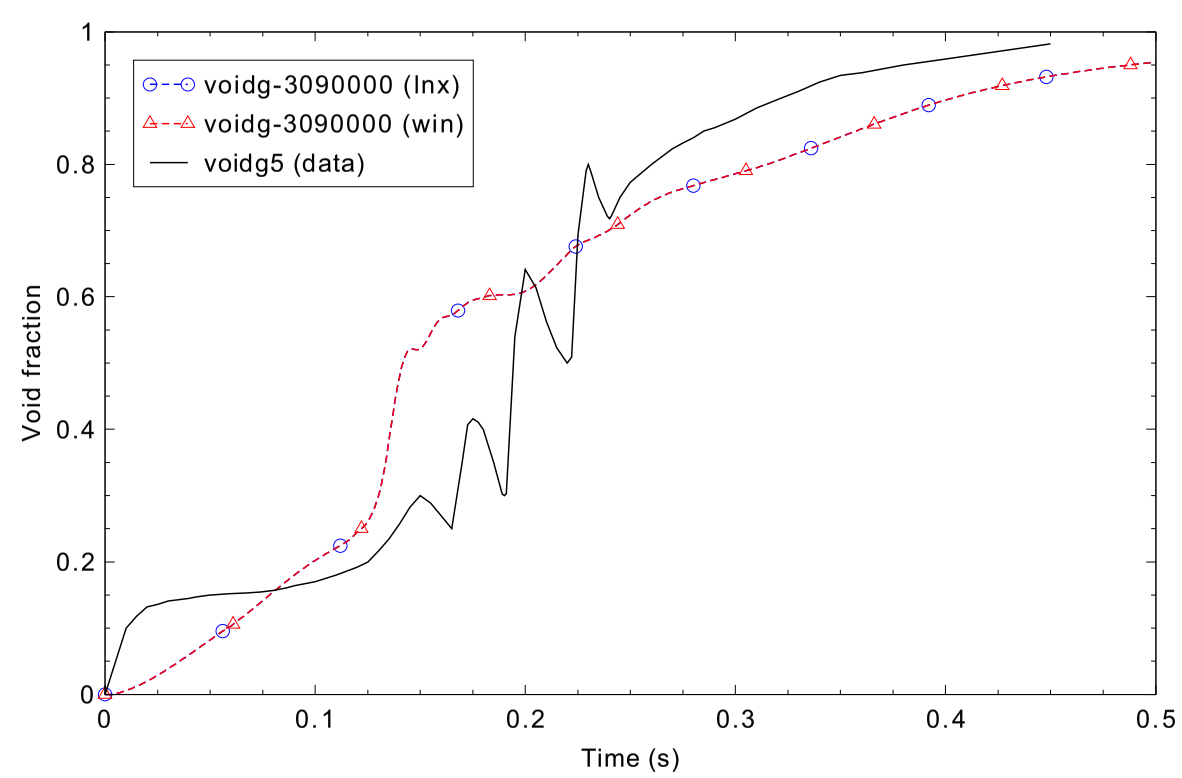

Figure 4.1-5. Measured and calculated void fractions for the Edwards-O'Brien blowdown test.

4.2 Marviken Critical Flow Test 21

Figures comparing simulations using Linux and Windows code versions are presented. Diagrams are included so that the figure numbering is the same as that in Volume III of the RELAP5-3D code manual. No differences were observed in the figures.

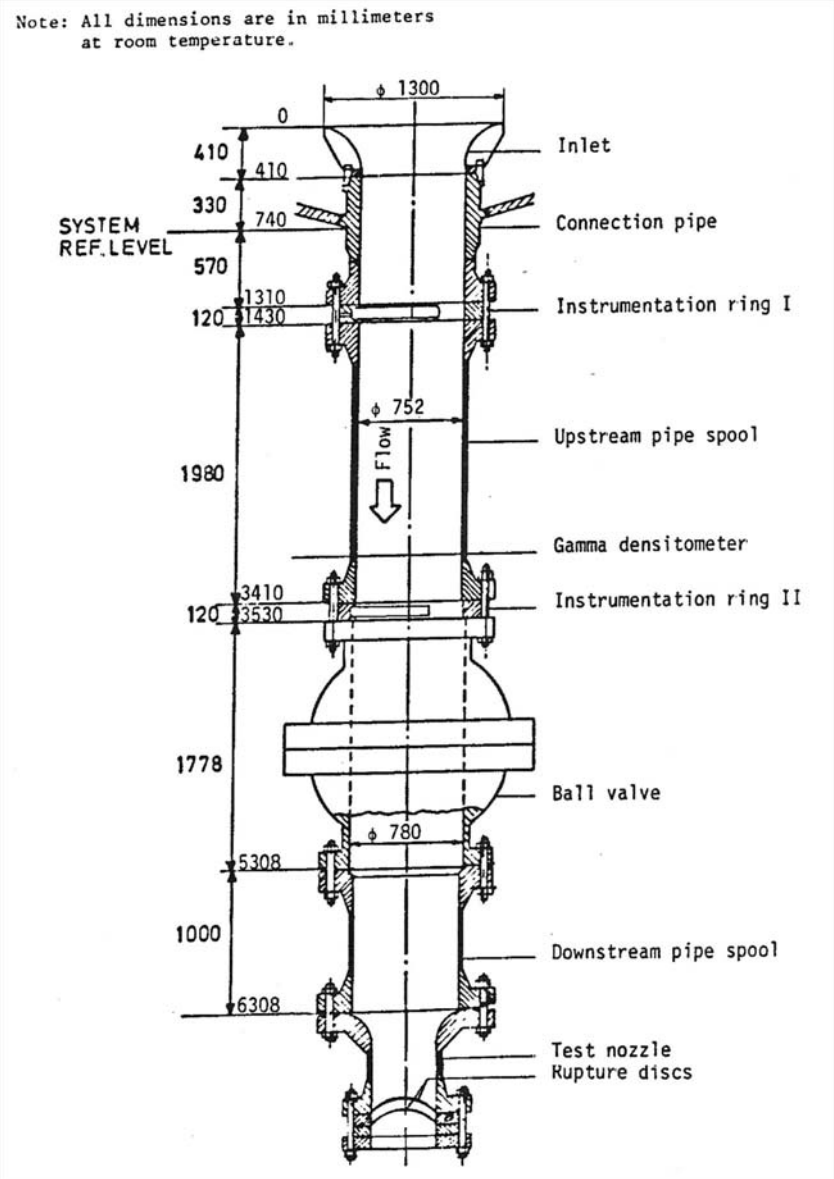

Figure 4.2-1. Marviken Critical Flow Test 21 discharge pipe.

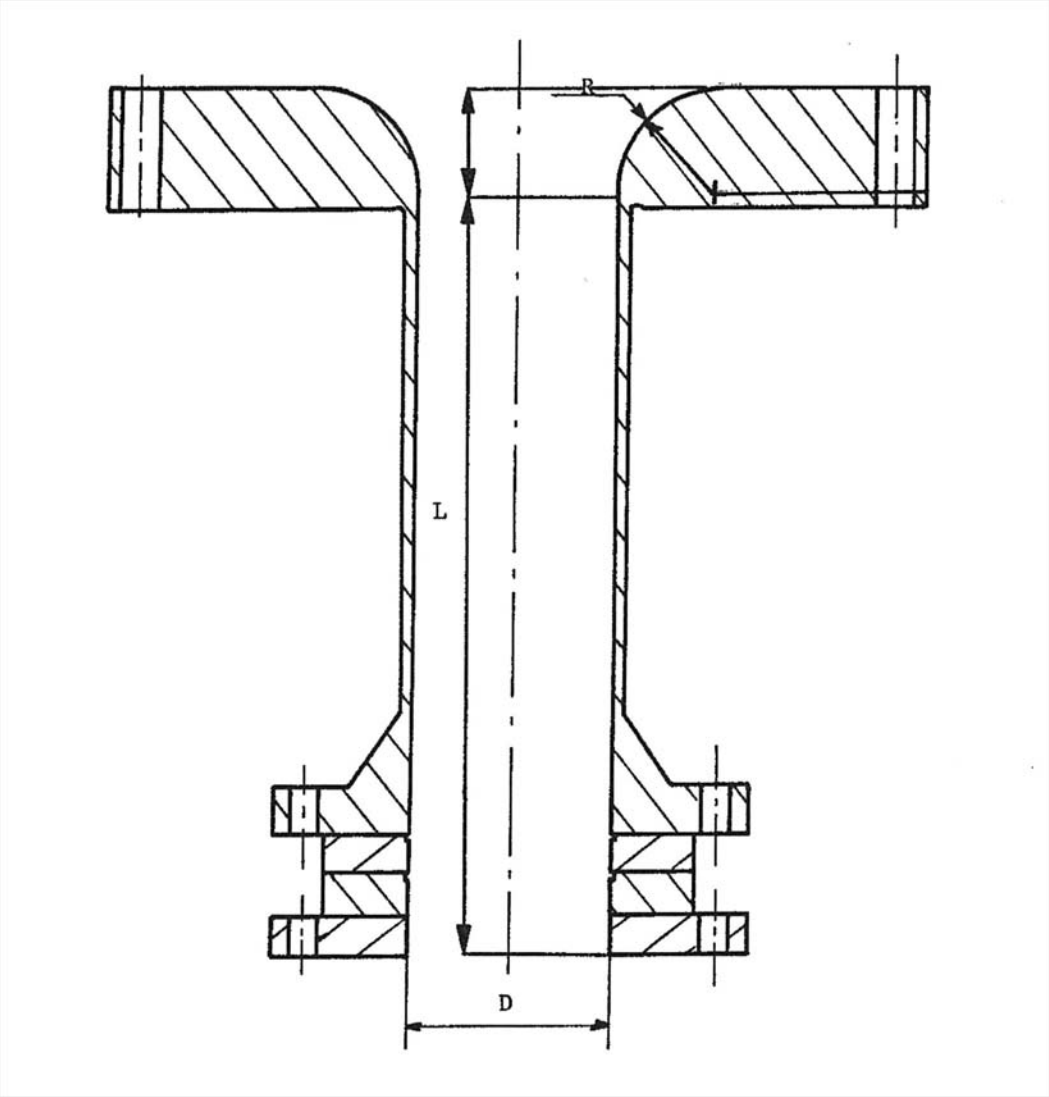

Figure 4.2-2. Marviken Critical Flow Test 21 test nozzle.

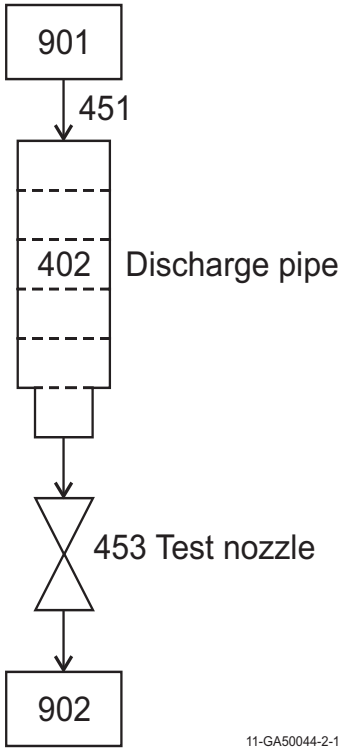

Figure 4.2-3. Marviken Critical Flow Test 21 nodalization diagram.

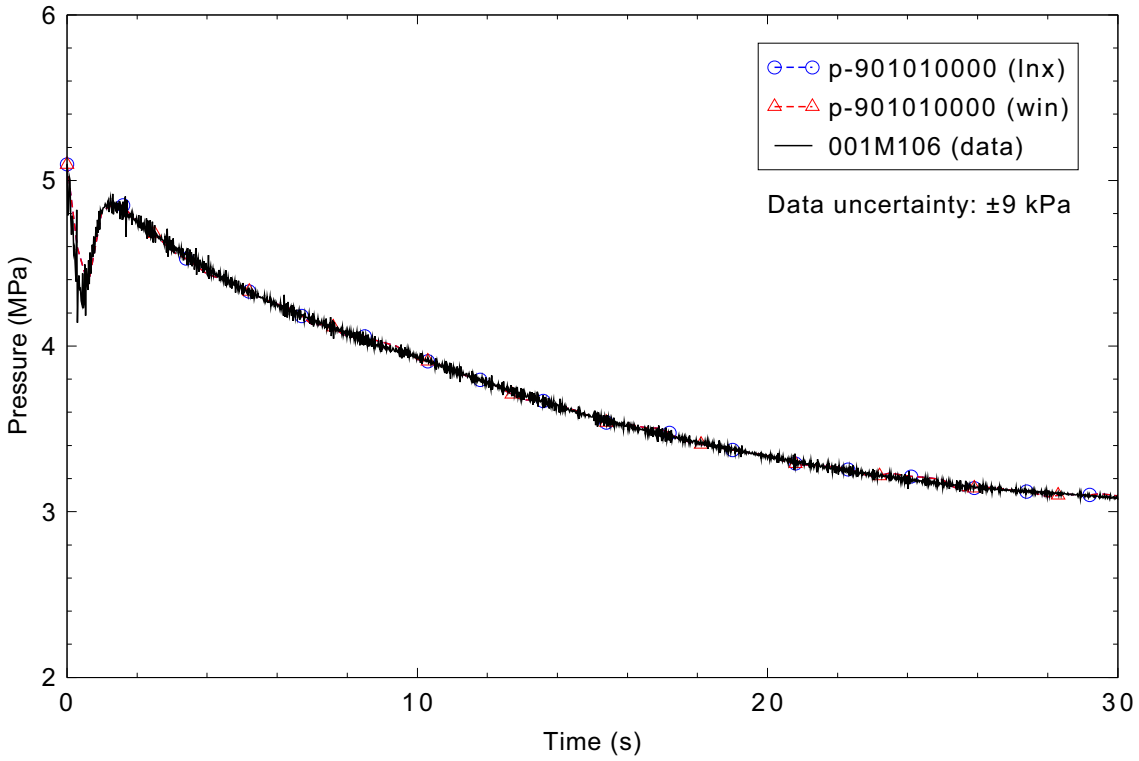

Figure 4.2-4. Marviken CFT 21 pressure at vessel bottom (boundary condition).

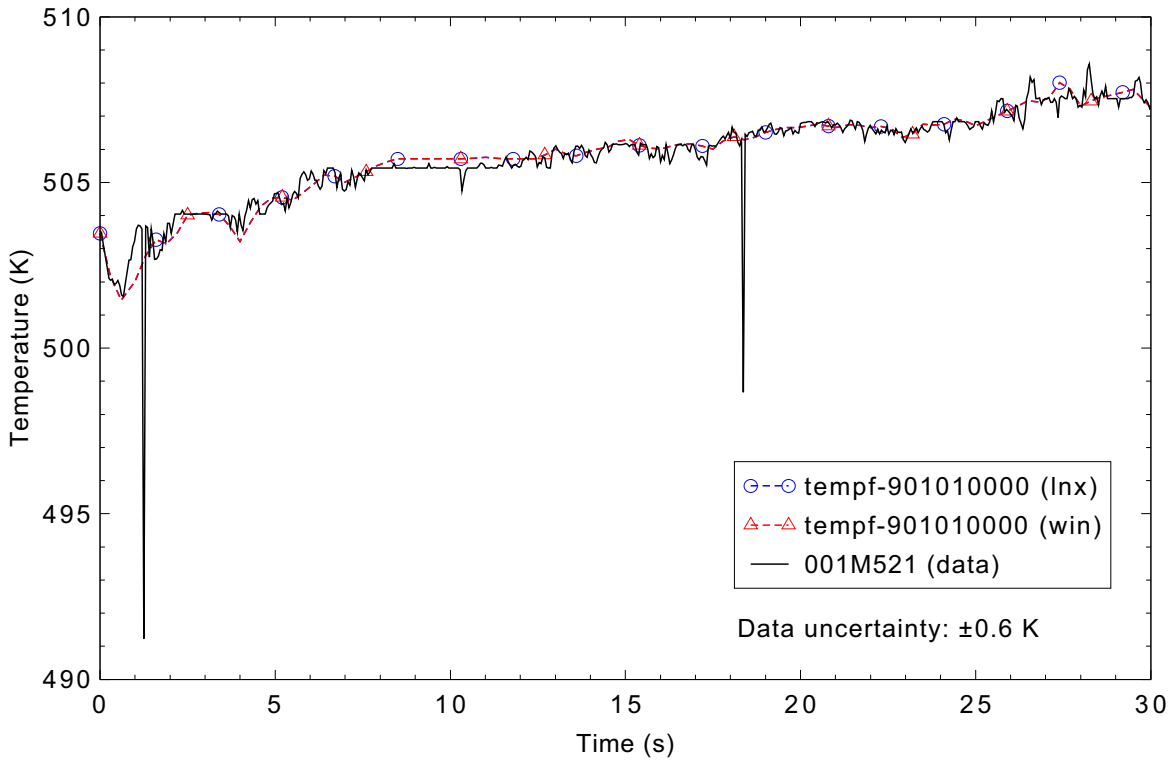

Figure 4.2-5. Marviken CFT 21 temperature at vessel bottom (boundary condition).

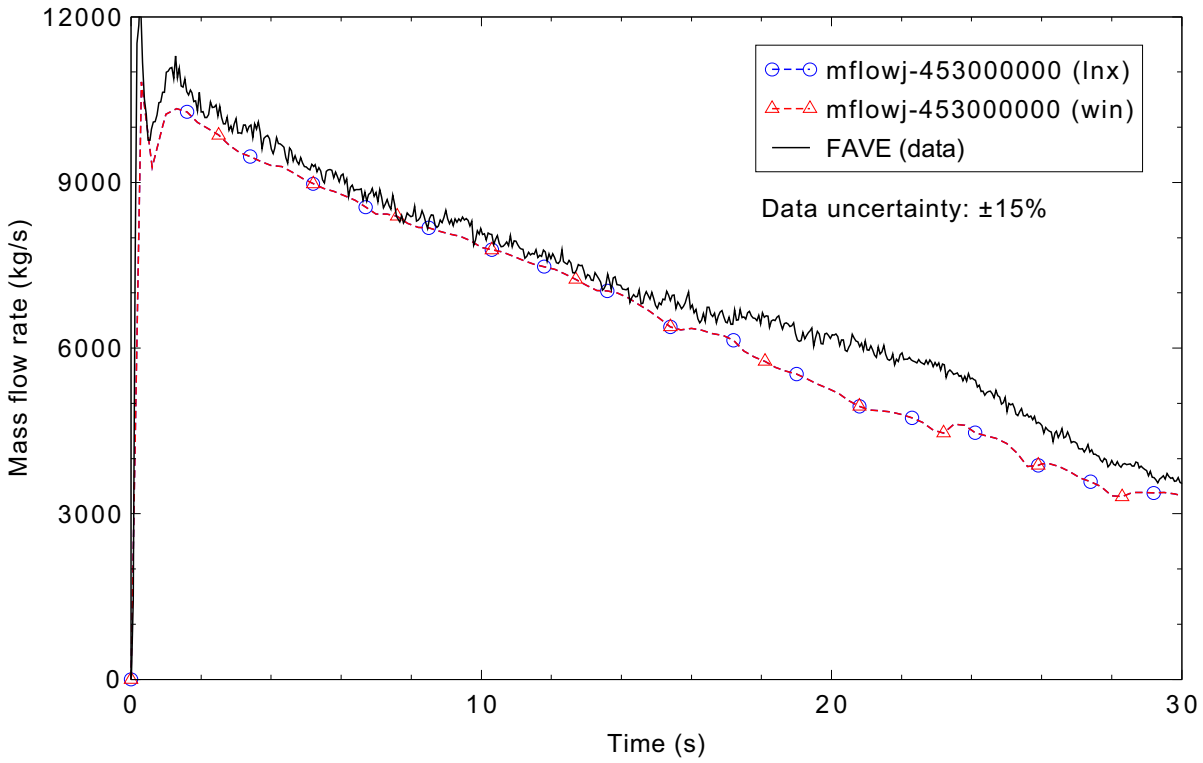

Figure 4.2-6. Measured and calculated mass flow rate for Marviken CFT 21.

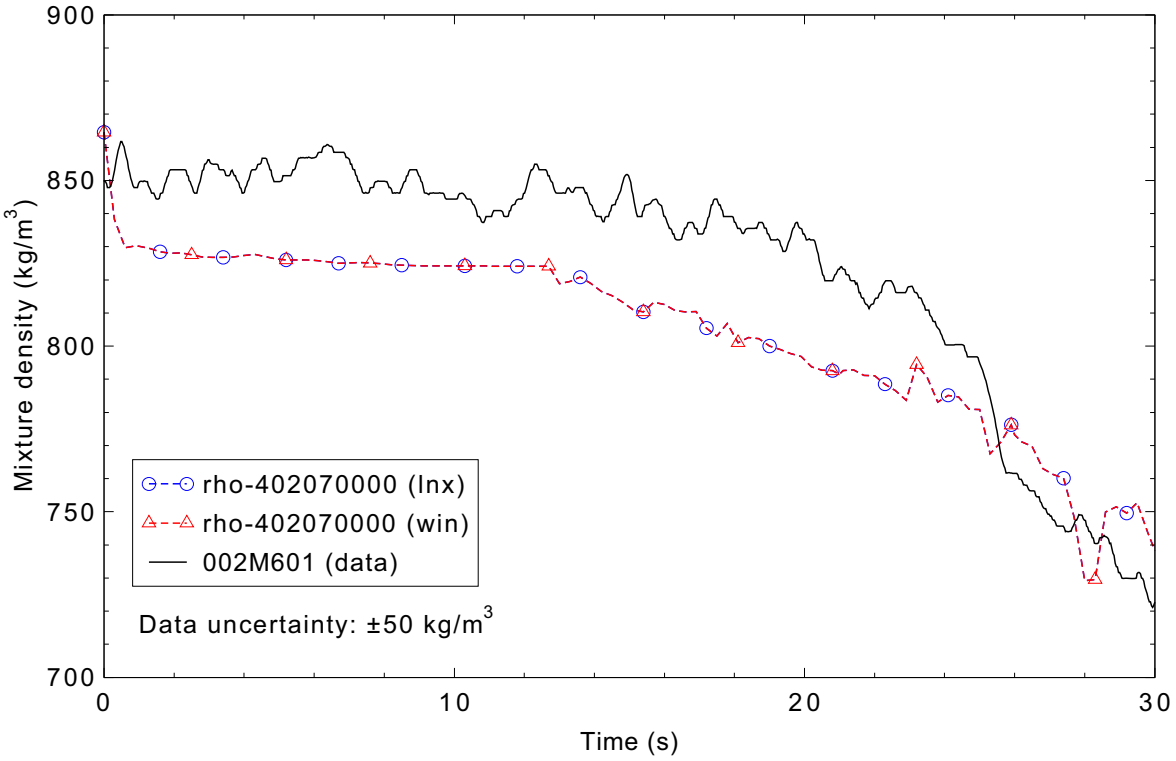

Figure 4.2-7. Measured and calculated mixture density in the discharge pipe for Marviken CFT 21.

4.3 Marviken Critical Flow Test 22

Figures comparing simulations using Linux and Windows code versions are presented. Diagrams are included so that the figure numbering is the same as that in Volume III of the RELAP5-3D code manual. No differences were observed in the figures.

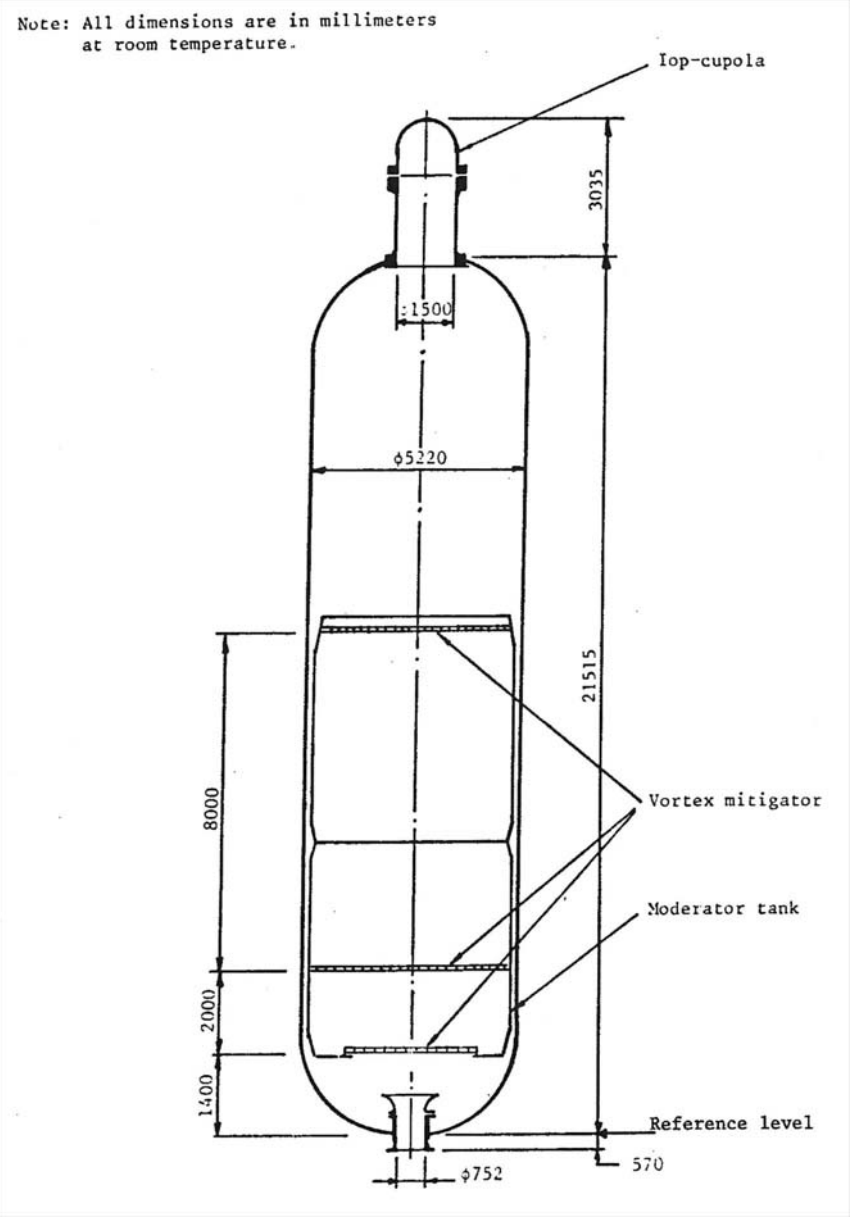

Figure 4.3-1. Marviken Critical Flow Test 22 pressure vessel.

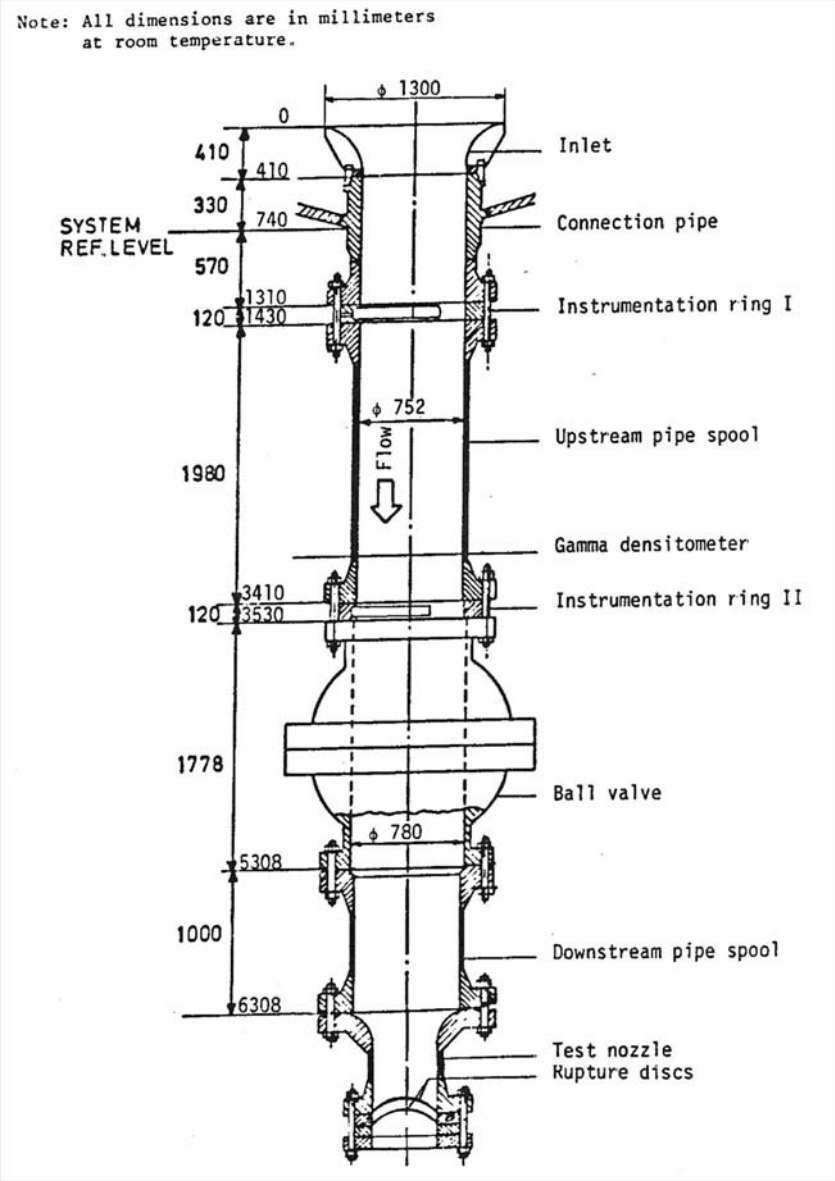

Figure 4.3-2. Marviken Critical Flow Test 22 discharge pipe, test nozzle, and rupture disk assembly.

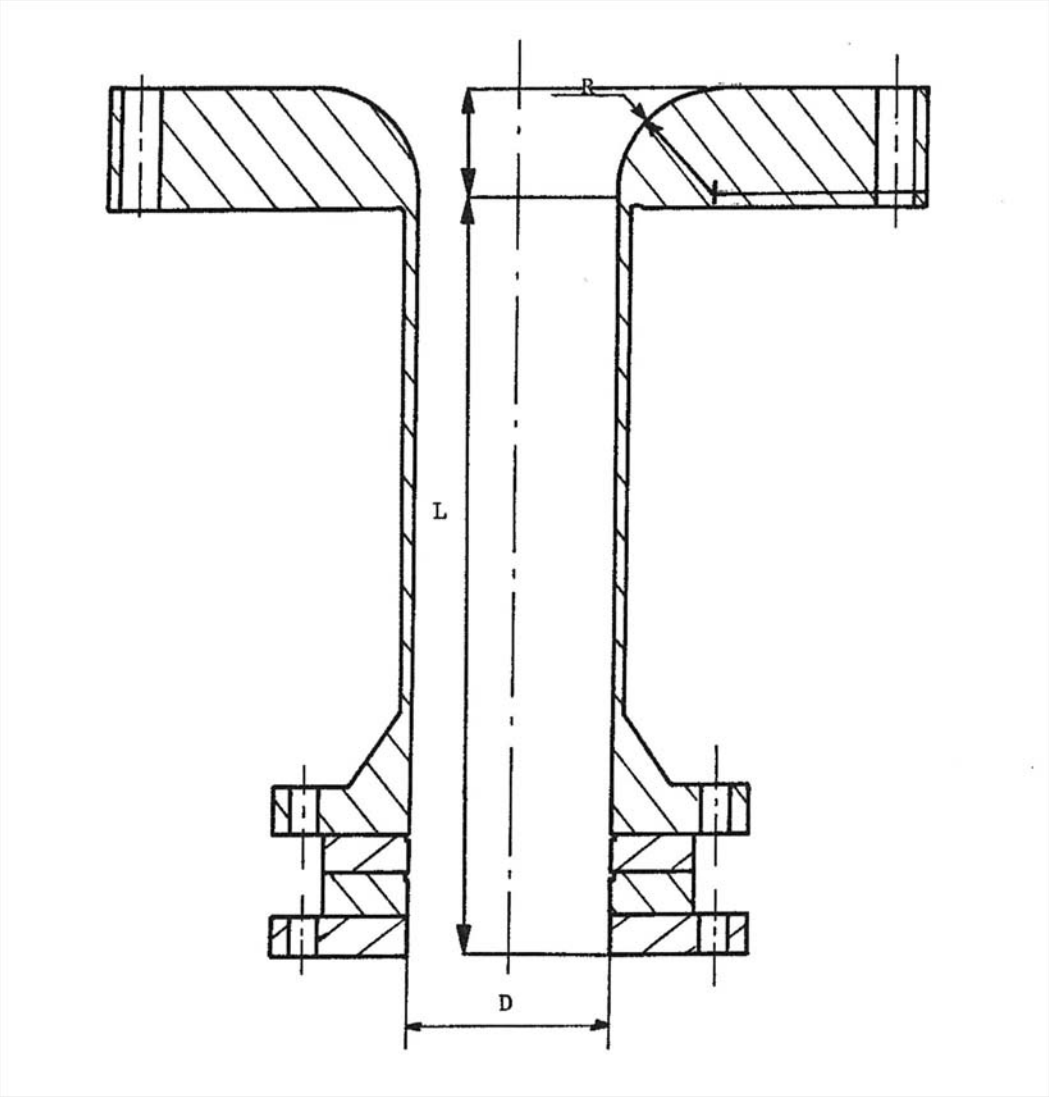

Figure 4.3-3. Marviken Critical Flow Test 22 test nozzle.

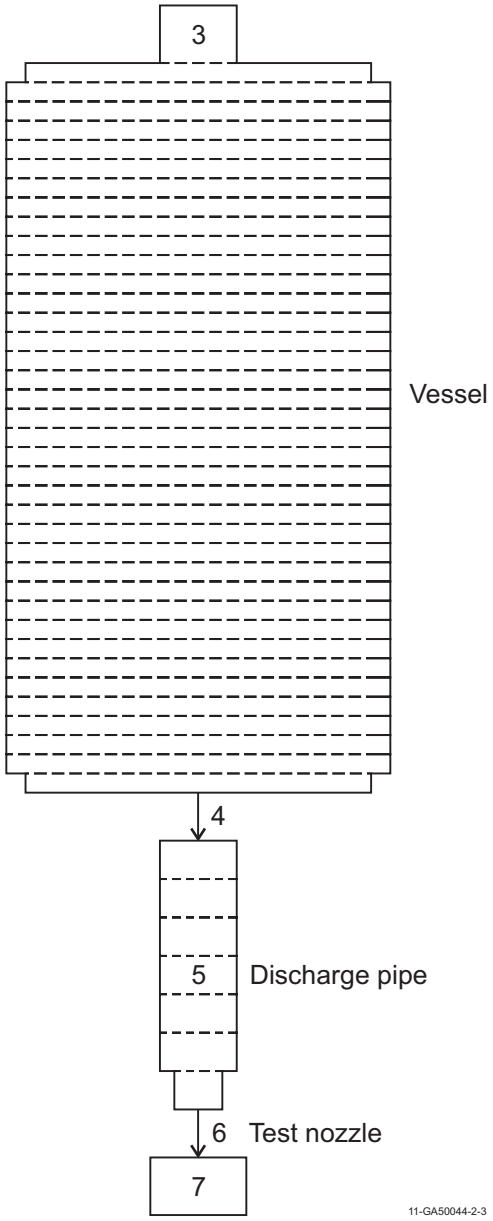

Figure 4.3-4. Marviken Critical Flow Test 22 nodalization diagram.

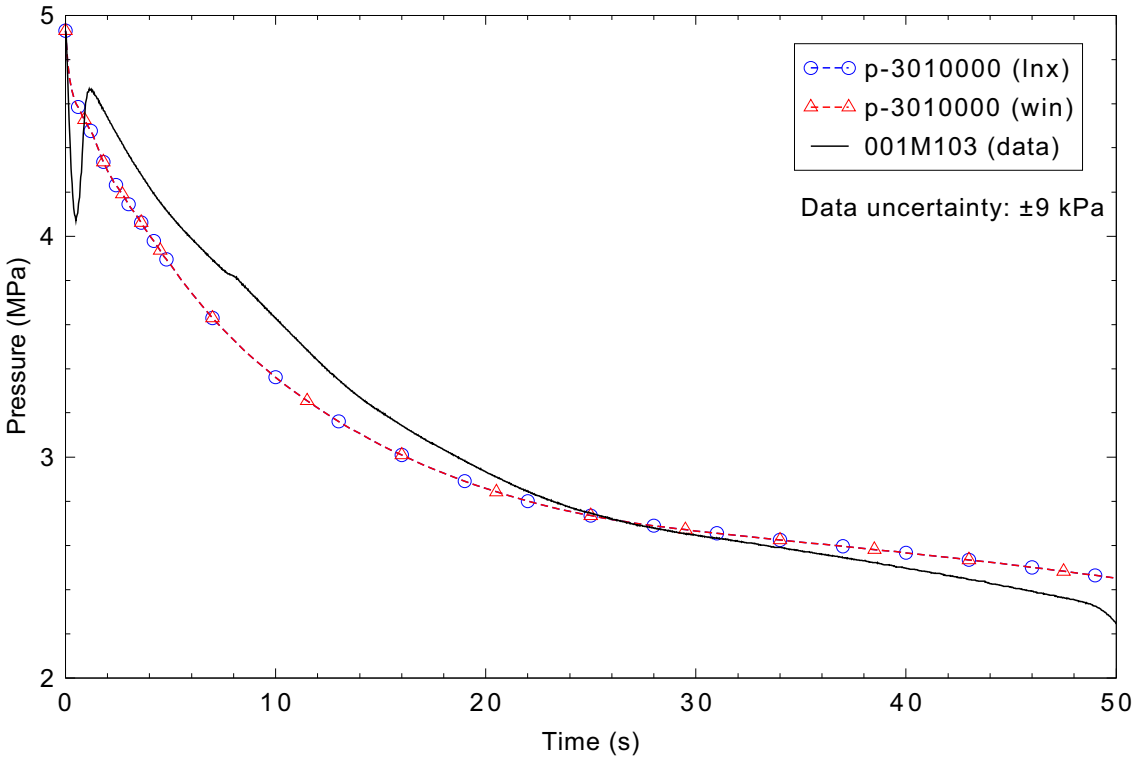

Figure 4.3-5. Measured and calculated vessel pressure for Marviken CFT 22.

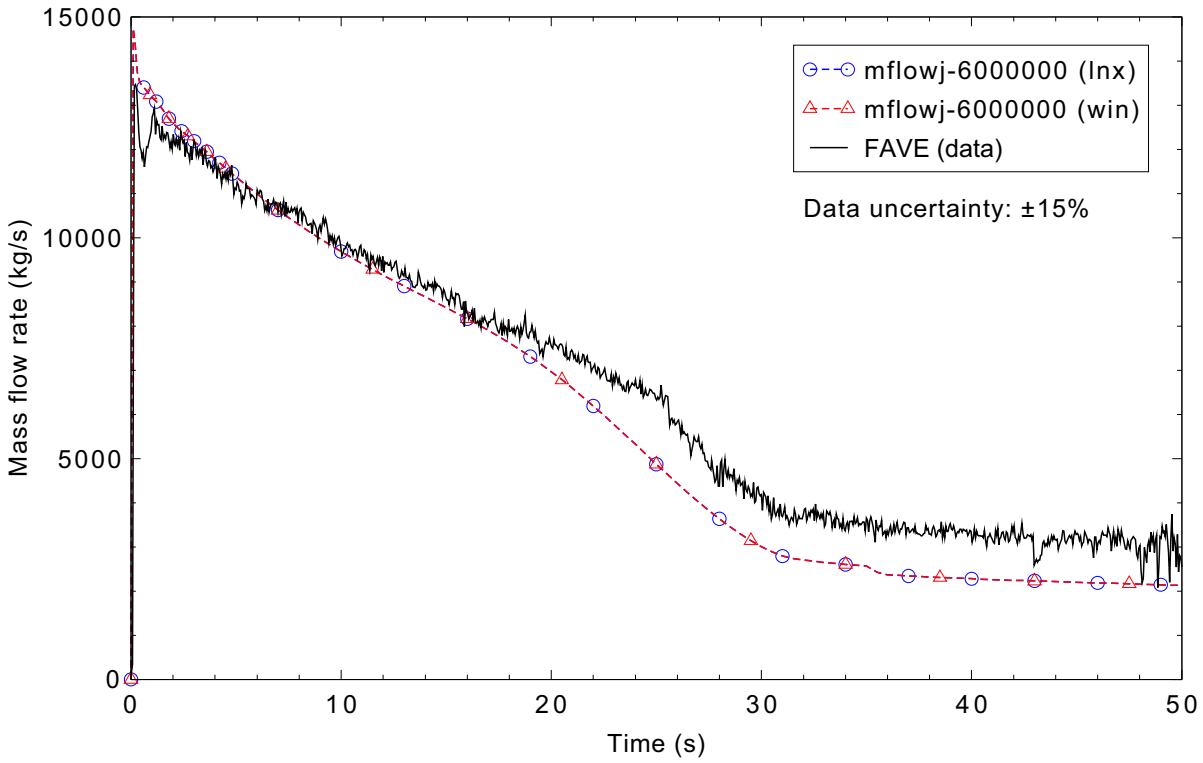

Figure 4.3-6. Measured and calculated mass flow rate for Marviken CFT 22.

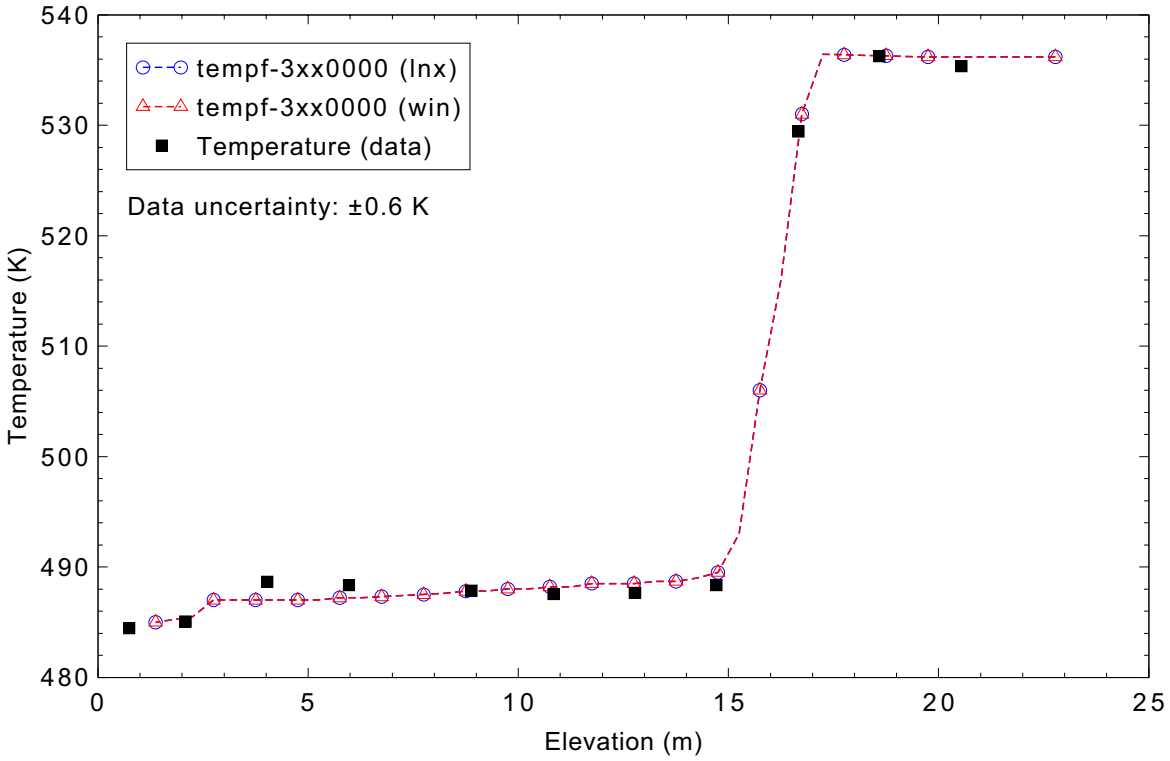

Figure 4.3-7. Measured and calculated temperature profile at 0 s for Marviken CFT 22.

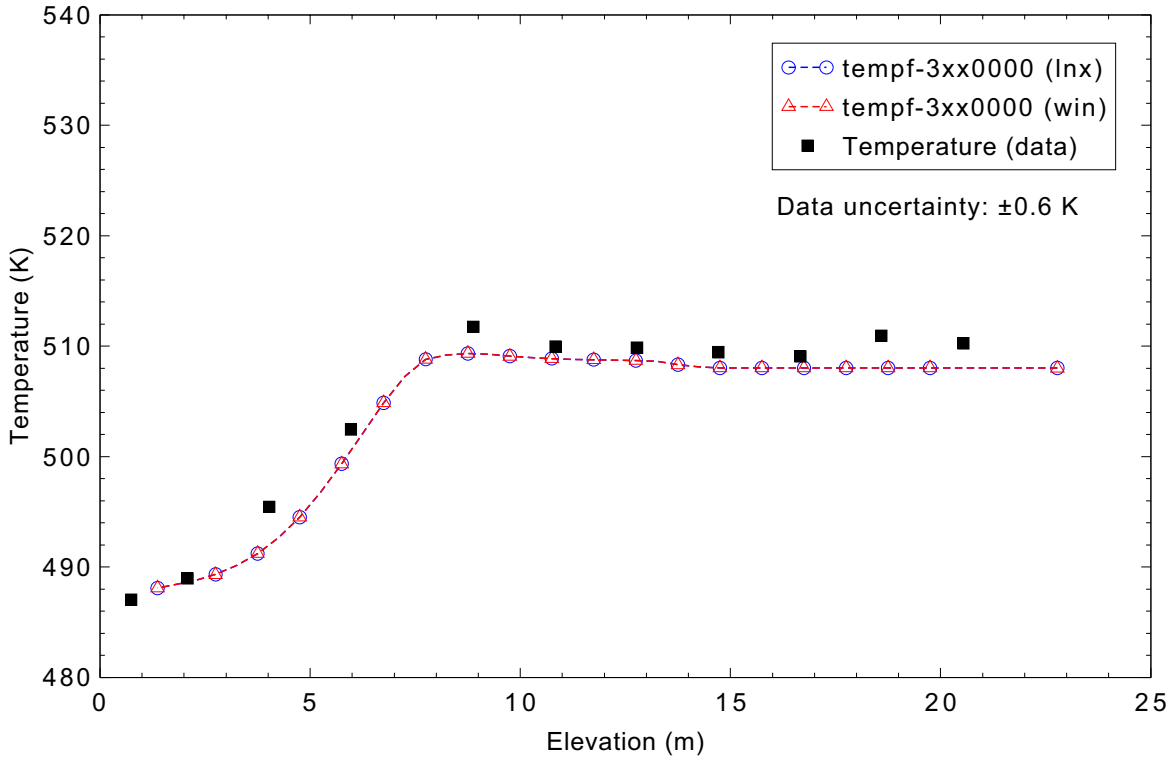

Figure 4.3-8. Measured and calculated temperature profile at 15 s for Marviken CFT 22.

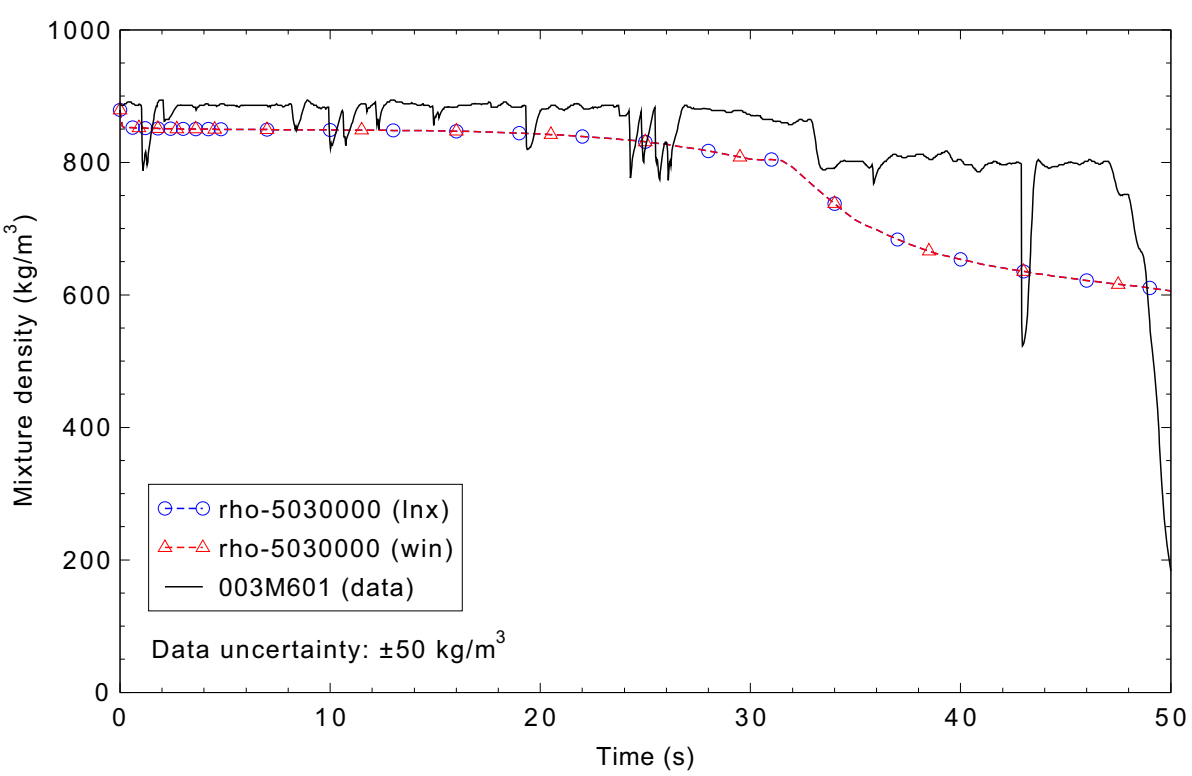

Figure 4.3-9. Measured and calculated mixture density in the discharge pipe for Marviken CFT 22.

4.4 Marviken Critical Flow Test 24

Figures comparing simulations using Linux and Windows code versions are presented. Diagrams are included so that the figure numbering is the same as that in Volume III of the RELAP5-3D code manual. No differences were observed in the figures.

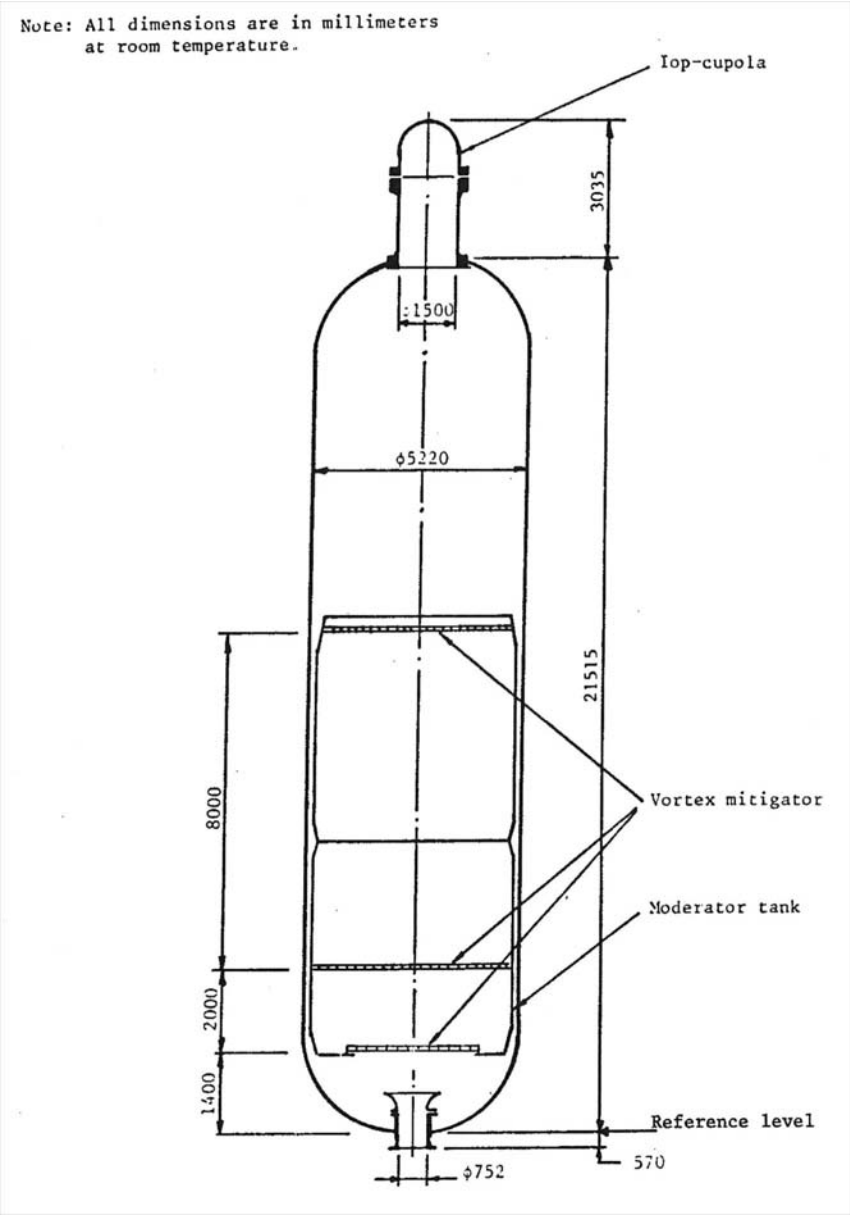

Figure 4.4-1. Marviken Critical Flow Test 24 pressure vessel.

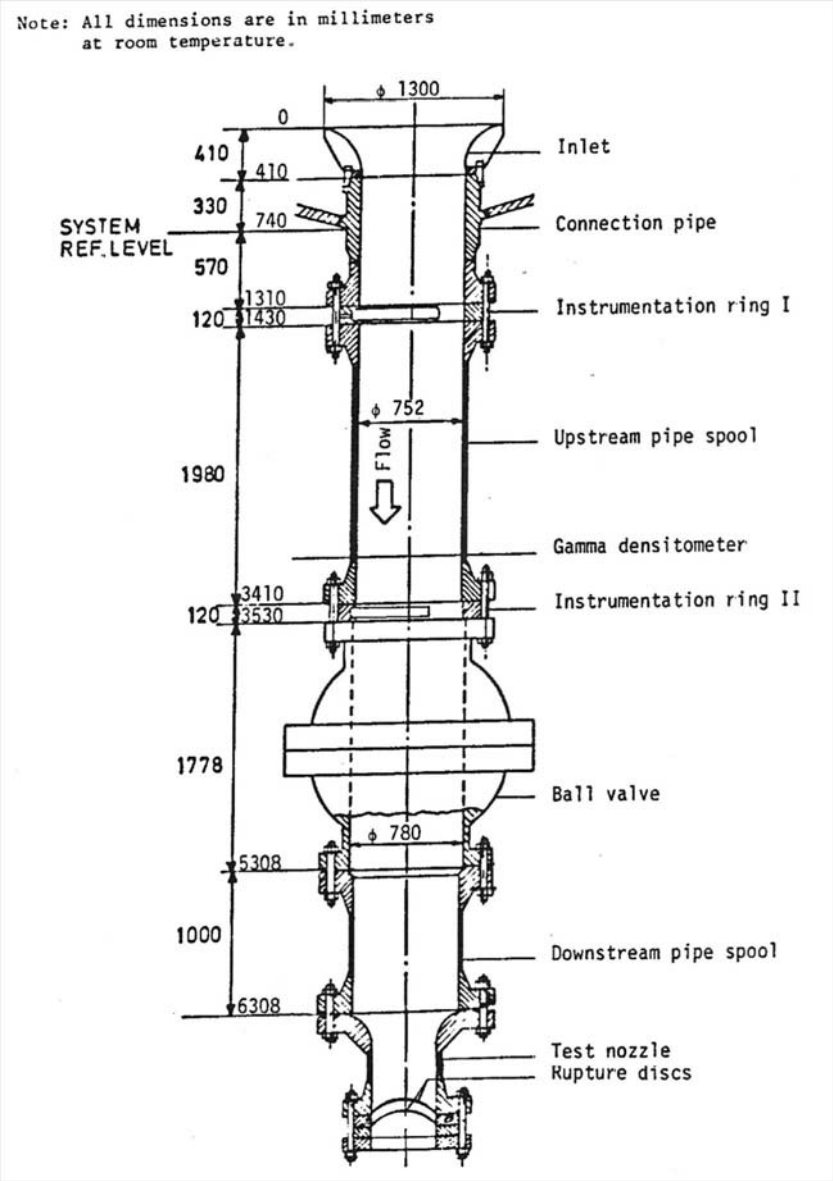

Figure 4.4-2. Marviken Critical Flow Test 24 discharge pipe, test nozzle, and rupture disk assembly.

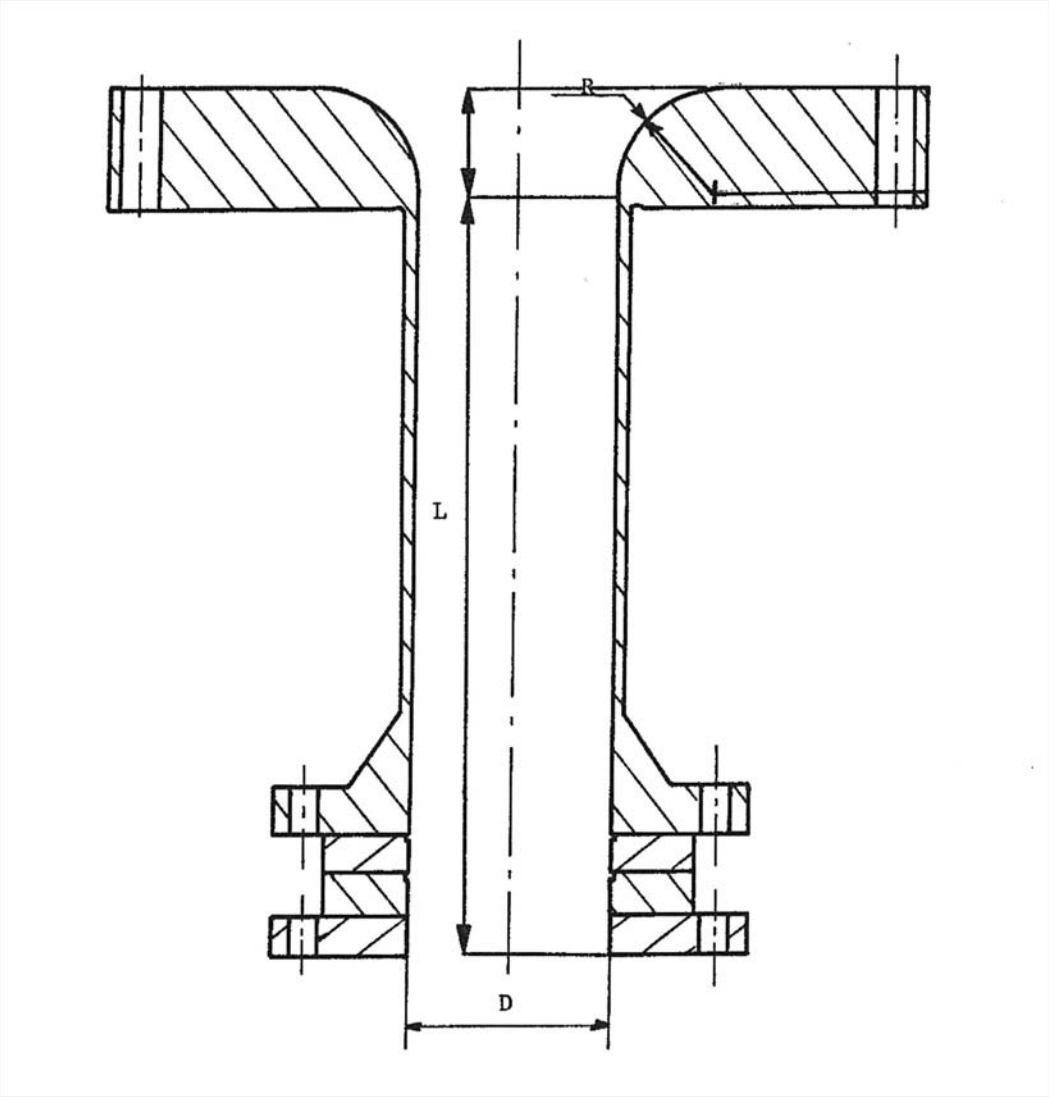

Figure 4.4-3. Marviken Critical Flow Test 24 test nozzle.

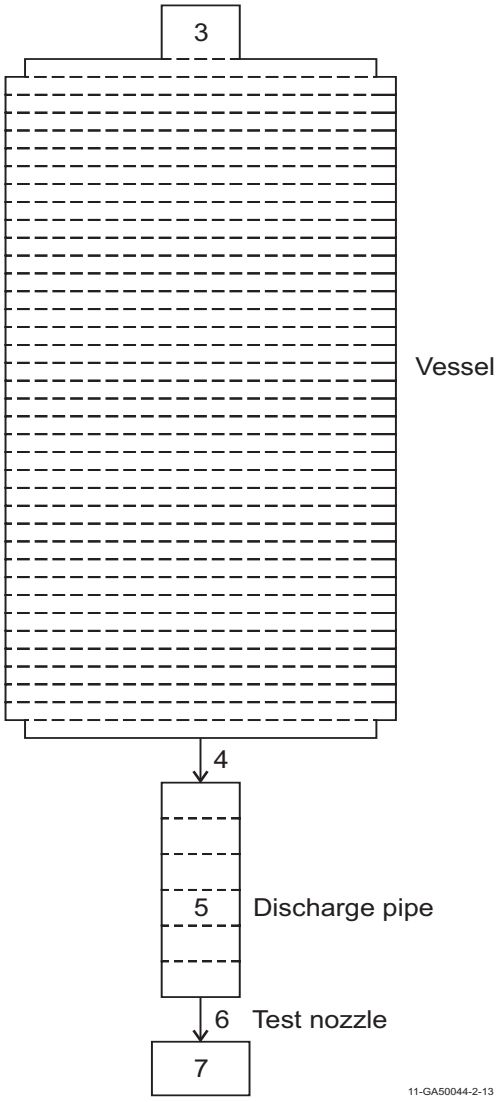

Figure 4.4-4. Marviken Critical Flow Test 24 nodalization diagram.

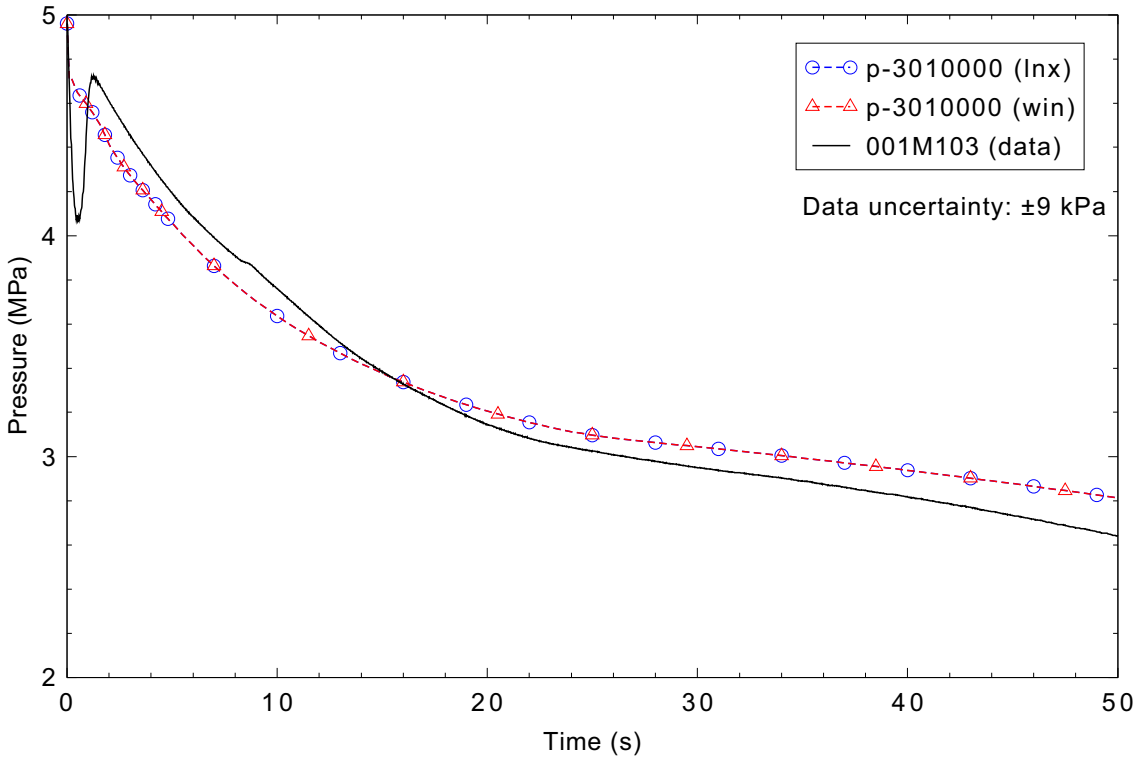

Figure 4.4-5. Measured and calculated vessel pressure for Marviken CFT 24.

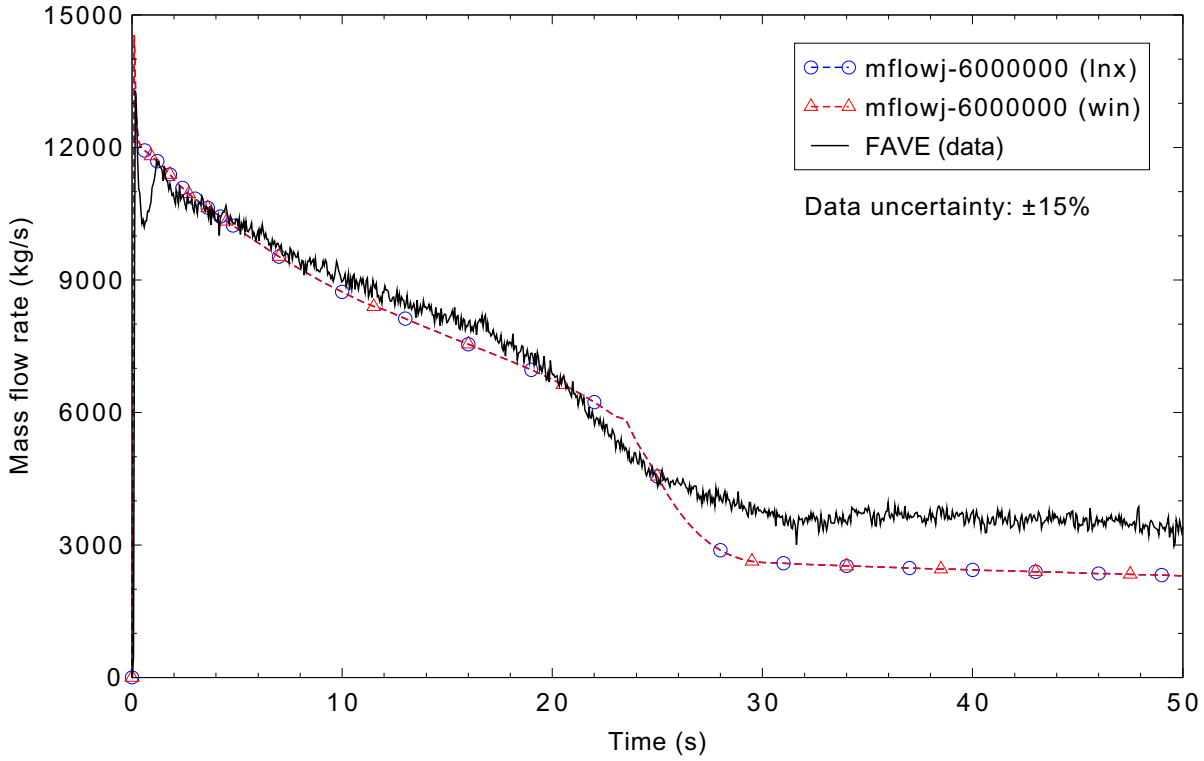

Figure 4.4-6. Measured and calculated mass flow rate for Marviken CFT 24.

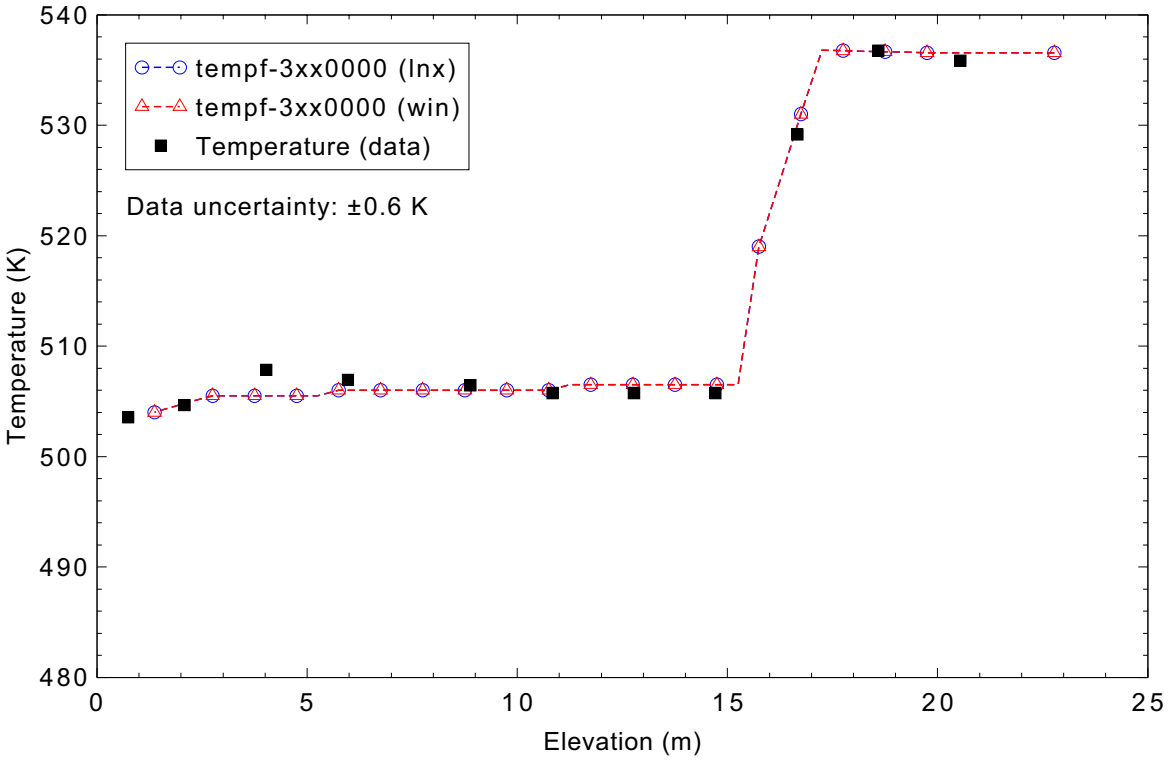

Figure 4.4-7. Measured and calculated vessel temperature profile at 0 s for Marviken CFT 24.

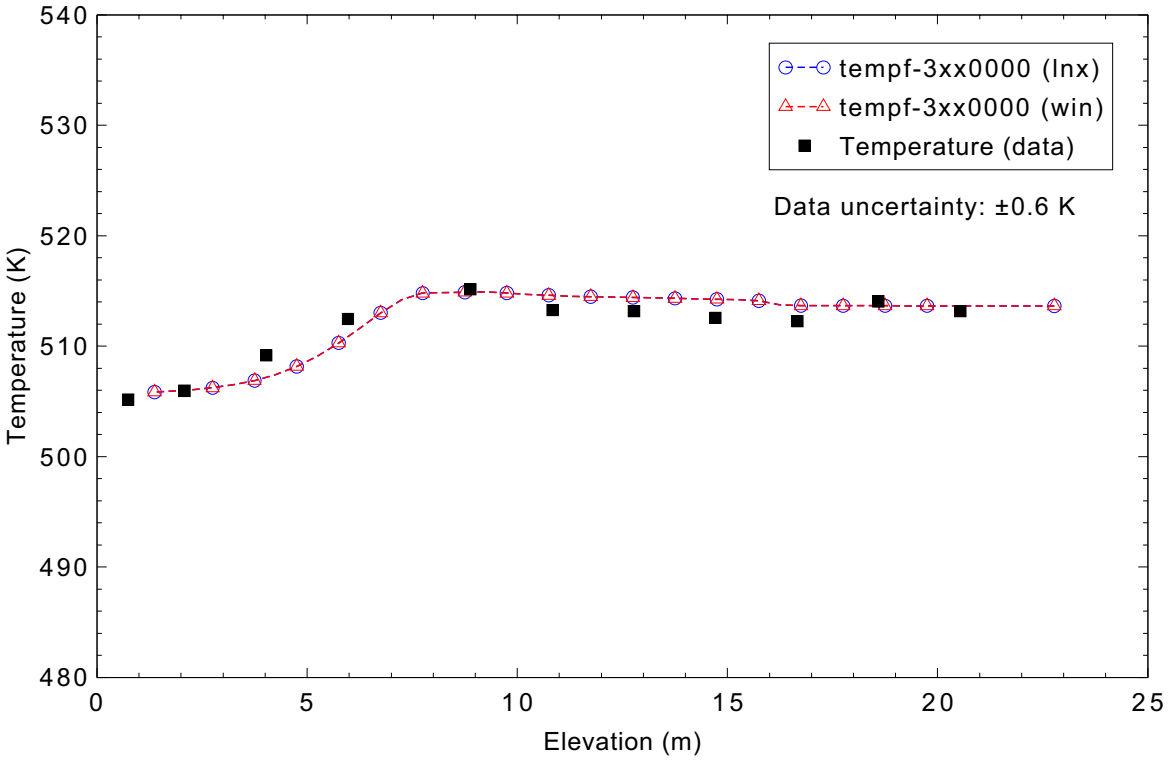

Figure 4.4-8. Measured and calculated vessel temperature profile at 15 s for Marviken CFT 24.

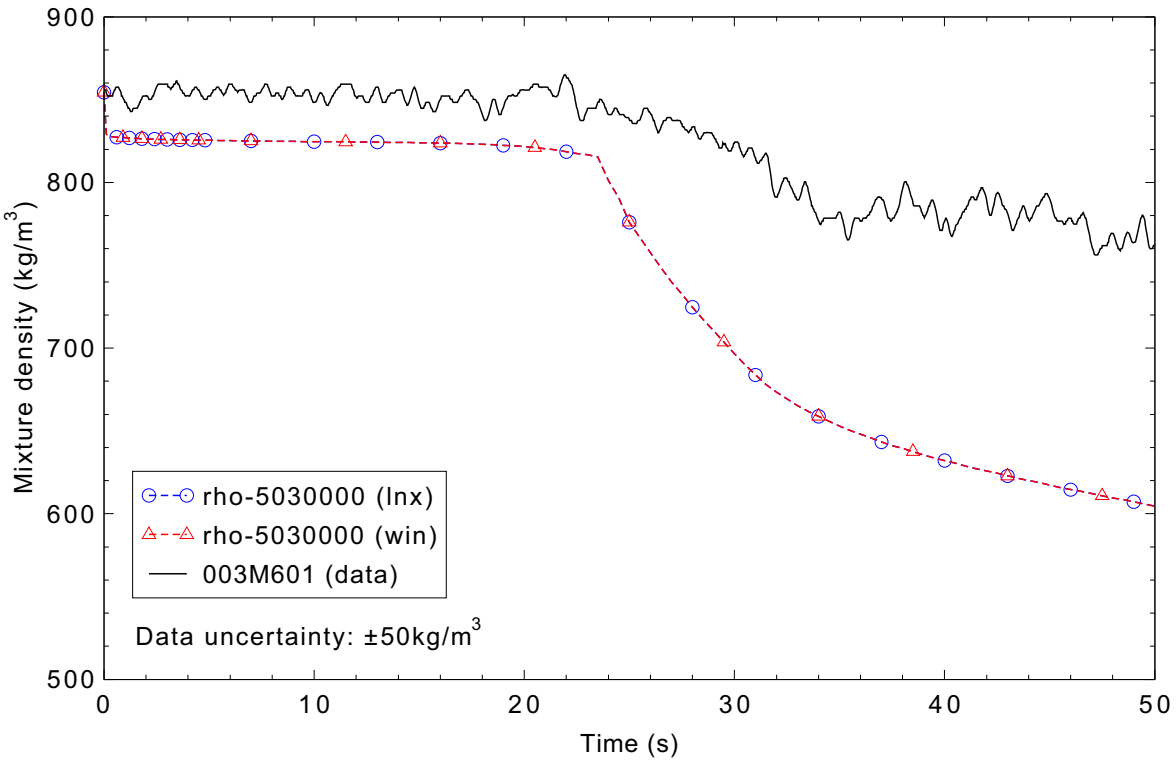

Figure 4.4-9. Measured and calculated mixture density in the discharge pipe for Marviken CFT 24.

4.5 Marviken Jet Impingement Test 11

Figures comparing simulations using Linux and Windows code versions are presented. Diagrams are included so that the figure numbering is the same as that in Volume III of the RELAP5-3D code manual. No differences were observed in the figures.

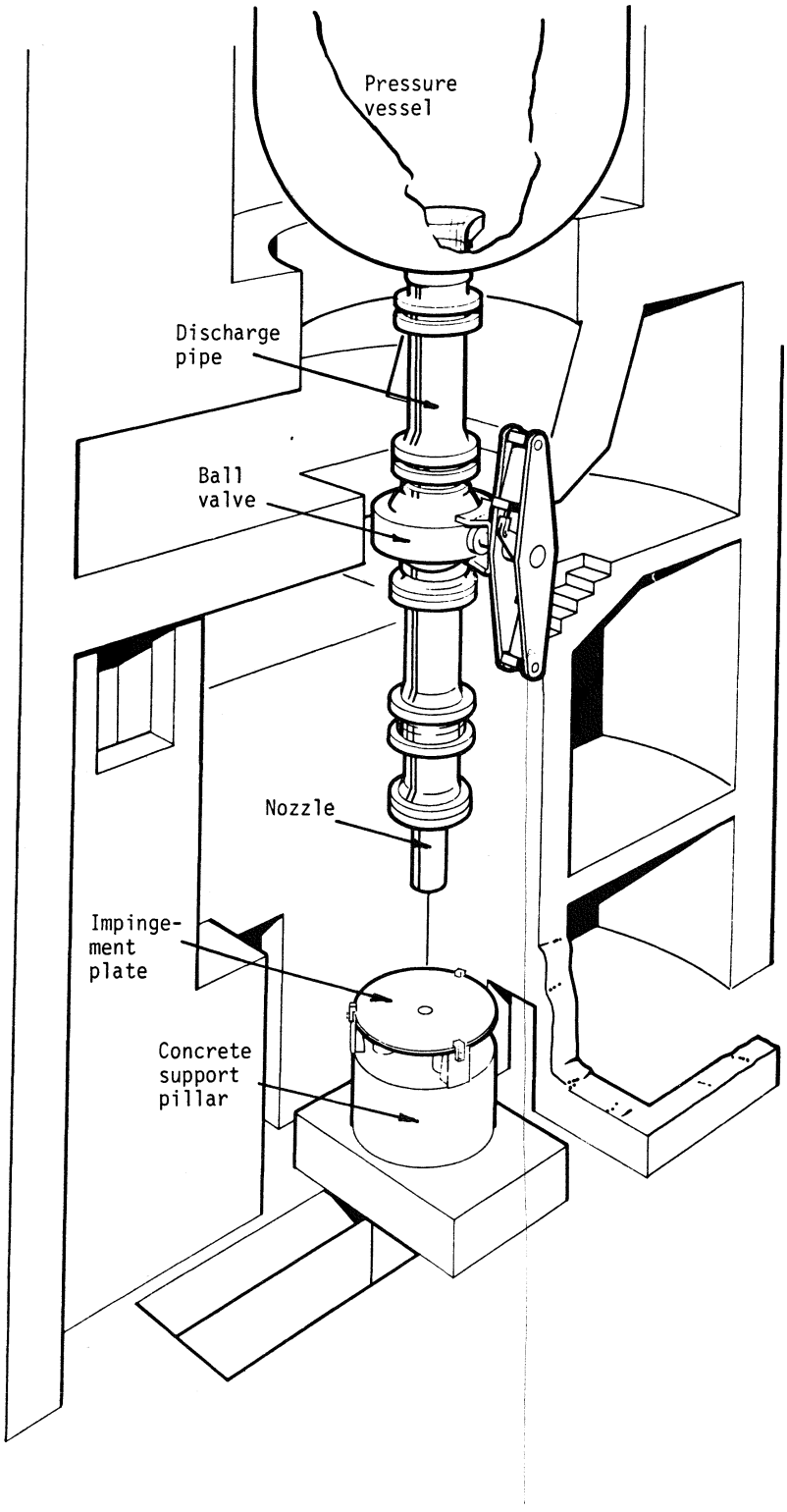

Figure 4.5-1. Test facility for Marviken JIT-11.

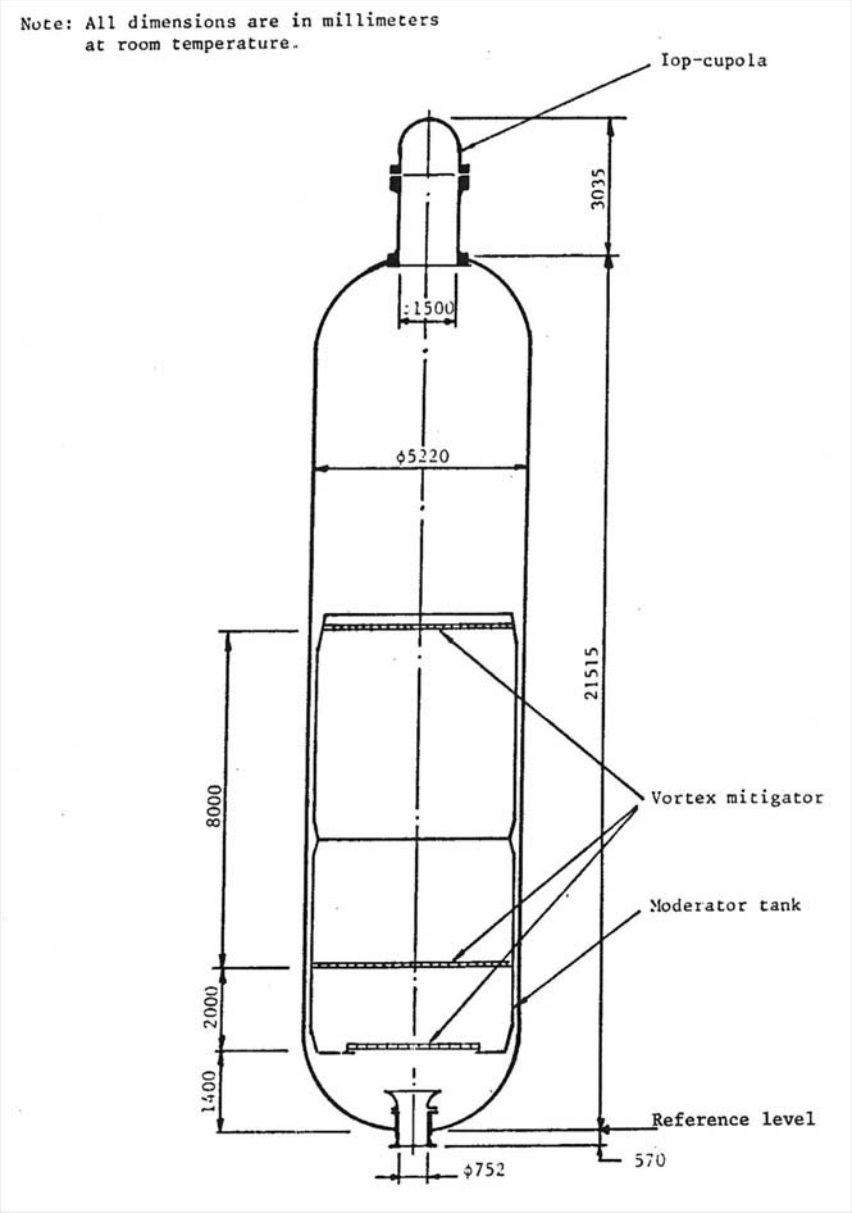

Figure 4.5-2. Pressure vessel for Marviken JIT-11.

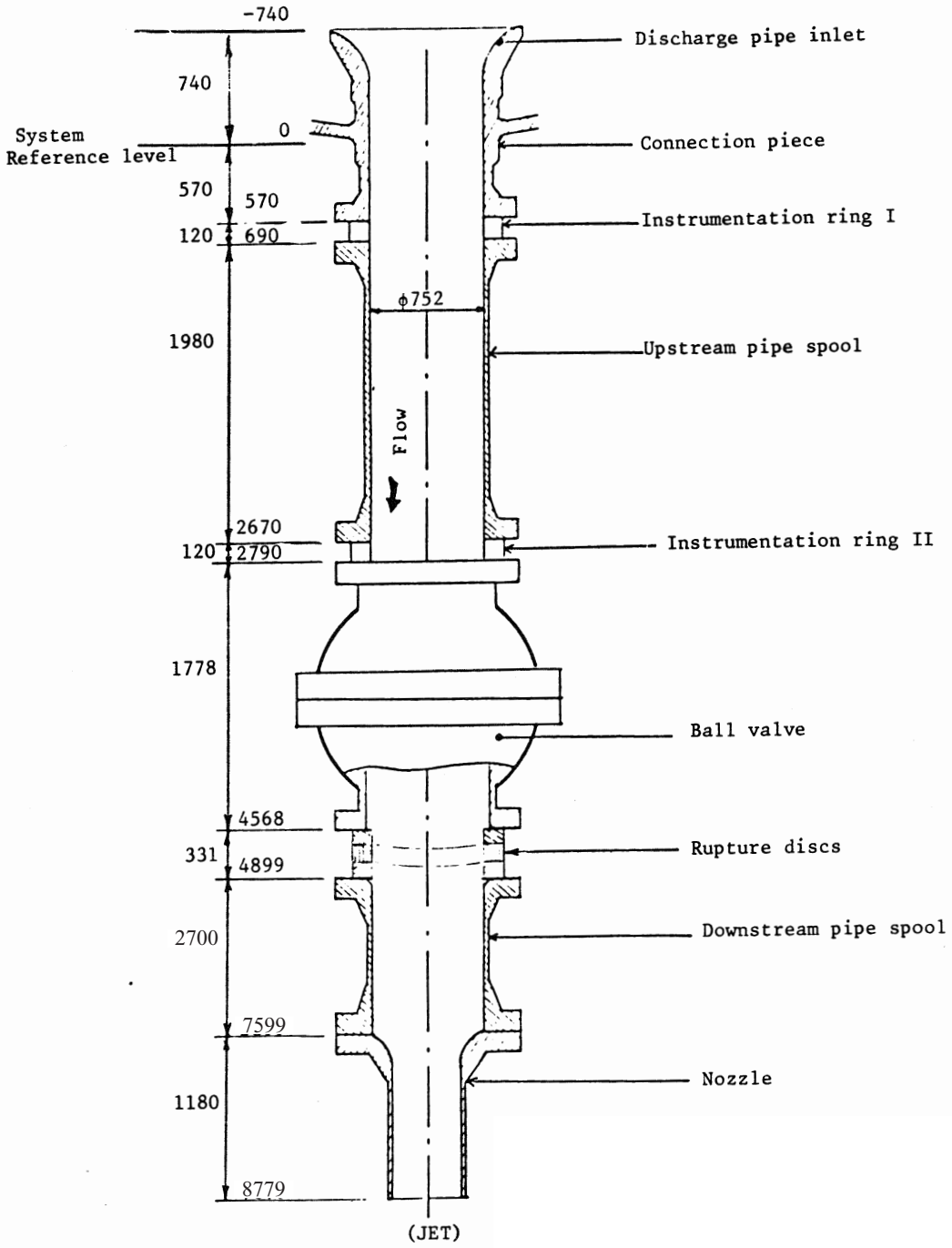

Figure 4.5-3. Discharge pipe for Marviken JIT-11.

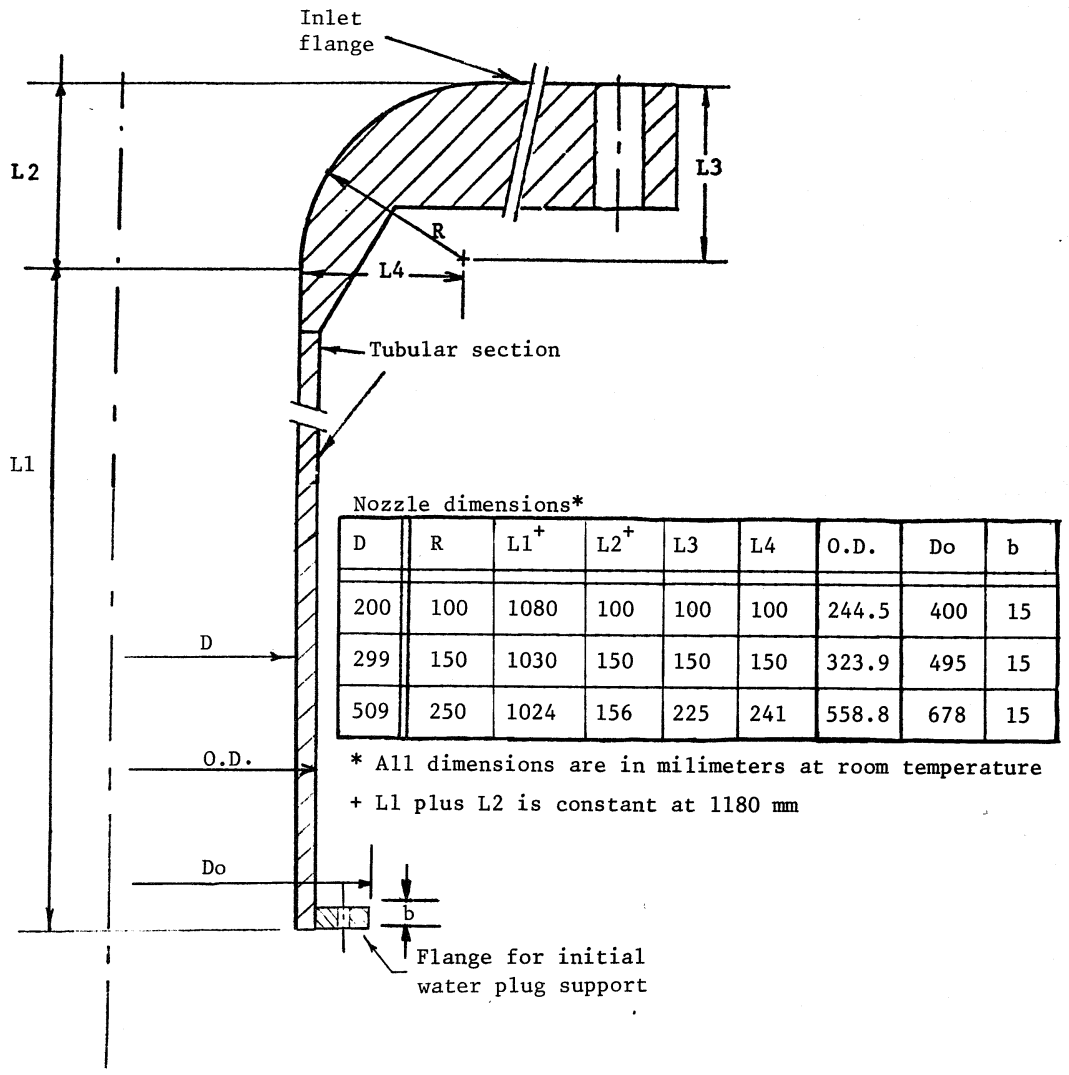

Nozzle dimensions*

D	R	L1+	L2+	L3	L4	O.D.	Do	b
200	100	1080	100	100	100	244.5	400	15
299	150	1030	150	150	150	323.9	495	15
509	250	1024	156	225	241	558.8	678	15

* All dimensions are in milimeters at room temperature

\+ L1 plus L2 is constant at 1180 mm

Figure 4.5-4. Nozzle for Marviken JIT-11.

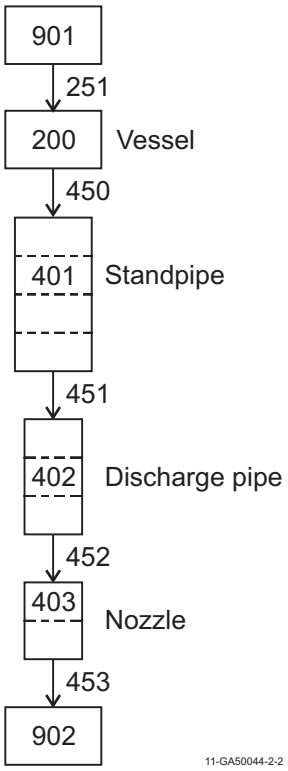

Figure 4.5-5. RELAP5-3D nodalization for Marviken JIT-11.

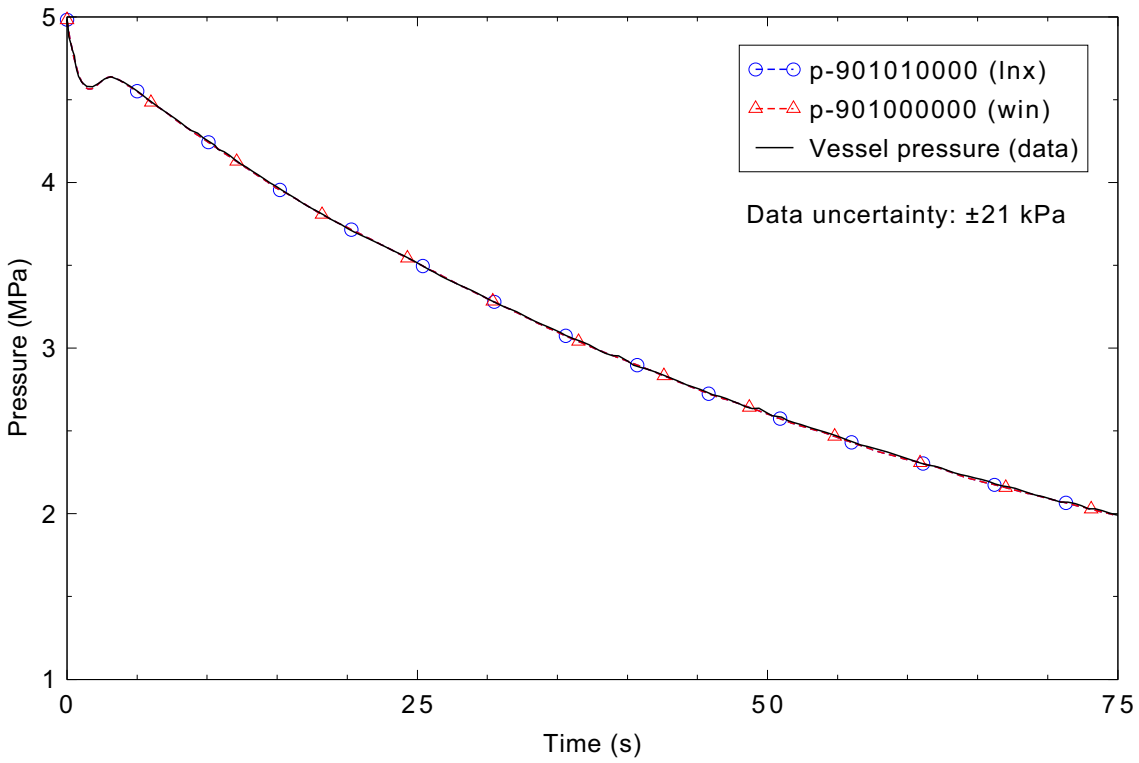

Figure 4.5-6. Vessel pressure boundary condition for Marviken JIT-11.

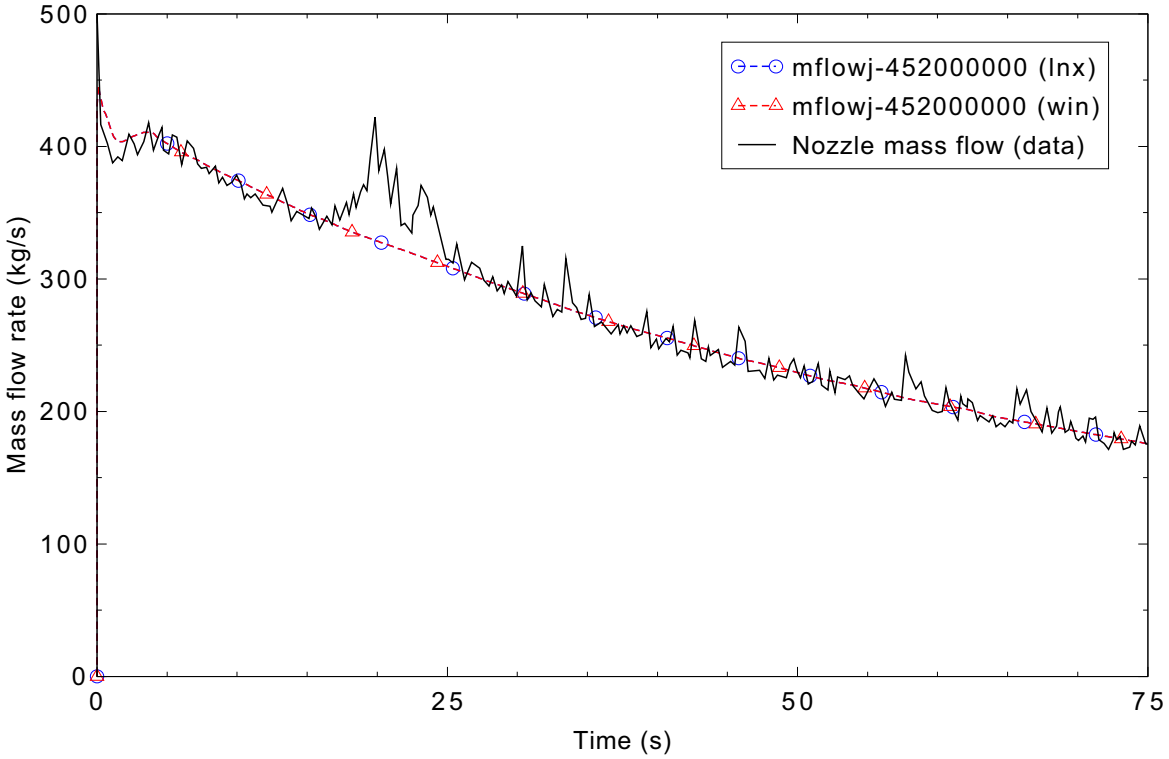

Figure 4.5-7. Measured and calculated mass flow rate for Marviken JIT-11.

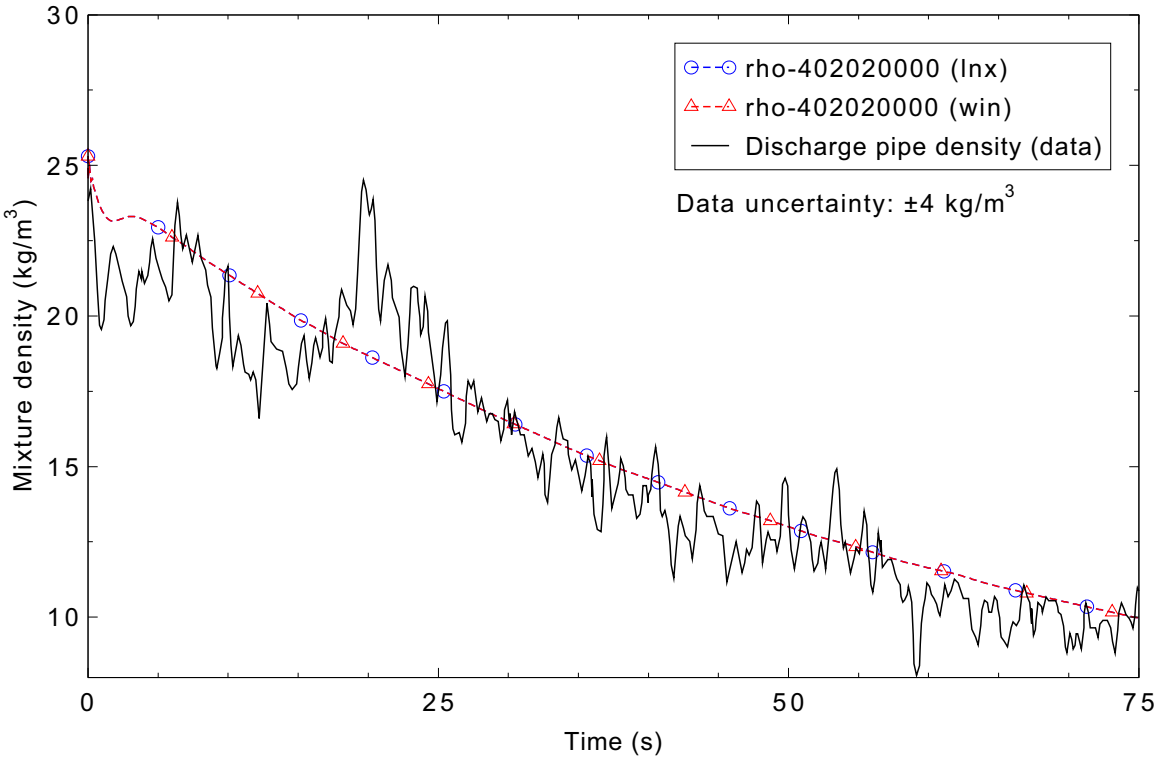

Figure 4.5-8. Measured and calculated mixture density in the discharge pipe for Marviken JIT-11.

4.6 Moby-Dick Air-Water

Figures comparing simulations using Linux and Windows code versions are presented. Diagrams are included so that the figure numbering is the same as that in Volume III of the RELAP5-3D code manual. No differences were observed in the figure.

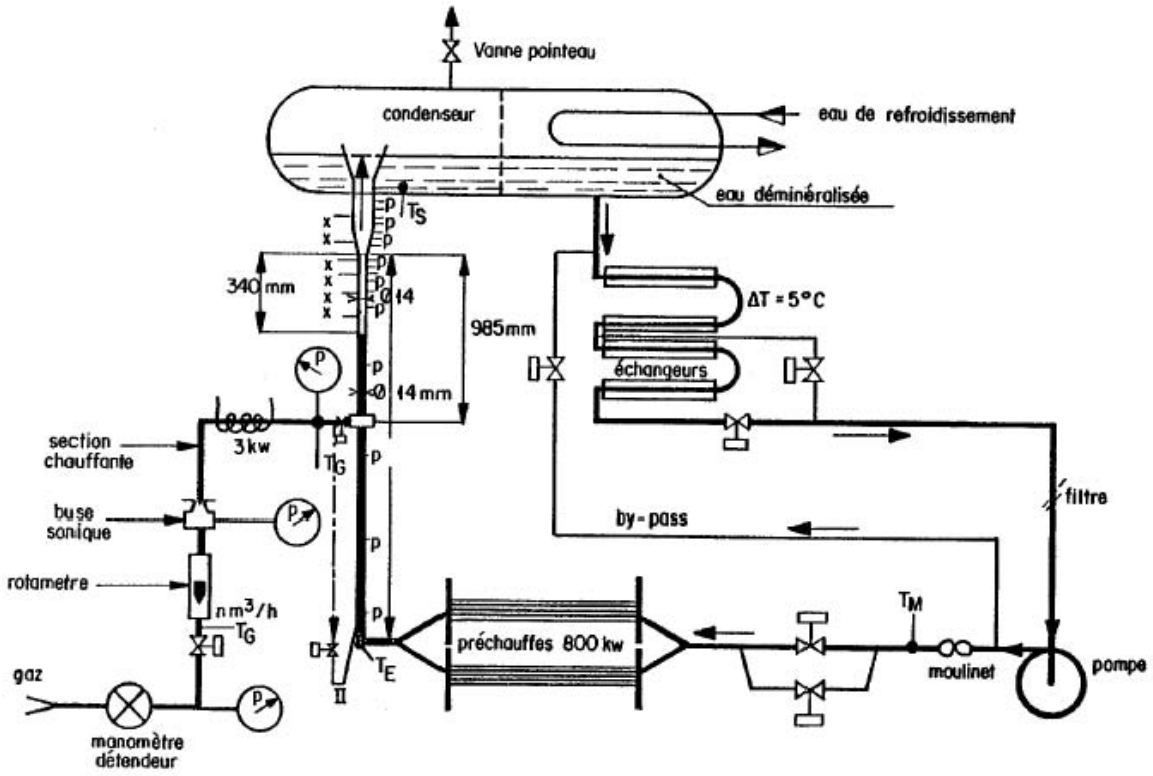

Figure 4.6-1. Moby-Dick test loop.

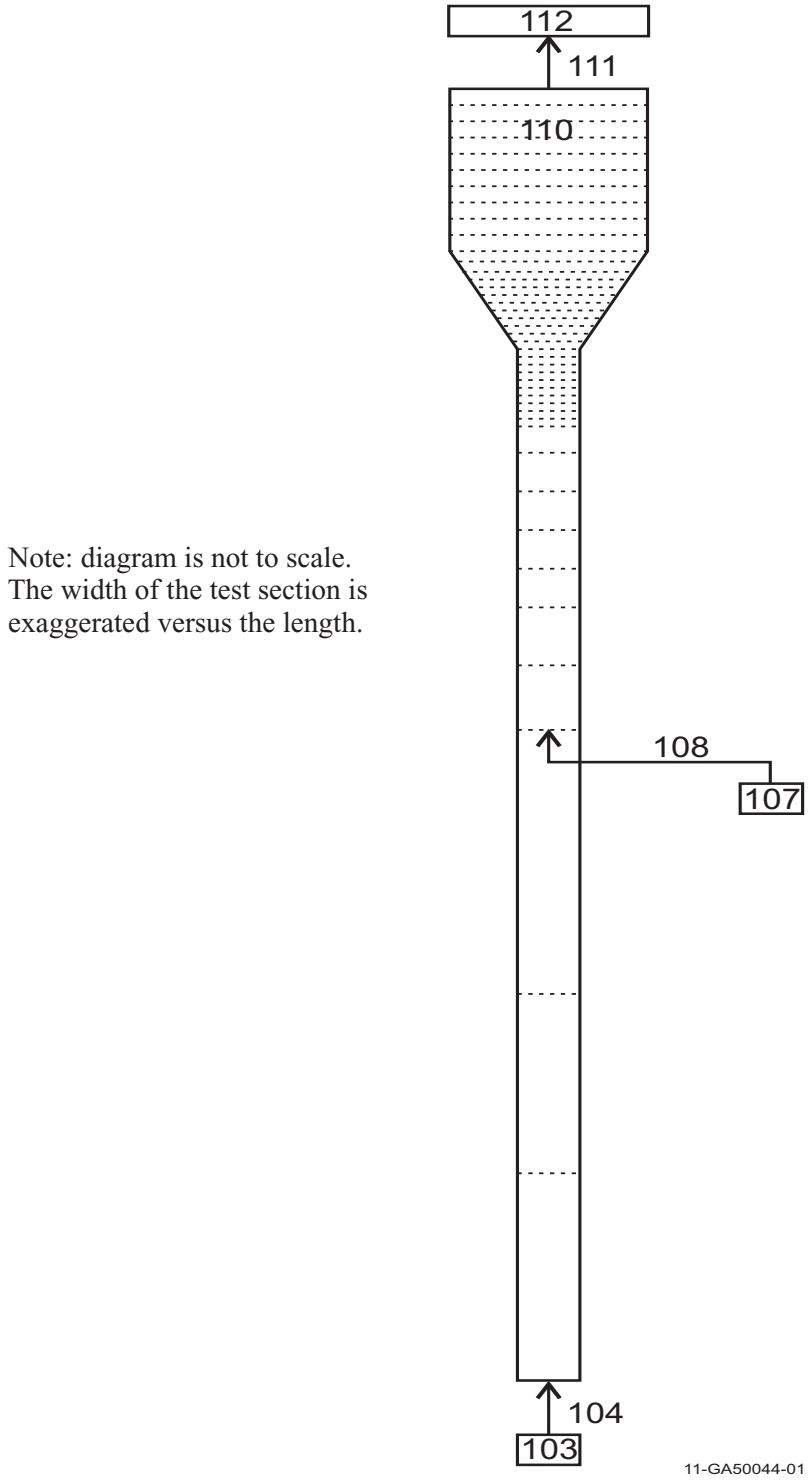

Figure 4.6-2. Nodalization diagram of the RELAP5-3D Moby-Dick experiment model.

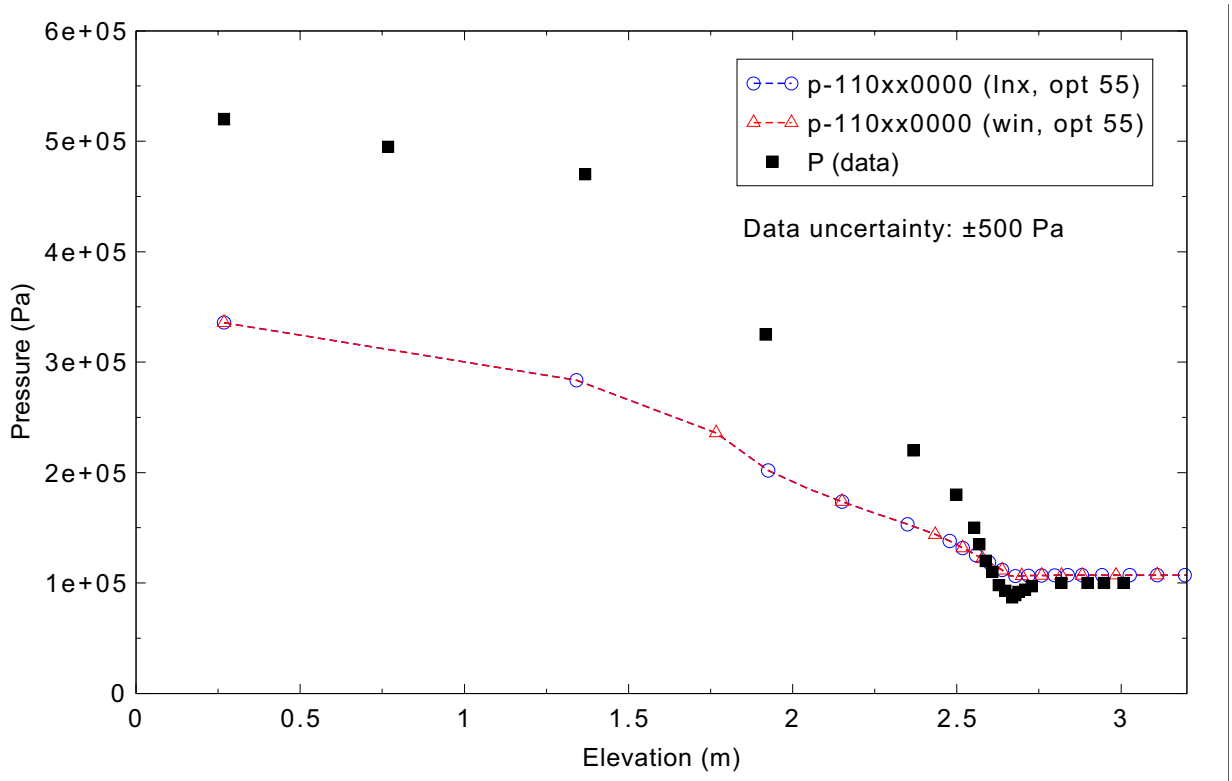

Figure 4.6-3. Measured and calculated axial pressure distribution for Moby-Dick Test 3141.

4.7 Christensen Test 15

Figures comparing simulations using Linux and Windows code versions are presented. Diagrams are included so that the figure numbering is the same as that in Volume III of the RELAP5-3D code manual. No differences were observed in the figure.

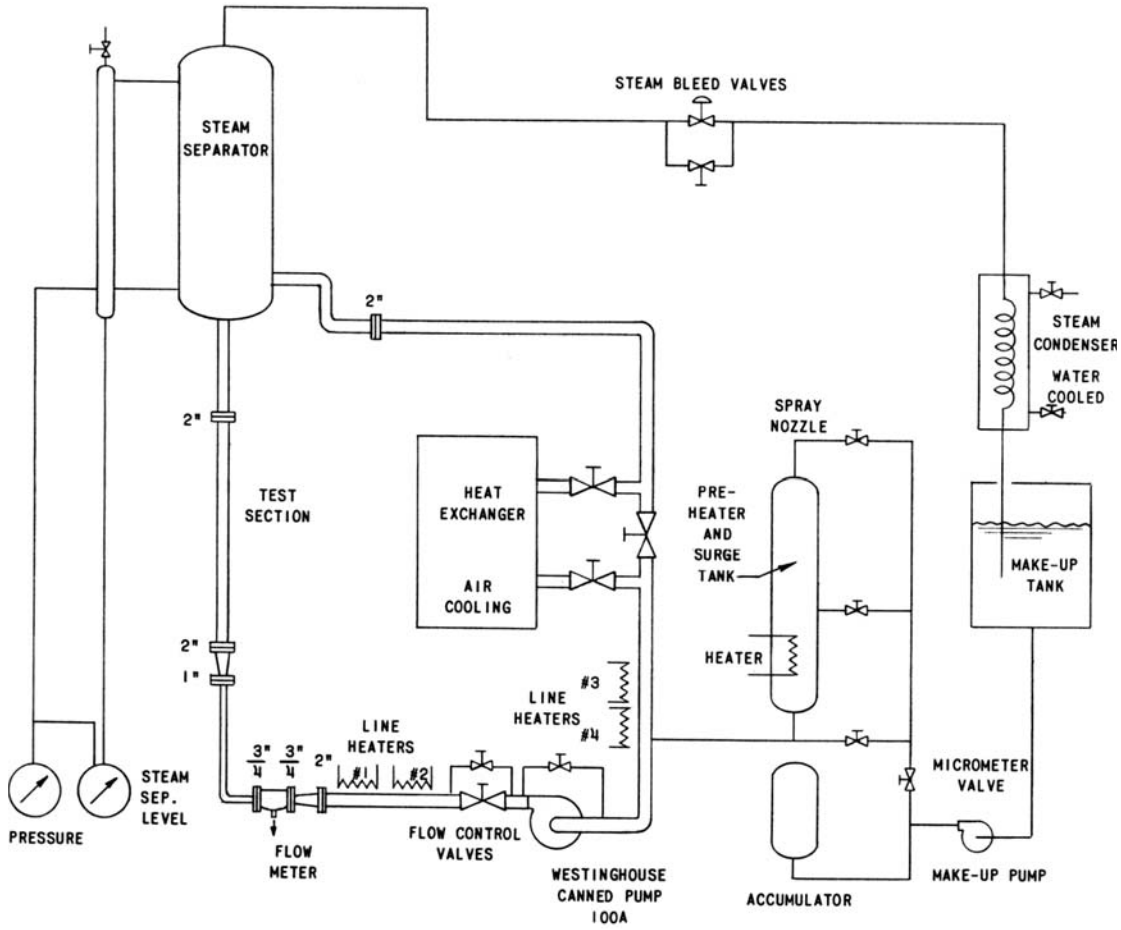

Figure 4.7-1. Test facility schematic for Christensen Test 15.

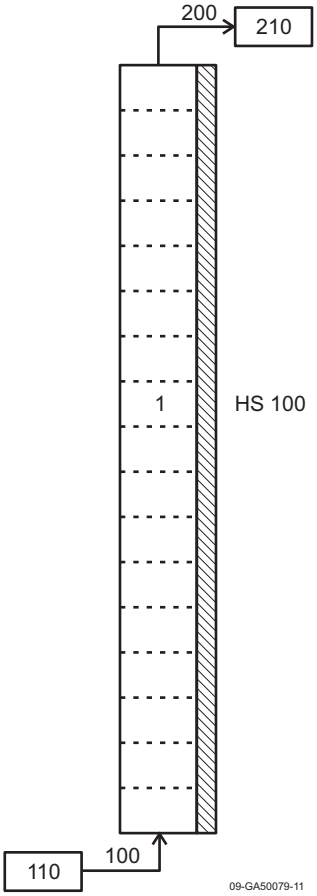

Figure 4.7-2. RELAP5-3D model nodalization for Christensen Test 15.

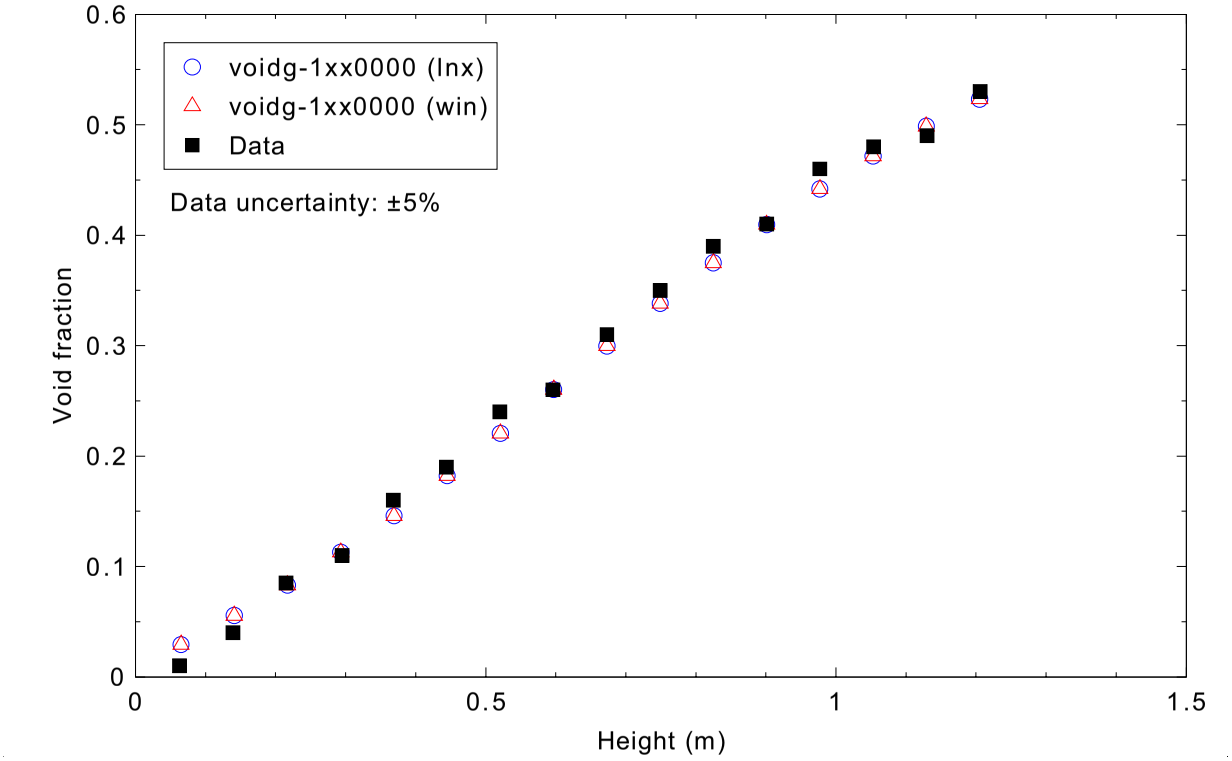

Figure 4.7-3. Measured and calculated test section void profiles for Christensen Test 15.

4.8 GE Level Swell - 1 ft - Test 1004-3

Figures comparing simulations using Linux and Windows code versions are presented. Diagrams are included so that the figure numbering is the same as that in Volume III of the RELAP5-3D code manual. No differences were observed in the figures.

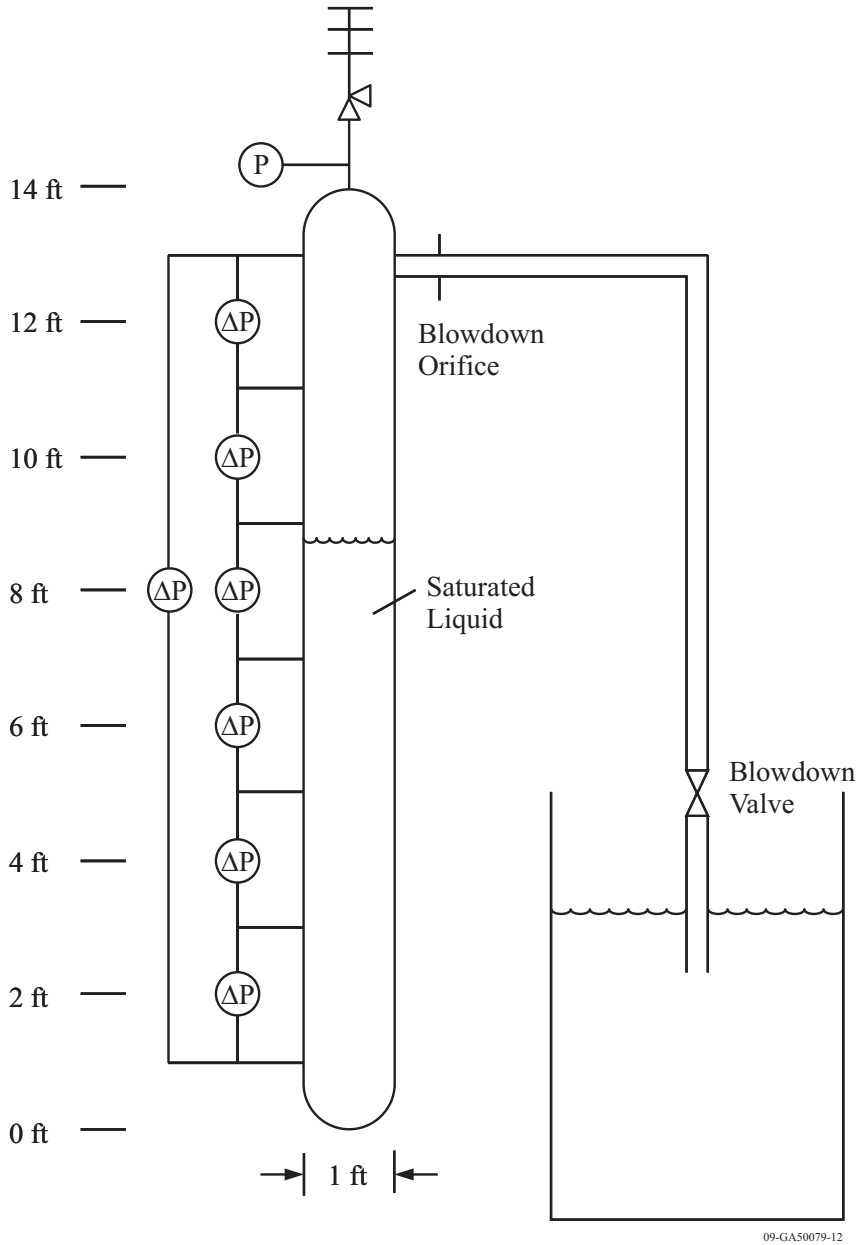

Figure 4.8-1. Test schematic for GE Small Blowdown Vessel Test 1004-3.

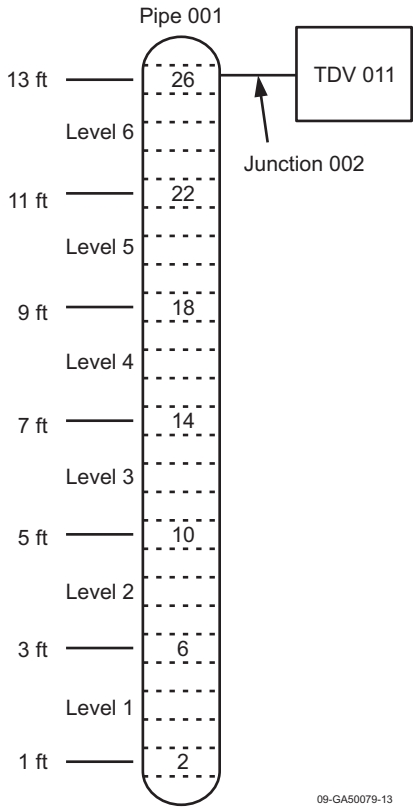

Figure 4.8-2. Nodalization diagram for GE Small Blowdown Vessel Test 1004-3.

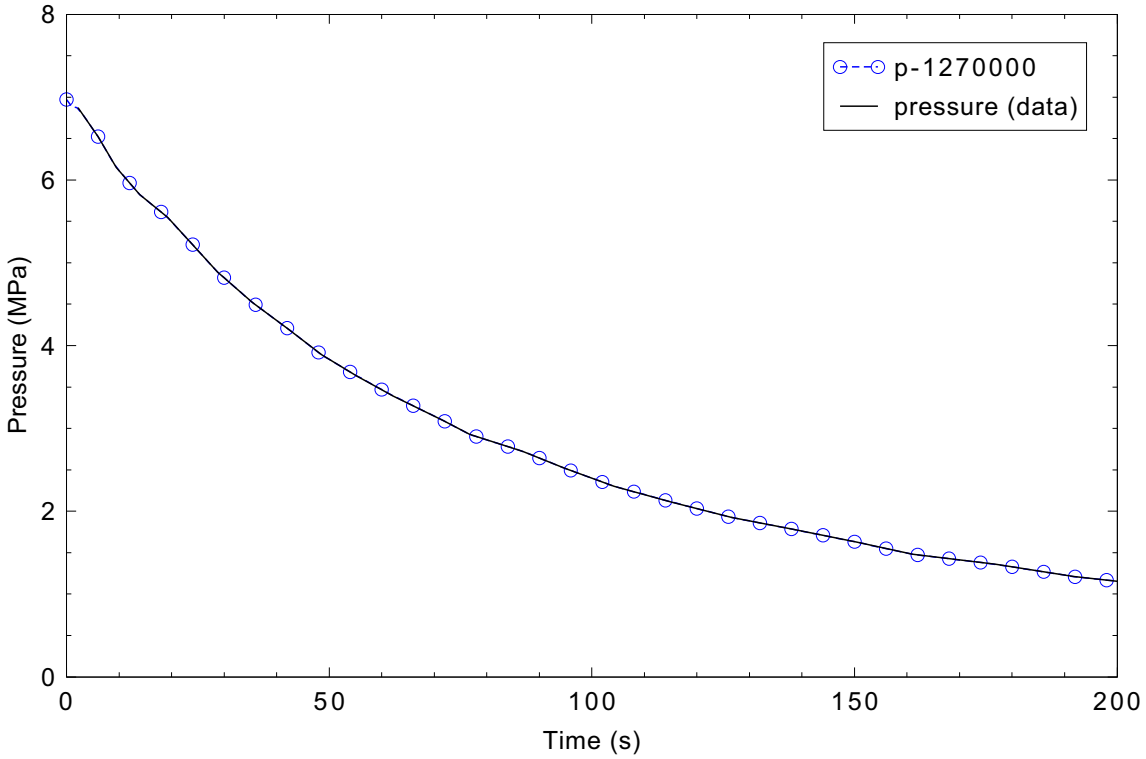

Figure 4.8-3. Comparison of experiment data with the pressure imposed by time-dependent volume 11.

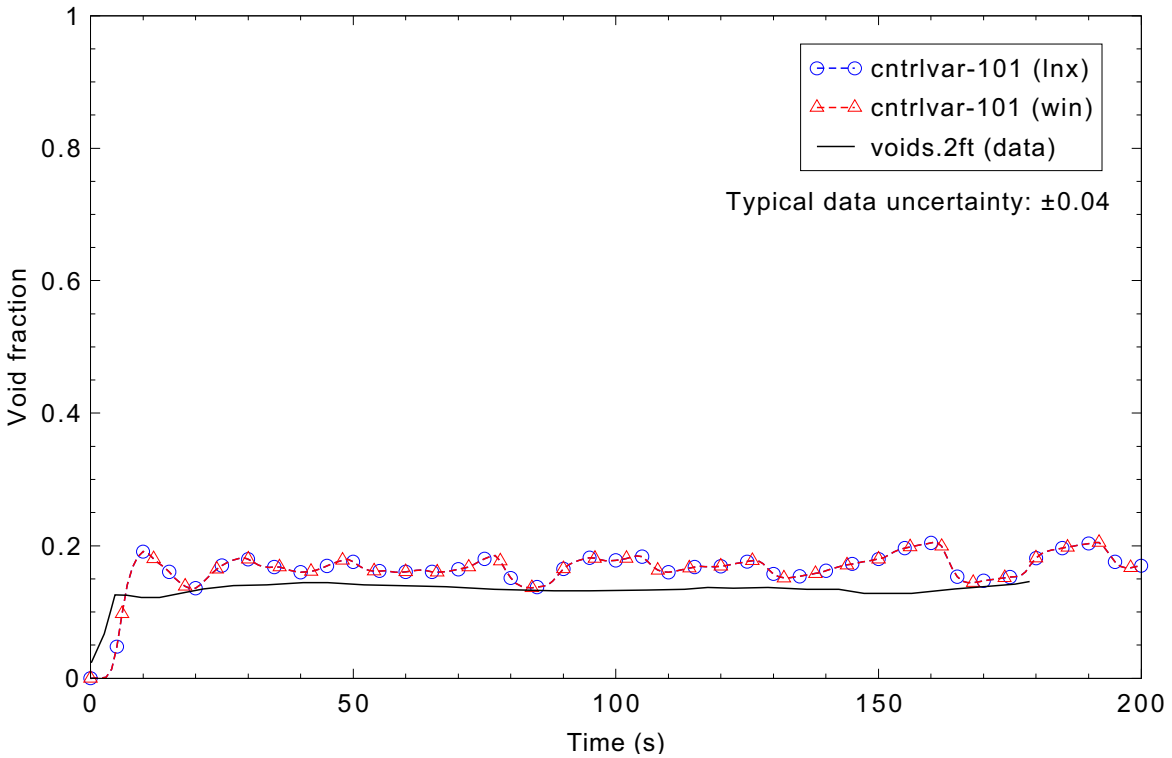

Figure 4.8-4. Measured and calculated void fraction at 2 ft (0.6 m) above the bottom of the vessel (level 1) for GE level swell Test 1004-3.

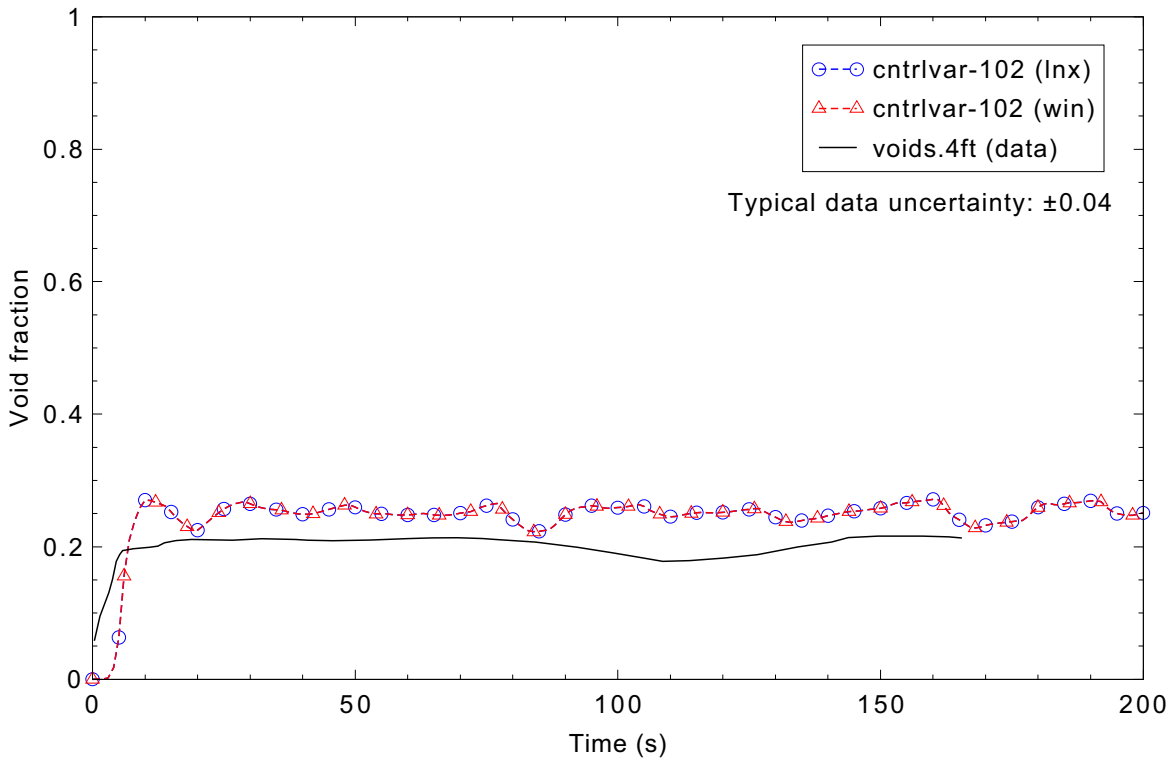

Figure 4.8-5. Measured and calculated void fraction at 4 ft (1.2 m) above the bottom of the vessel (level 2) for GE level swell Test 1004-3.

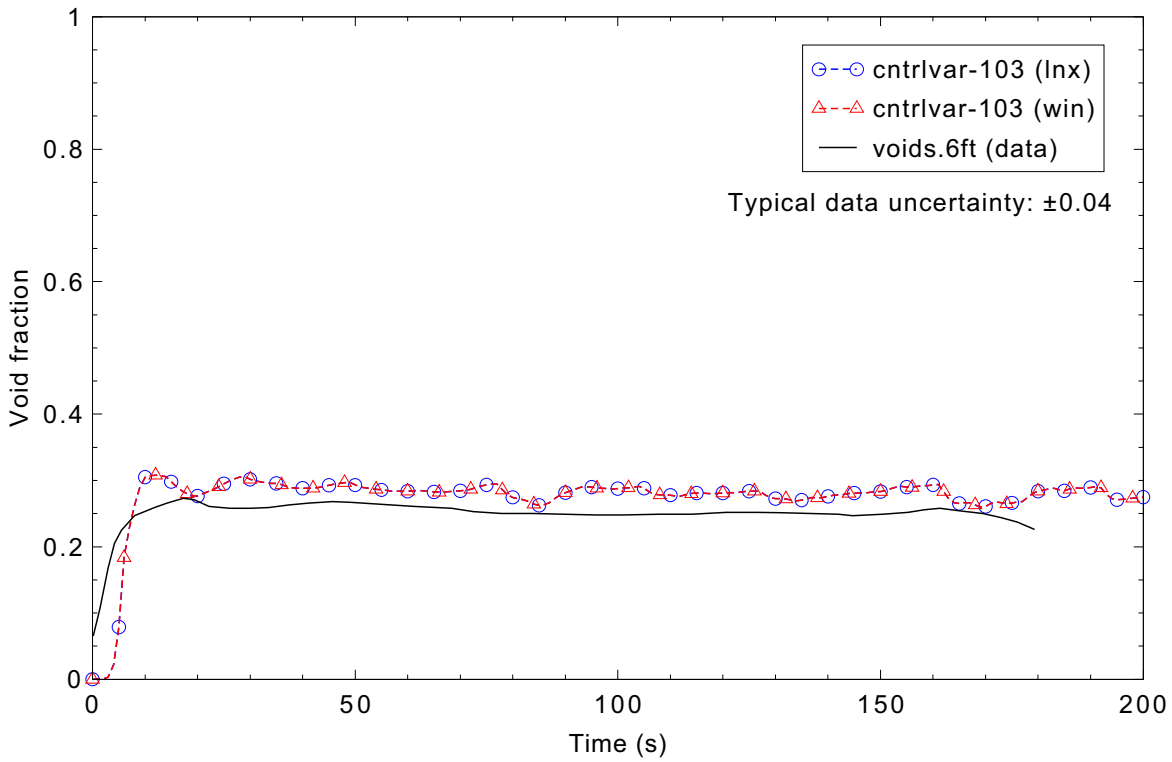

Figure 4.8-6. Measured and calculated void fraction at 6 ft (1.8 m) above the bottom of the vessel (level 3) for GE level swell Test 1004-3.

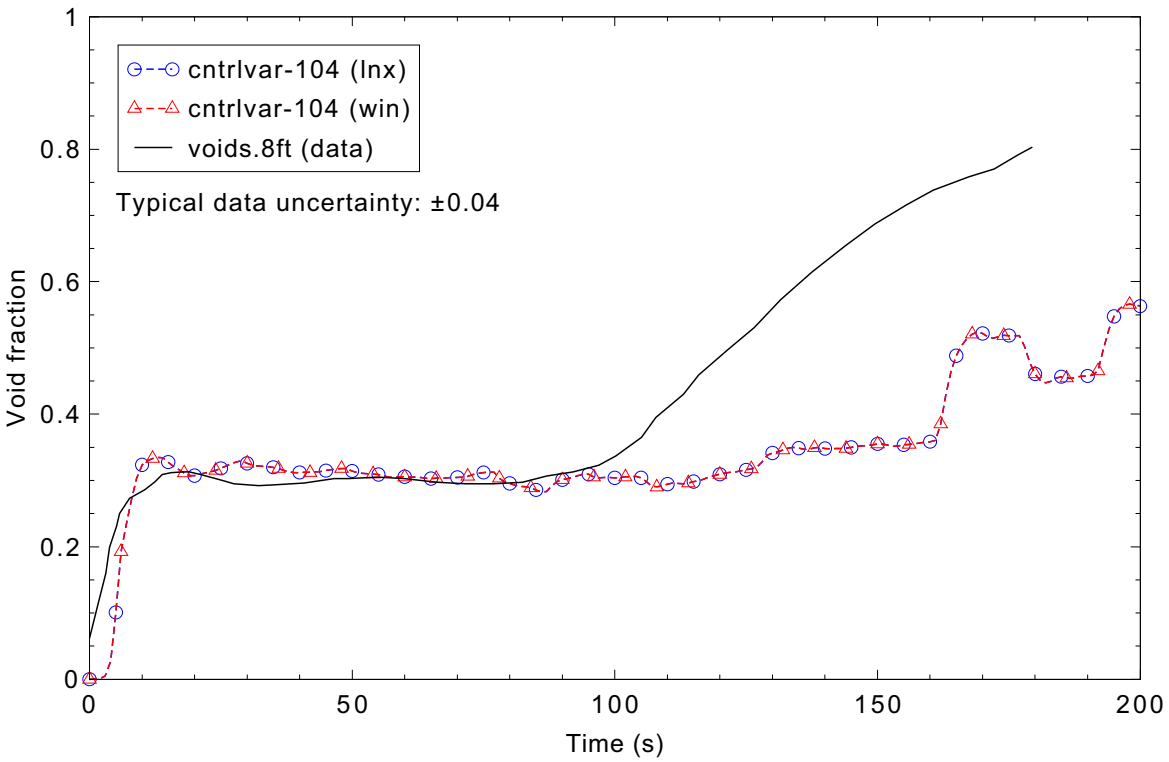

Figure 4.8-7. Measured and calculated void fraction at 8 ft (2.4 m) above the bottom of the vessel (level 4) for GE level swell Test 1004-3.

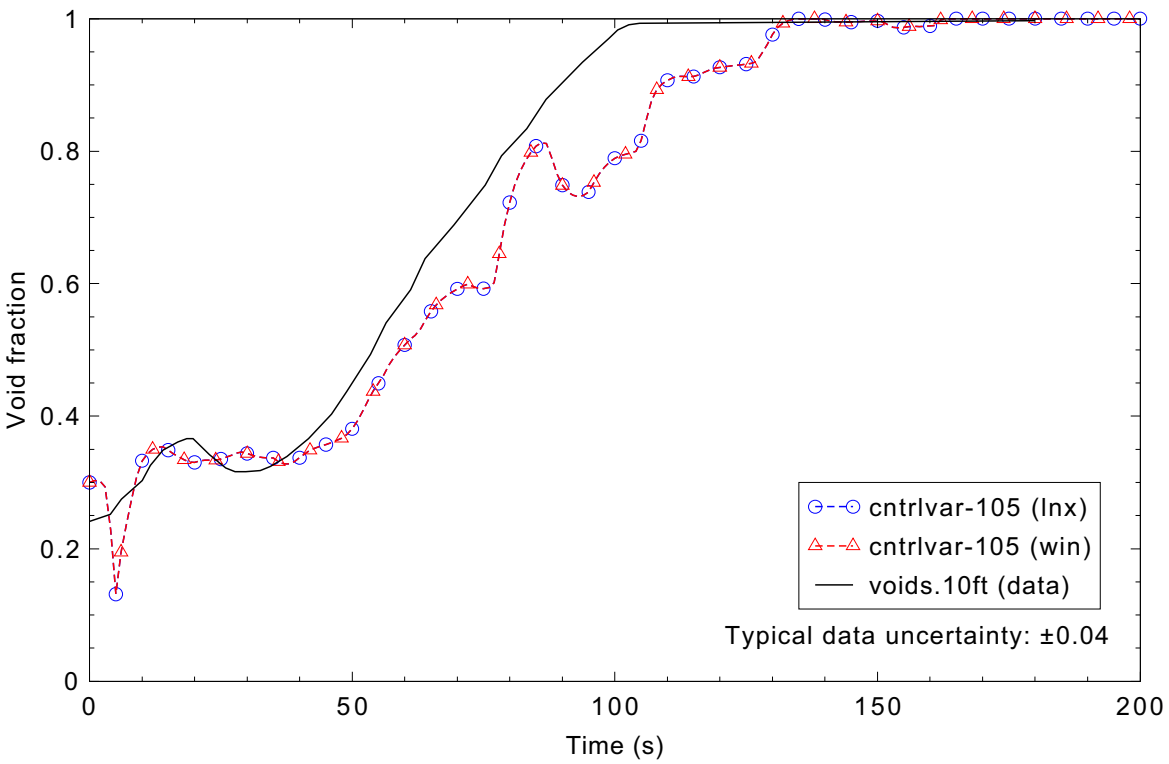

Figure 4.8-8. Measured and calculated void fraction at 10 ft (3.0 m) above the bottom of the vessel (level 5) for GE level swell Test 1004-3.

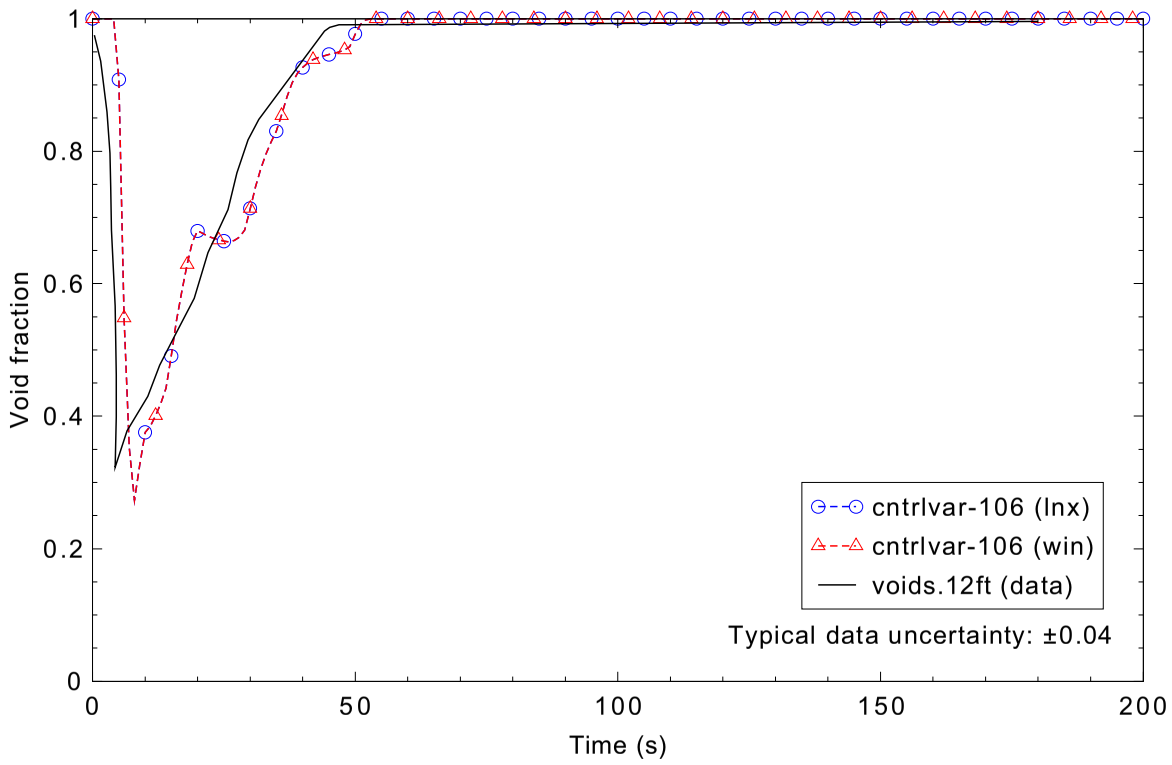

Figure 4.8-9. Measured and calculated void fraction at 12 ft (3.7 m) above the bottom of the vessel (level 6) for GE level swell Test 1004-3.

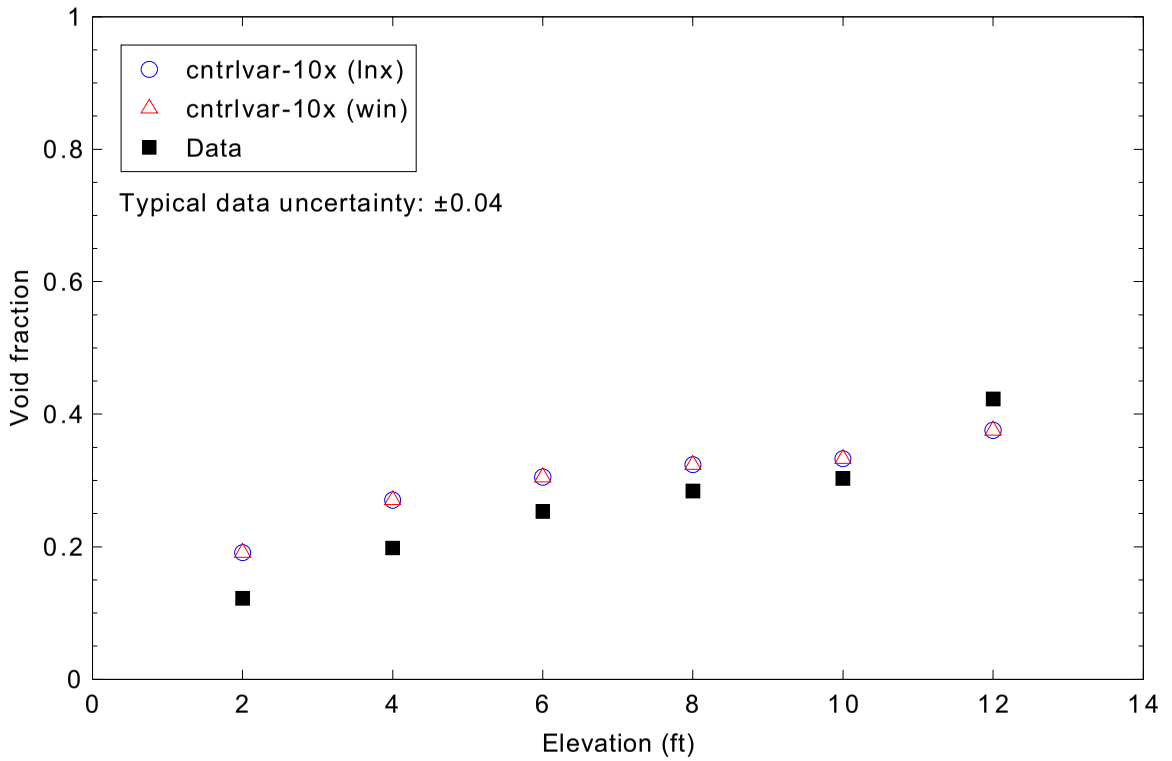

Figure 4.8-10. Measured and calculated void fraction profile in the vessel at 10 s for GE level swell Test 1004-3.

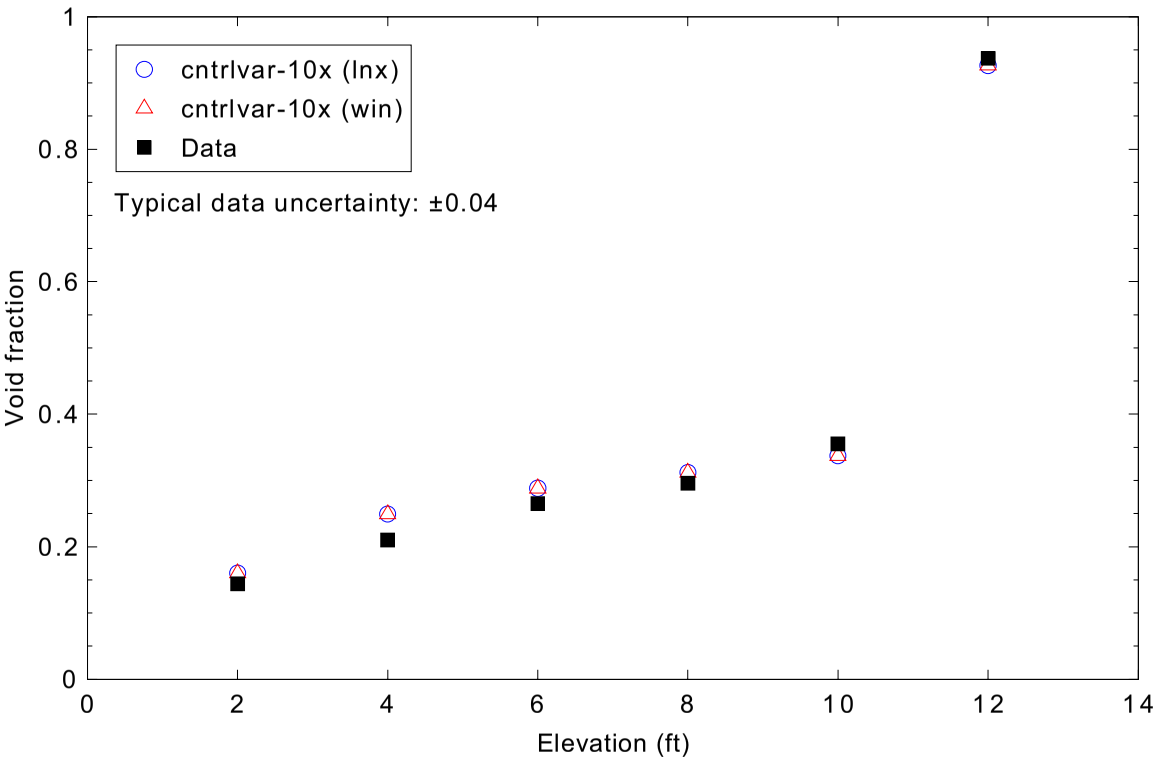

Figure 4.8-11. Measured and calculated void fraction profile in the vessel at 40 s for GE level swell Test 1004-3.

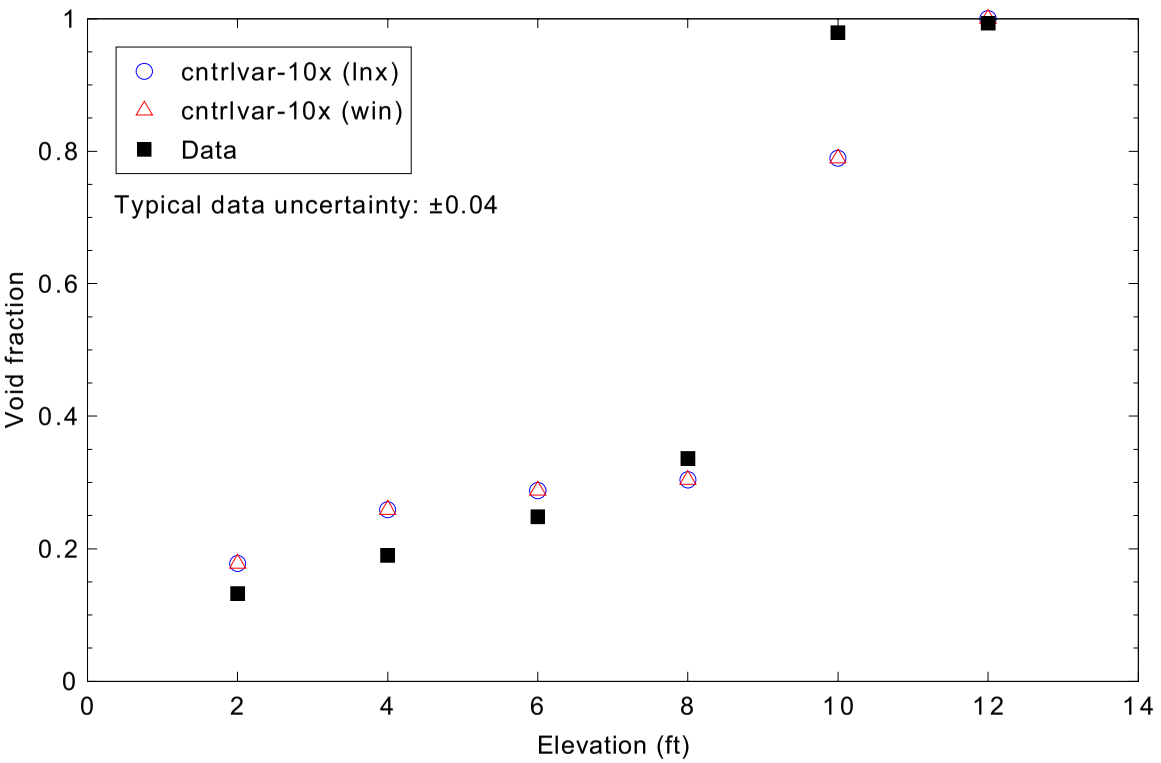

Figure 4.8-12. Measured and calculated void fraction profile in the vessel at 100 s for GE level swell Test 1004-3.

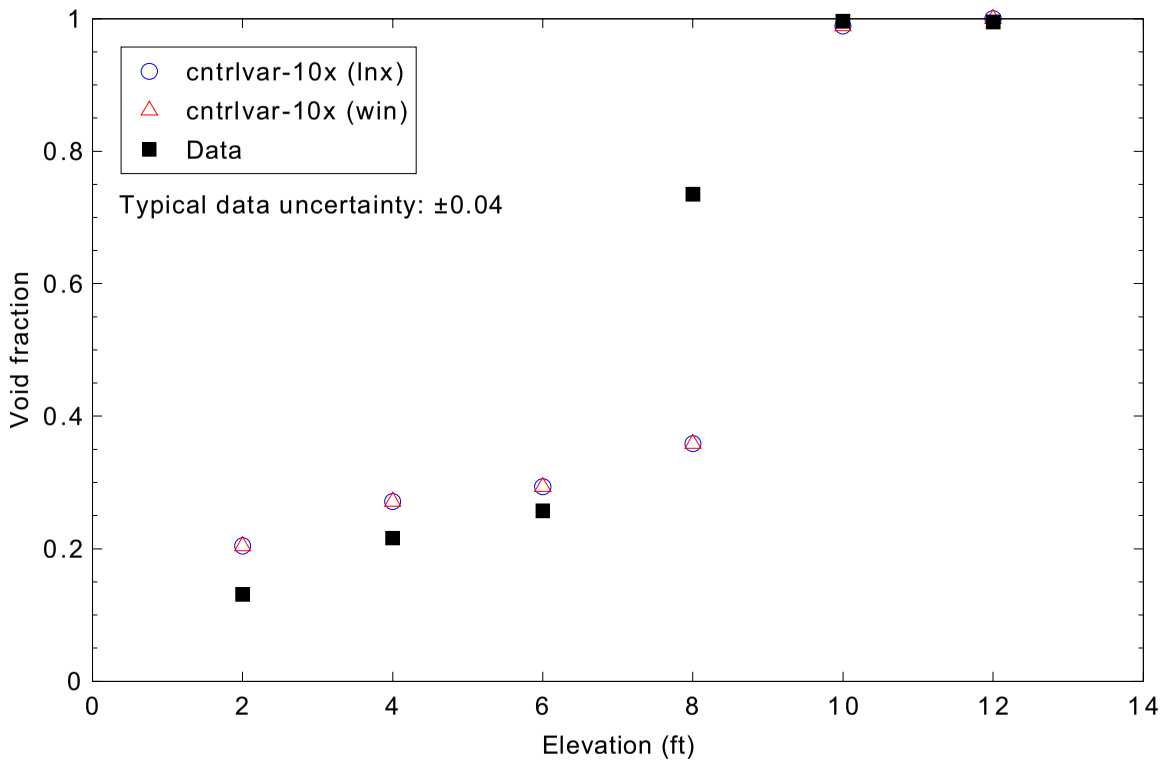

Figure 4.8-13. Measured and calculated void fraction profile in the vessel at 160 s for GE level swell Test 1004-3.

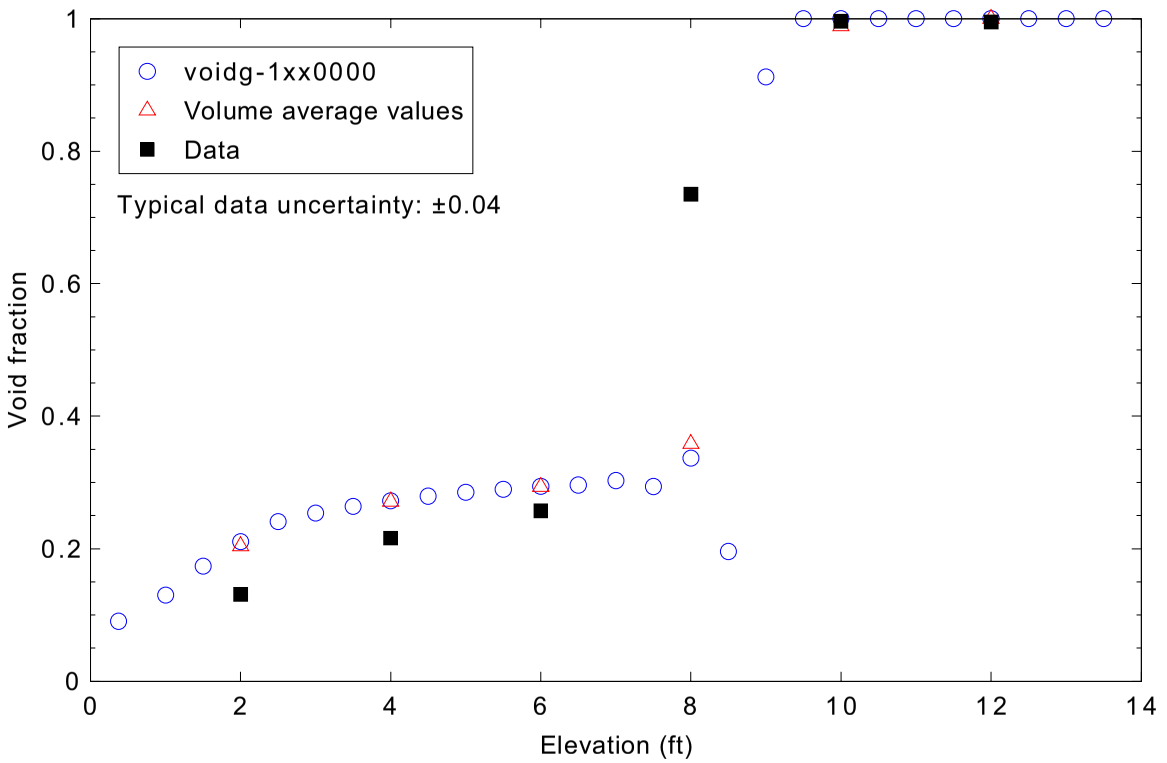

Figure 4.8-14. Volume and volume-average void fractions at 160 s for GE level swell Test 1004-3 (semi-implicit calculations).

4.9 GE Level Swell - 4 ft - Test 5801-15

Figures comparing simulations using Linux and Windows code versions are presented. Diagrams are included so that the figure numbering is the same as that in Volume III of the RELAP5-3D code manual. No differences were observed in the figures.

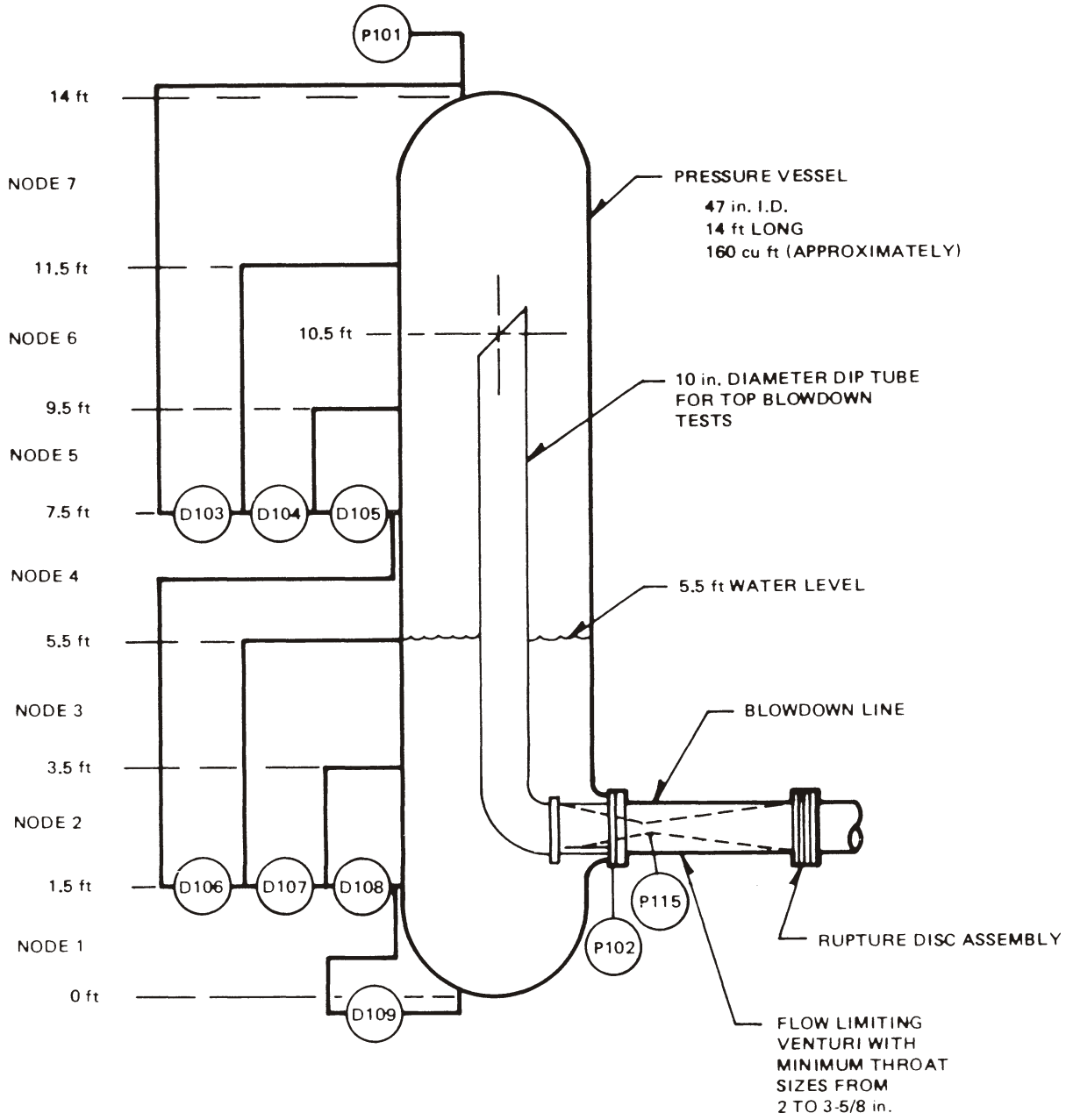

Figure 4.9-1. GE Large Blowdown Vessel schematic diagram.

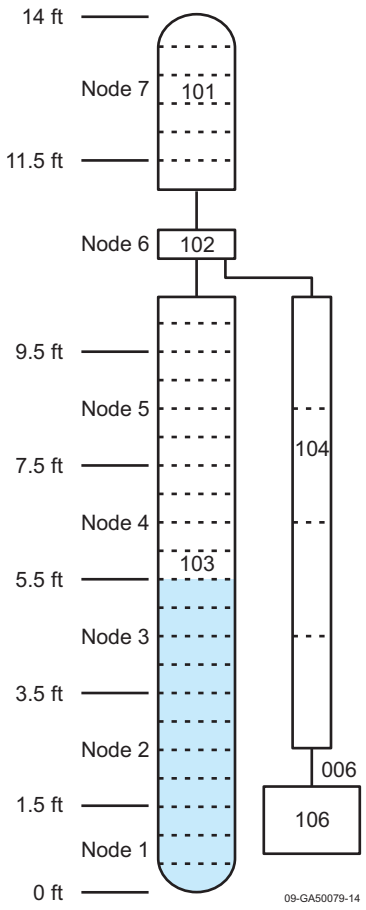

Figure 4.9-2. Nodalization diagram for GE Large Blowdown Vessel Test 5801-15.

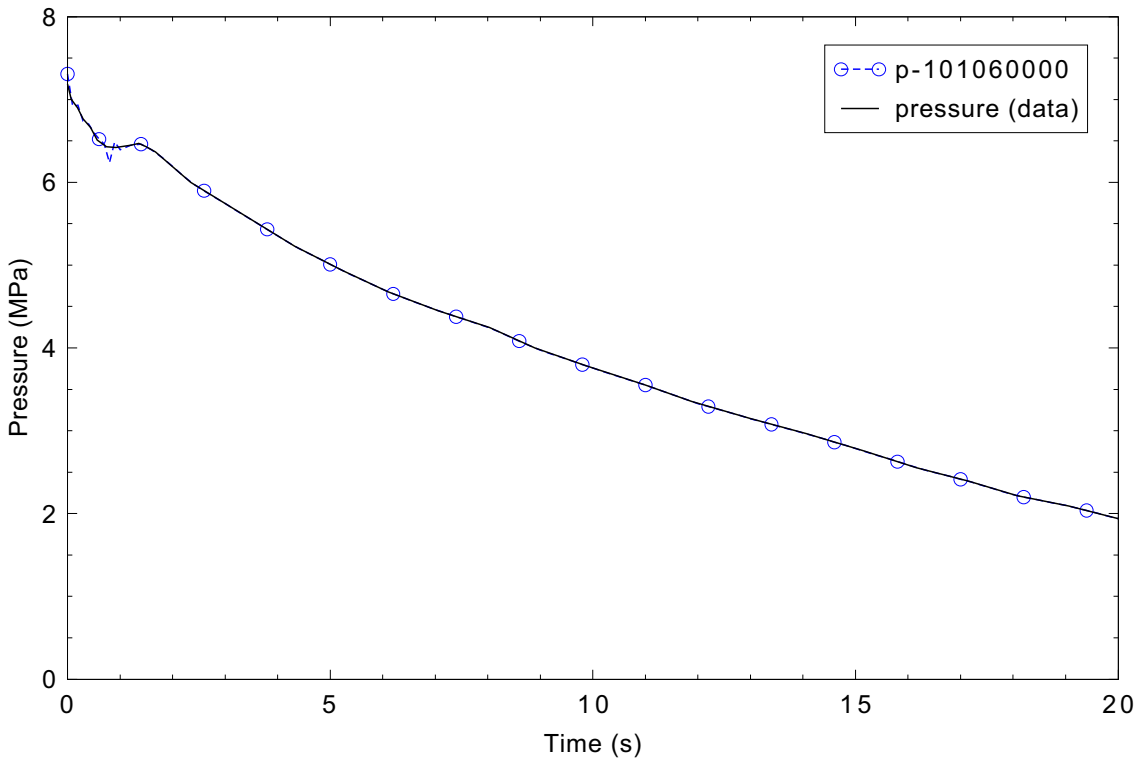

Figure 4.9-3. Comparison of experiment data with the pressure imposed by time-dependent volume 106.

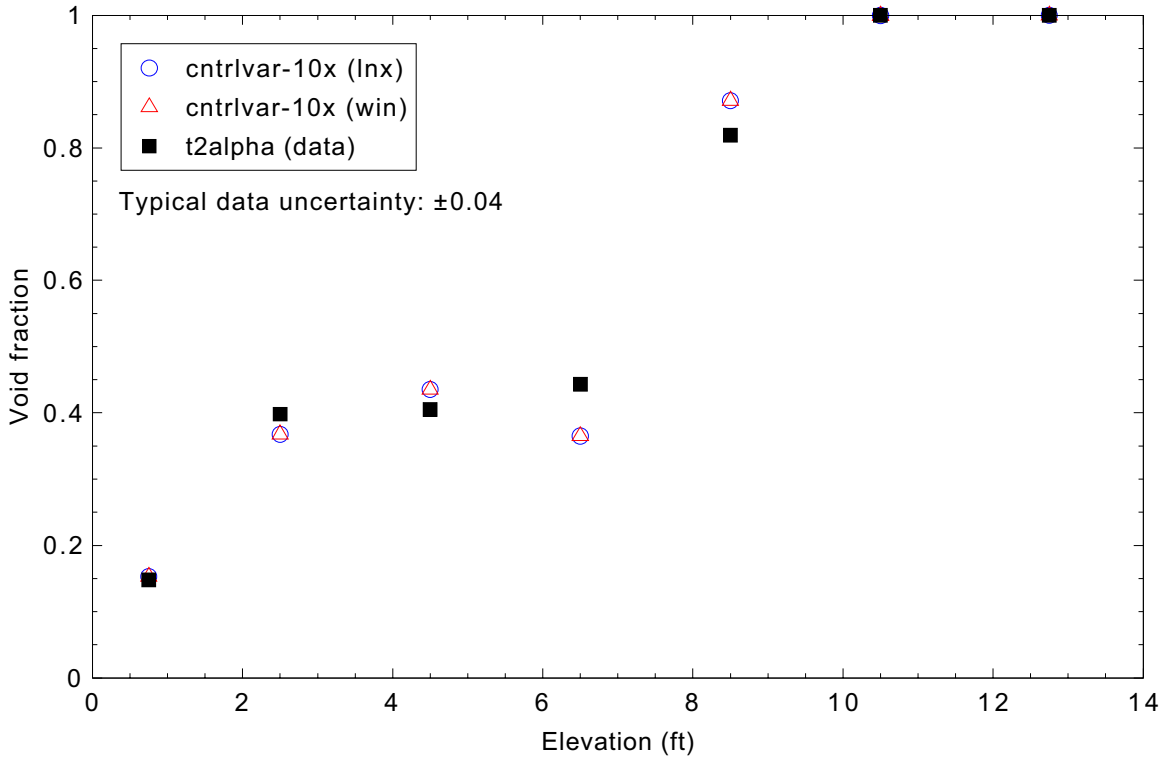

Figure 4.9-4. Measured and calculated void fraction profile in the vessel at 2 s for GE level swell Test 5801-15.

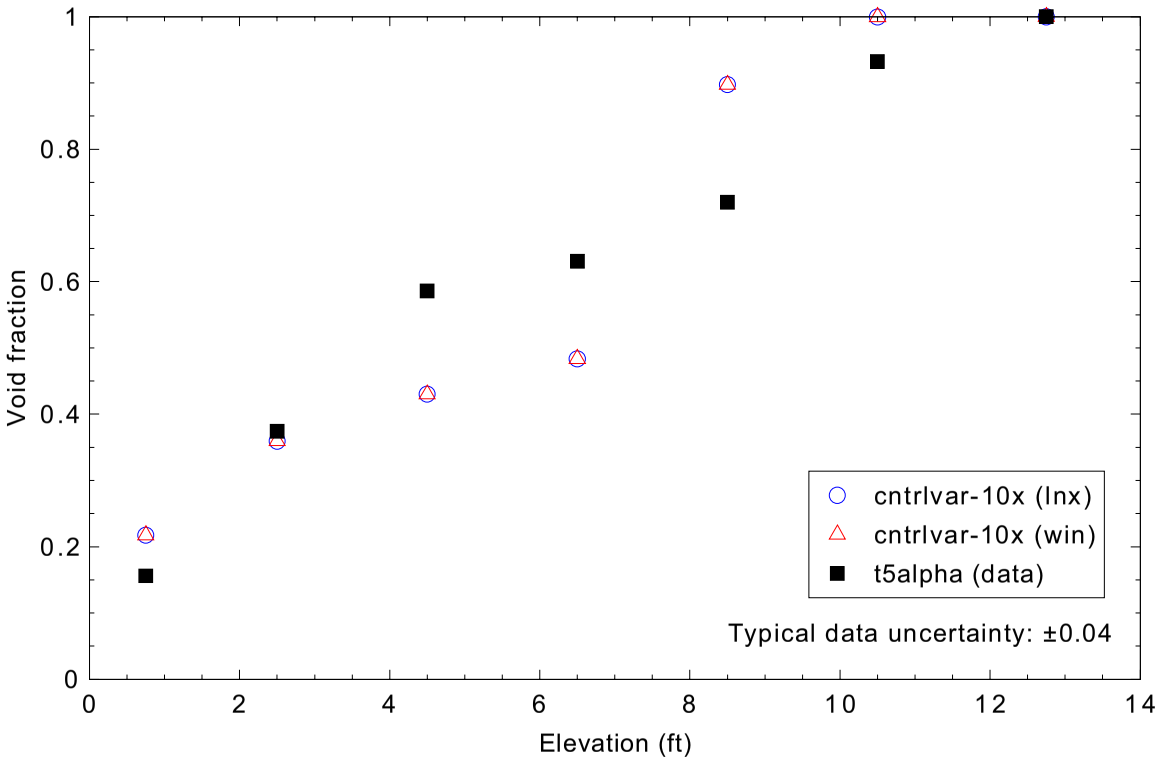

Figure 4.9-5. Measured and calculated void fraction profile in the vessel at 5 s for GE level swell Test 5801-15.

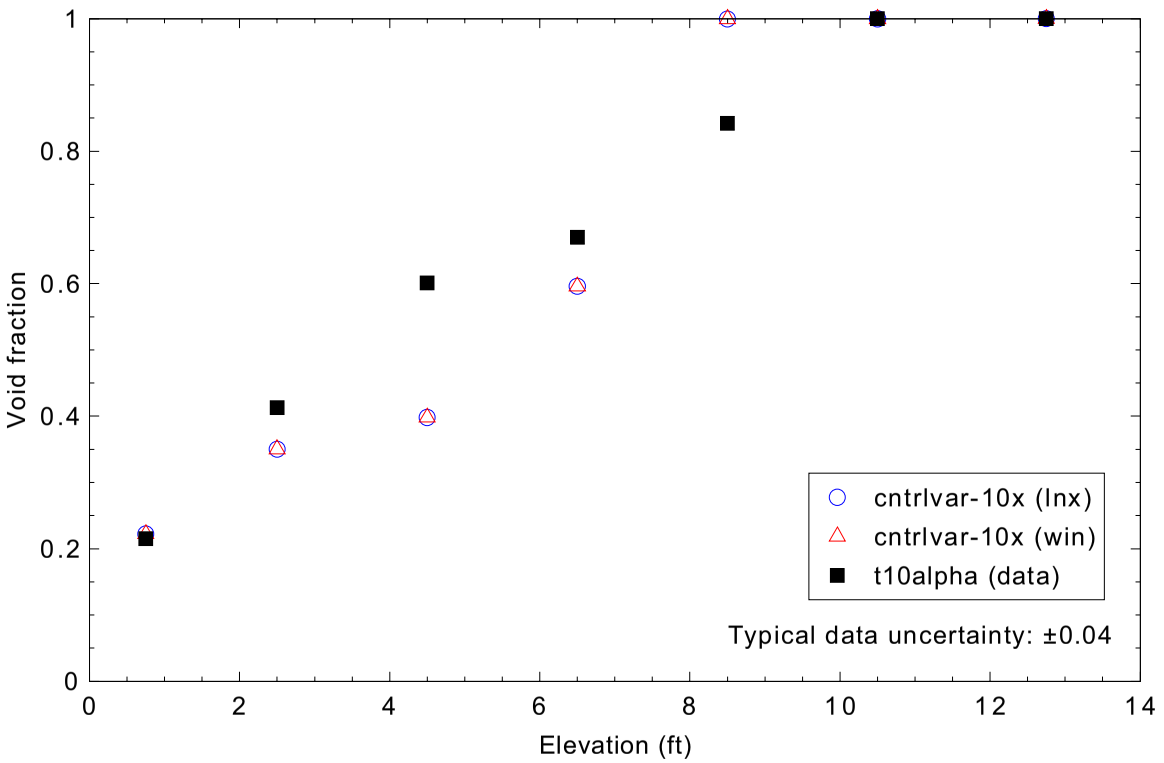

Figure 4.9-6. Measured and calculated void fraction profile in the vessel at 10 s for GE level swell Test 5801-15.

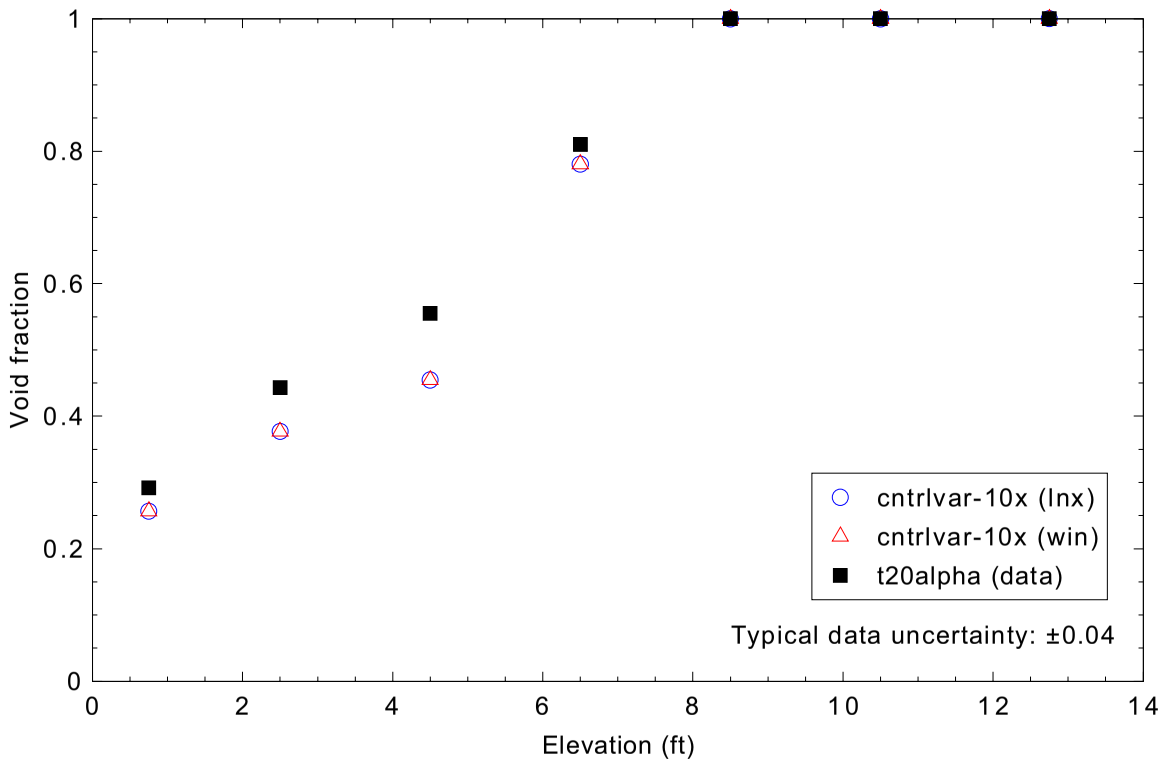

Figure 4.9-7. Measured and calculated void fraction profile in the vessel at 20 s for GE level swell Test 5801-15.

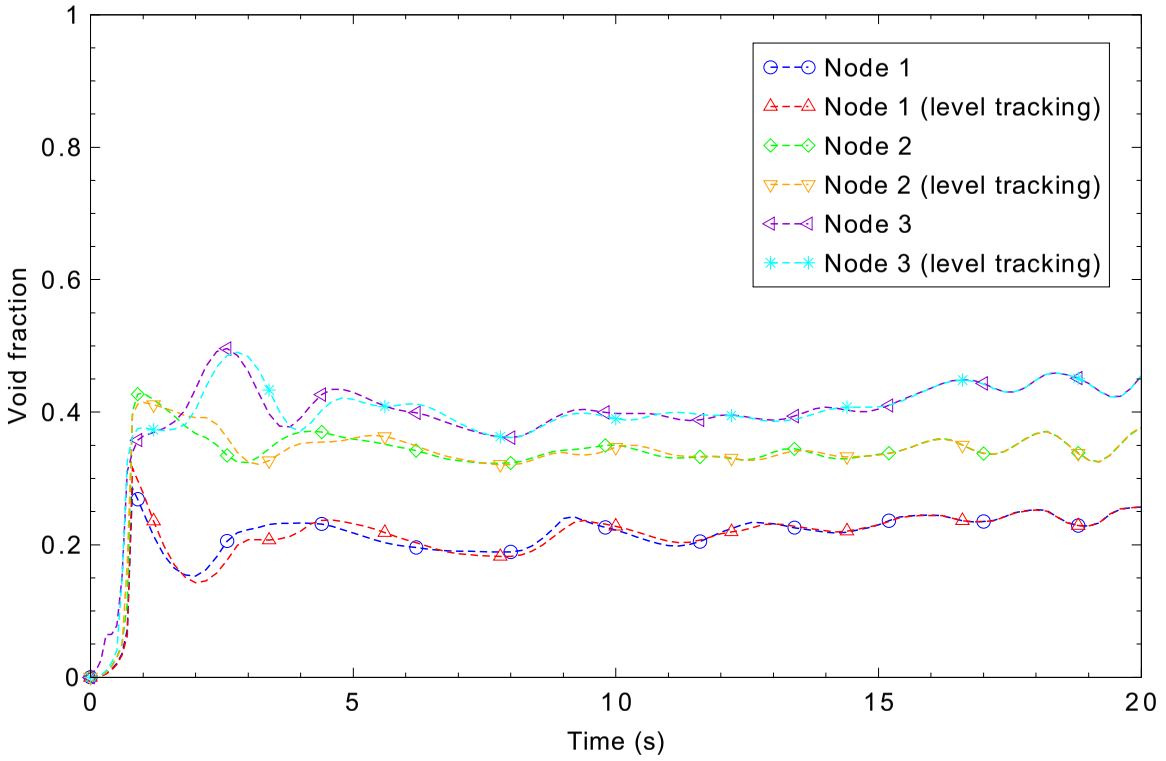

Figure 4.9-8. Effect of level tracking model on calculated void fractions for levels 1-3 using the semi-implicit solution scheme.

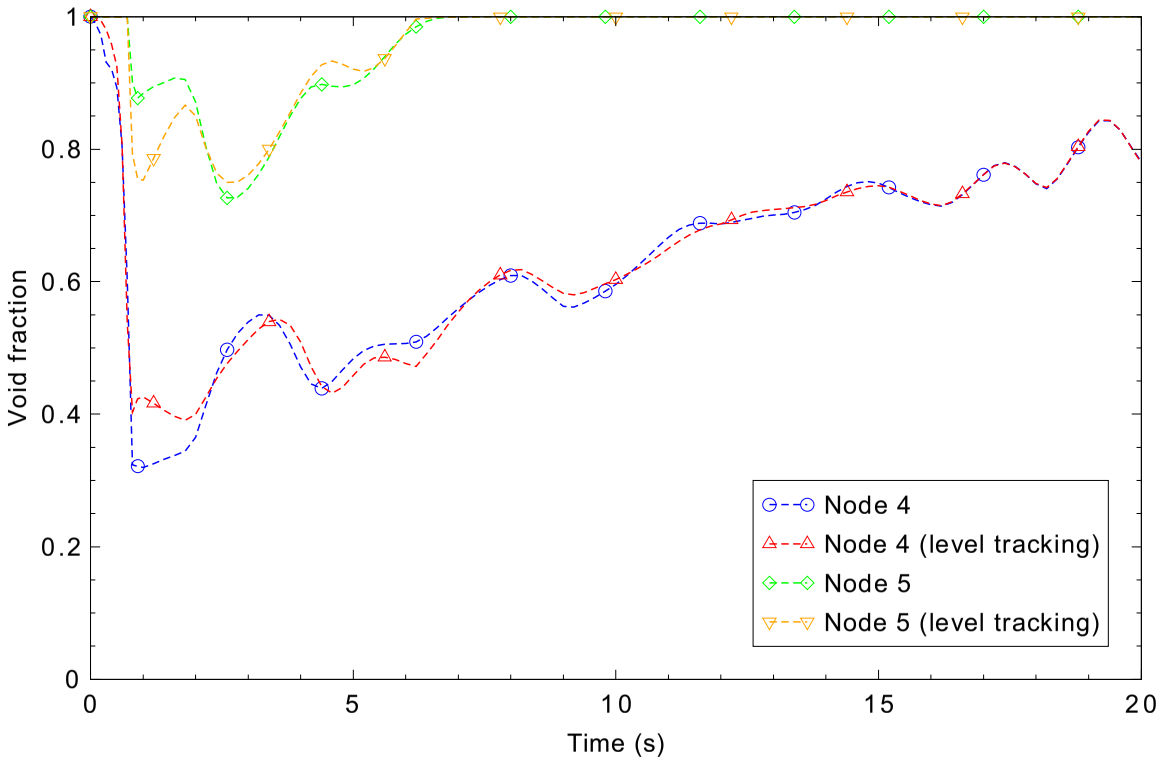

Figure 4.9-9. Effect of level tracking model on calculated void fractions for levels 4 and 5 using the semi-implicit solution scheme.

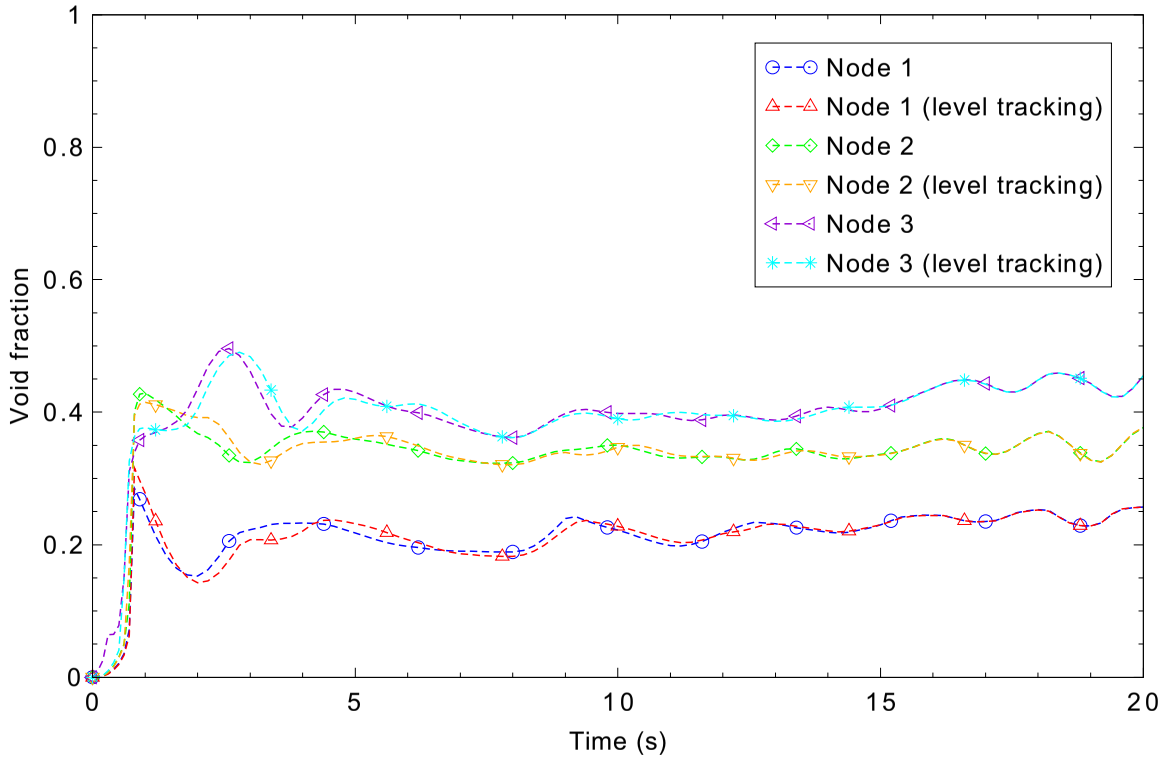

Figure 4.9-10. Effect of level tracking model on calculated void fractions for levels 1-3 using the nearly-implicit solution scheme.

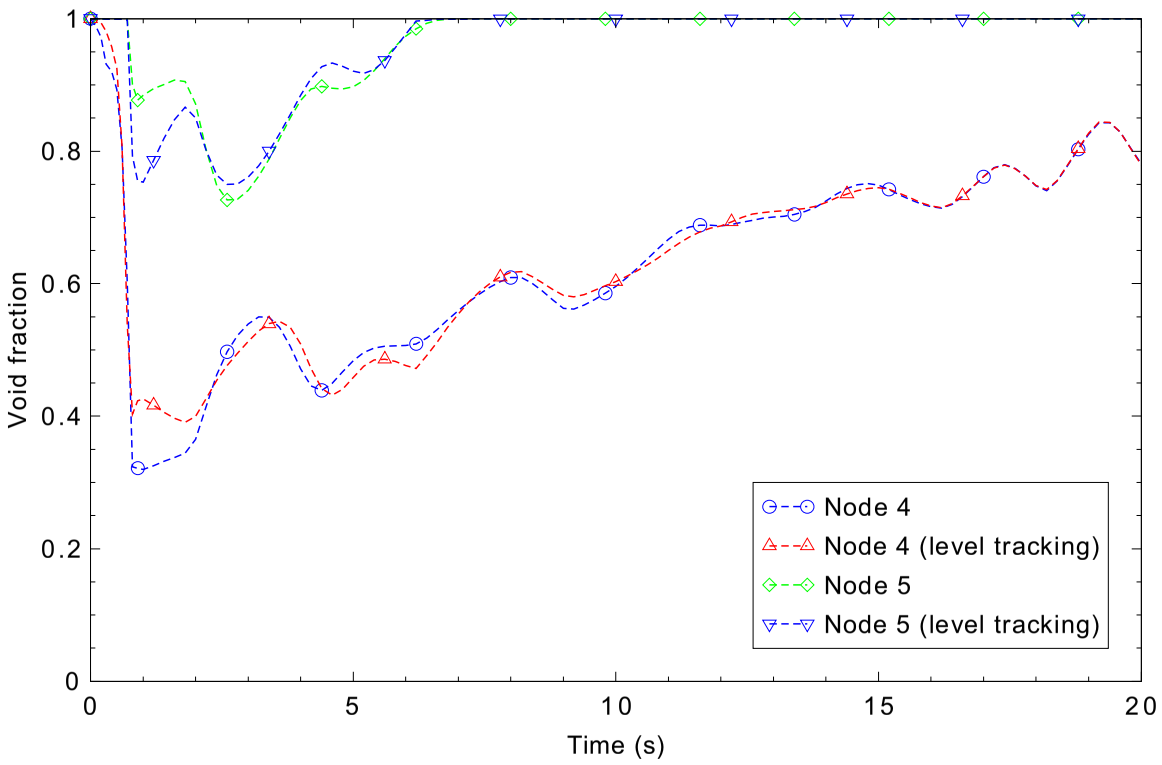

Figure 4.9-11. Effect of level tracking model on calculated void fractions for levels 4 and 5 using the nearly-implicit solution scheme.

4.10 Bennett Heated Tube Tests 5358, 5294, and 5394

Figures comparing simulations using Linux and Windows code versions are presented. Diagrams are included so that the figure numbering is the same as that in Volume III of the RELAP5-3D code manual. No differences were observed in the figures.

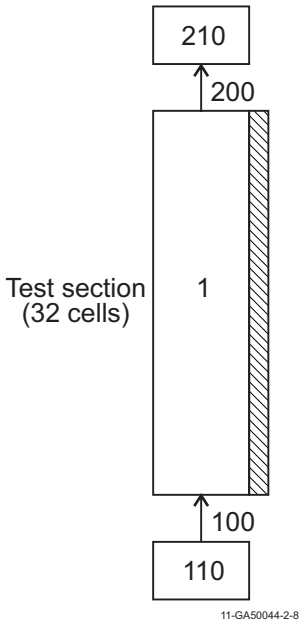

Figure 4.10-1. Nodalization diagram for the Bennett test facility.

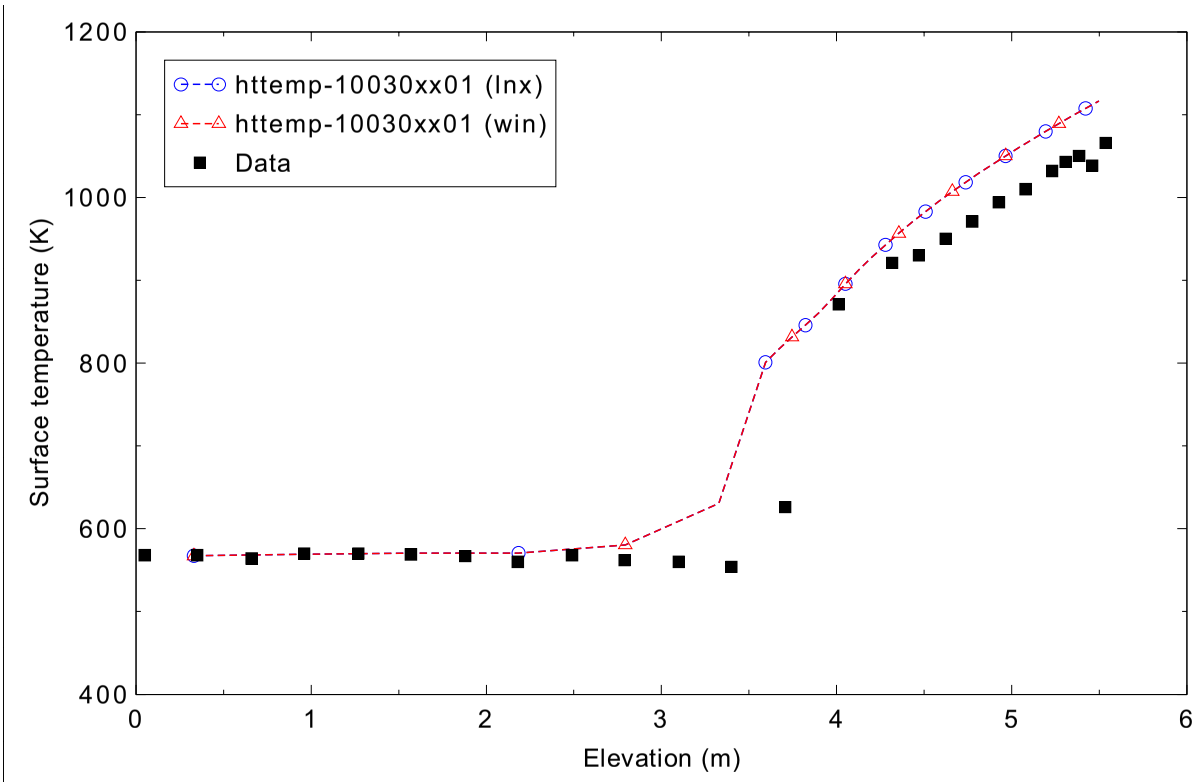

Figure 4.10-2. Measured and calculated axial wall temperatures for Bennett heated tube low mass flux Test 5358.

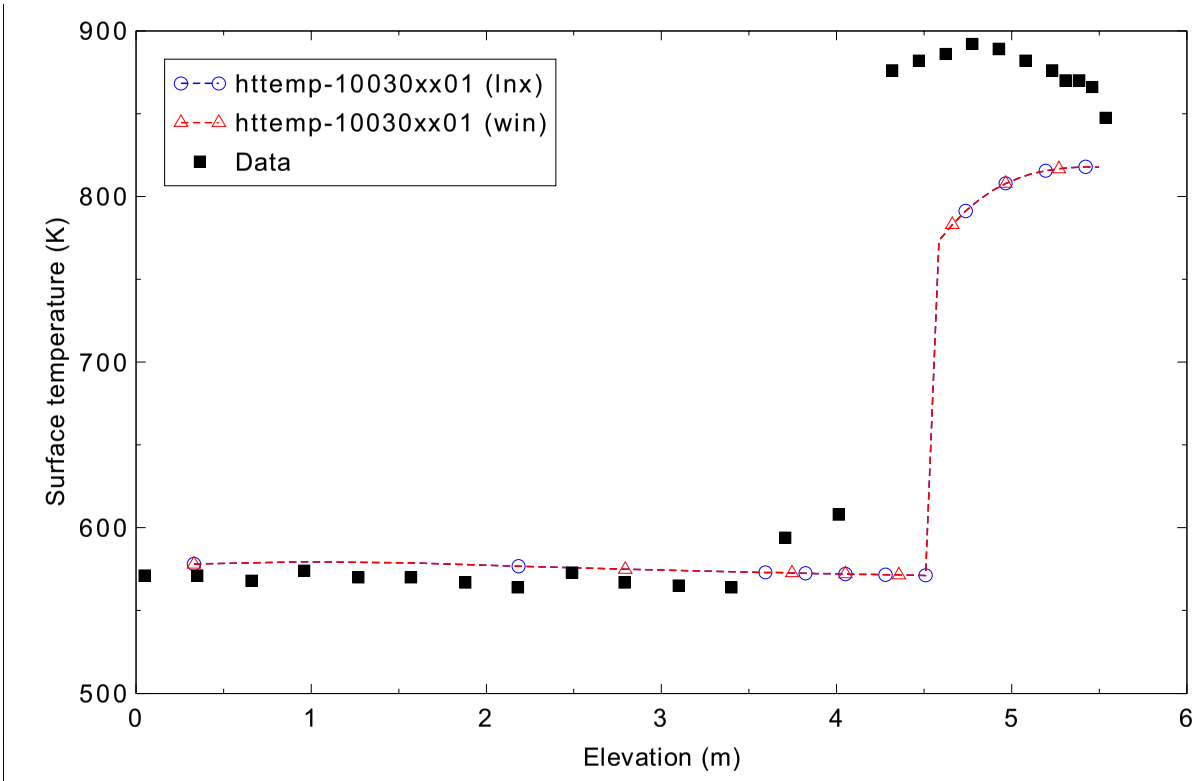

Figure 4.10-3. Measured and calculated axial wall temperatures for Bennett heated tube intermediate mass flux Test 5294.

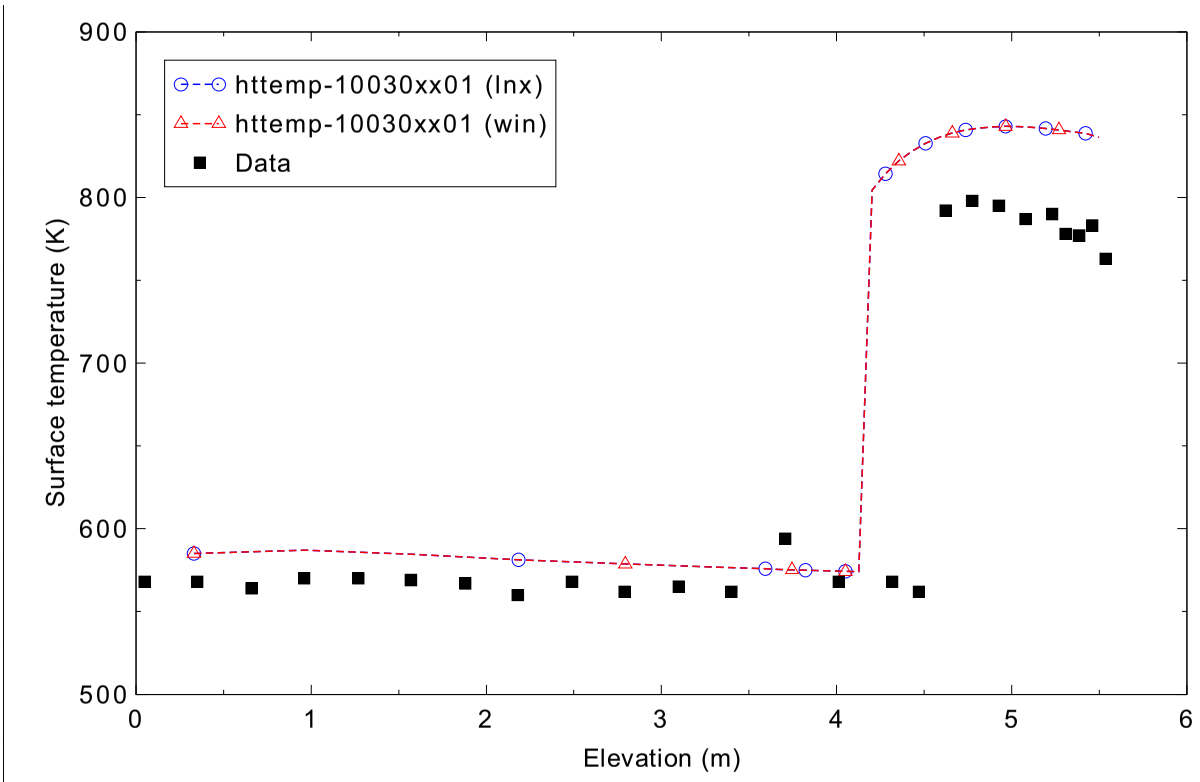

Figure 4.10-4. Measured and calculated axial wall temperatures for Bennett heated tube high mass flux Test 5394.

4.11 ORNL THTF Tests 3.07.9B, 3.07.9N, 3.07.9W and 3.09.10I

Figures comparing simulations using Linux and Windows code versions are presented. Diagrams are included so that the figure numbering is the same as that in Volume III of the RELAP5-3D code manual. No differences were observed in the figures.

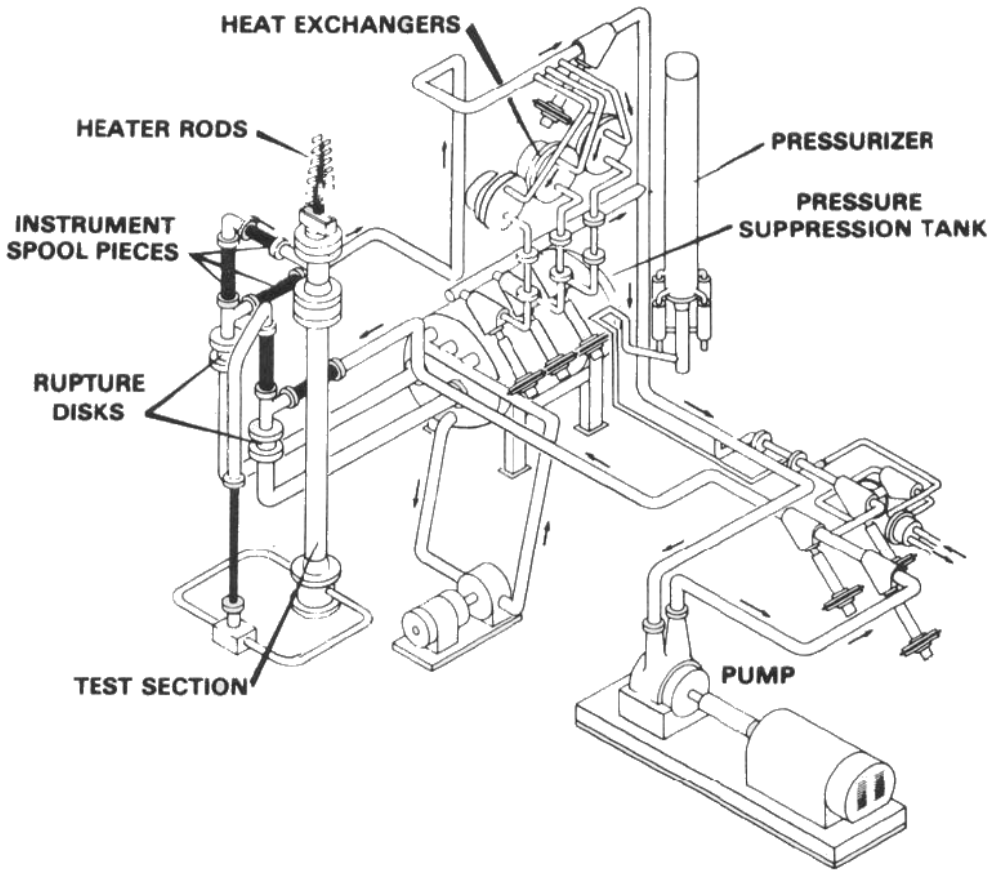

Figure 4.11-1. Experiment setup of the ORNL Thermal Hydraulic Test Facility (THTF) steady state film boiling tests.

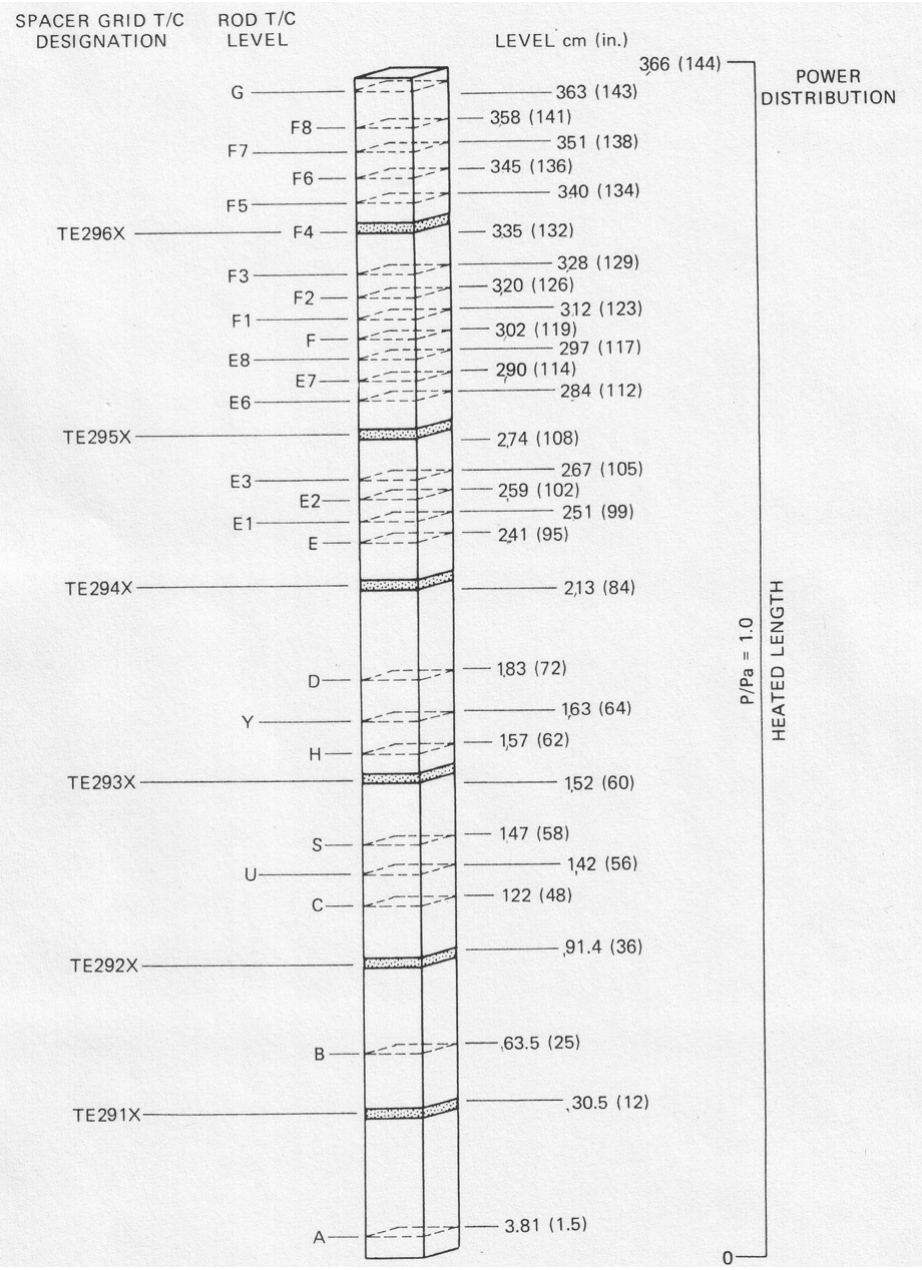

Figure 4.11-2. Test section of the ORNL Thermal Hydraulic Test Facility.

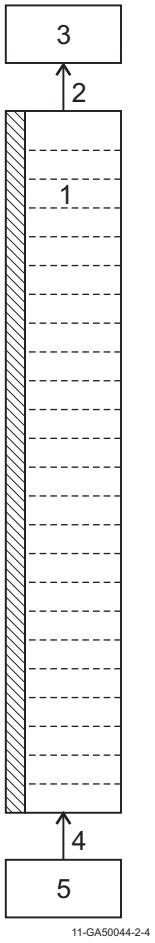

Figure 4.11-3. Nodalization diagram for the ORNL THTF steady state experiments.

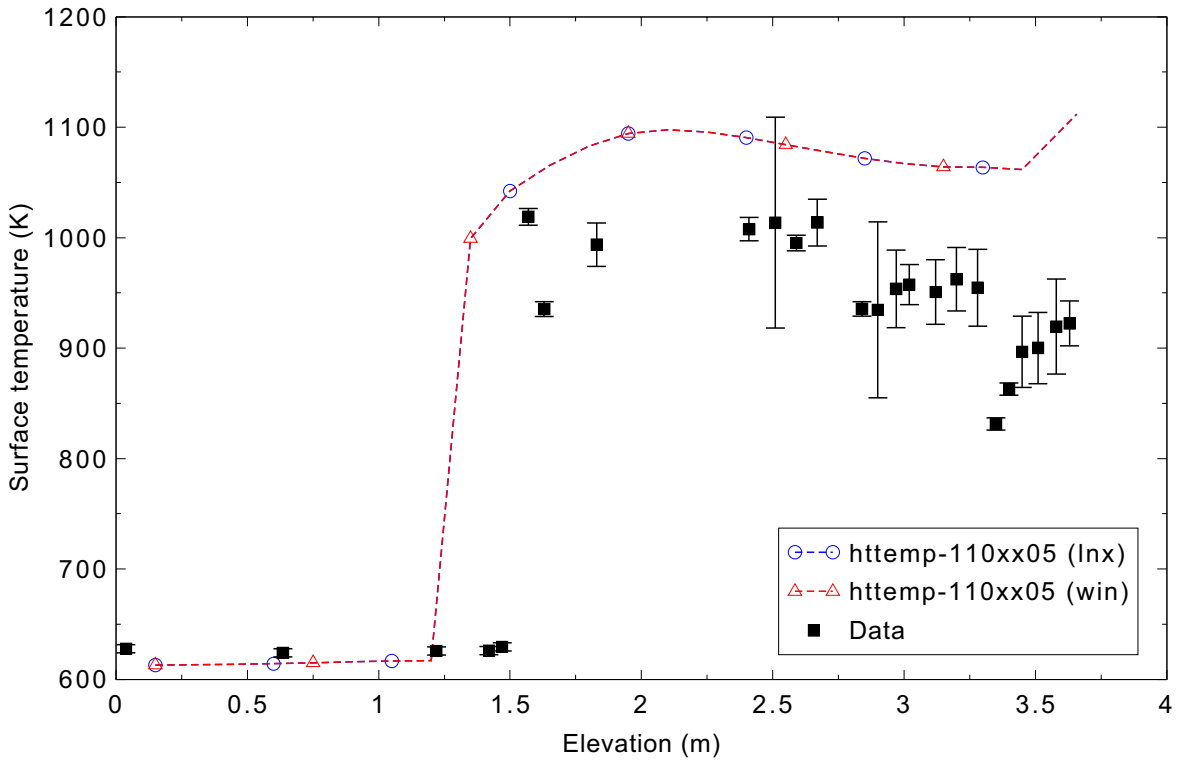

Figure 4.11-4. Measured and calculated steady state rod surface temperatures for ORNL THTF Test 3.07.9B.

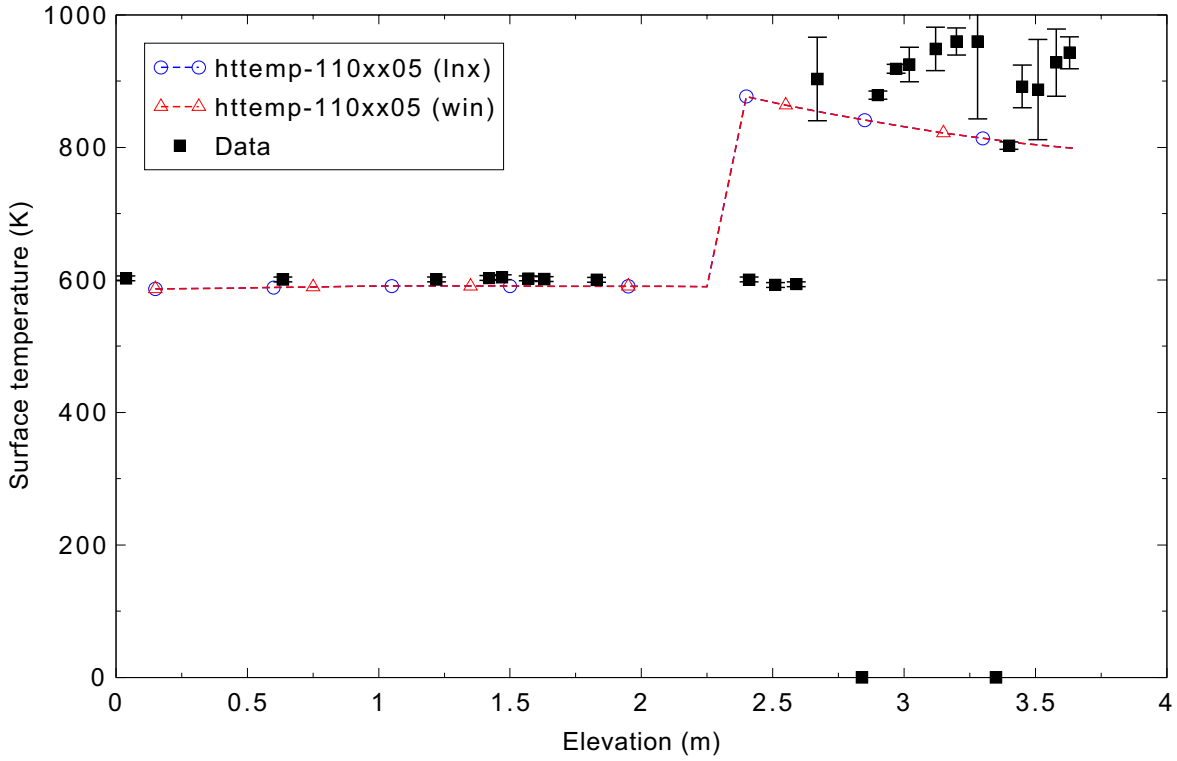

Figure 4.11-5. Measured and calculated steady state rod surface temperatures for ORNL THTF Test 3.07.9N.

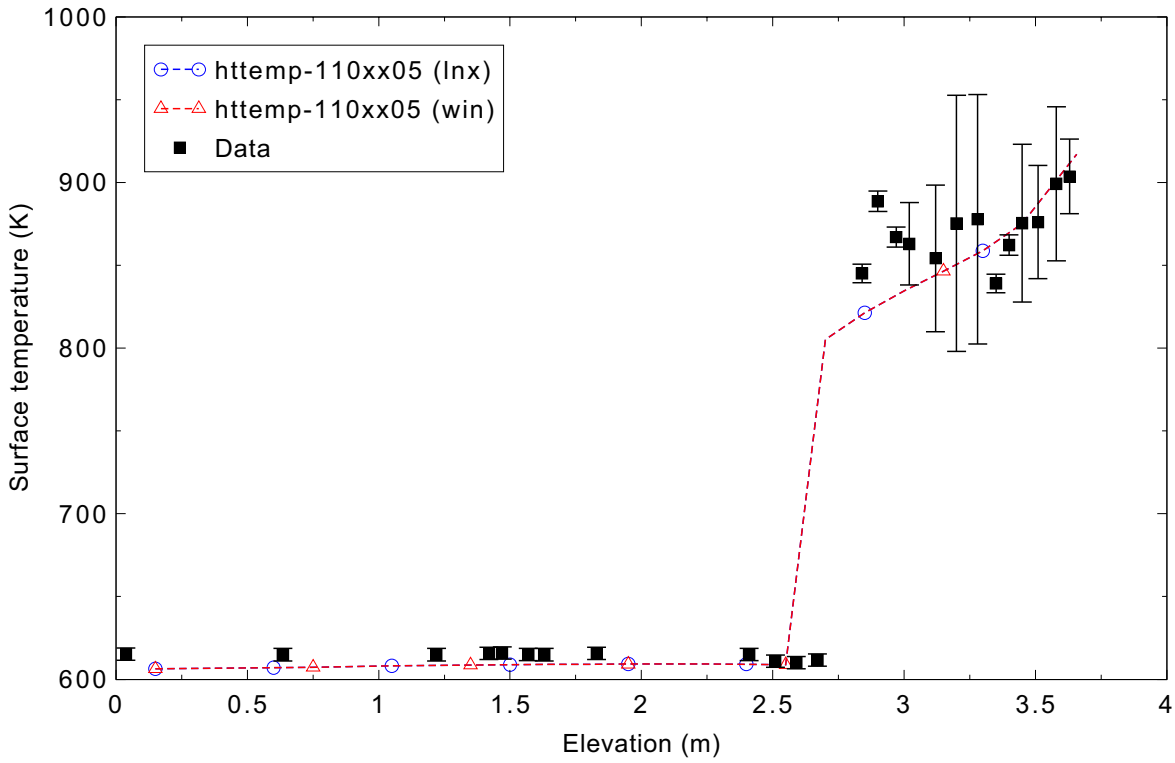

Figure 4.11-6. Measured and calculated steady state rod surface temperatures for ORNL THTF Test 3.07.9W.

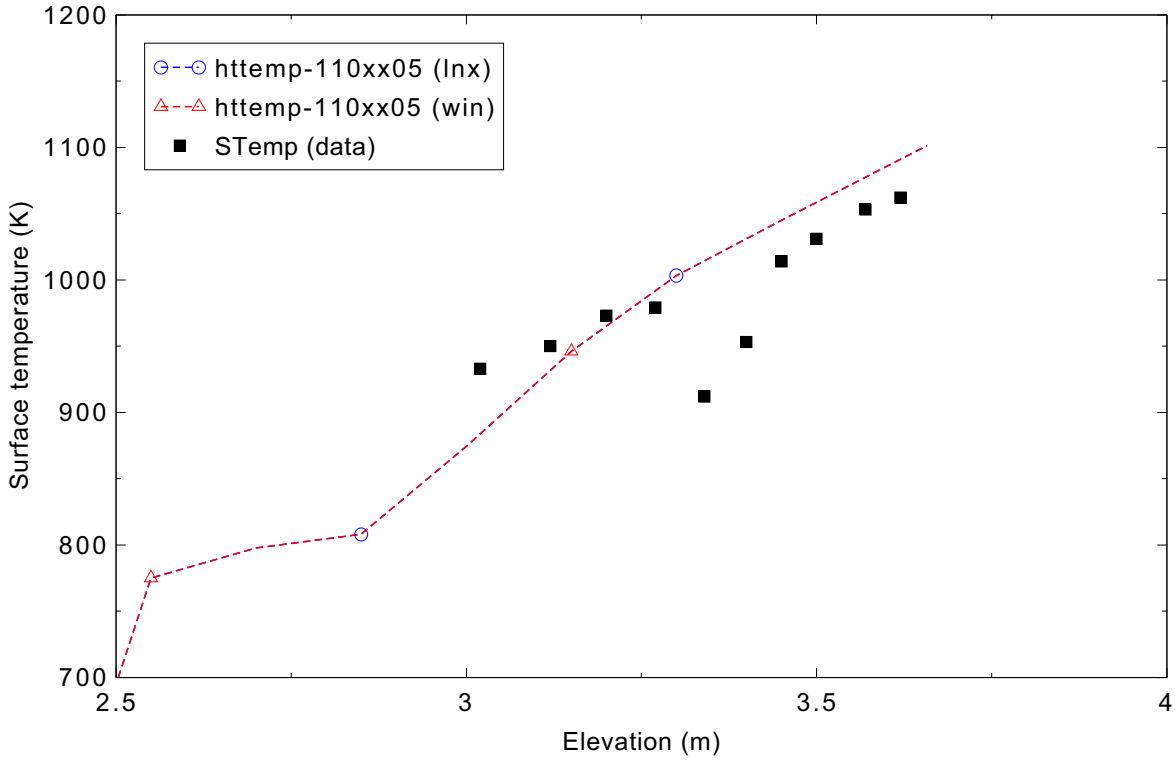

Figure 4.11-7. Measured and calculated steady state axial rod surface temperatures for ORNL THTF Test 3.09.10I.

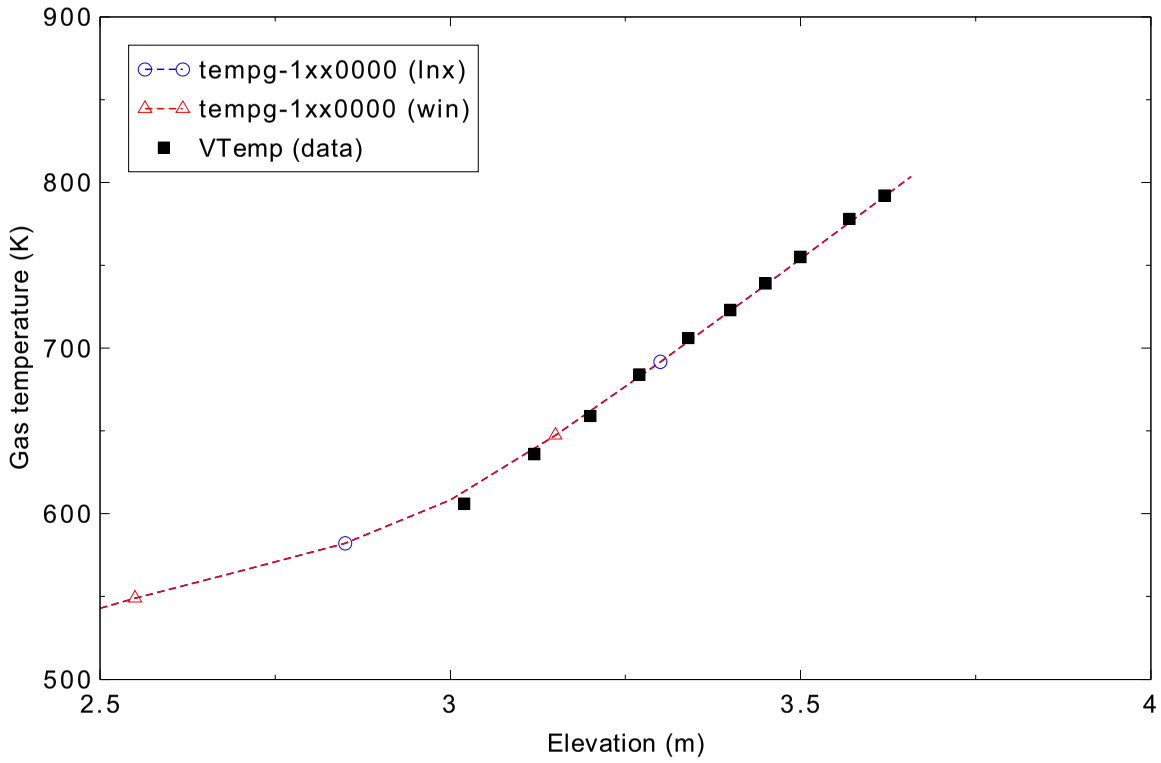

Figure 4.11-8. Measured and calculated steady state axial gas temperatures for ORNL THTF Test 3.09.10I.

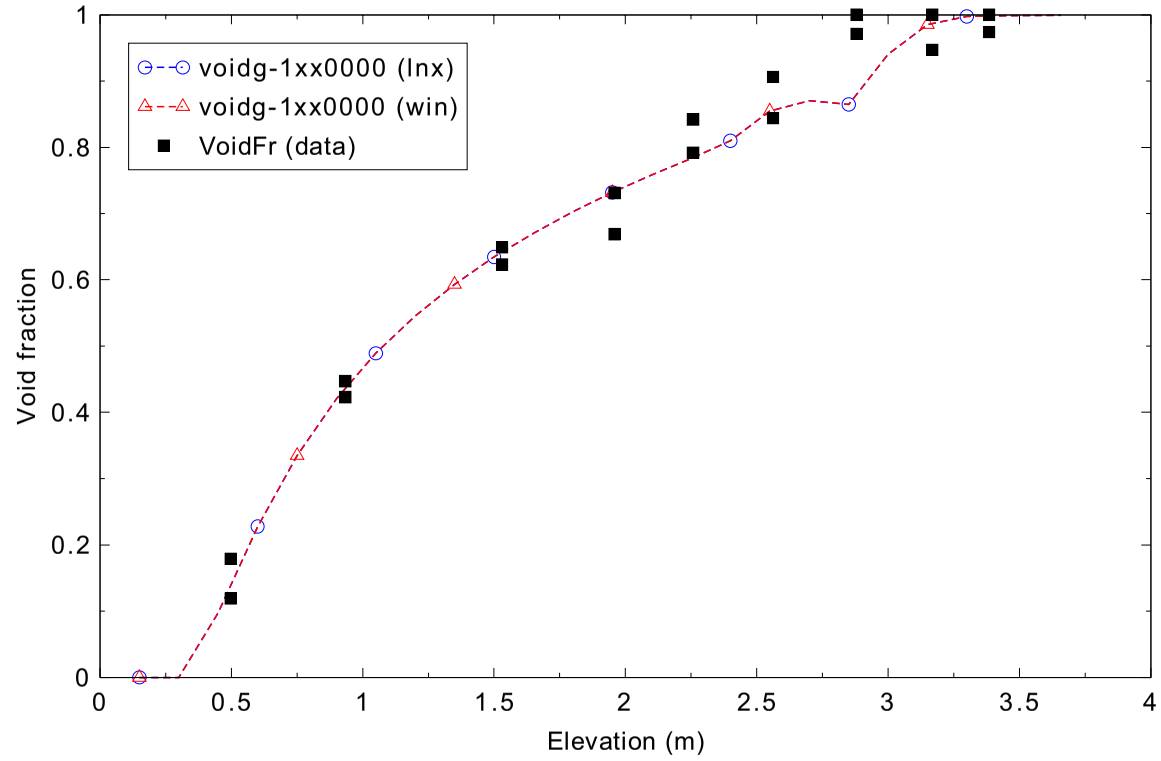

Figure 4.11-9. Measured and calculated steady state axial void fractions for ORNL THTF Test 3.09.10I.

4.12 Royal Institute of Technology Tube Test 261

Figures comparing simulations using Linux and Windows code versions are presented. Diagrams are included so that the figure numbering is the same as that in Volume III of the RELAP5-3D code manual. No differences were observed in the figures.

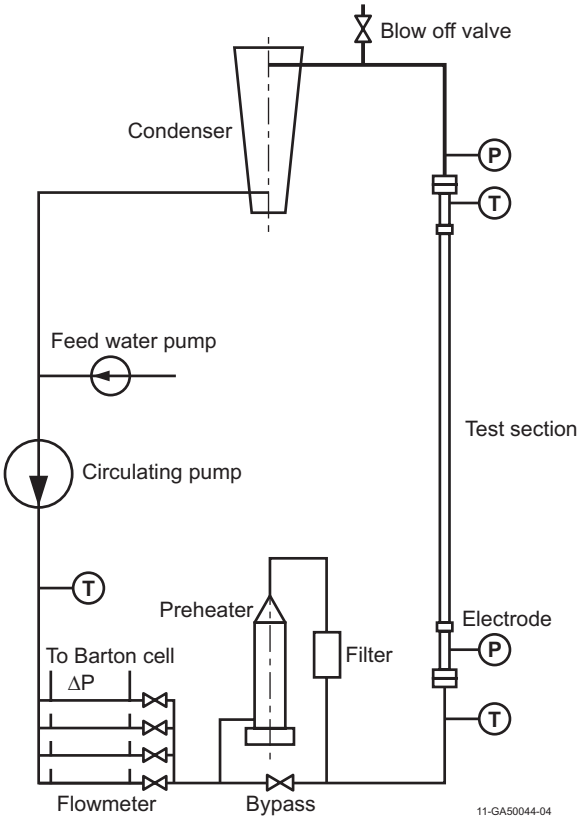

Figure 4.12-1. RIT Tube Test facility diagram.

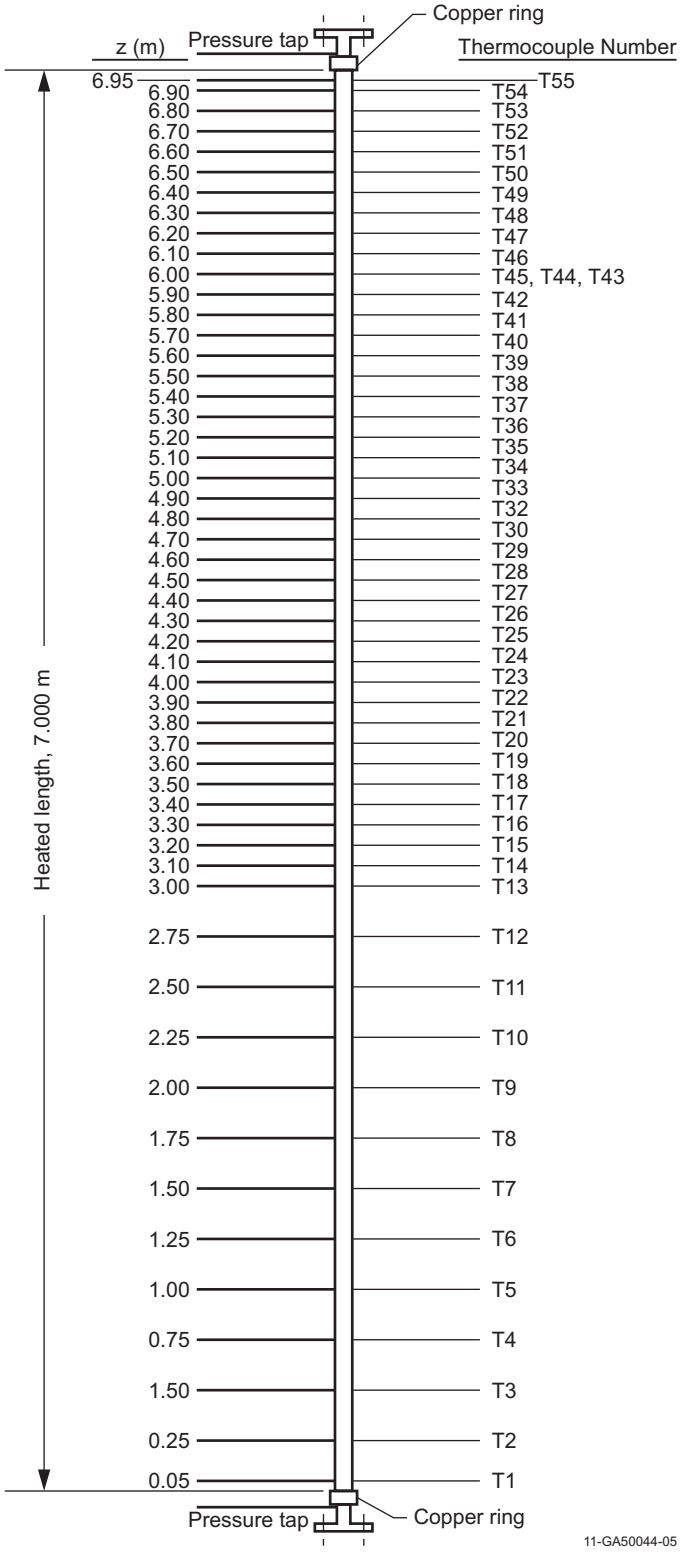

Figure 4.12-2. Locations of temperature measurements for RIT Tube Test 261.

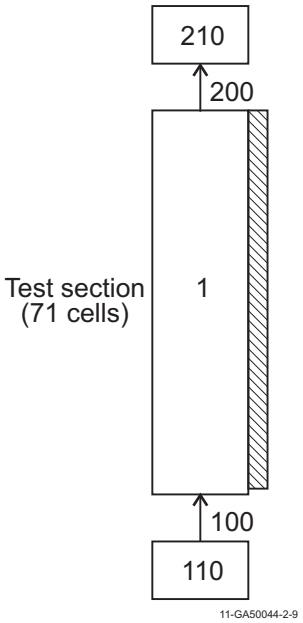

Figure 4.12-3. Nodalization diagram for the RIT test facility.

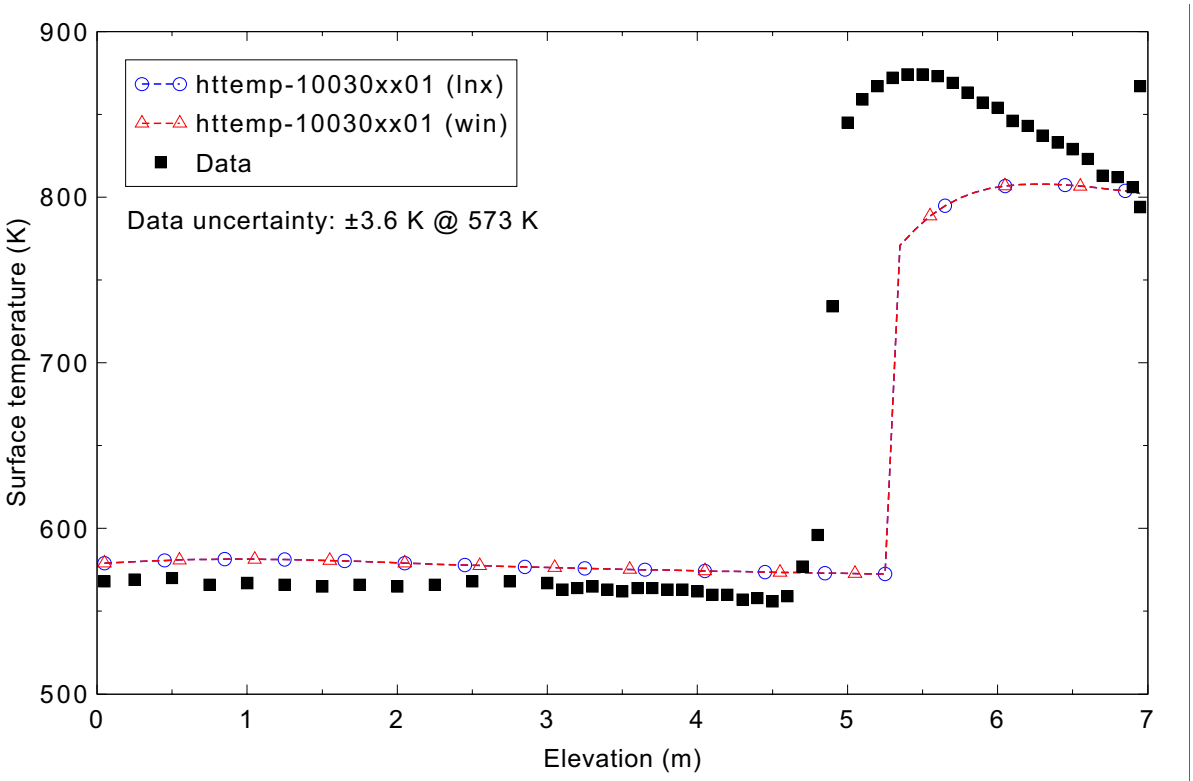

Figure 4.12-4. Measured and calculated tube surface temperatures for RIT Tube Test 261 with the default CHF model.

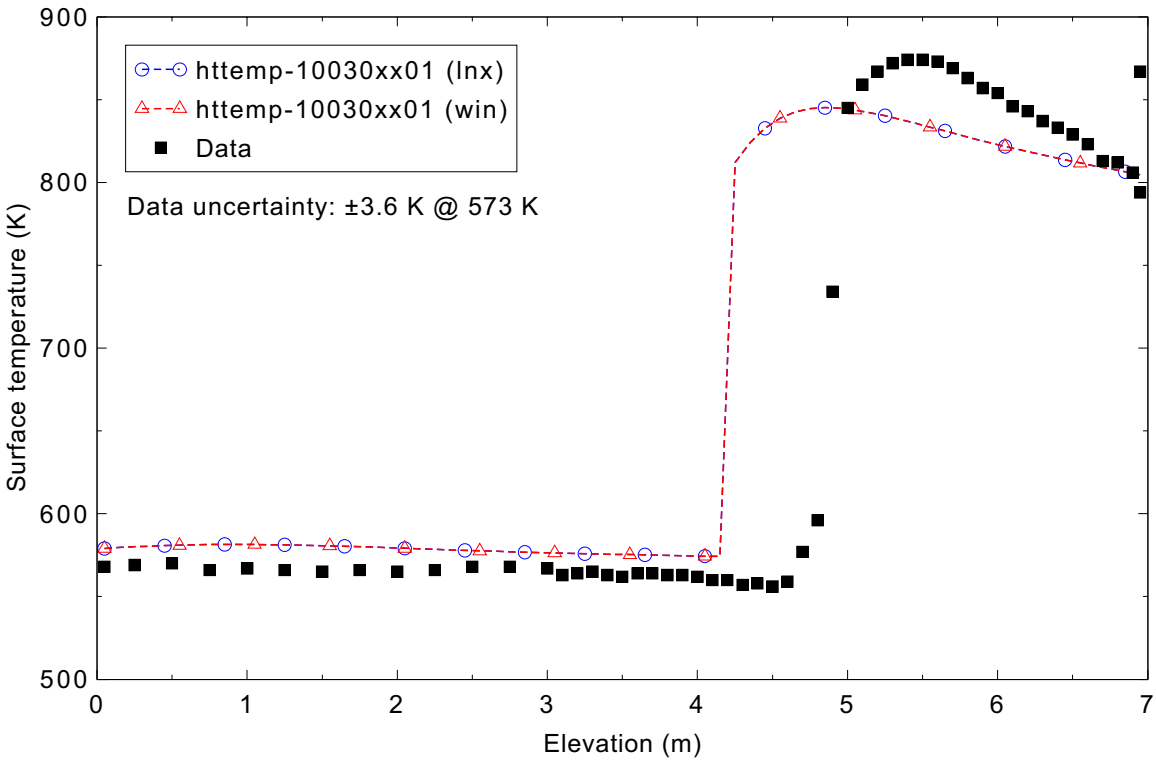

Figure 4.12-5. Measured and calculated tube surface temperatures for RIT Tube Test 261 with the PG-CHF model.

4.13 FLECHT SEASET Test 31504

Figures comparing simulations using Linux and Windows code versions are presented. Diagrams are included so that the figure numbering is the same as that in Volume III of the RELAP5-3D code manual. Noticeable differences were observed in Figures 4.13-15, 16, 19, 20, 21, and 22.

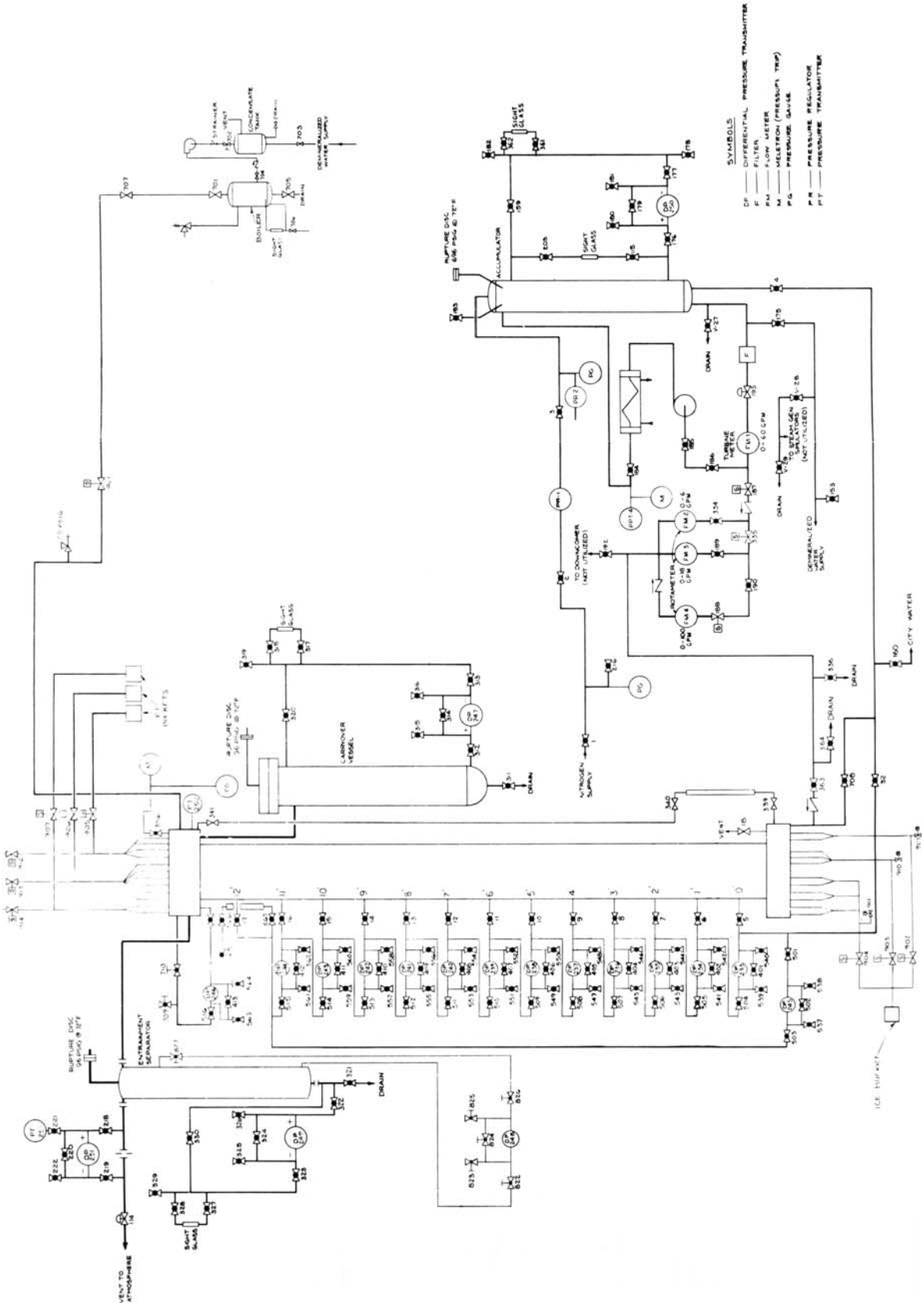

Figure 4.13-1. FLECHT SEASET unblocked bundle flow diagram for forced reflood.

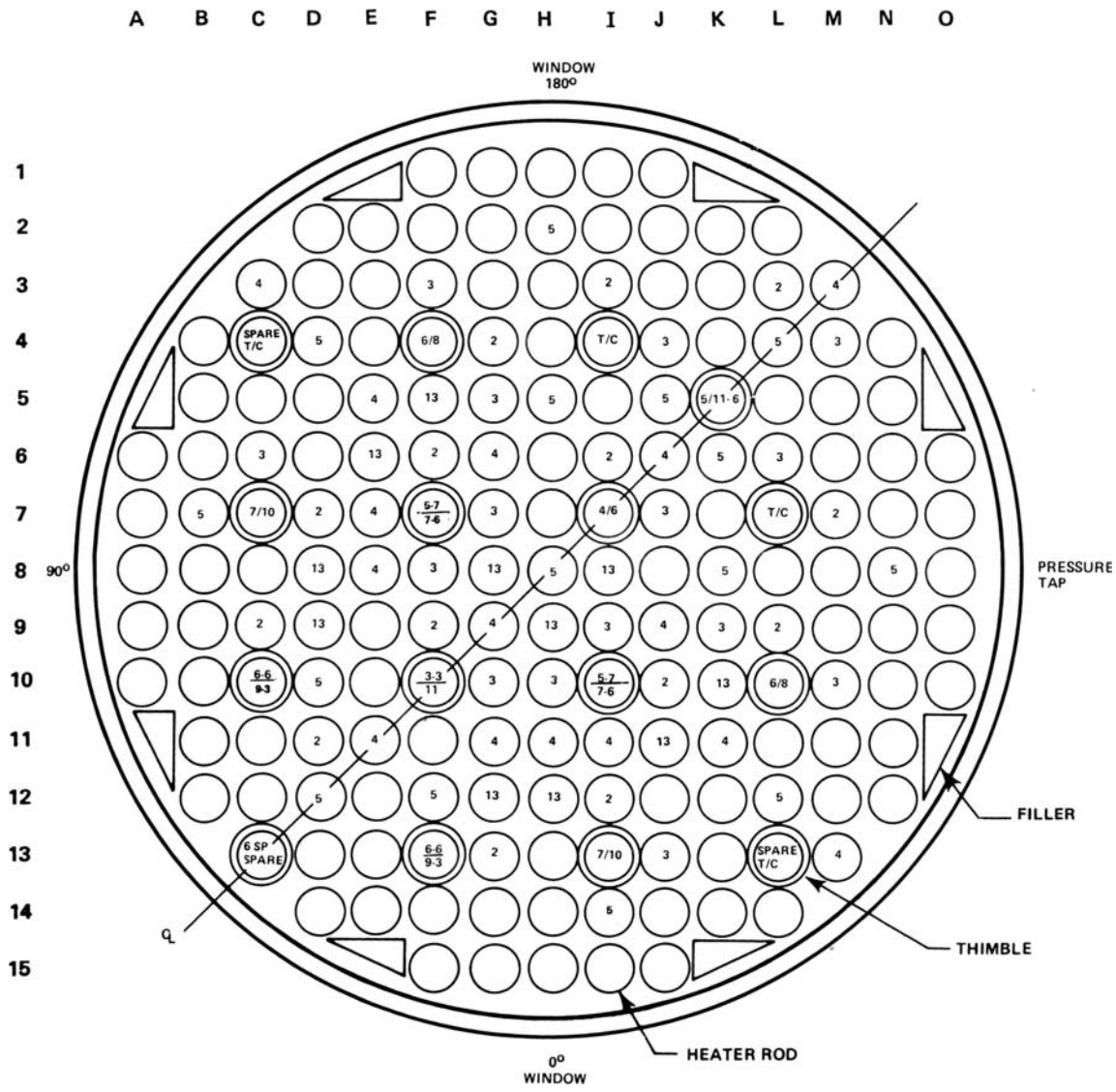

Figure 4.13-2. FLECHT SEASET bundle cross section.

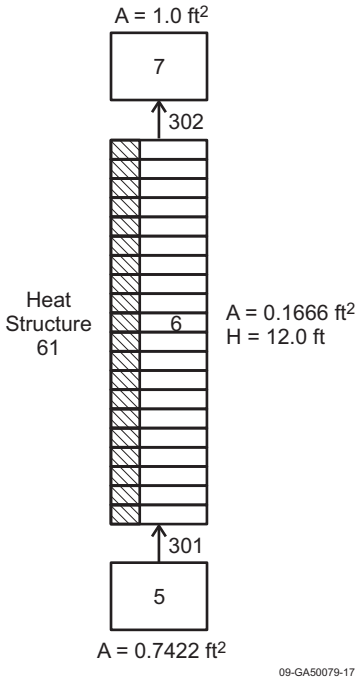

Figure 4.13-3. RELAP5-3D nodalization for the FLECHT SEASET forced reflood experiments.

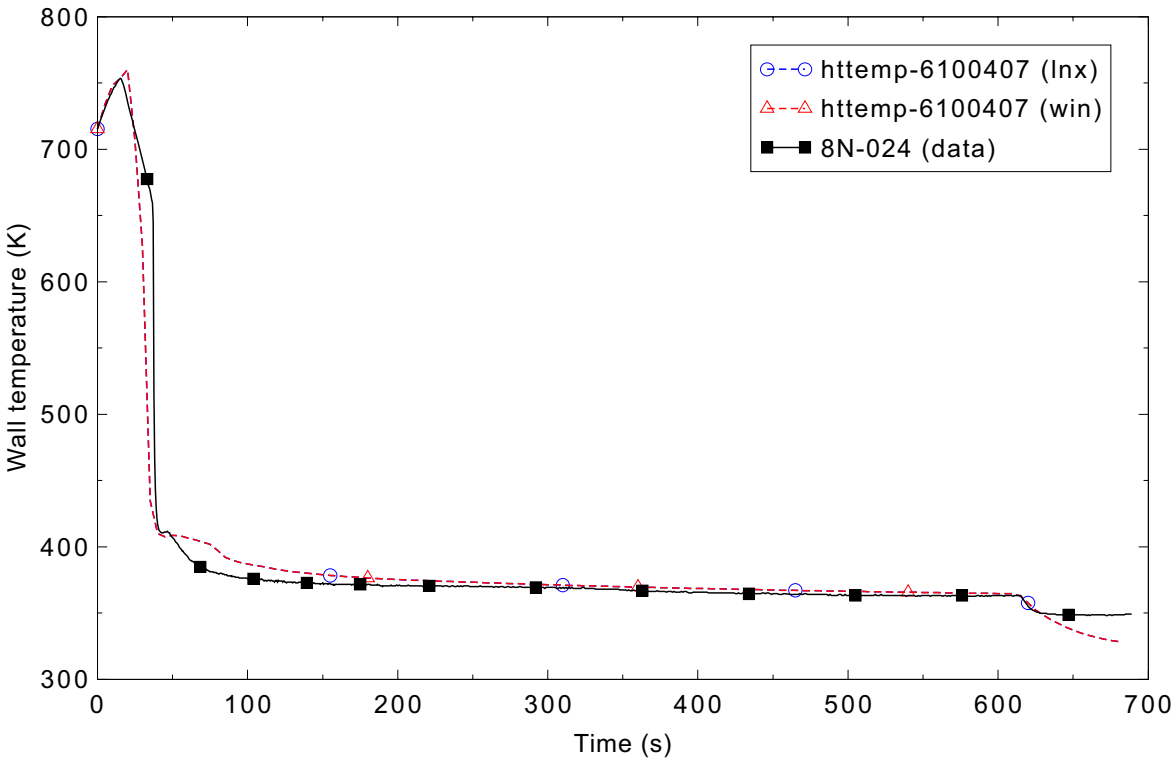

Figure 4.13-4. Measured and calculated rod surface temperatures for FLECHT SEASET forced reflood Test 31504 at the 0.62-m (24-in.) elevation.

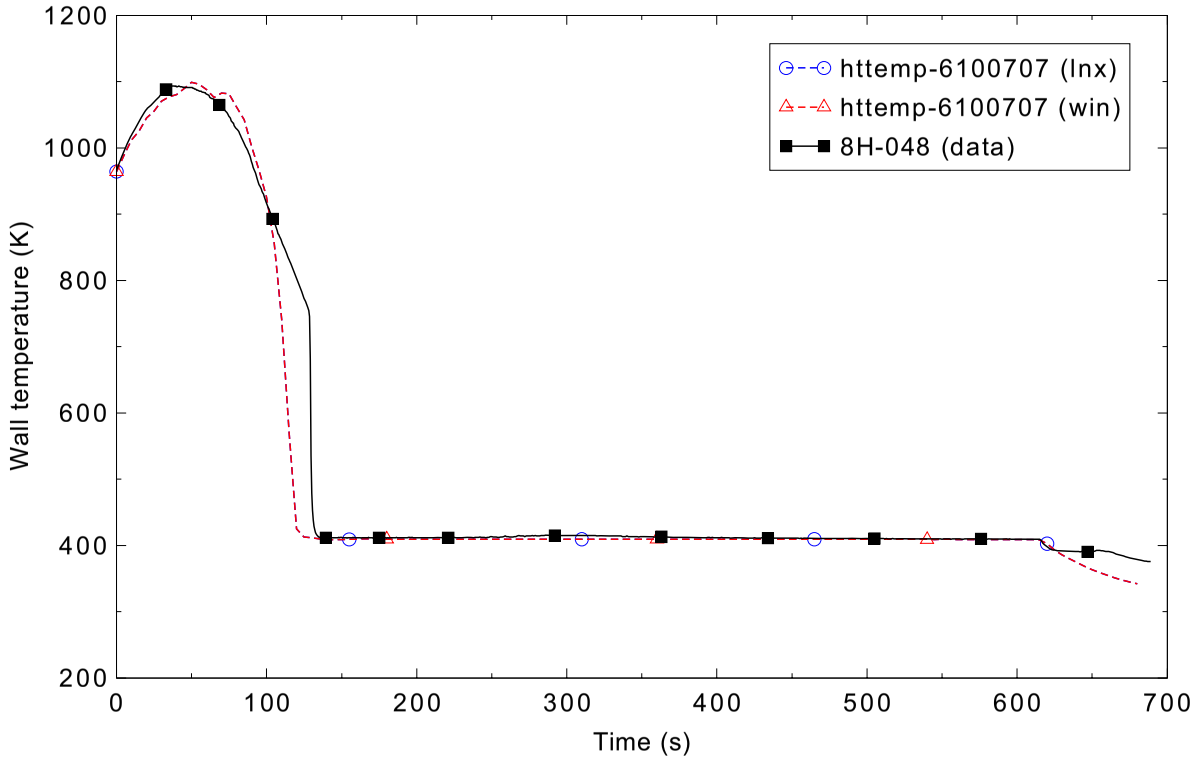

Figure 4.13-5. Measured and calculated rod surface temperatures for FLECHT SEASET forced reflood Test 31504 at the 1.23-m (48-in.) elevation

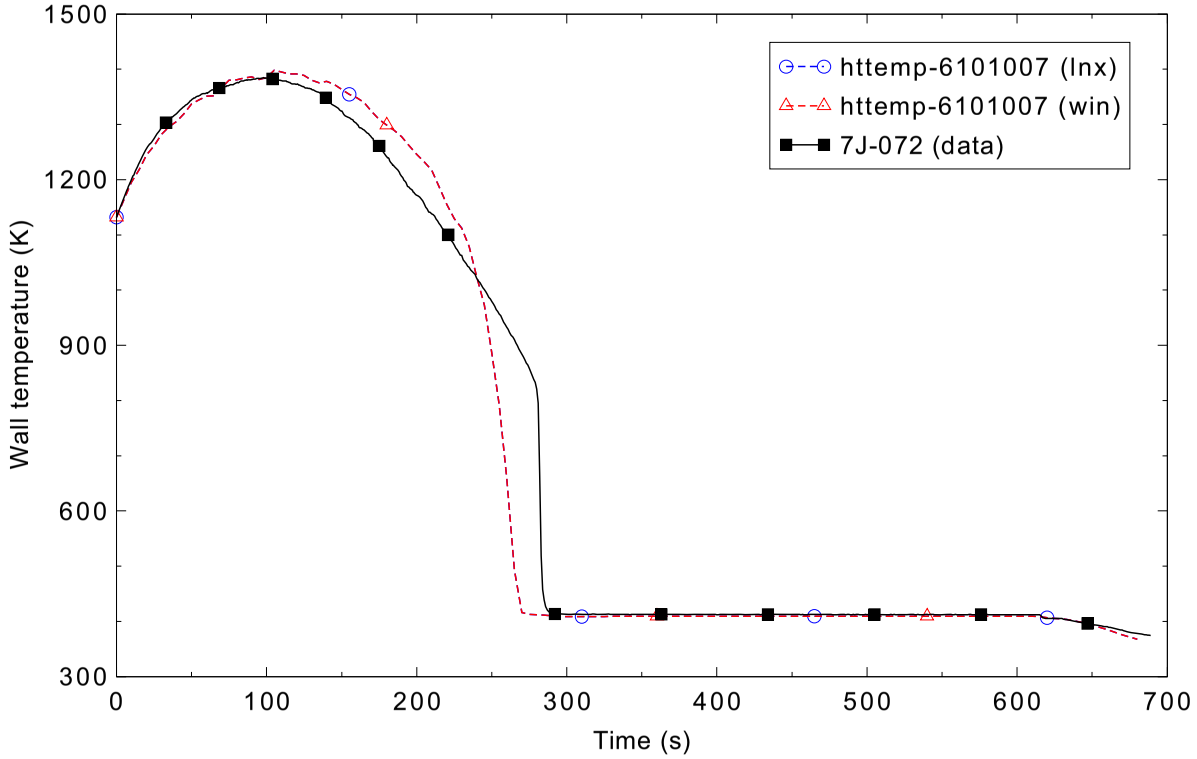

Figure 4.13-6. Measured and calculated rod surface temperatures for FLECHT SEASET forced reflood Test 31504 at the 1.85-m (72-in.) elevation.

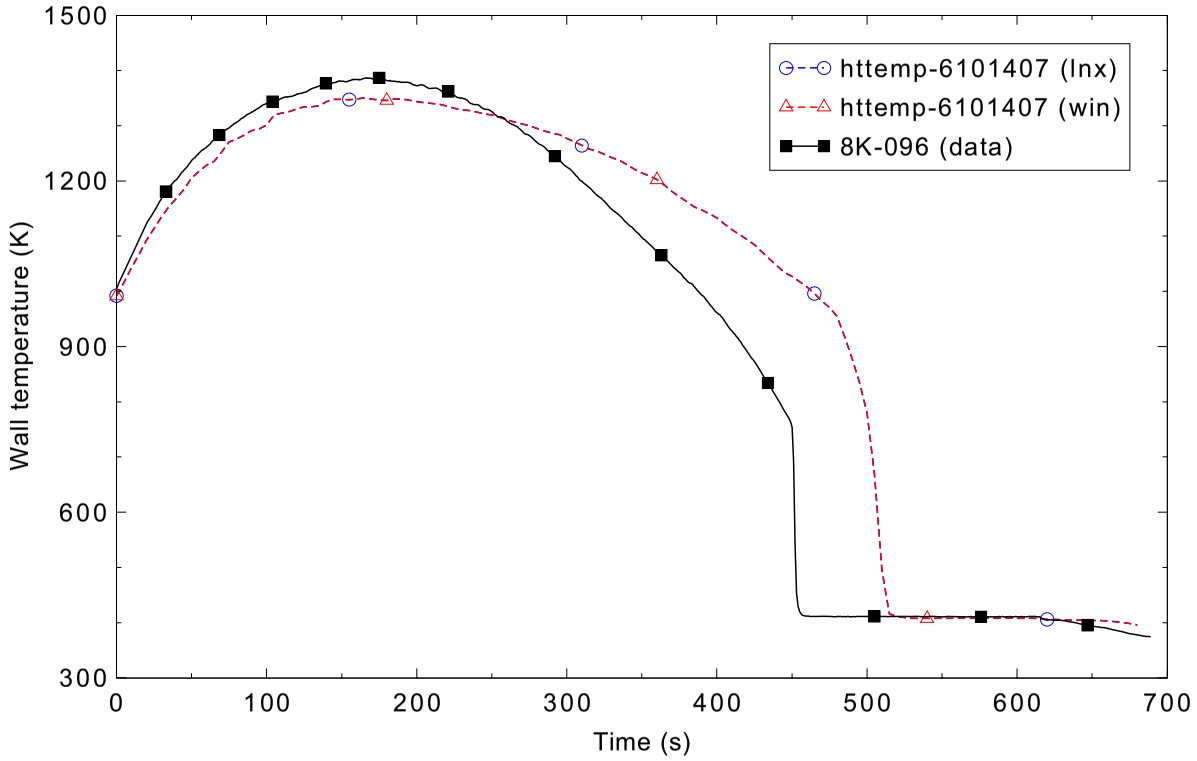

Figure 4.13-7. Measured and calculated rod surface temperatures for FLECHT SEASET forced reflood Test 31504 at the 2.46-m (96-in.) elevation.

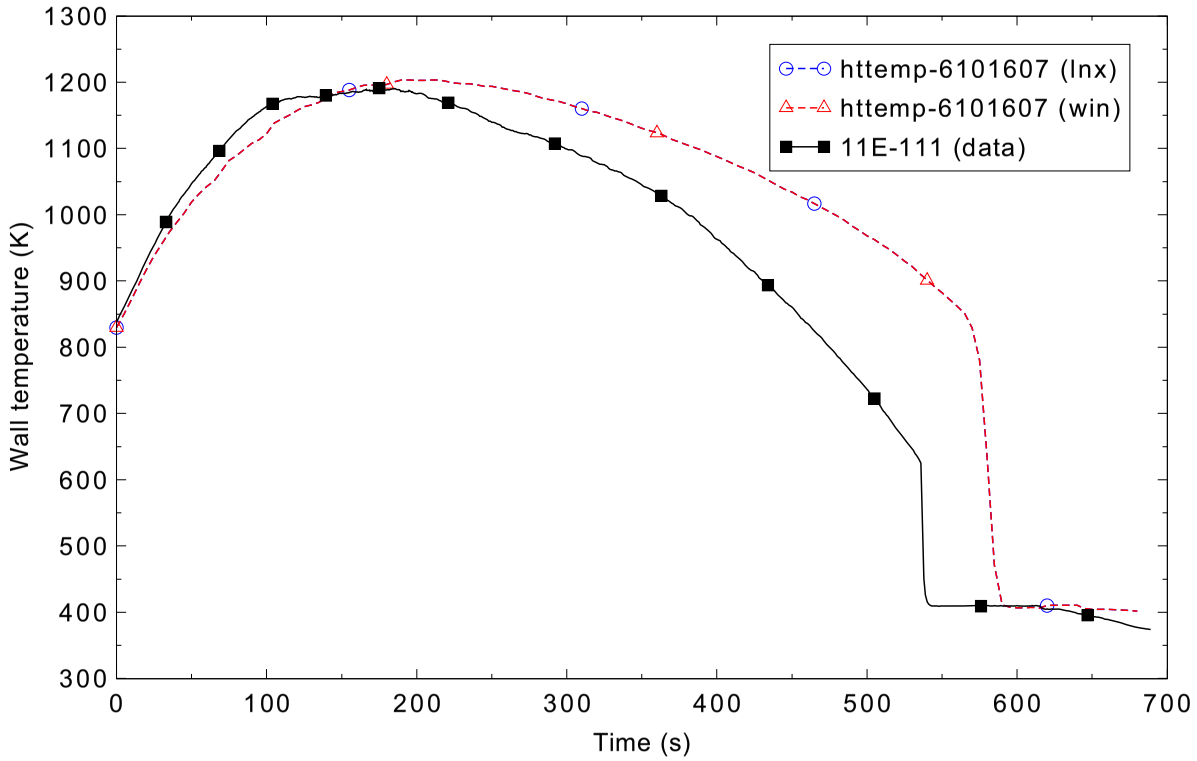

Figure 4.13-8. Measured and calculated rod surface temperatures for FLECHT SEASET forced reflood Test 31504 at the 2.85-m (111-in.) elevation.

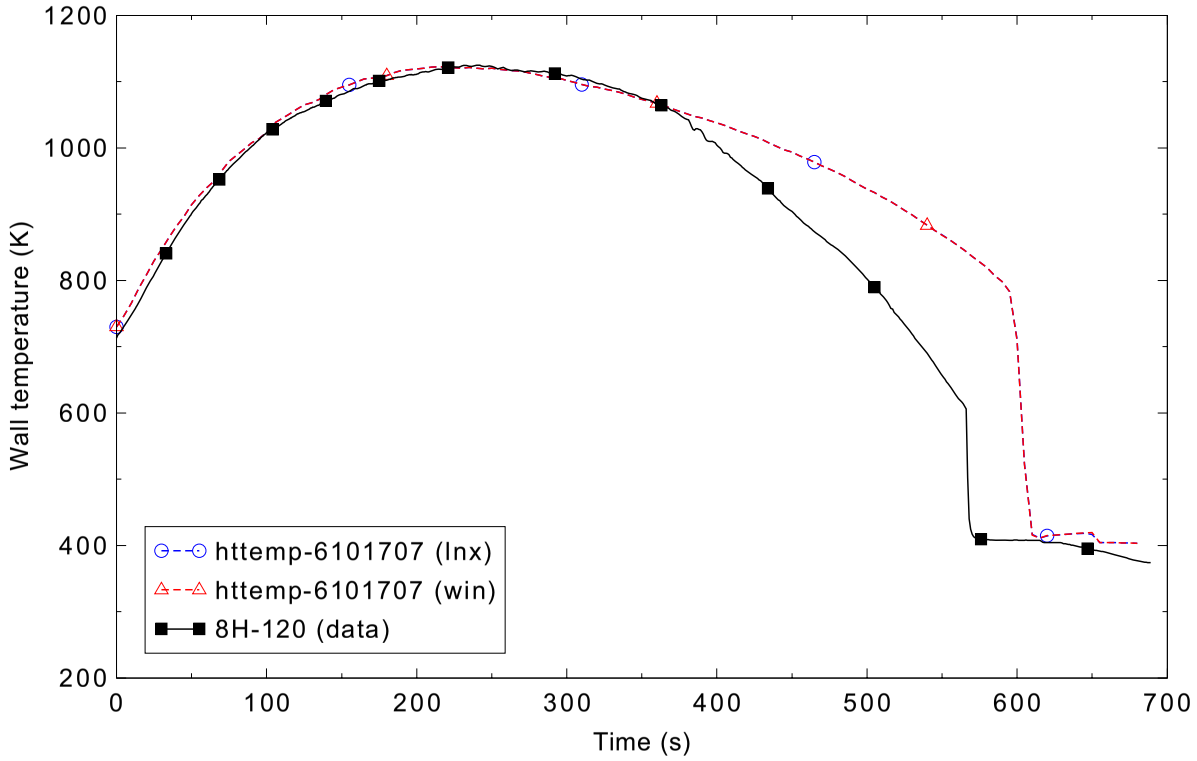

Figure 4.13-9. Measured and calculated rod surface temperatures for FLECHT SEASET forced reflood Test 31504 at the 3.08-m (120-in.) elevation.

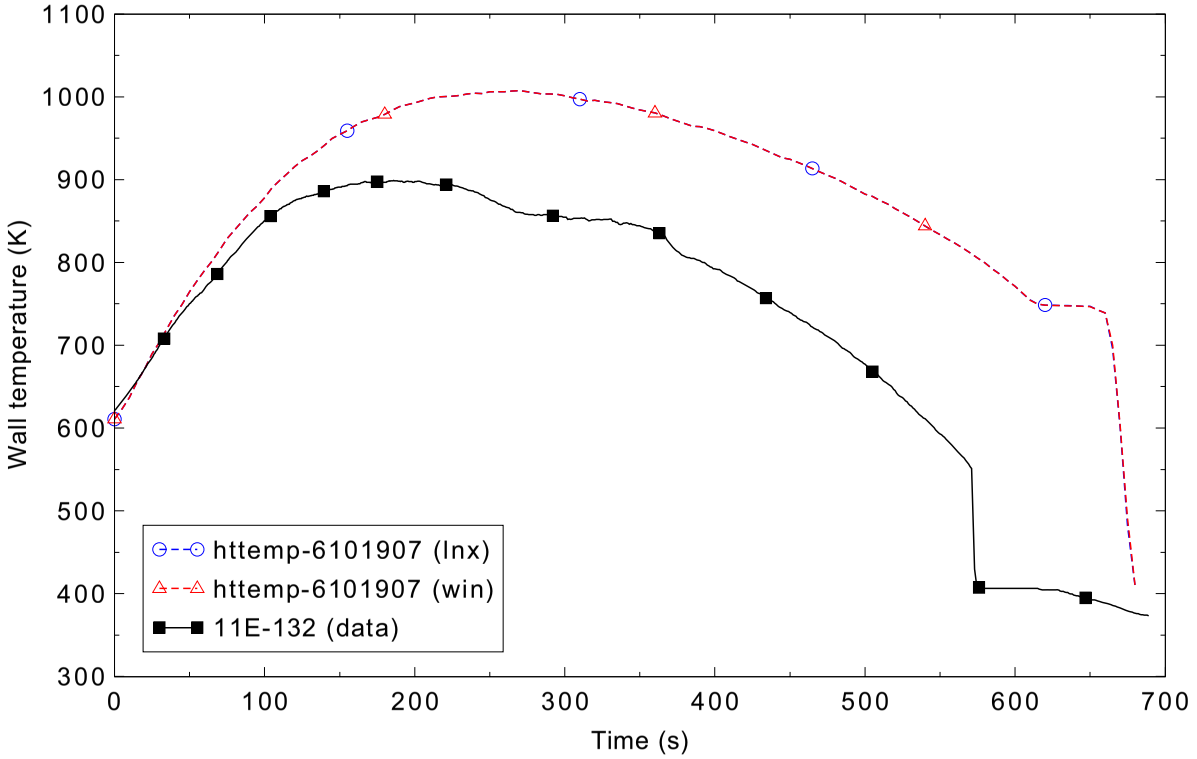

Figure 4.13-10. Measured and calculated rod surface temperatures for FLECHT SEASET forced reflood Test 31504 at the 3.38-m (132-in.) elevation.

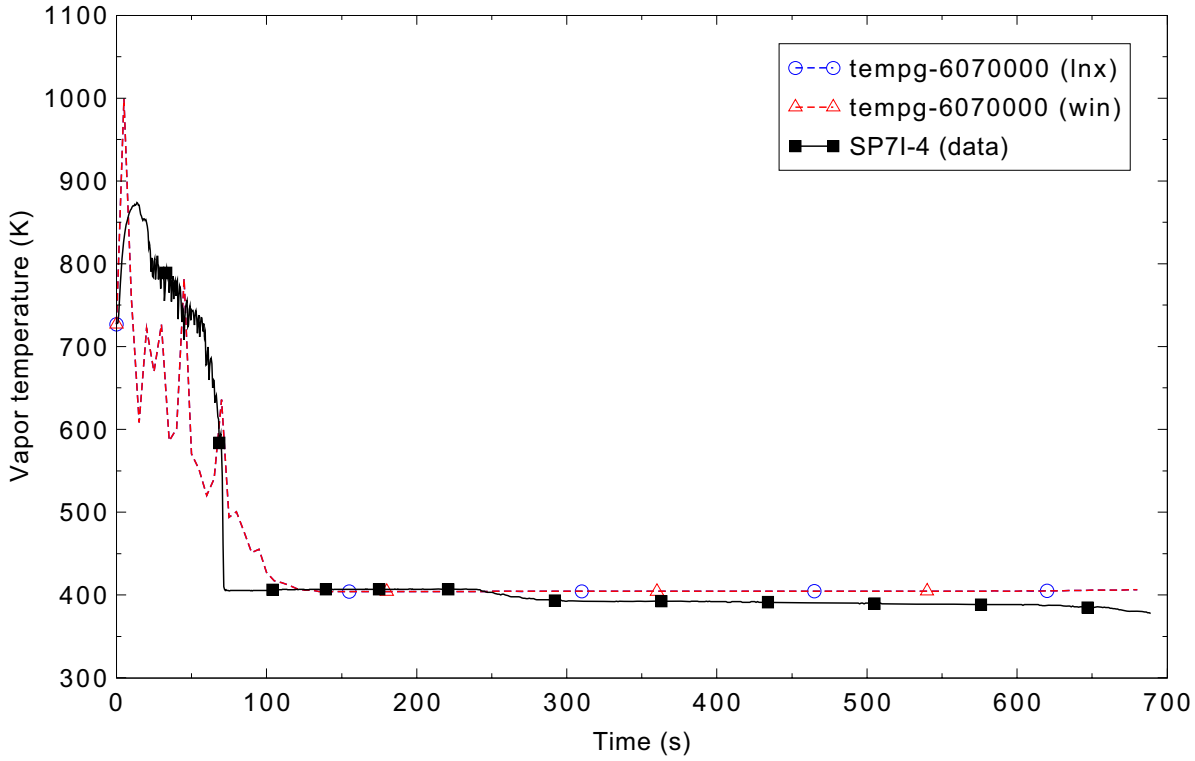

Figure 4.13-11. Measured and calculated steam temperatures for FLECHT SEASET forced reflood Test 31504 at the 1.23-m (4-ft) elevation.

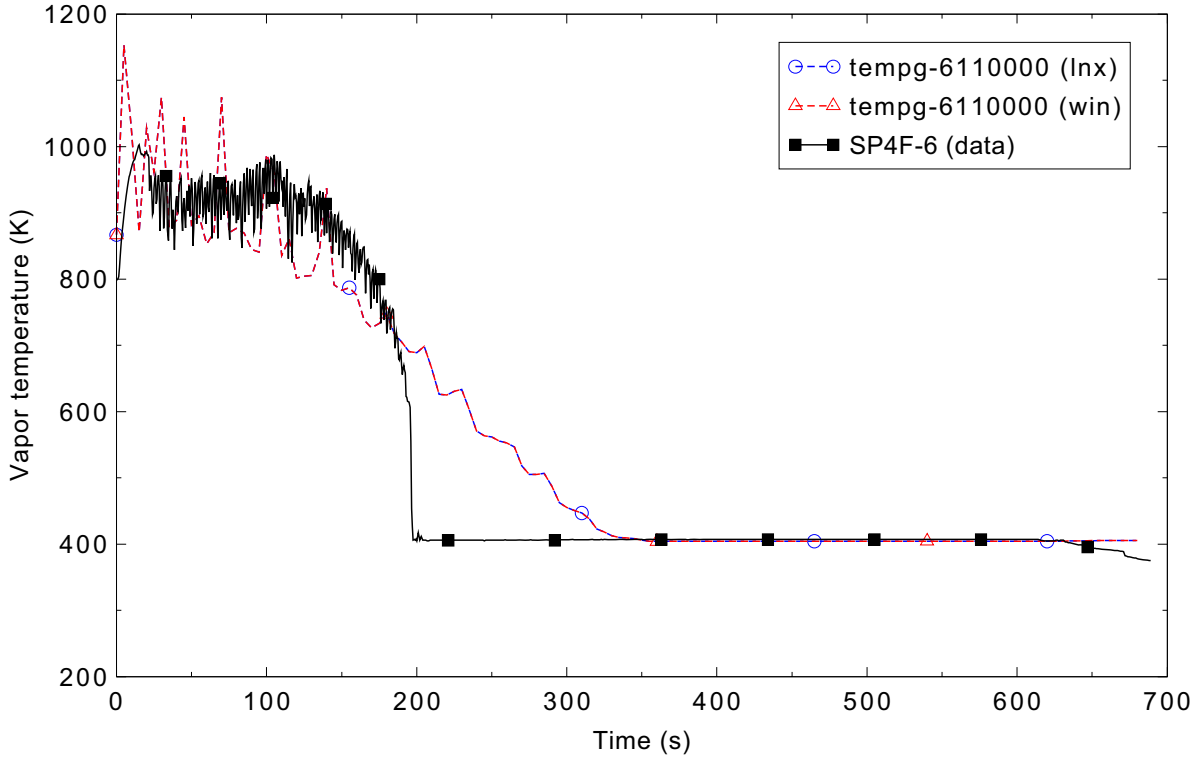

Figure 4.13-12. Measured and calculated steam temperatures for FLECHT SEASET forced reflood Test 31504 at the 1.85-m (6-ft) elevation.

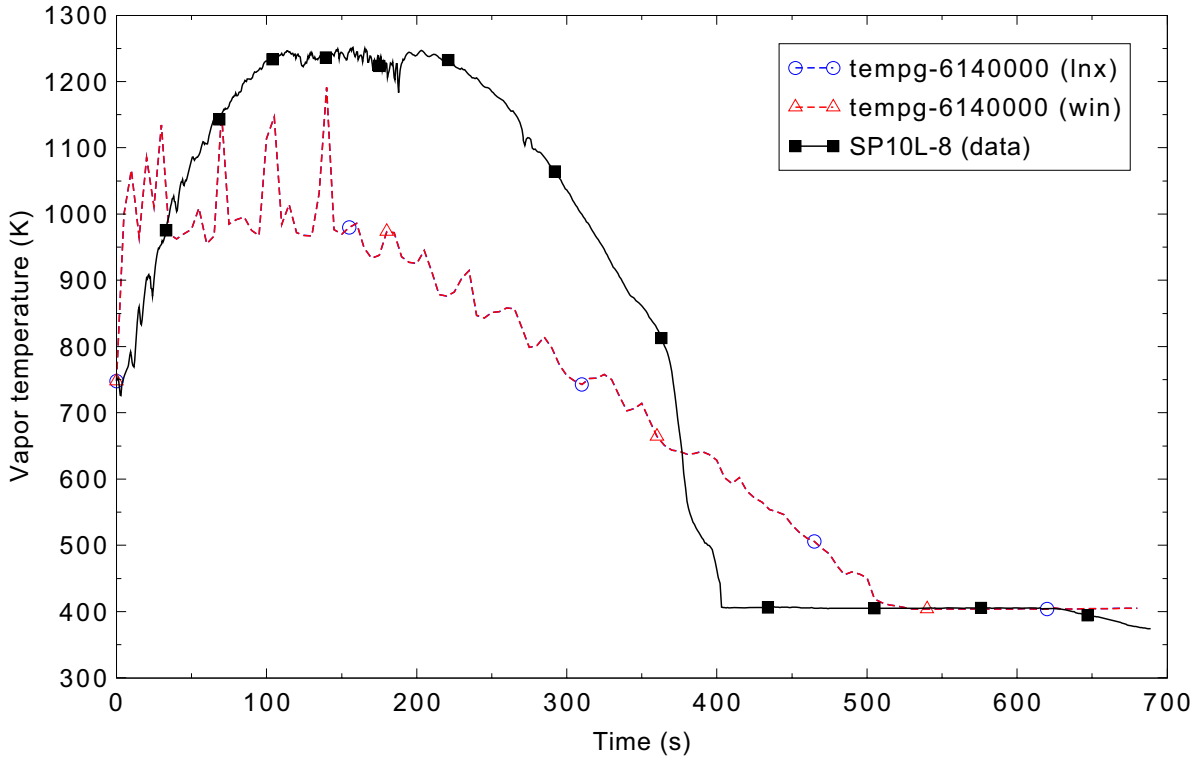

Figure 4.13-13. Measured and calculated steam temperatures for FLECHT SEASET forced reflood Test 31504 at the 2.46-m (8-ft) elevation.

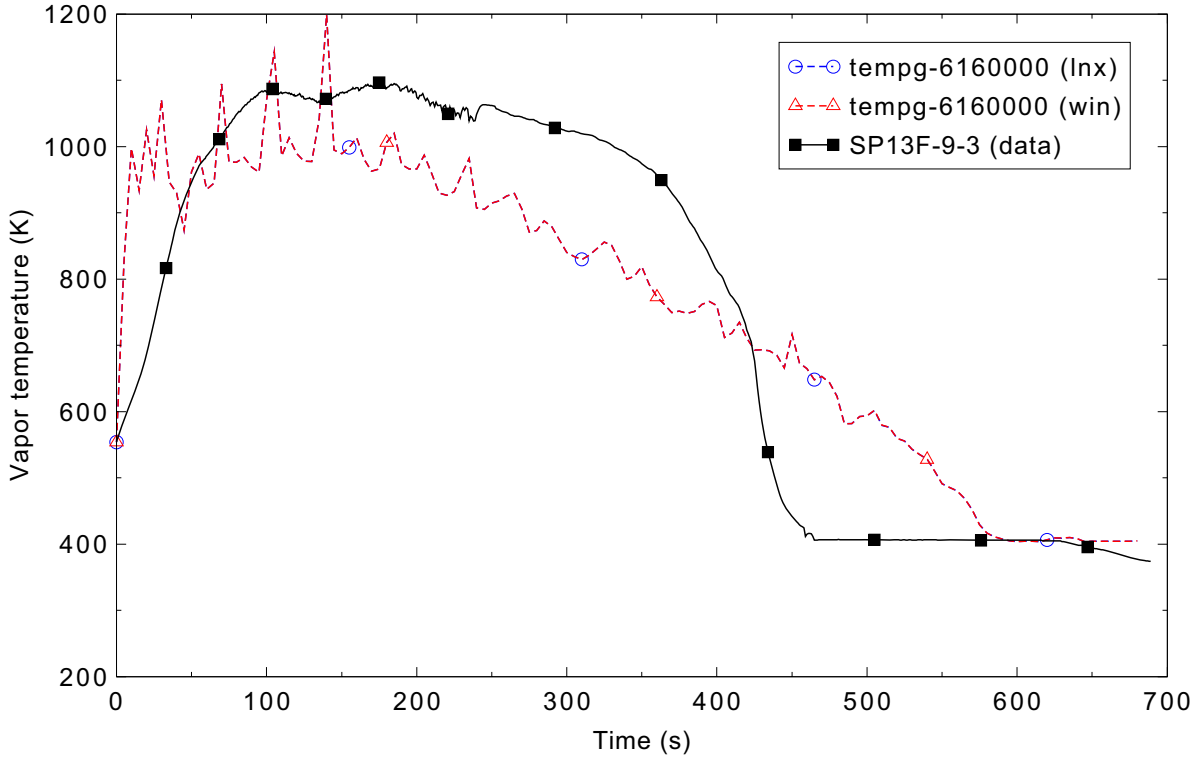

Figure 4.13-14. Measured and calculated steam temperatures for FLECHT SEASET forced reflood Test 31504 at the 2.85-m (9.25-ft) elevation.

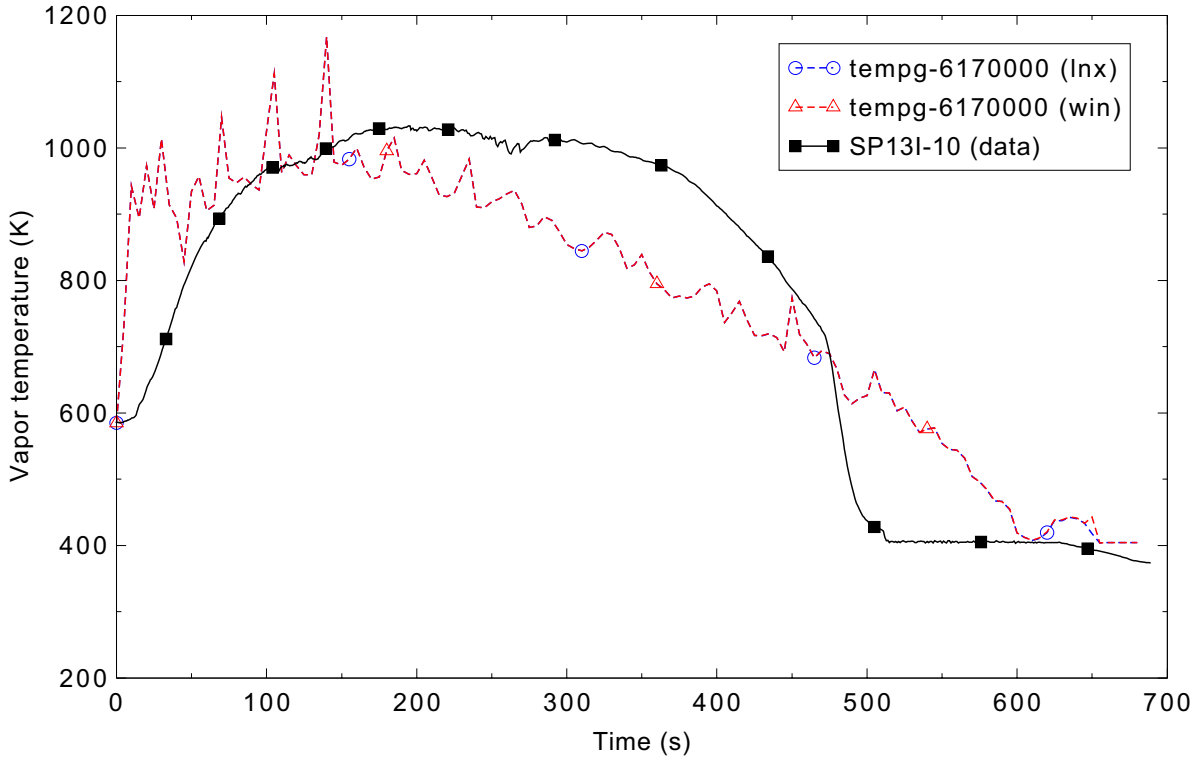

Figure 4.13-15. Measured and calculated steam temperatures for FLECHT SEASET forced reflood Test 31504 at the 3.08-m (10-ft) elevation.

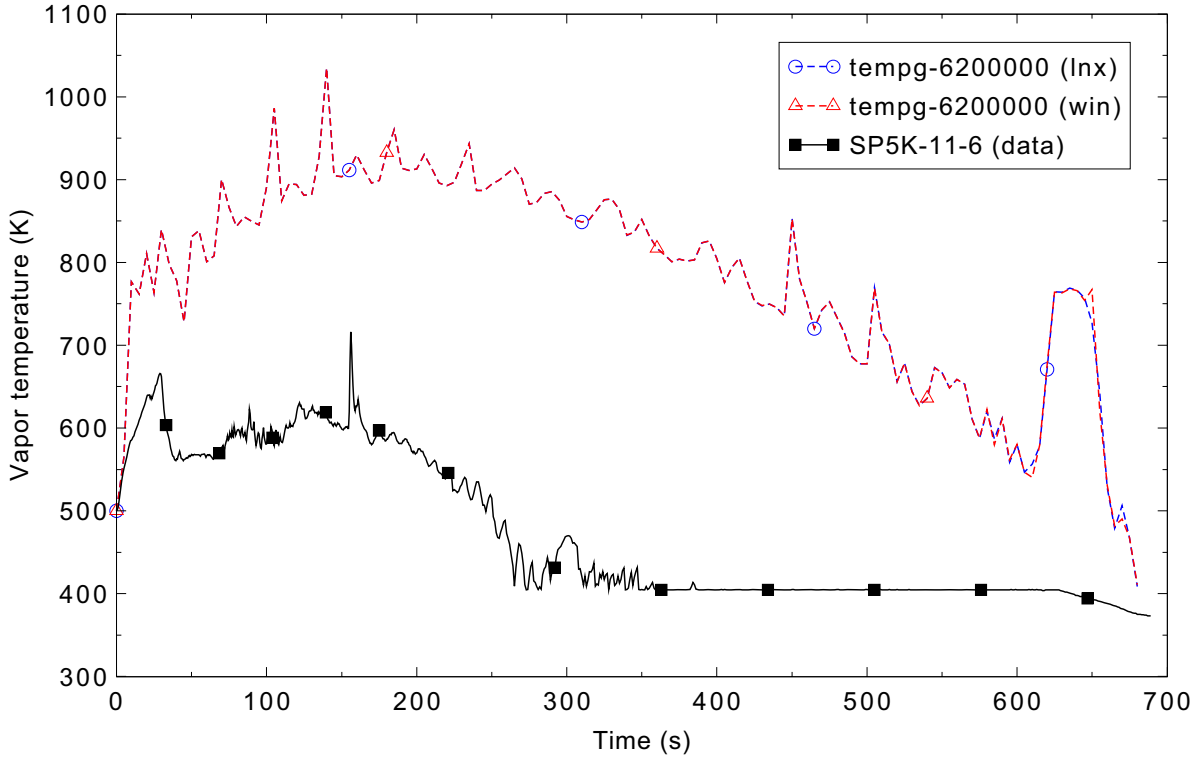

Figure 4.13-16. Measured and calculated steam temperatures for FLECHT SEASET forced reflood Test 31504 at the 3.54-m (11.5-ft) elevation.

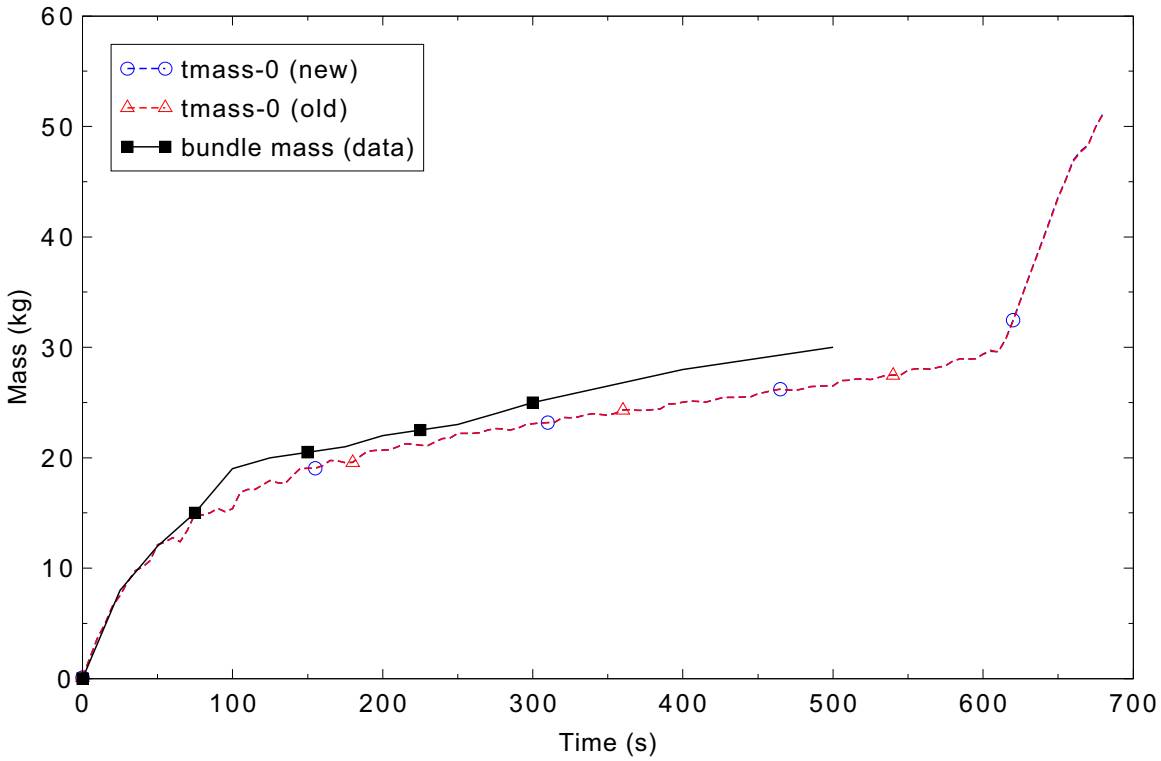

Figure 4.13-17. Measured and calculated total bundle mass inventory for FLECHT SEASET forced reflood Test 31504.

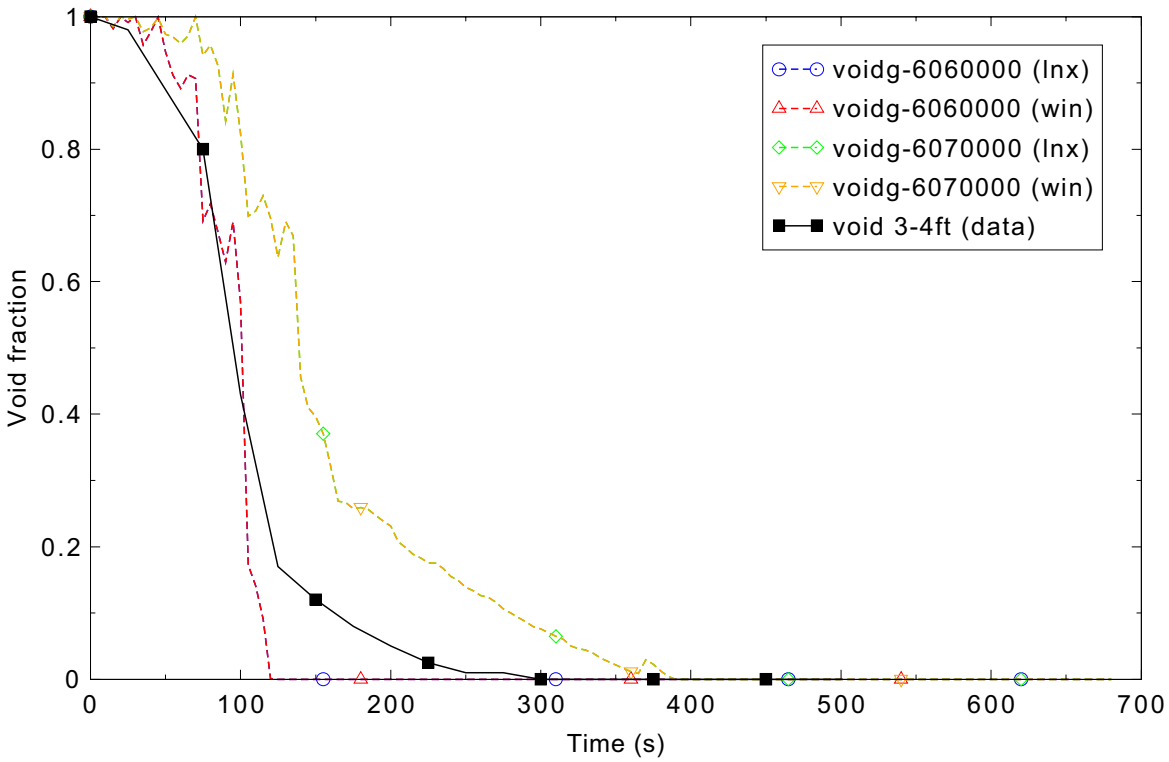

Figure 4.13-18. Measured and calculated void fractions at 0.92 to 1.23-m (3 to 4-ft) elevations for FLECHT SEASET forced reflood Test 31504.

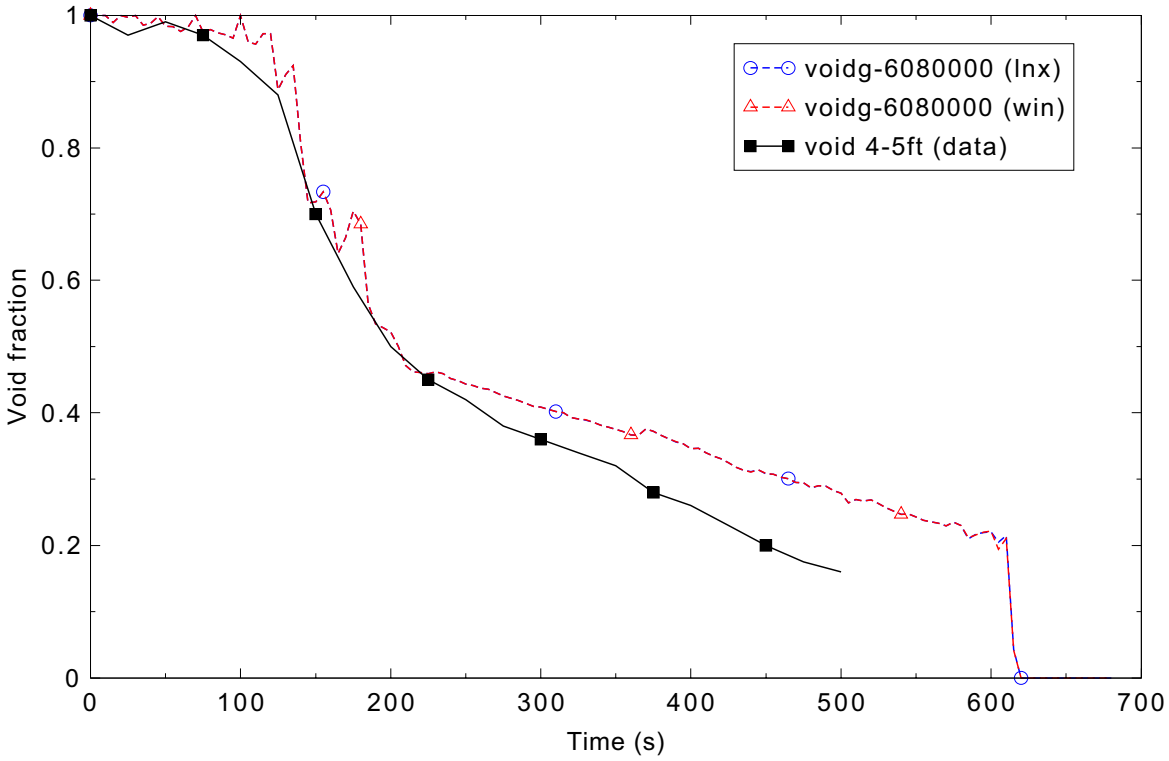

Figure 4.13-19. Measured and calculated void fractions at 1.23 to 1.54-m (4 to 5-ft) elevations for FLECHT SEASET forced reflood Test 31504.

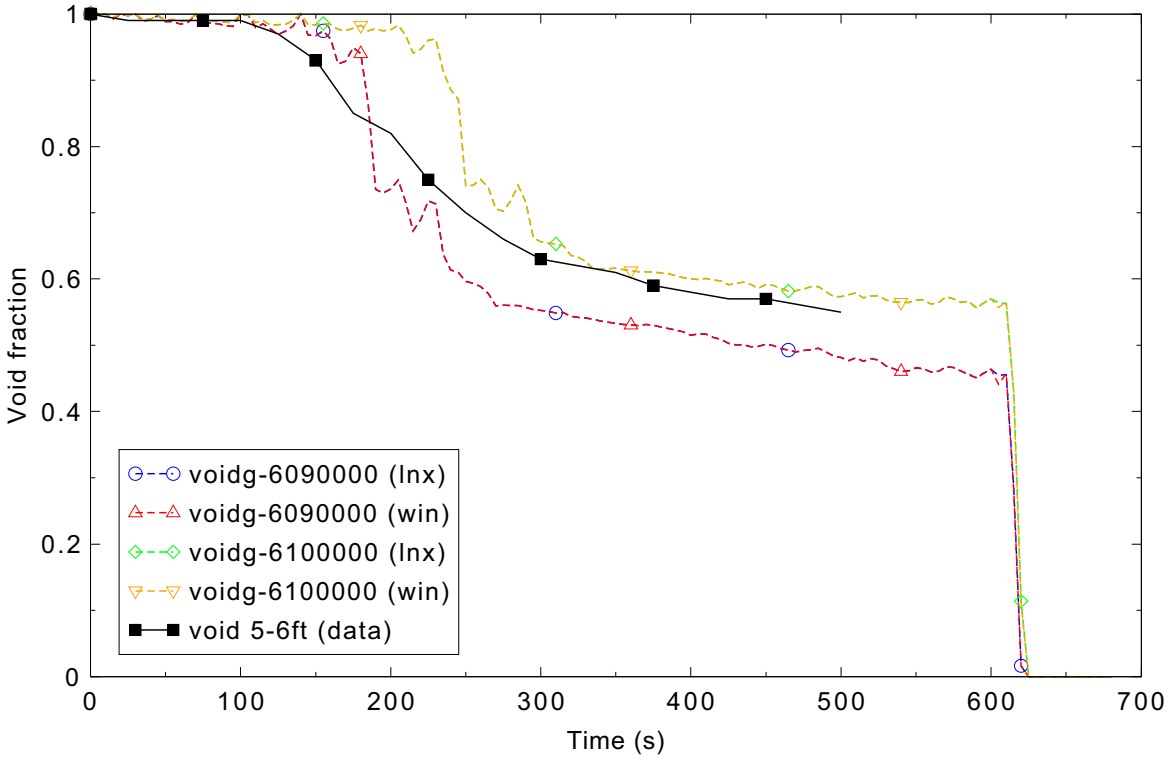

Figure 4.13-20. Measured and calculated void fractions at 1.54 to 1.85-m (5 to 6-ft) elevations for FLECHT SEASET forced reflood Test 31504.

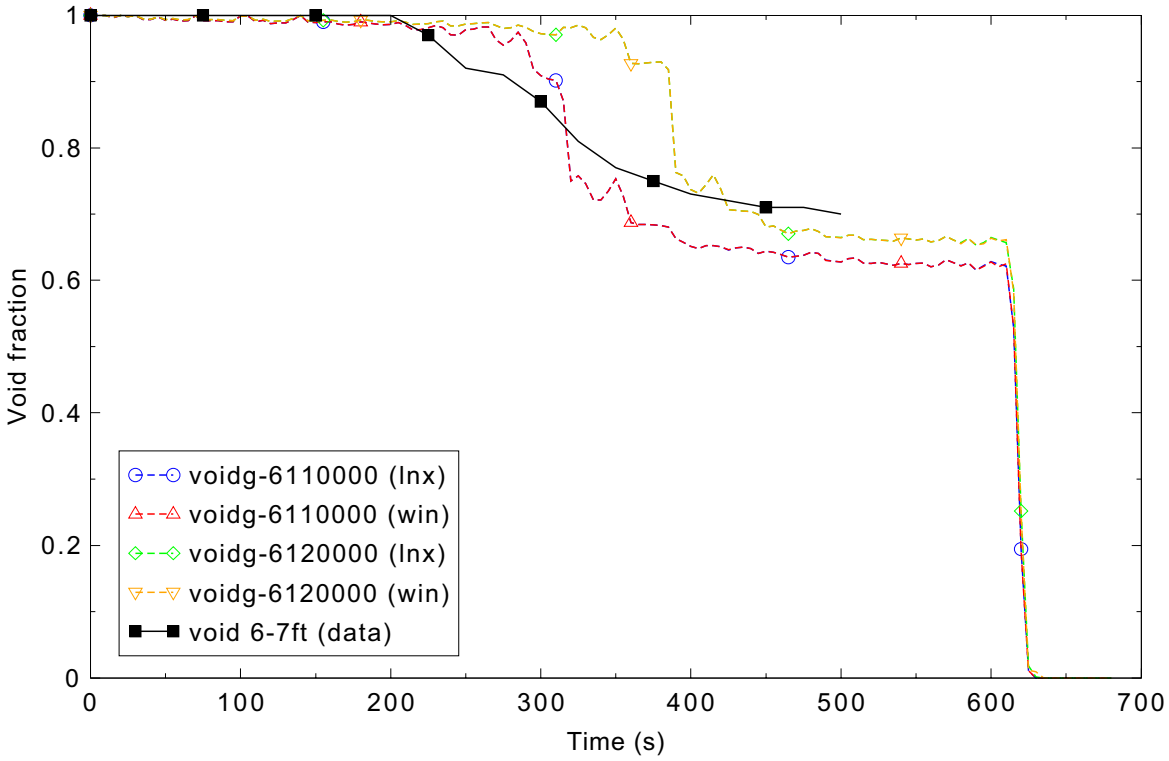

Figure 4.13-21. Measured and calculated void fractions at 1.85 to 2.15-m (6 to 7-ft) elevations for FLECHT SEASET forced reflood Test 31504.

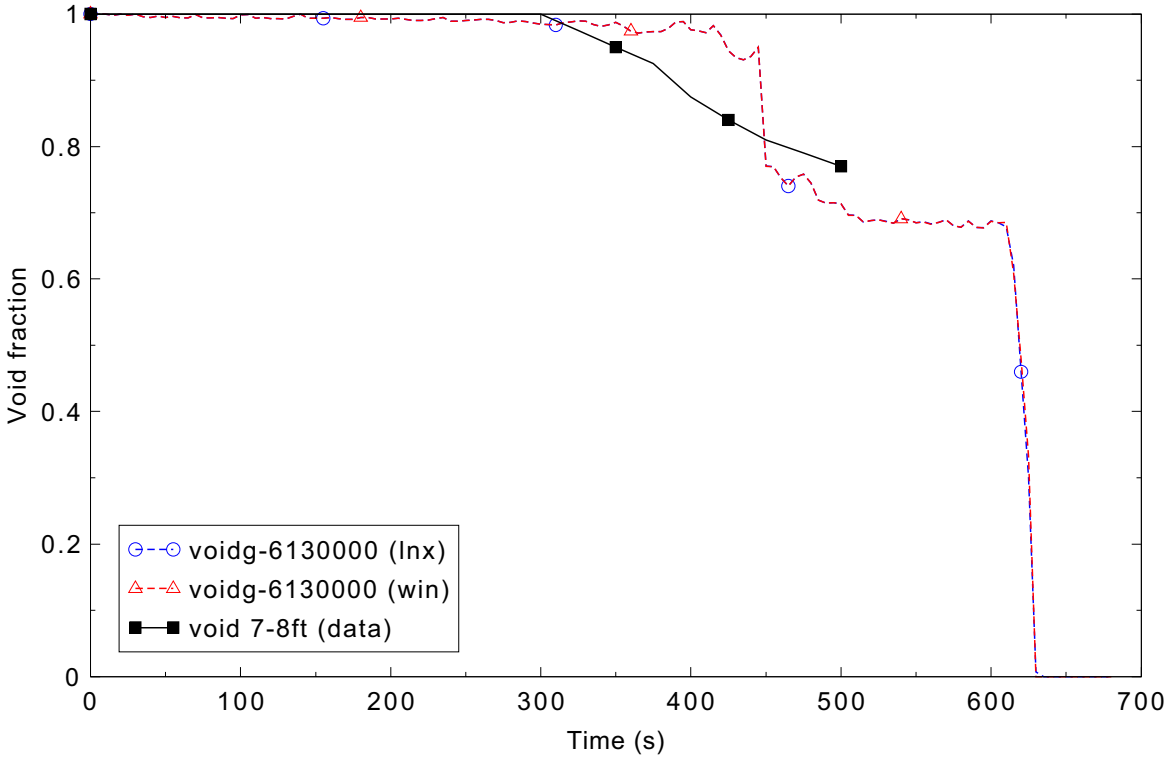

Figure 4.13-22. Measured and calculated void fractions at 2.15 to 2.46-m (7 to 8-ft) elevations for FLECHT SEASET forced reflood Test 31504.

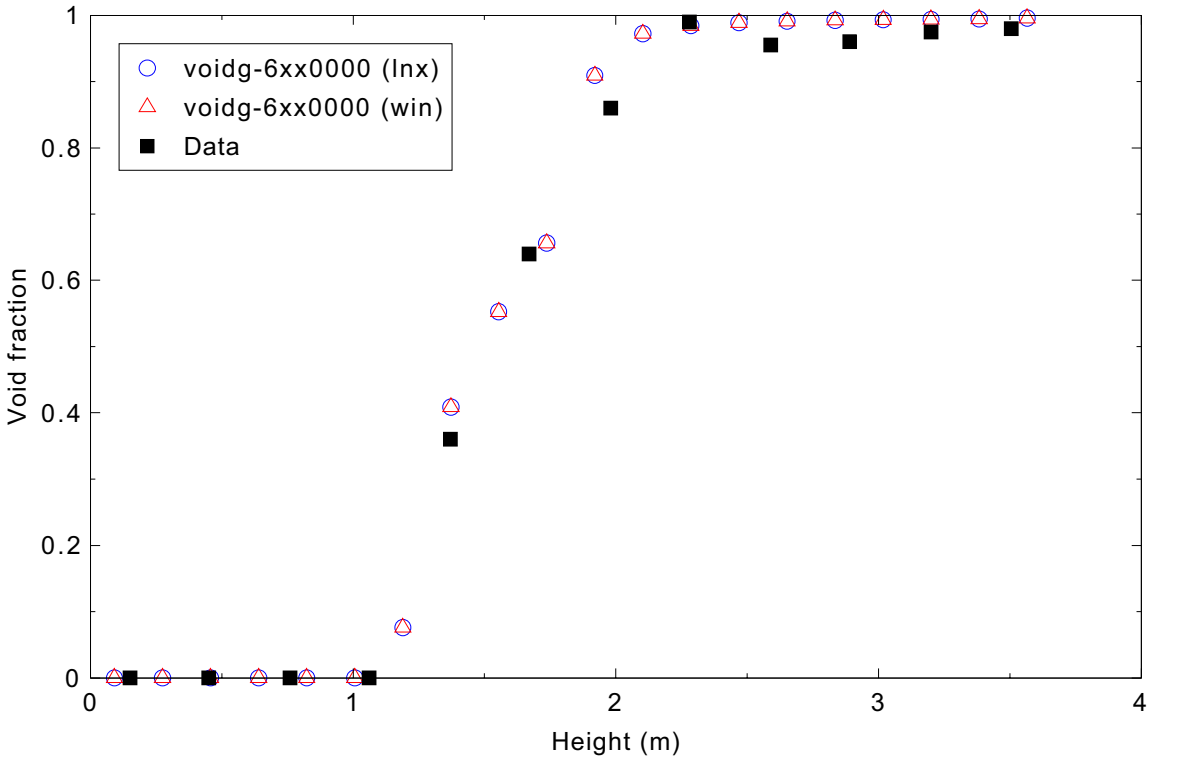

Figure 4.13-23. Measured and calculated axial void profile at 300 s for FLECHT SEASET forced reflood Test 31504.

4.14 FLECHT SEASET Test 31701

Figures comparing simulations using Linux and Windows code versions are presented. Diagrams are included so that the figure numbering is the same as that in Volume III of the RELAP5-3D code manual. Noticeable differences were observed in Figures 4.14-7, 8, 9, 10, 11, 14, 15, 16, 17, and 18.

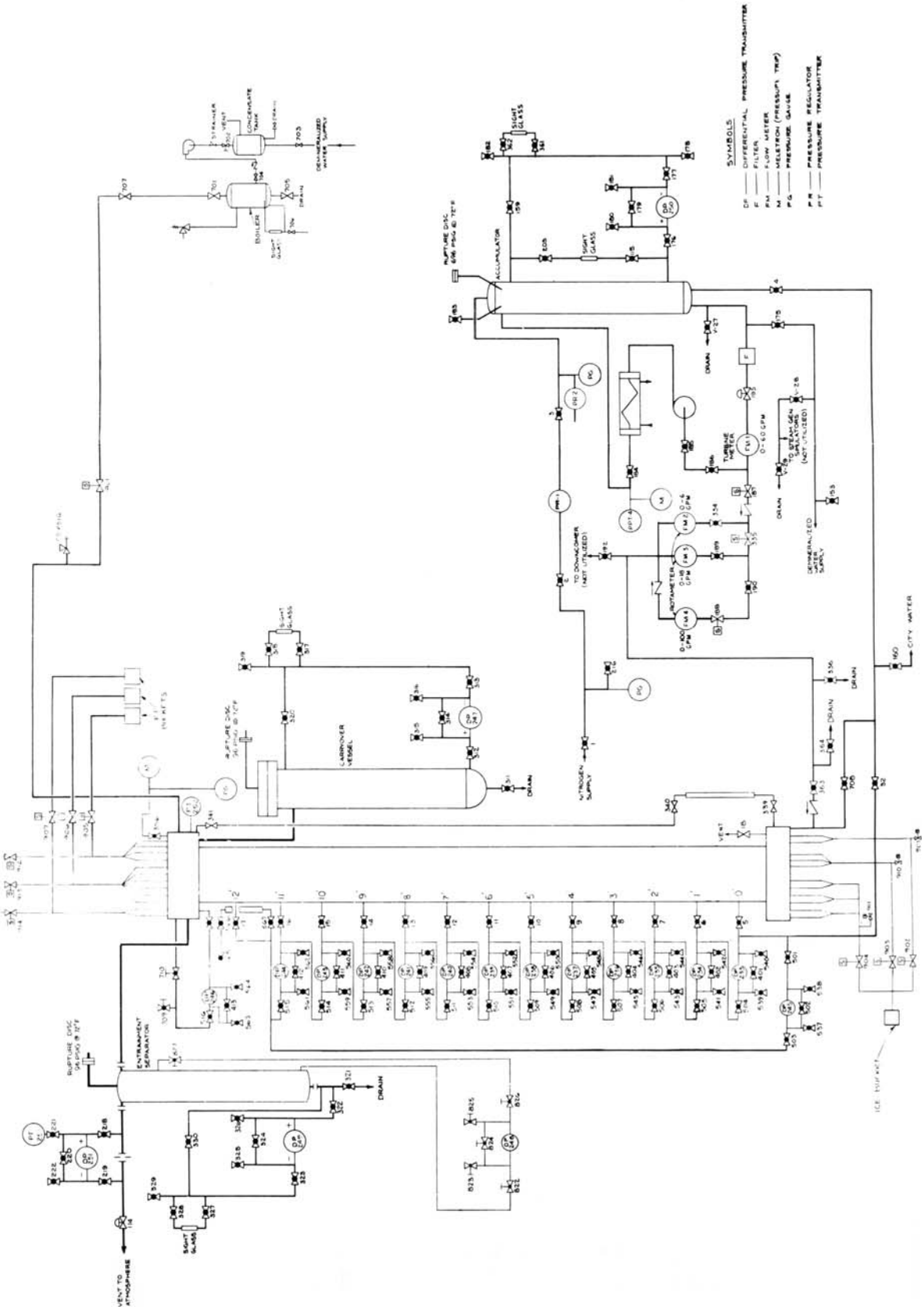

Figure 4.14-1. FLECHT SEASET unblocked bundle flow diagram for forced reflood.

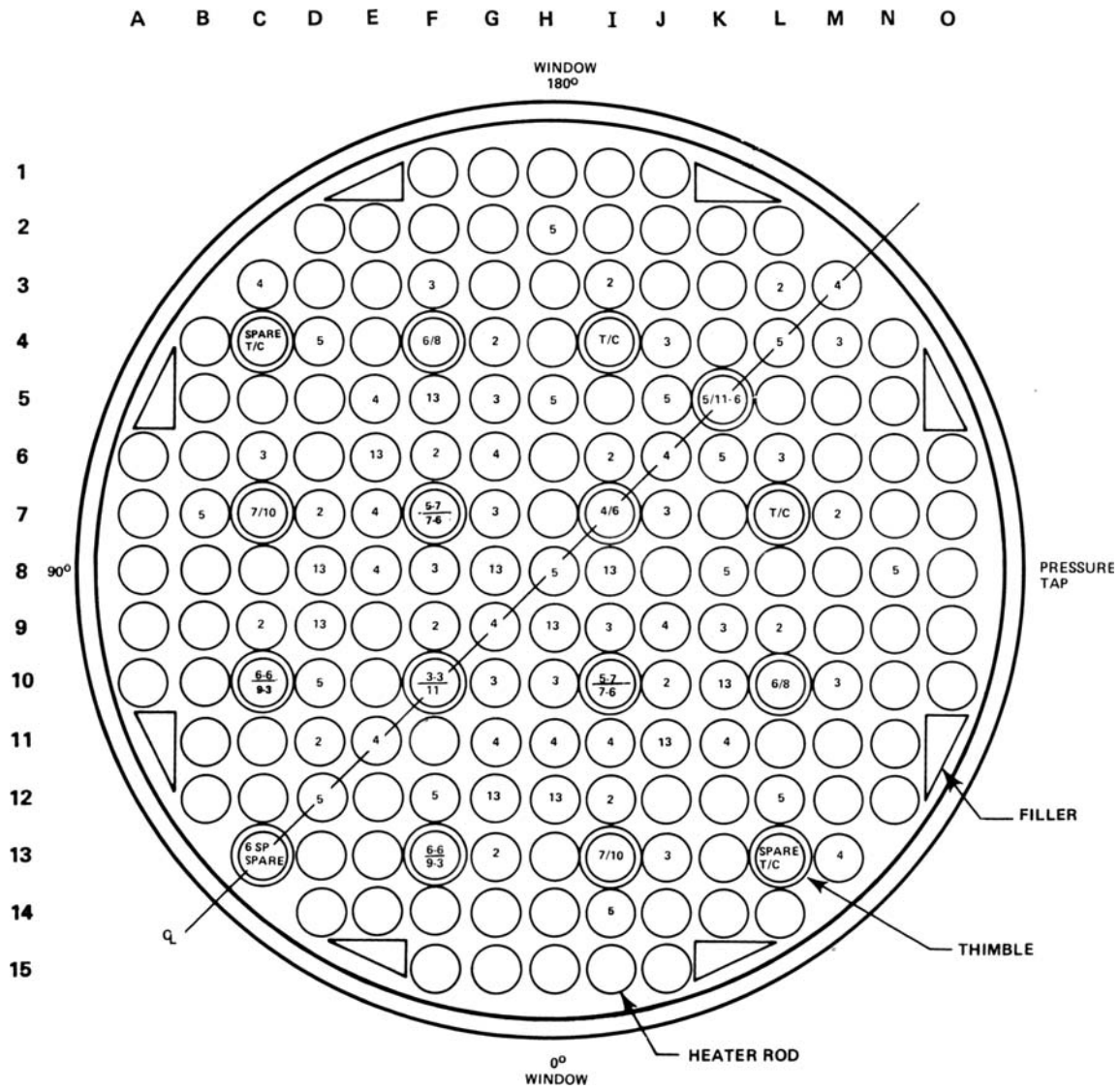

Figure 4.14-2. FLECHT SEASET bundle cross section.

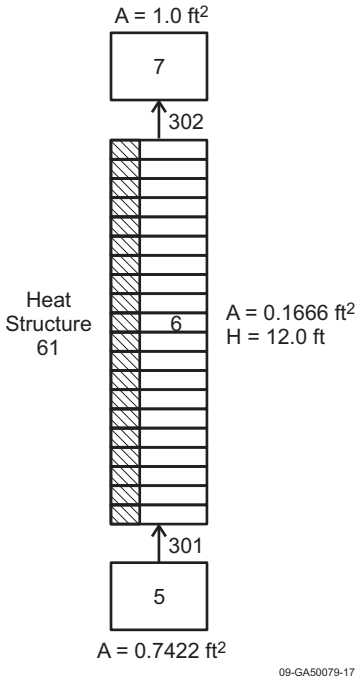

Figure 4.14-3. RELAP5-3D nodalization for the FLECHT SEASET forced reflood experiments.

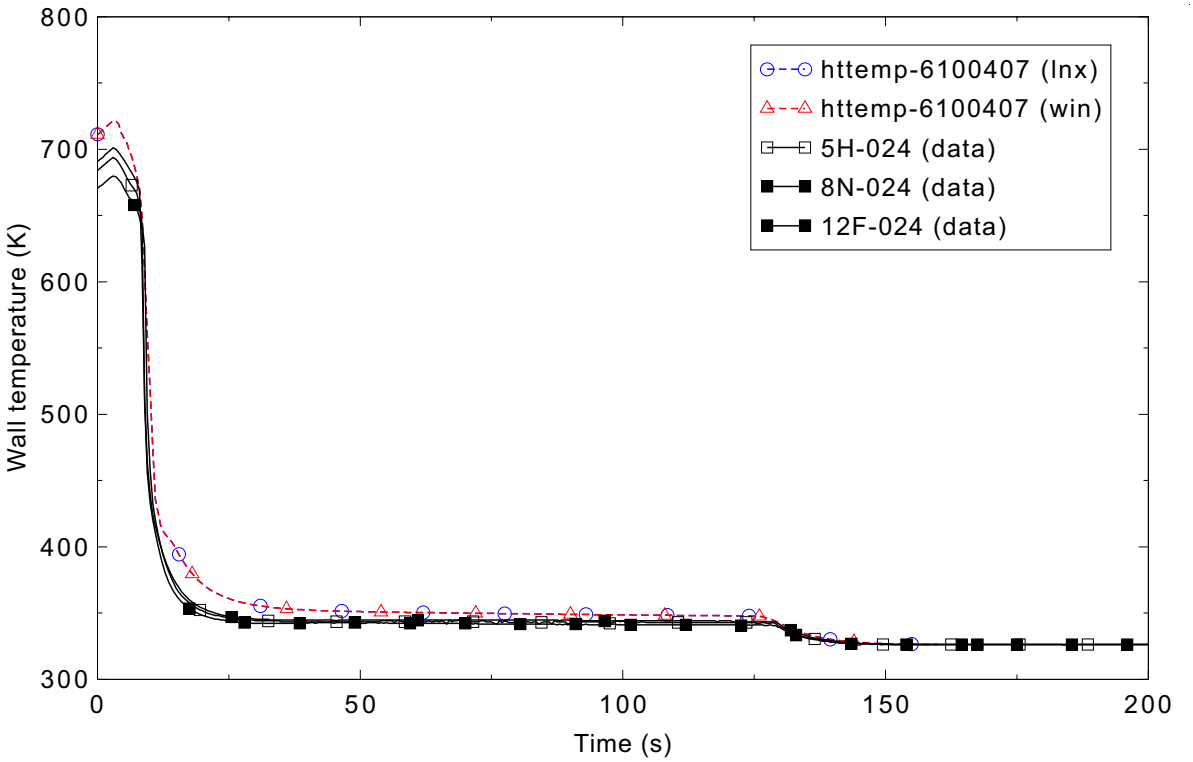

Figure 4.14-4. Measured and calculated rod surface temperatures for FLECHT SEASET forced reflood Test 31701 at the 0.62-m (24-in.) elevation.

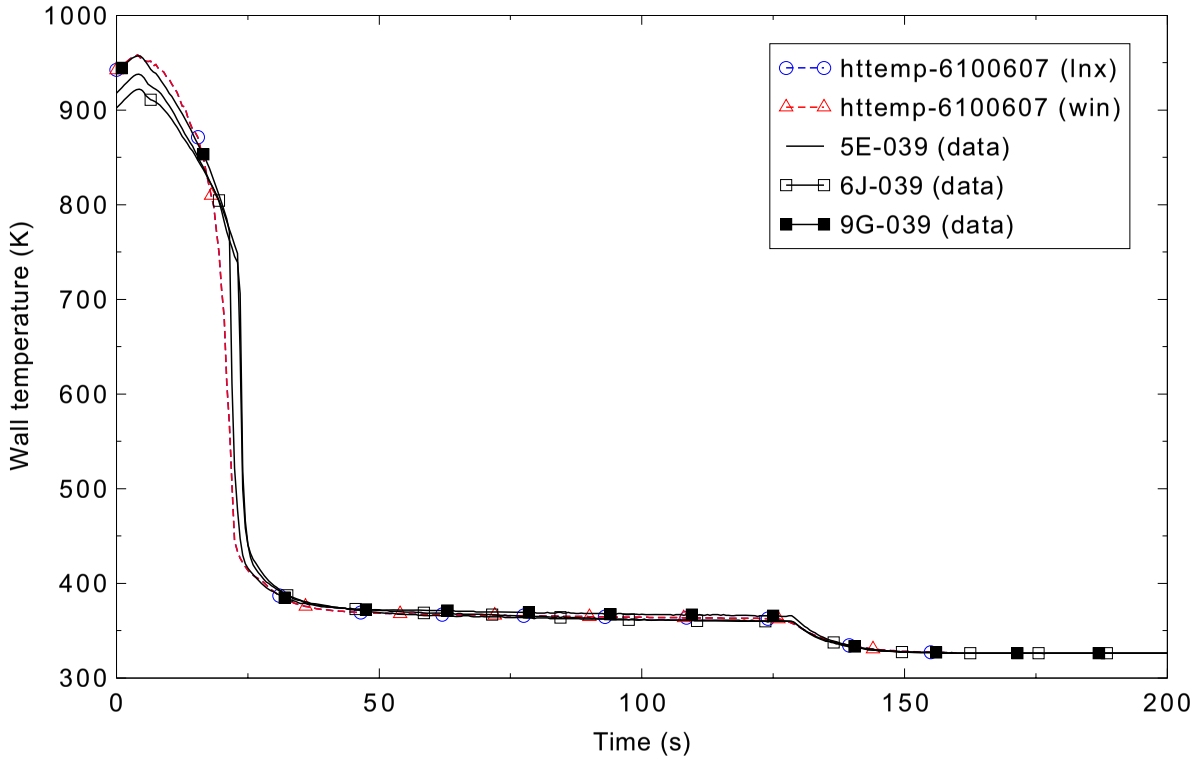

Figure 4.14-5. Measured and calculated rod surface temperatures for FLECHT SEASET forced reflood Test 31701 at the 0.99-m (39-in.) elevation.

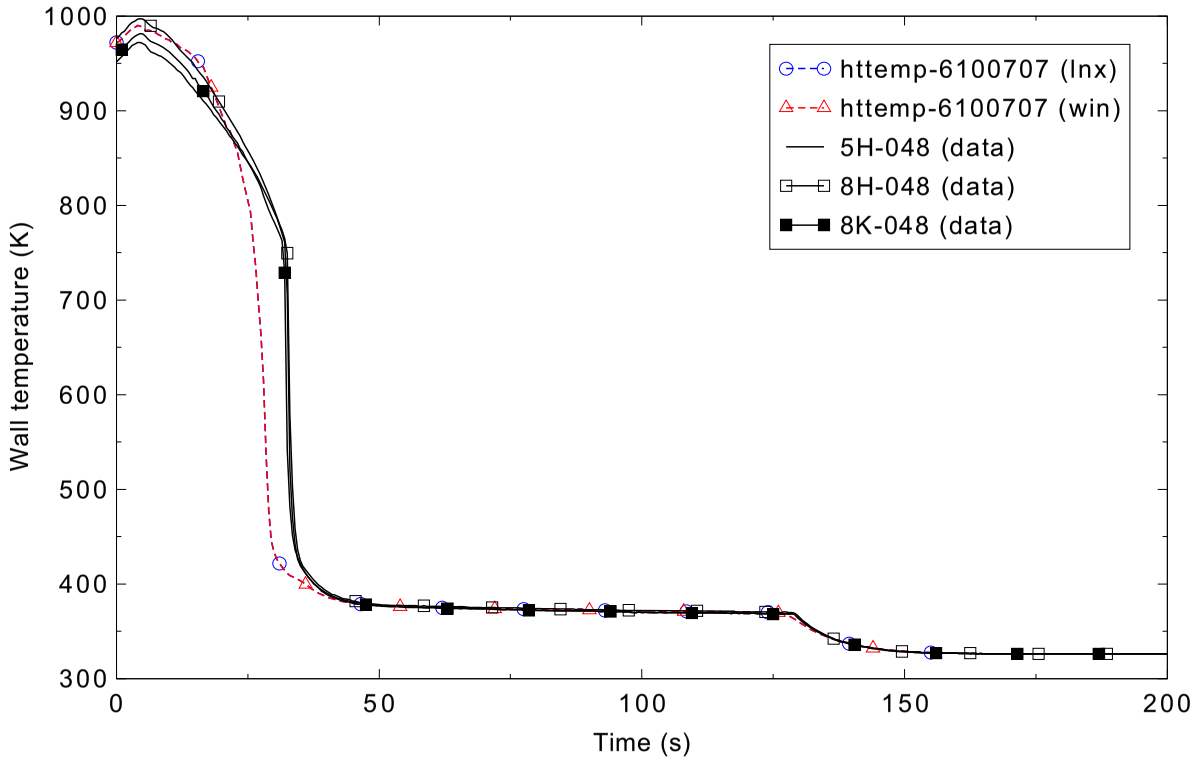

Figure 4.14-6. Measured and calculated rod surface temperatures for FLECHT SEASET forced reflood Test 31701 at the 1.22-m (48-in.) elevation.

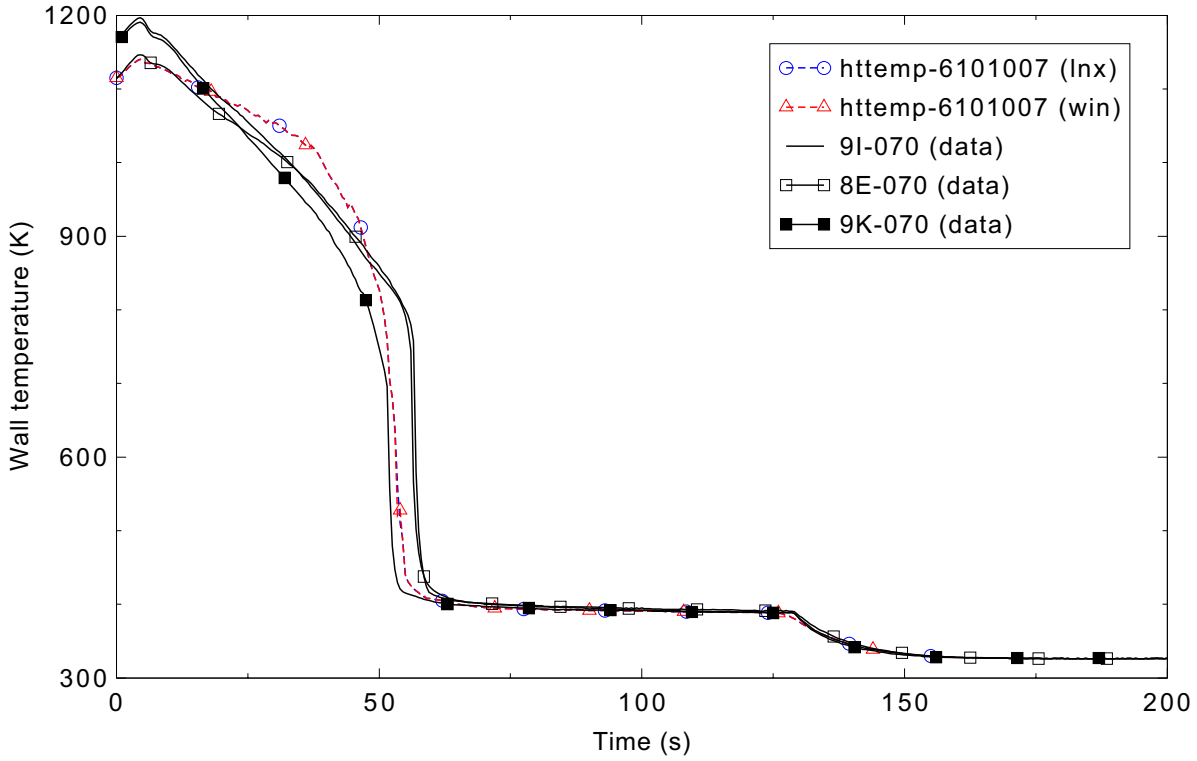

Figure 4.14-7. Measured and calculated rod surface temperatures for FLECHT SEASET forced reflood Test 31701 at the 1.78-m (70-in.) elevation.

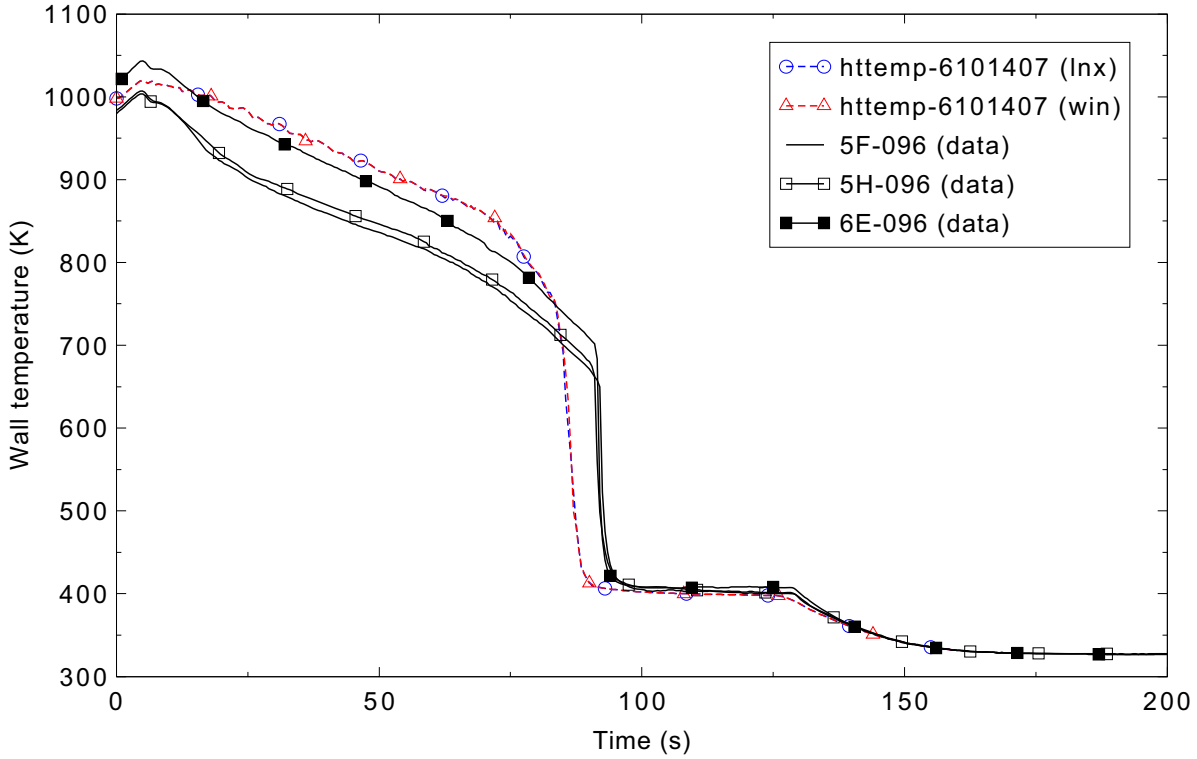

Figure 4.14-8. Measured and calculated rod surface temperatures for FLECHT SEASET forced reflood Test 31701 at the 2.46-m (96-in.) elevation.

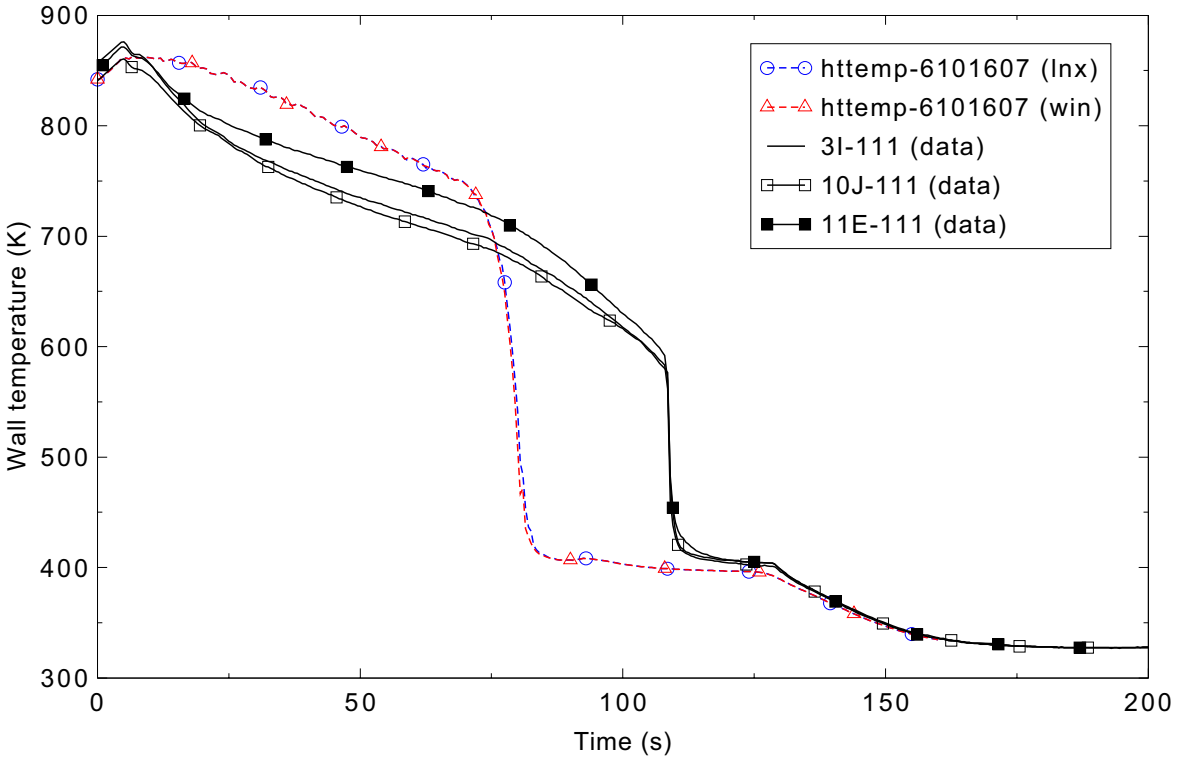

Figure 4.14-9. Measured and calculated rod surface temperatures for FLECHT SEASET forced reflood Test 31701 at the 2.85-m (111-in.) elevation.

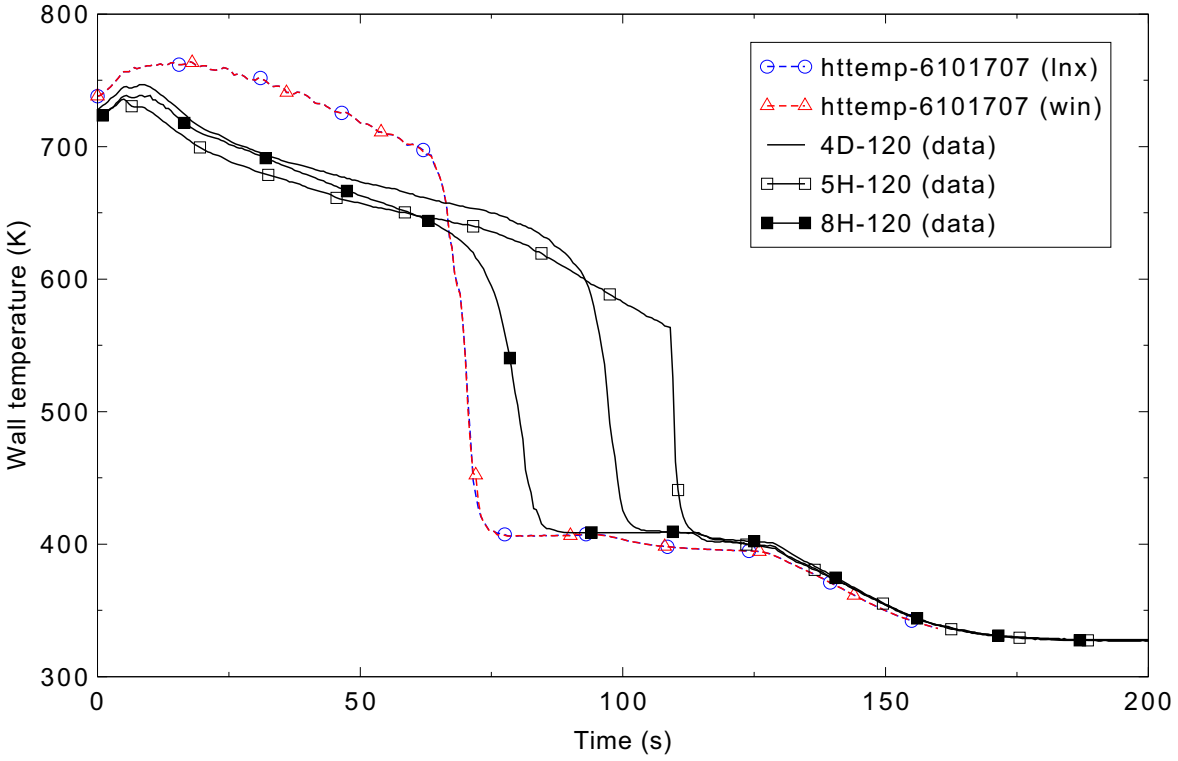

Figure 4.14-10. Measured and calculated rod surface temperatures for FLECHT SEASET forced reflood Test 31701 at the 3.08-m (120-in.) elevation.

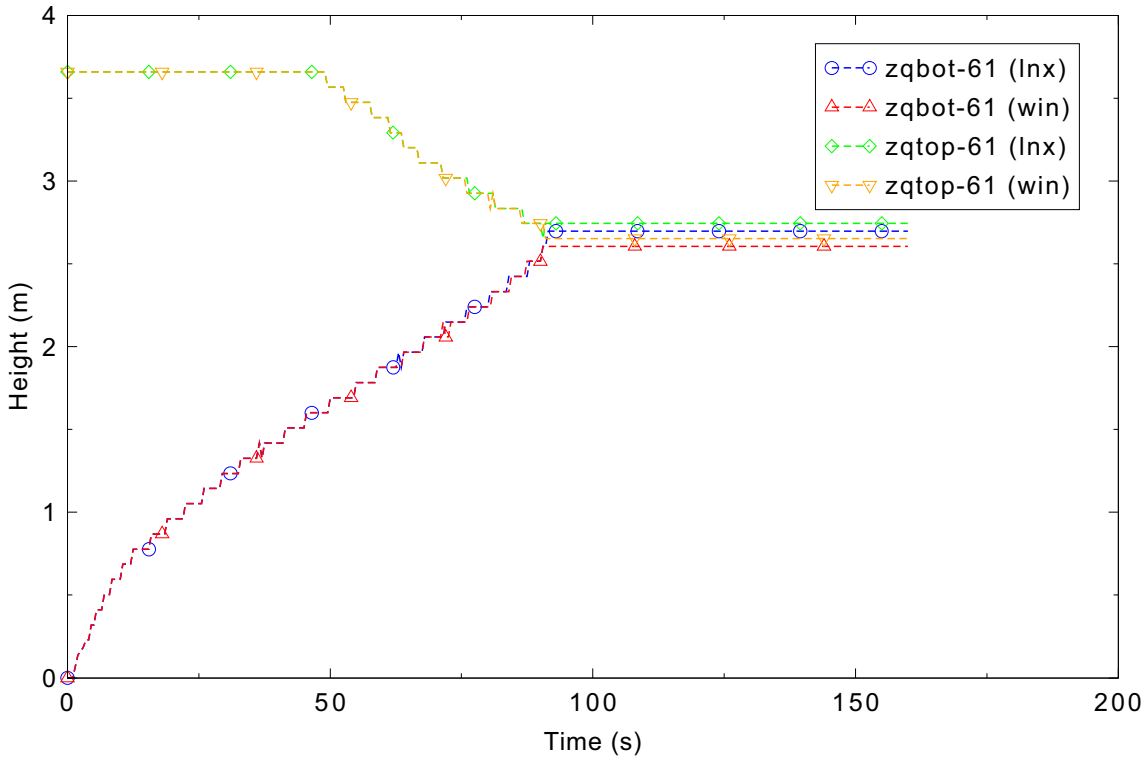

Figure 4.14-11. RELAP5-3D calculated rod bundle bottom and top quench behavior for FLECHT SEASET forced reflood Test 31701.

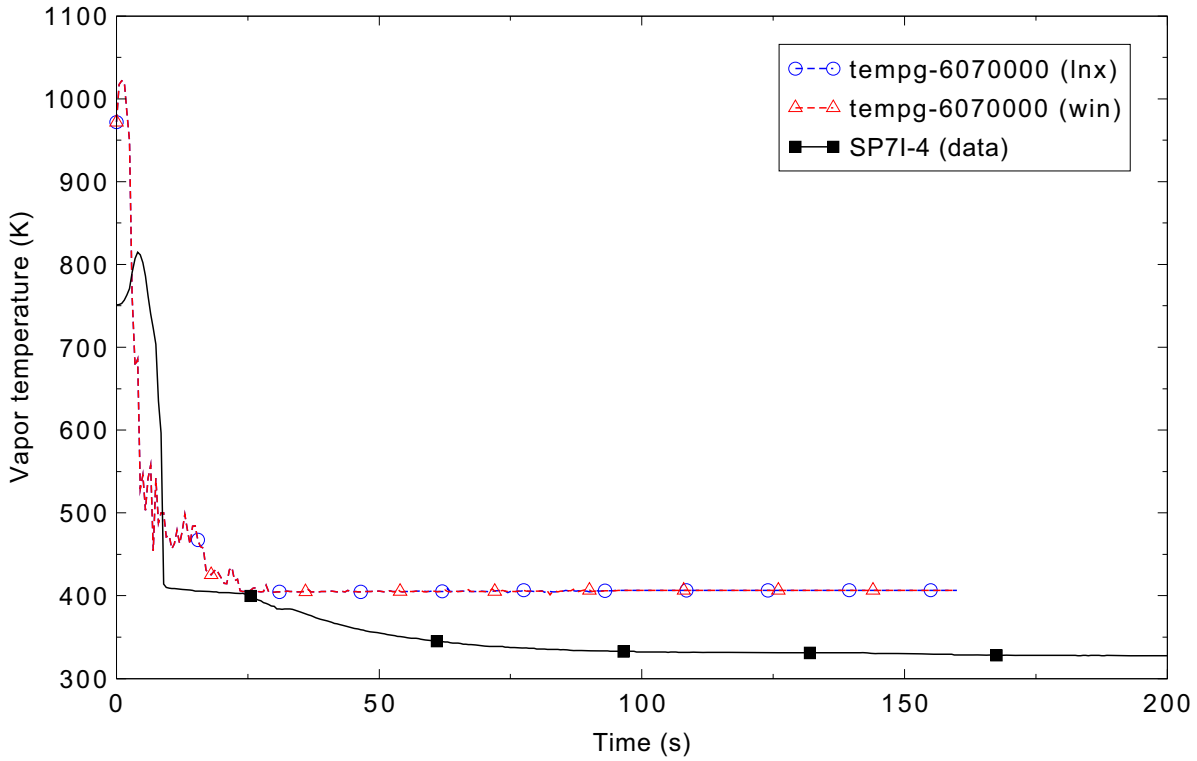

Figure 4.14-12. Measured and calculated steam temperatures for FLECHT SEASET forced reflood Test 31701 at the 1.23-m (4-ft) elevation.

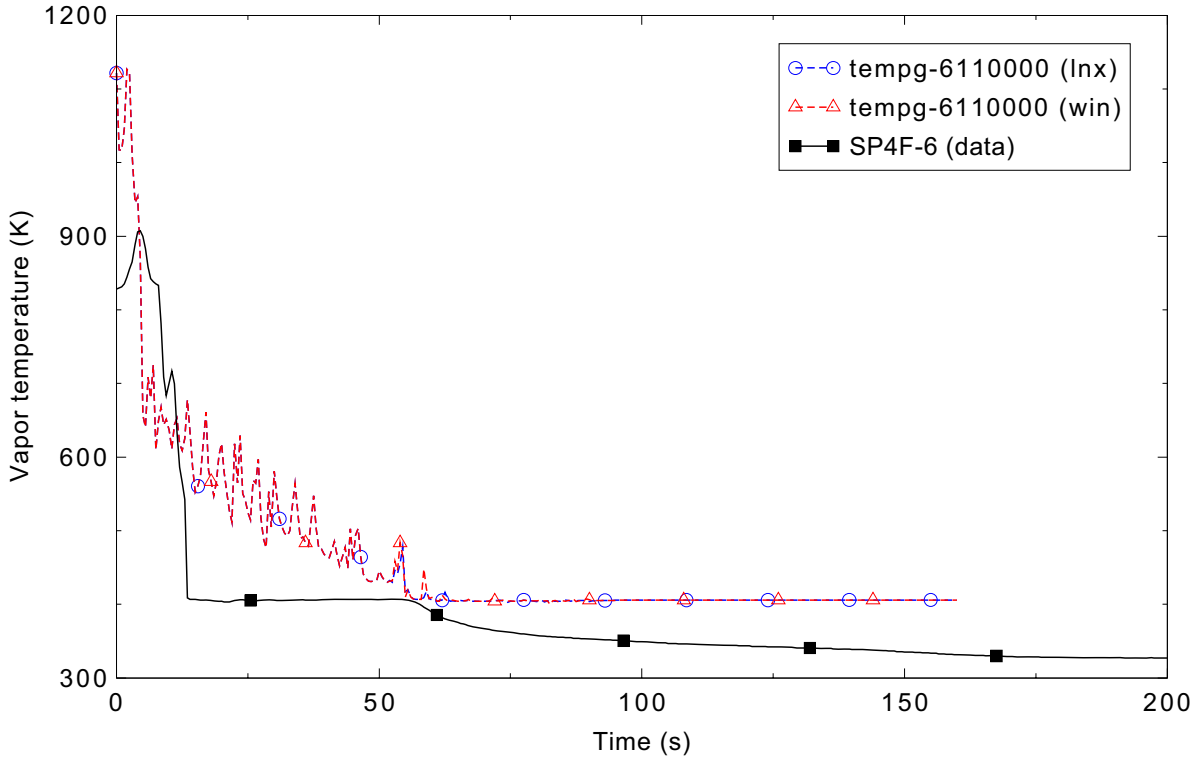

Figure 4.14-13. Measured and calculated steam temperatures for FLECHT SEASET forced reflood Test 31701 at the 1.85-m (6-ft) elevation.

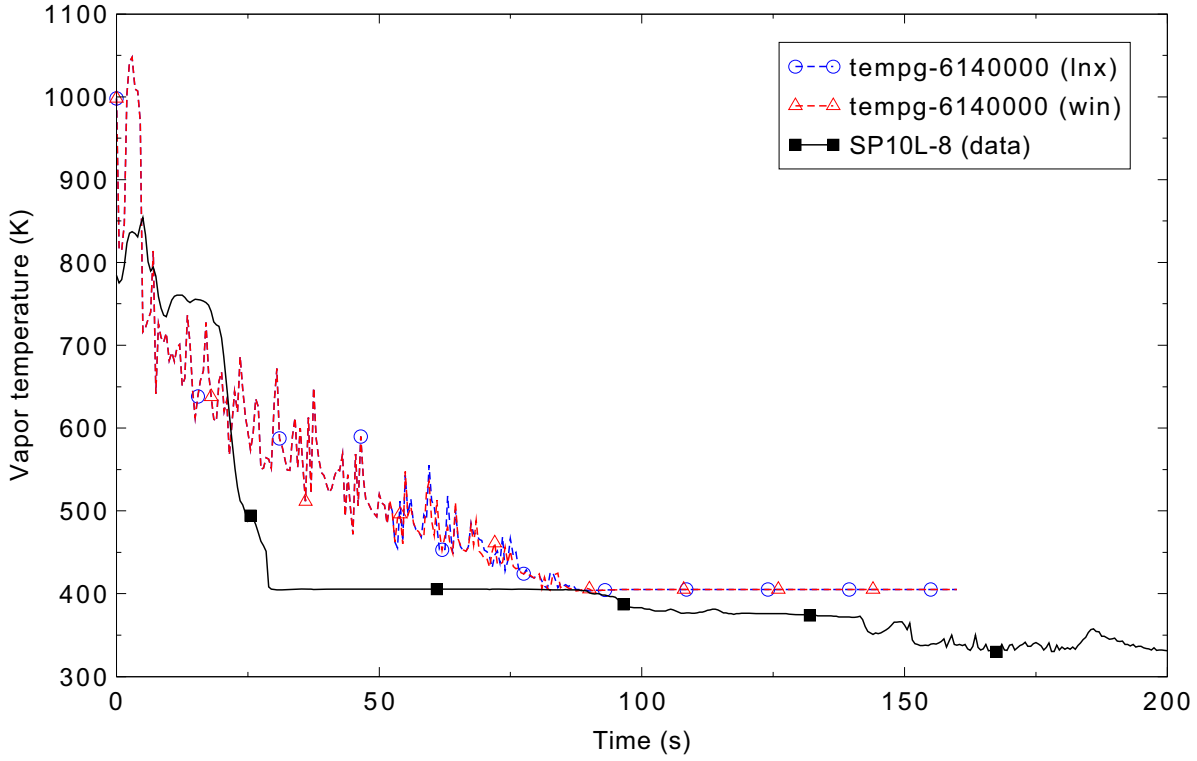

Figure 4.14-14. Measured and calculated steam temperatures for FLECHT SEASET forced reflood Test 31701 at the 2.46-m (8-ft) elevation.

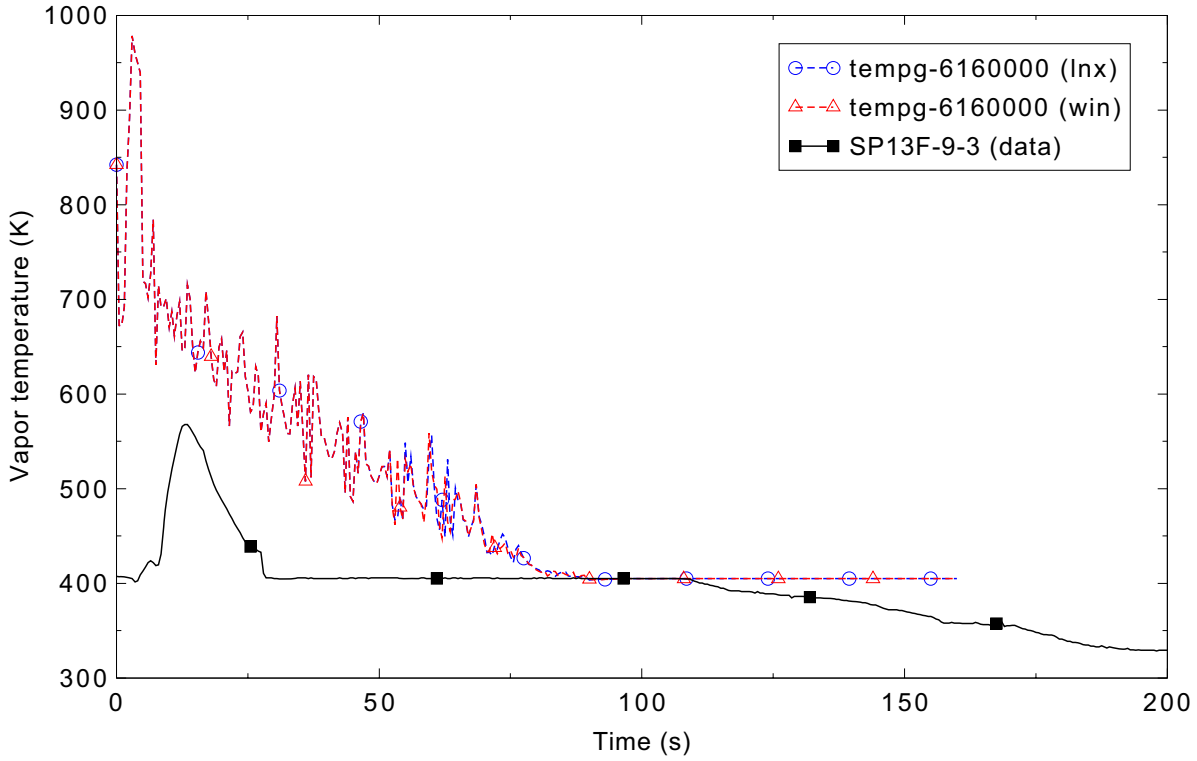

Figure 4.14-15. Measured and calculated steam temperatures for FLECHT SEASET forced reflood Test 31701 at the 2.85-m (9.25-ft) elevation.

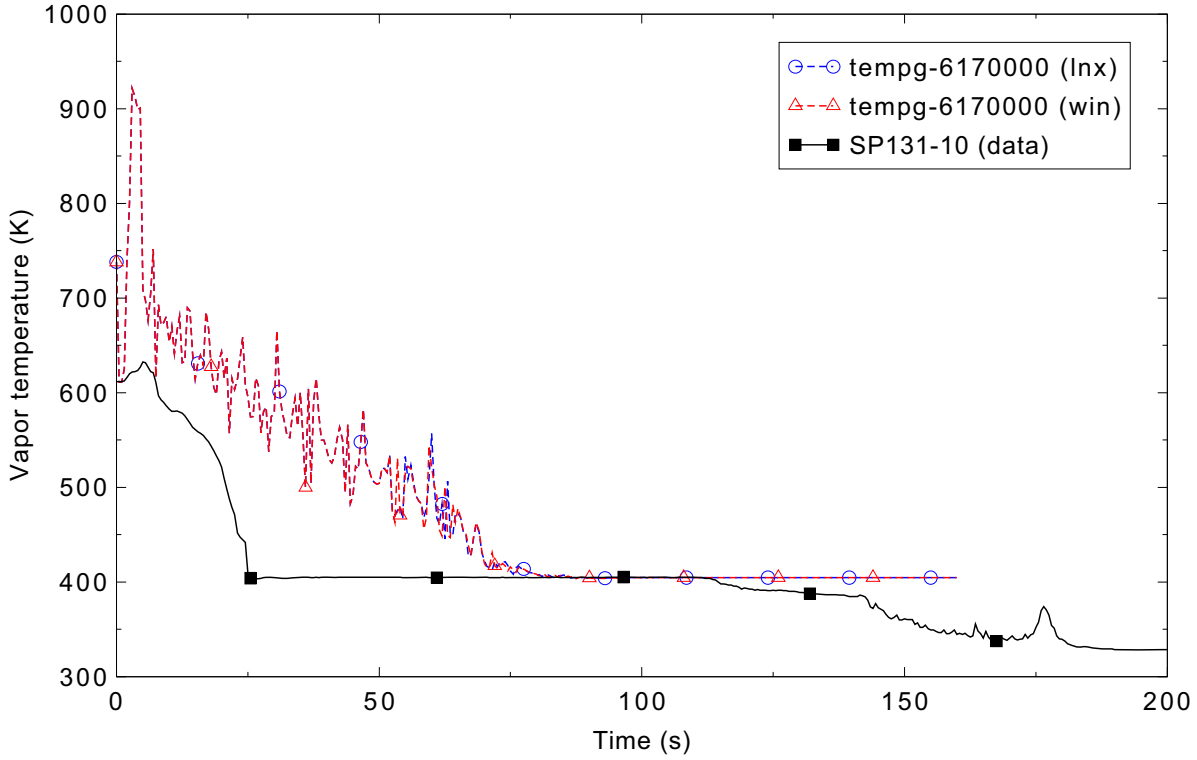

Figure 4.14-16. Measured and calculated steam temperatures for FLECHT SEASET forced reflood Test 31701 at the 3.08-m (10-ft) elevation.

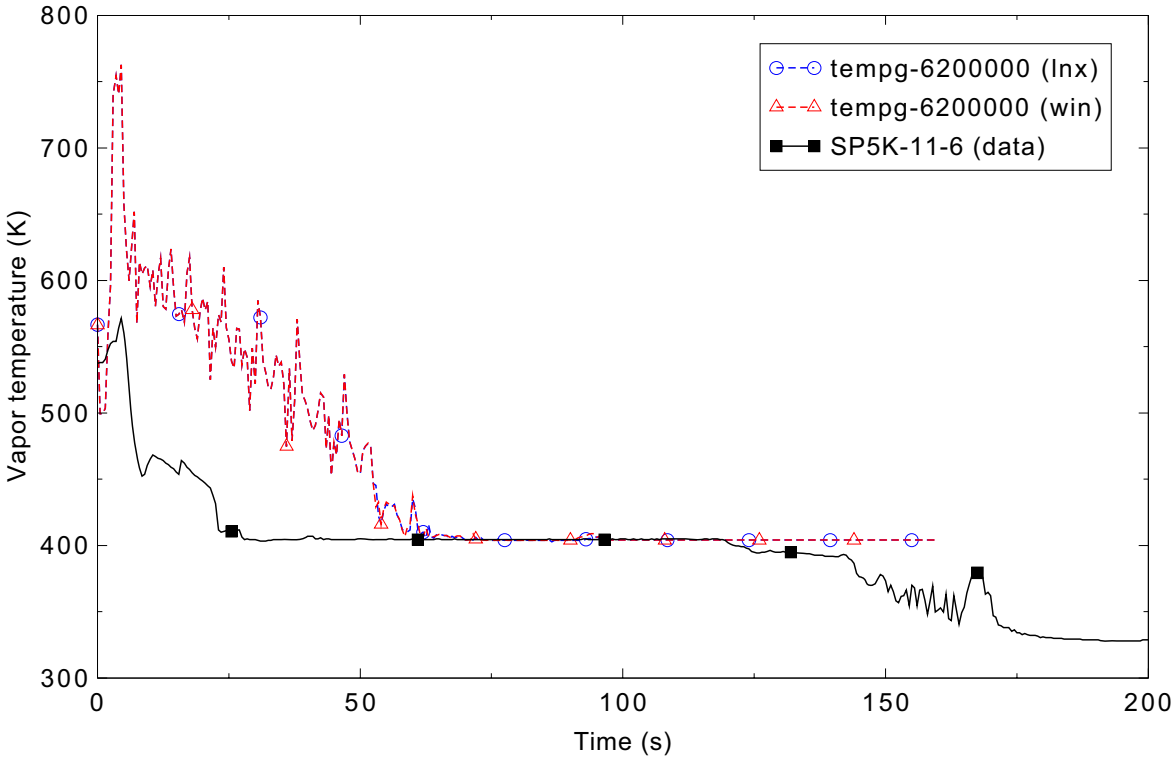

Figure 4.14-17. Measured and calculated steam temperatures for FLECHT SEASET forced reflood Test 31701 at the 3.54-m (11.5-ft) elevation.

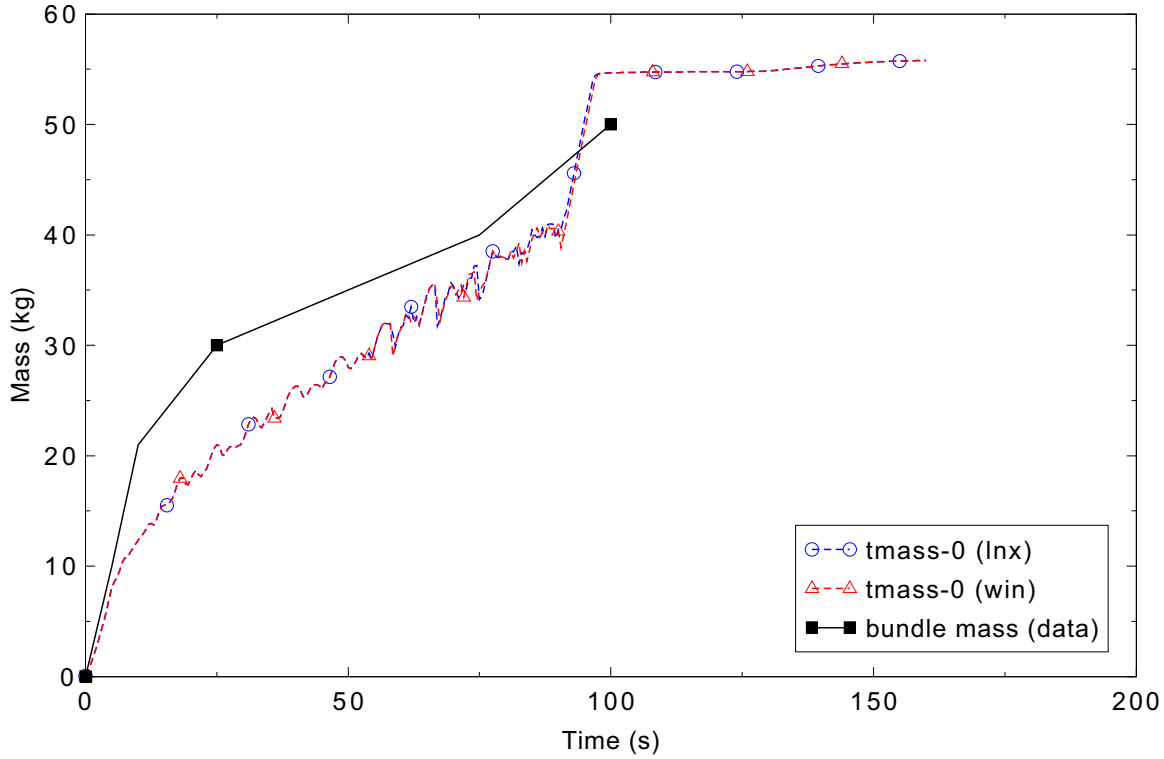

Figure 4.14-18. Measured and calculated total bundle mass inventory for FLECHT SEASET forced reflood Test 31701.

4.15 Dukler-Smith Air-Water Flooding

Figures comparing simulations using Linux and Windows code versions are presented. Diagrams are included so that the figure numbering is the same as that in Volume III of the RELAP5-3D code manual. No differences were observed in the figures.

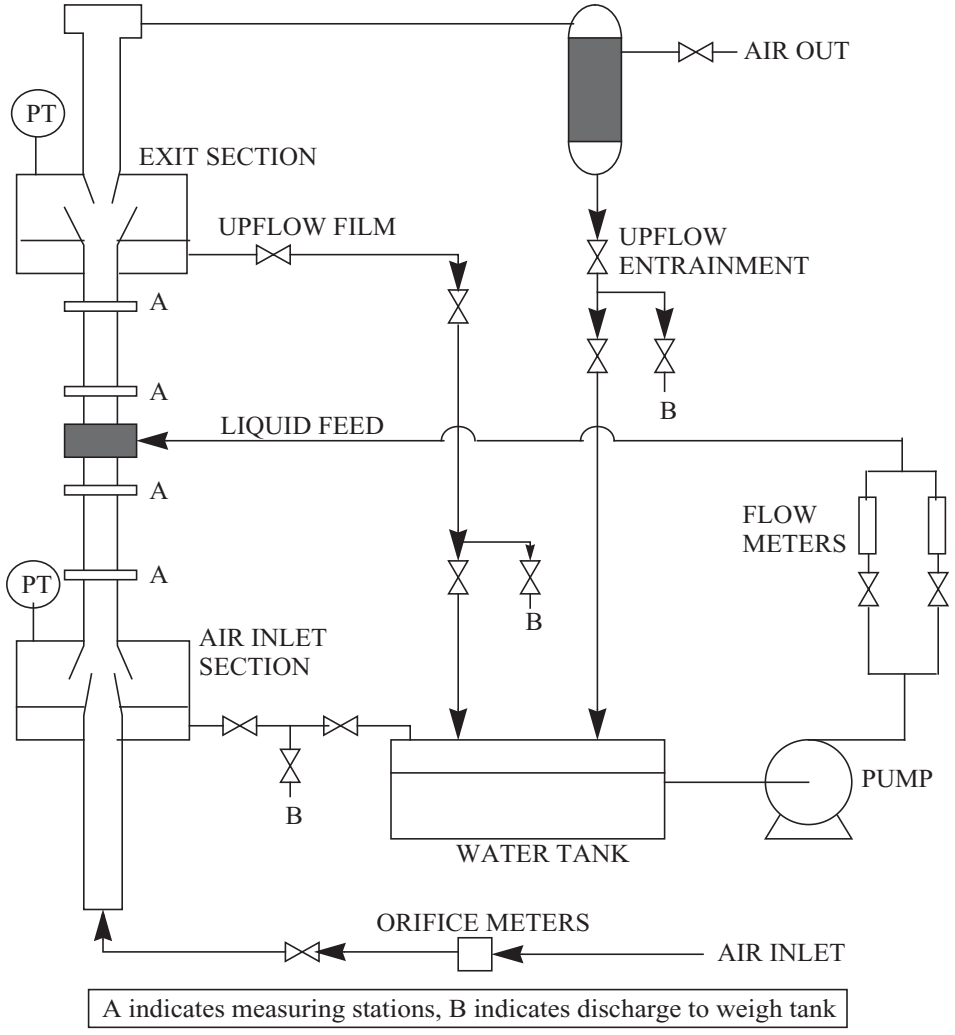

Figure 4.15-1. Schematic of the Dukler-Smith Air-Water Test Facility.

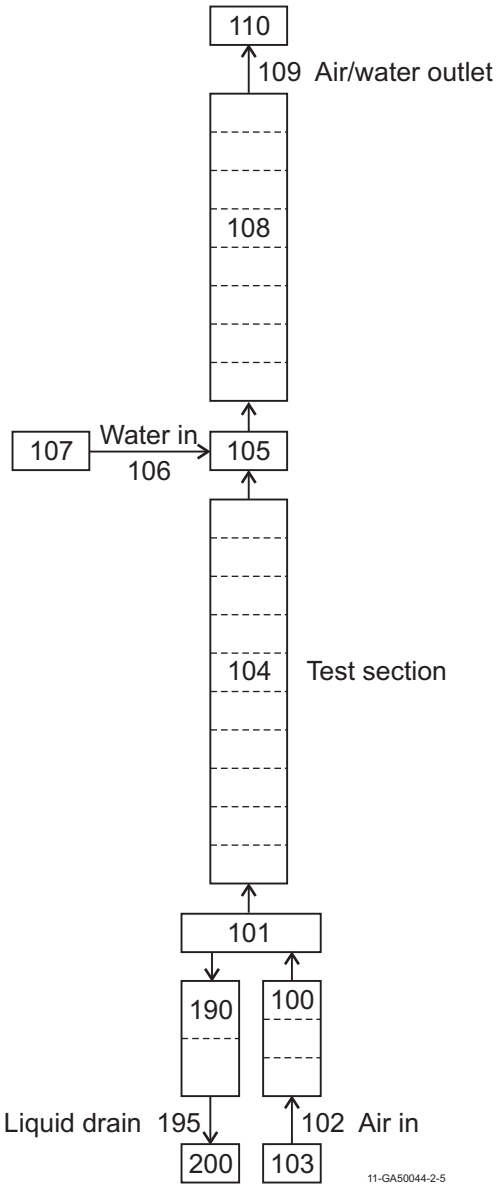

Figure 4.15-2. Nodalization diagram for the Dukler-Smith test facility.

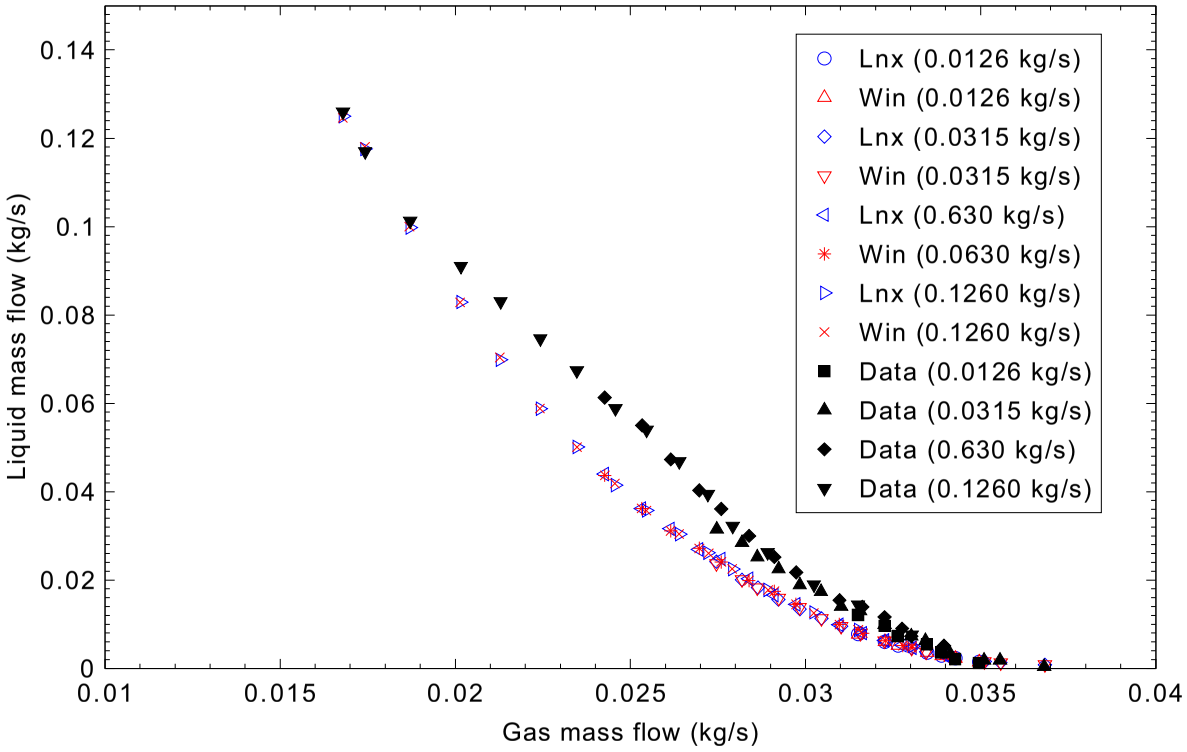

Figure 4.15-3. Comparison of RELAP5-3D predictions to Dukler-Smith data.

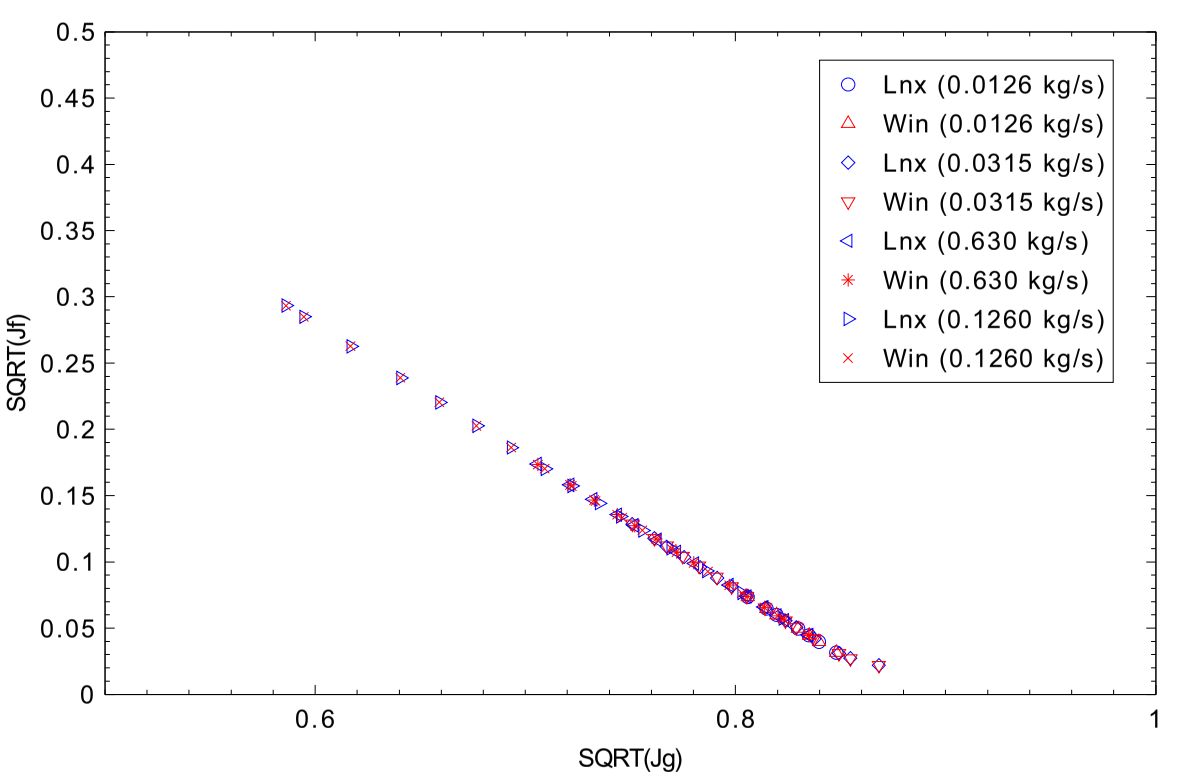

Figure 4.15-4. RELAP5-3D calculated superficial liquid velocity versus superficial gas velocity for the Dukler-Smith test.

4.16 UPTF Downcomer CCFL Test 6, Run 131

Figures comparing simulations using Linux and Windows code versions are presented. Diagrams are included so that the figure numbering is the same as that in Volume III of the RELAP5-3D code manual. Noticeable differences were observed in Figures 4.16-5, 6, 7, and 8.

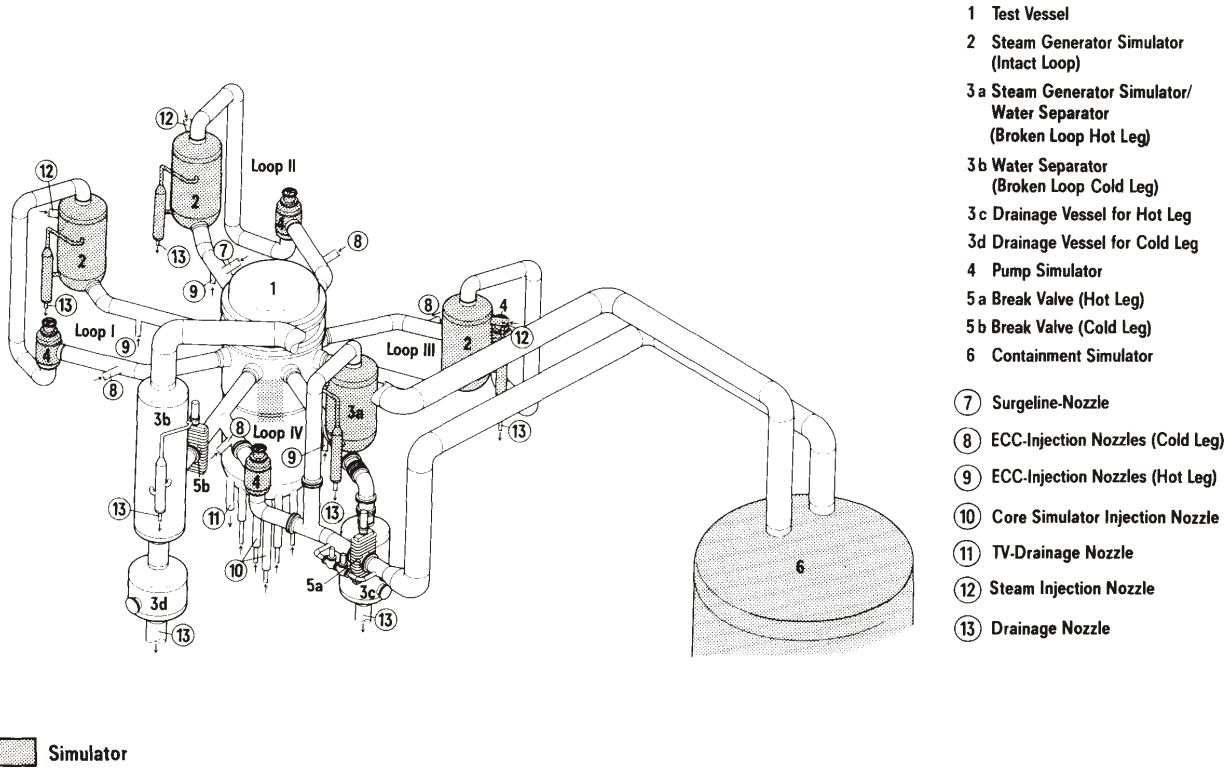

Figure 4.16-1. Schematic of the UPTF.

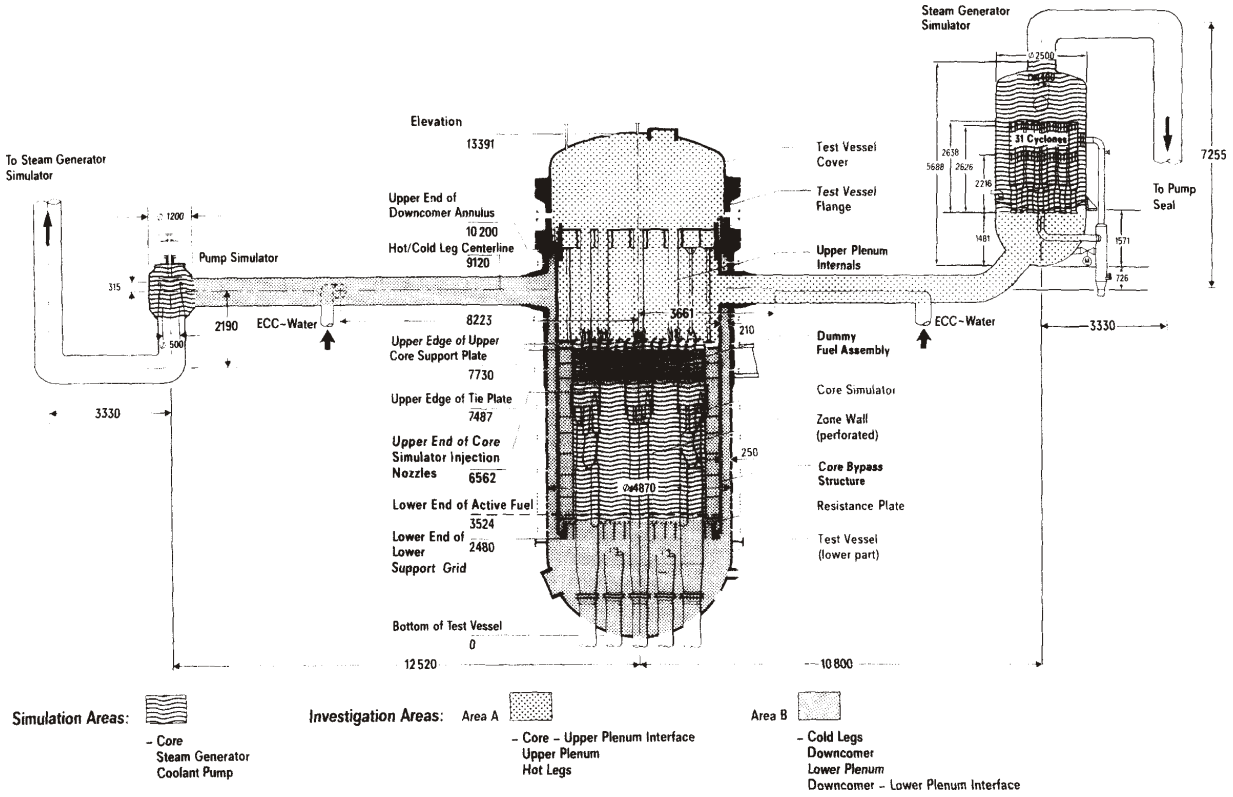

Figure 4.16-2. Key dimensions of the UPTF.

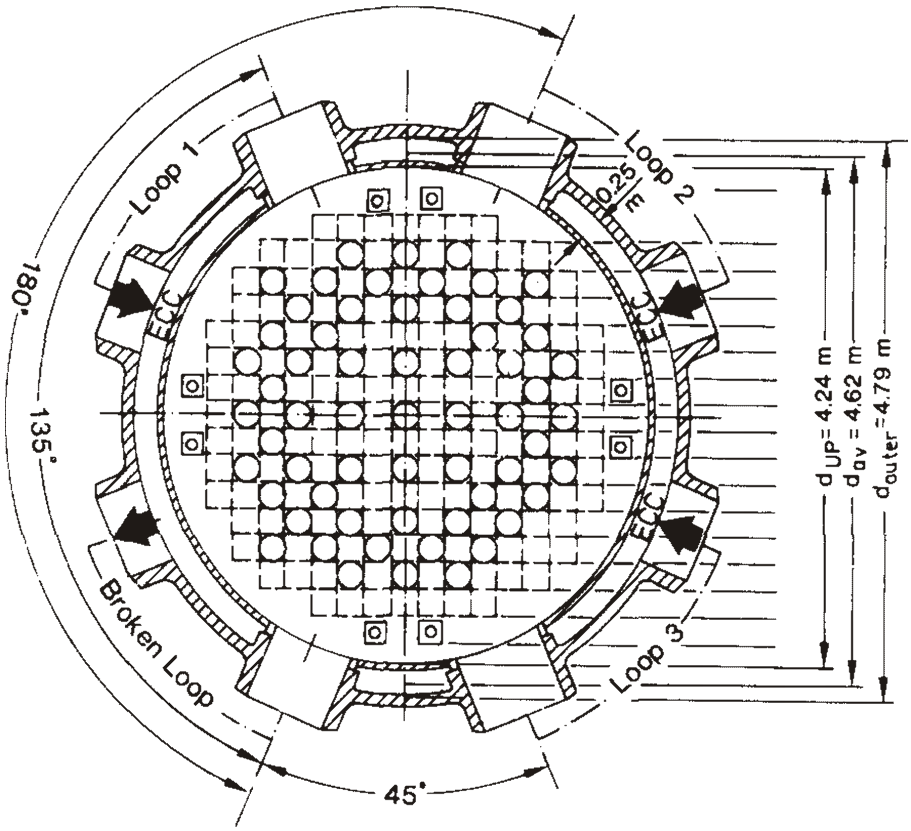

Figure 4.16-3. Cross-section of the UPTF reactor vessel.

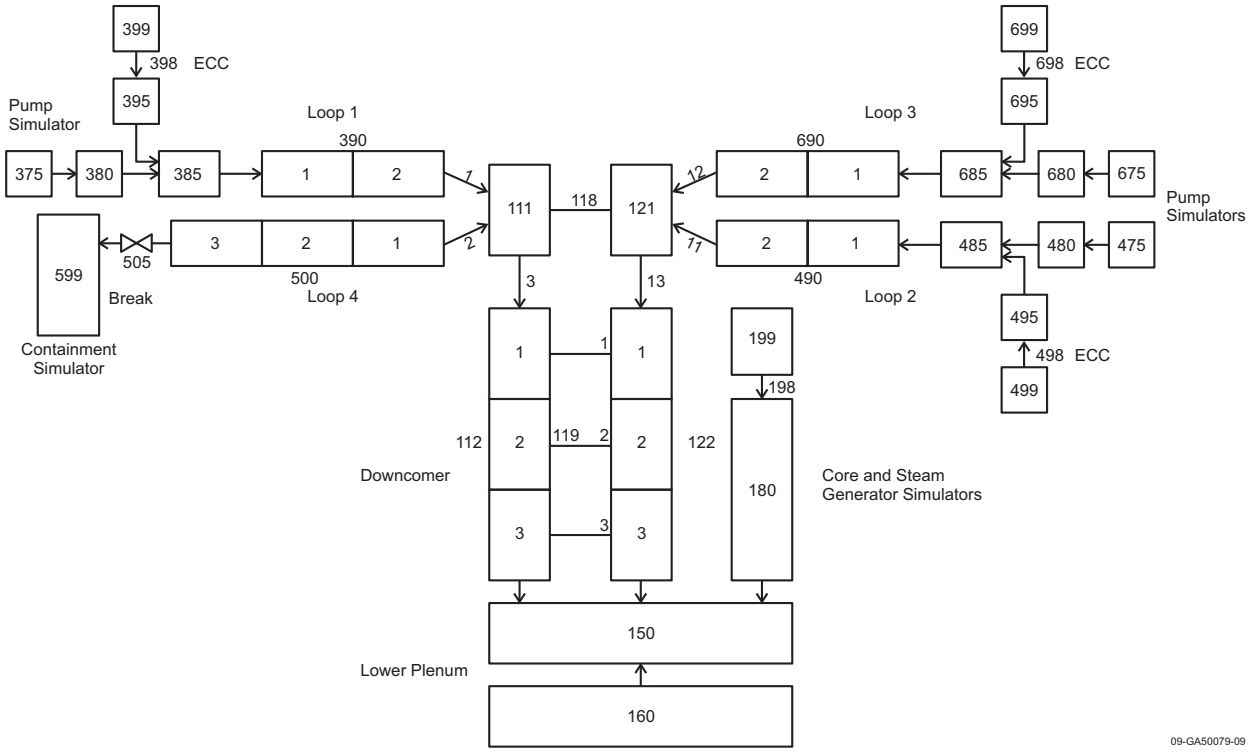

Figure 4.16-4. RELAP5-3D nodalization for UPTF Test 6.

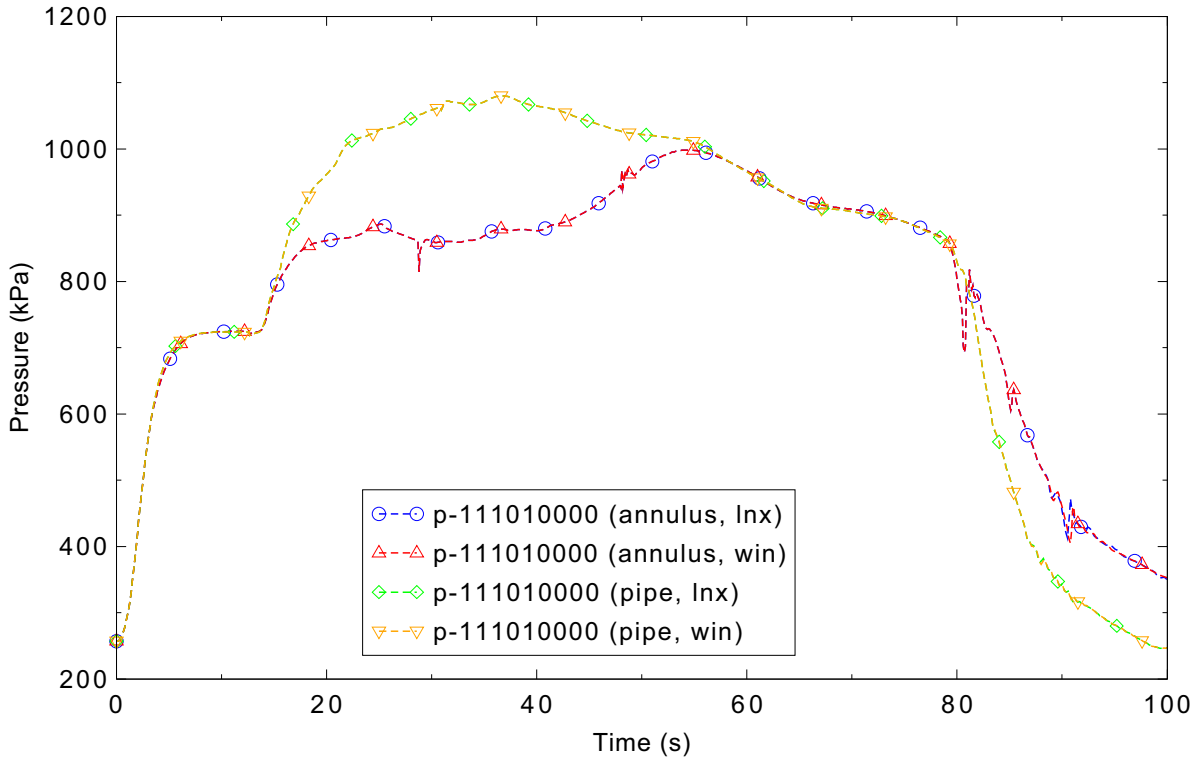

Figure 4.16-5. Downcomer pressure in UPTF Test 6, Run 131.

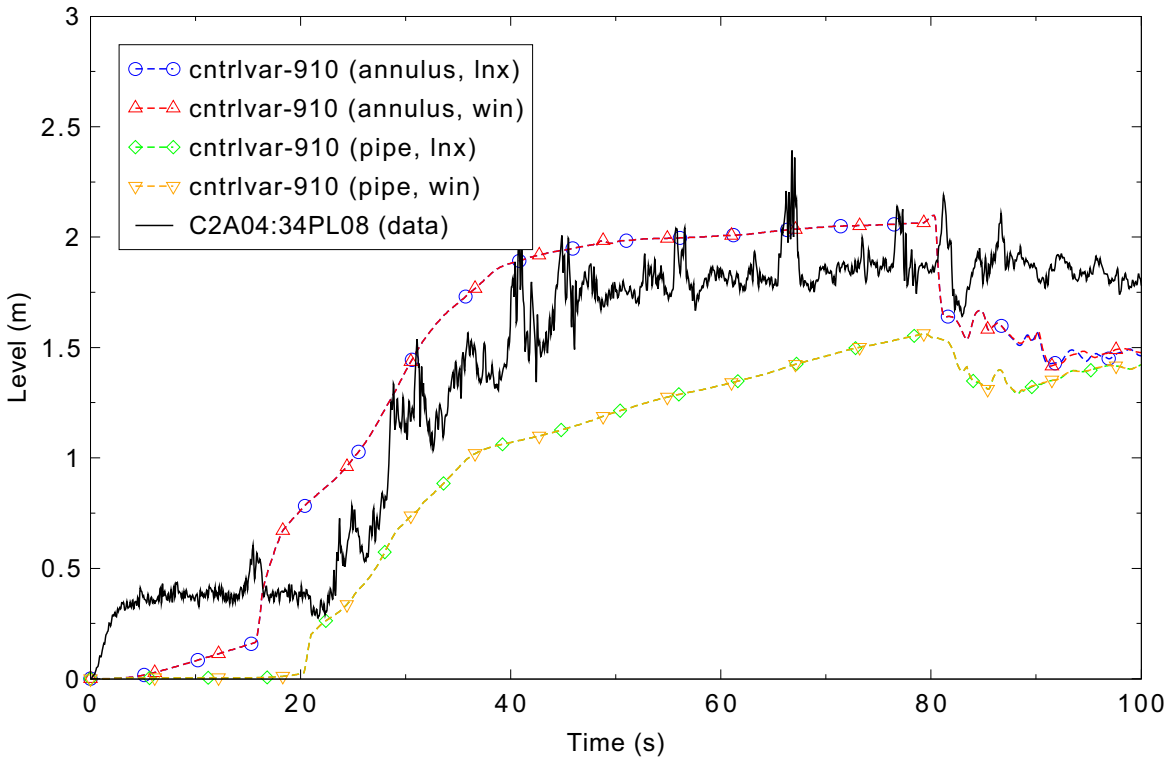

Figure 4.16-6. Collapsed liquid level in the lower plenum in UPTF Test 6, Run 131.

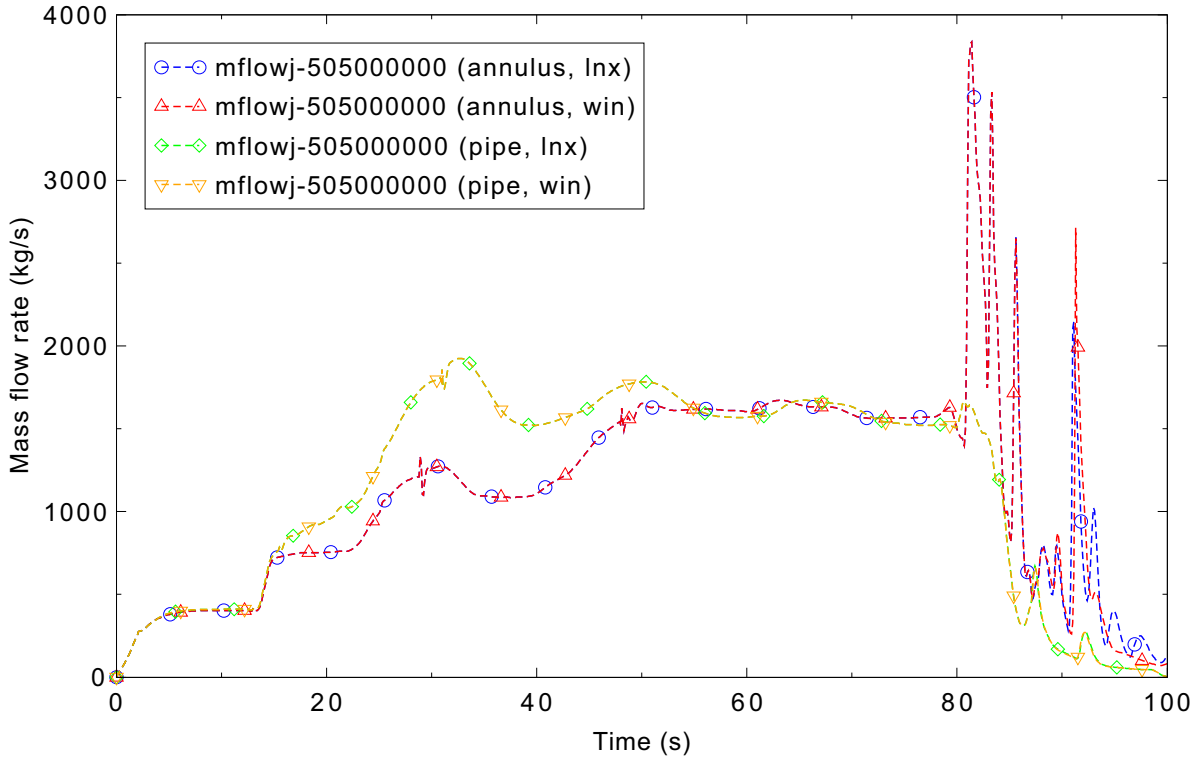

Figure 4.16-7. Break mass flow in UPTF Test 6, Run 131.

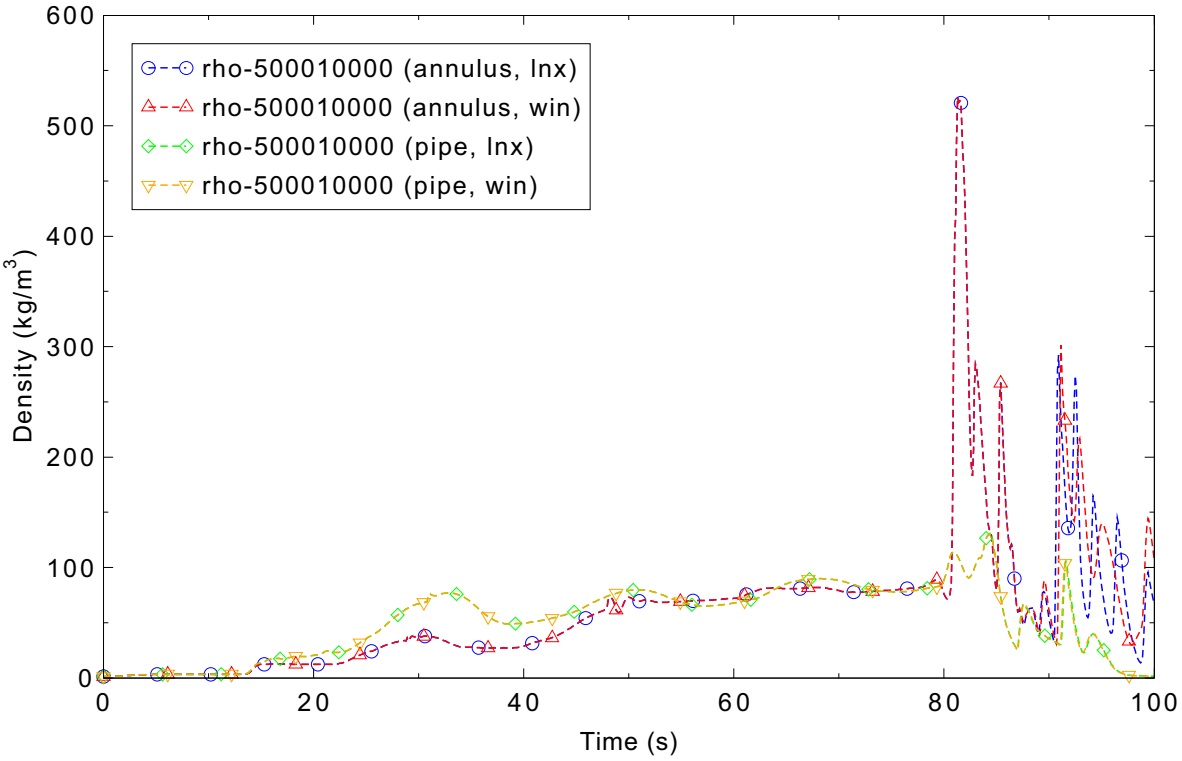

Figure 4.16-8. Fluid density in the broken cold leg in UPTF Test 6, Run 131.

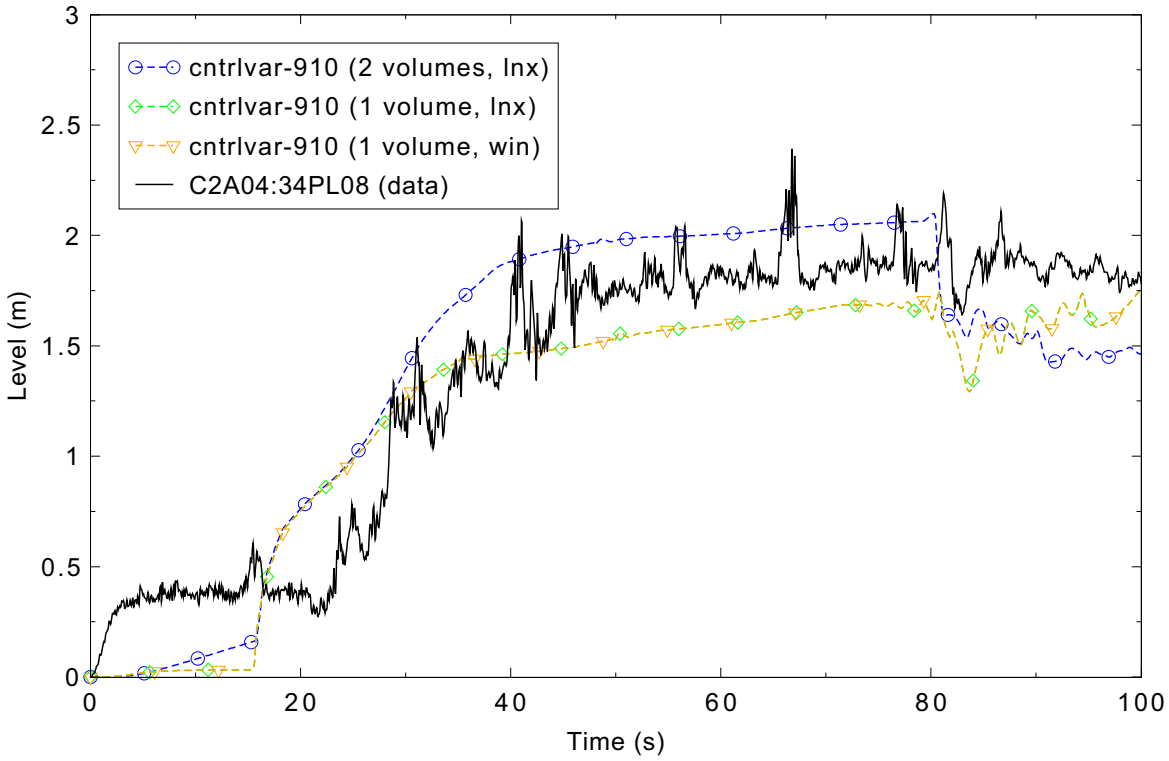

Figure 4.16-9. The effect of nodalization on collapsed liquid level in UPTF Test 6, Run 131.

4.17 MIT Pressurizer Test ST4

Figures comparing simulations using Linux and Windows code versions are presented. Diagrams are included so that the figure numbering is the same as that in Volume III of the RELAP5-3D code manual. No differences were observed in the figures.

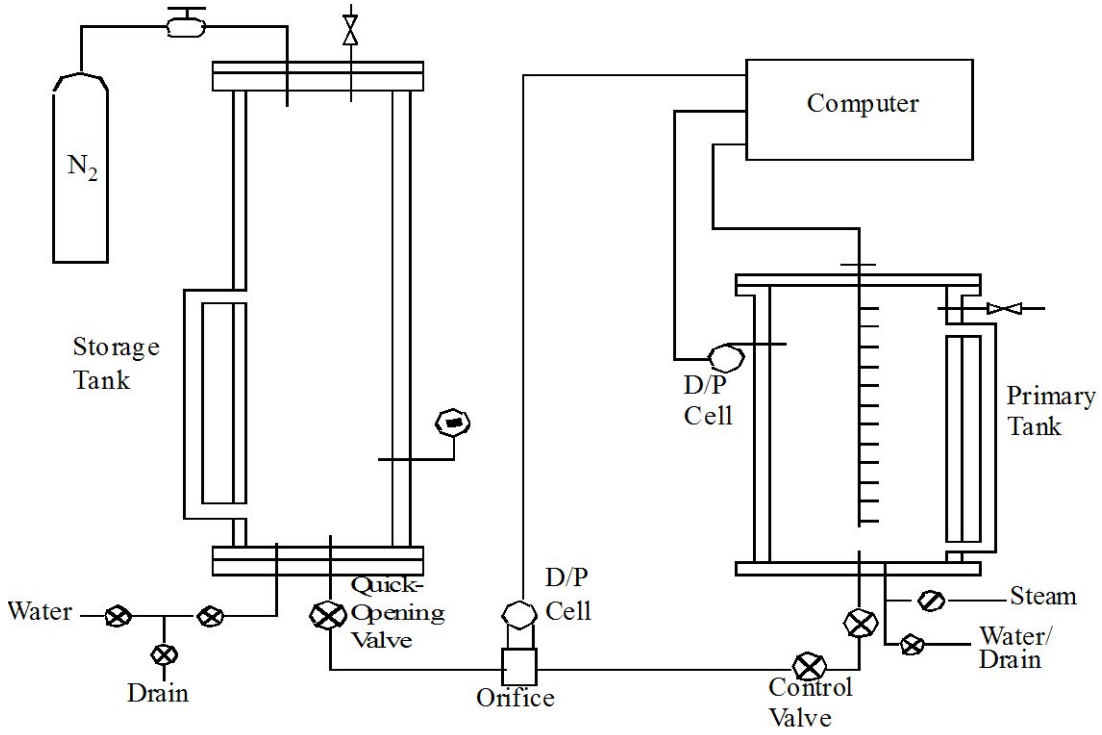

Figure 4.17-1. Schematic of MIT pressurizer test facility.

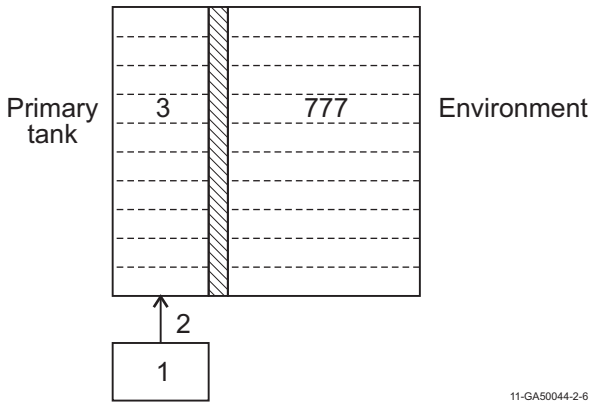

Figure 4.17-2. RELAP5-3D nodalization of MIT pressurizer.

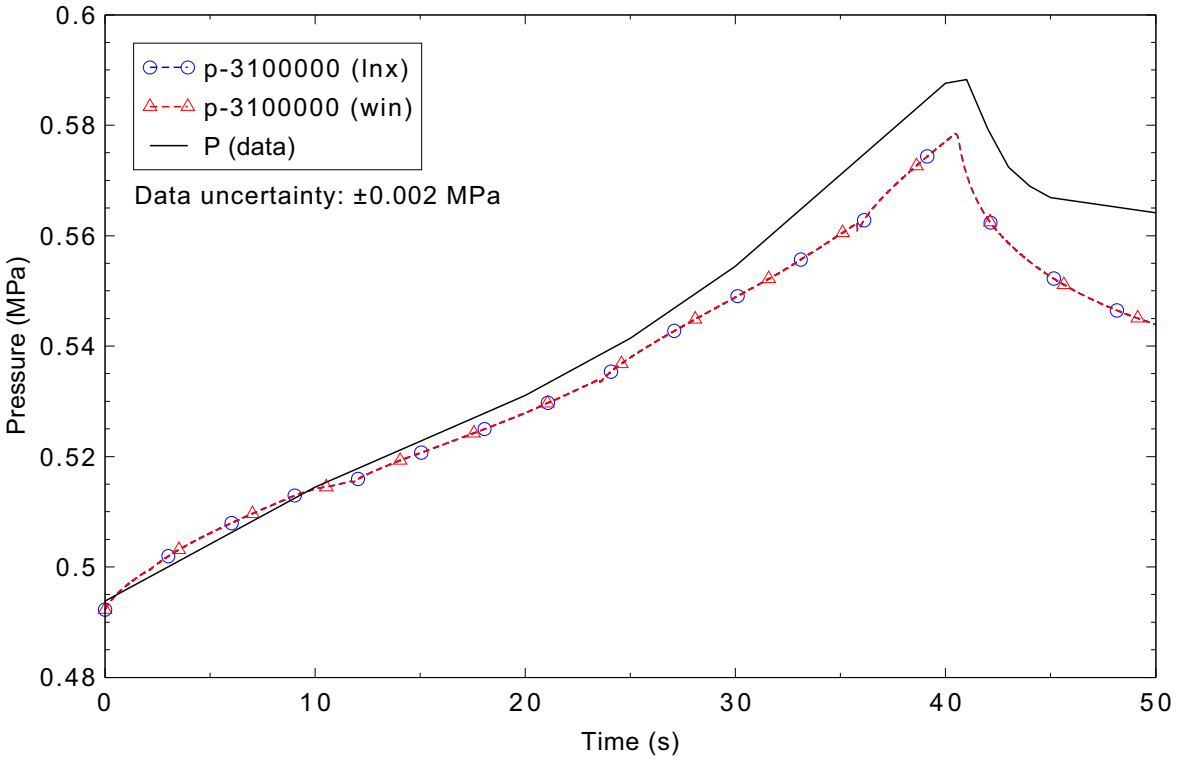

Figure 4.17-3. Measured and calculated pressure at the top of the tank for MIT pressurizer Test ST4.

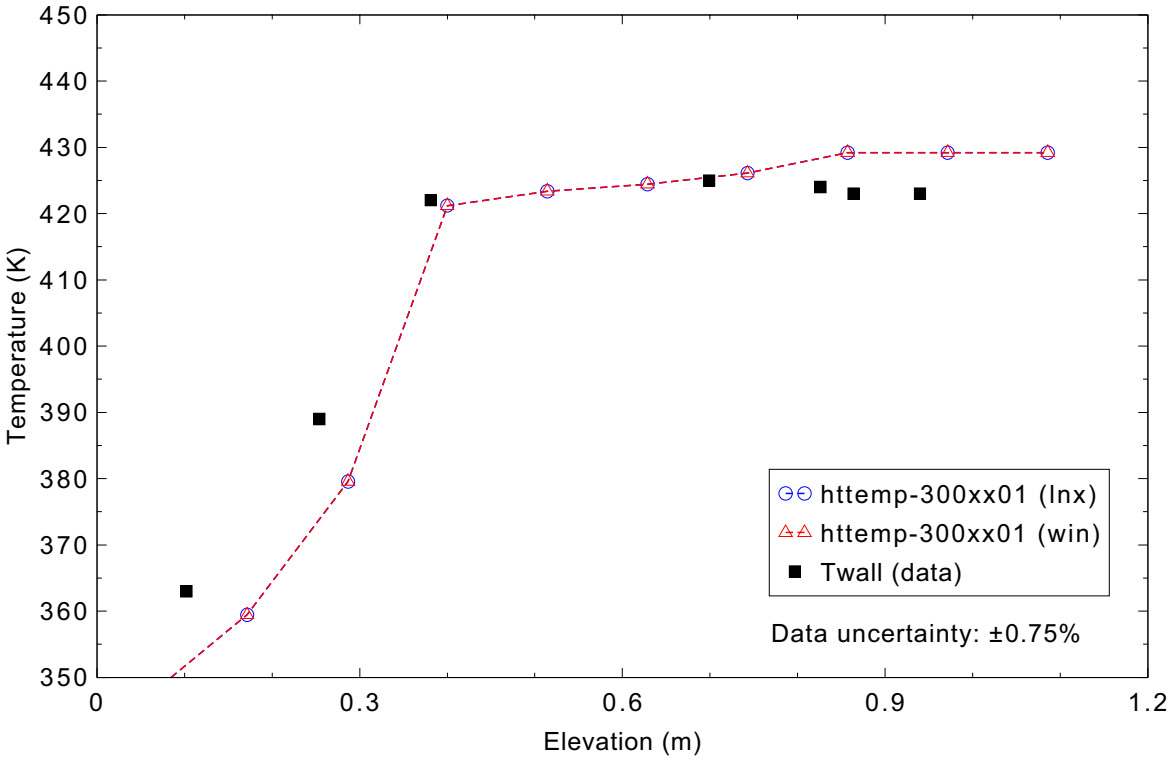

Figure 4.17-4. Measured and calculated wall temperature profile at 35 s for MIT pressurizer Test ST4.

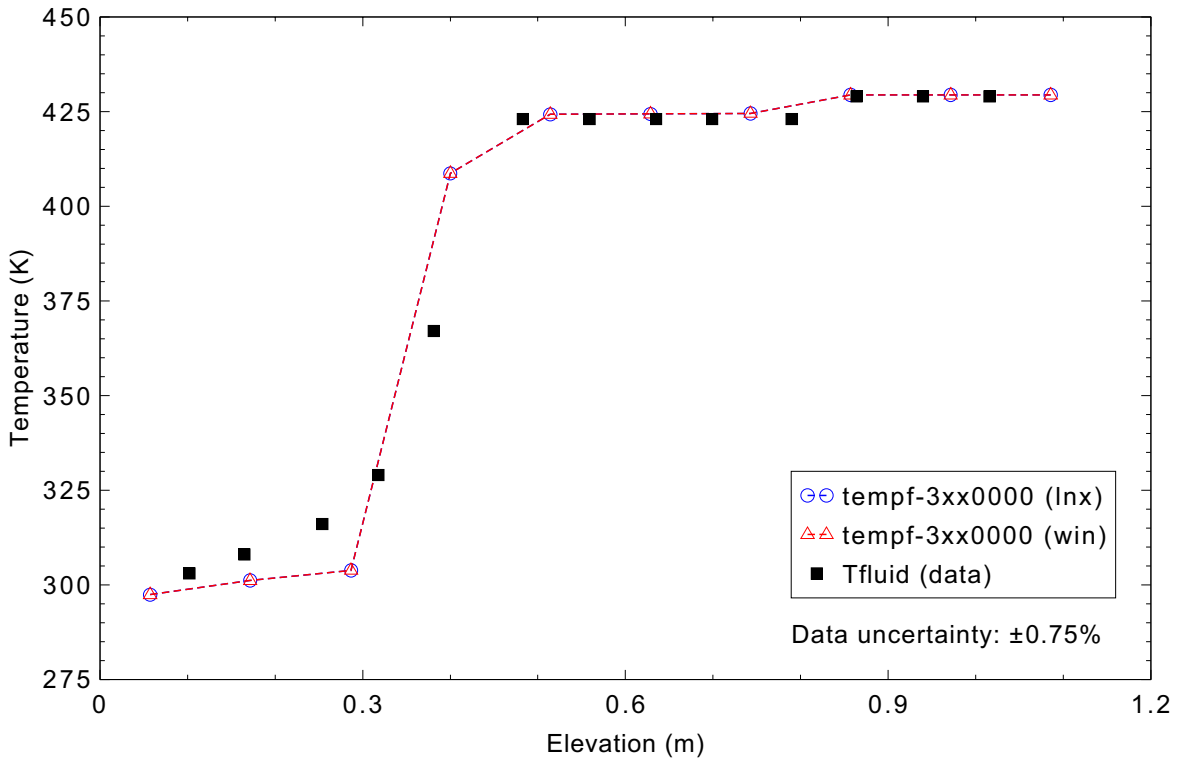

Figure 4.17-5. Measured and calculated fluid temperature profile at 35 s for MIT pressurizer Test ST4.

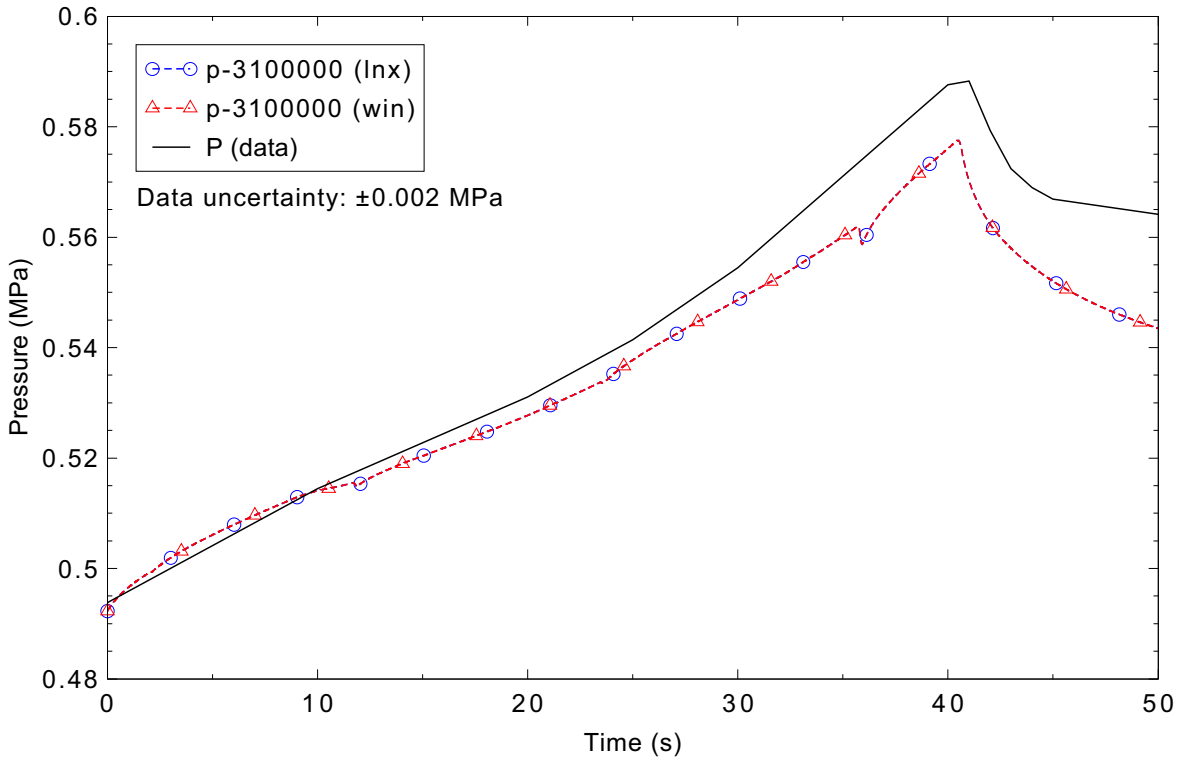

Figure 4.17-6. Measured and calculated pressure at the top of the tank for MIT pressurizer Test ST4 with the mixture level tracking turned off.

4.18 Neptunus Test Y05

Figures comparing simulations using Linux and Windows code versions are presented. Diagrams are included so that the figure numbering is the same as that in Volume III of the RELAP5-3D code manual. No differences were observed in the figures.

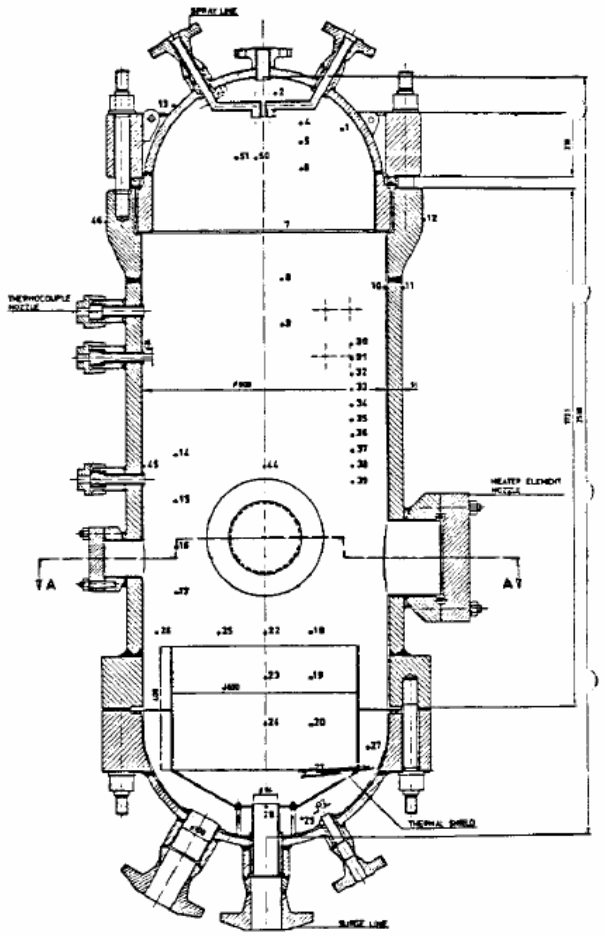

Figure 4.18-1. Neptunus test facility pressurizer.

.

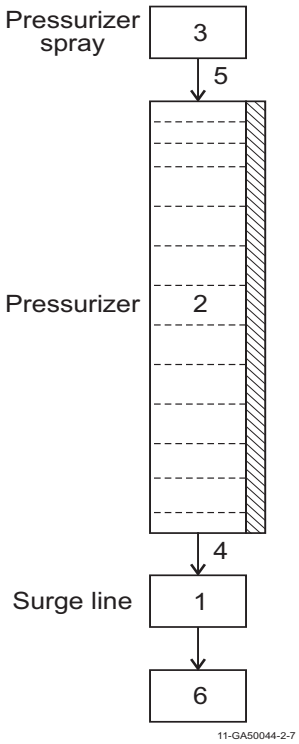

Figure 4.18-2. Nodalization diagram for the Neptunus pressurizer model.

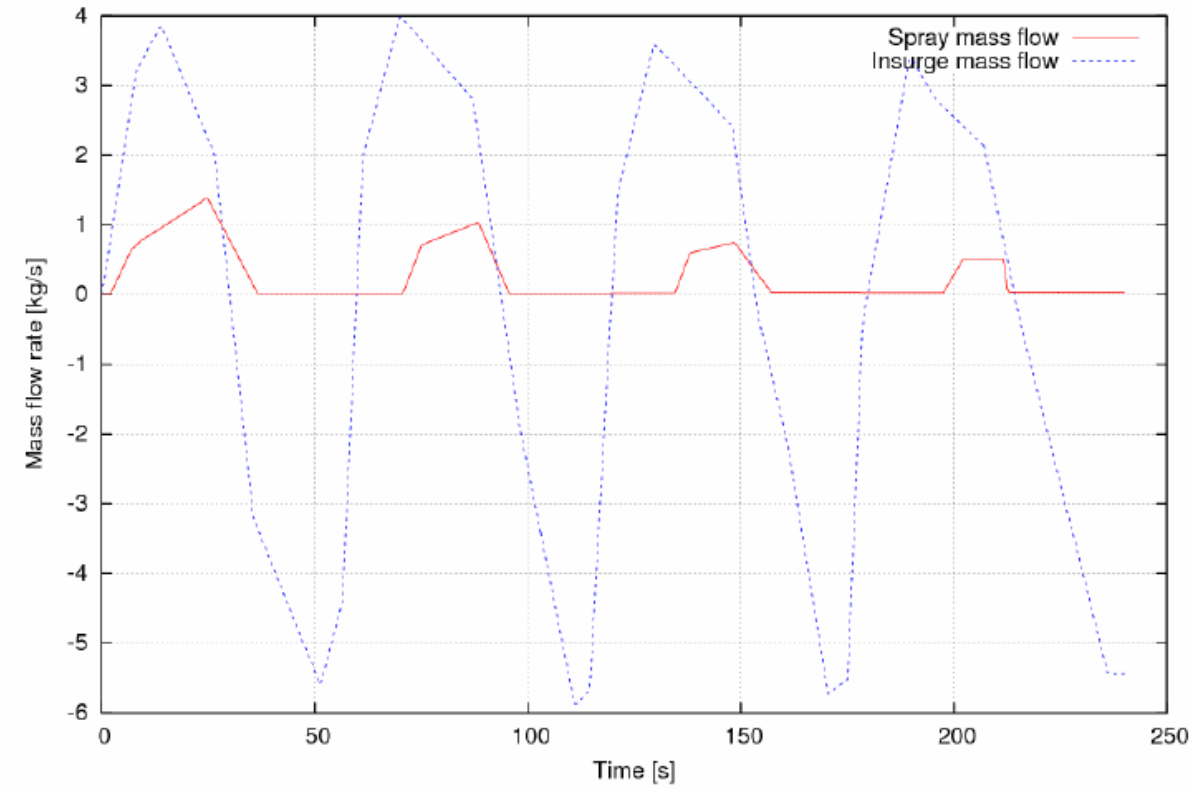

Figure 4.18-3. Transient boundary condition flow rates for Neptunus Test Y05.

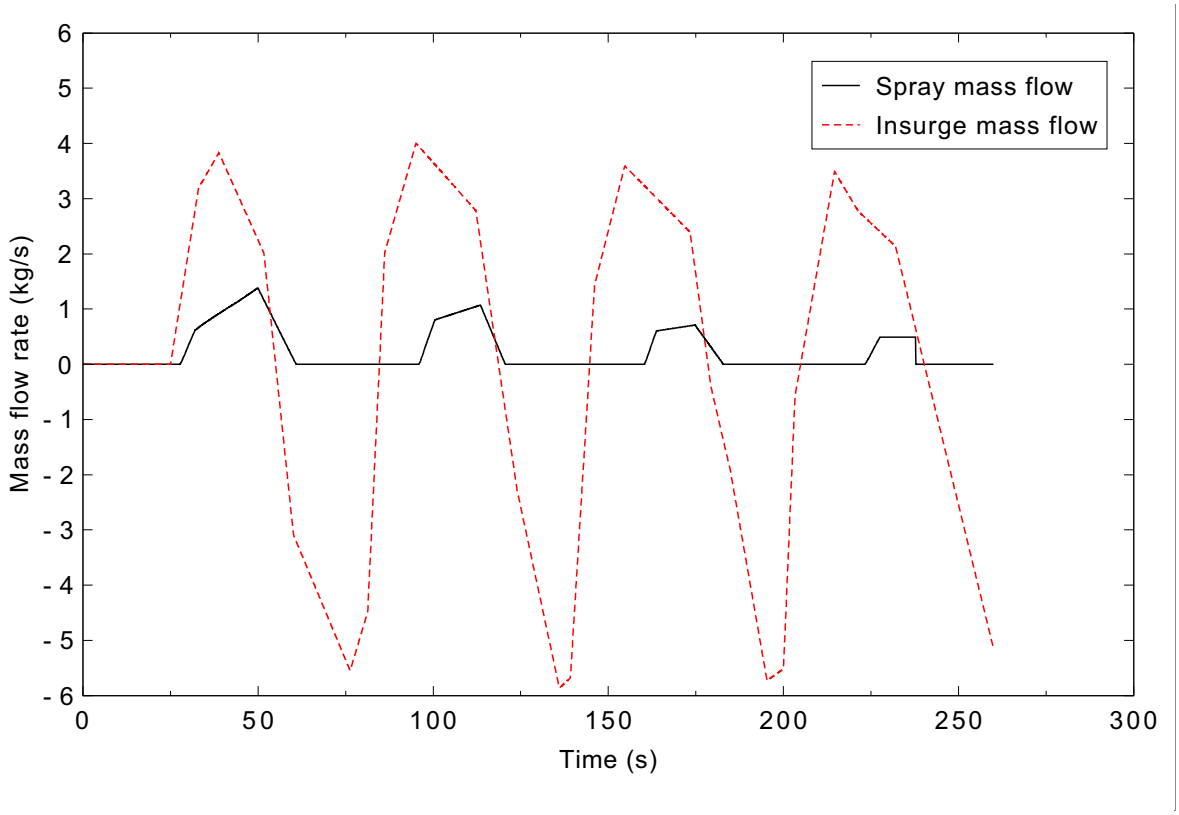

Figure 4.18-4. RELAP5-3D model input boundary flows for Neptunus Test Y05.

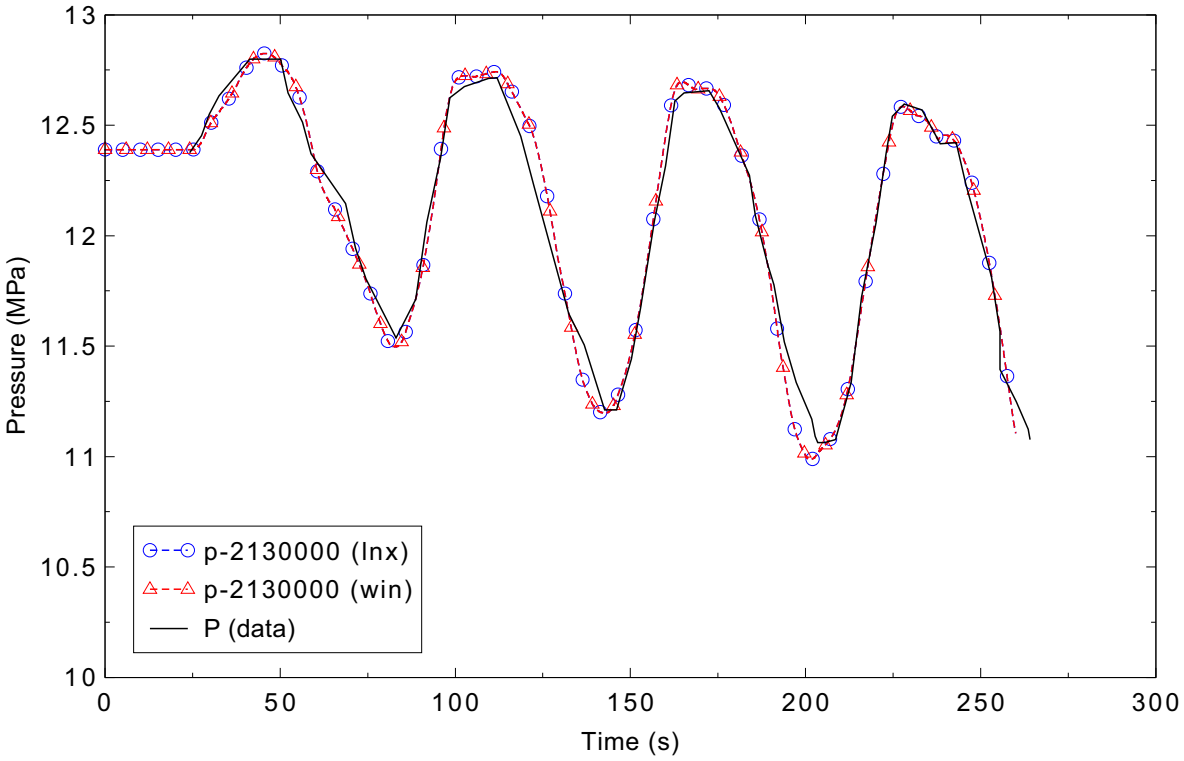

Figure 4.18-5. Measured and calculated pressurizer dome pressure for Neptunus Test Y05.

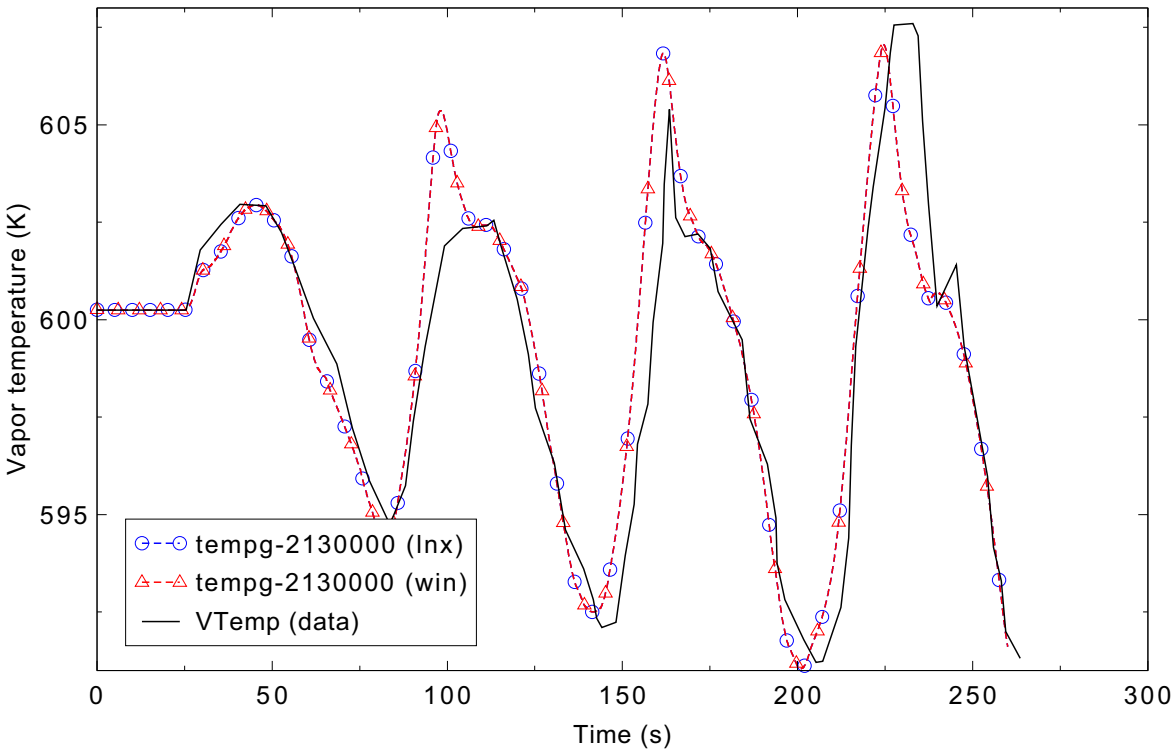

Figure 4.18-6. Measured and calculated pressurizer steam temperature for Neptunus Test Y05.

4.19 MB2 Test 1712

Figures comparing simulations using Linux and Windows code versions are presented. Diagrams are included so that the figure numbering is the same as that in Volume III of the RELAP5-3D code manual. No differences were observed in the figures.

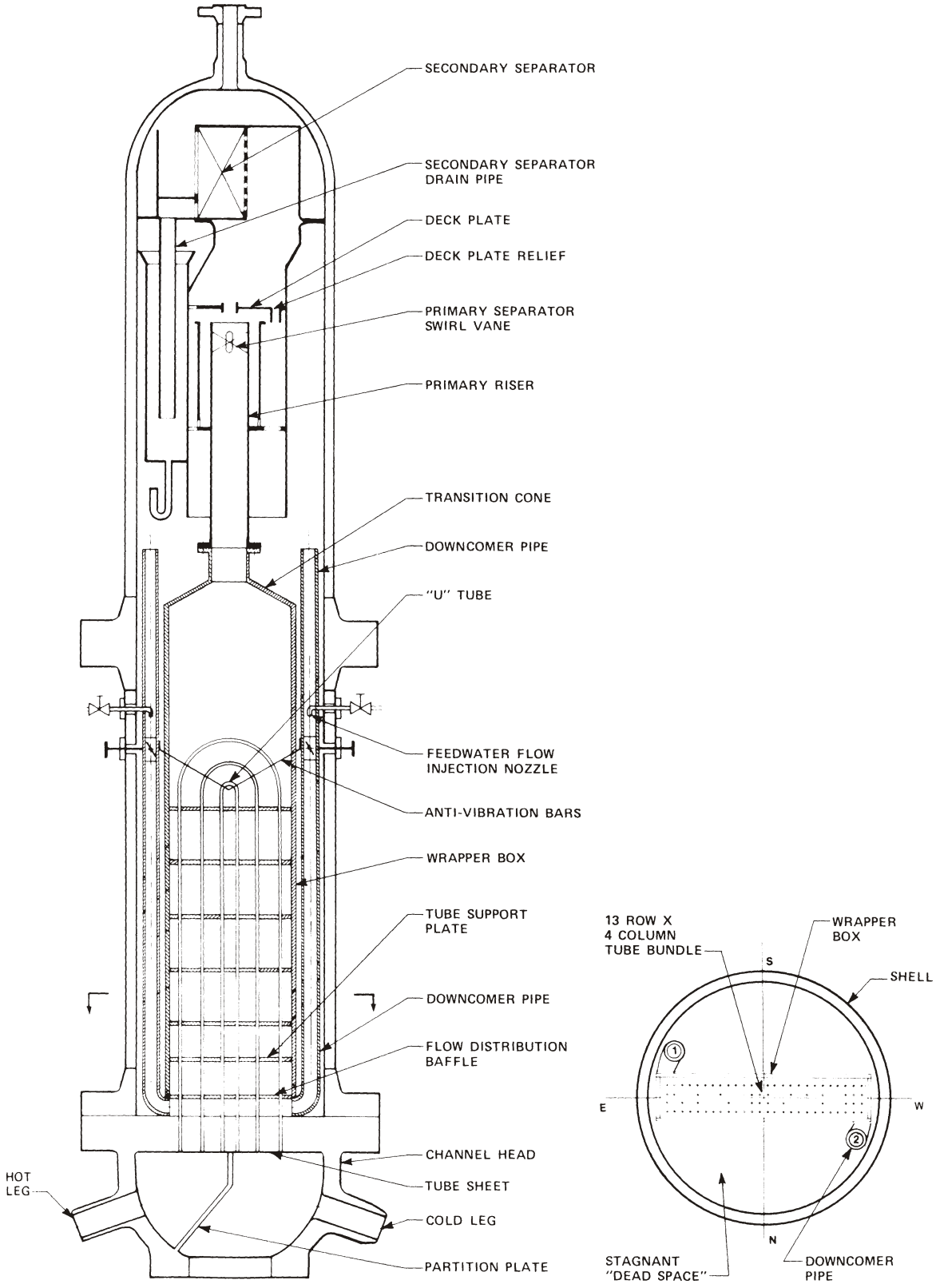

Figure 4.19-1. MB-2 schematic diagram.

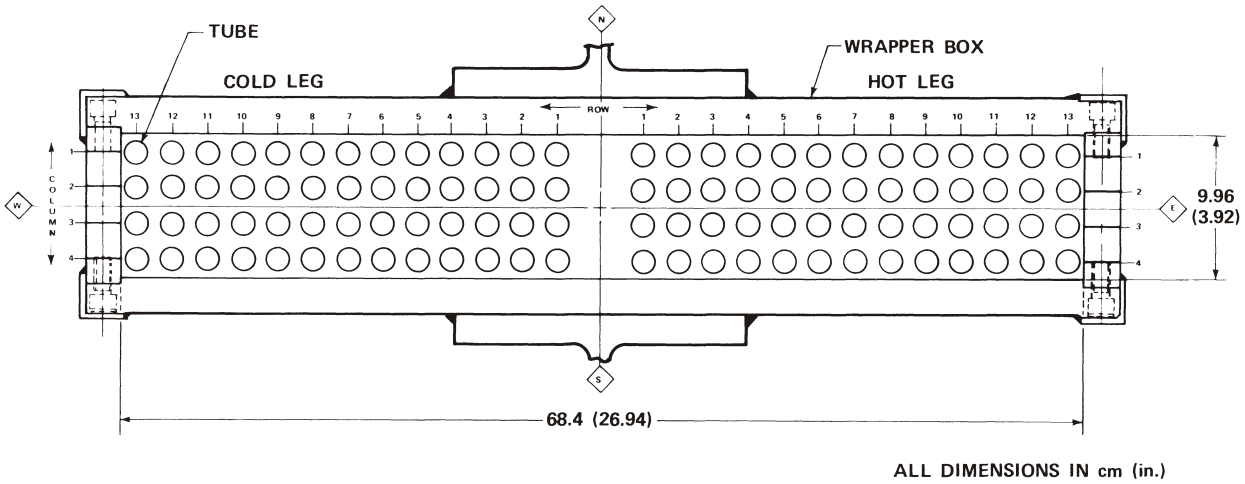

Figure 4.19-2. MB-2 tube bundle cross section.

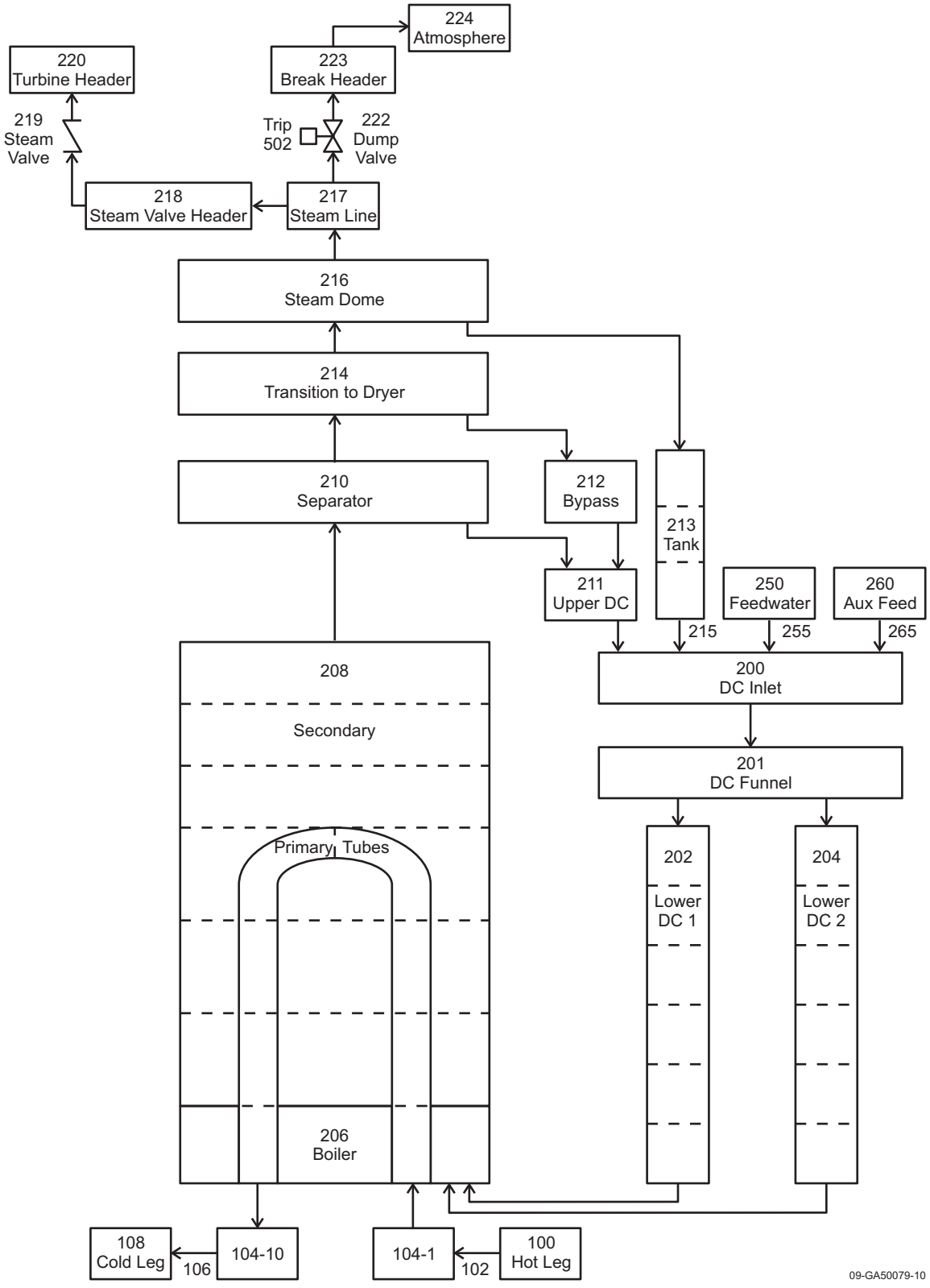

Figure 4.19-3. Nodalization diagram for MB-2 LOF Test 1712.

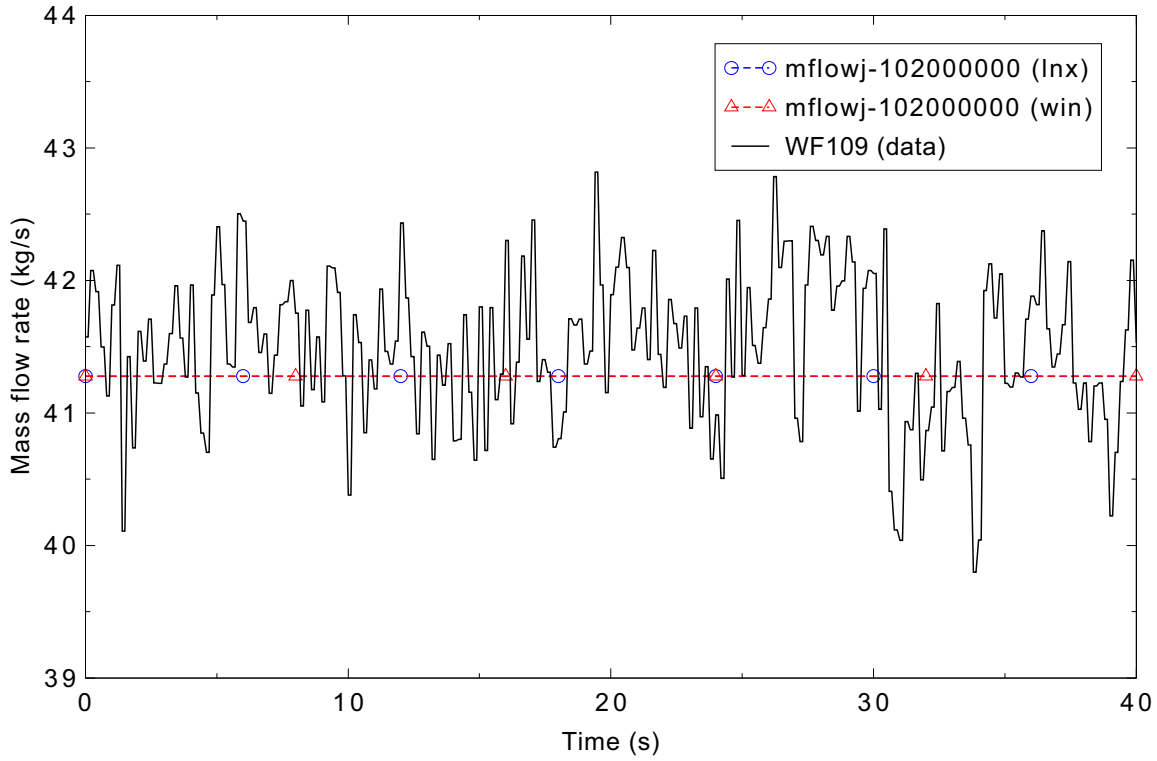

Figure 4.19-4. Measured and RELAP5-3D primary flow rate during MB-2 steady state Test 1712.

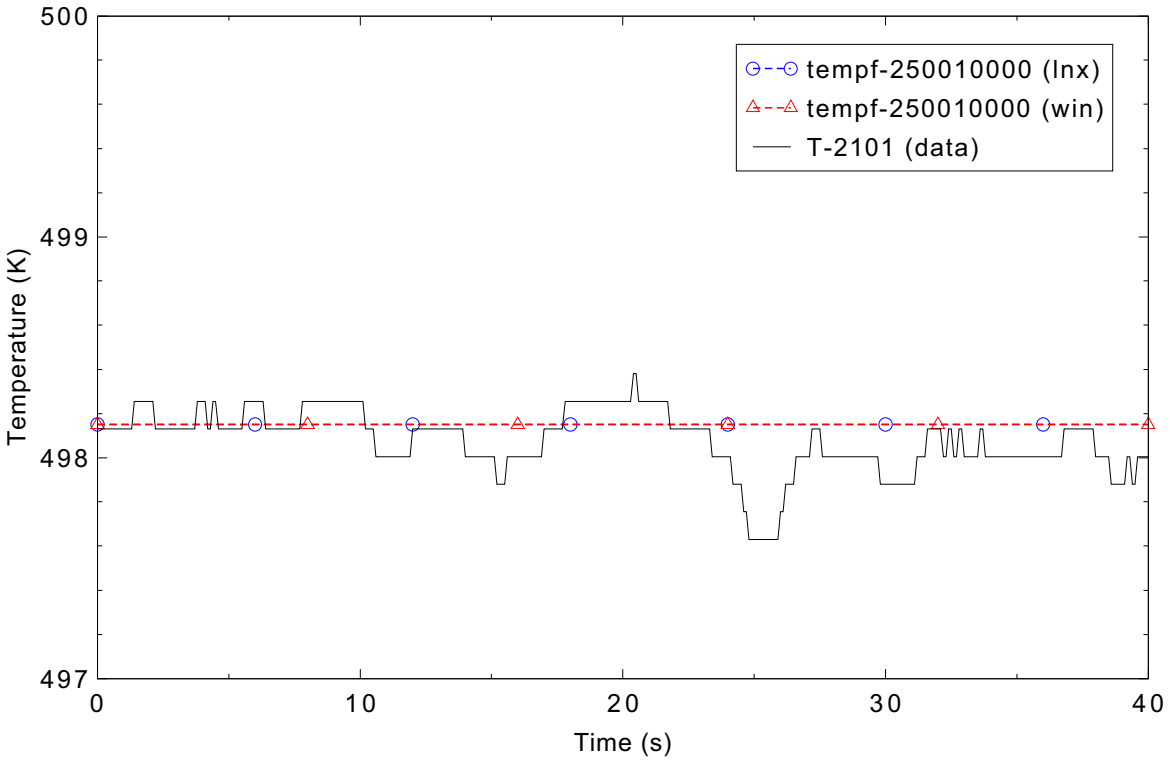

Figure 4.19-5. Measured and RELAP5-3D main feed water temperature during MB-2 steady state Test 1712.

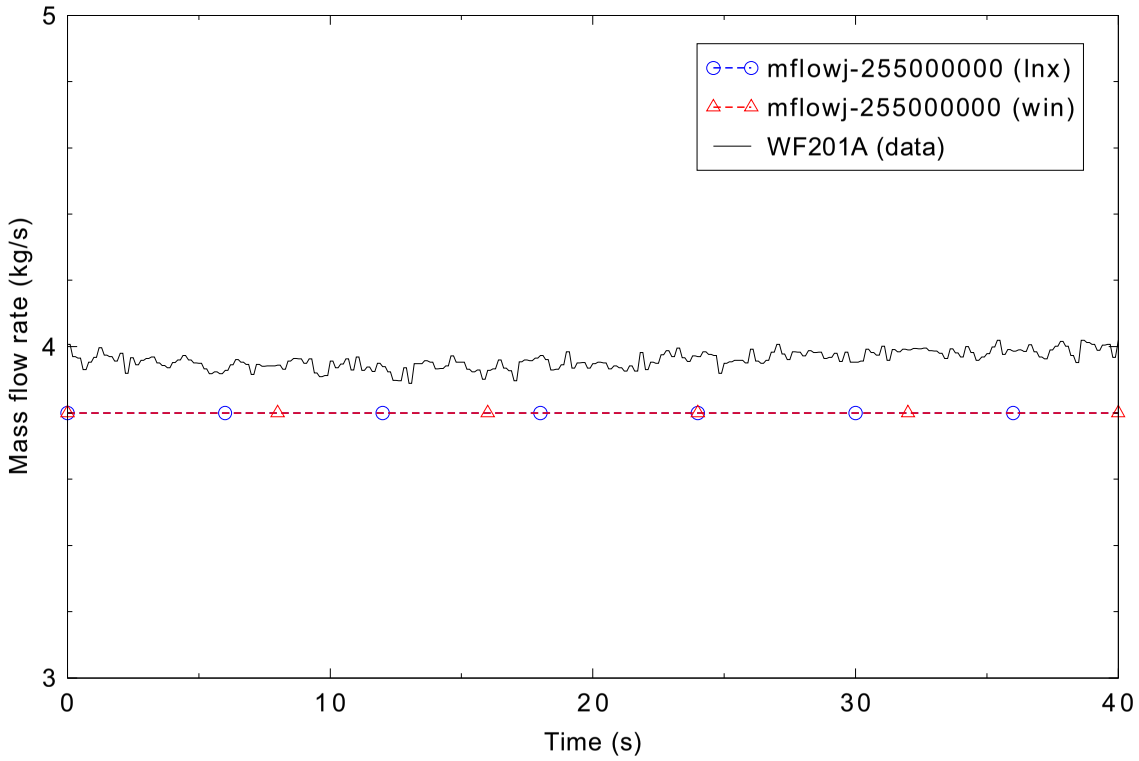

Figure 4.19-6. Measured and calculated main feed water flow rate during MB-2 steady state Test 1712.

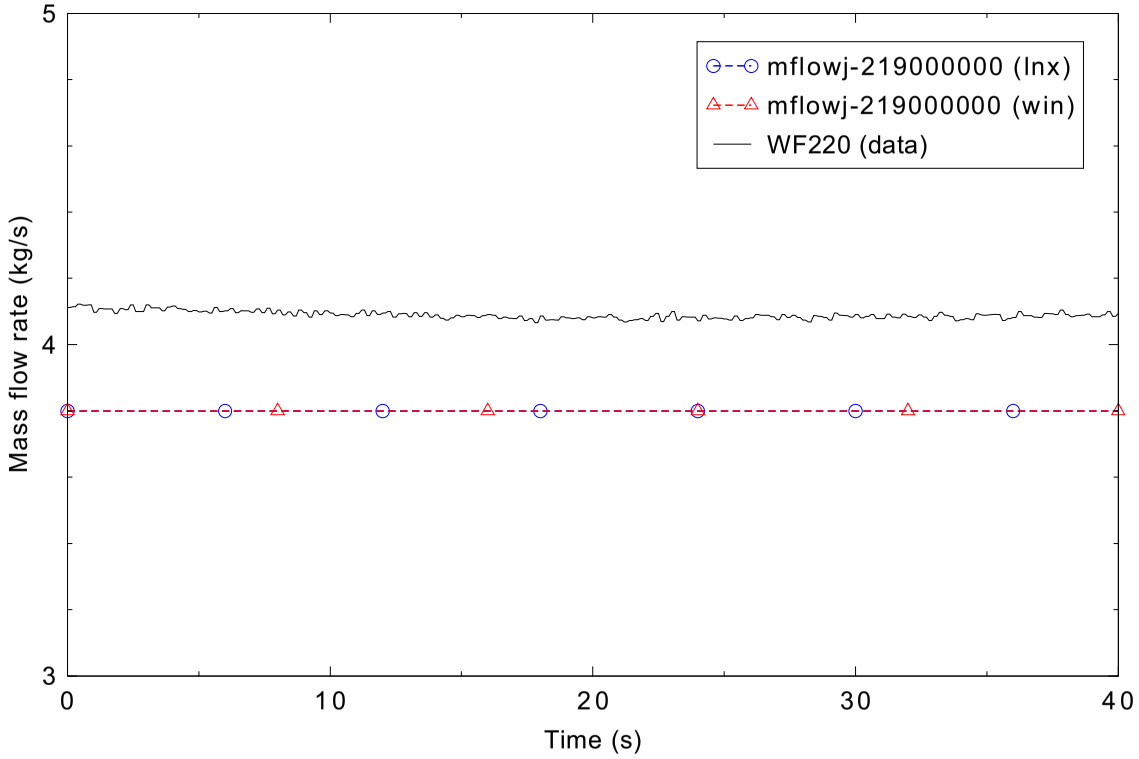

Figure 4.19-7. Measured and calculated steam flow rate during MB-2 steady state Test 1712.

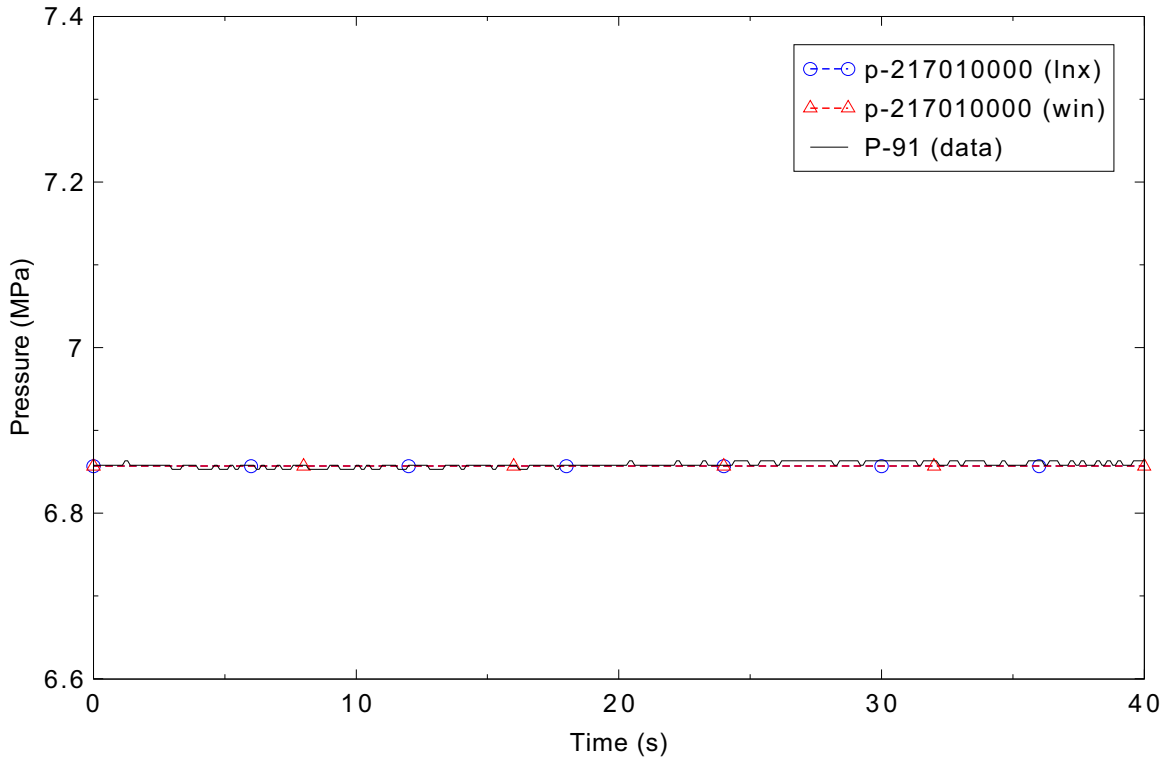

Figure 4.19-8. Measured and calculated steam line pressure during MB-2 steady state Test 1712.

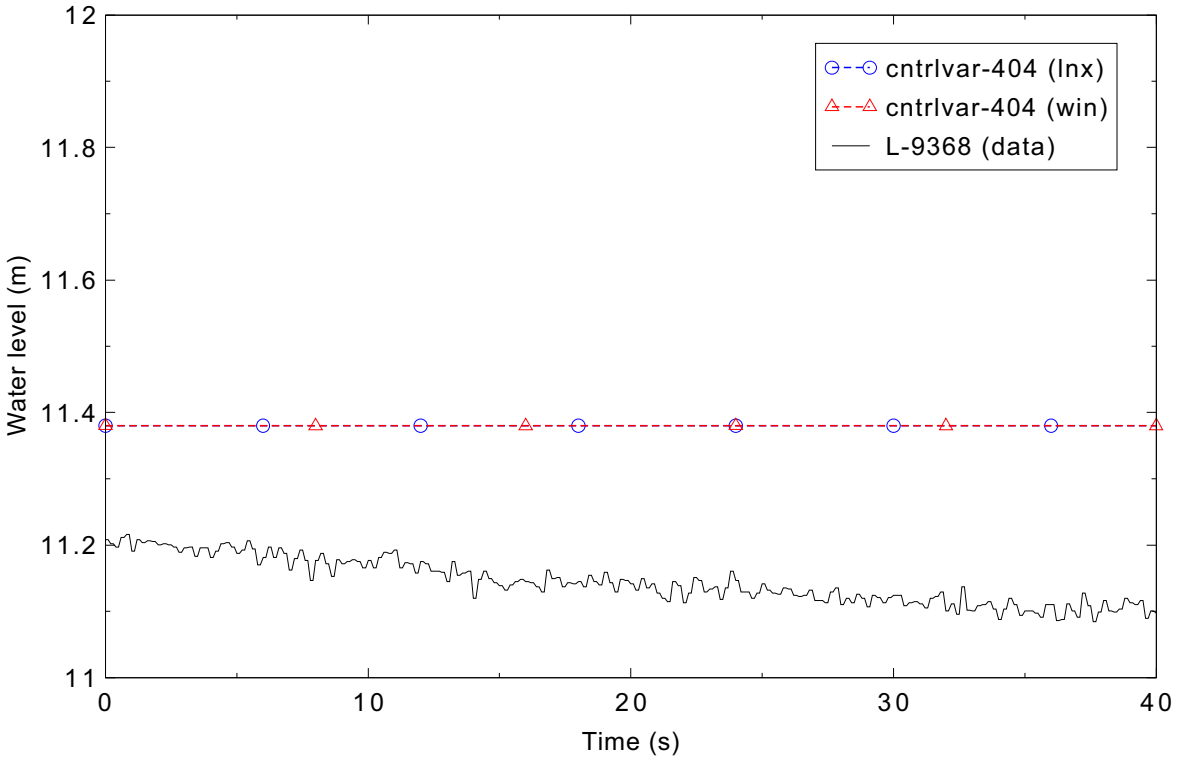

Figure 4.19-9. Measured and calculated narrow range water level during MB-2 steady state Test 1712.

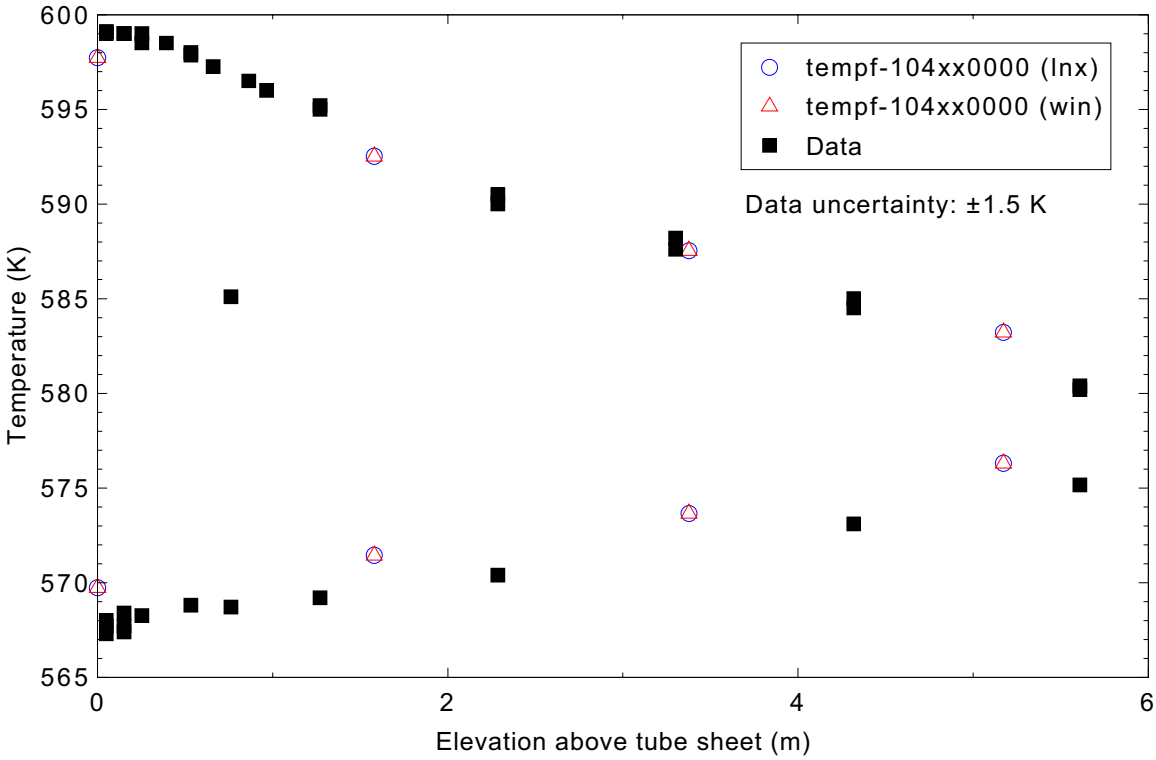

Figure 4.19-10. Measured and calculated primary side fluid temperatures during MB-2 steady state Test 1712.

4.20 LOFT Experiment L3-1

Figures comparing simulations using Linux and Windows code versions are presented. Diagrams are included so that the figure numbering is the same as that in Volume III of the RELAP5-3D code manual. No differences were observed in the figures.

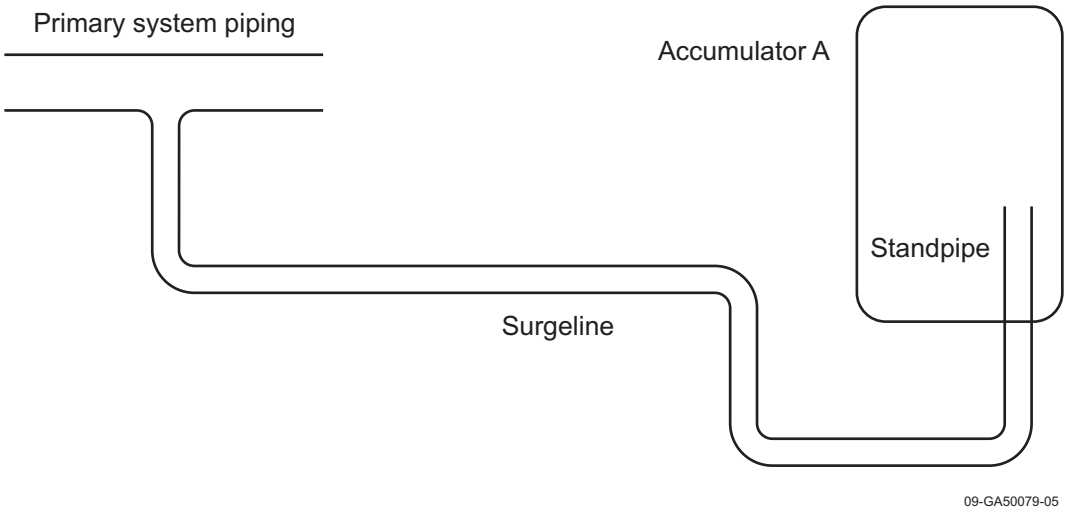

Figure 4.20-1. LOFT Experiment L3-1 Accumulator A and surgeline schematic.

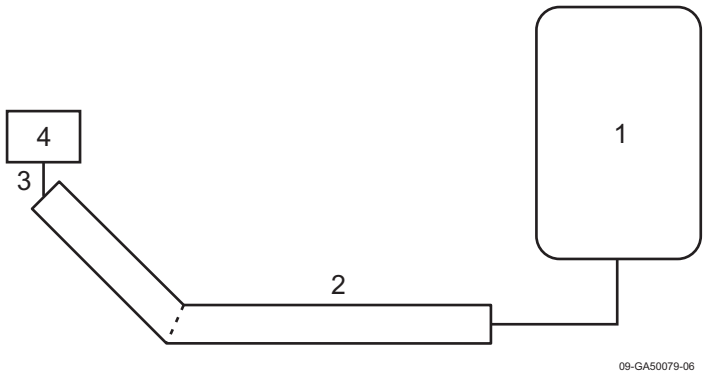

Figure 4.20-2. RELAP5 LOFT Experiment L3-1 accumulator model nodalization.

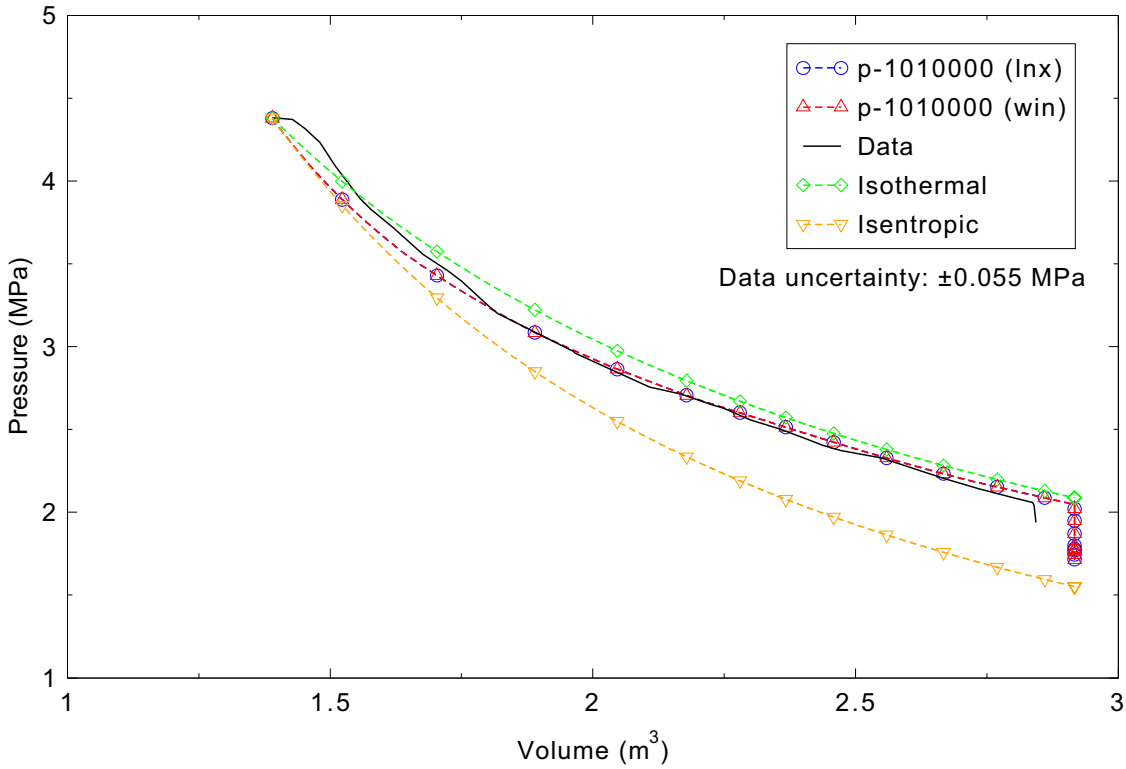

Figure 4.20-3. Measured and calculated accumulator gas dome pressure versus volume for LOFT Experiment L3-1.

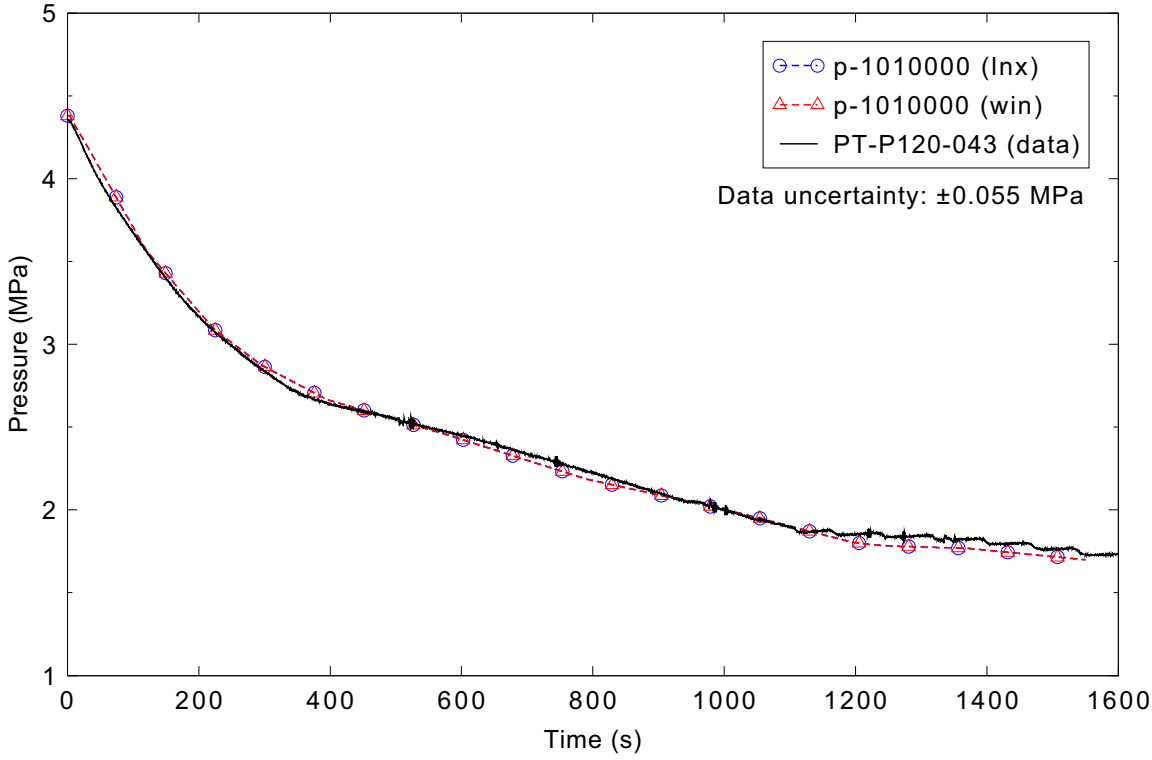

Figure 4.20-4. Measured and calculated accumulator gas dome pressure for LOFT Experiment L3-1.

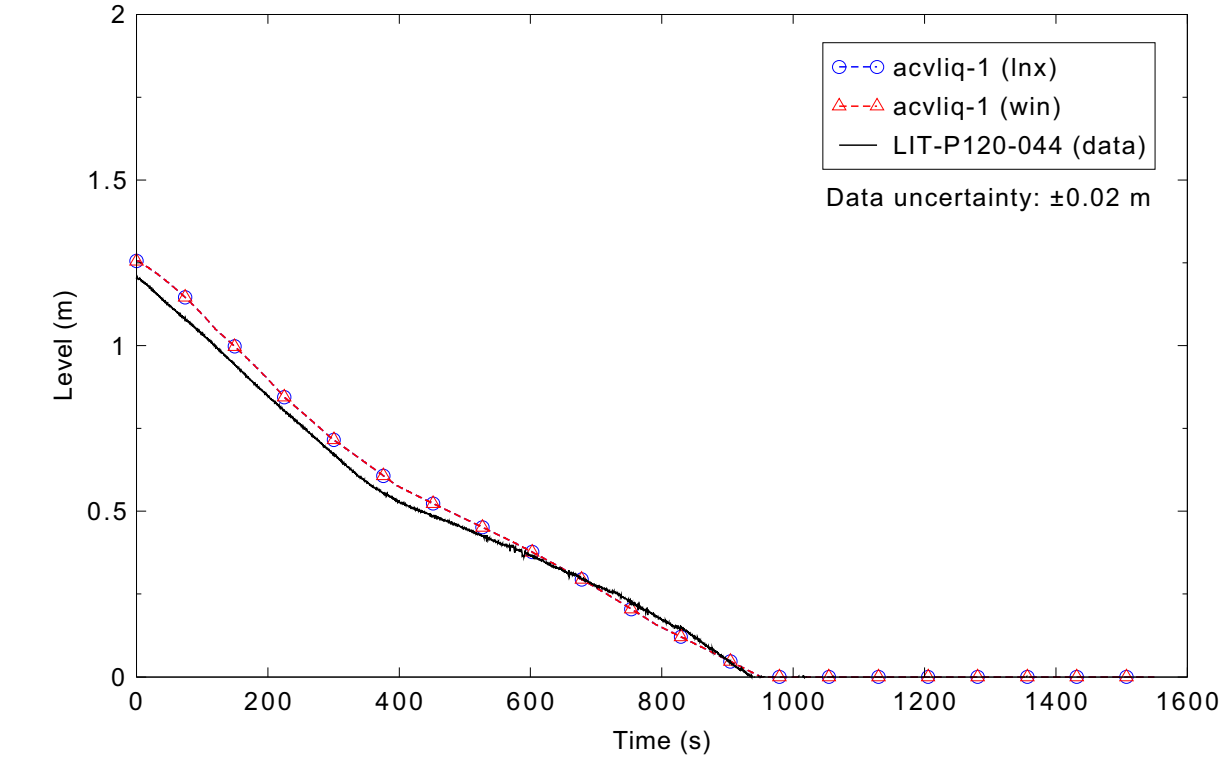

Figure 4.20-5. Measured and calculated accumulator liquid level for LOFT Experiment L3-1.

4.21 Full-Scale Reactor Coolant Pump

Figures comparing simulations using Linux and Windows code versions are presented. Diagrams are included so that the figure numbering is the same as that in Volume III of the RELAP5-3D code manual. No differences were observed in the figures.

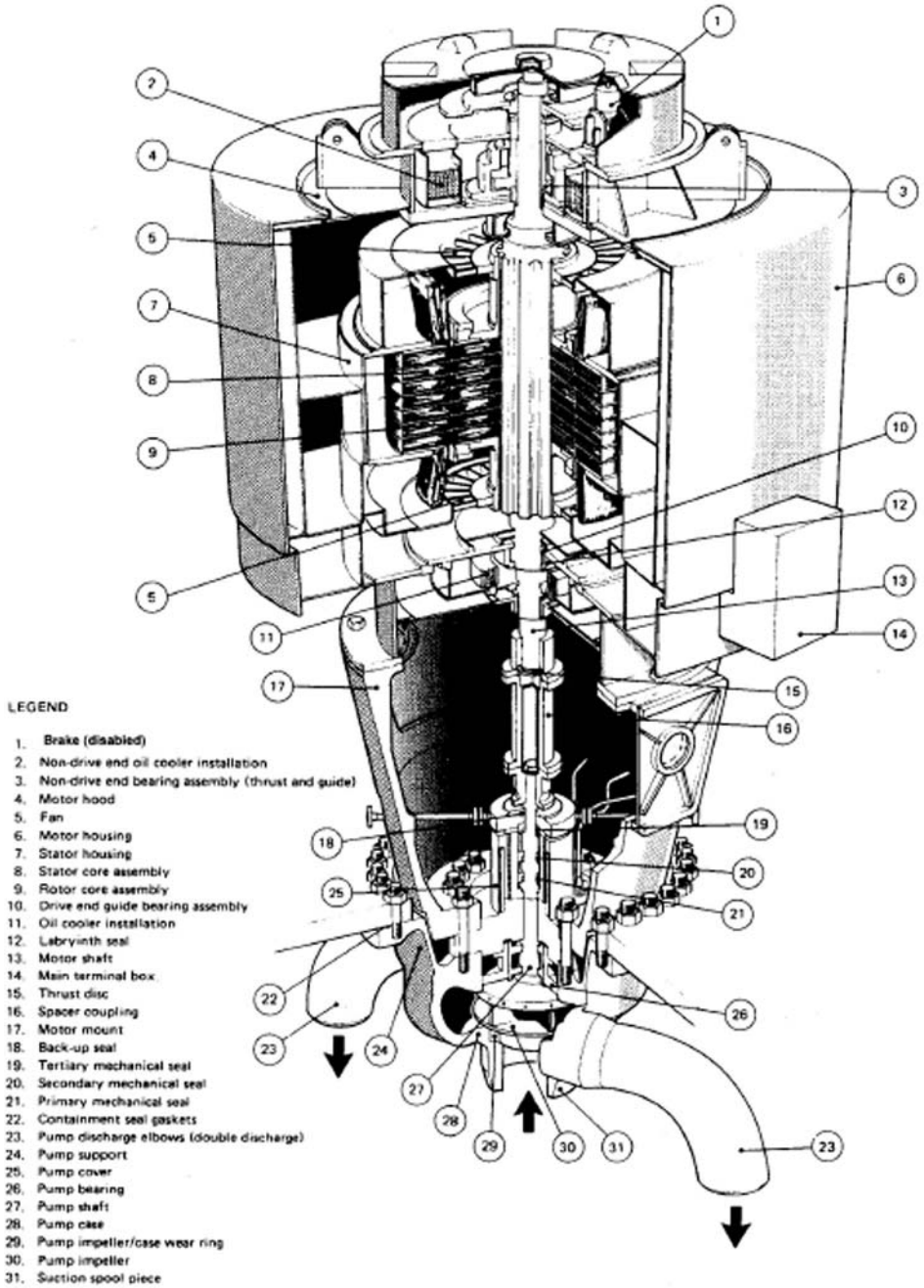

Figure 4.21-1. Full-size reactor coolant pump.

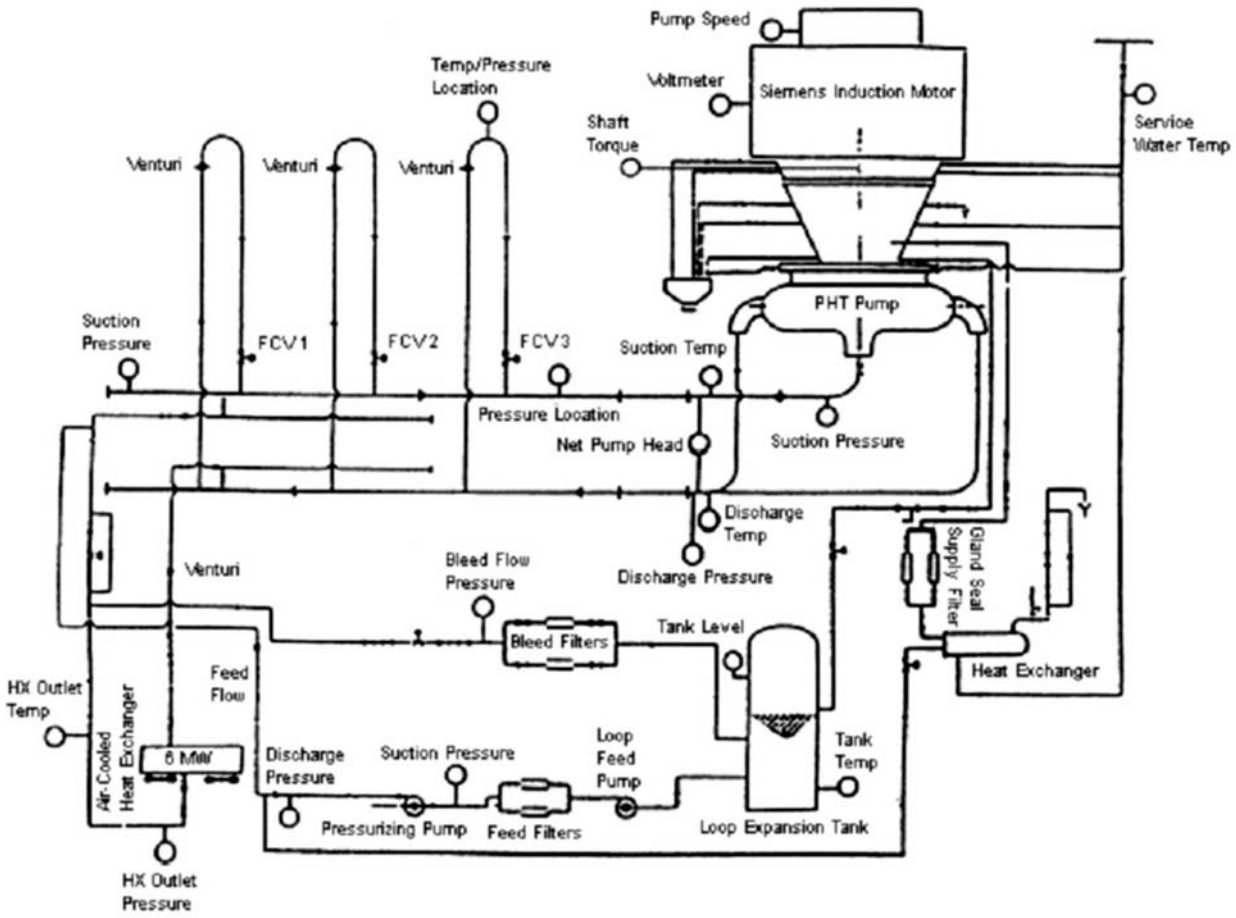

Figure 4.21-2. Schematic of the OHT test loop.

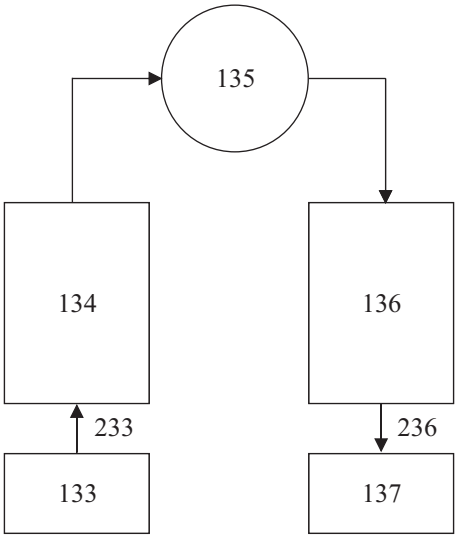

Figure 4.21-3. RELAP5-3D nodalization for the OHT pump tests.

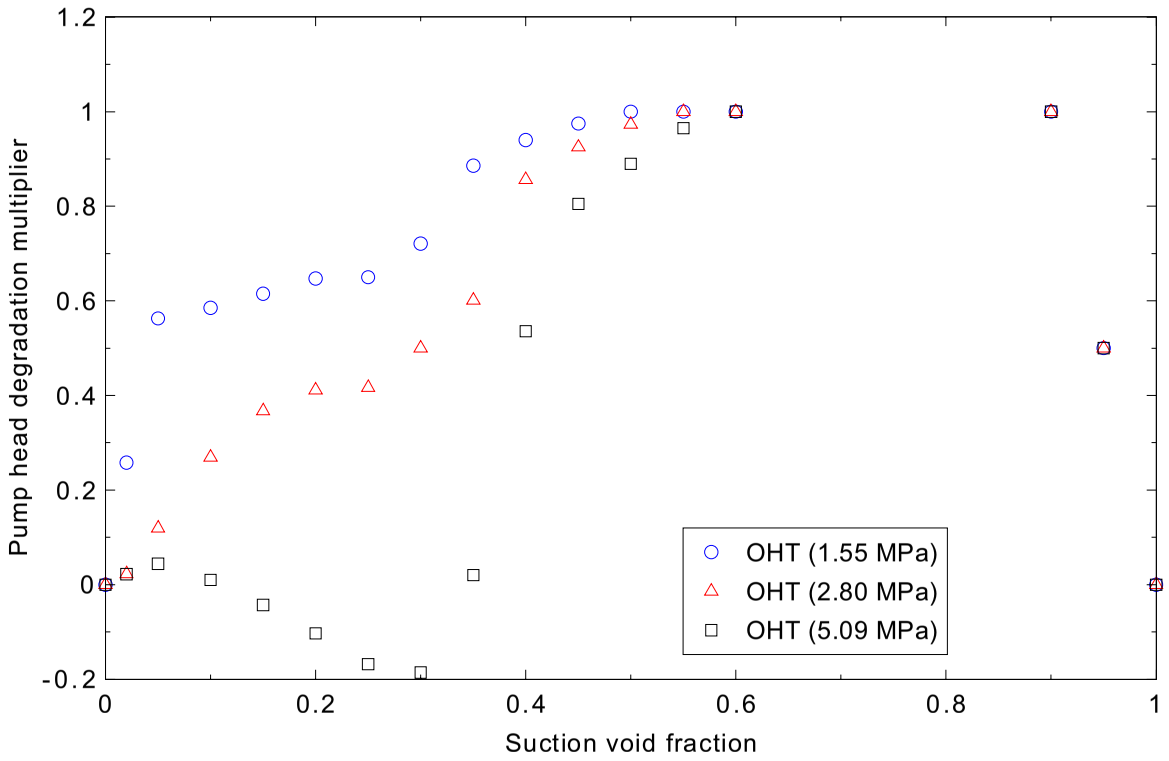

Figure 4.21-4. OHT pump head degradation multipliers.

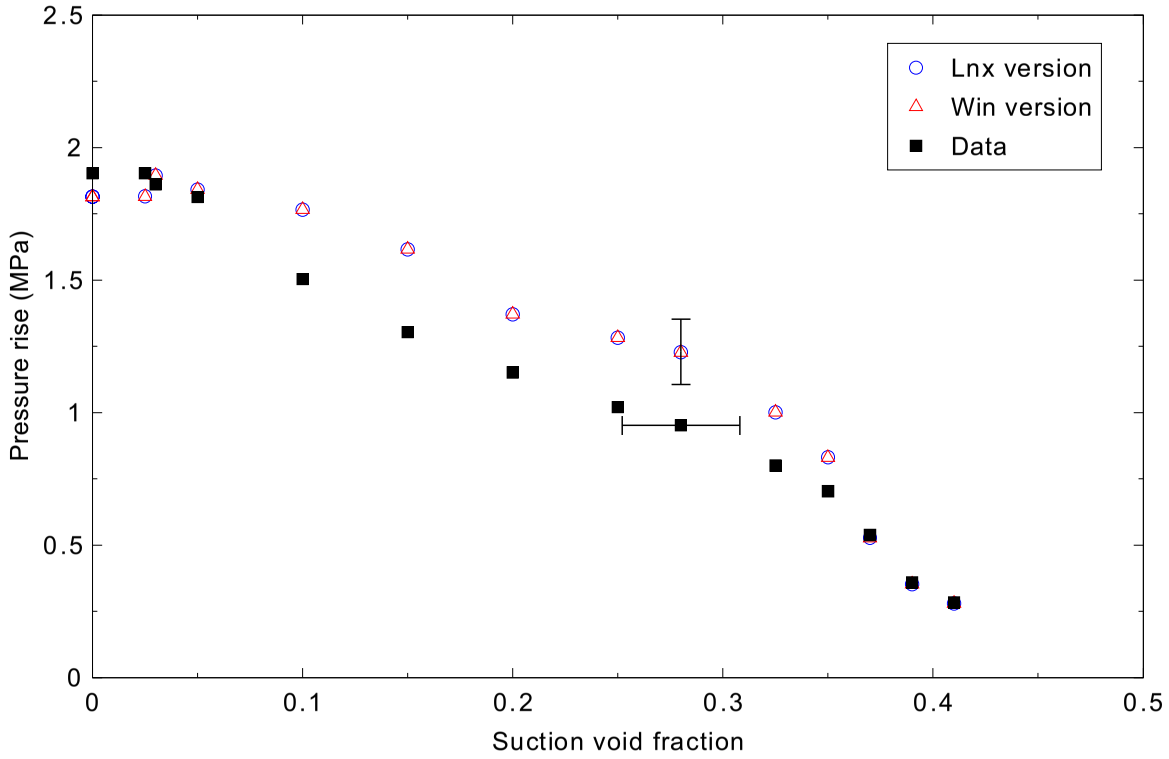

Figure 4.21-5. Pump differential pressures for a suction pressure of 2.80 MPa for the reactor coolant pump case.

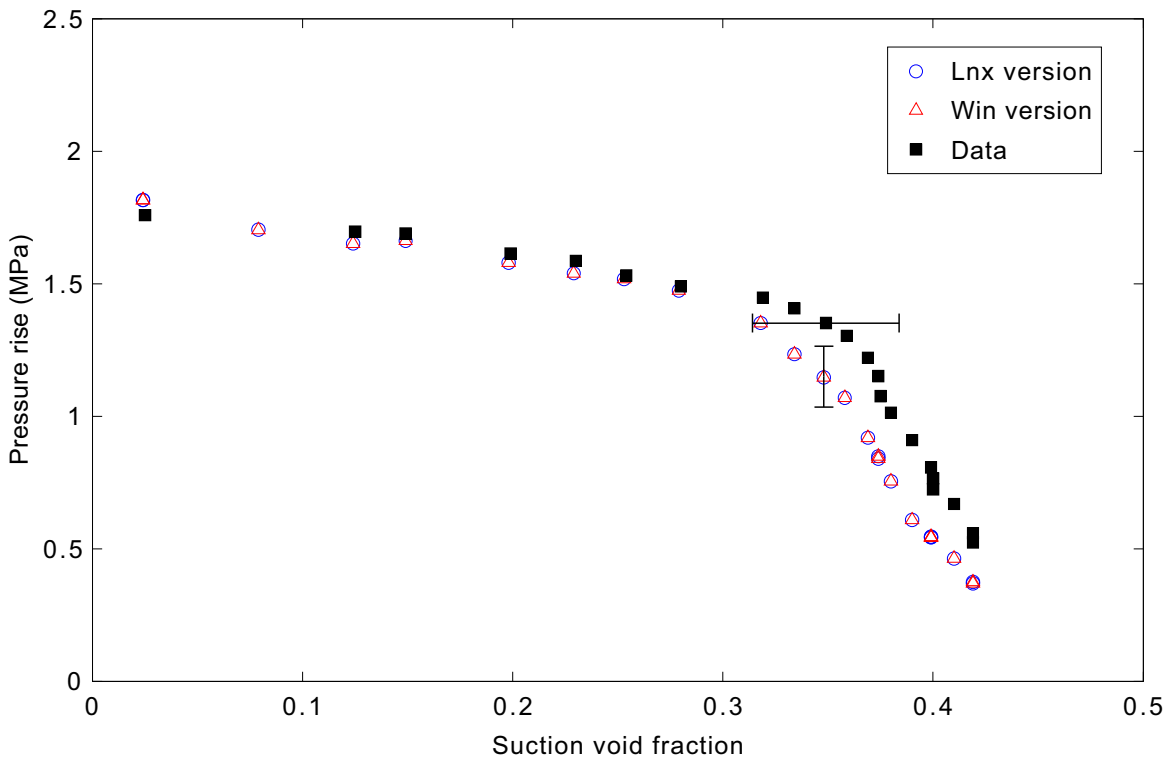

Figure 4.21-6. Pump differential pressures for a suction pressure of 4.69 MPa for the reactor coolant pump case.

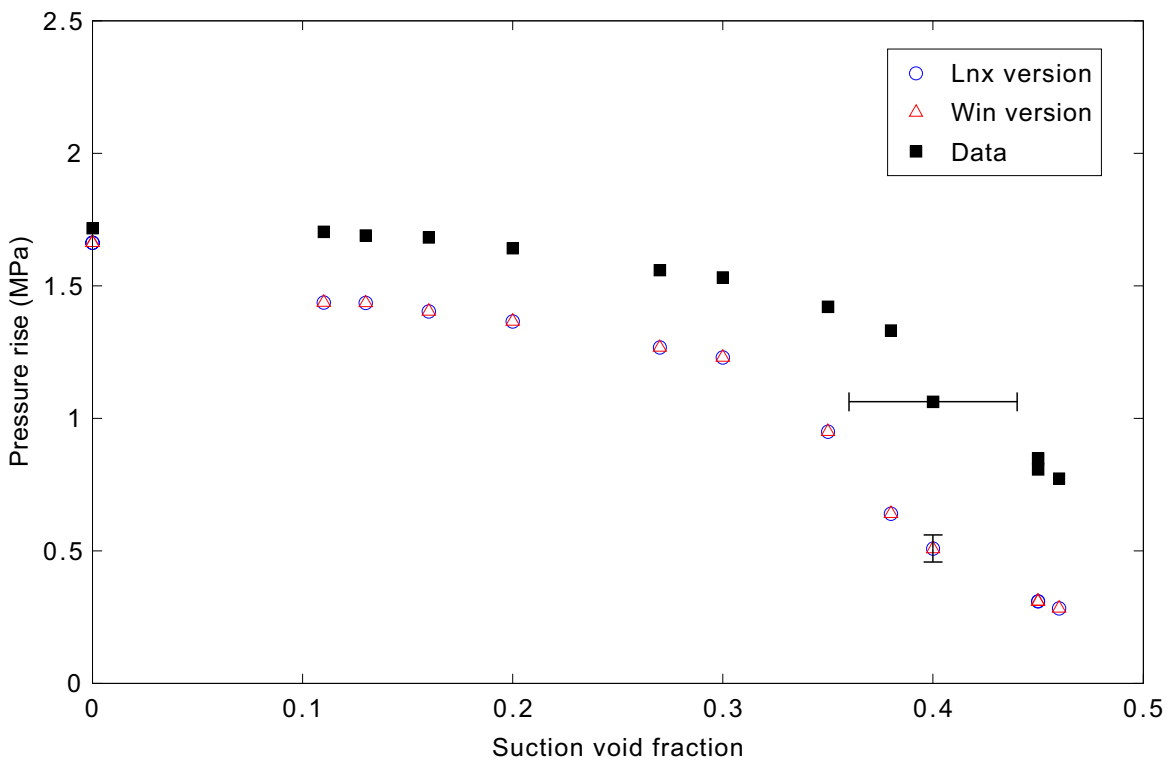

Figure 4.21-7. Pump differential pressures for a suction pressure of 6.42 MPa for the reactor coolant pump case.

4.22 GE 1/6-Scale Jet Pump

Figures comparing simulations using Linux and Windows code versions are presented. Diagrams are included so that the figure numbering is the same as that in Volume III of the RELAP5-3D code manual. No differences were observed in the figures.

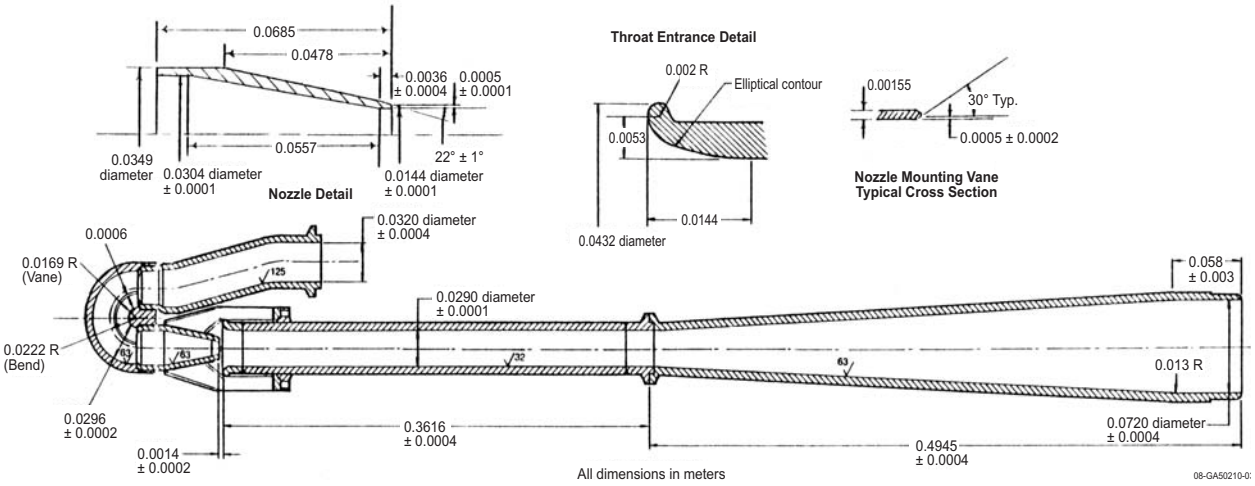

Figure 4.22-1. 1/6-scale model jet pump.

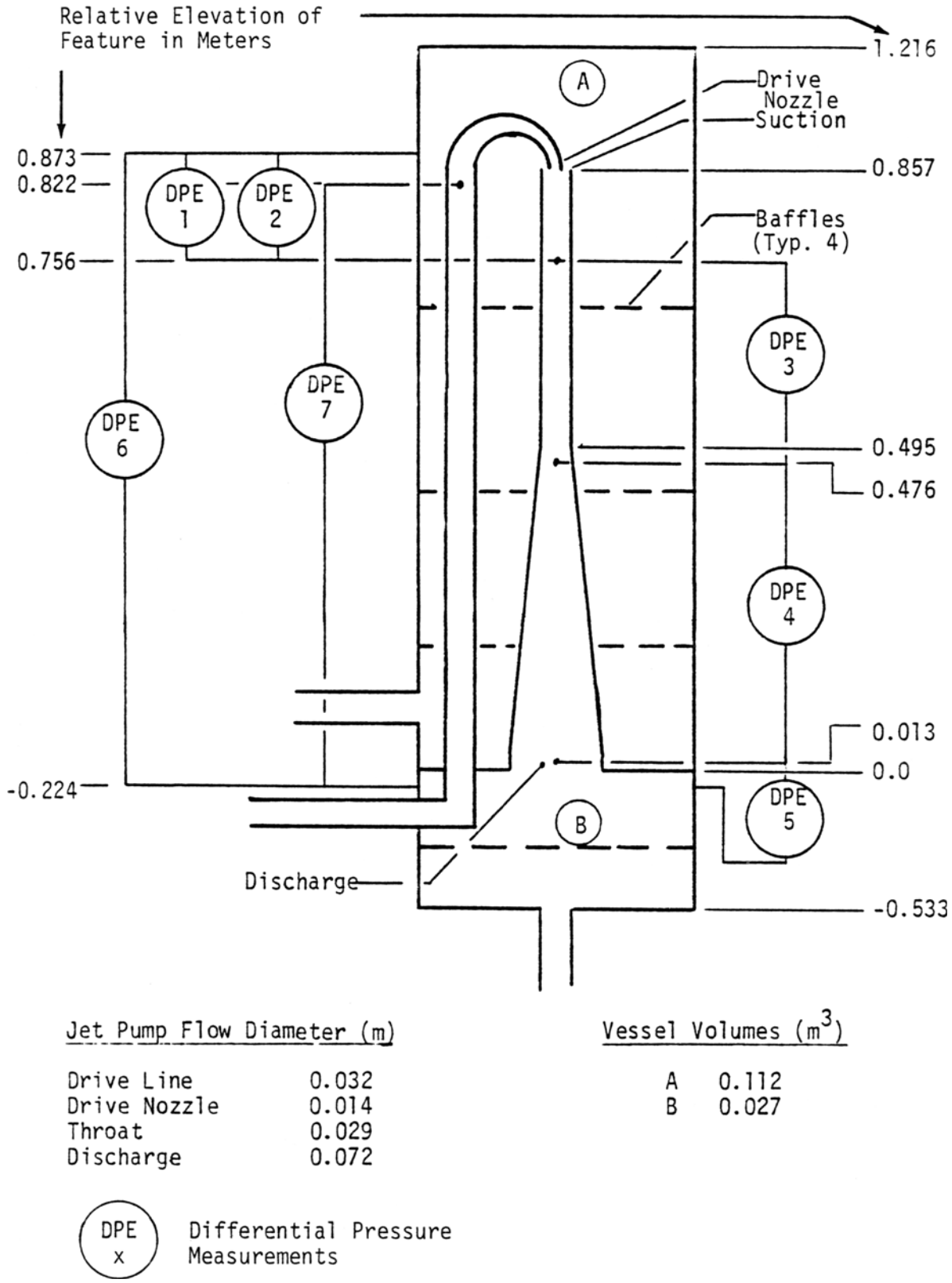

Jet Pump Flow Diameter (m)	
Drive Line	0.032
Drive Nozzle	0.014
Throat	0.029
Discharge	0.072

Vessel Volumes (m^3)	
A	0.112
B	0.027

DPE x — Differential Pressure Measurements

Figure 4.22-2. Schematic of the jet pump and vessel.

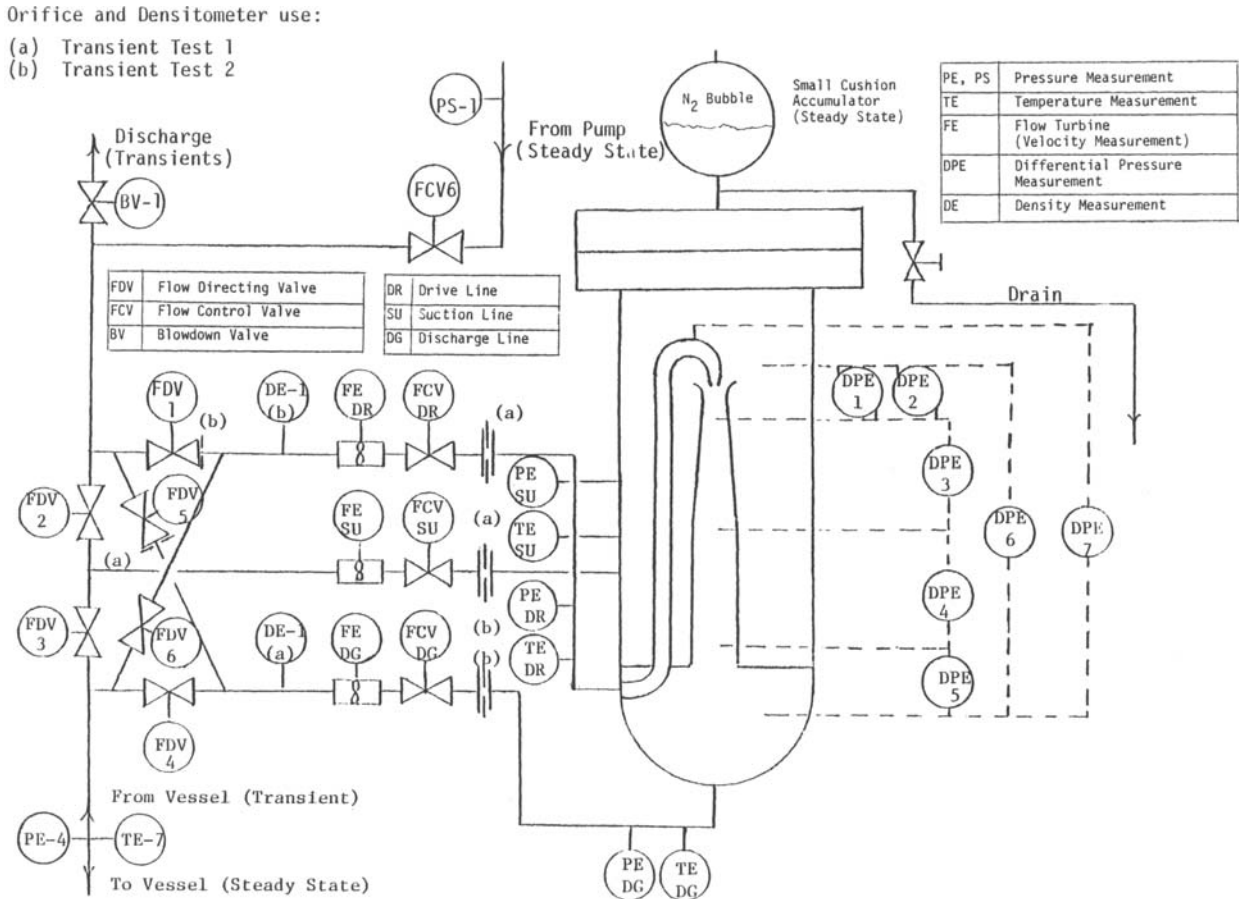

Figure 4.22-3. Jet pump test assembly and instrumentation.

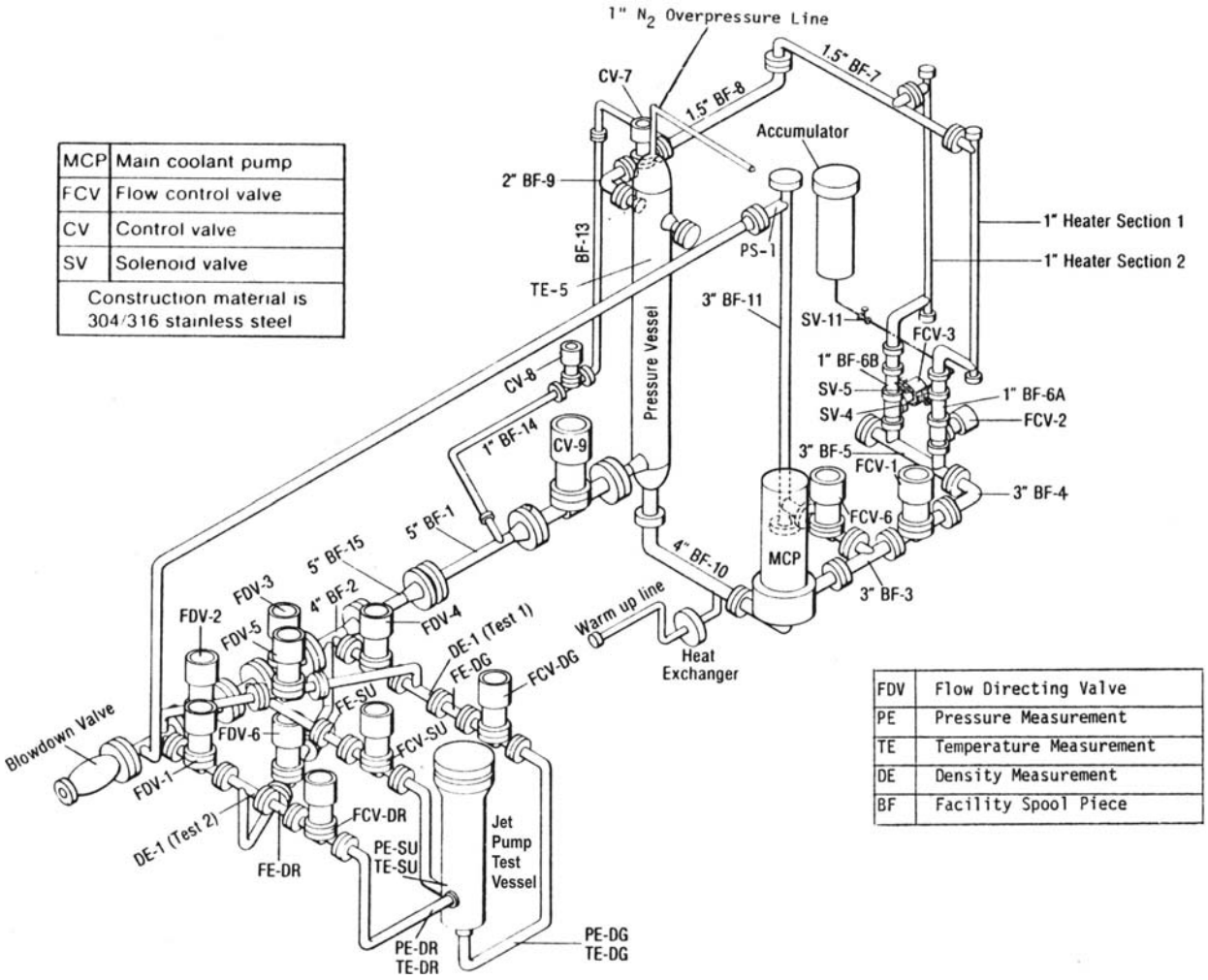

Figure 4.22-4. Jet pump assembly and blowdown facility schematic.

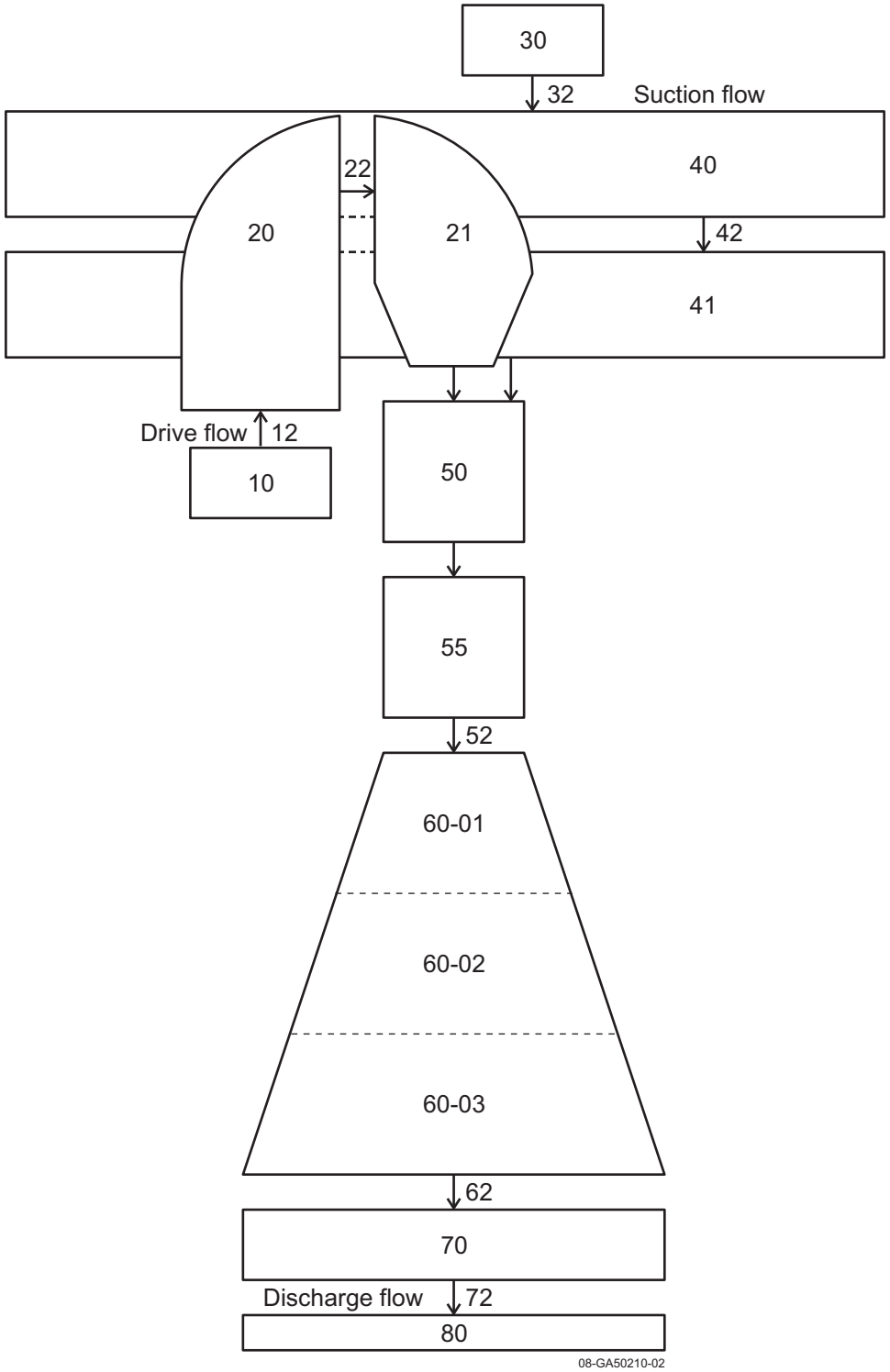

Figure 4.22-5. RELAP5-3D nodalization for the 1/6-scale jet pump test.

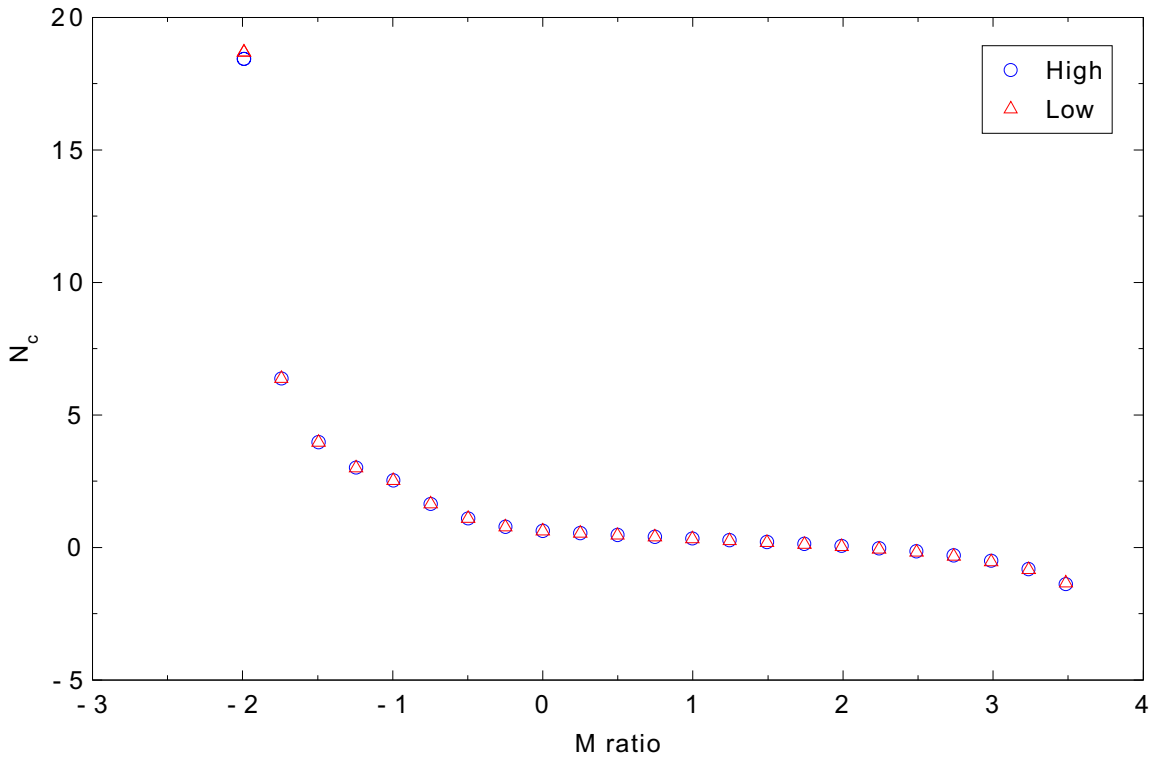

Figure 4.22-6. Calculated flow parameters for forward drive flows at high and low pressure and temperature for the 1/6-scale jet pump case.

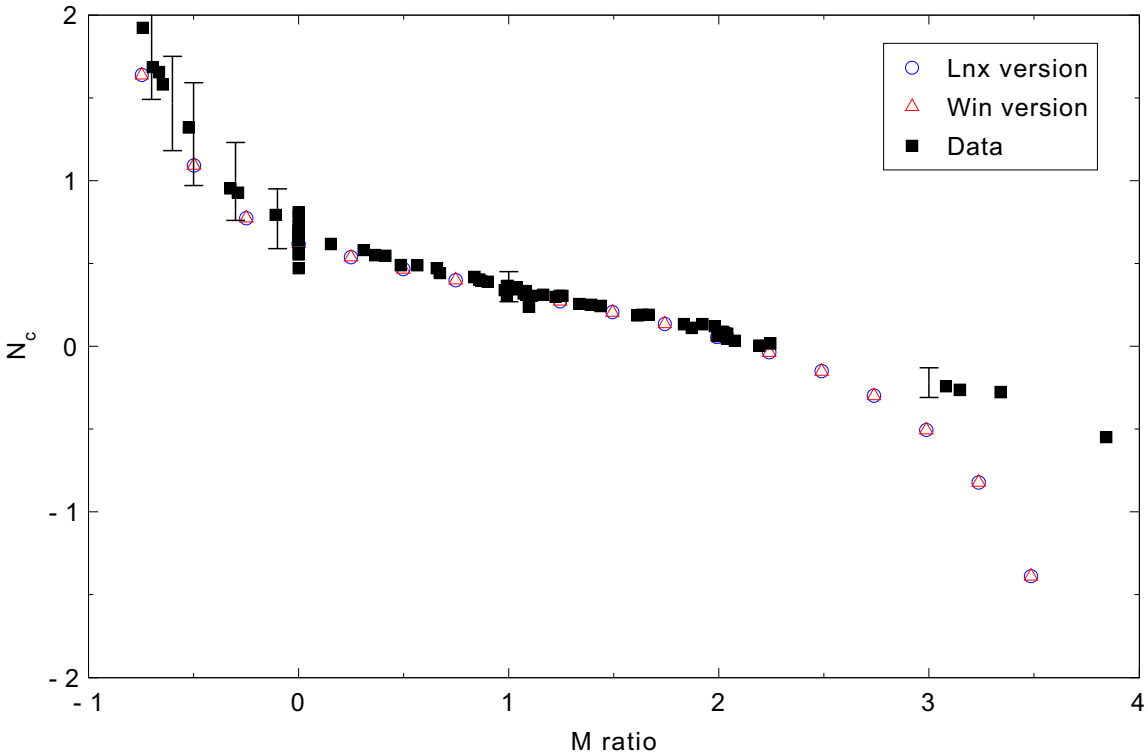

Figure 4.22-7. Measured and calculated flow parameters for forward drive flows for the 1/6-scale jet pump case.

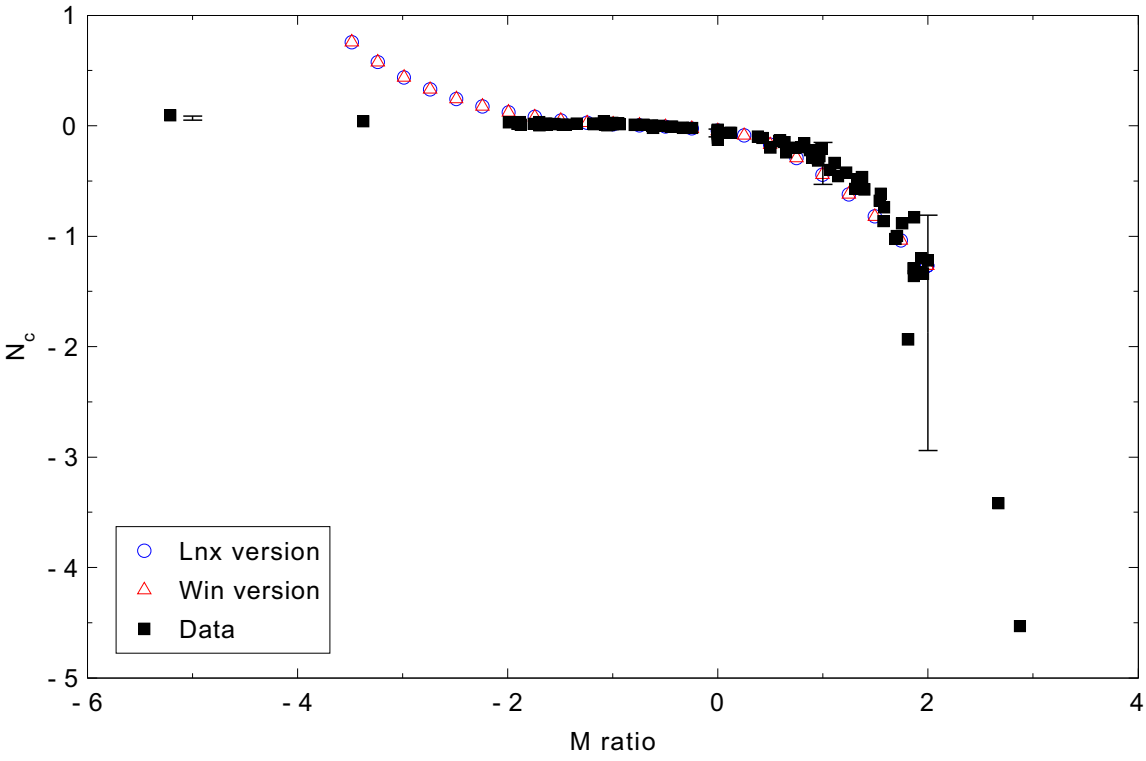

Figure 4.22-8. Measured and calculated flow parameters for reverse drive flows for the 1/6-scale jet pump case.

5. INTEGRAL EFFECTS CASES

This chapter presents the integral effects assessment case results.

5.1 LOFT Experiment L3-7

Figures comparing simulations using Linux and Windows code versions are presented. Diagrams are included so that the figure numbering is the same as that in Volume III of the RELAP5-3D code manual. A noticeable difference was observed in Figure 5.1-4.

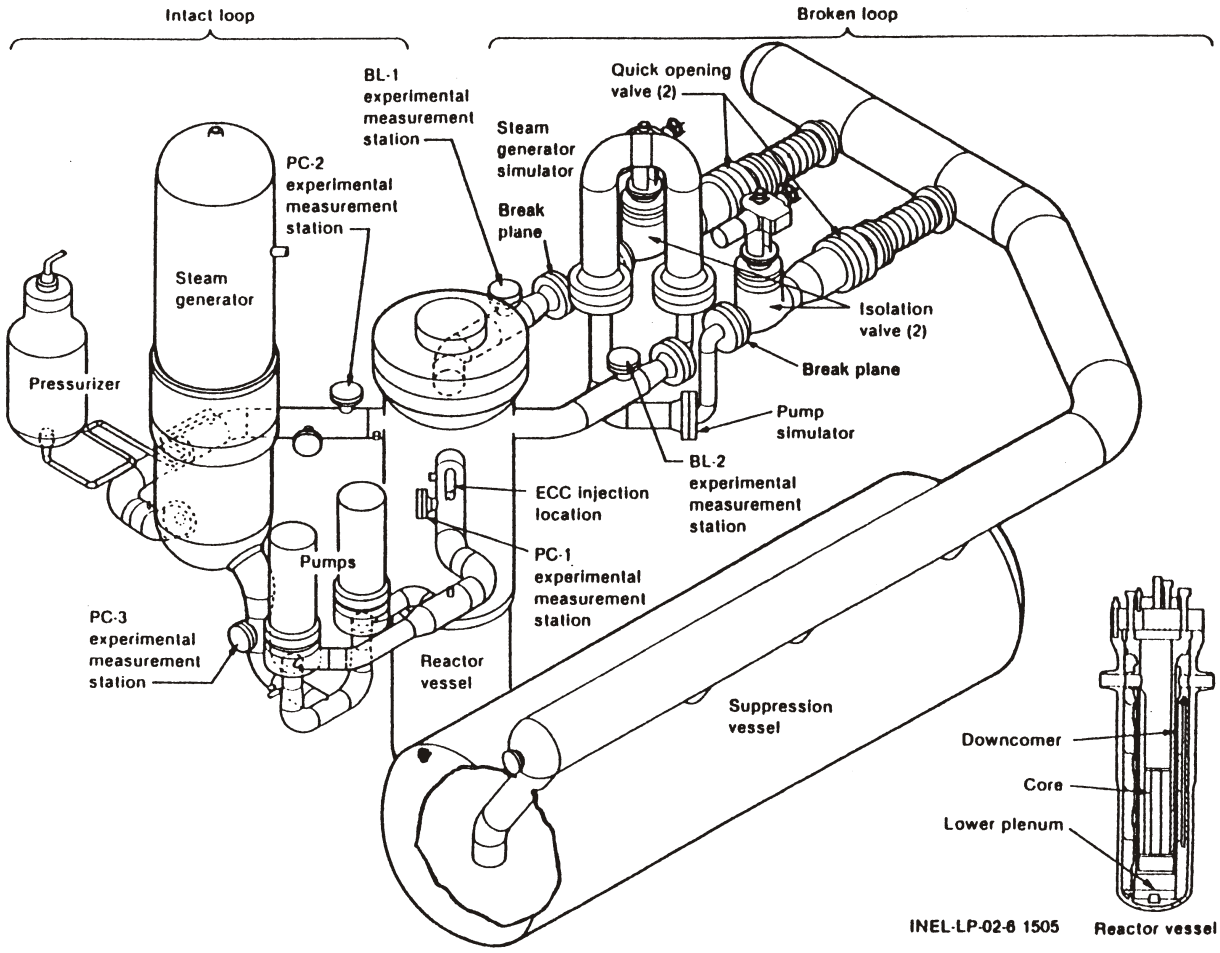

Figure 5.1-1. Schematic of the LOFT facility.

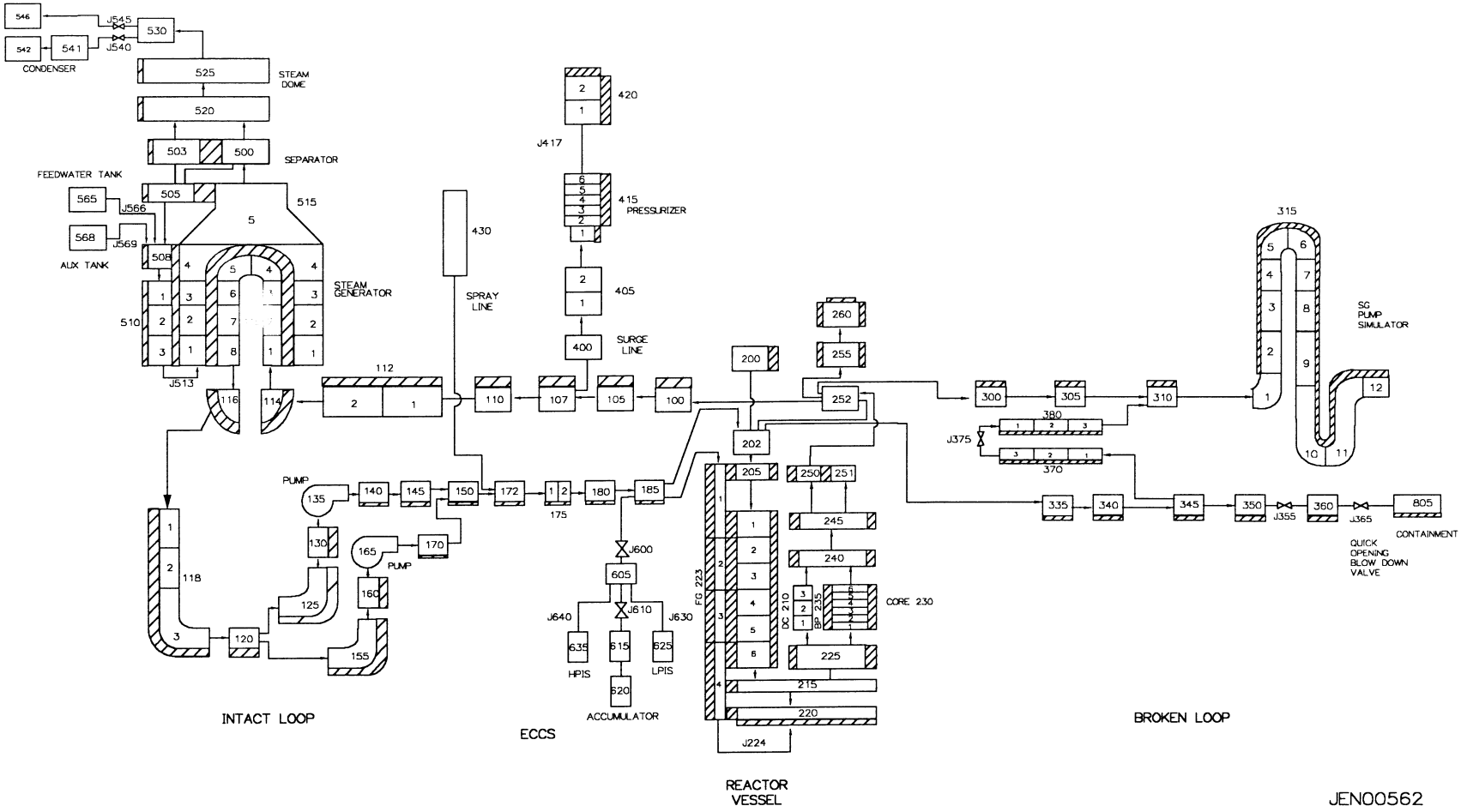

Figure 5.1-2. RELAP5-3D nodalization for the LOFT facility Experiment L3-7.

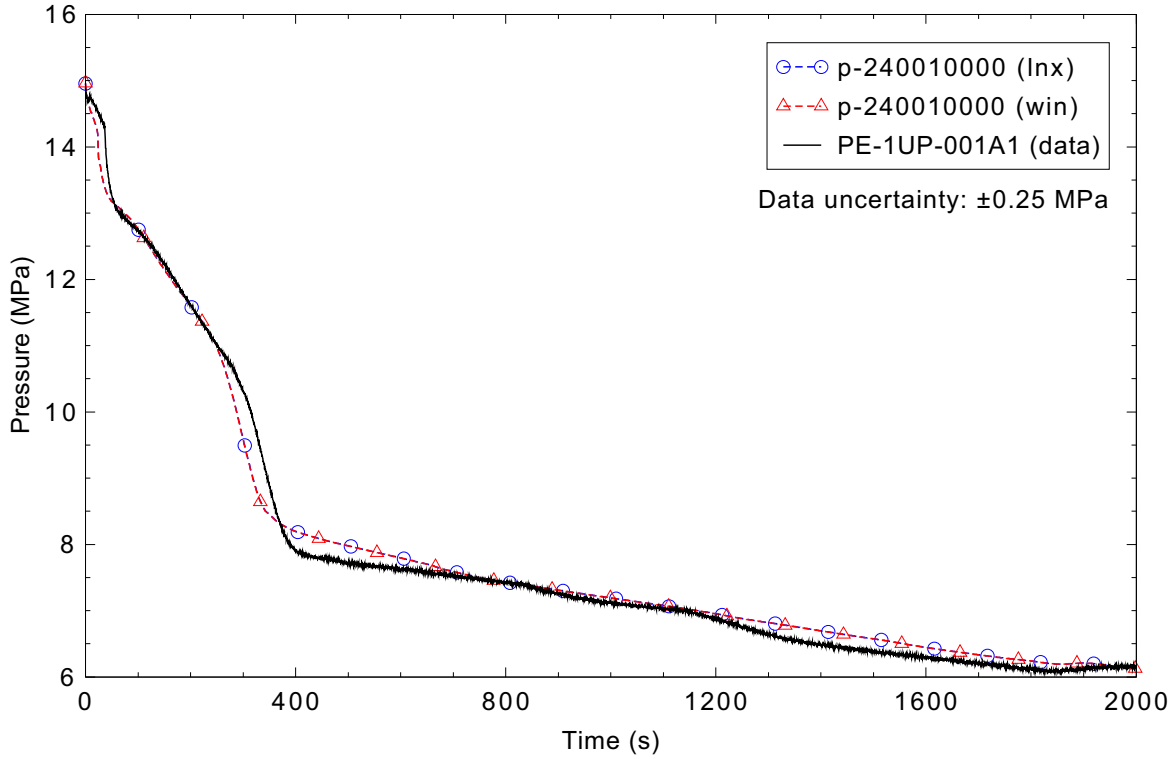

Figure 5.1-3. Measured and calculated reactor vessel upper plenum pressure for LOFT Experiment L3-7.

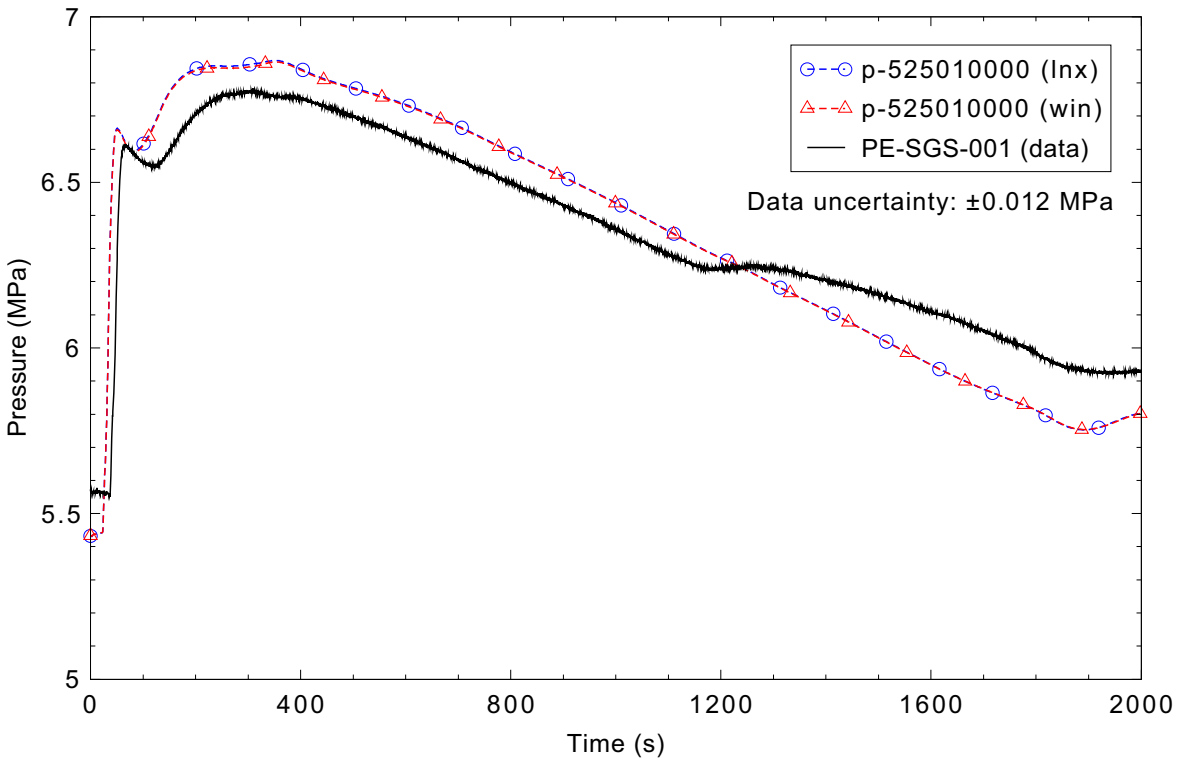

Figure 5.1-4. Measured and calculated steam generator secondary pressure for LOFT Experiment L3-7.

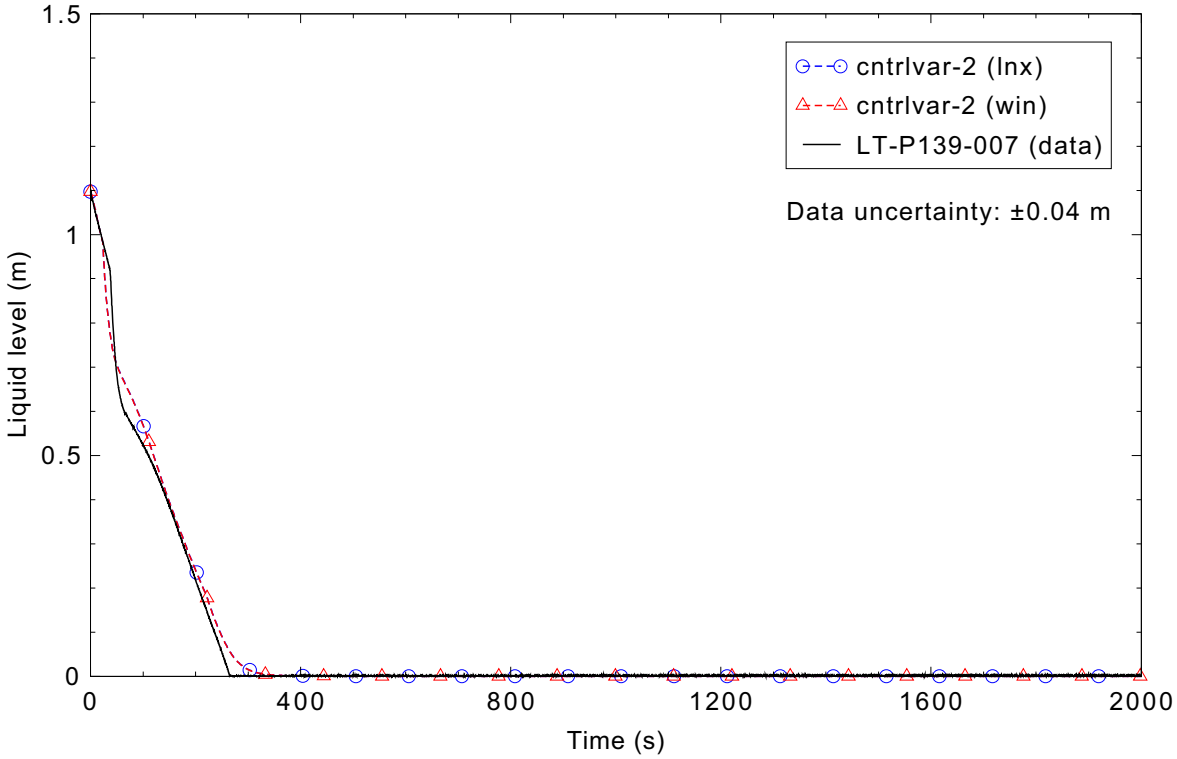

Figure 5.1-5. Measured and calculated pressurizer liquid level for LOFT Experiment L3-7.

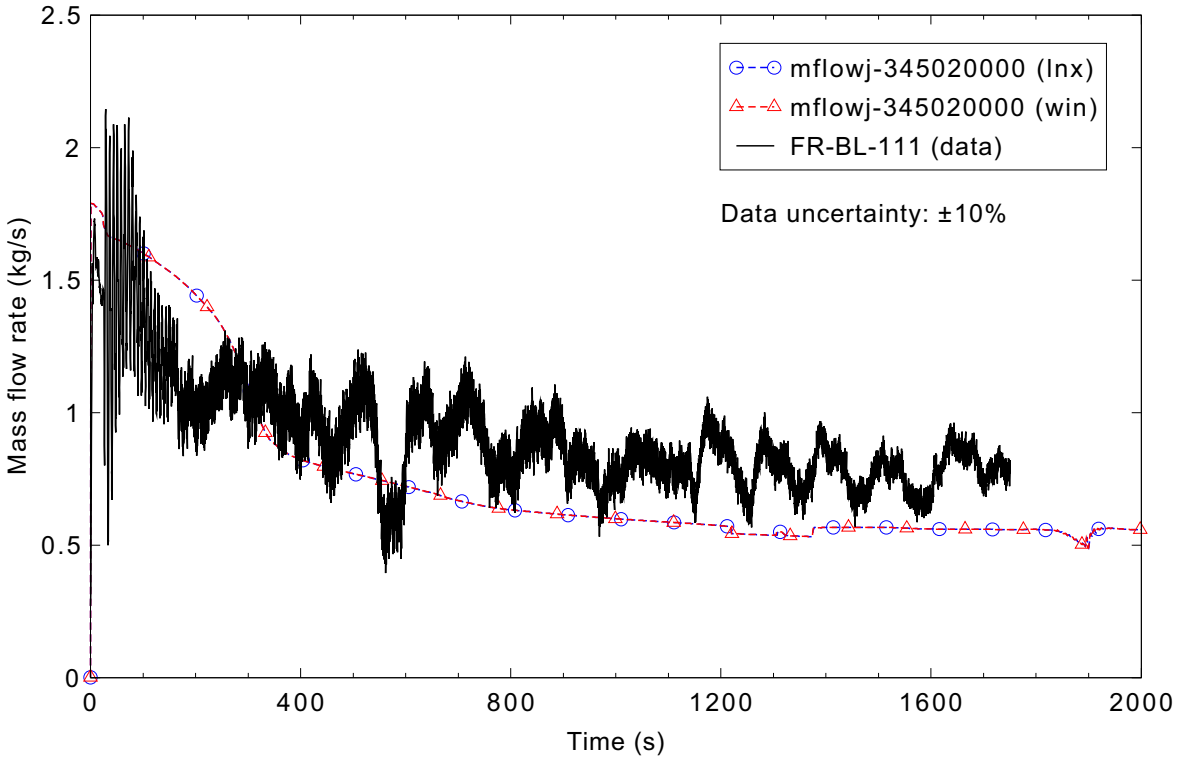

Figure 5.1-6. Measured and calculated break flow rate for LOFT Experiment L3-7.

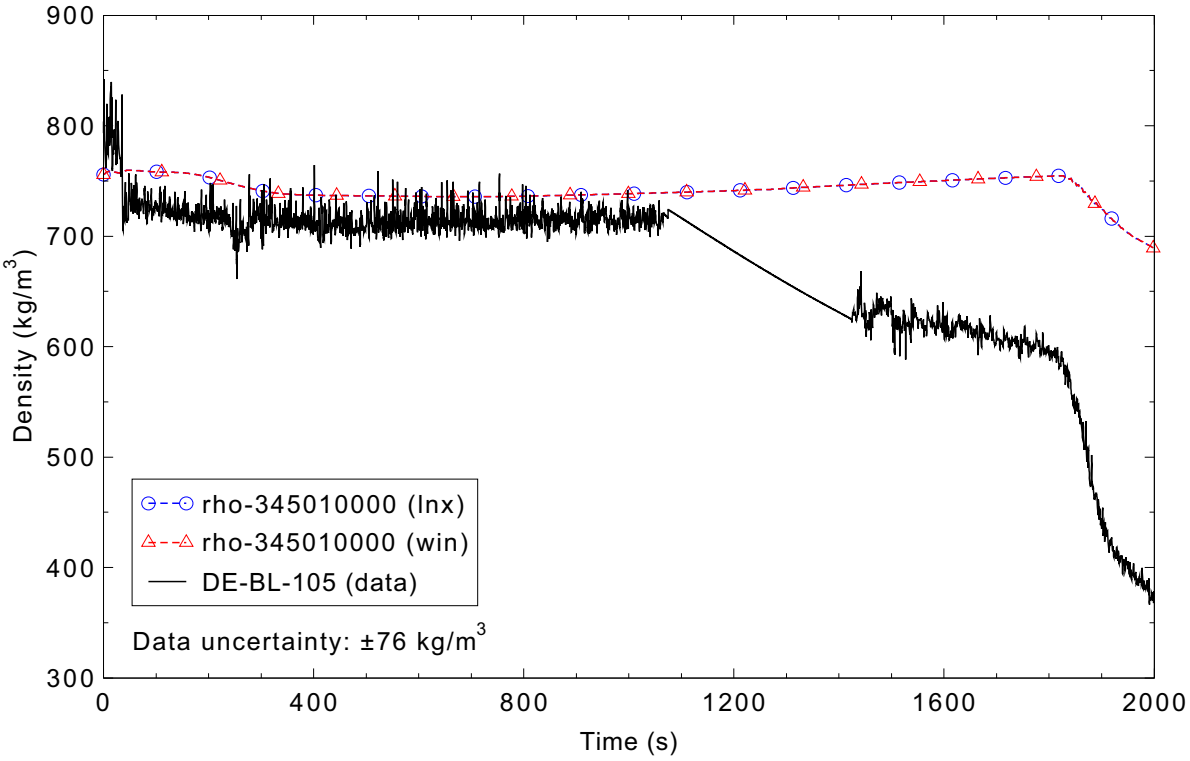

Figure 5.1-7. Measured and calculated broken loop cold leg fluid density for LOFT Experiment L3-7.

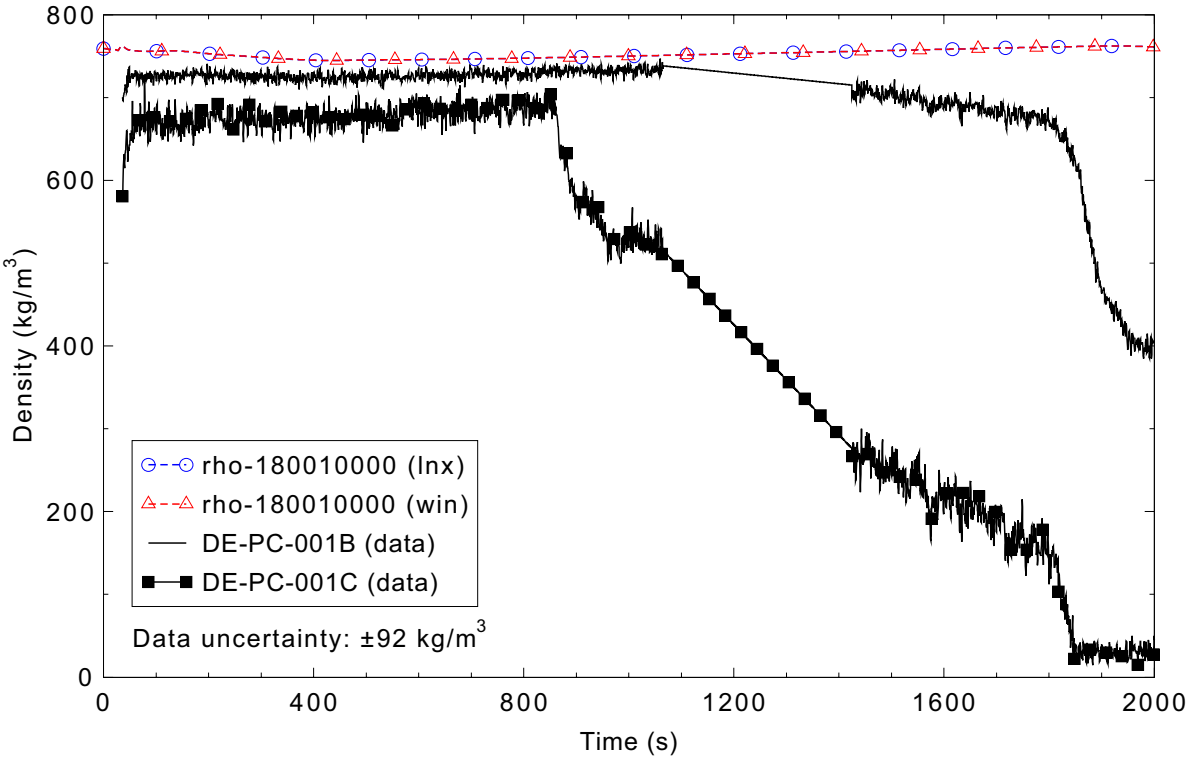

Figure 5.1-8. Measured and calculated intact loop cold leg fluid density for LOFT Experiment L3-7.

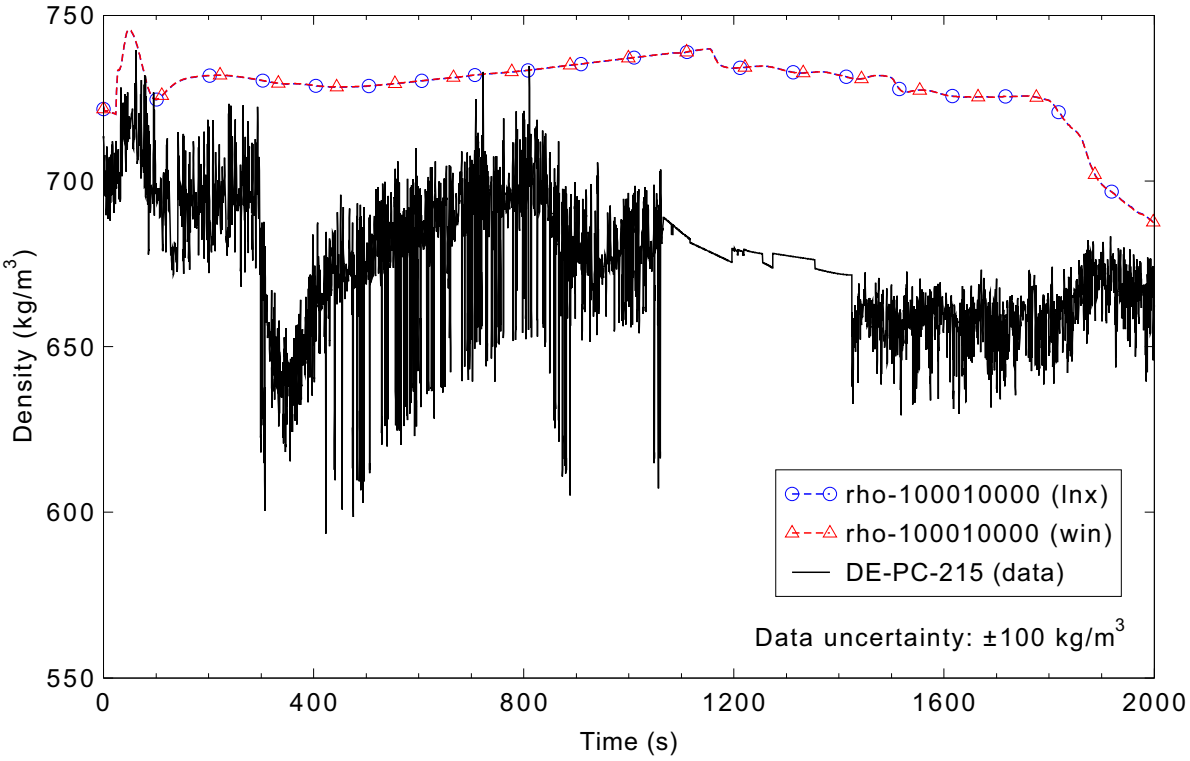

Figure 5.1-9. Measured and calculated intact loop hot leg fluid density for LOFT Experiment L3-7.

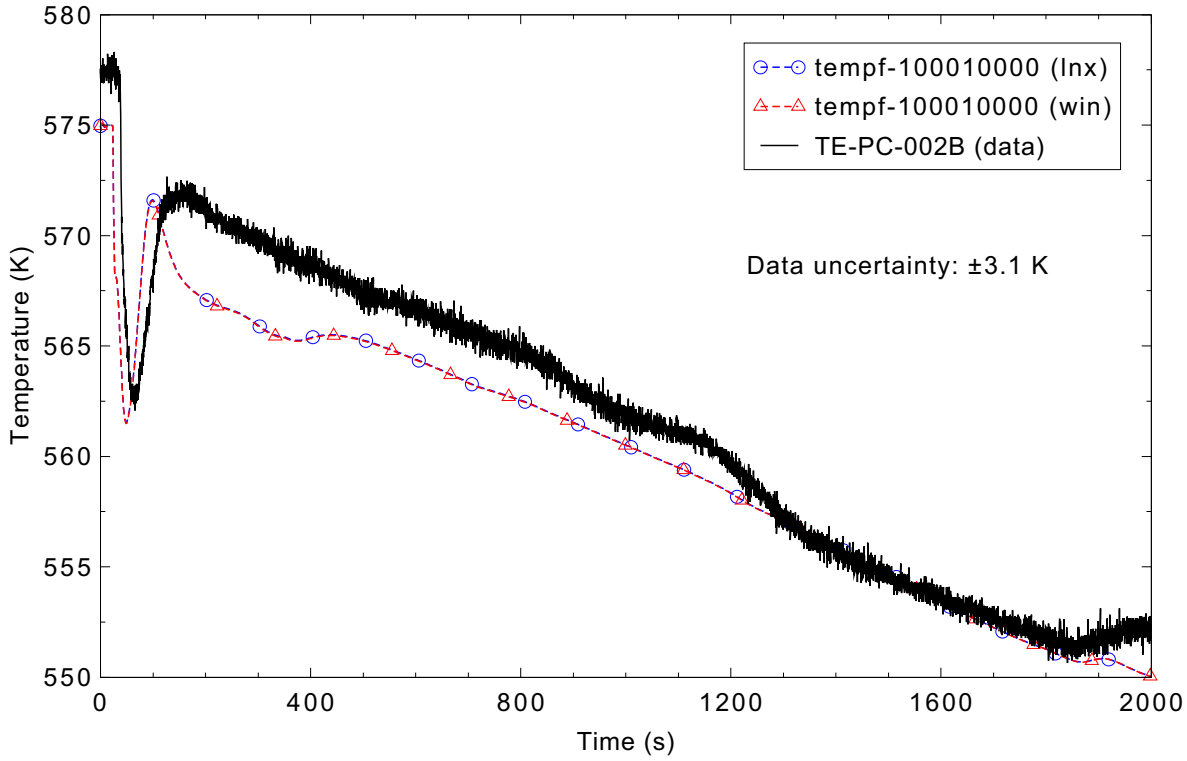

Figure 5.1-10. Measured and calculated intact loop hot leg fluid temperature for LOFT Experiment L3-7.

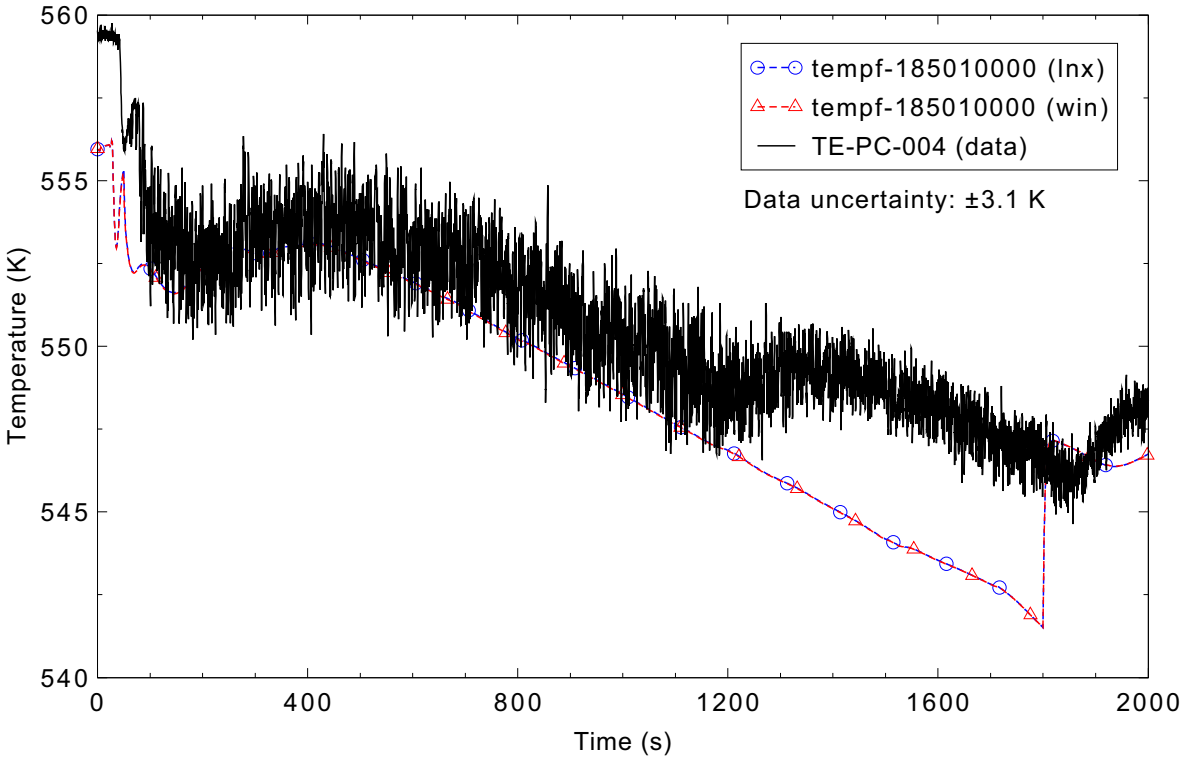

Figure 5.1-11. Measured and calculated intact loop cold leg fluid temperature for LOFT Experiment L3-7.

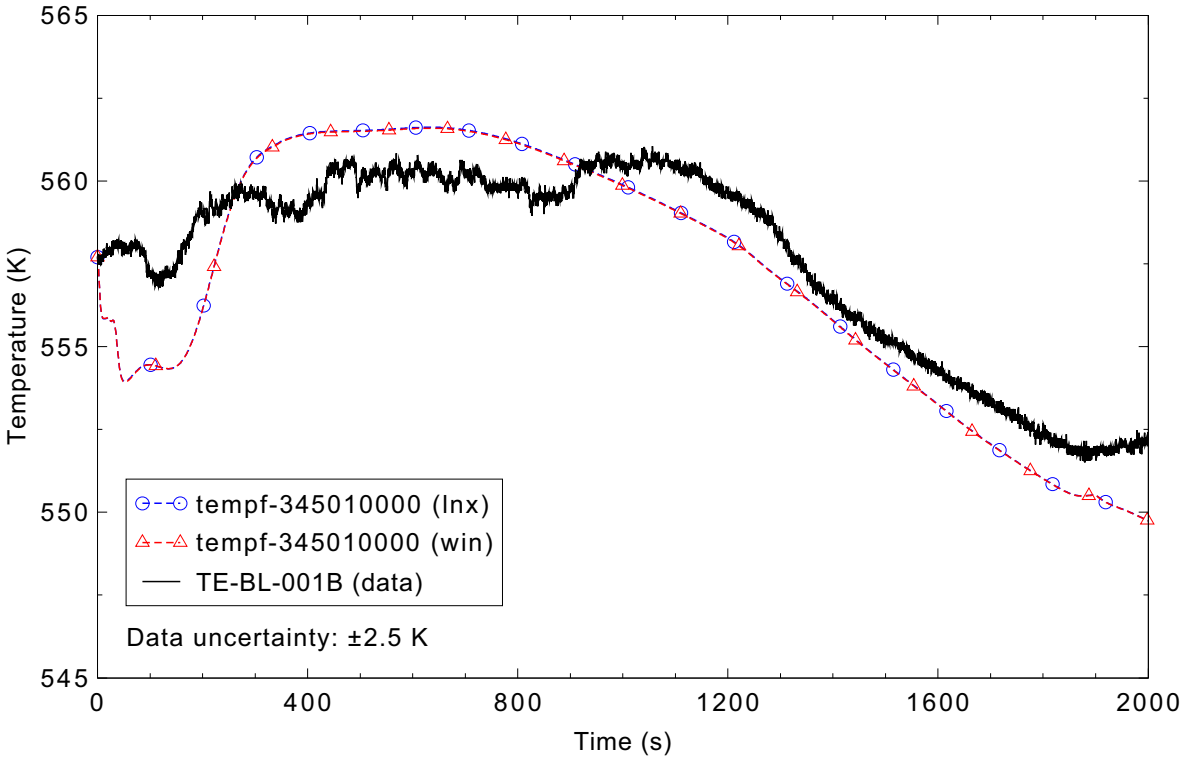

Figure 5.1-12. Measured and calculated broken loop cold leg fluid temperature for LOFT Experiment L3-7.

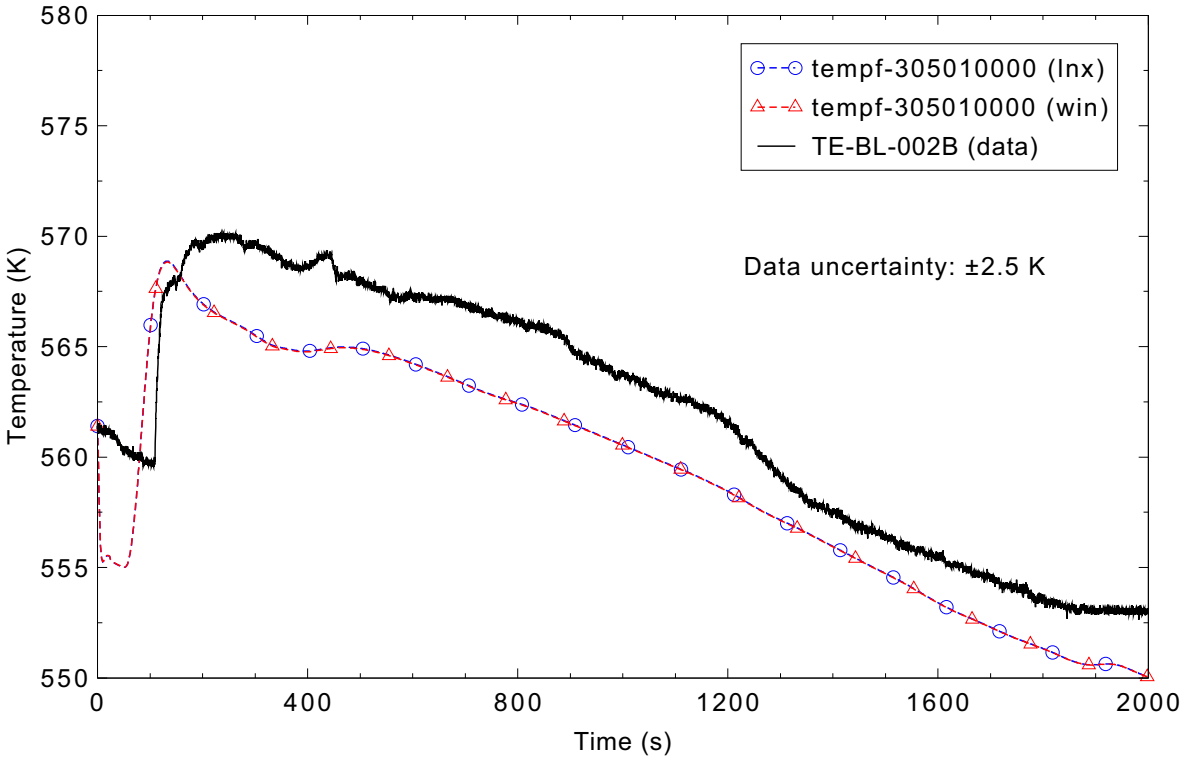

Figure 5.1-13. Measured and calculated broken loop hot leg fluid temperature for LOFT Experiment L3-7.

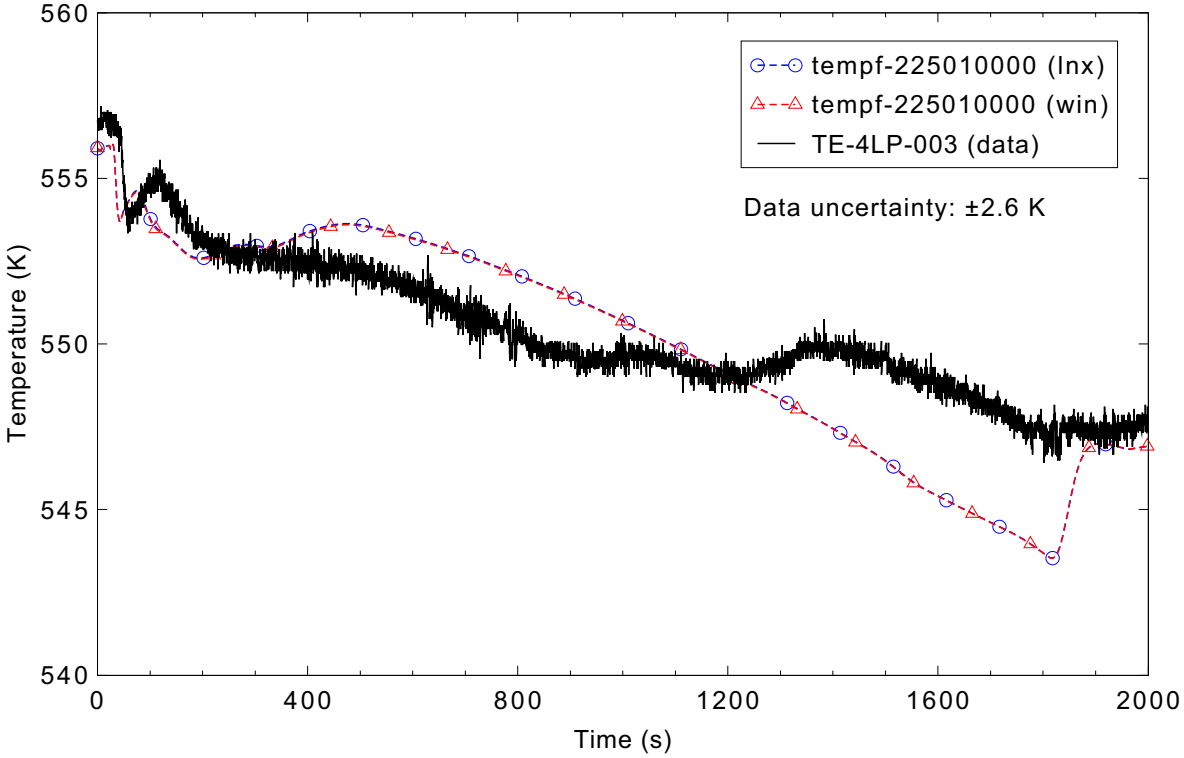

Figure 5.1-14. Measured and calculated core inlet fluid temperature for LOFT Experiment L3-7.

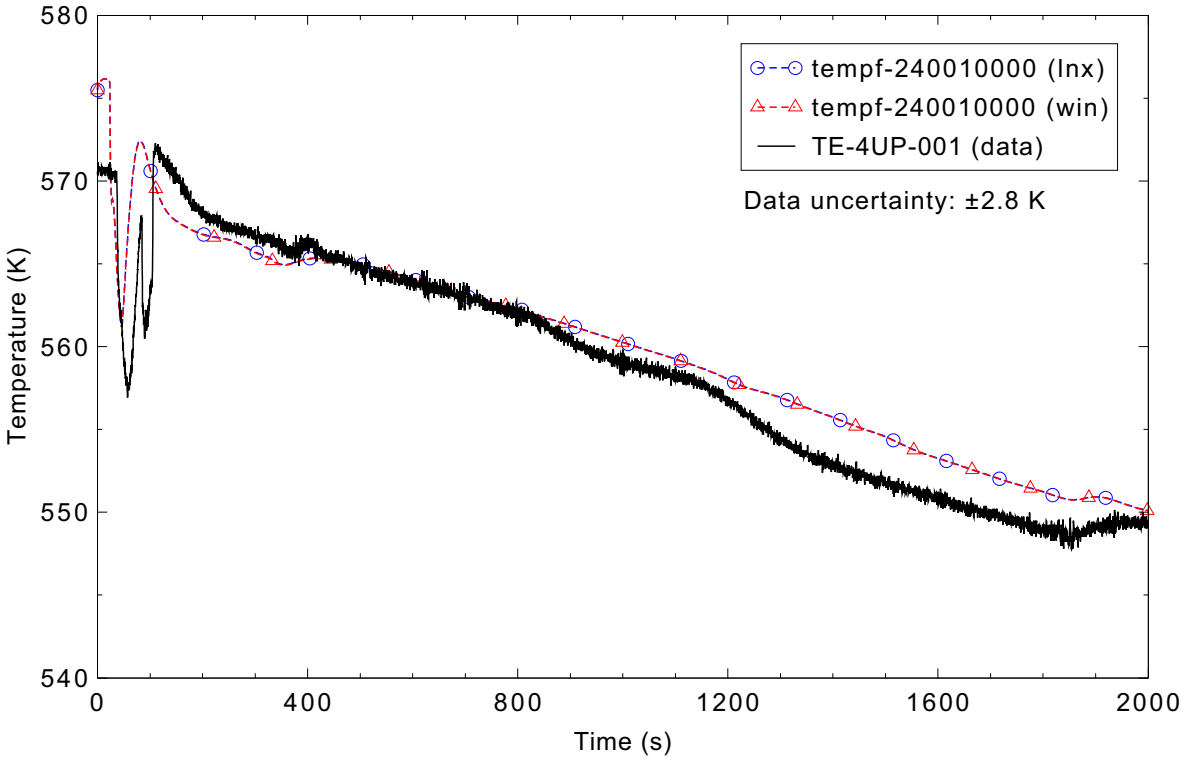

Figure 5.1-15. Measured and calculated reactor vessel upper plenum fluid temperature for LOFT Experiment L3-7.

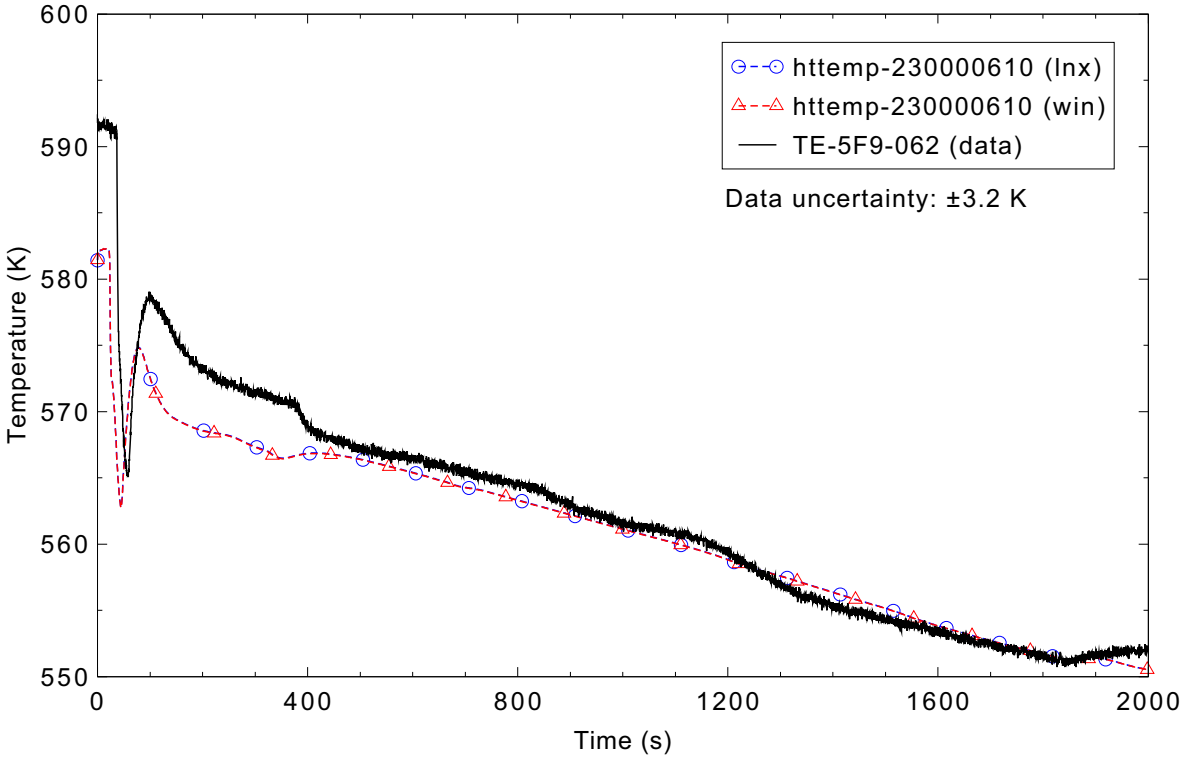

Figure 5.1-16. Measured and calculated fuel cladding surface temperature 1.57 m above the bottom of the fuel for LOFT Experiment L3-7.

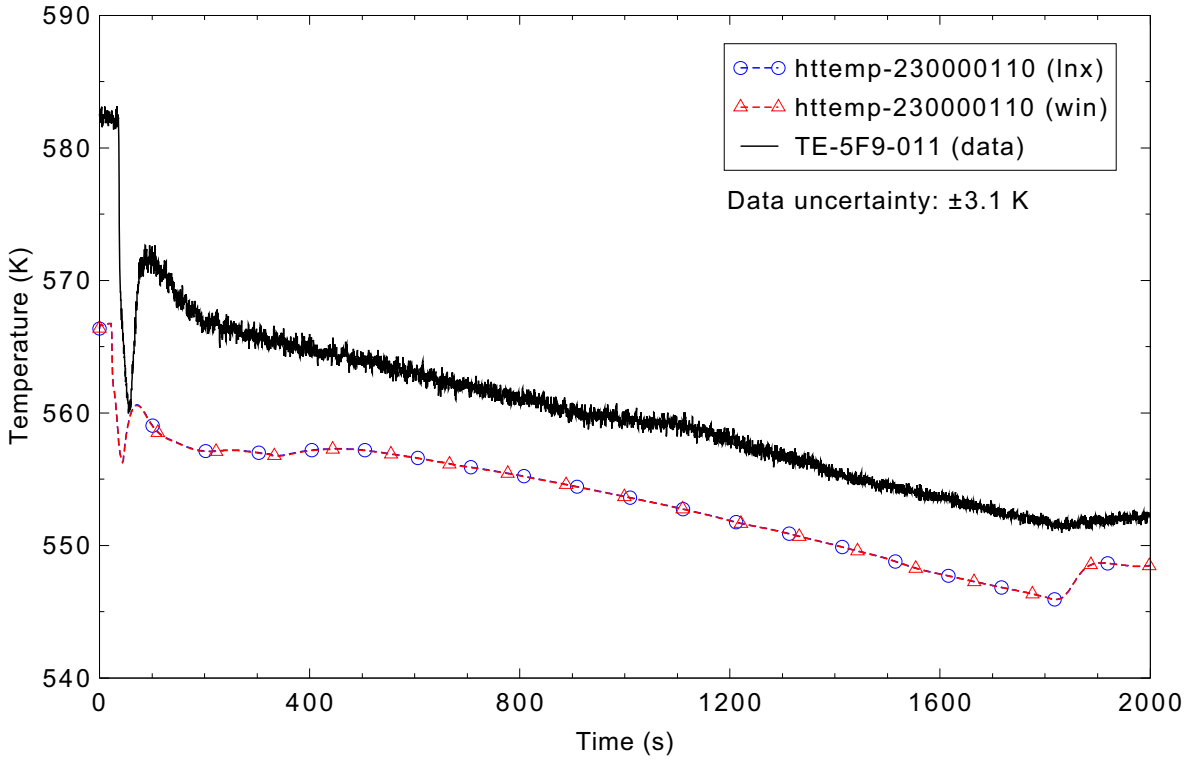

Figure 5.1-17. Measured and calculated fuel cladding surface temperature 0.28 m above the bottom of the fuel for LOFT Experiment L3-7.

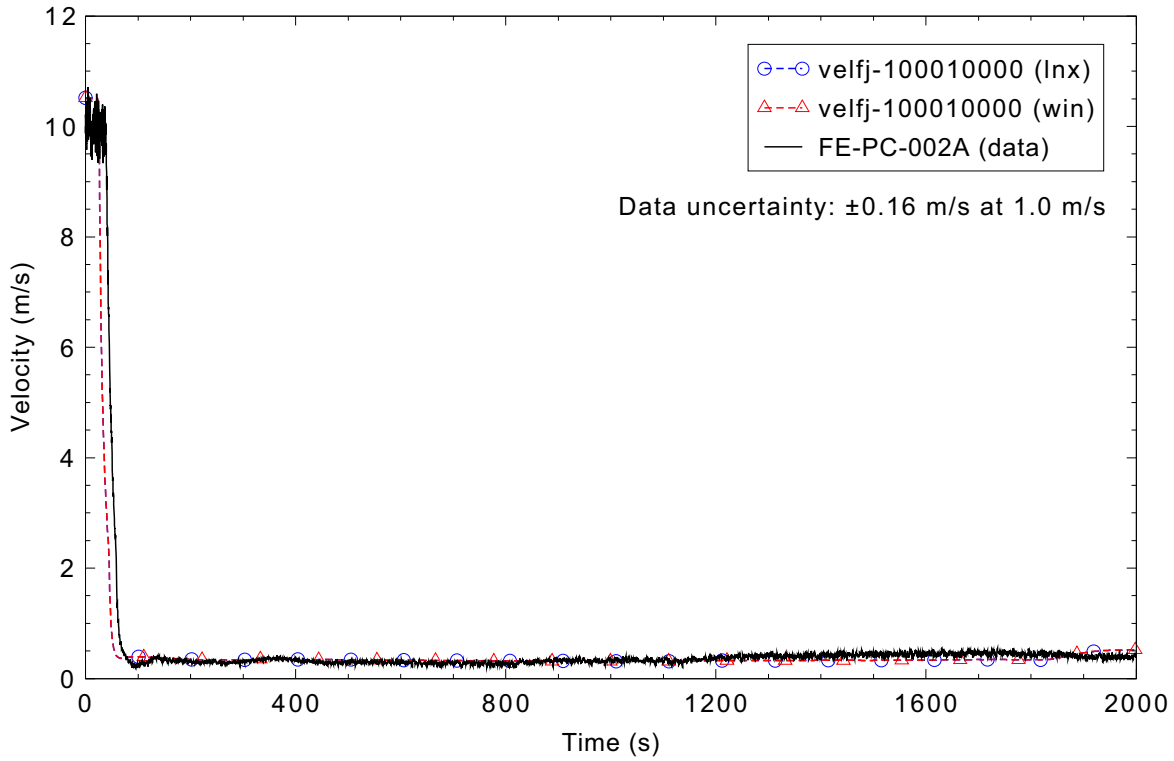

Figure 5.1-18. Measured and calculated hot leg fluid velocity for LOFT Experiment L3-7.

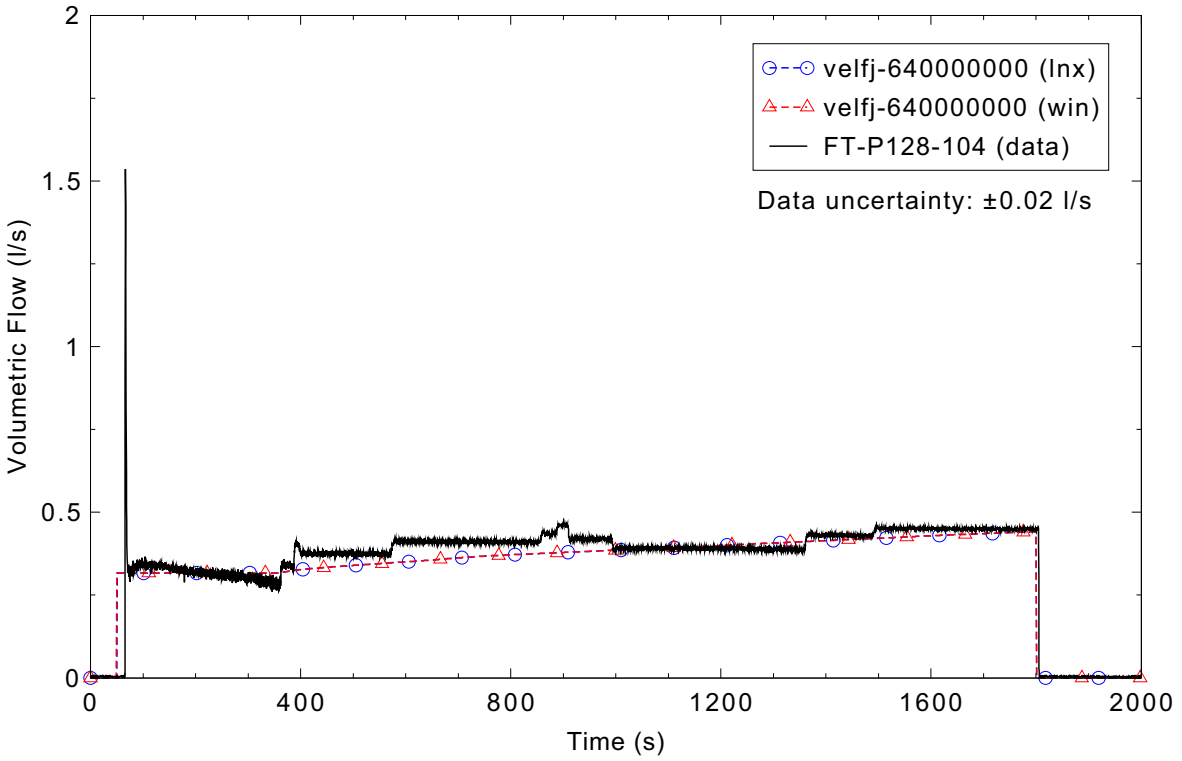

Figure 5.1-19. Measured and calculated HPIS volumetric flow for LOFT Experiment L3-7.

5.2 ROSA-IV Test SB-CL-18

Figures comparing simulations using Linux and Windows code versions are presented. Diagrams are included so that the figure numbering is the same as that in Volume III of the RELAP5-3D code manual. Significant differences were observed in Figures 5.2-16, 17, and 18. Noticeable differences were observed in Figures 5.2-4, 6, 8, 9, 10, 11, 12, 13, 14, 15, 19, 20, 21, 22, 23, and 24.

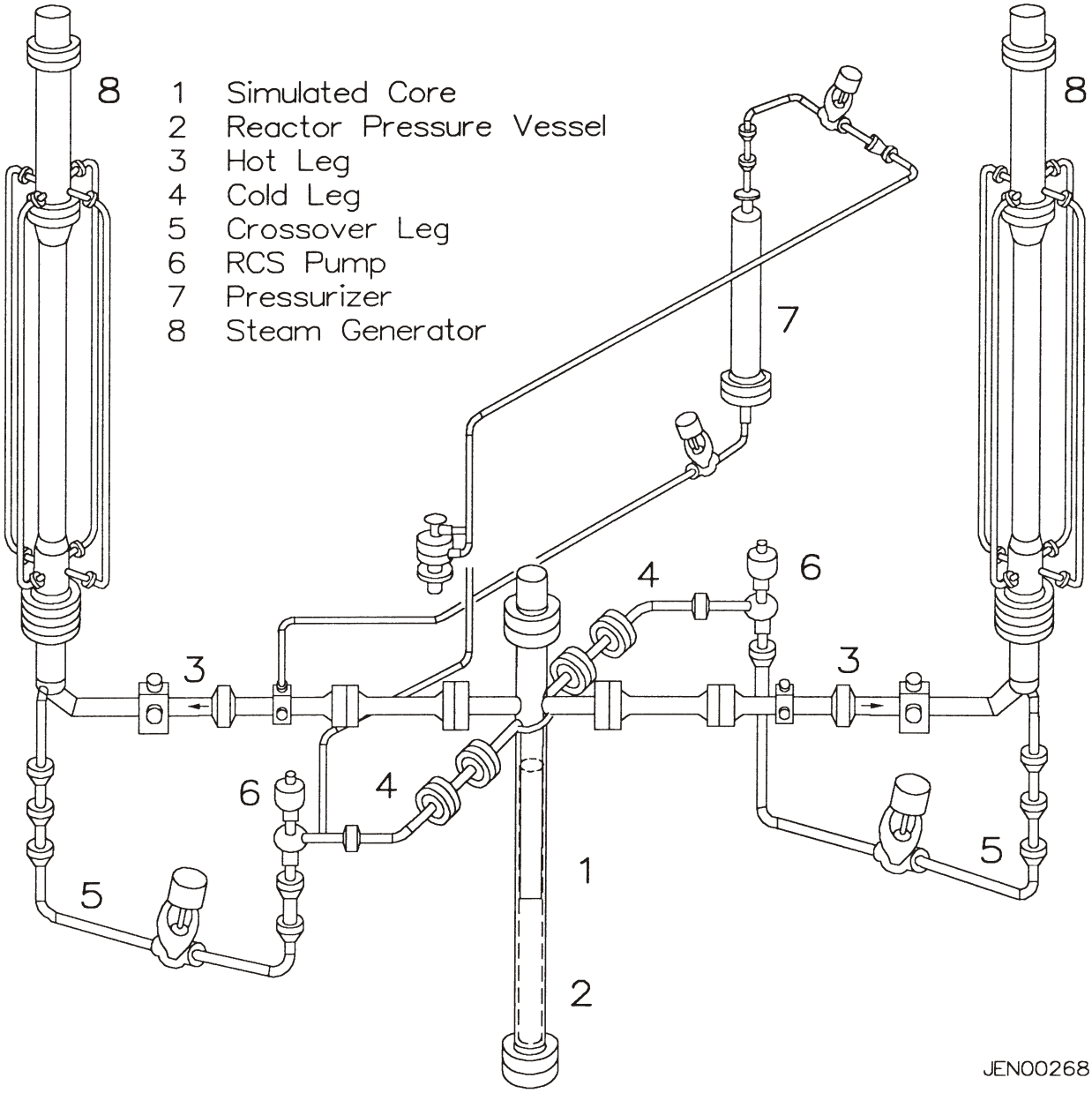

Figure 5.2-1. Schematic of the ROSA-IV large scale test facility (LSTF).

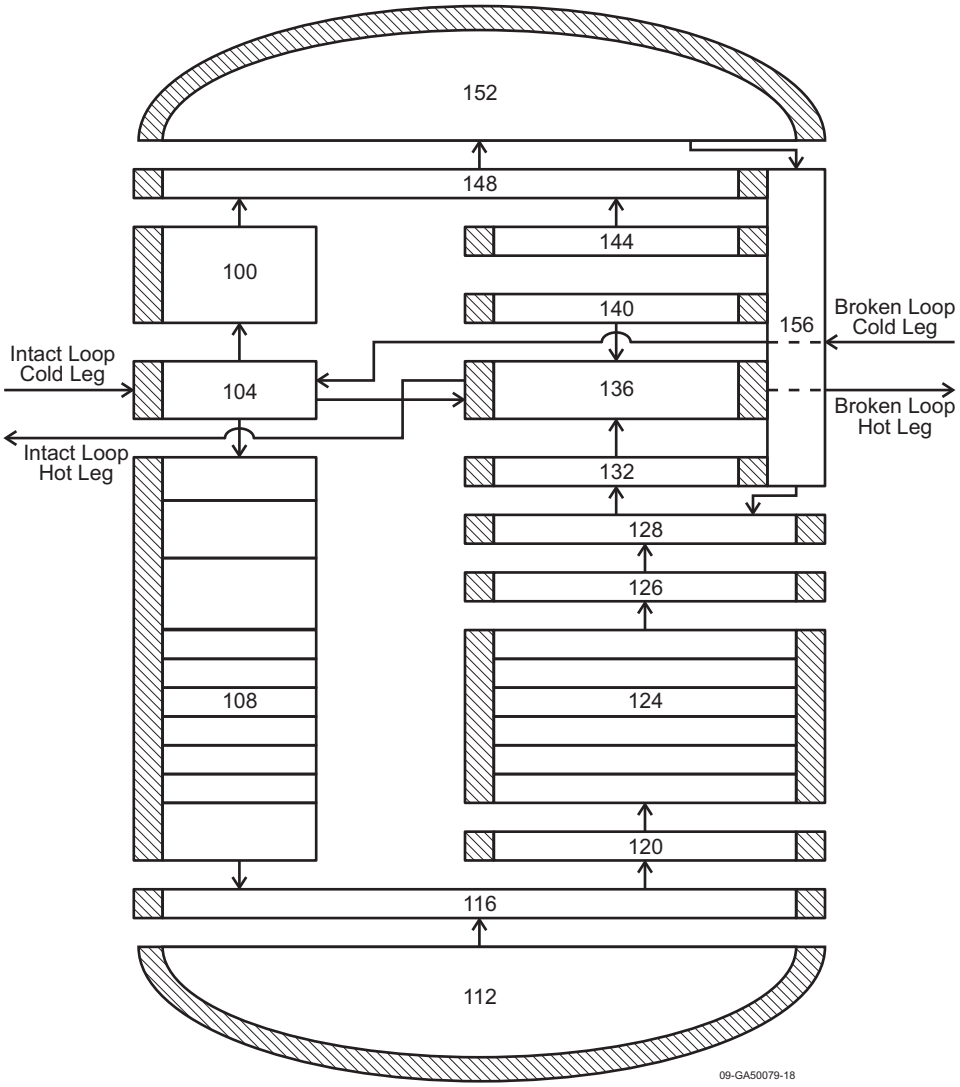

Figure 5.2-2. RELAP5 input model reactor vessel nodalization for ROSA-IV SB-CL-18 test.

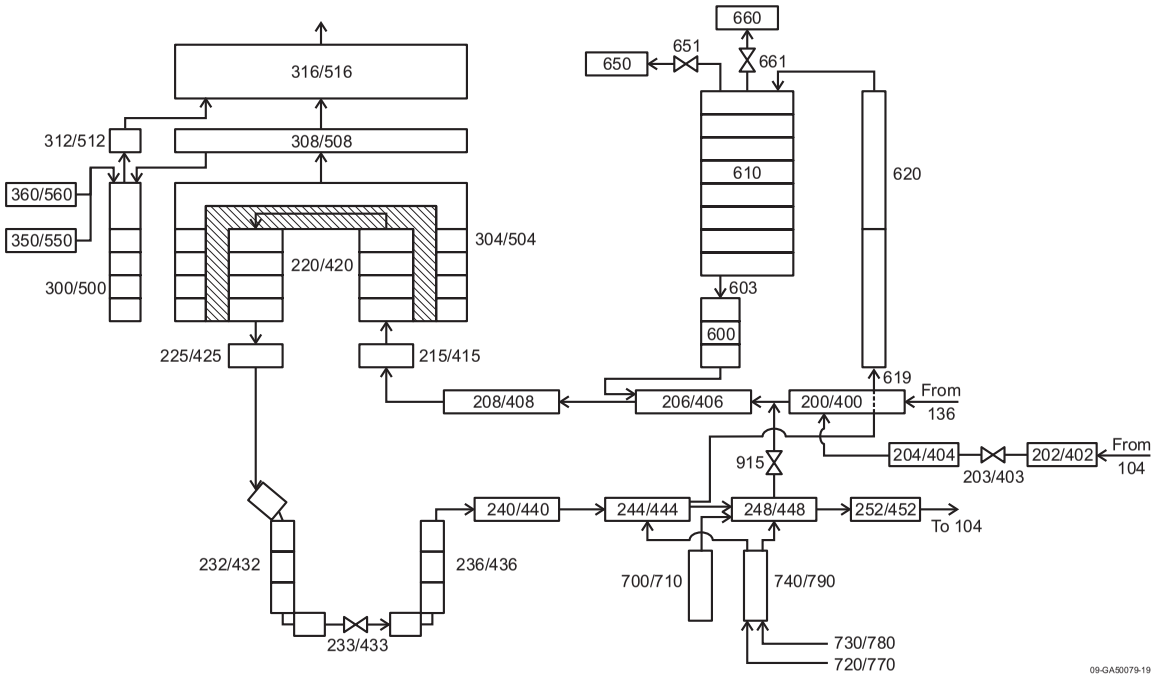

Figure 5.2-3. RELAP5-3D input model loop nodalization for ROSA-IV SB-CL-18 test.

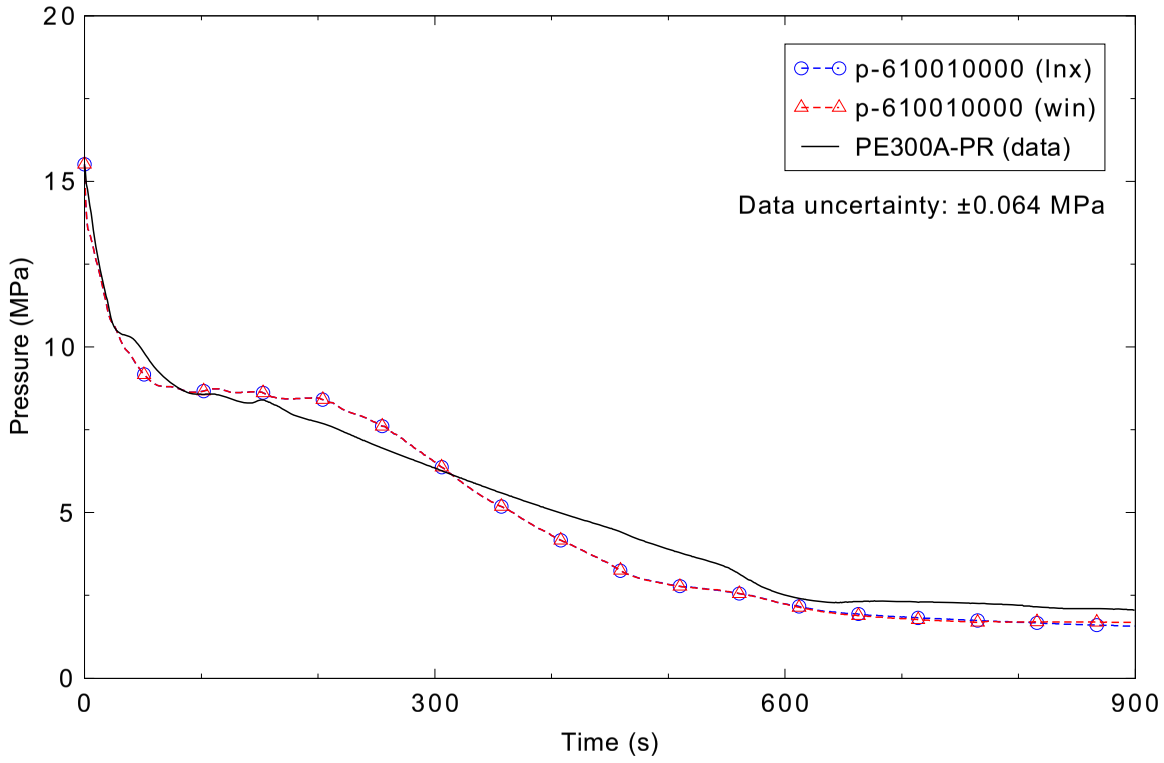

Figure 5.2-4. Measured and calculated pressurizer pressure, ROSA-IV Test SB-CL-18.

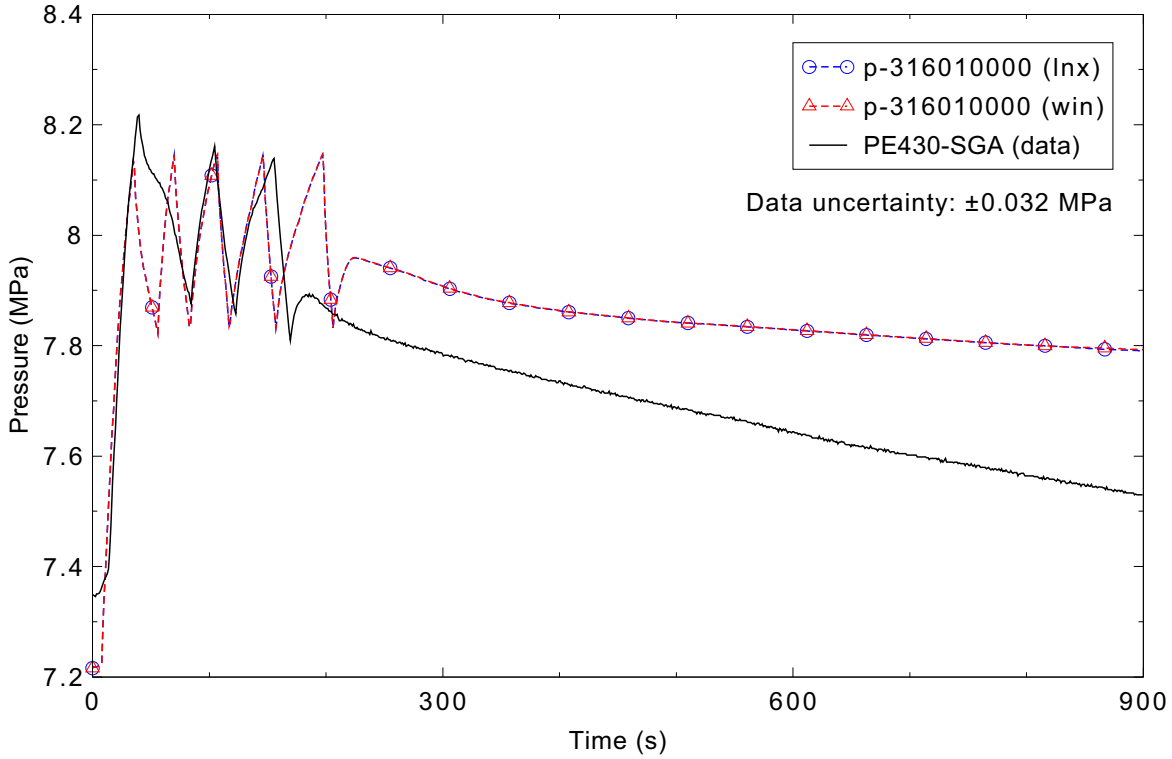

Figure 5.2-5. Measured and calculated pressure of steam generator A, ROSA-IV Test SB-CL-18.

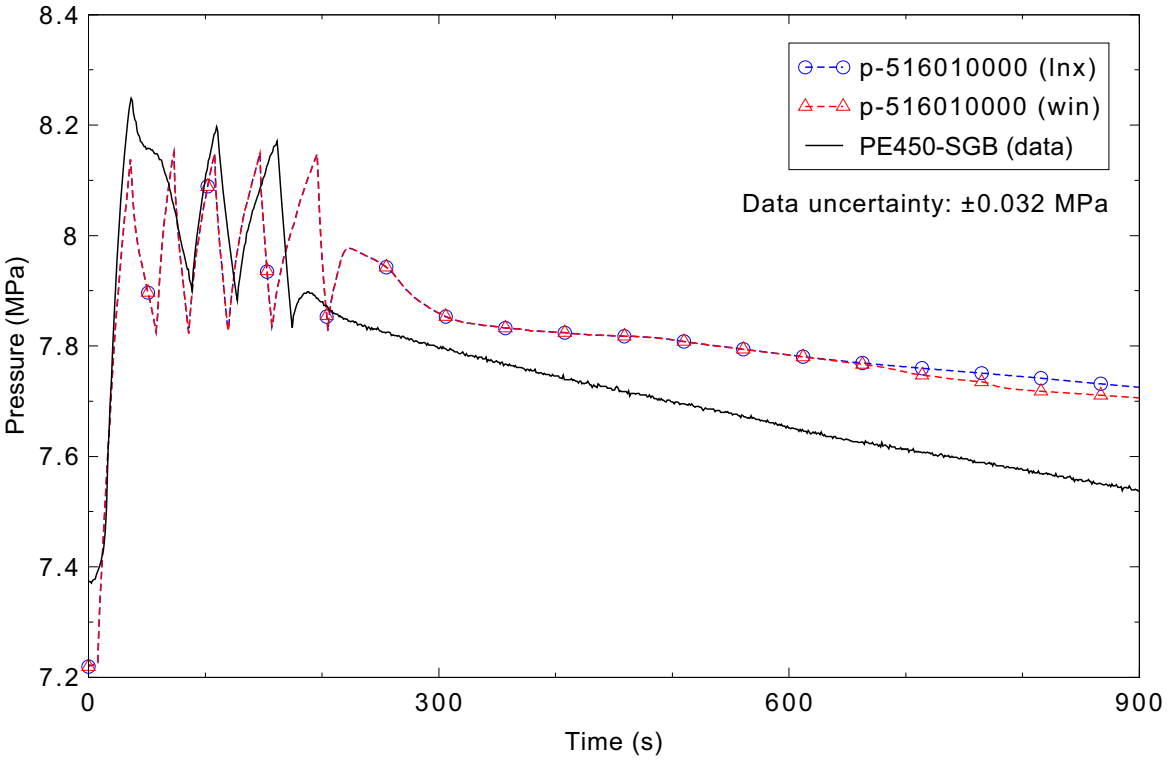

Figure 5.2-6. Measured and calculated pressure of steam generator B, ROSA-IV Test SB-CL-18.

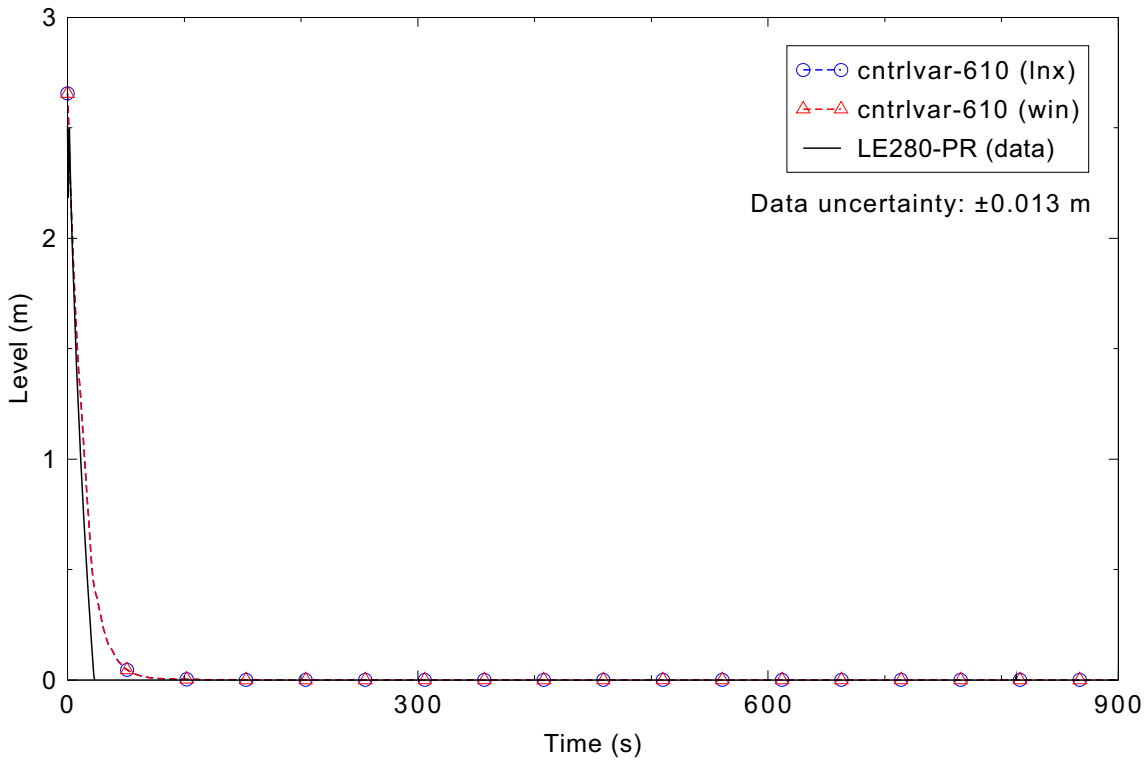

Figure 5.2-7. Measured and calculated pressurizer liquid level, ROSA-IV Test SB-CL-18.

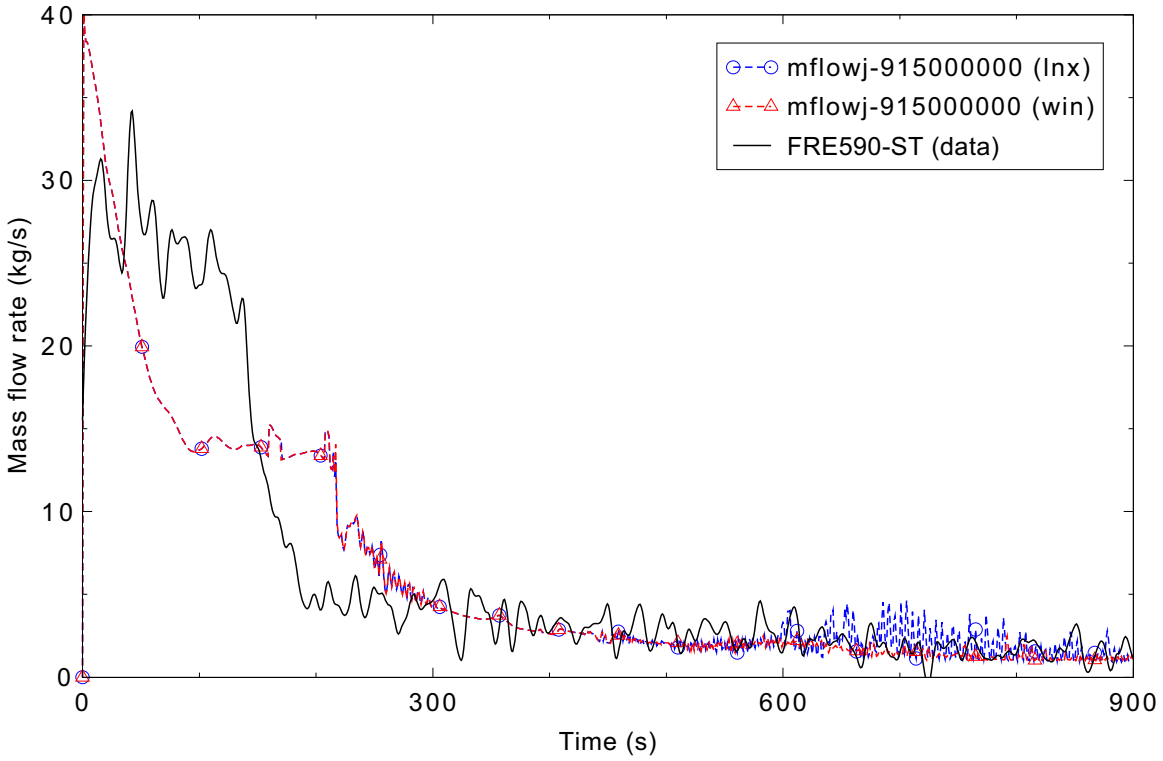

Figure 5.2-8. Measured and calculated break mass flow rate, ROSA-IV Test SB-CL-18.

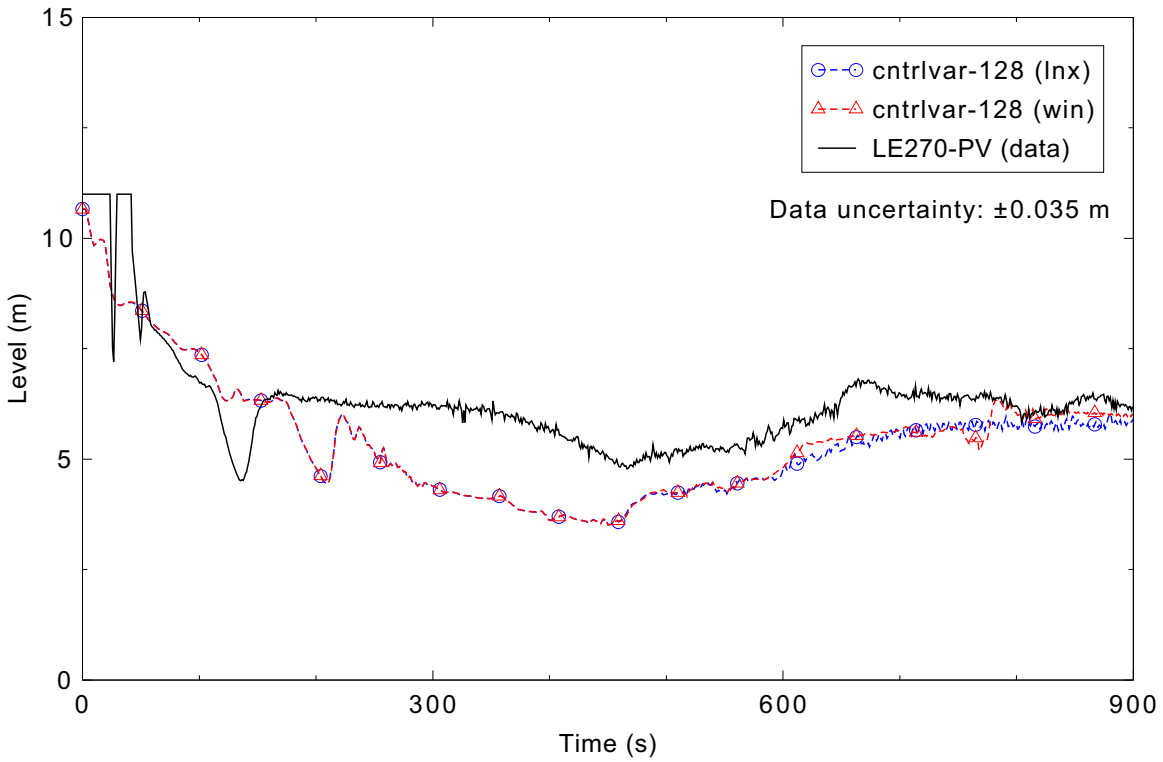

Figure 5.2-9. Measured and calculated vessel liquid level, ROSA-IV Test SB-CL-18.

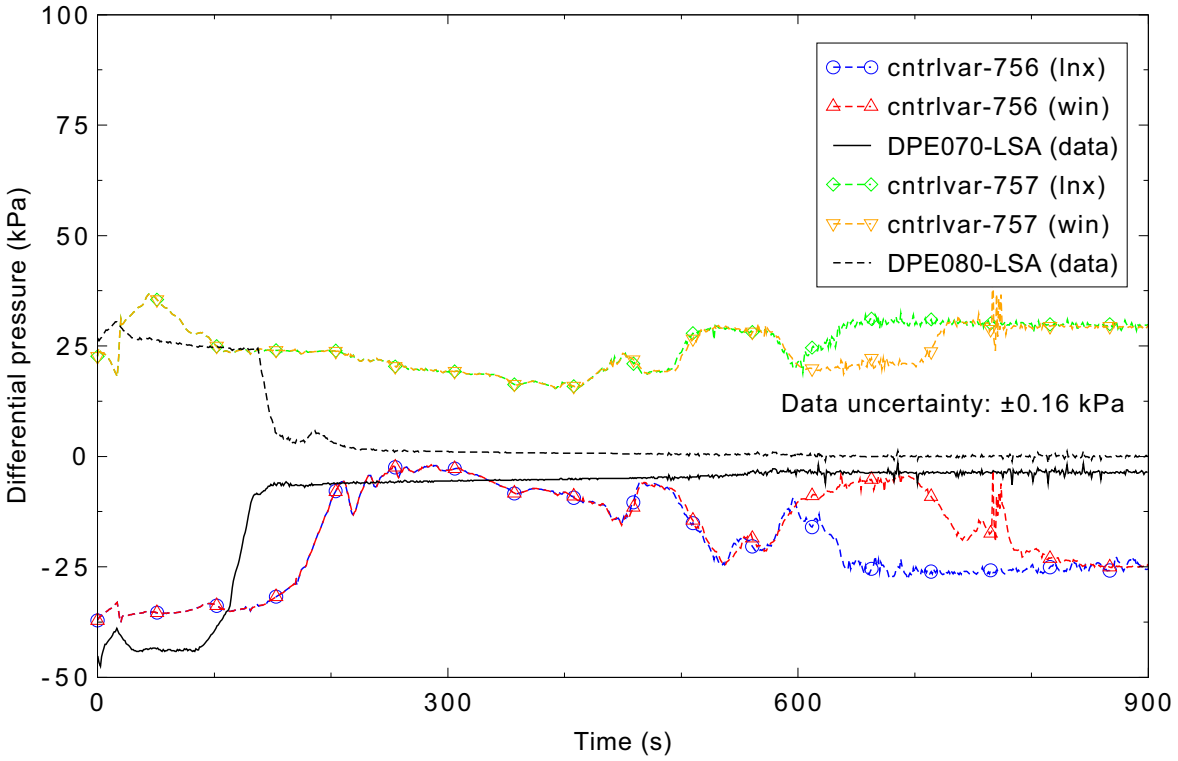

Figure 5.2-10. Measured and calculated differential pressures across loop seal A, ROSA-IV Test SB-CL-18.

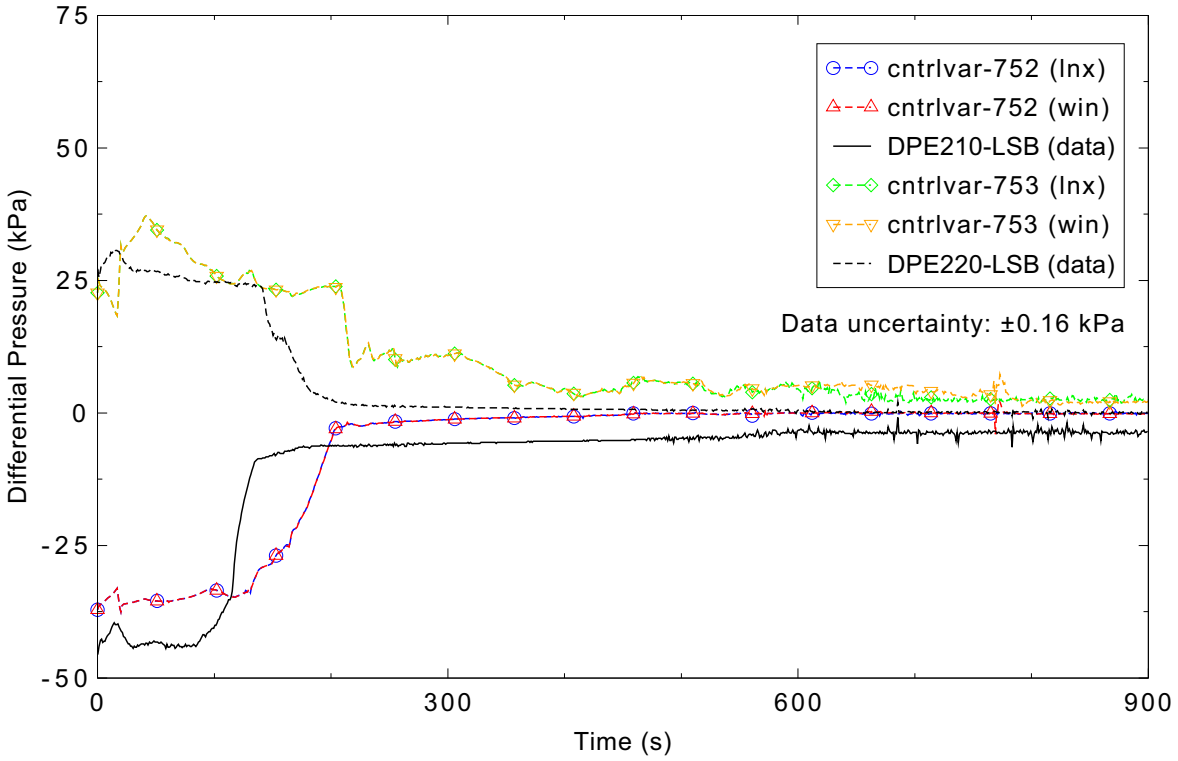

Figure 5.2-11. Measured and calculated differential pressures across loop seal B, ROSA-IV Test SB-CL-18.

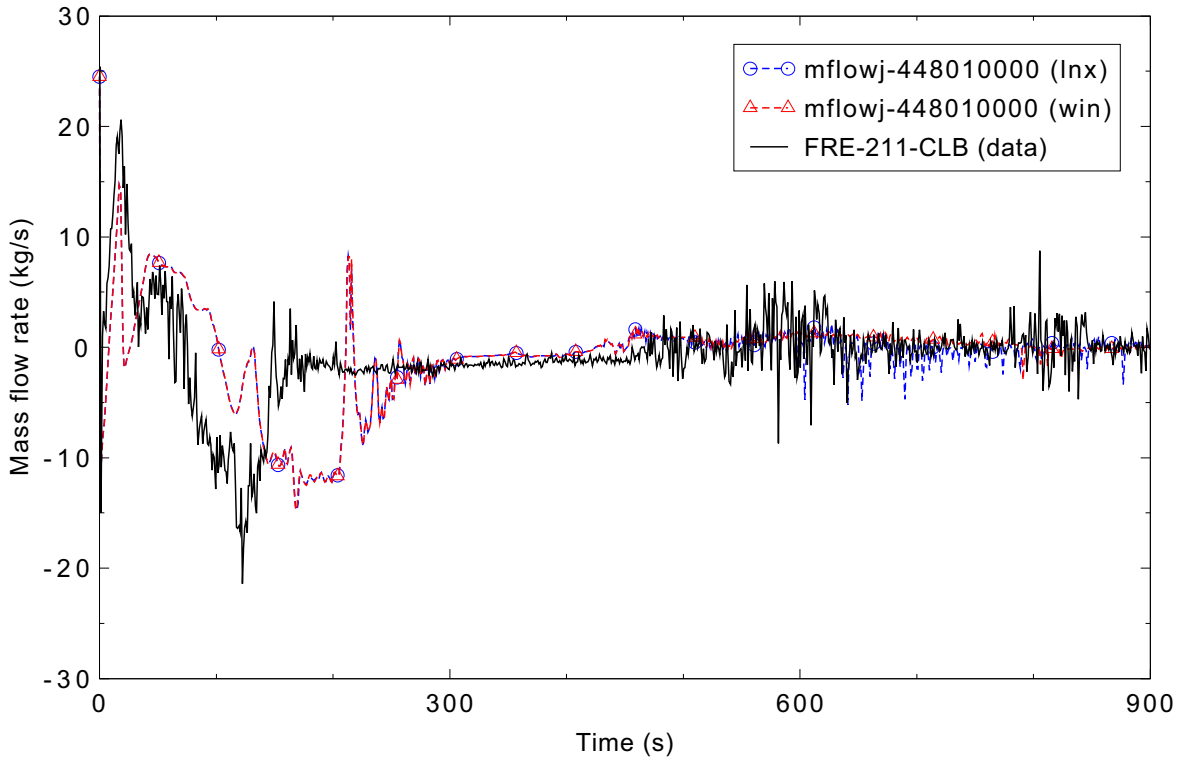

Figure 5.2-12. Measured and calculated mass flow rate in the broken loop cold leg, ROSA-IV Test SB-CL-18.

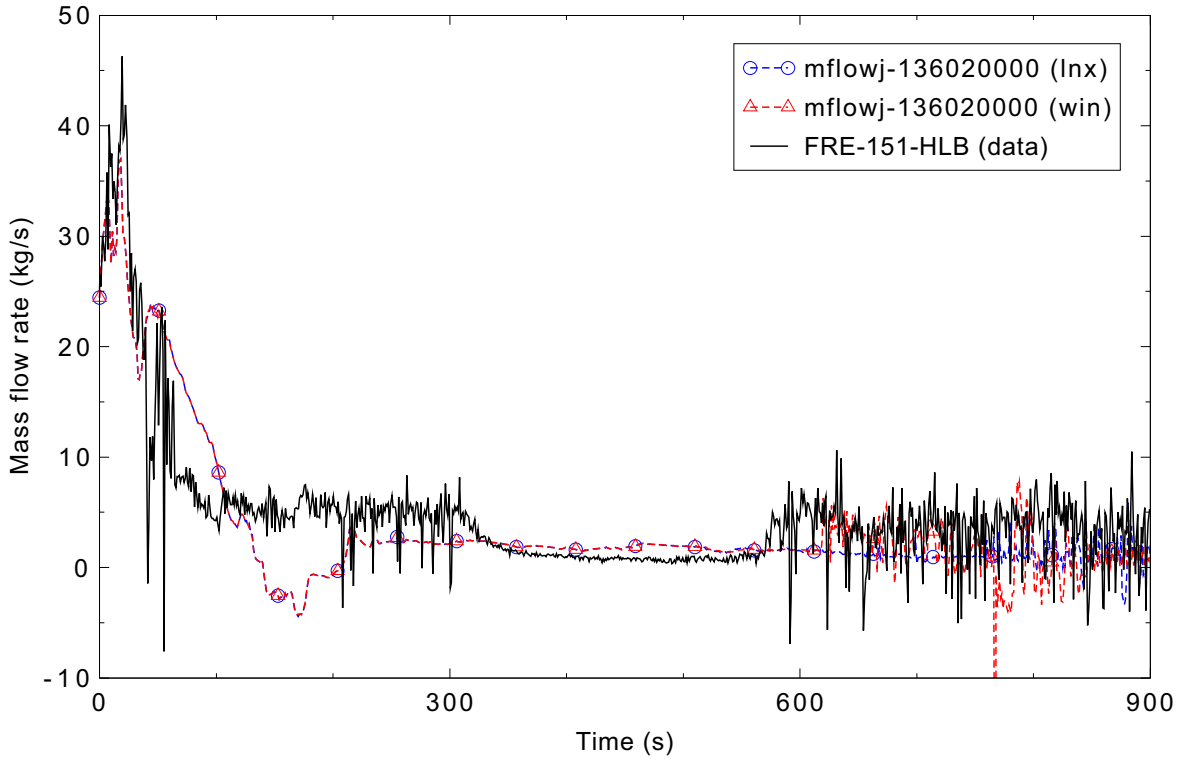

Figure 5.2-13. Measured and calculated mass flow rate in the broken loop hot leg, ROSA-IV Test SB-CL-18.

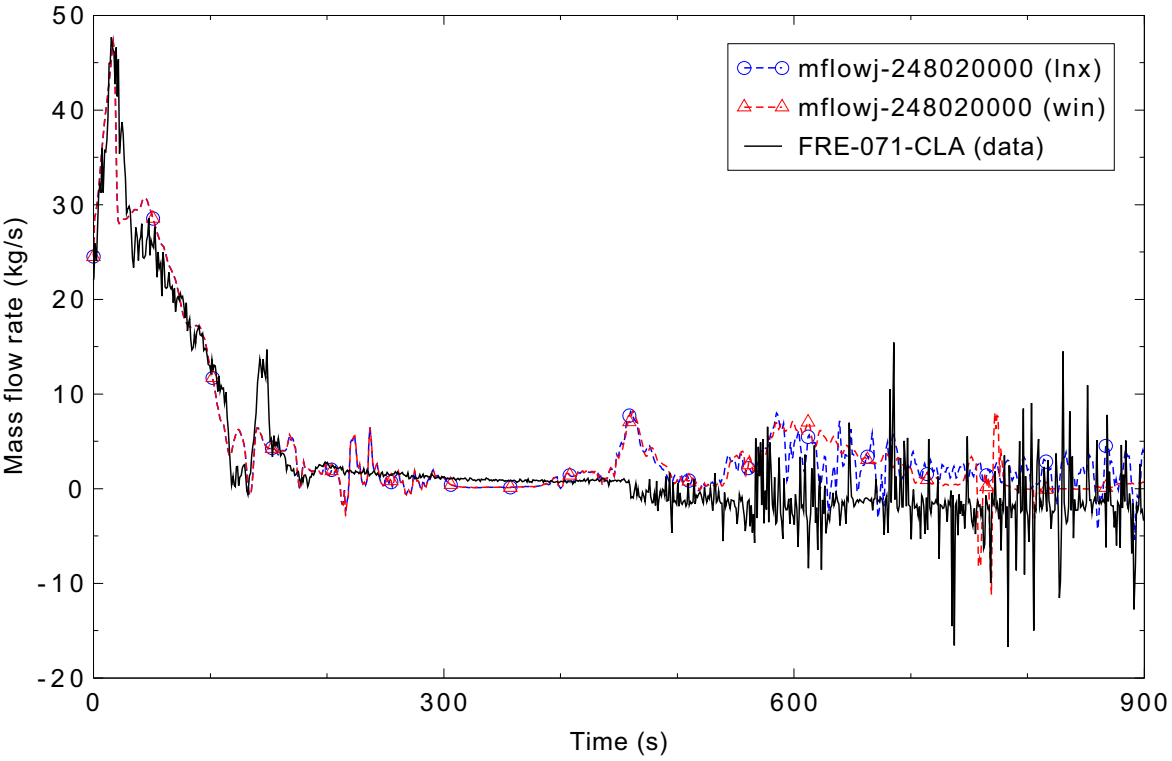

Figure 5.2-14. Measured and calculated mass flow rate in the intact loop cold leg, ROSA-IV Test SB-CL-18.

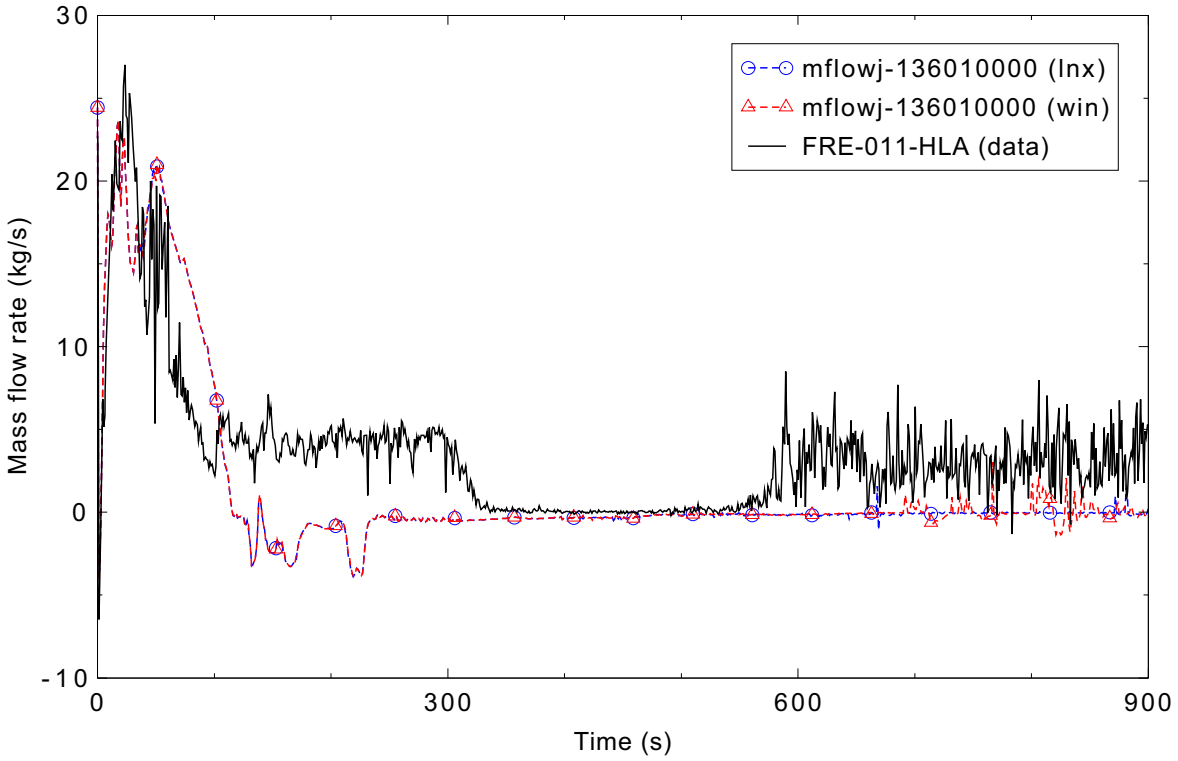

Figure 5.2-15. Measured and calculated mass flow rate in the intact loop hot leg, ROSA-IV Test SB-CL-18.

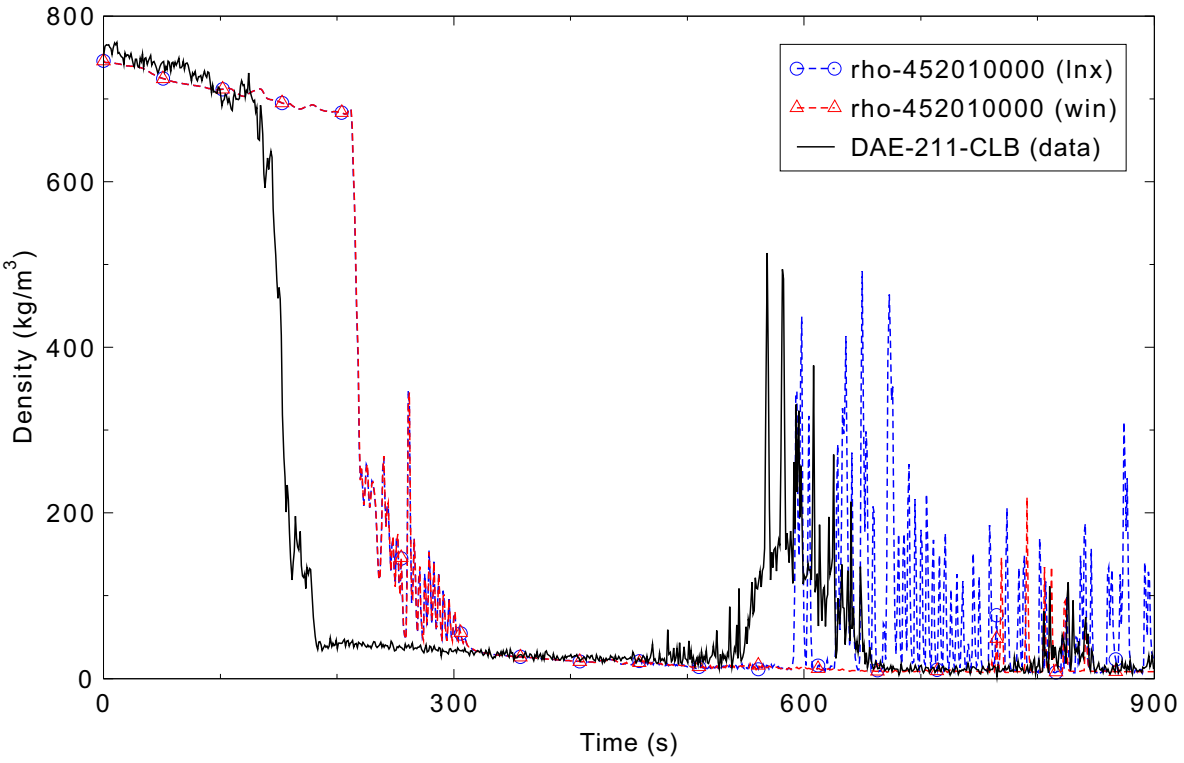

Figure 5.2-16. Measured and calculated density in the broken loop cold leg, ROSA-IV Test SB-CL-18.

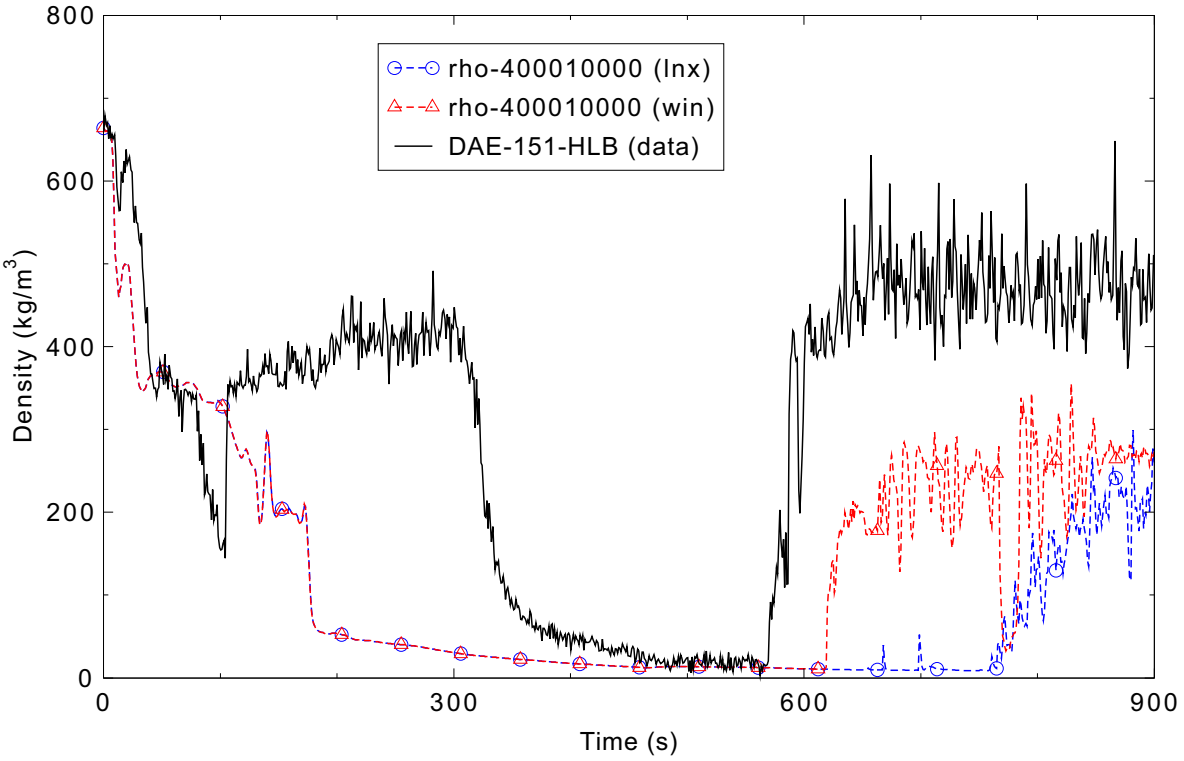

Figure 5.2-17. Measured and calculated density in the broken loop hot leg, ROSA-IV Test SB-CL-18.

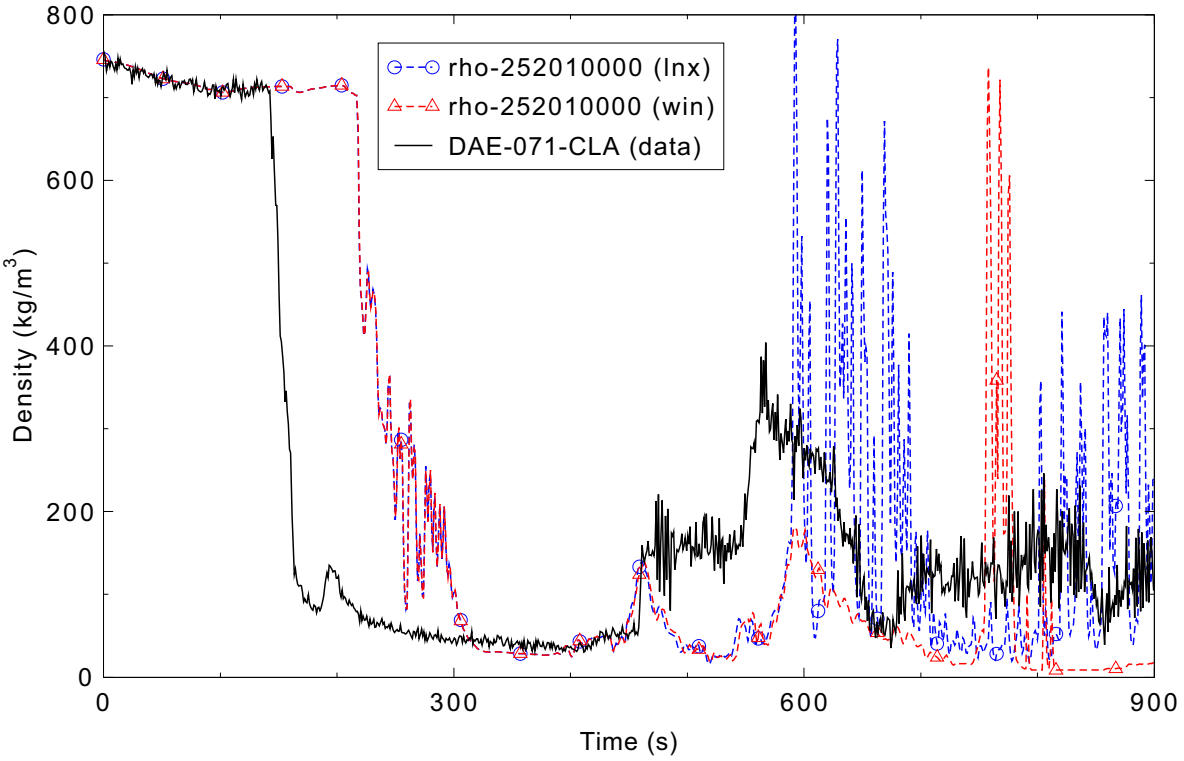

Figure 5.2-18. Measured and calculated density in the intact loop cold leg, ROSA-IV Test SB-CL-18.

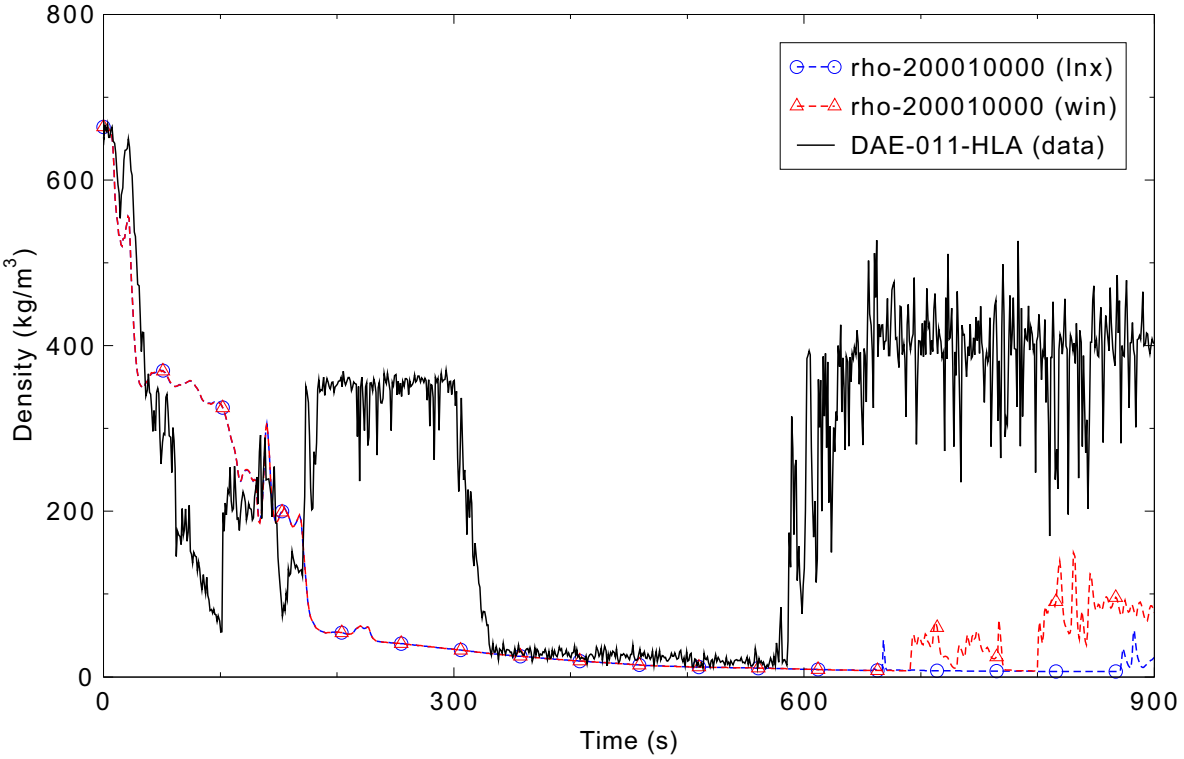

Figure 5.2-19. Measured and calculated density in the intact loop hot leg, ROSA-IV Test SB-CL-18.

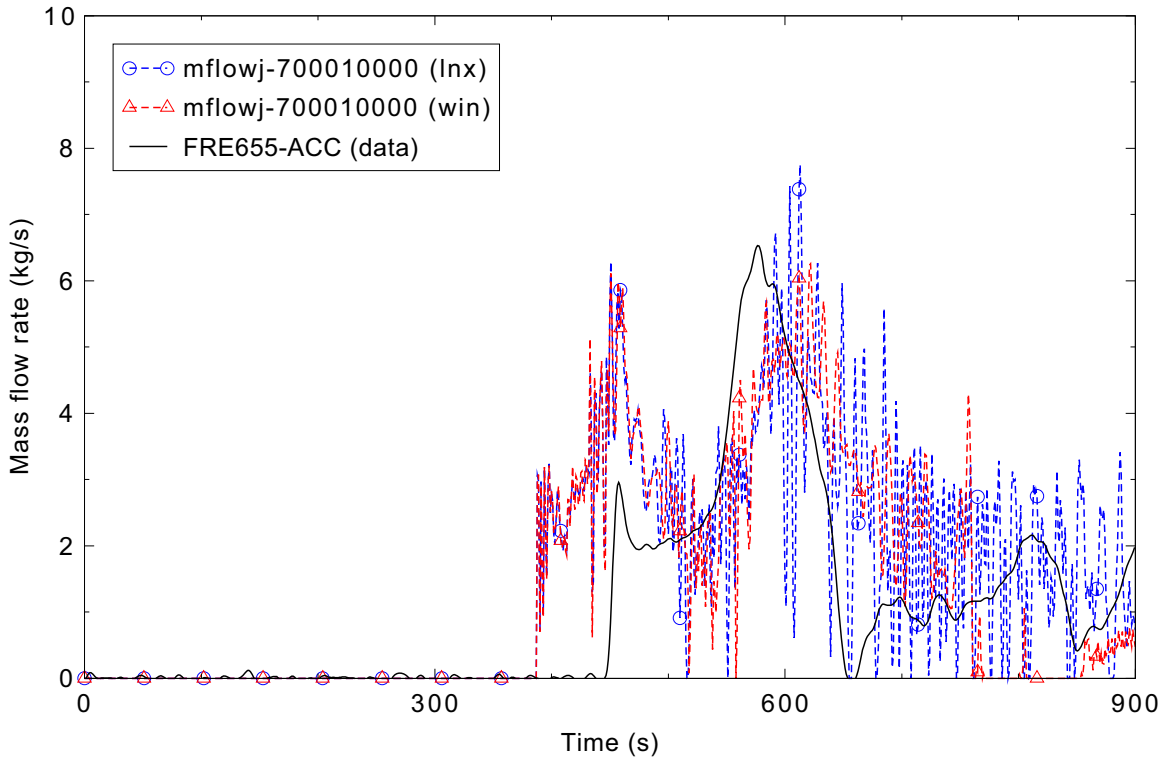

Figure 5.2-20. Measured and calculated mass flow rate accumulator-cold, ROSA-IV Test SB-CL-18.

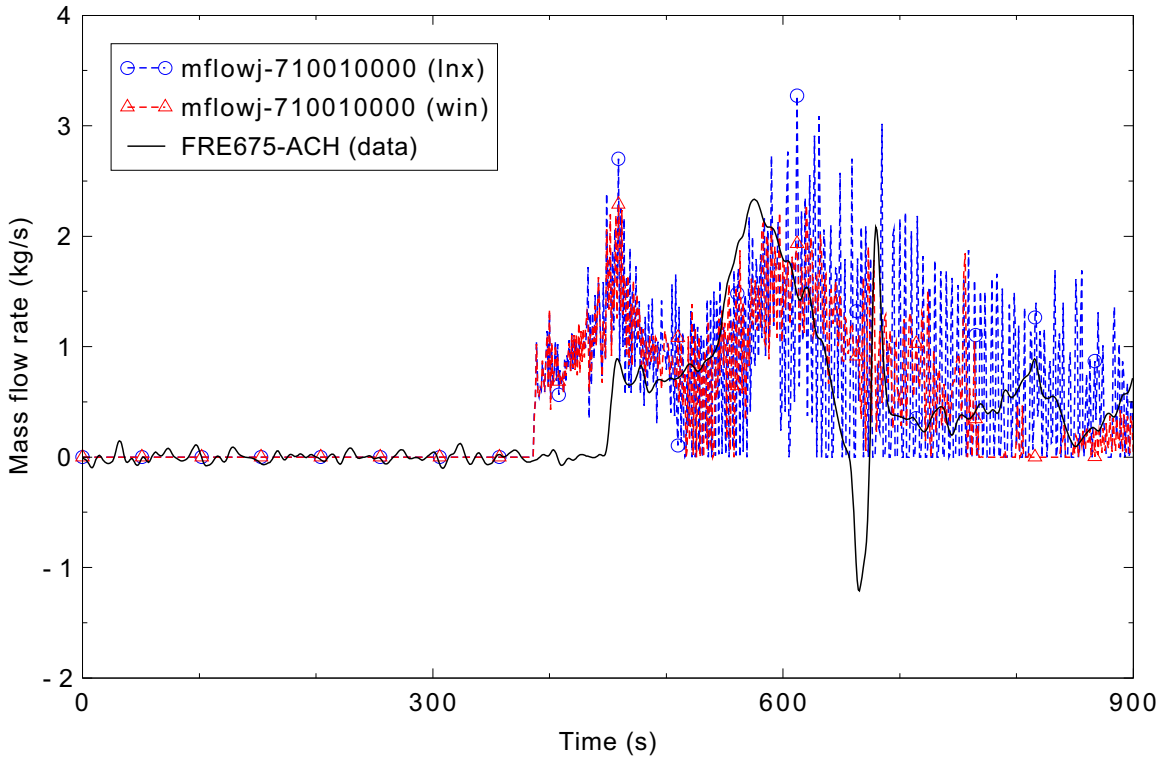

Figure 5.2-21. Measured and calculated mass flow rate accumulator-hot, ROSA-IV Test SB-CL-18.

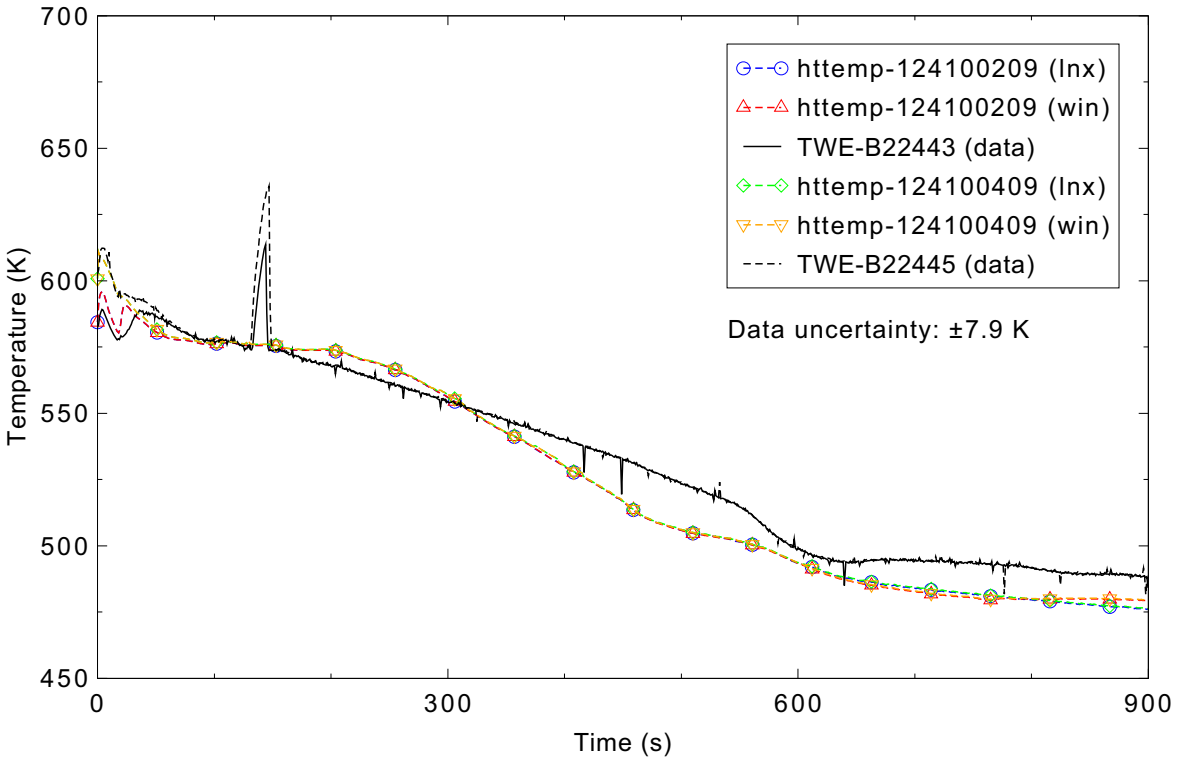

Figure 5.2-22. Measured and calculated heater rod surface temperature for axial levels 3 (1.018 m) and 5 (1.830 m), ROSA-IV Test SB-CL-18.

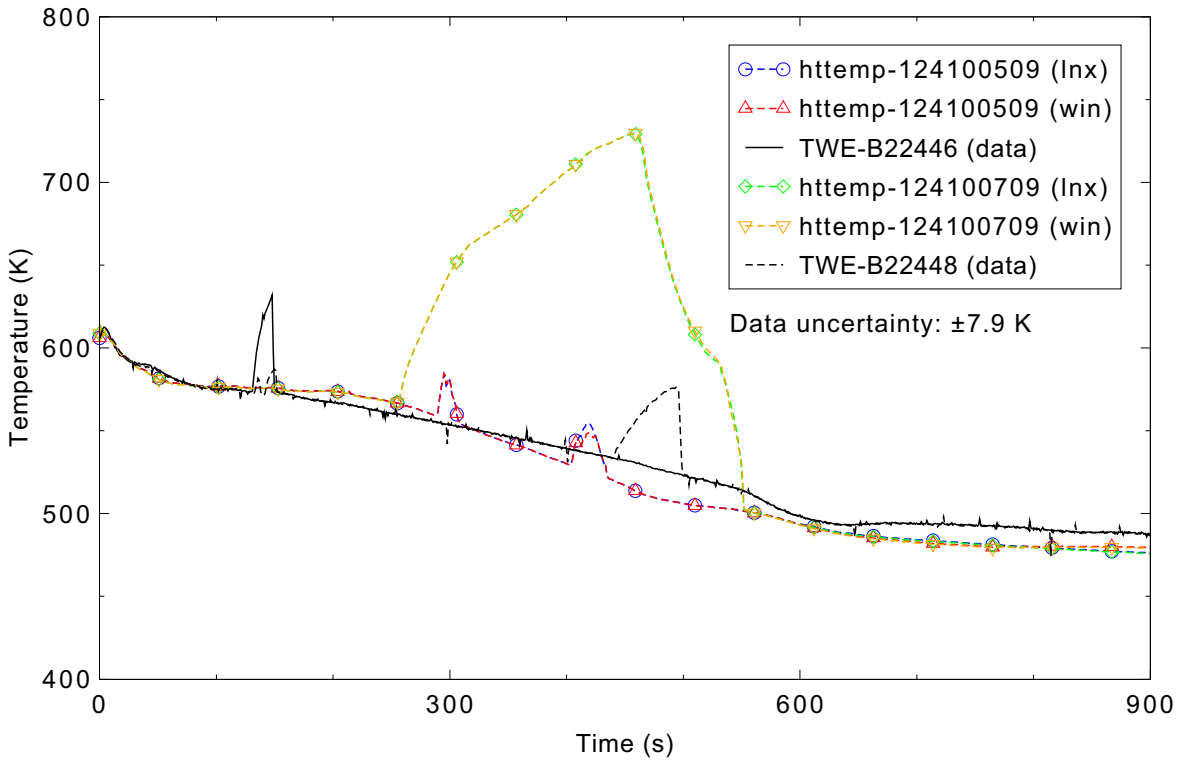

Figure 5.2-23. Measured and calculated heater rod surface temperature for axial levels 6 (2.236 m) and 8 (3.048 m), ROSA-IV Test SB-CL-18.

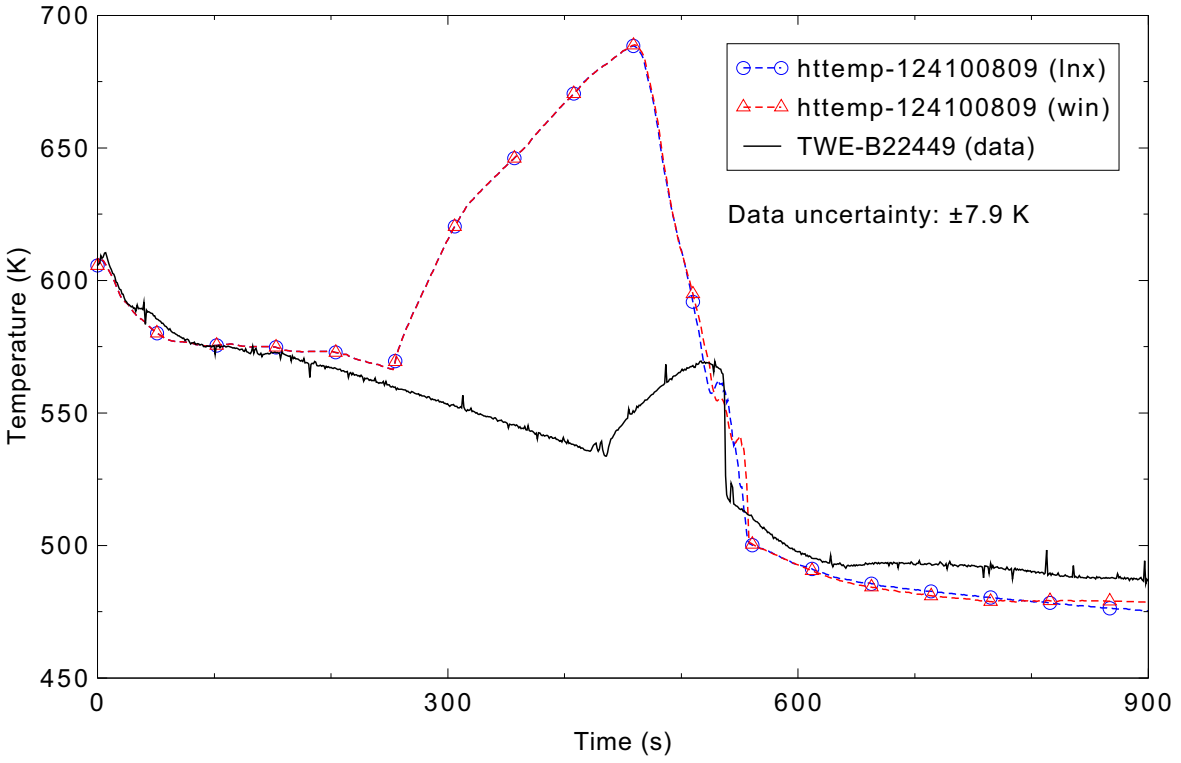

Figure 5.2-24. Measured and calculated heater rod surface temperature for axial level 9 (3.610 m), ROSA-IV Test SB-CL-18.

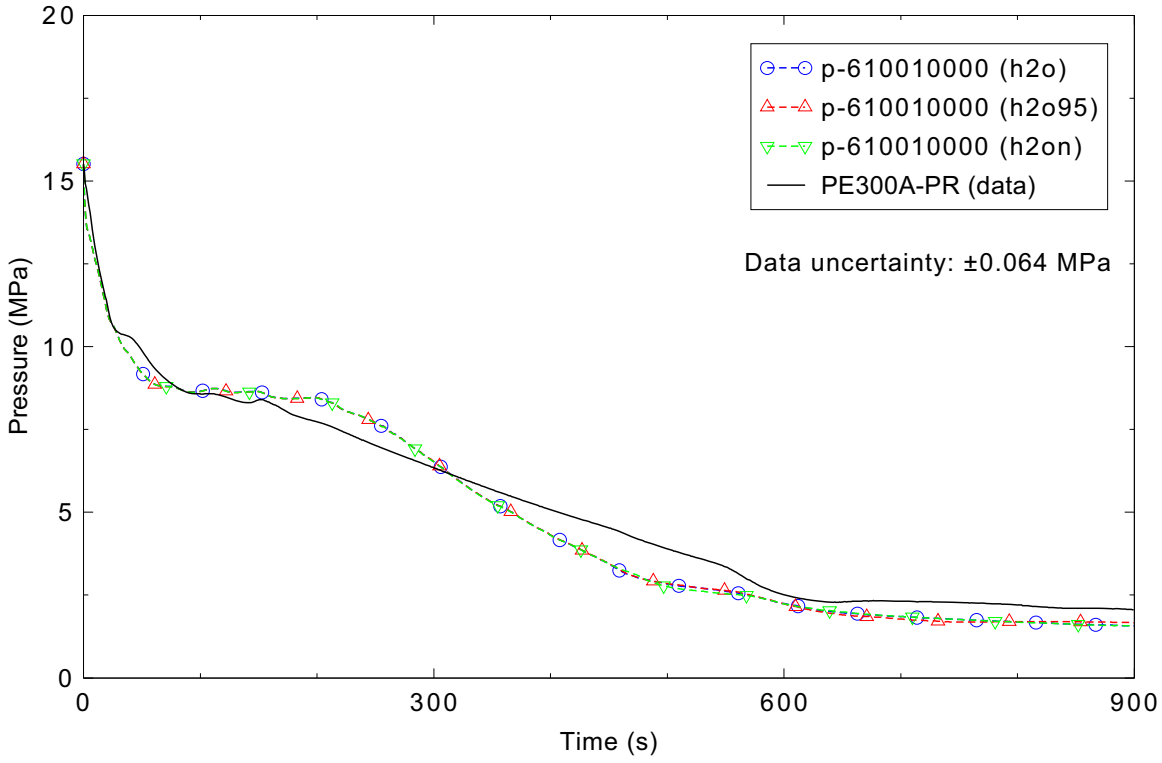

Figure 5.2-25. Measured and calculated pressurizer pressure for different water properties, ROSA-IV Test SB-CL-18.

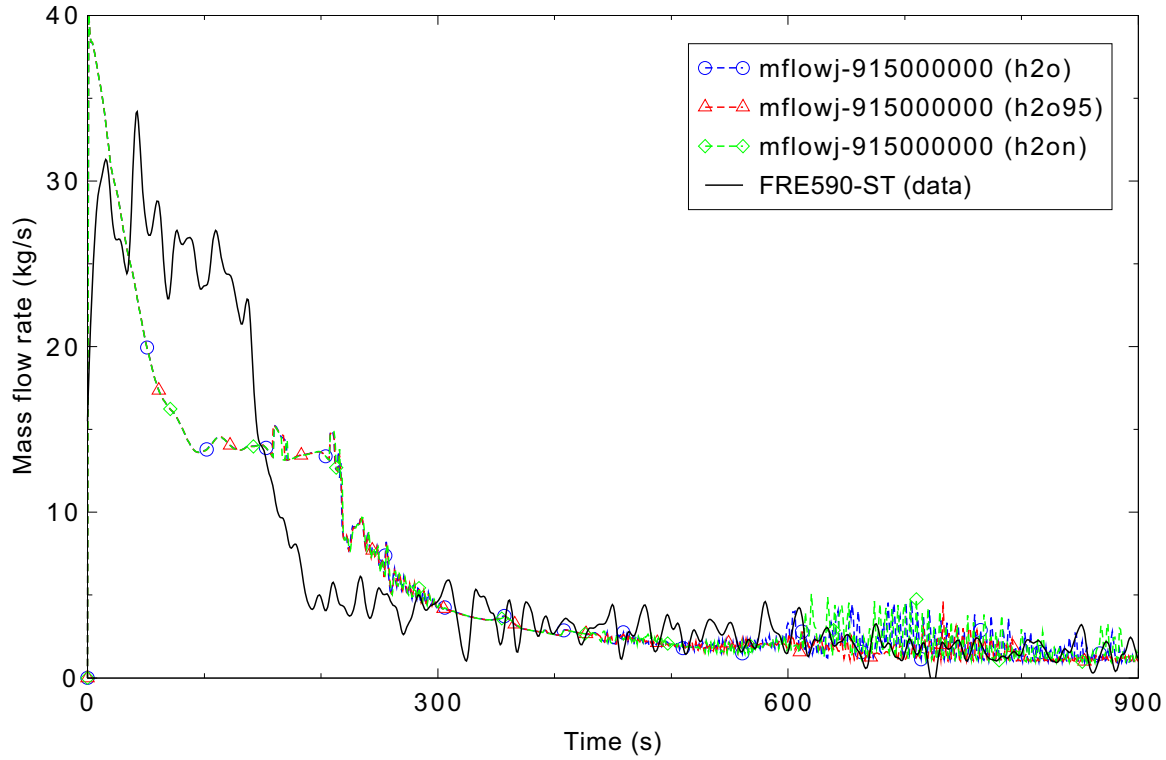

Figure 5.2-26. Measured and calculated break mass flow rate for different water properties, ROSA-IV Test SB-CL-18.

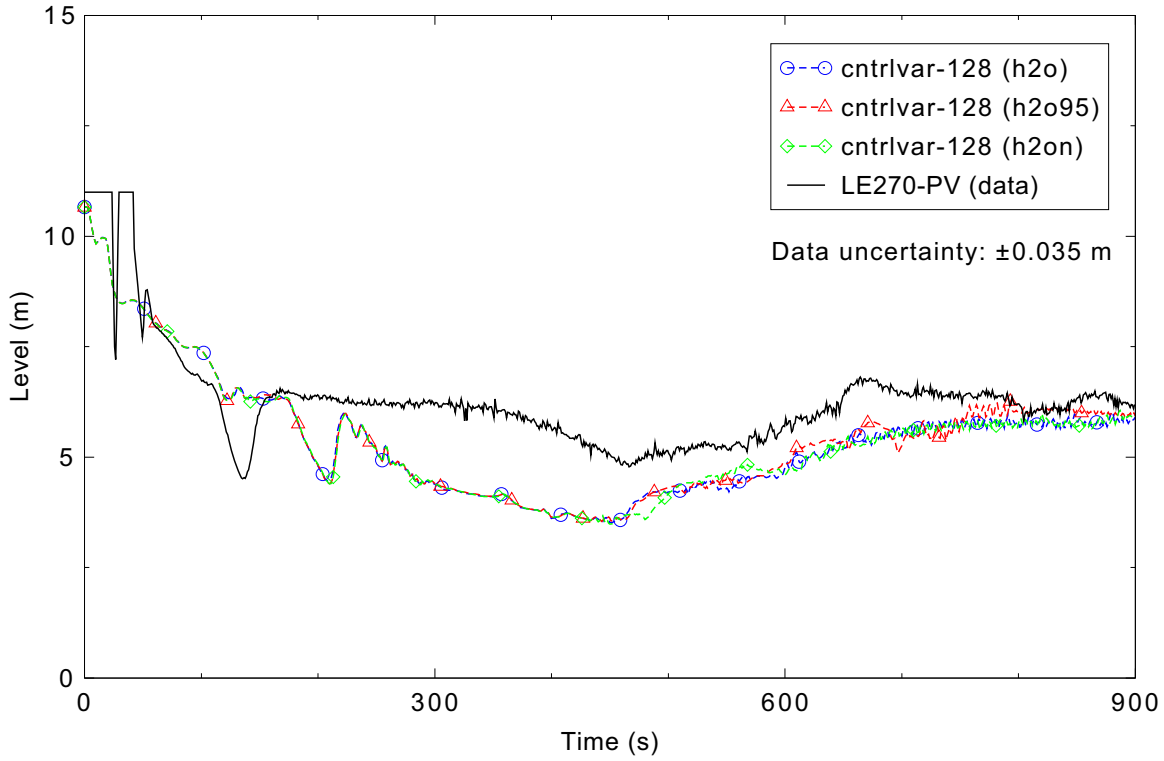

Figure 5.2-27. Measured and calculated vessel liquid level for different water properties, ROSA-IV Test SB-CL-18.

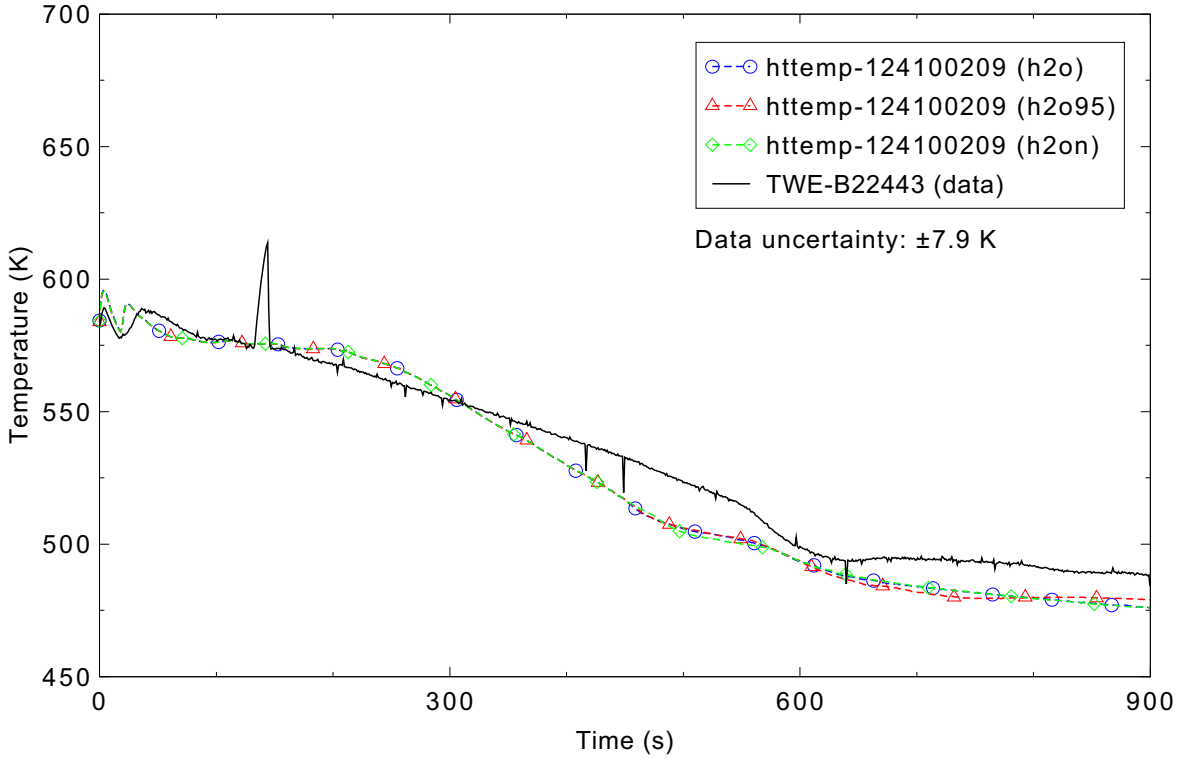

Figure 5.2-28. Measured and calculated heater rod surface temperature for axial level 3 (1.018 m) and different water properties, ROSA-IV Test SB-CL-18.

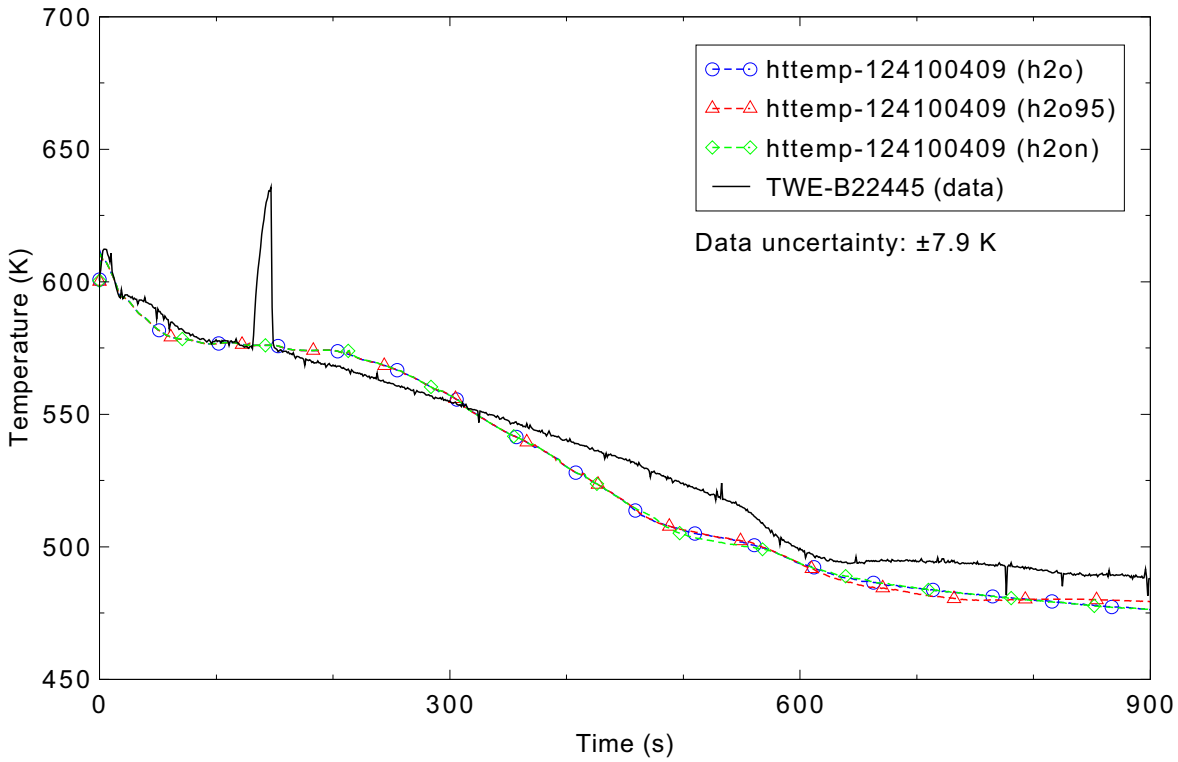

Figure 5.2-29. Measured and calculated heater rod surface temperature for axial level 5 (1.830 m) and different water properties, ROSA-IV Test SB-CL-18.

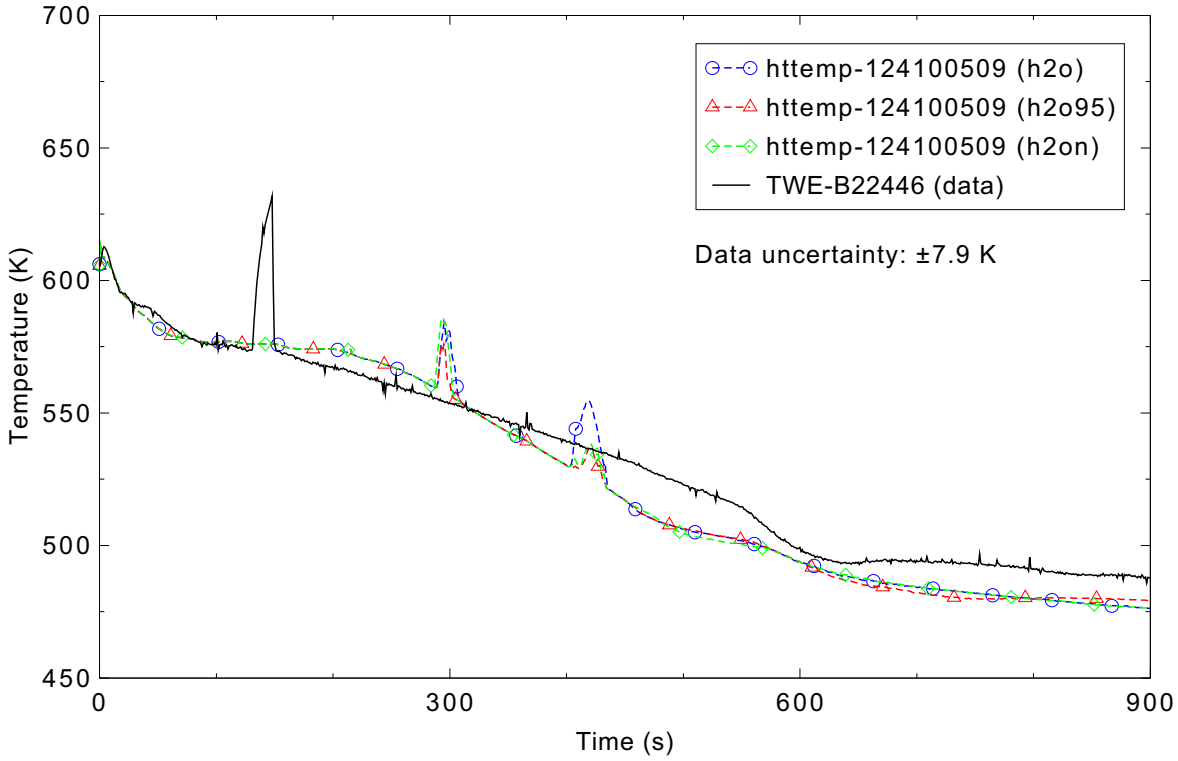

Figure 5.2-30. Measured and calculated heater rod surface temperature for axial level 6 (2.236 m) and different water properties, ROSA-IV Test SB-CL-18.

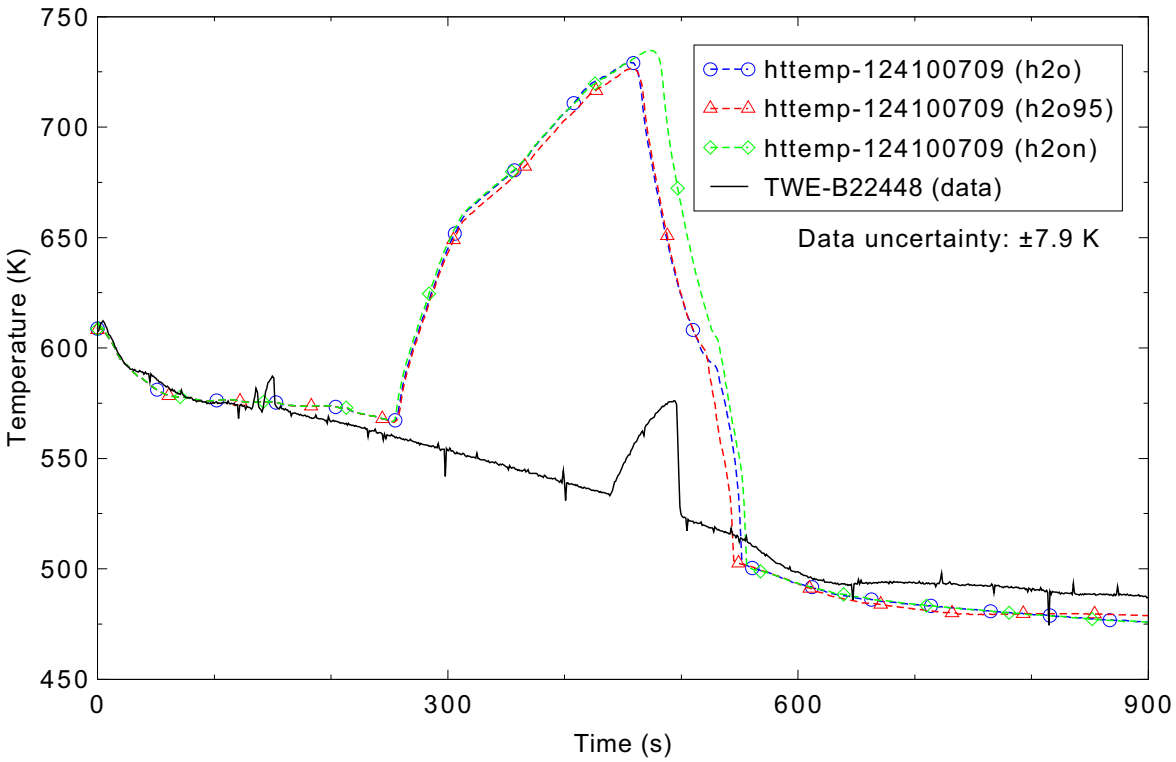

Figure 5.2-31. Measured and calculated heater rod surface temperature for axial level 8 (3.048 m) and different water properties, ROSA-IV Test SB-CL-18.

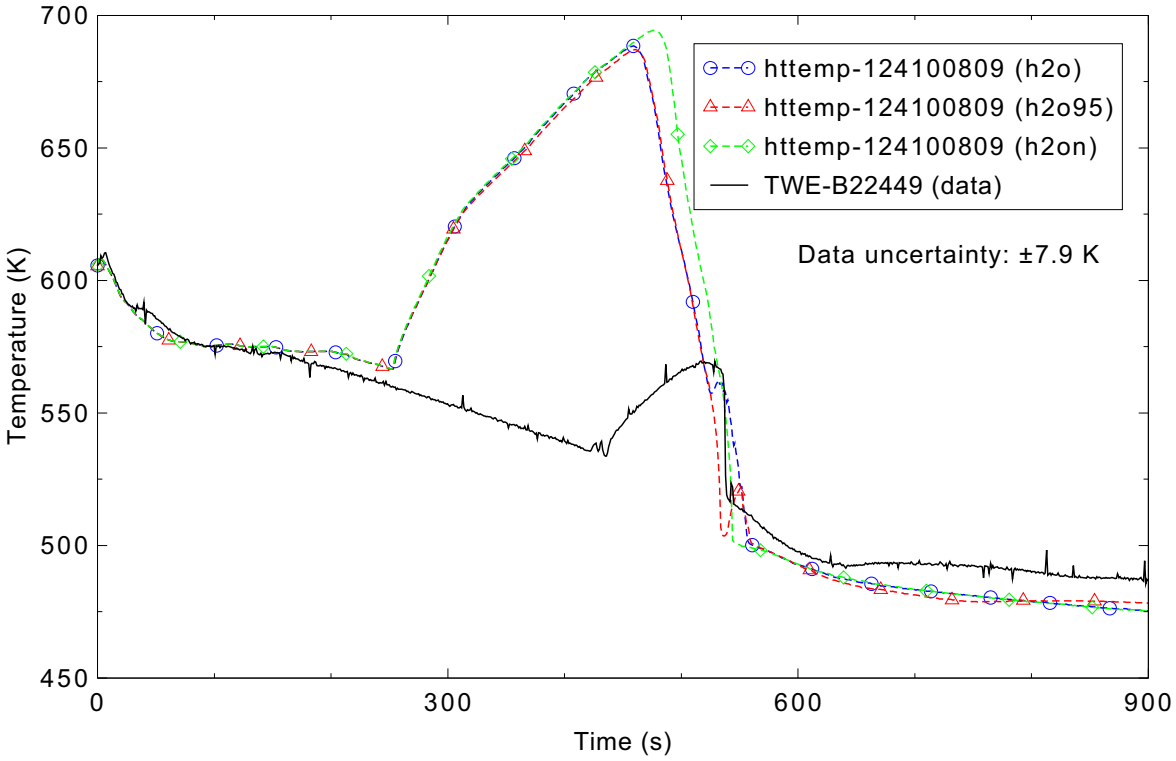

Figure 5.2-32. Measured and calculated heater rod surface temperature for axial level 9 (3.610 m) and different water properties, ROSA-IV Test SB-CL-18.

5.3 Semiscale NC Tests 1, 2, 3, and 10

Figures comparing simulations using Linux and Windows code versions are presented. Diagrams are included so that the figure numbering is the same as that in Volume III of he RELAP5-3D code manual. Noticeable differences were observed in Figures 5.3-10, 20, 21, 22, and 23.

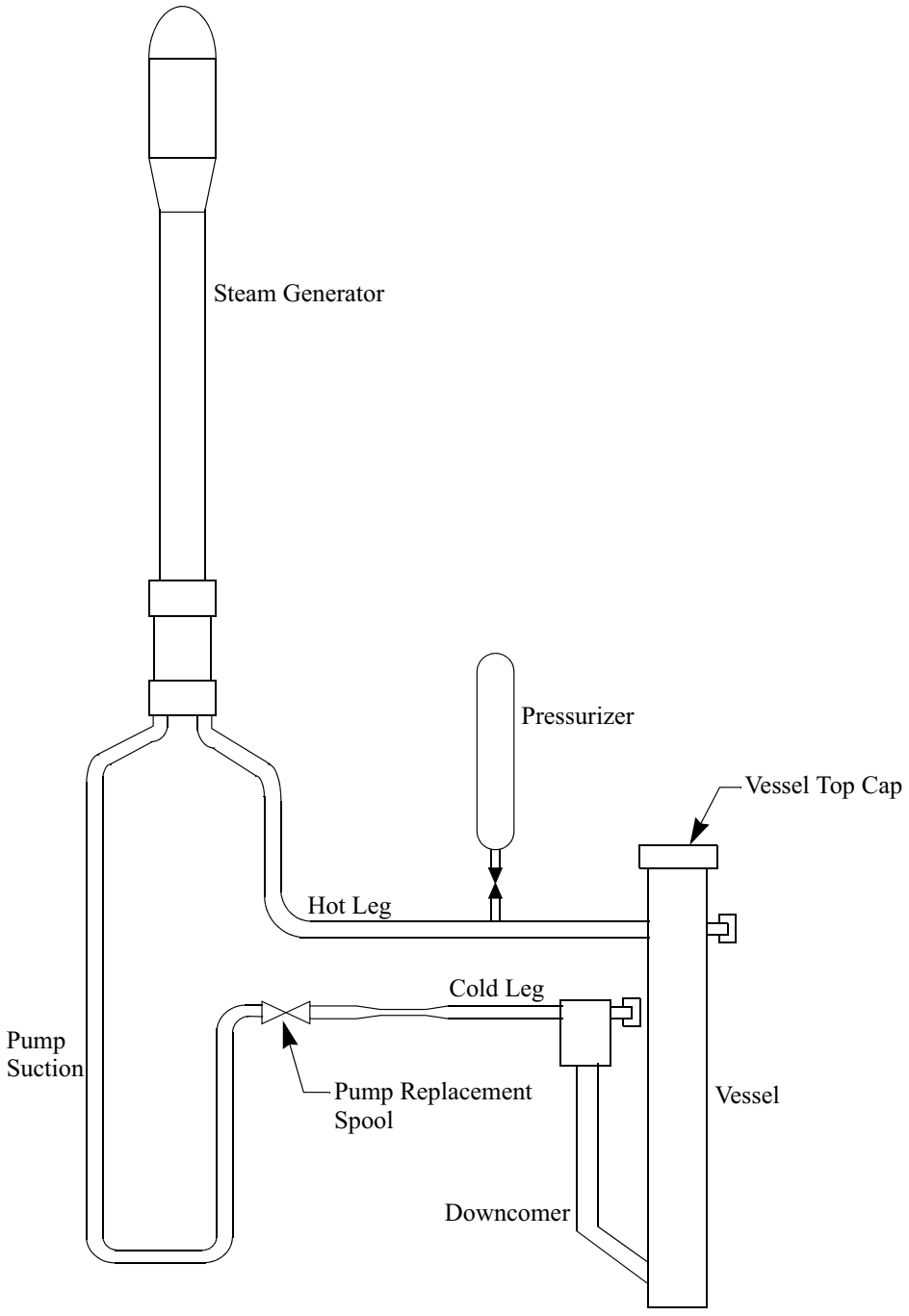

Figure 5.3-1. Semiscale Mod-2A single-loop configuration.

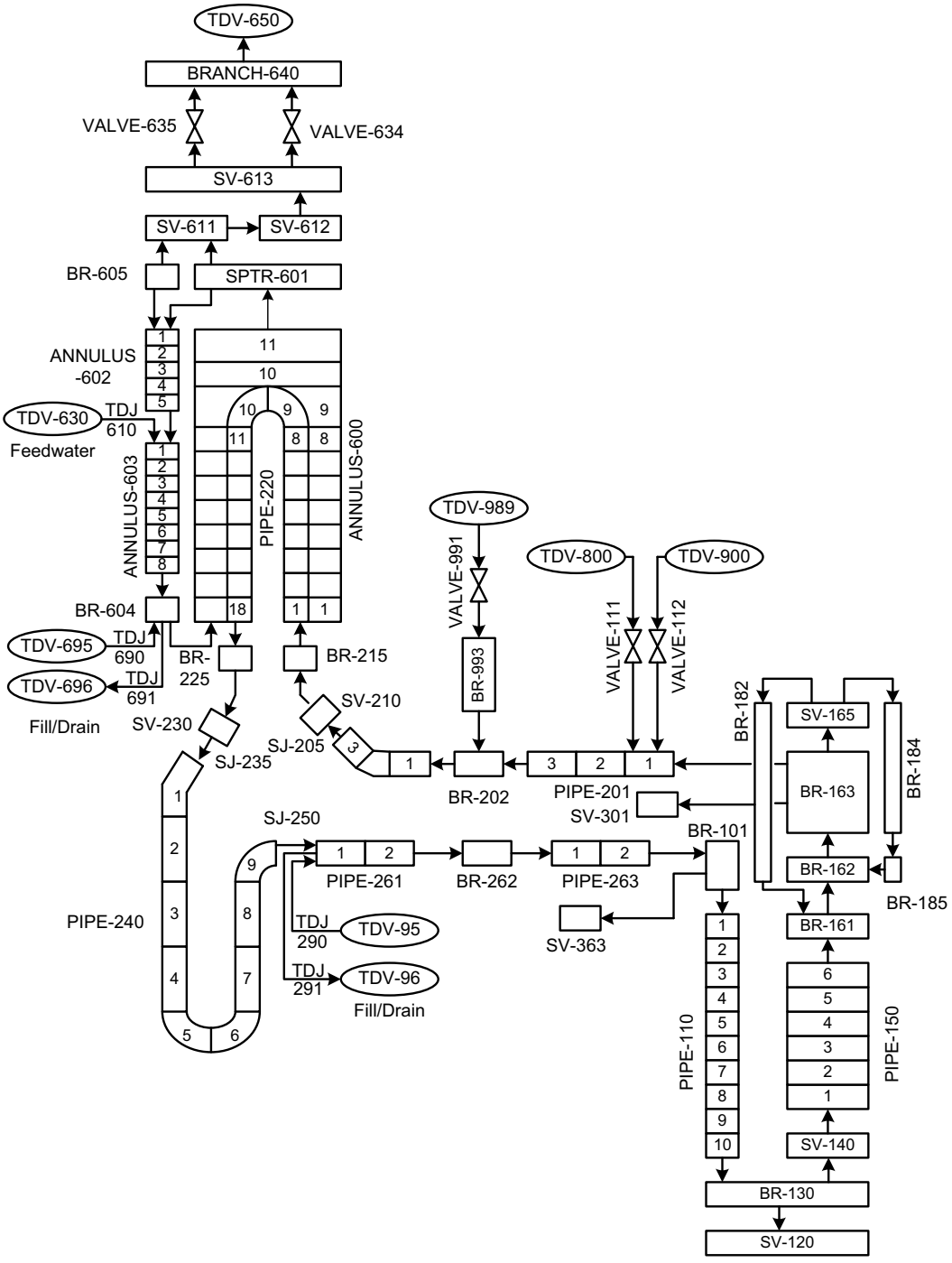

Figure 5.3-2. Nodalization of RELAP5-3D Semiscale natural circulation test model.

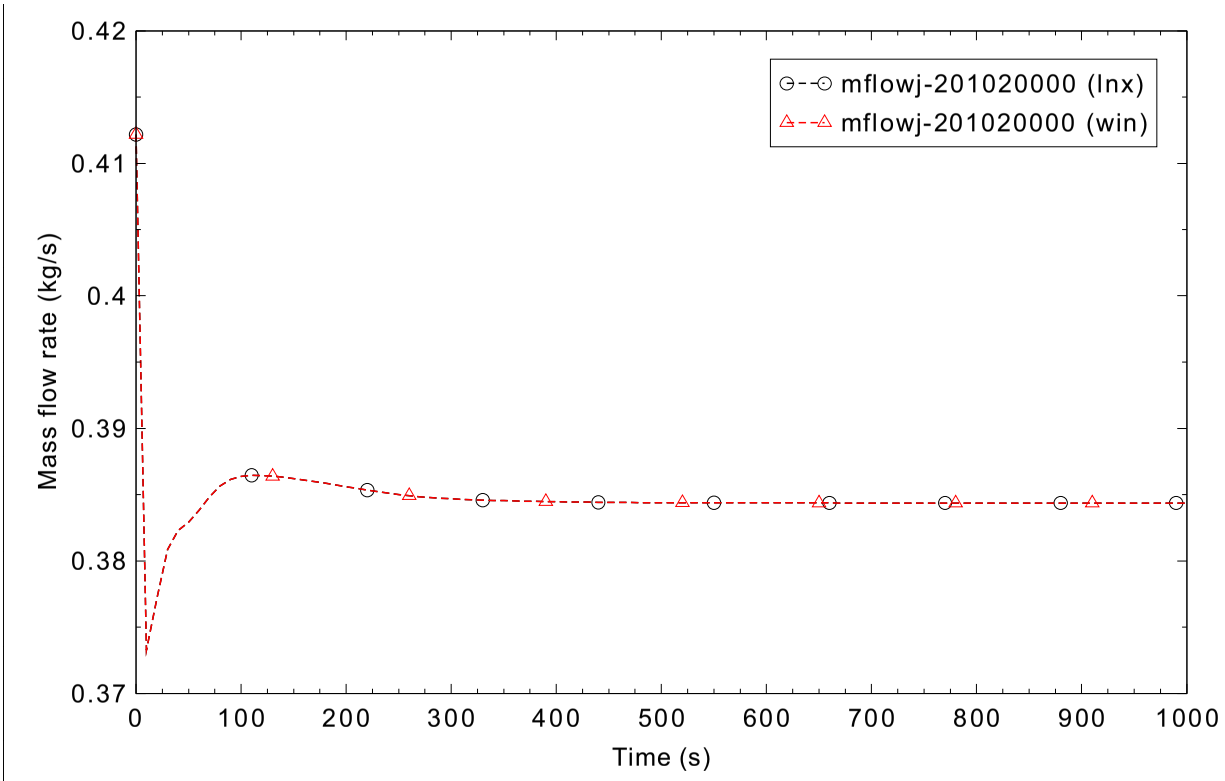

Figure 5.3-3. Calculated primary system mass flow rate at 60 kW core power for Semiscale Test S-NC-1.

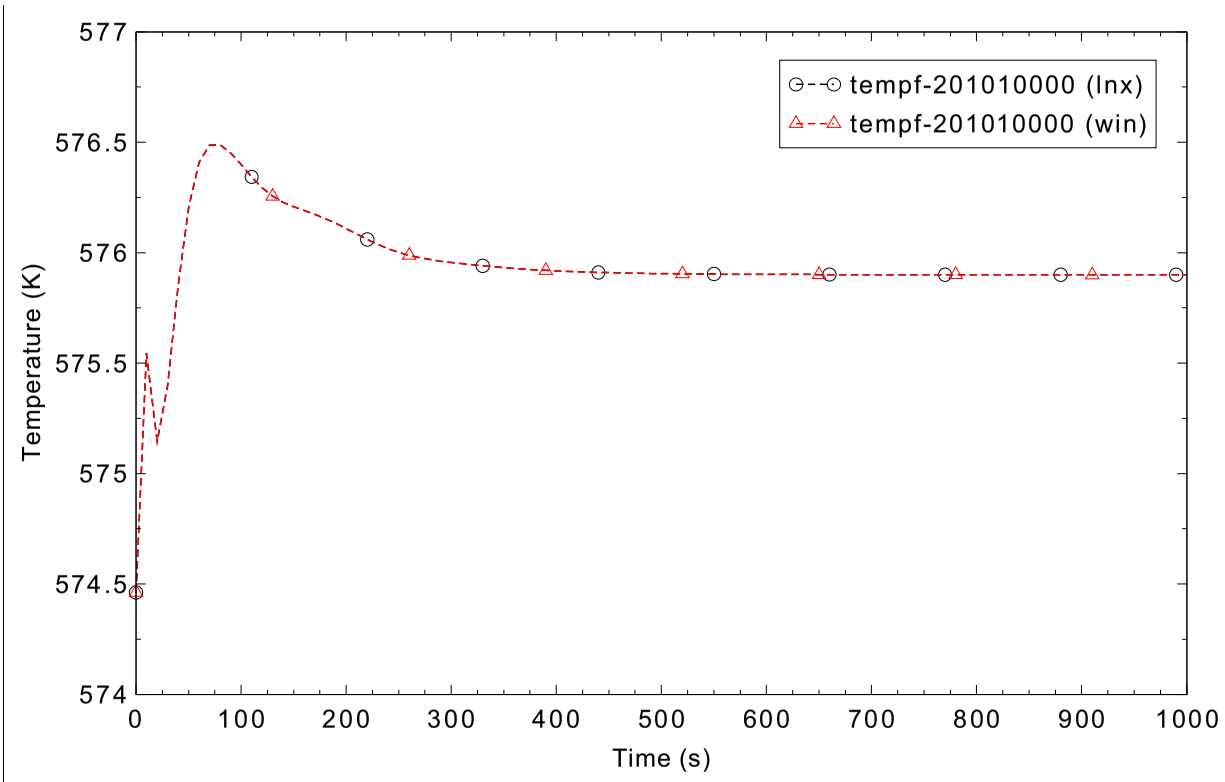

Figure 5.3-4. Calculated hot leg liquid temperature at 60 kW core power for Semiscale Test S-NC-1.

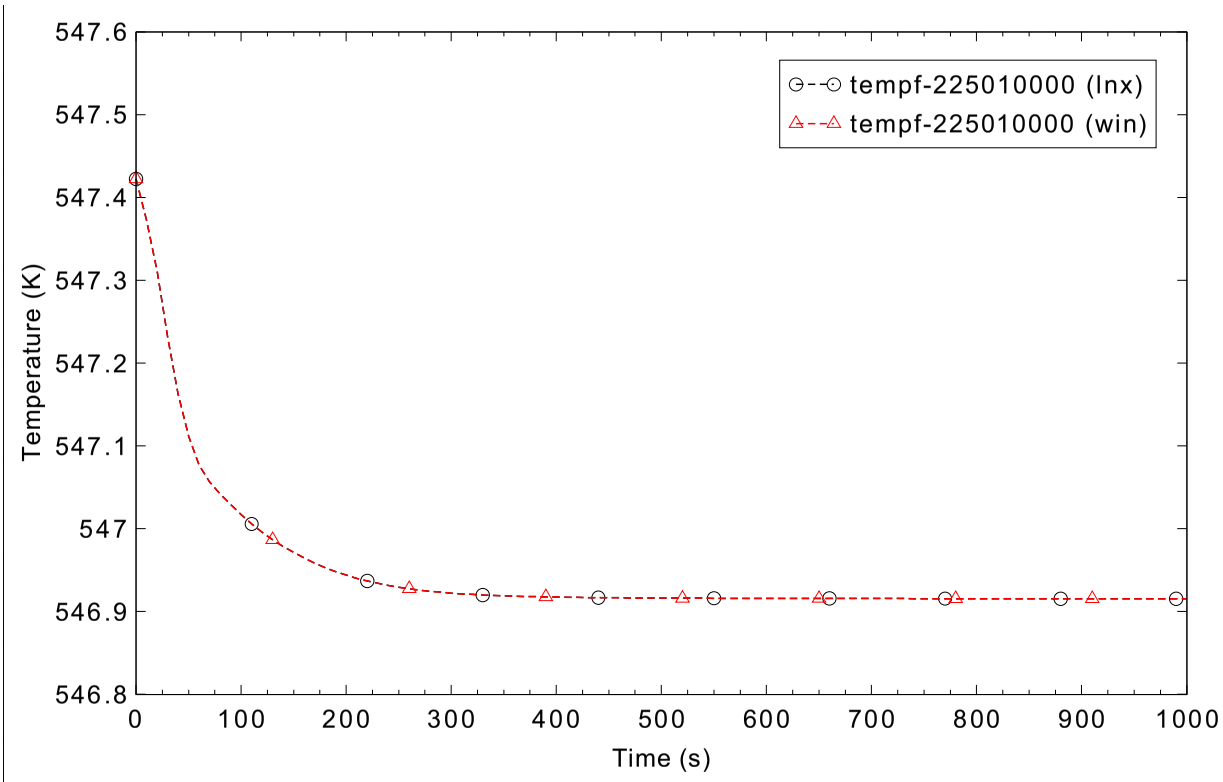

Figure 5.3-5. Calculated cold leg liquid temperature at 60 kW core power for Semiscale Test S-NC-1.

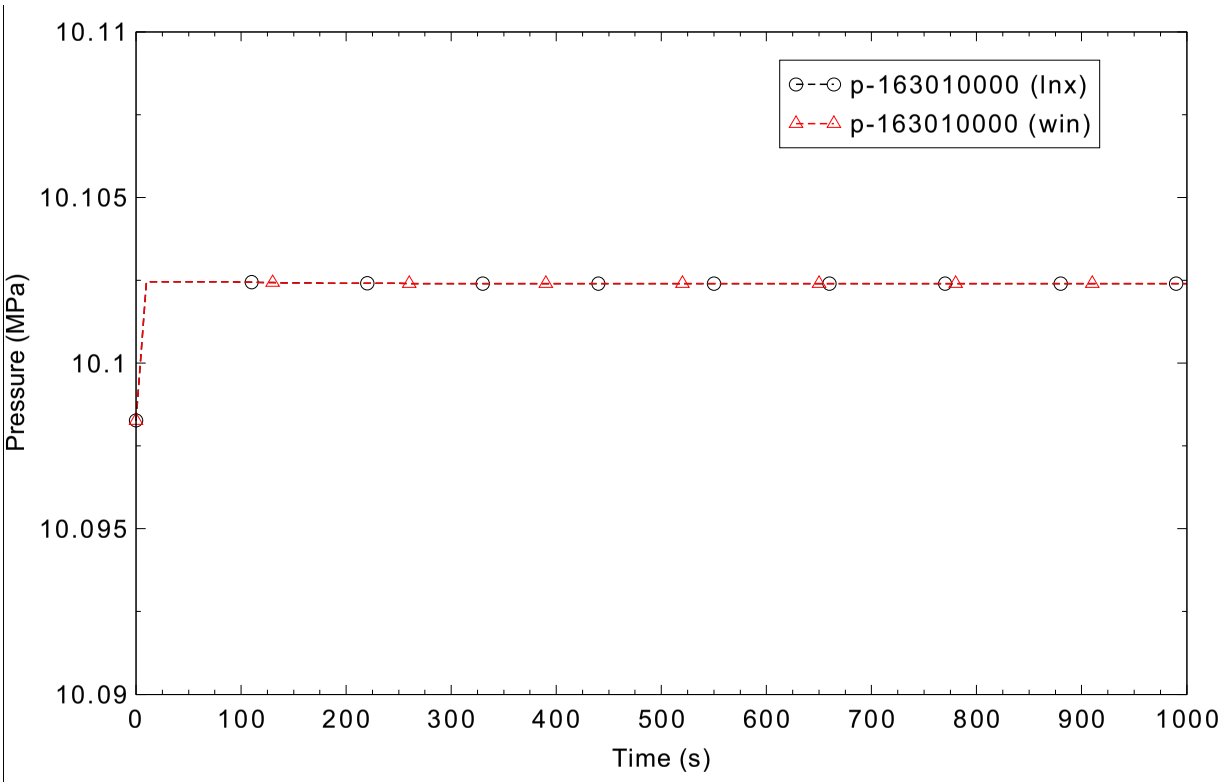

Figure 5.3-6. Calculated primary system pressure at 60 kW core power for Semiscale Test S-NC-1.

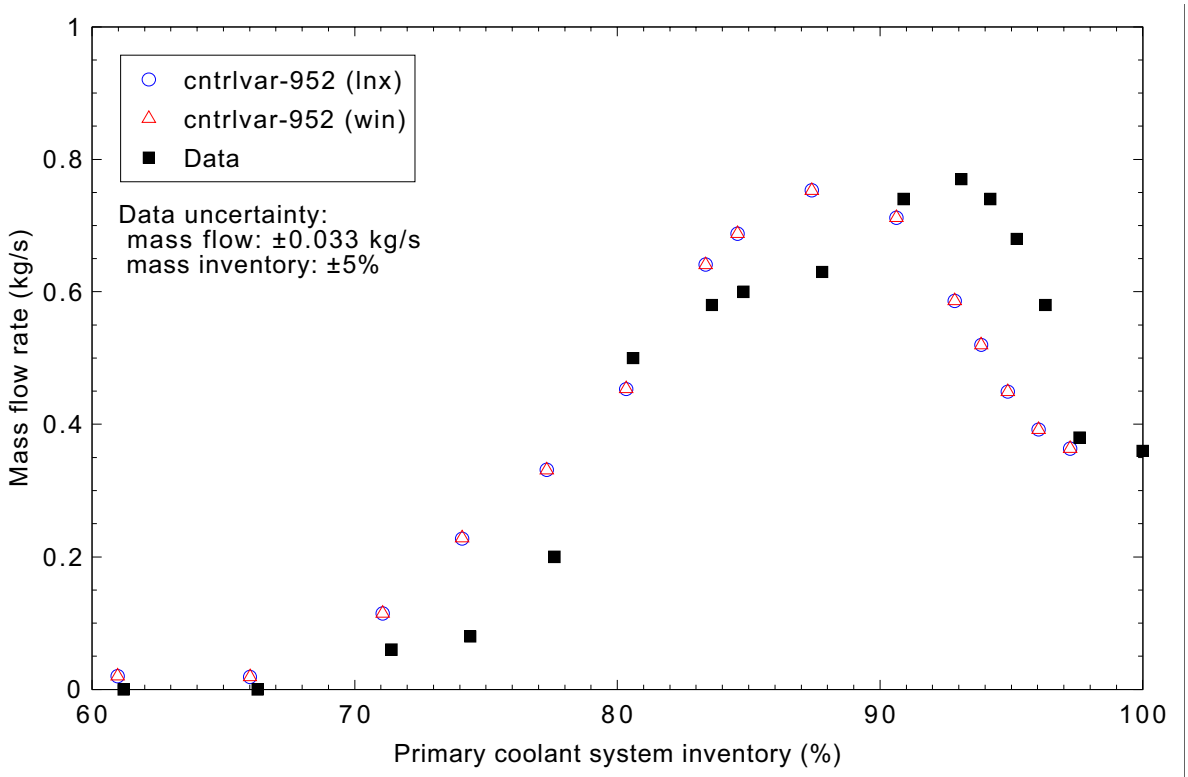

Figure 5.3-7. Measured and calculated primary system mass flow rate at 60 kW core power for Semiscale Test S-NC-2.

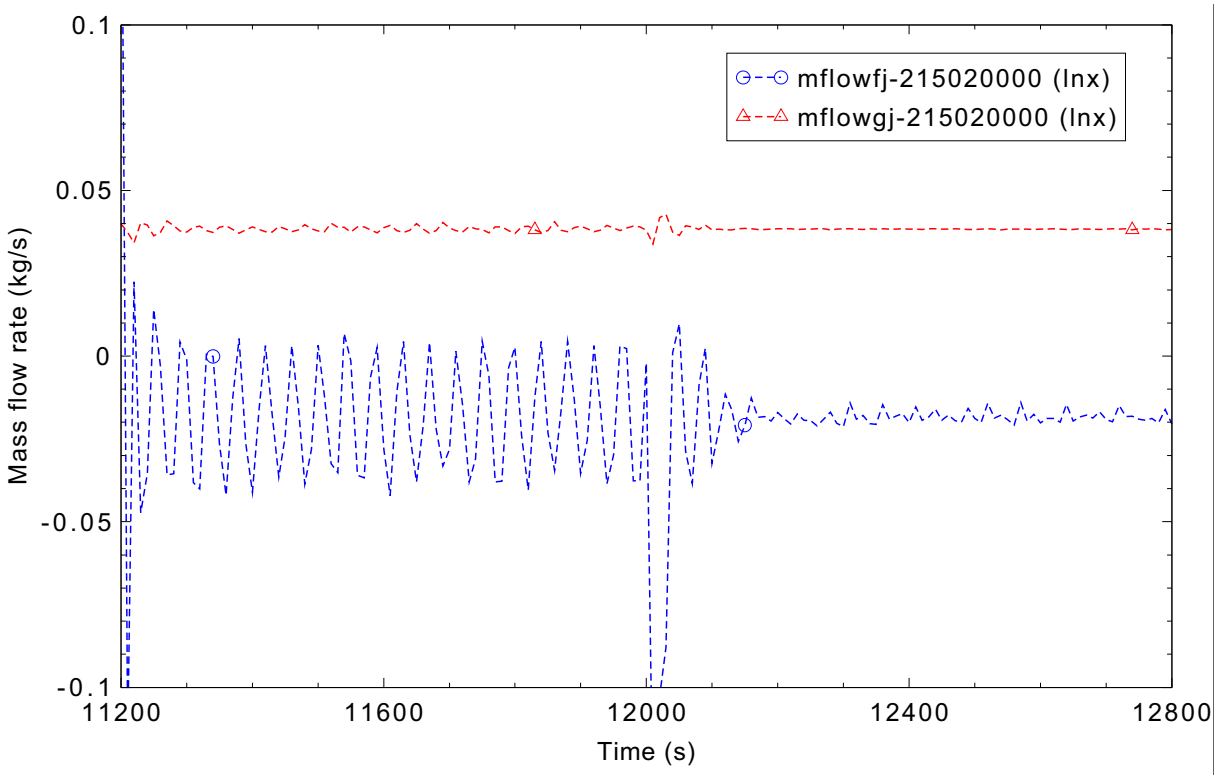

Figure 5.3-8. Calculated primary system liquid and vapor mass flow rates at 60 kW core power for Semiscale Test S-NC-2.

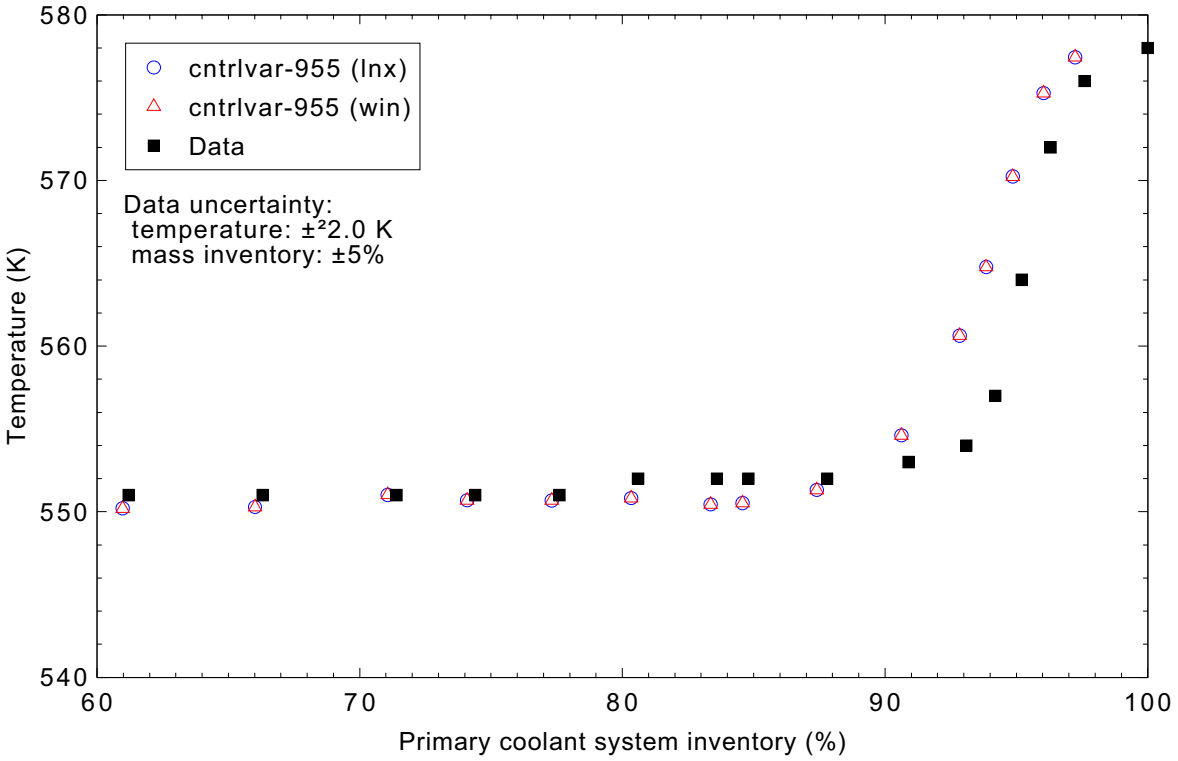

Figure 5.3-9. Measured and calculated hot leg liquid temperature at 60 kW core power for Semiscale Test S-NC-2.

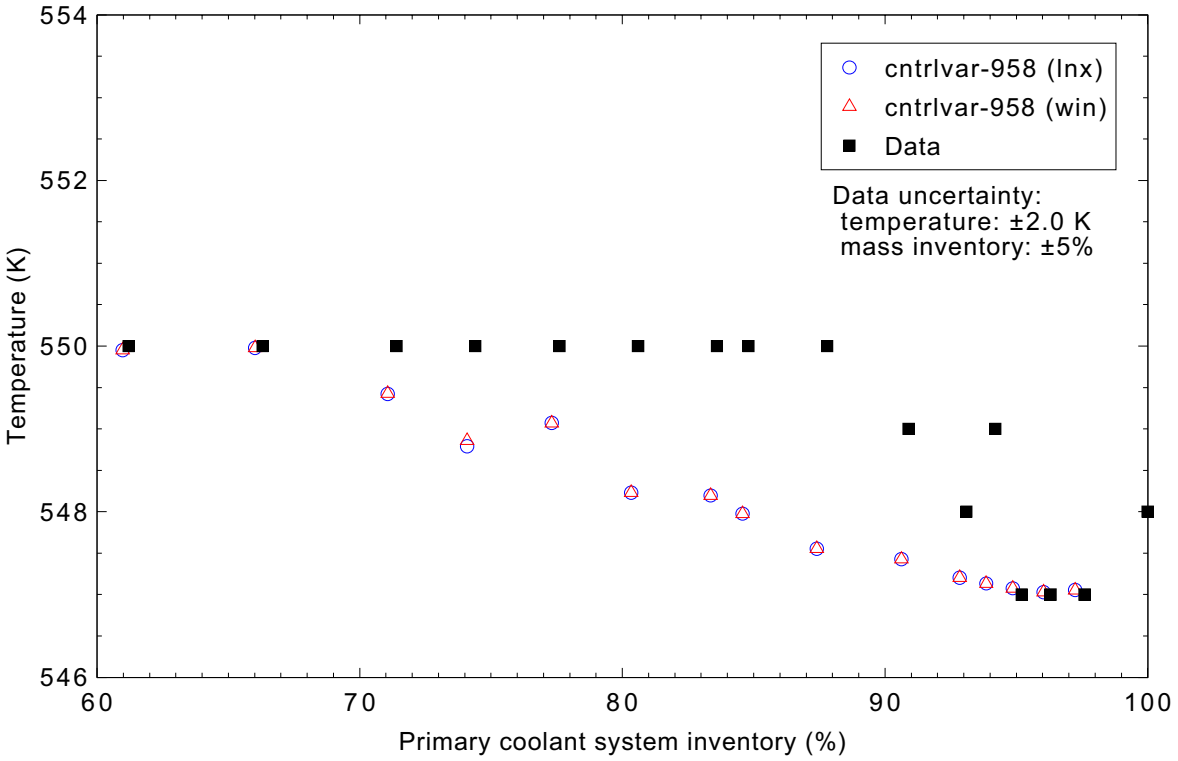

Figure 5.3-10. Measured and calculated cold leg liquid temperature at 60 kW core power for Semiscale Test S-NC-2.

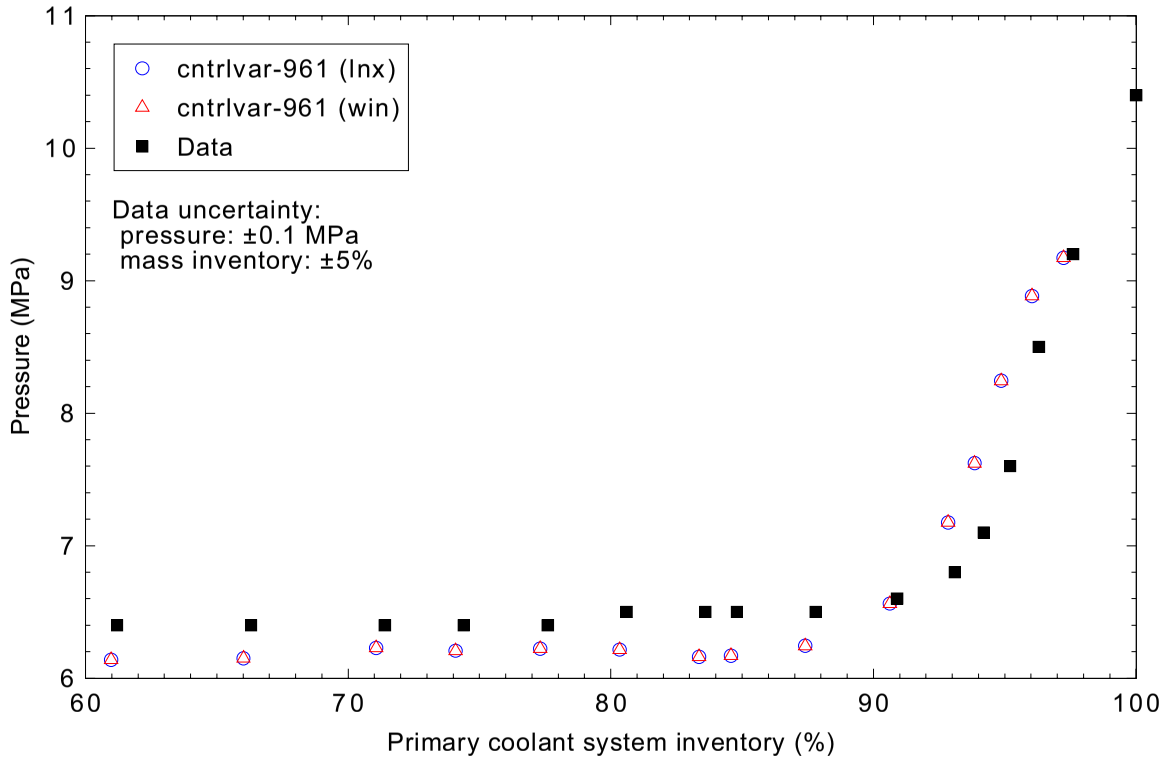

Figure 5.3-11. Measured and calculated reactor vessel upper plenum pressure at 60 kW core power for Semiscale Test S-NC-2.

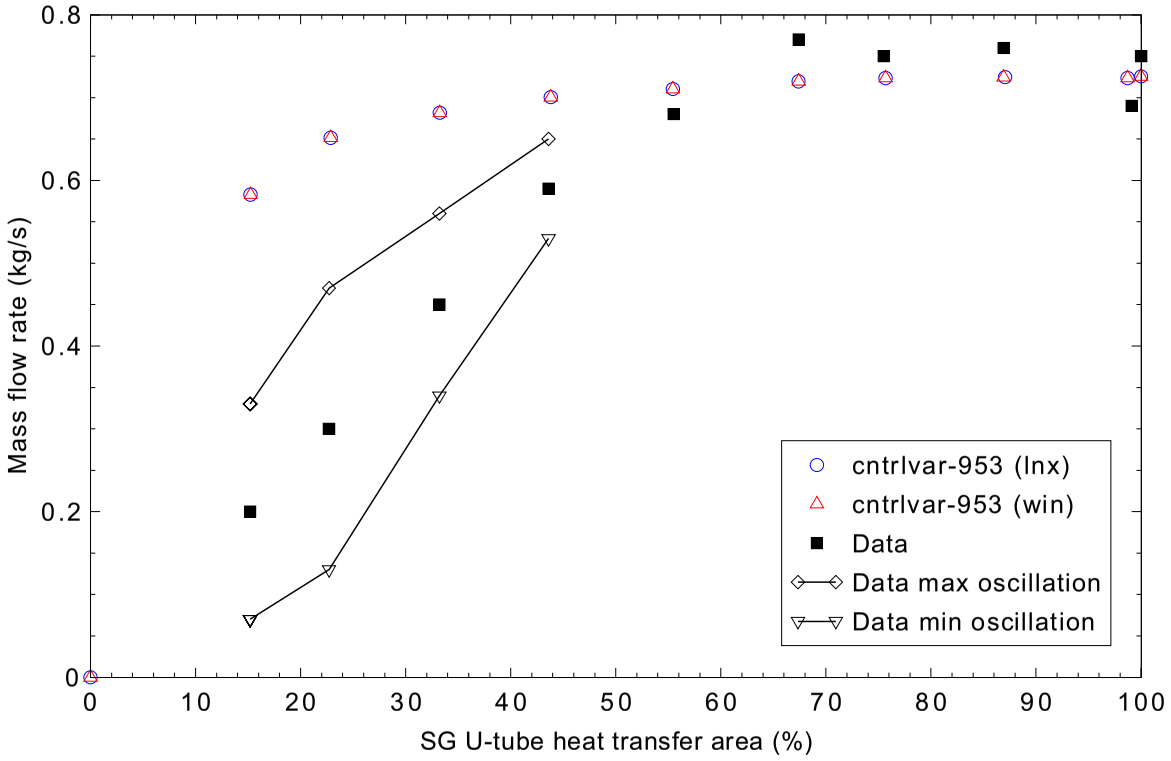

Figure 5.3-12. Measured and calculated primary system mass flow rate for Semiscale Test S-NC-3.

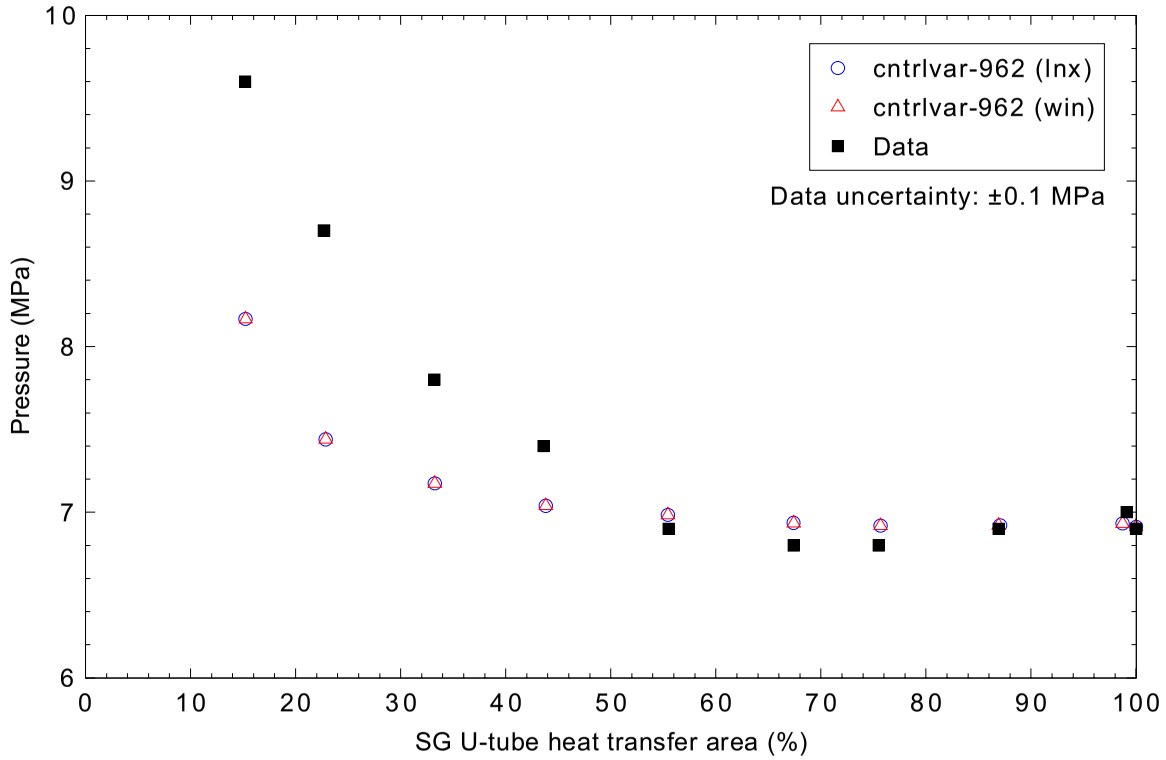

Figure 5.3-13. Measured and calculated primary system pressure for Semiscale Test S-NC-3.

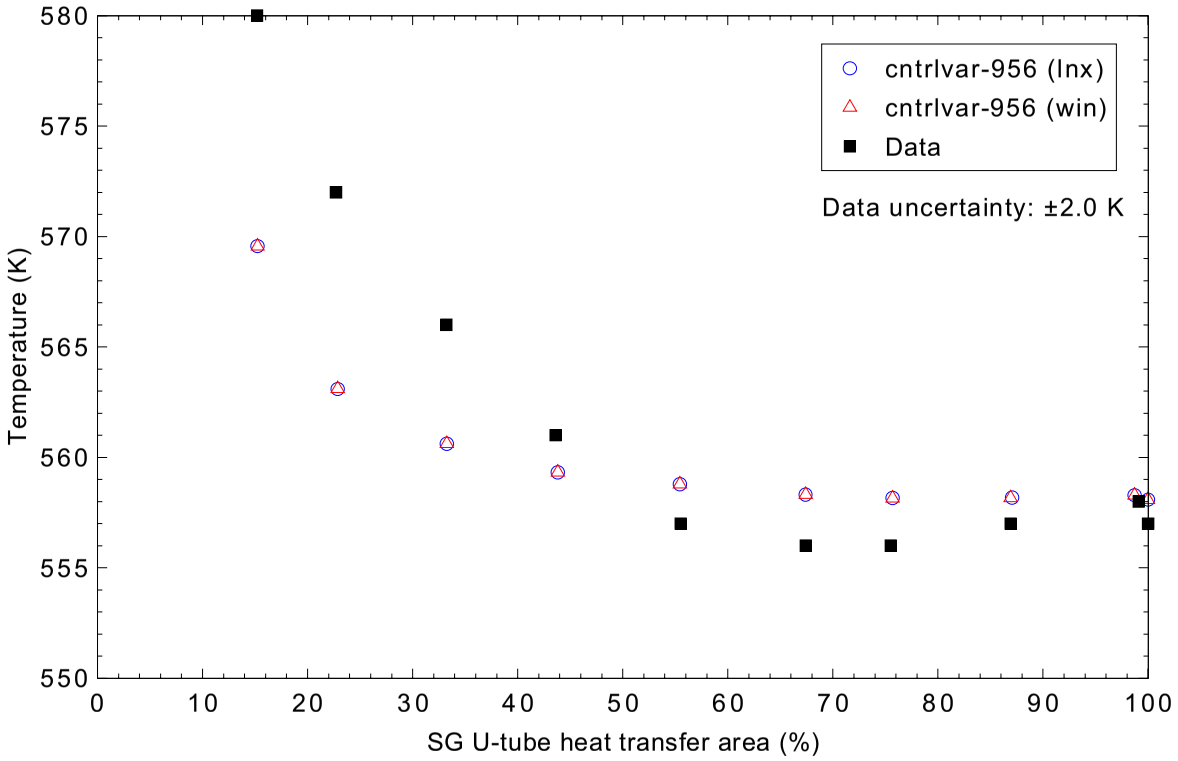

Figure 5.3-14. Measured and calculated hot leg liquid temperature for Semiscale Test S-NC-3.

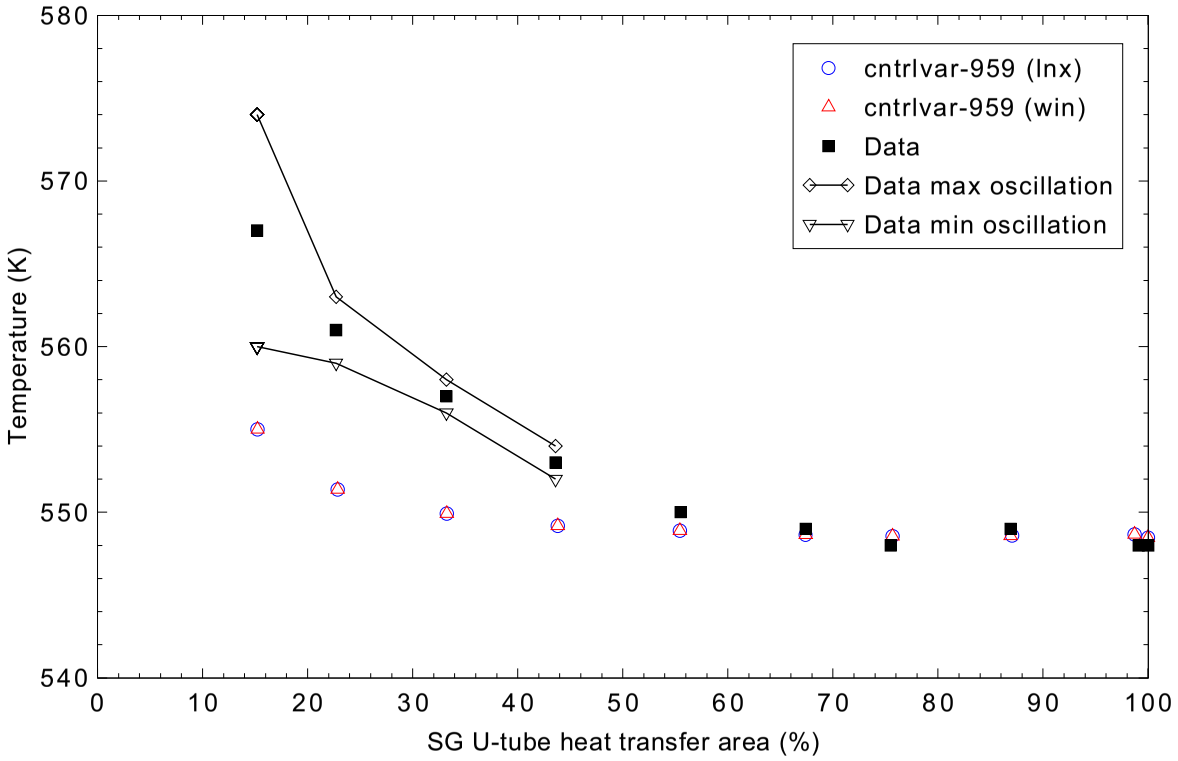

Figure 5.3-15. Measured and calculated cold leg liquid temperature for Semiscale Test S-NC-3.

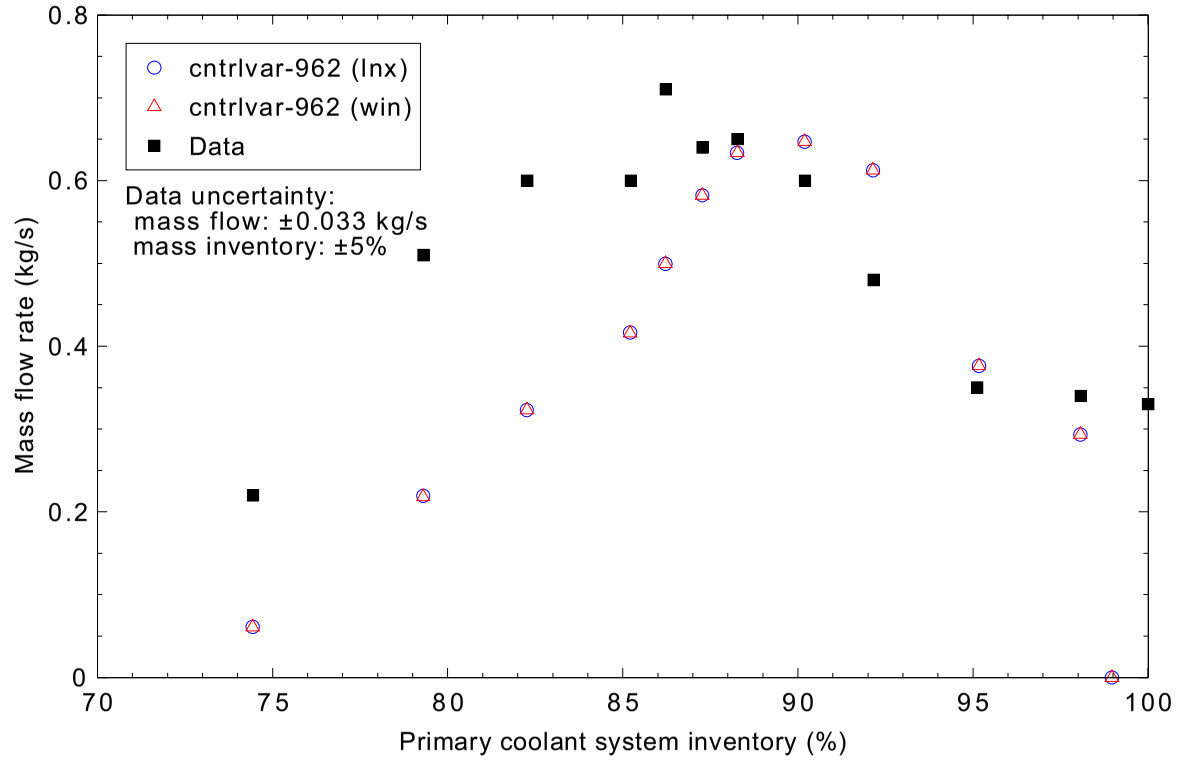

Figure 5.3-16. Measured and calculated primary system mass flow rate for Semiscale Test S-NC-10 Part 2.

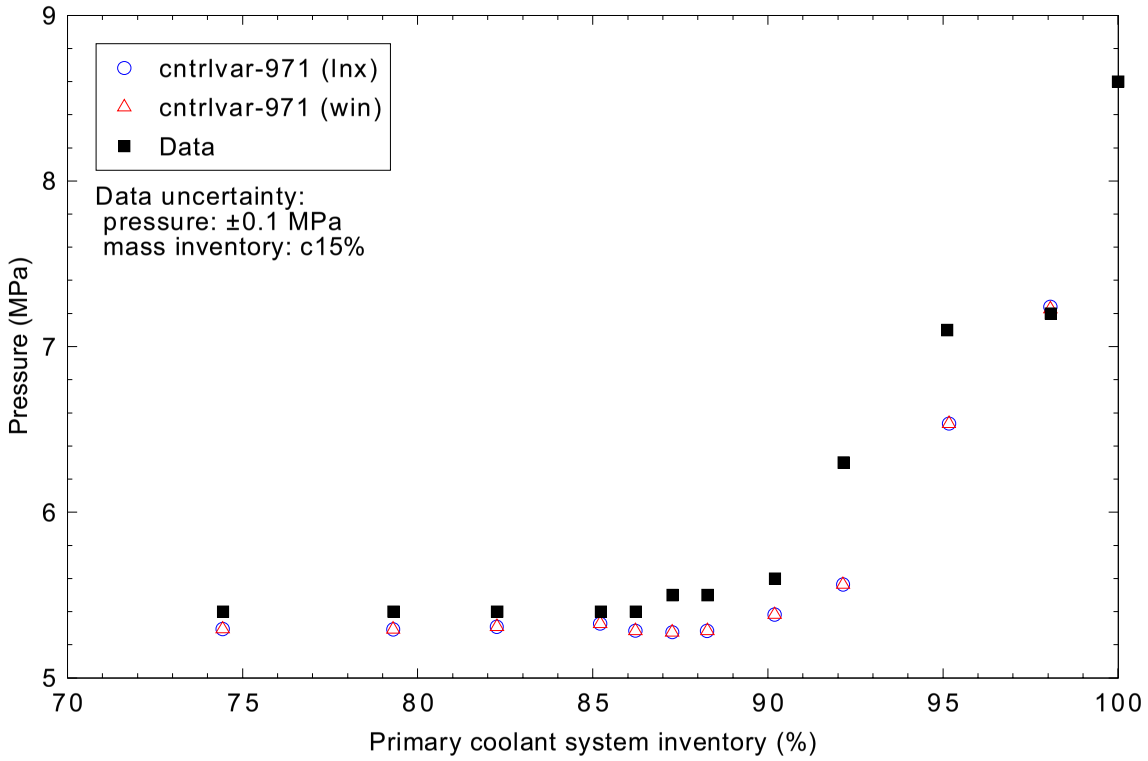

Figure 5.3-17. Measured and calculated primary system pressures for Semiscale Test S-NC-10 Part 2.

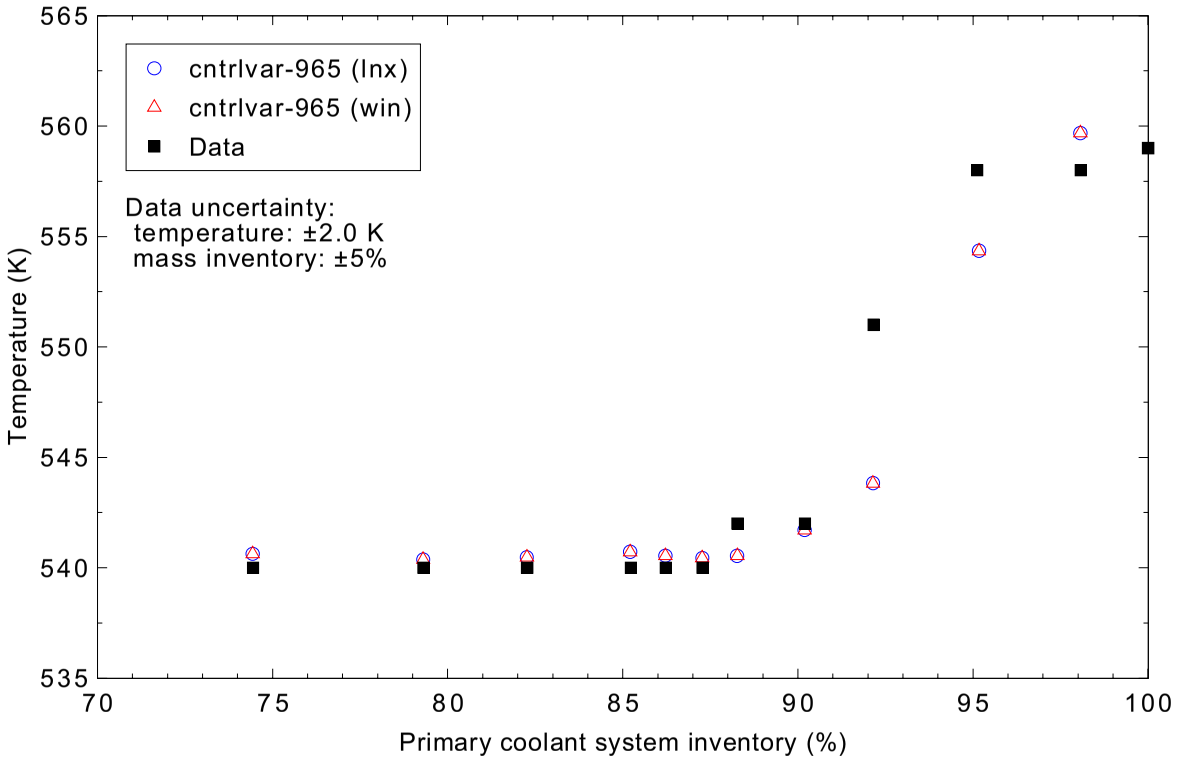

Figure 5.3-18. Measured and calculated hot leg liquid temperatures for Semiscale Test S-NC-10 Part 2.

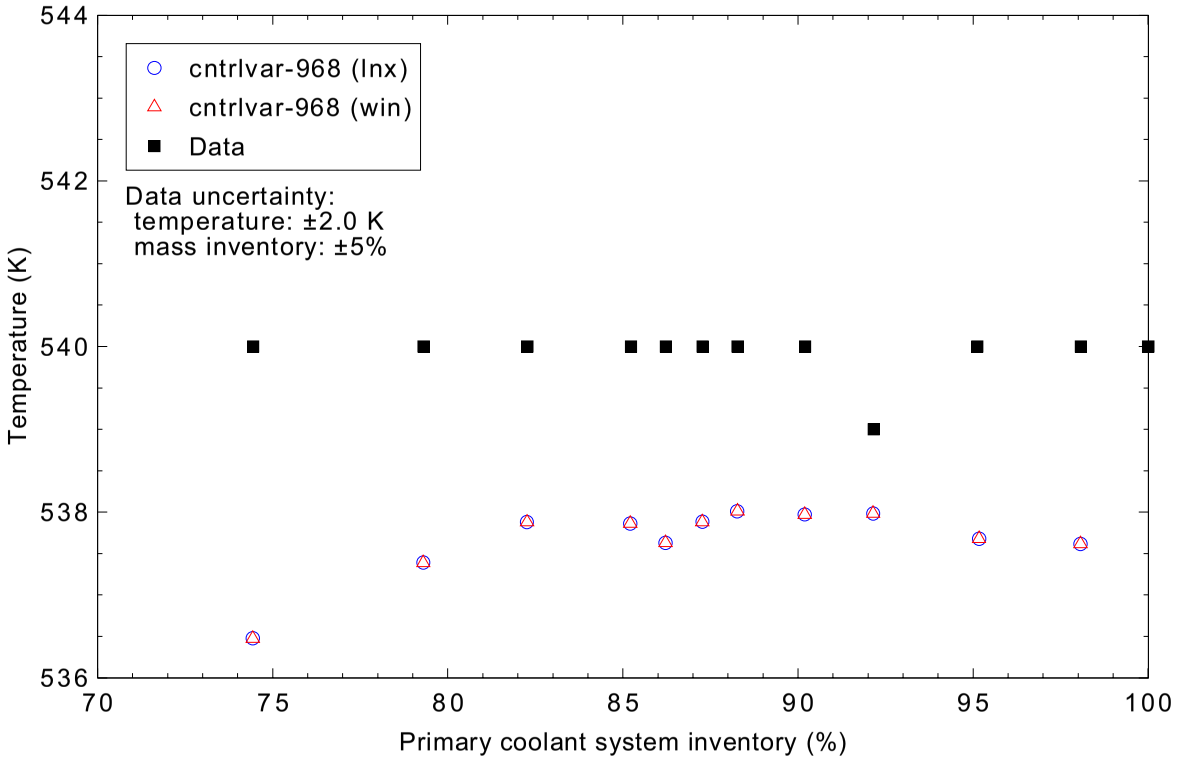

Figure 5.3-19. Measured and calculated cold leg liquid temperatures for Semiscale Test S-NC-10 Part 2.

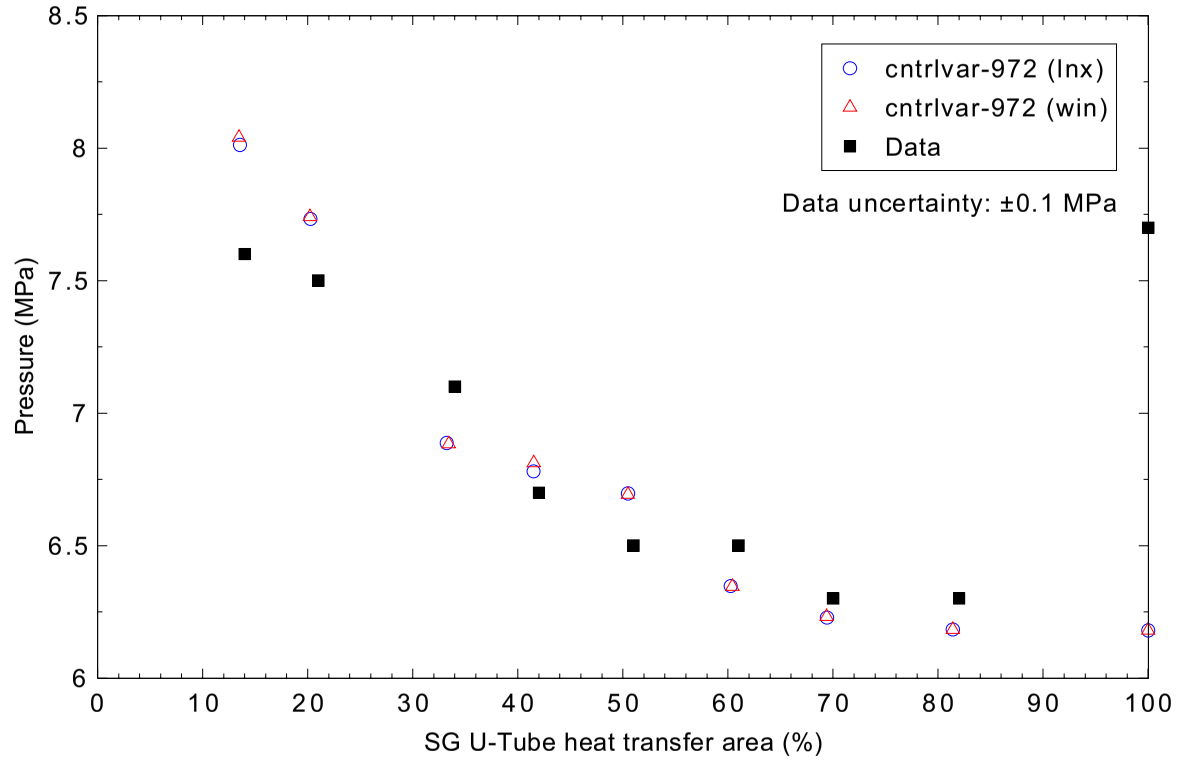

Figure 5.3-20. Measured and calculated primary system pressure for Semiscale Test S-NC-10 Part 3.

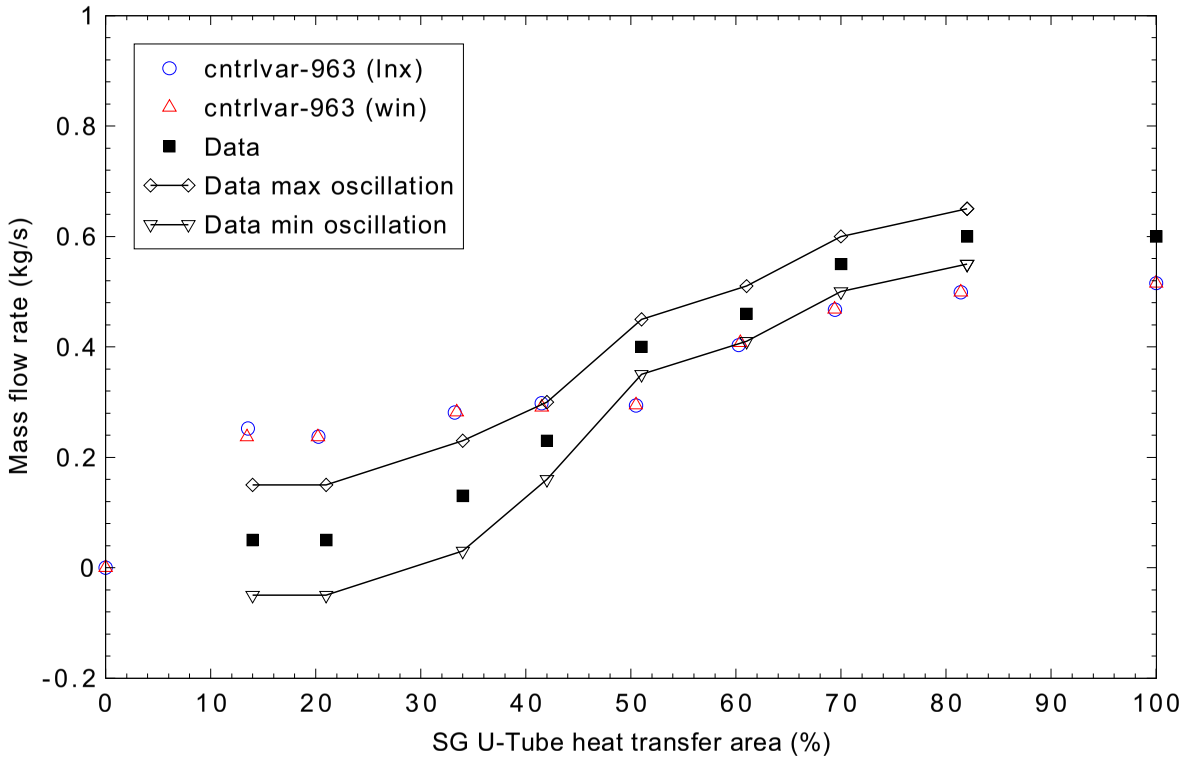

Figure 5.3-21. Measured and calculated primary system mass flow rate for Semiscale Test S-NC-10 Part 3.

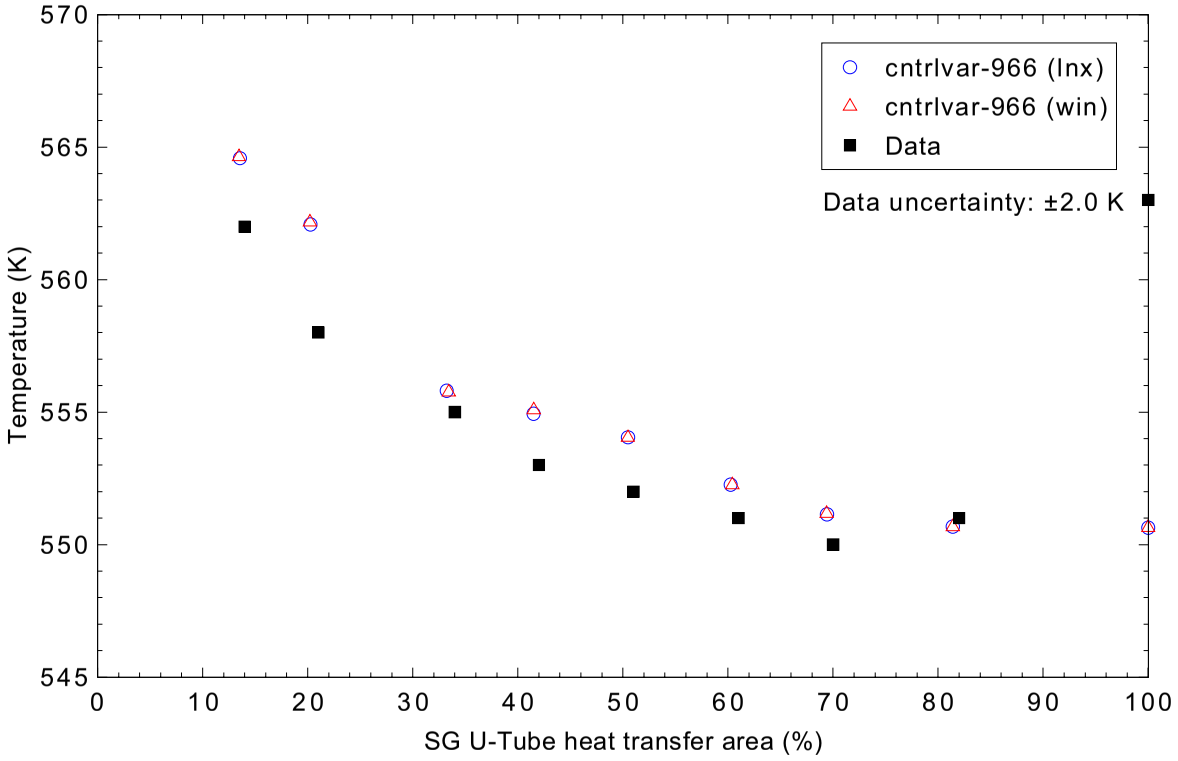

Figure 5.3-22. Measured and calculated hot leg liquid temperature for Semiscale Test S-NC-10 Part 3.

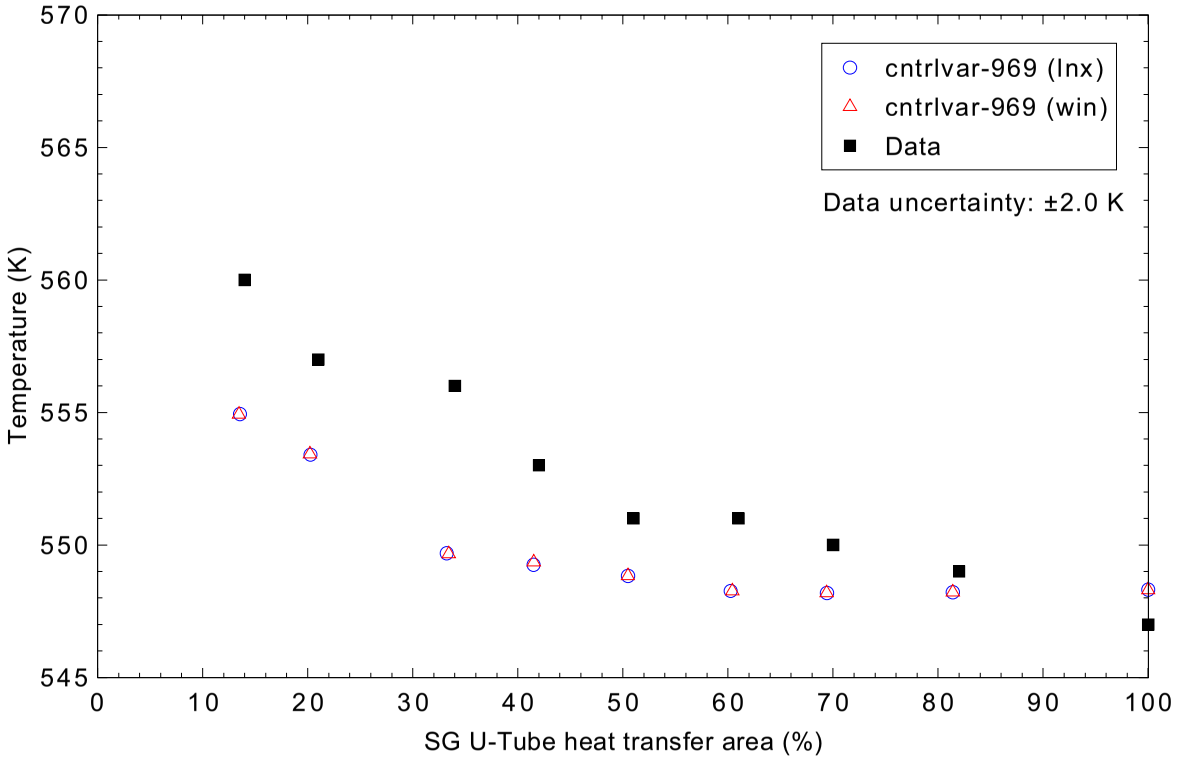

Figure 5.3-23. Measured and calculated cold leg liquid temperature for Semiscale Test S-NC-10 Part 3.

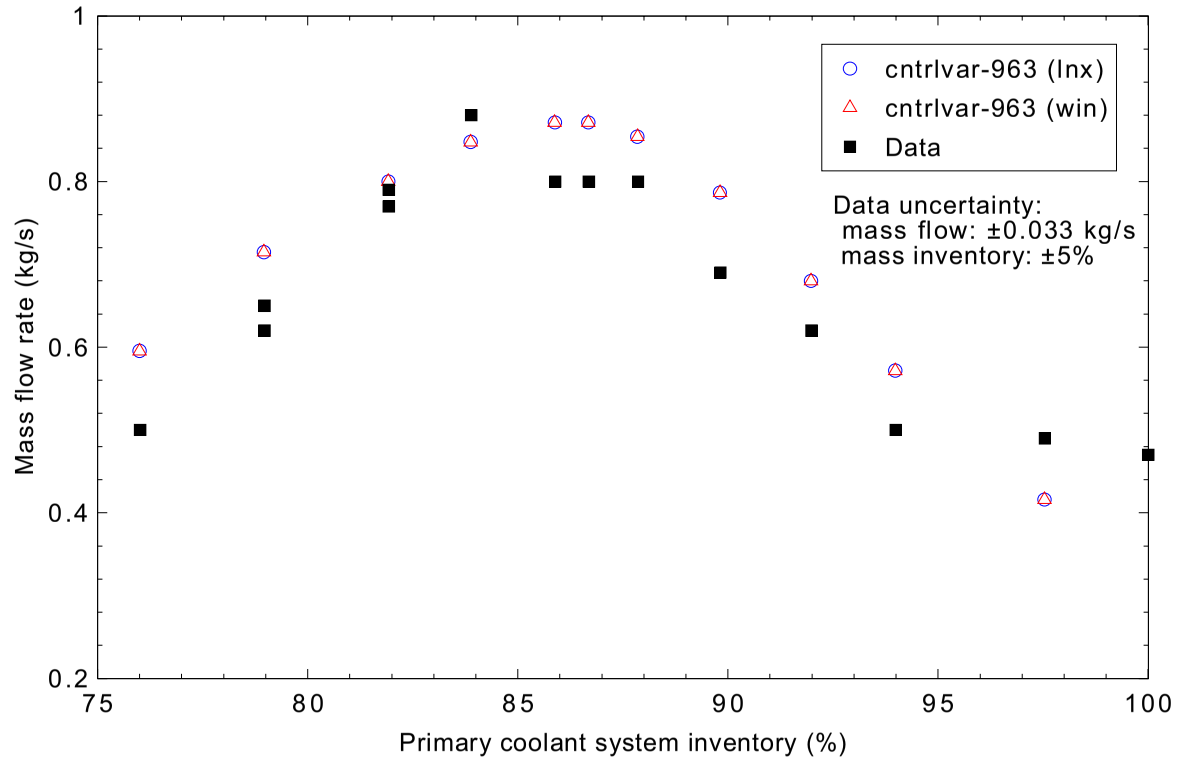

Figure 5.3-24. Measured and calculated primary system mass flow rate for Semiscale Test S-NC-10 Part 4 with core power of 100 kW.

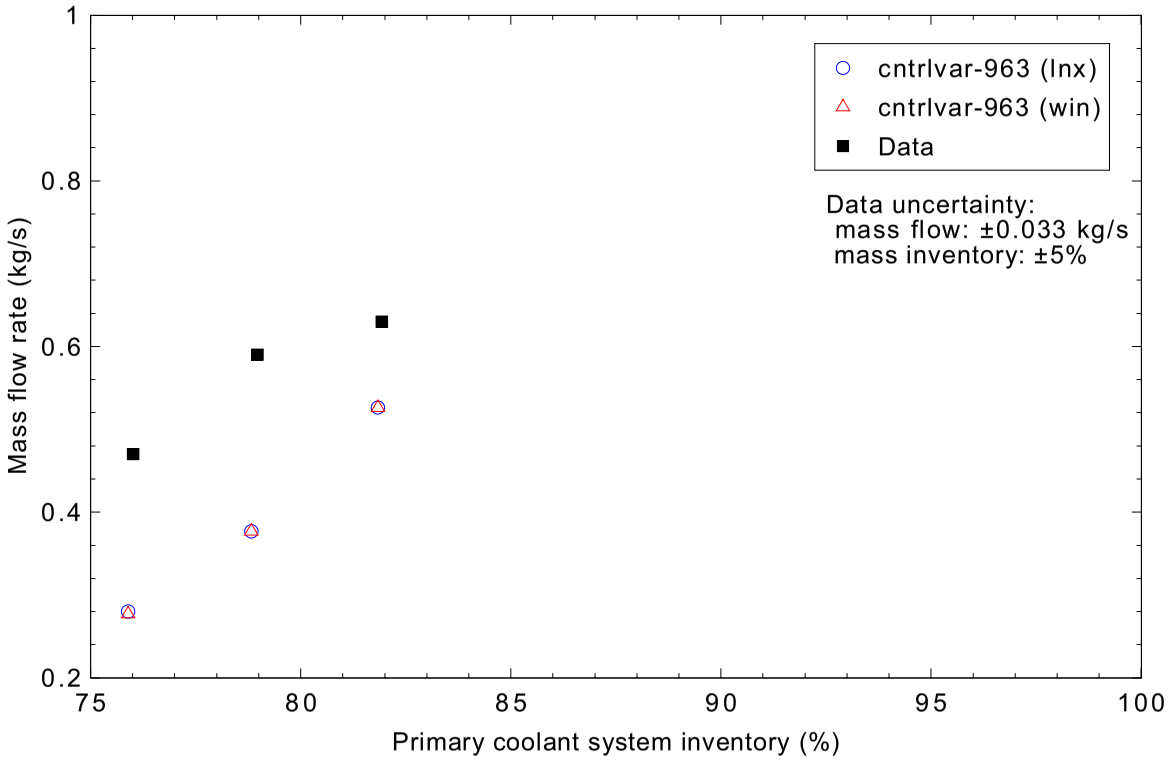

Figure 5.3-25. Measured and calculated primary system mass flow rate for Semiscale Test S-NC-10 Part 4 with core power of 60 kW.

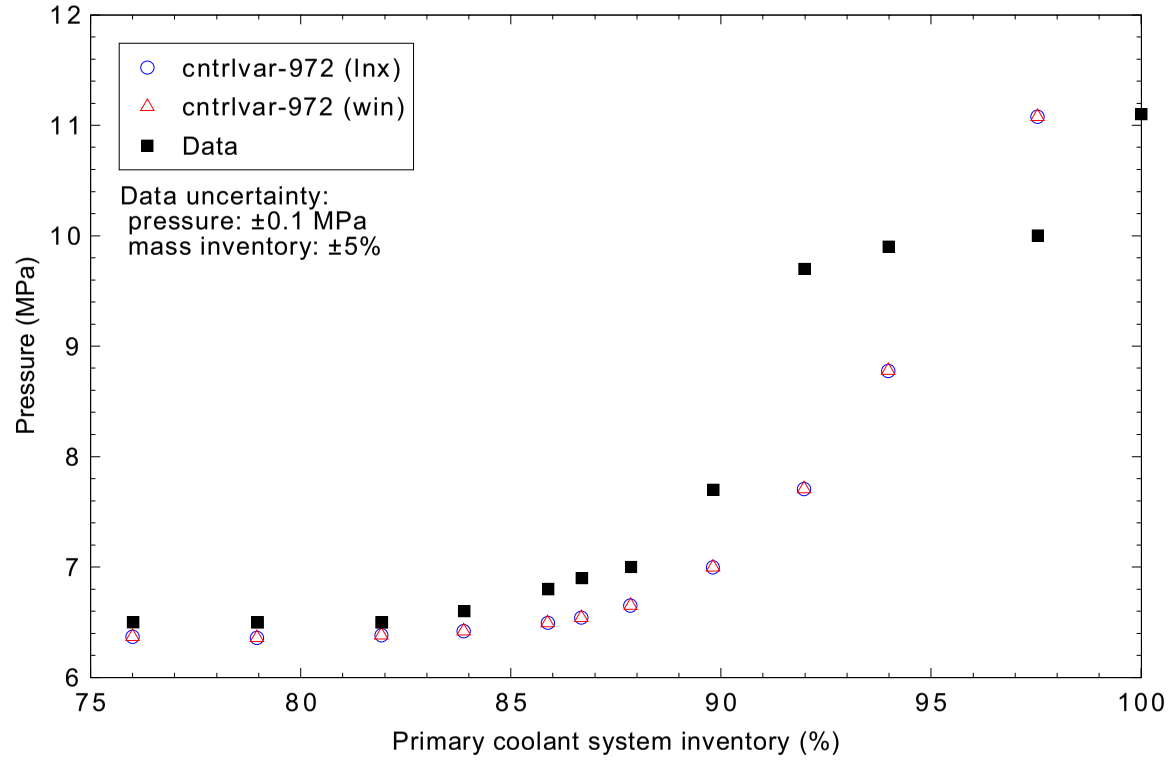

Figure 5.3-26. Measured and calculated primary system pressures for Semiscale Test S-NC-10 Part 4 with core power of 100 kW.

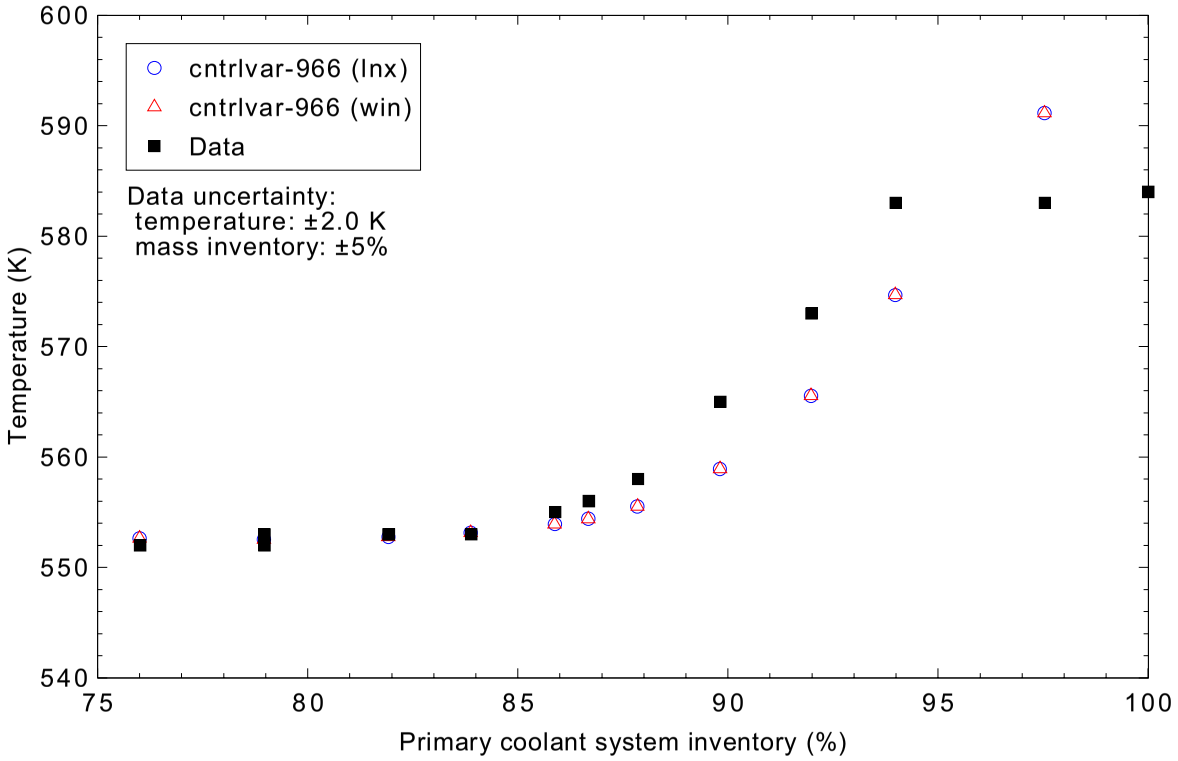

Figure 5.3-27. Measured and calculated hot leg liquid temperatures for Semiscale Test S-NC-10 Part 4 with core power of 100 kW.

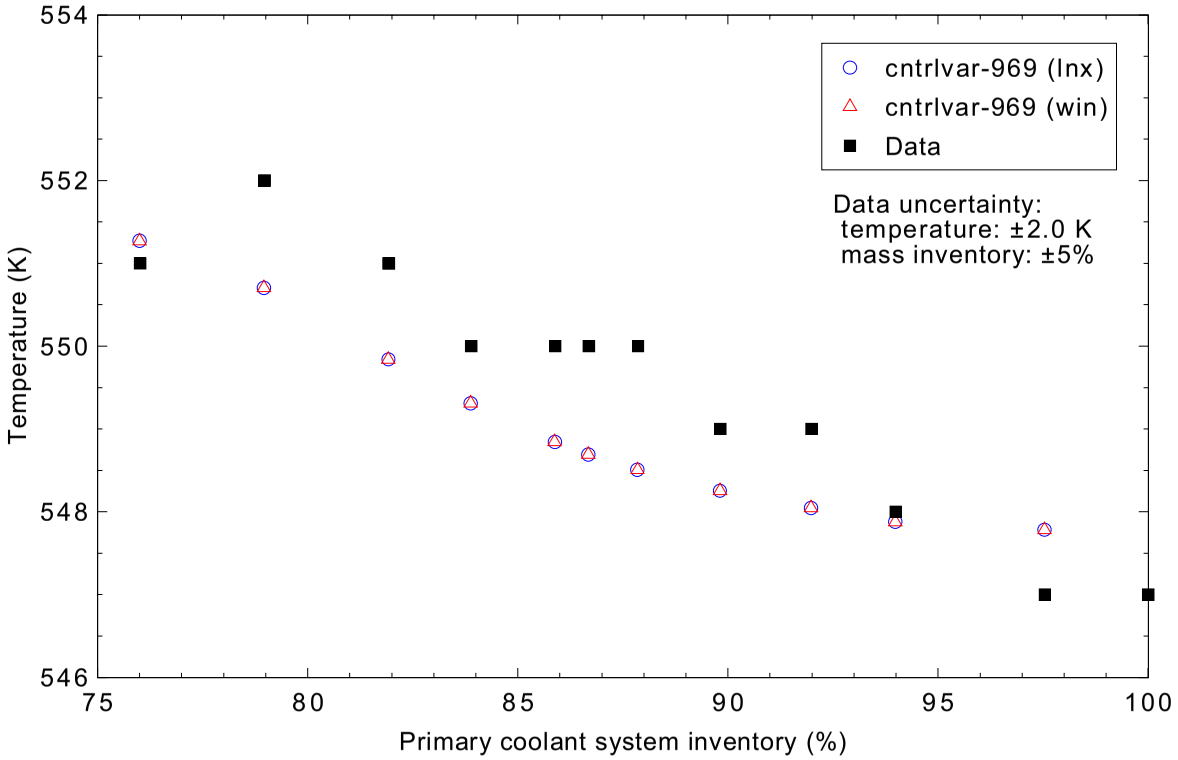

Figure 5.3-28. Measured and calculated cold leg liquid temperatures for Semiscale Test S-NC-10 Part 4 with core power of 100 kW.

5.4 LOBI Test A1-04R (Large Break)

Figures comparing simulations using Linux and Windows code versions are presented. Diagrams are included so that the figure numbering is the same as that in Volume III of the RELAP5-3D code manual. Noticeable differences were observed in Figures 5.4-5, 6, 7, 8, 9, 10, 11, 12, 13, 14, 15, 16, 17, 18, 19, and 20.

.

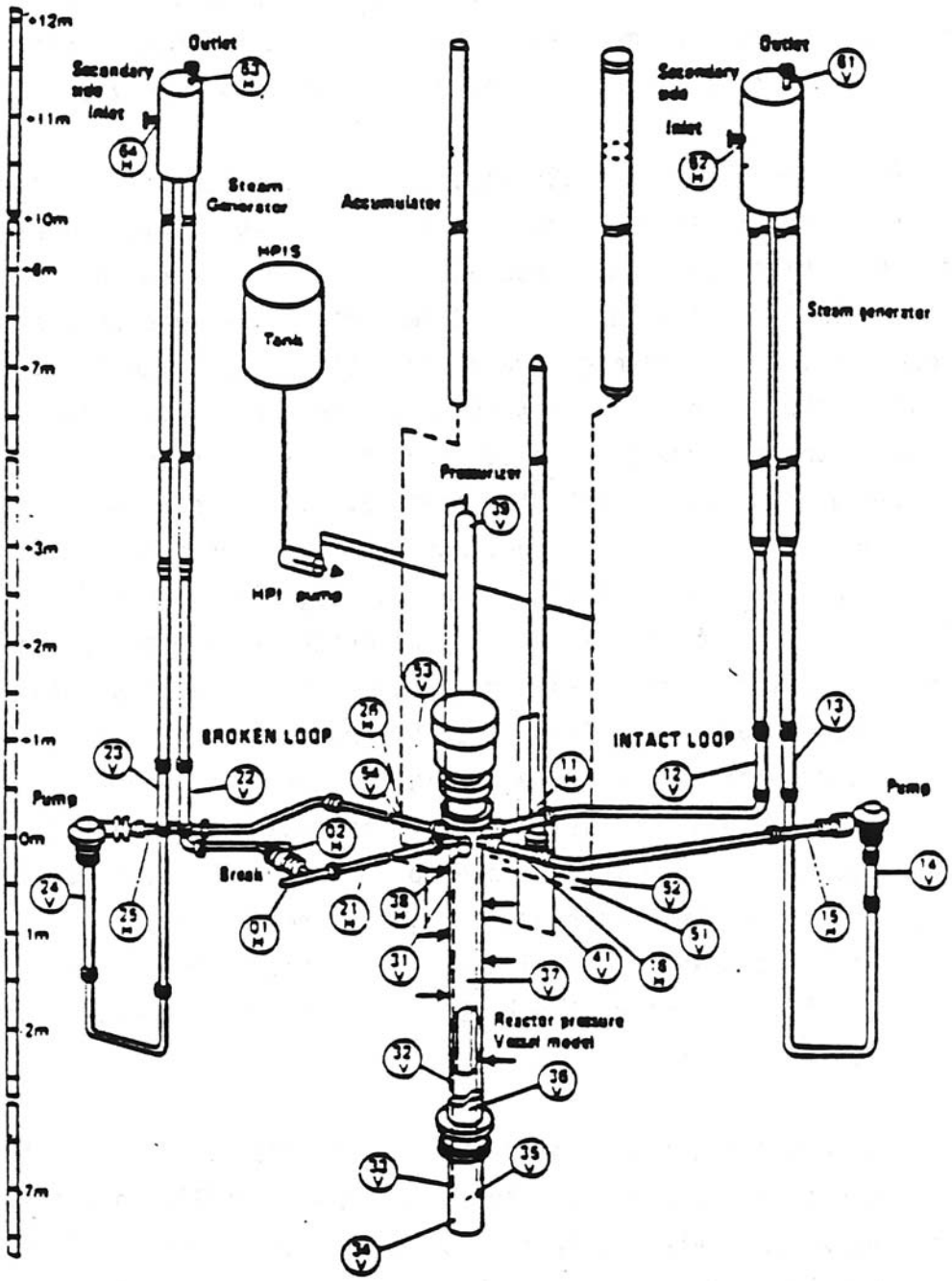

Figure 5.4-1. Schematic of LOBI facility.

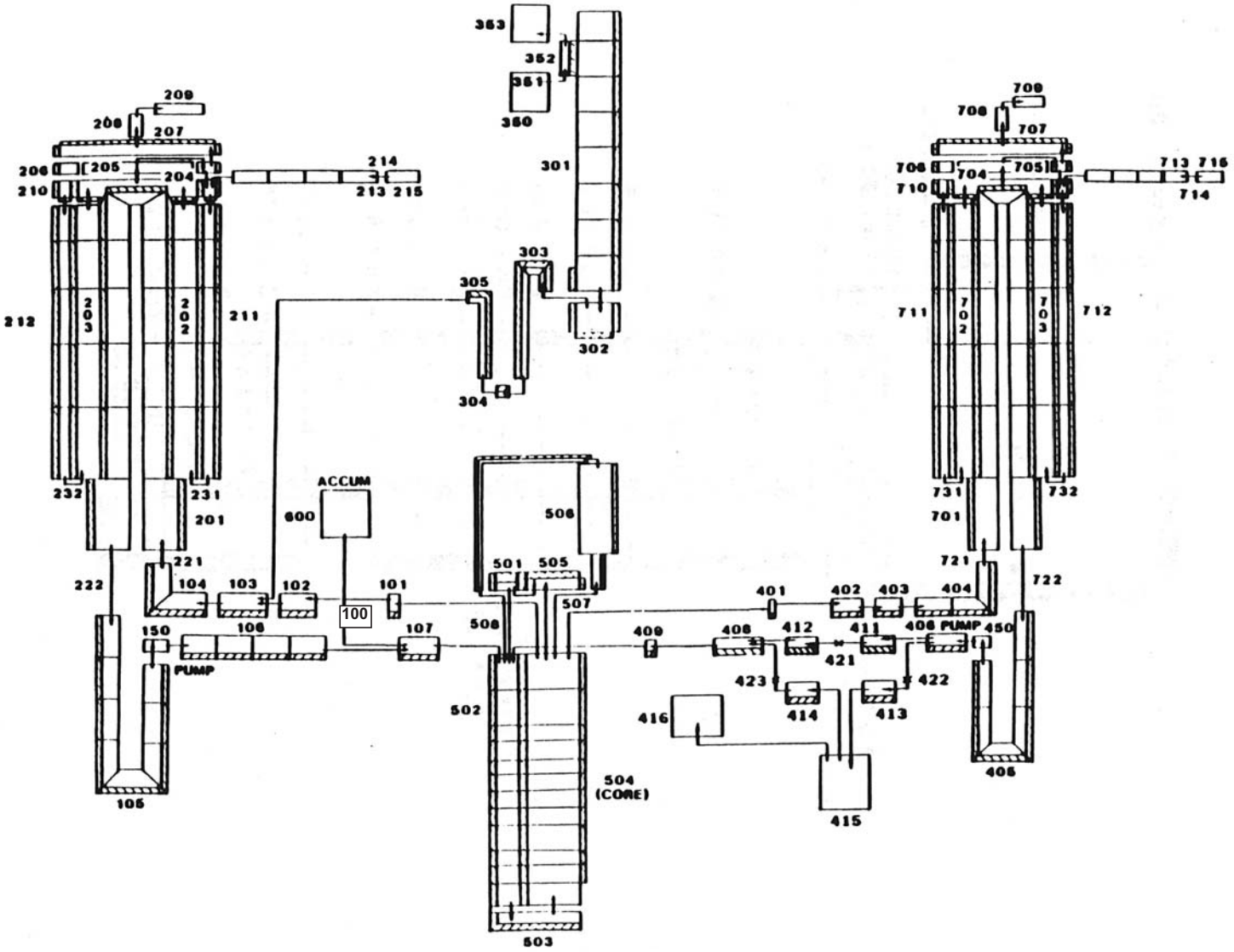

Figure 5.4-2. Noding diagram for the LOBI facility.

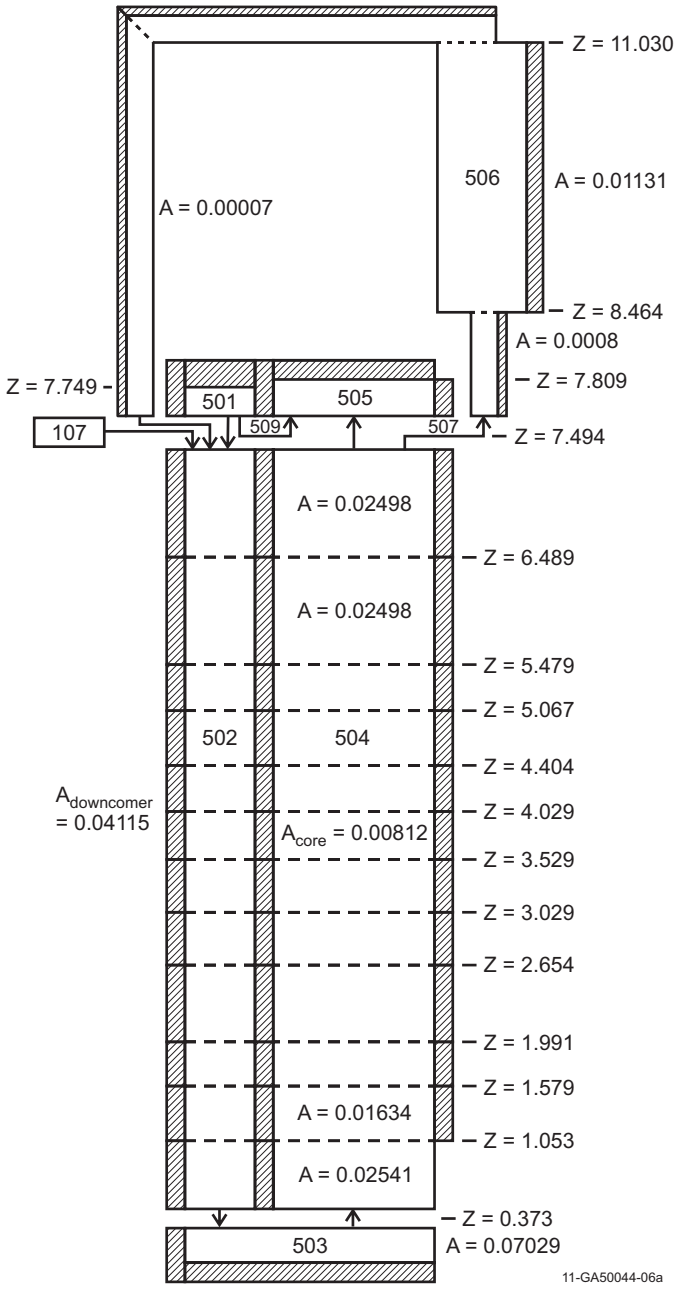

Figure 5.4-3. LOBI reactor vessel nodalization.

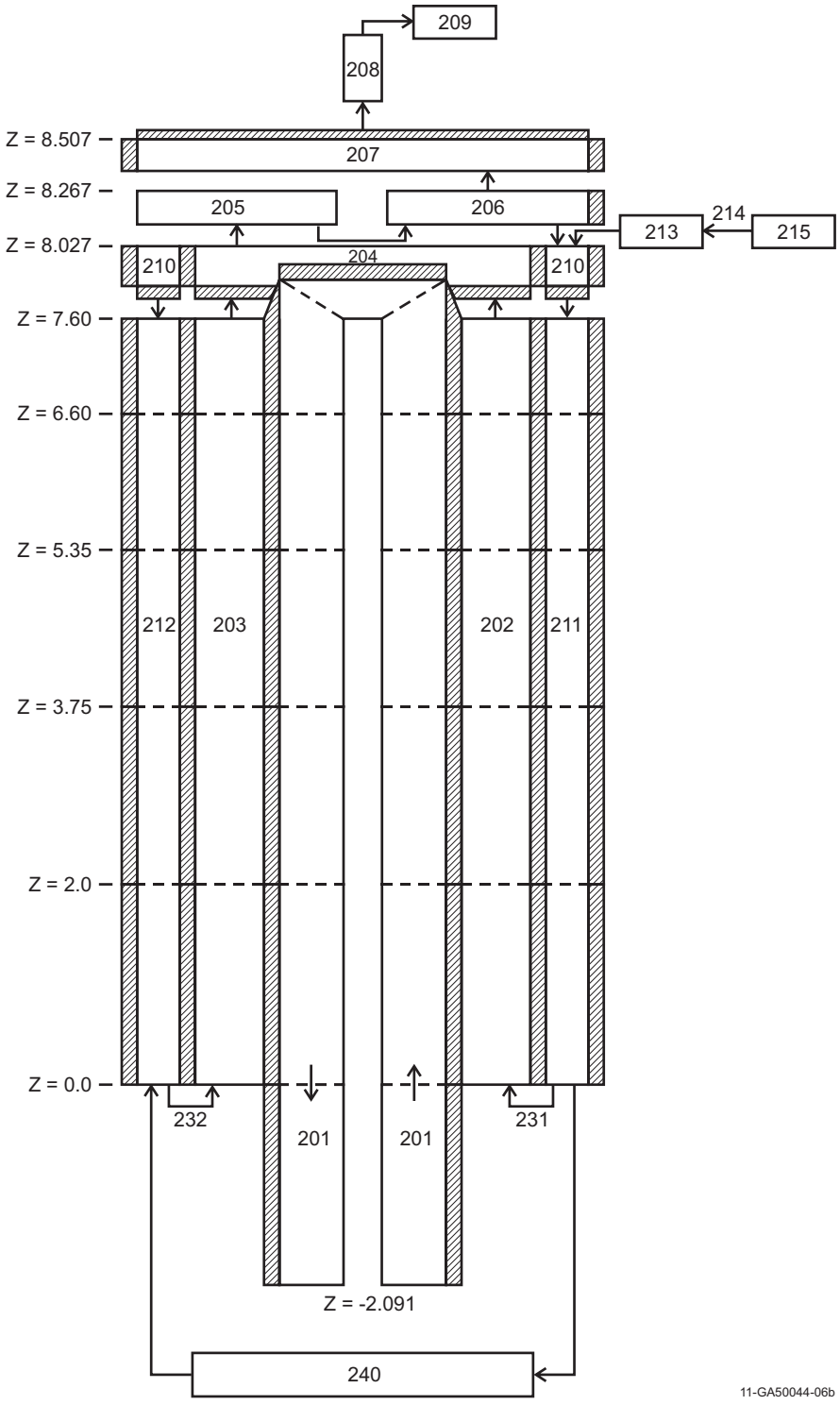

Figure 5.4-4. LOBI steam generator nodalization.

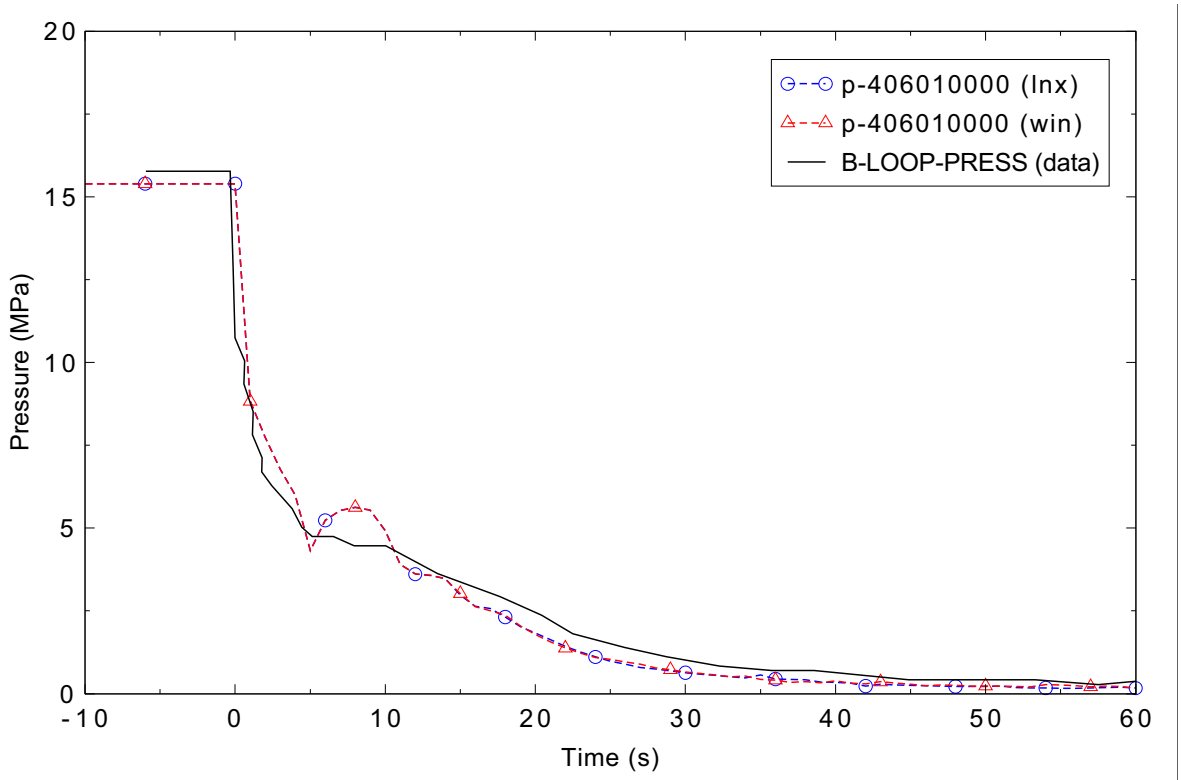

Figure 5.4-5. Broken loop pressure behavior for LOBI Test A1-04R.

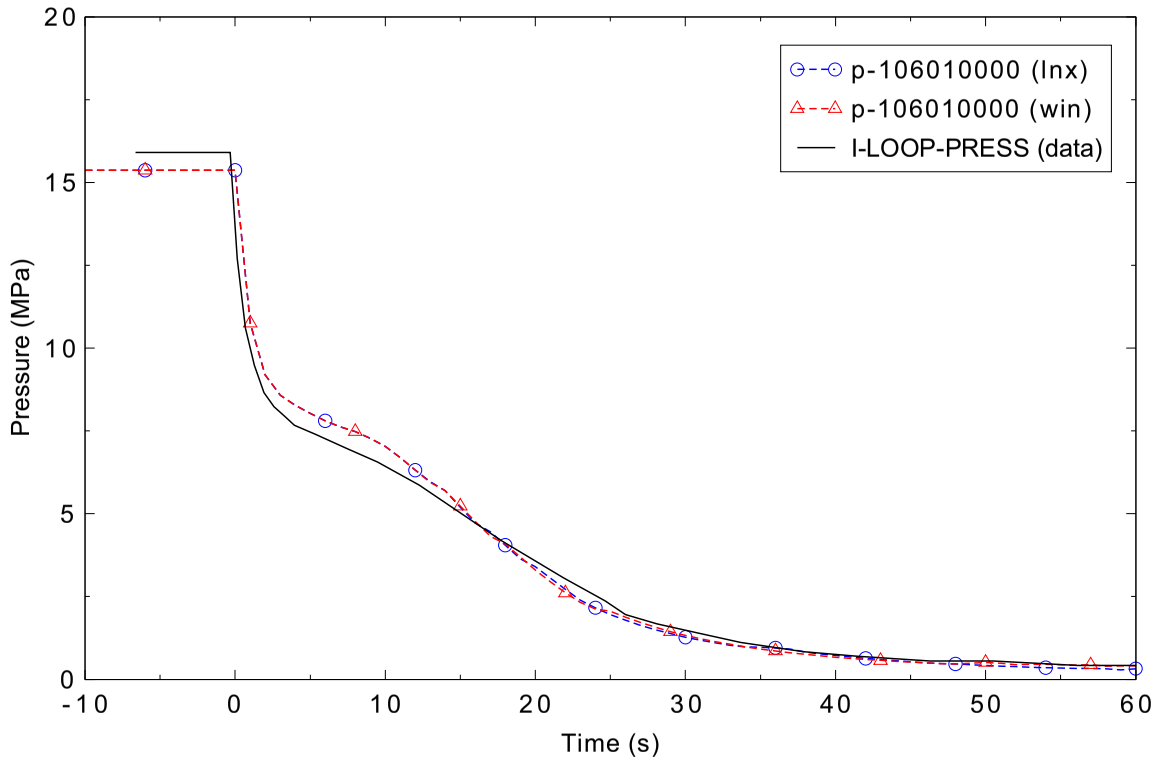

Figure 5.4-6. Intact loop pressure behavior for LOBI Test A1-04R.

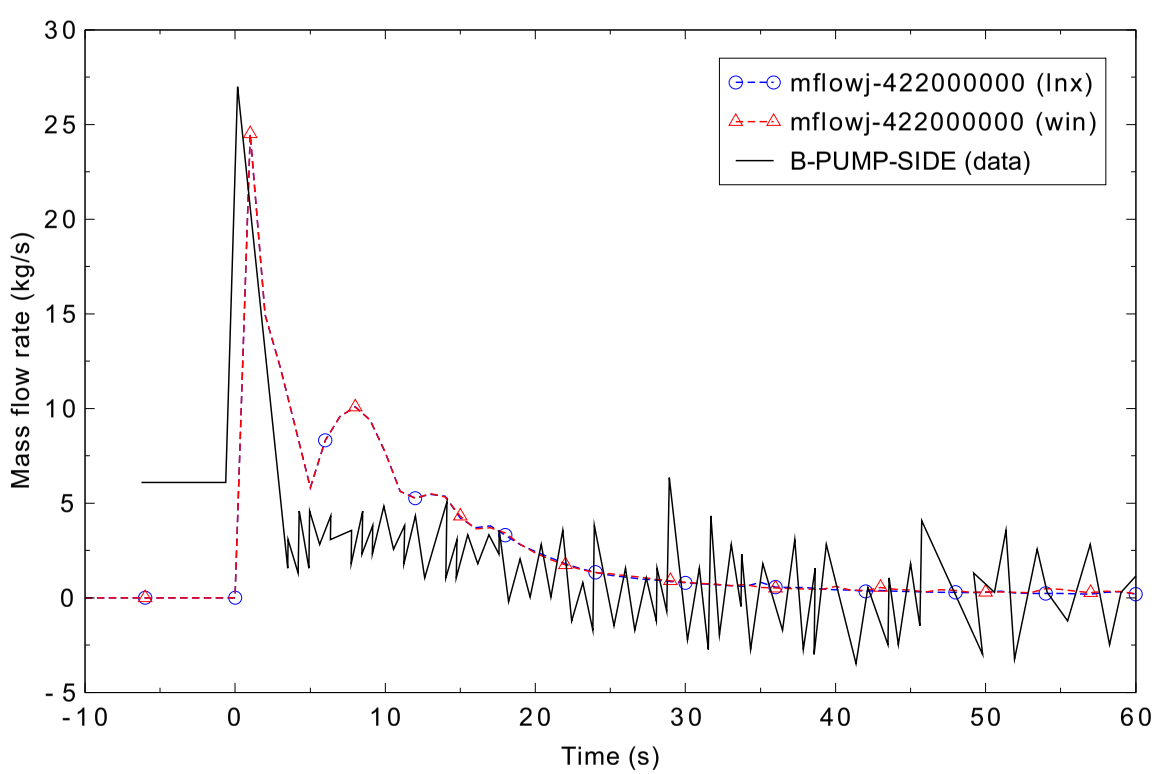

Figure 5.4-7. Broken loop mass flow rate (pump side) for LOBI Test A1-04R.

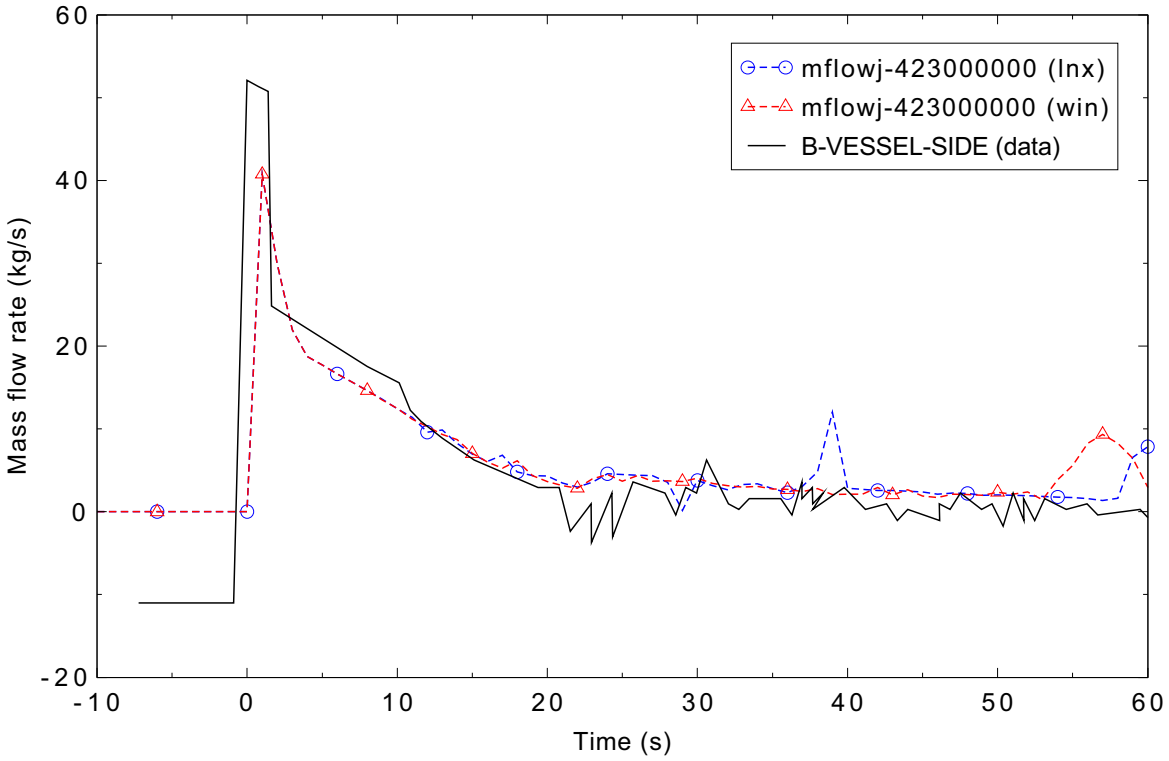

Figure 5.4-8. Broken loop mass flow rate (vessel side) for LOBI Test A1-04R.

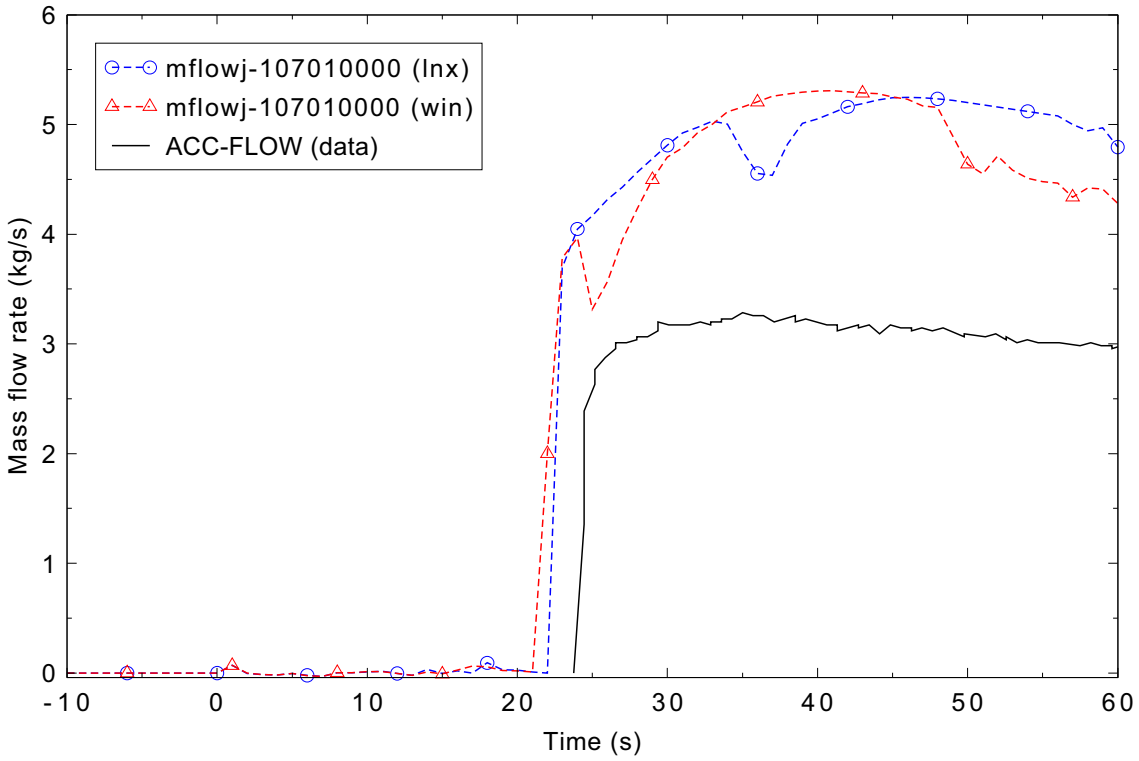

Figure 5.4-9. Accumulator discharge flow rate for LOBI Test A1-04R.

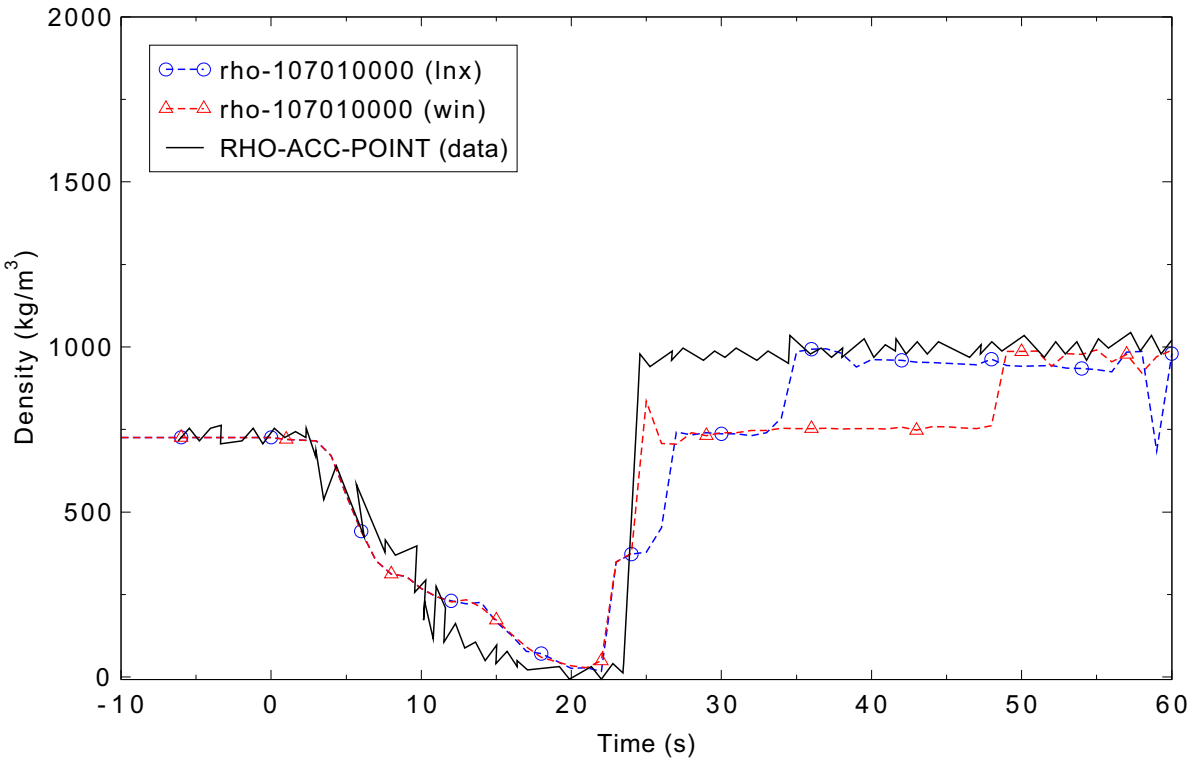

Figure 5.4-10. Fluid density at the accumulator injection point for LOBI Test A1-04R.

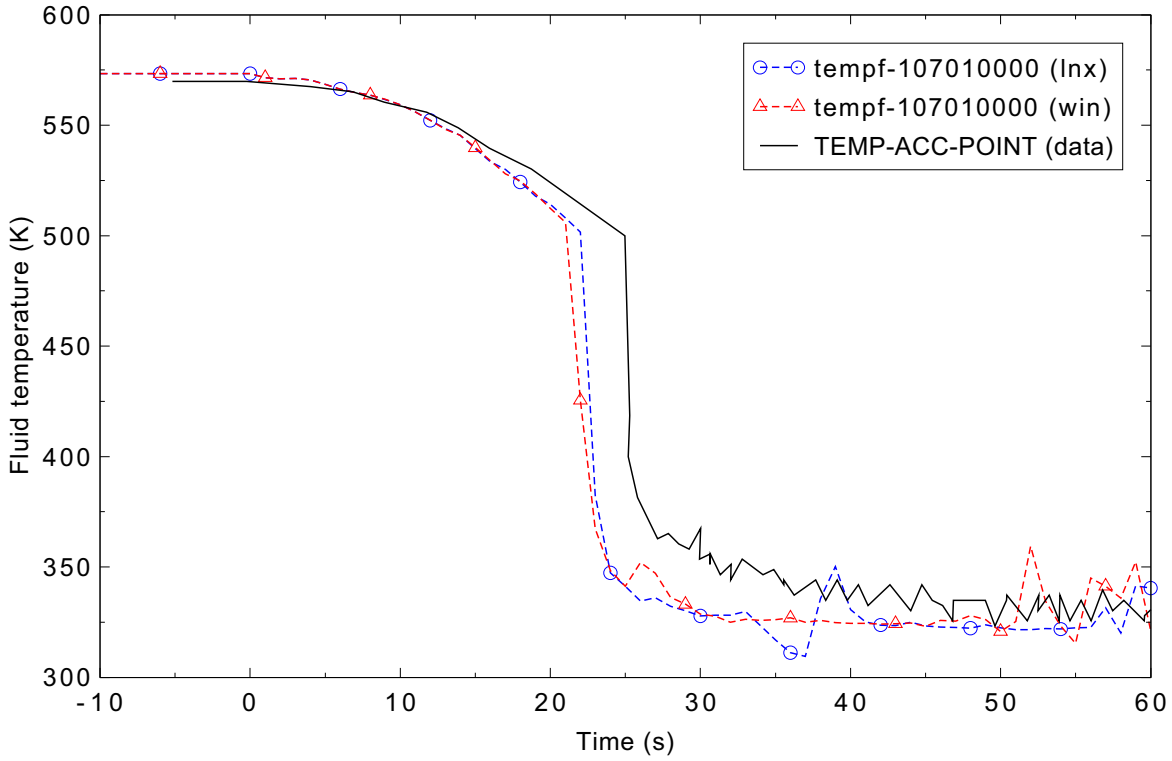

Figure 5.4-11. Measured and calculated fluid temperature at the accumulator injection point for LOBI Test A1-04R.

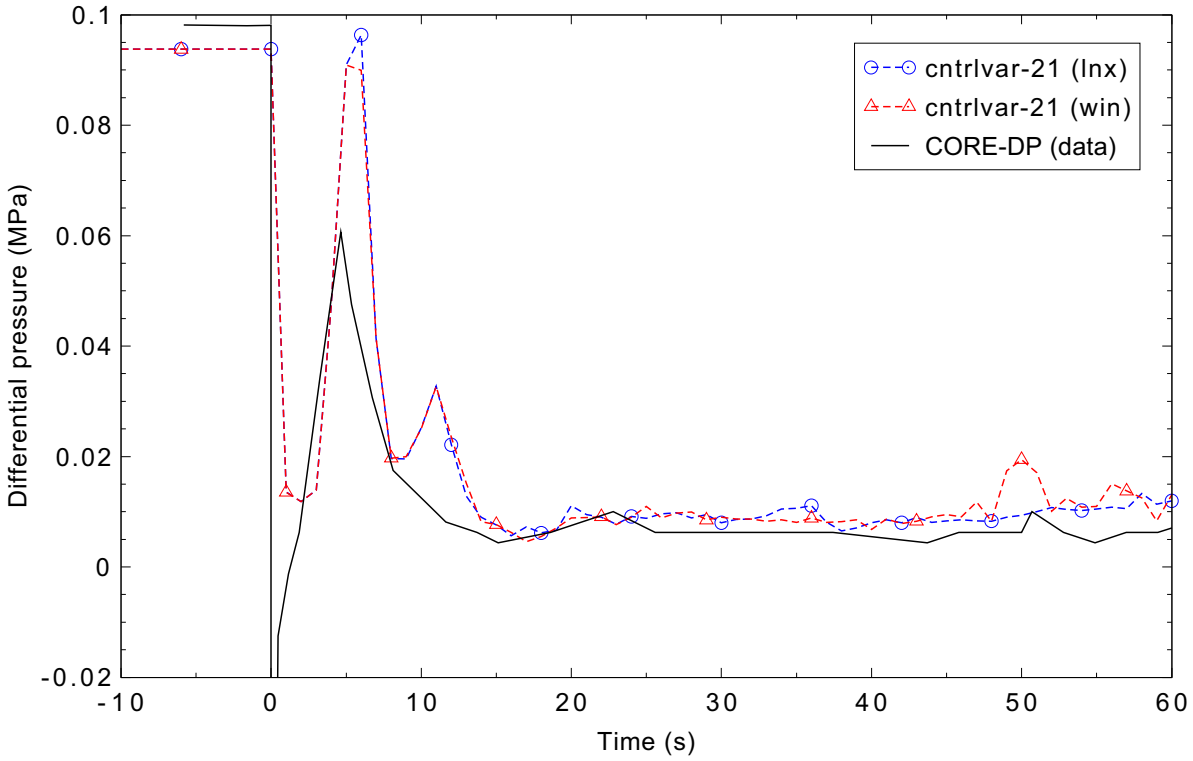

Figure 5.4-12. Measured and calculated core differential pressure for LOBI Test A1-04R.

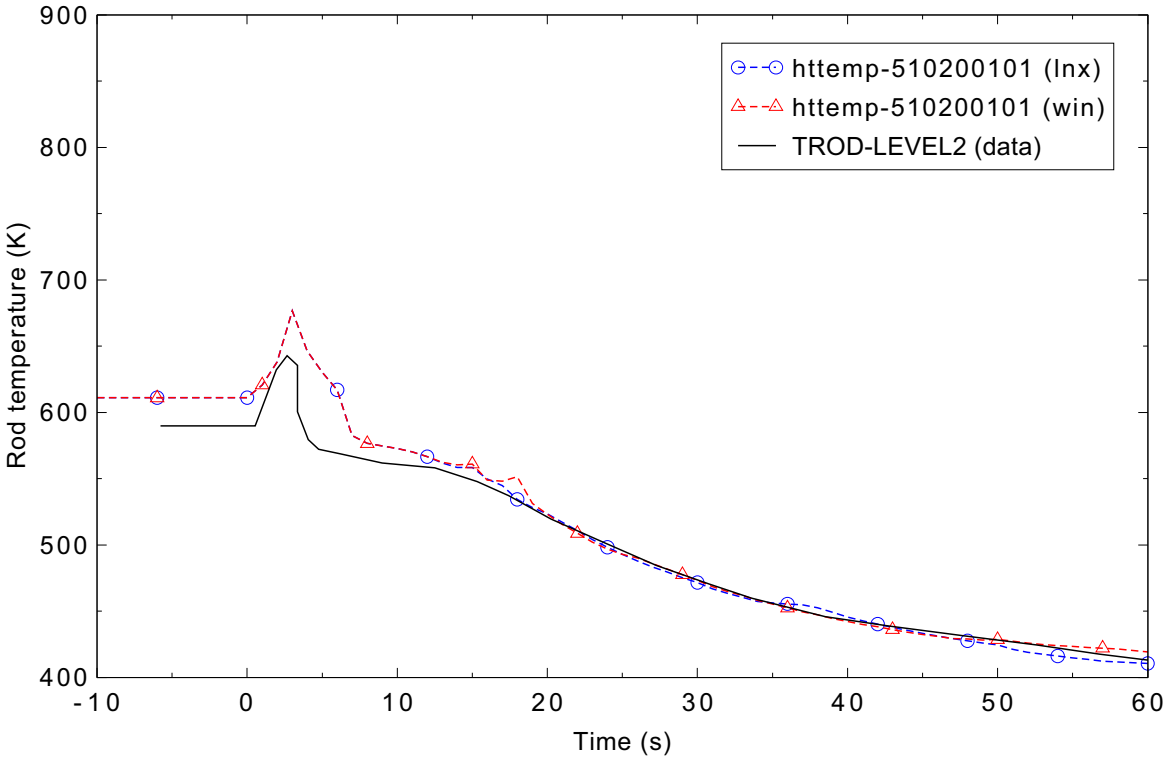

Figure 5.4-13. Measured and calculated lower core heater rod temperature (Level 2) for LOBI Test A1-04R.

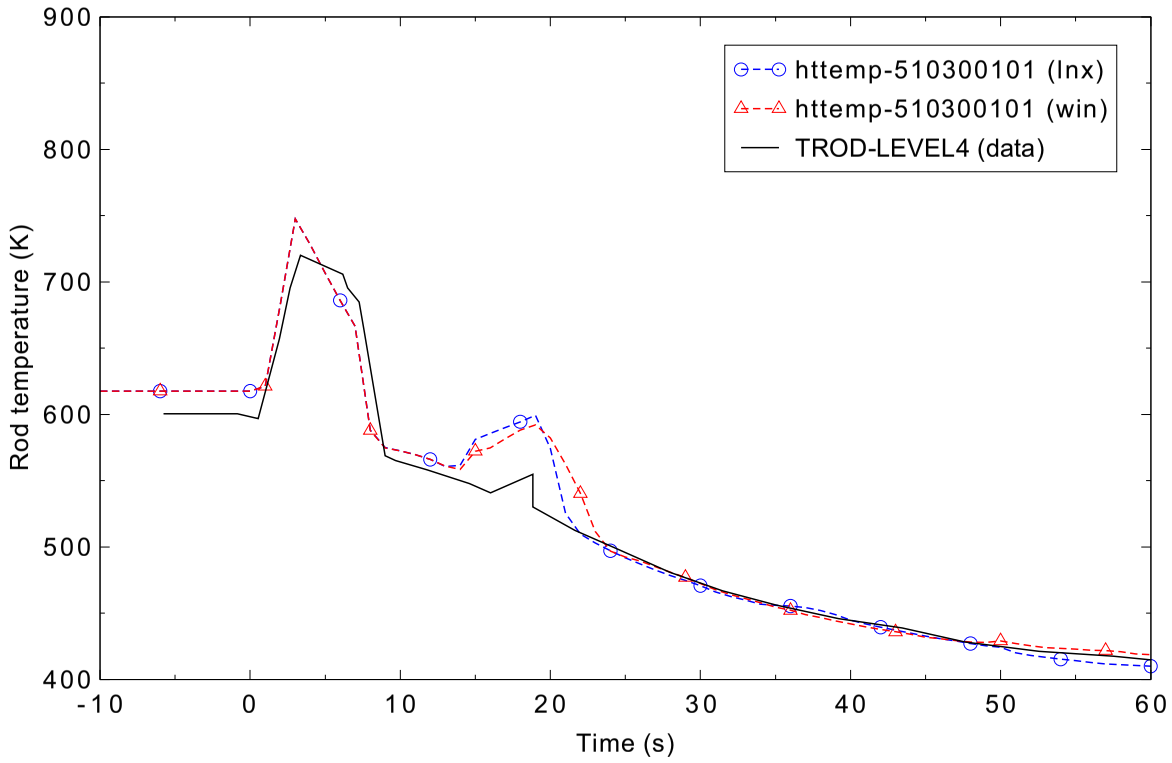

Figure 5.4-14. Measured and calculated lower core heater rod temperature (Level 4) for LOBI Test A1-04R.

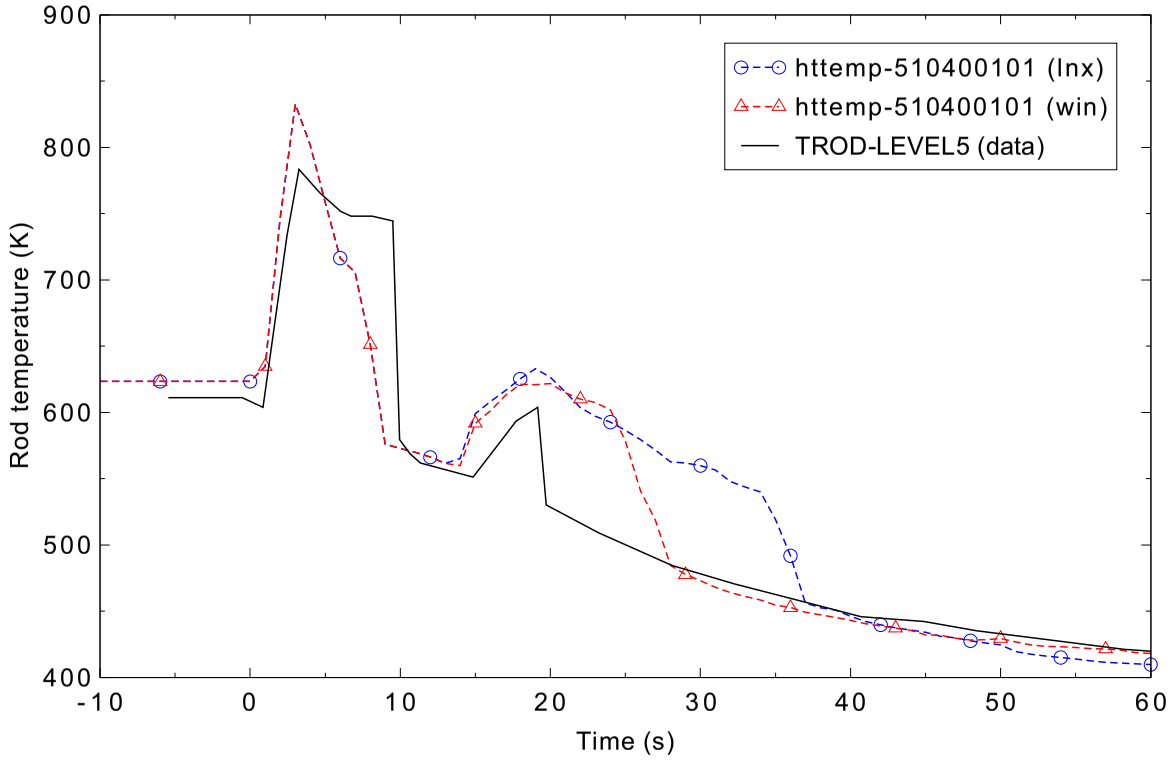

Figure 5.4-15. Measured and calculated mid-core heater rod temperature (Level 5) for LOBI Test A1-04R.

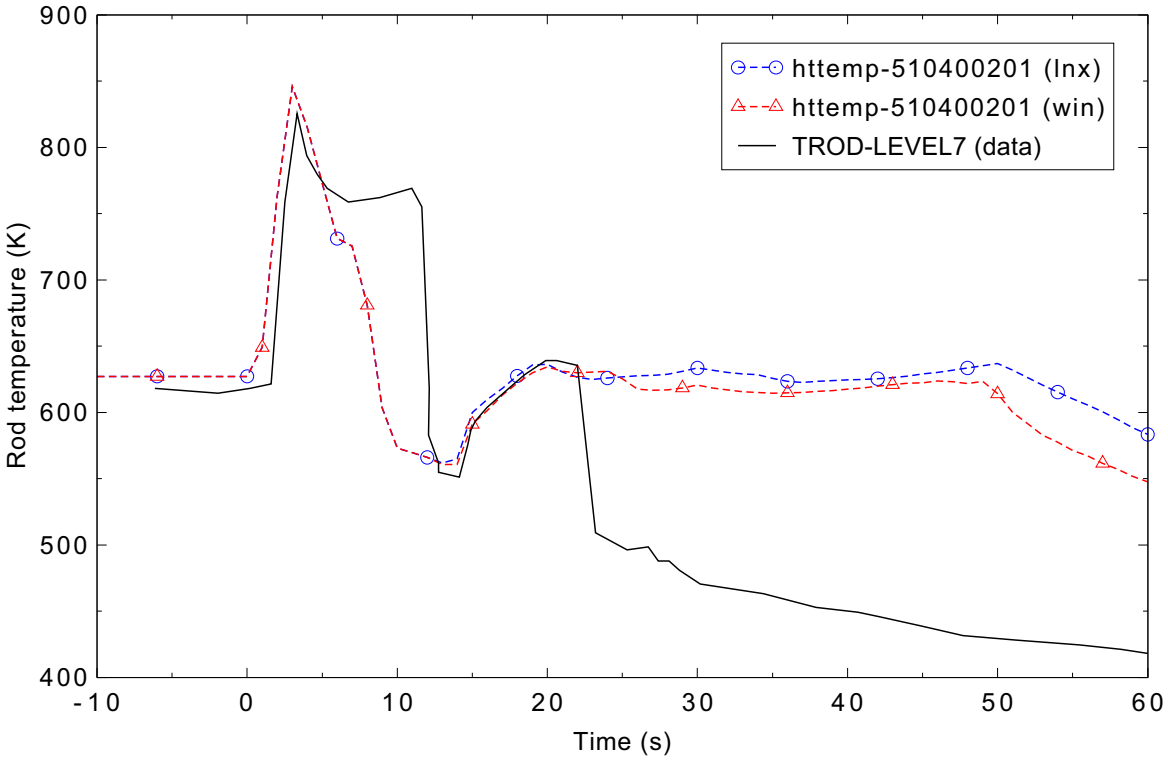

Figure 5.4-16. Measured and calculated mid-core heater rod temperature (Level 6) for LOBI Test A1-04R.

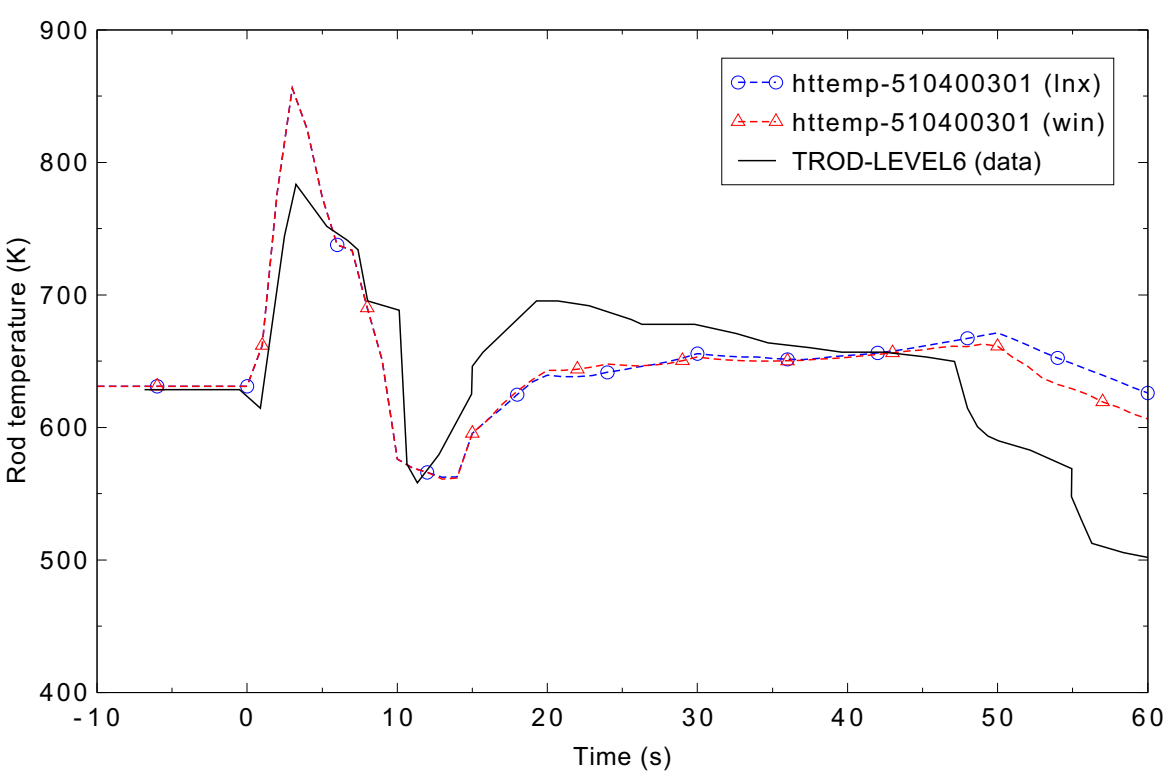

Figure 5.4-17. Measured and calculated mid-core heater rod temperature (Level 7) for LOBI Test A1-04R.

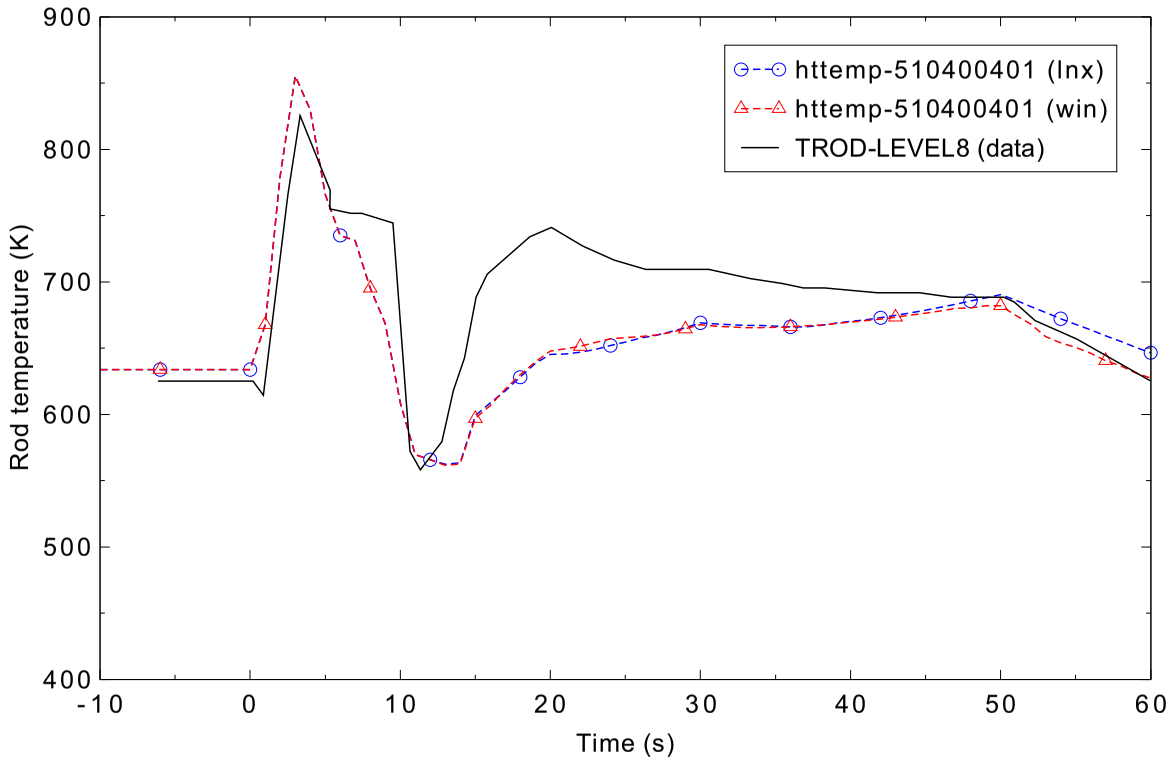

Figure 5.4-18. Measured and calculated mid-core heater temperature (Level 8) for LOBI Test A1-04R.

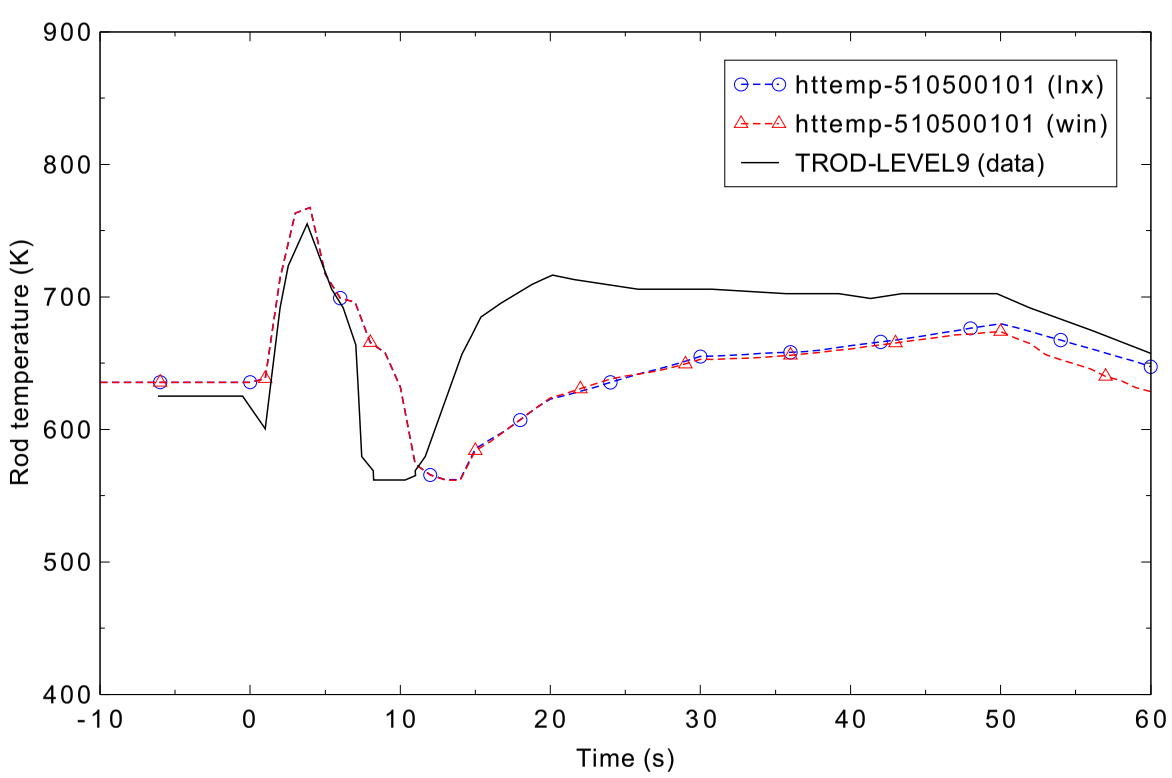

Figure 5.4-19. Measured and calculated upper core heater rod temperature (Level 9) for LOBI Test A1-04R.

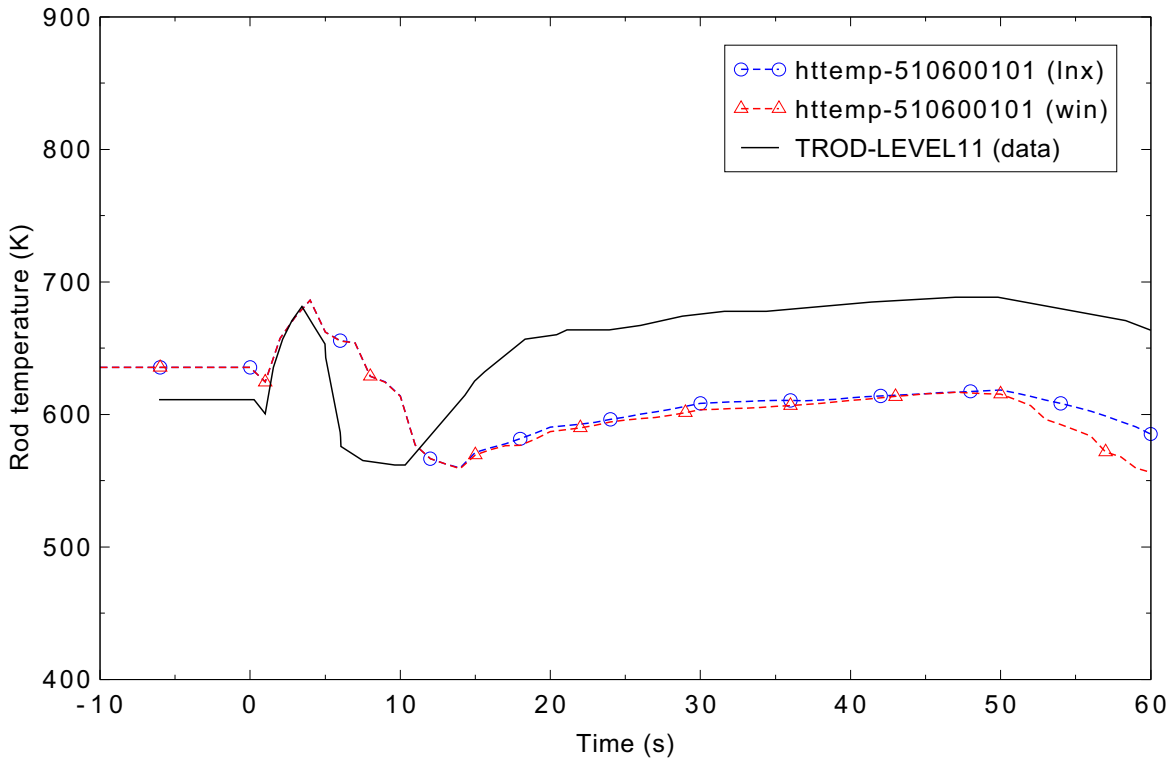

Figure 5.4-20. Measured and calculated upper core heater rod temperature (Level 11) for LOBI Test A1-04R.

5.5 LOFT Experiment L2-5 (1-D)

Figures comparing simulations using Linux and Windows code versions are presented. Diagrams are included so that the figure numbering is the same as that in Volume III of the RELAP5-3D code manual. A significant difference was observed in Figure 5.5-11. Noticeable differences were observed in Figures 5.5-3, 4, 6, 7, 8, 9, 10, 12, 13, 14, 15, 17, 18, 19, 20, 21, 22, 23, 24, 25, 26, 27, 28, 29, 30, 31, and 32.

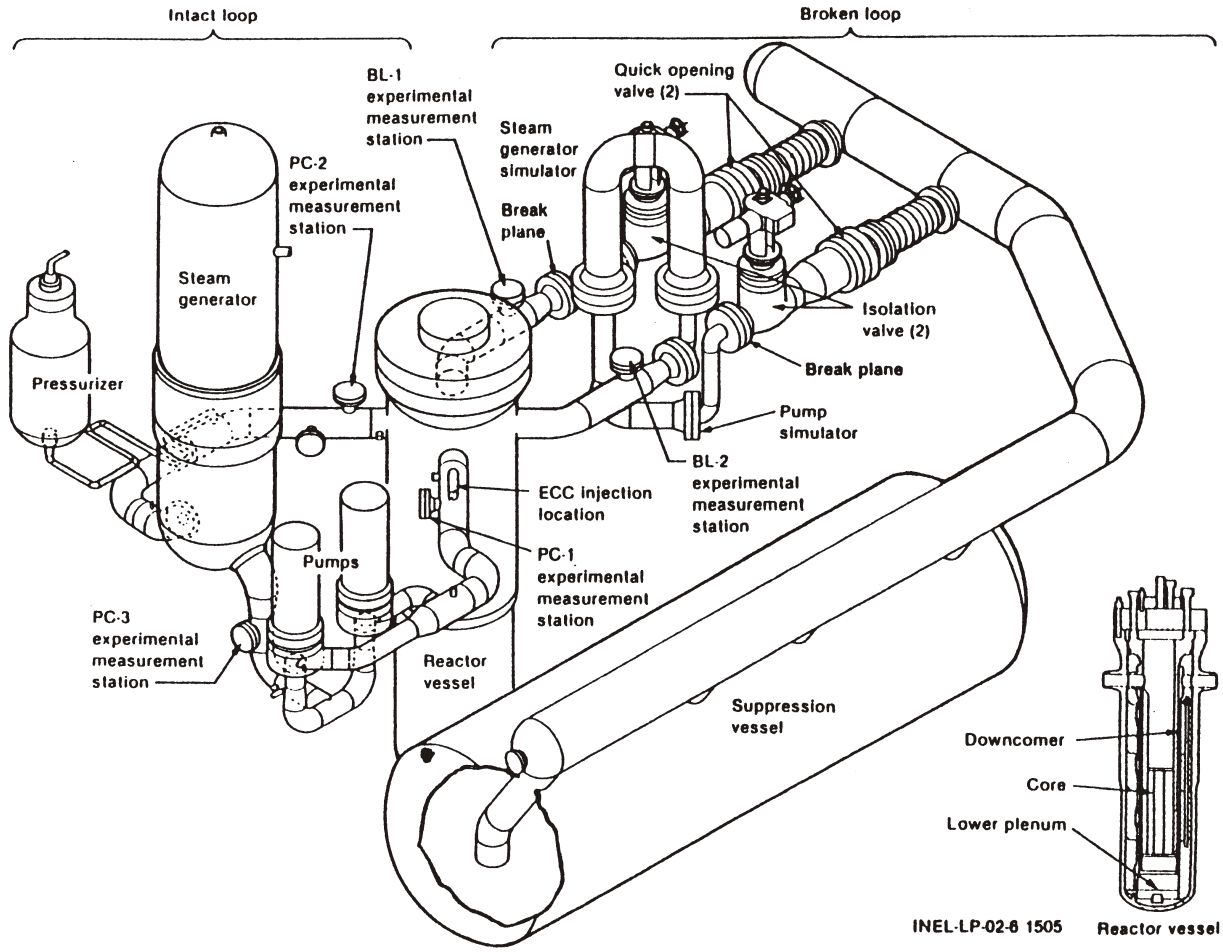

Figure 5.5-1. Schematic of the LOFT facility.

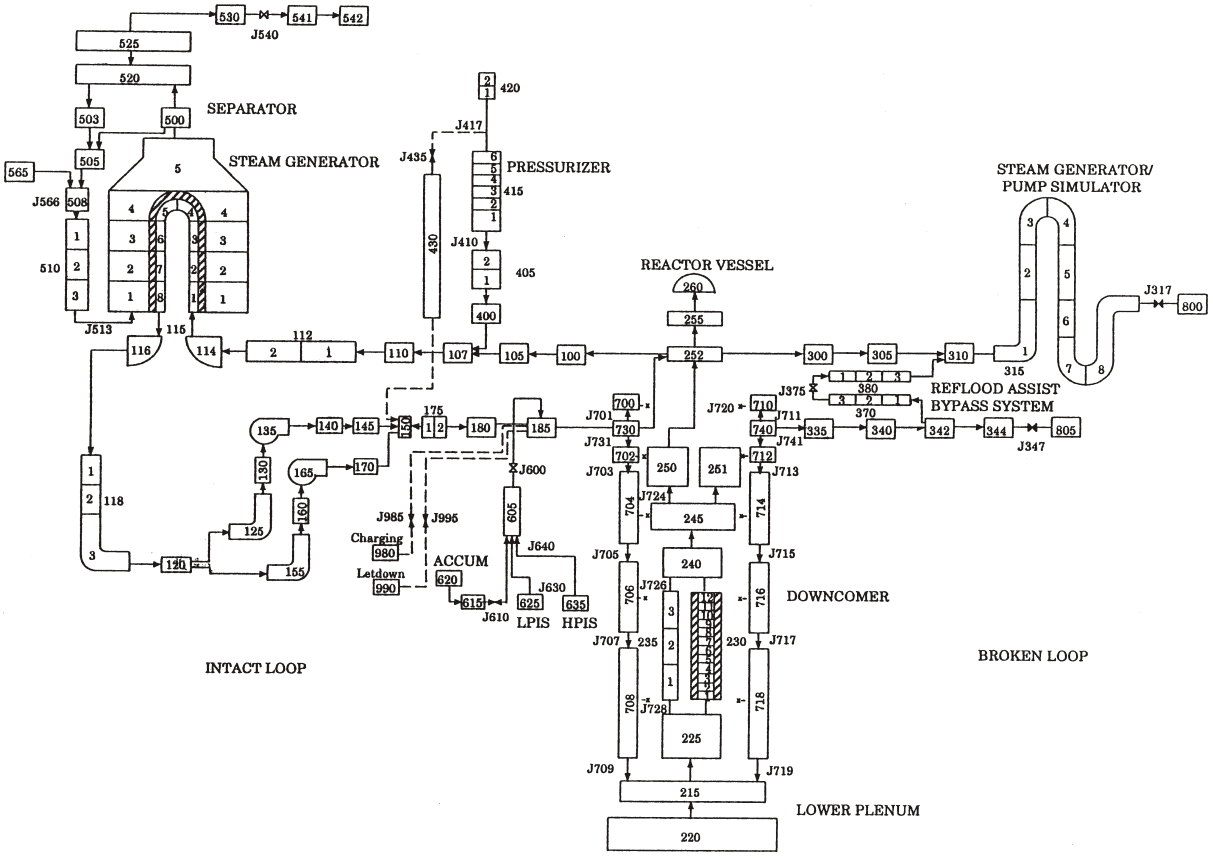

Figure 5.5-2. RELAP5-3D nodalization for the LOFT facility Experiment L2-5 (1-D vessel).

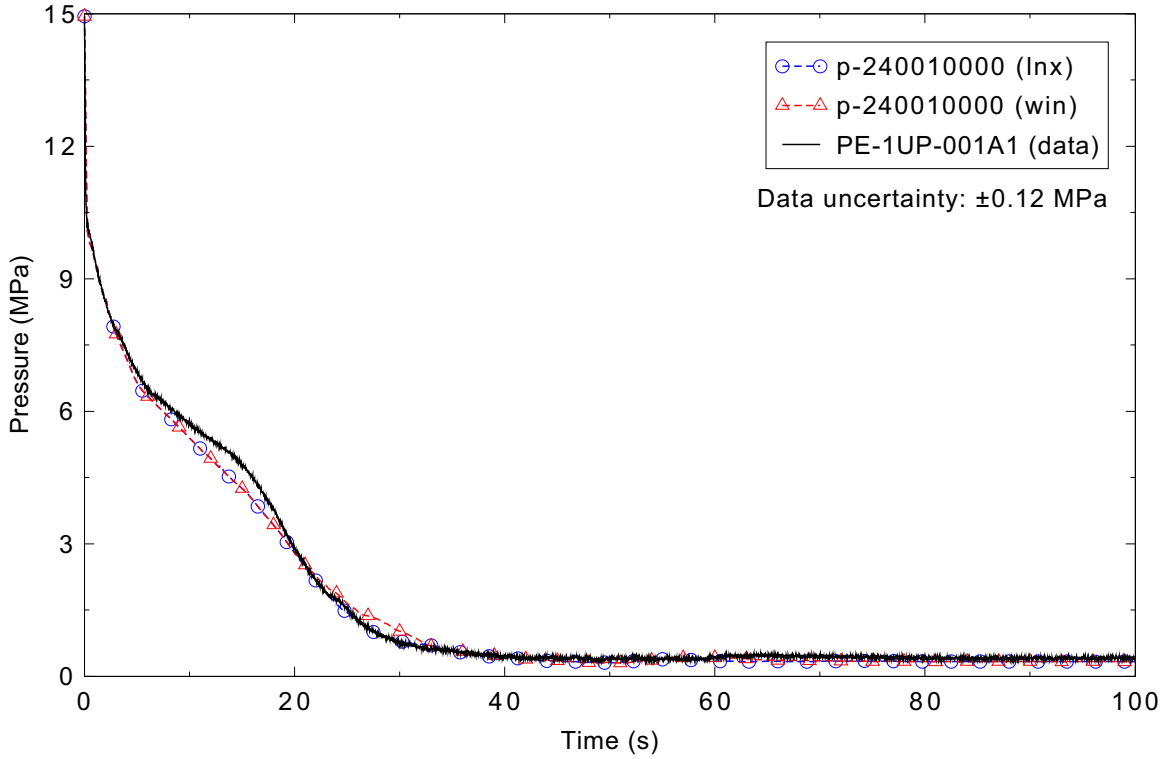

Figure 5.5-3. Measured and calculated reactor vessel upper plenum pressure for the LOFT Experiment L2-5 1-D case.

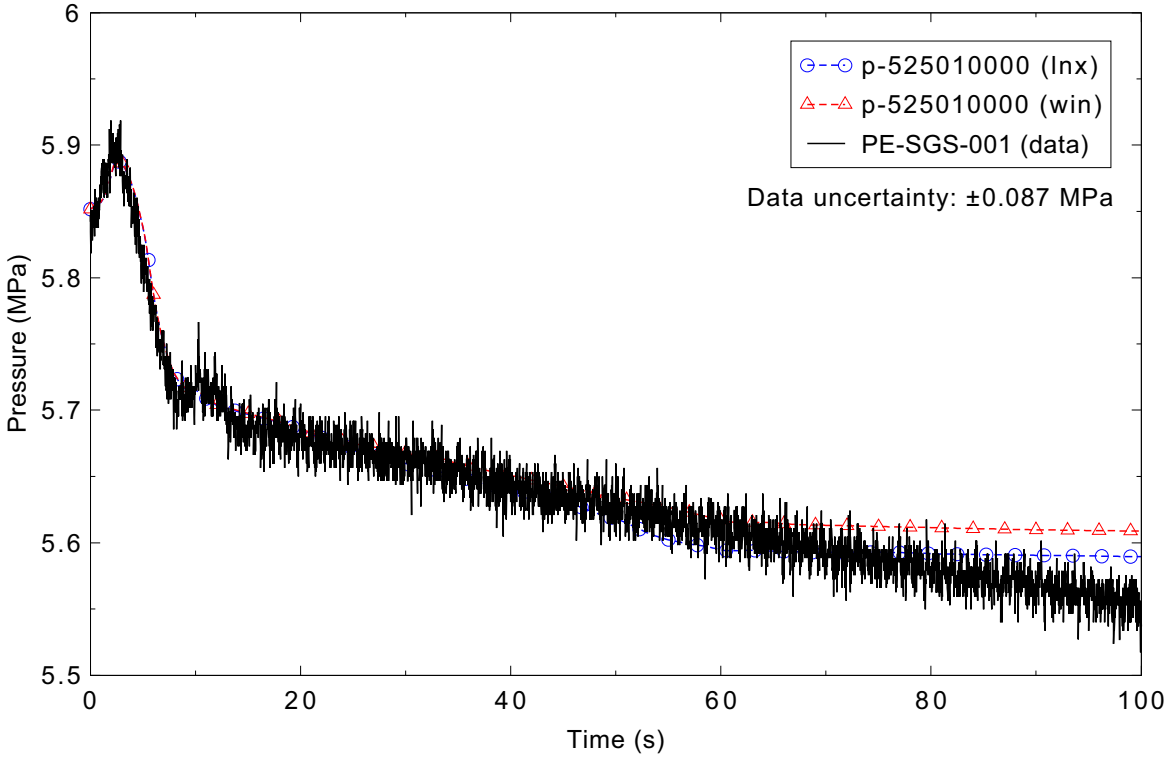

Figure 5.5-4. Measured and calculated steam generator pressure for the LOFT Experiment L2-5 1-D case.

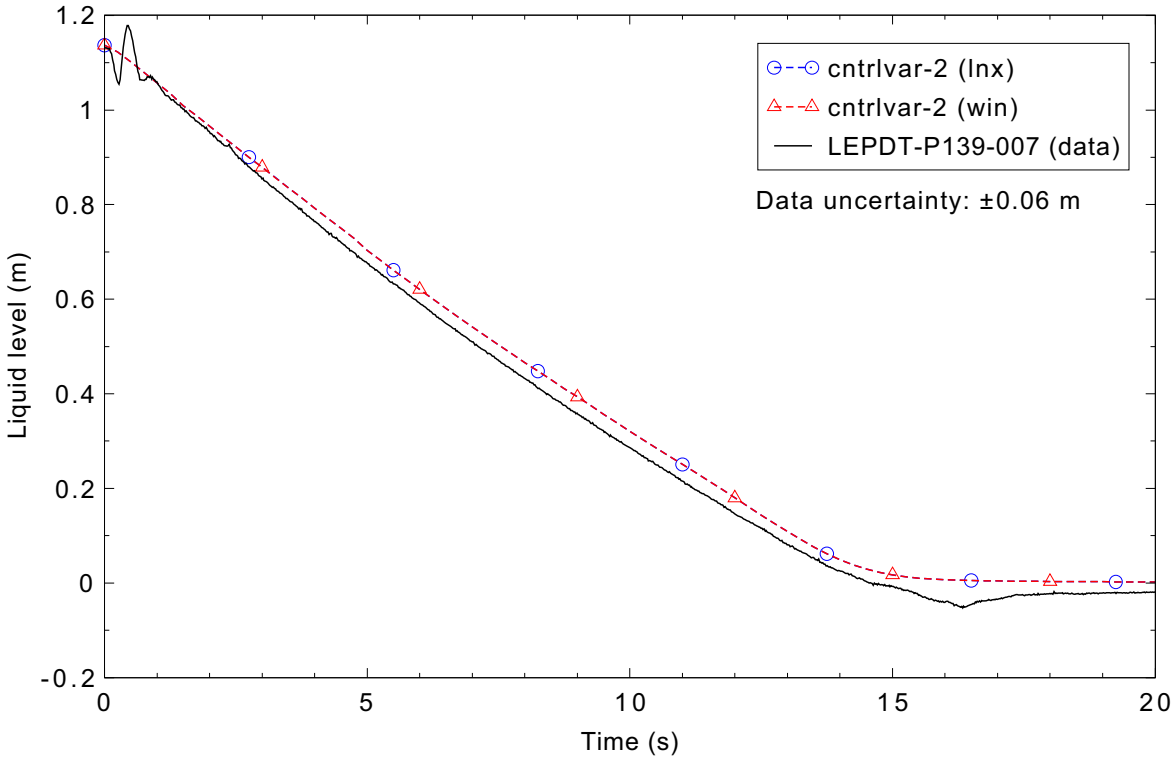

Figure 5.5-5. Measured and calculated pressurizer liquid level for the LOFT Experiment L2-5 1-D case.

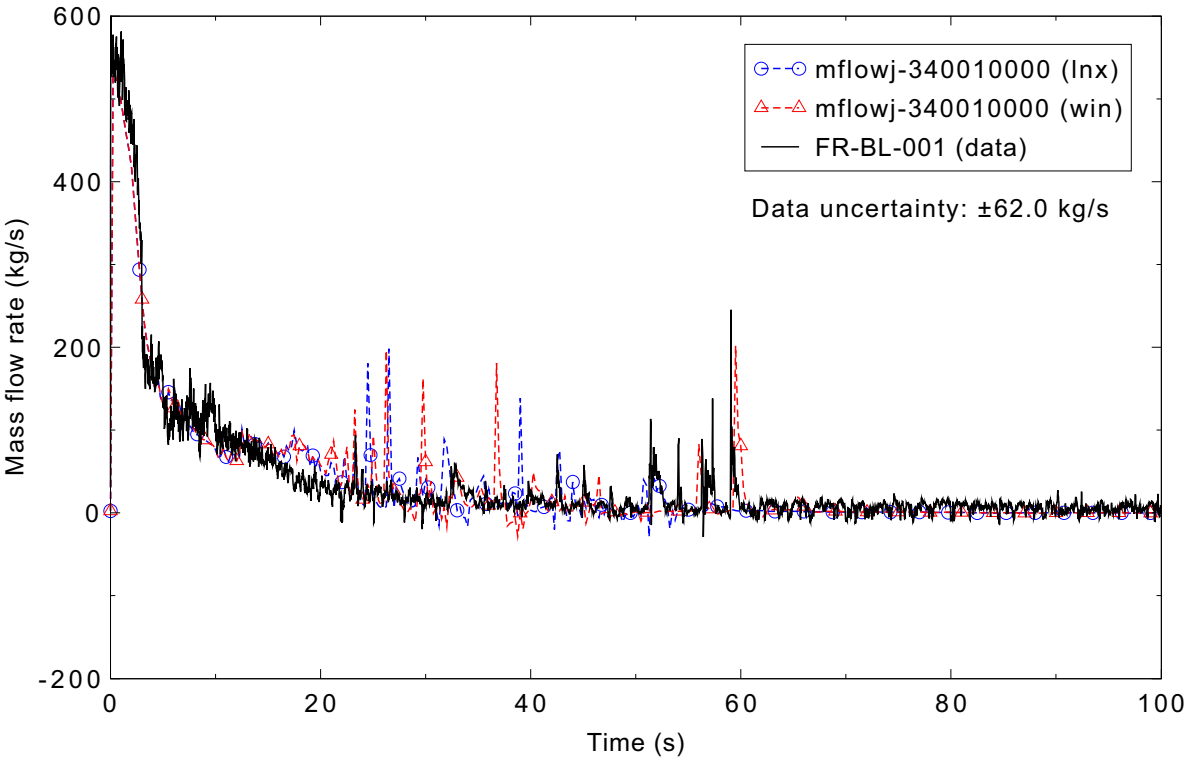

Figure 5.5-6. Measured and calculated mass flow rate in the broken loop cold leg for the LOFT Experiment L2-5 1-D case.

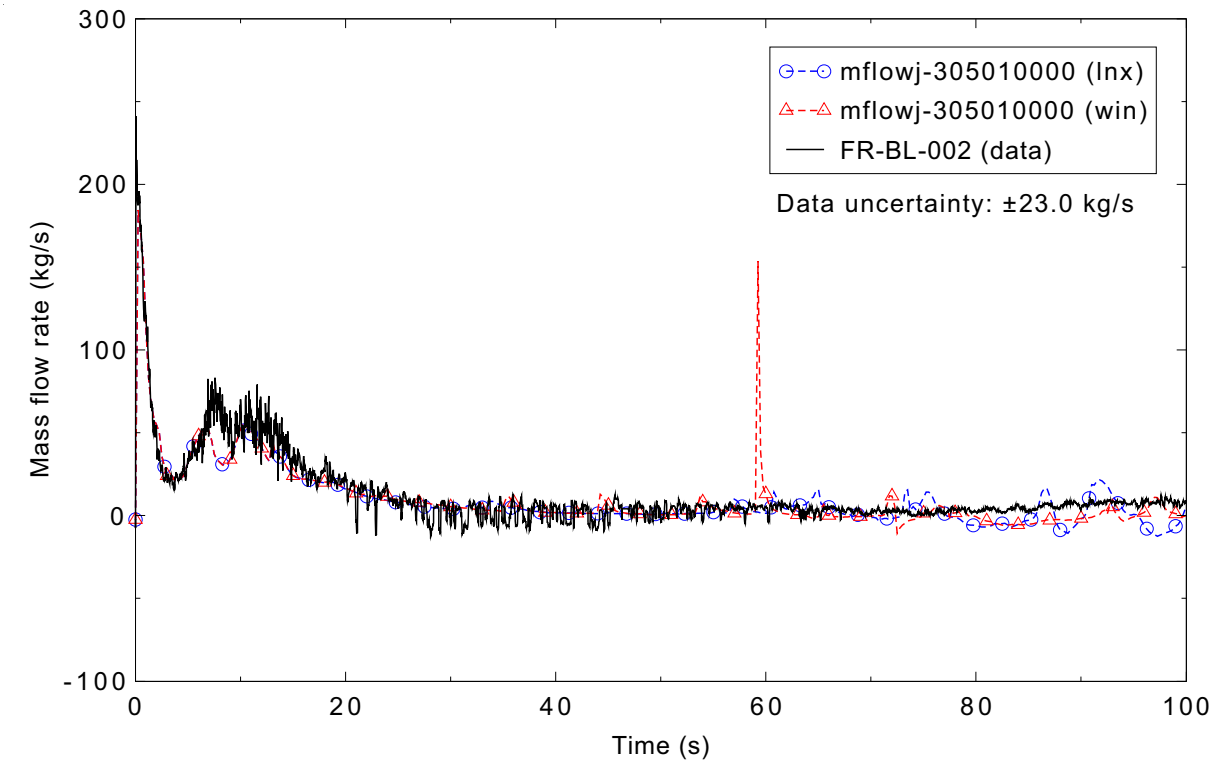

Figure 5.5-7. Measured and calculated mass flow rate in the broken loop hot leg for the LOFT Experiment L2-5 1-D case.

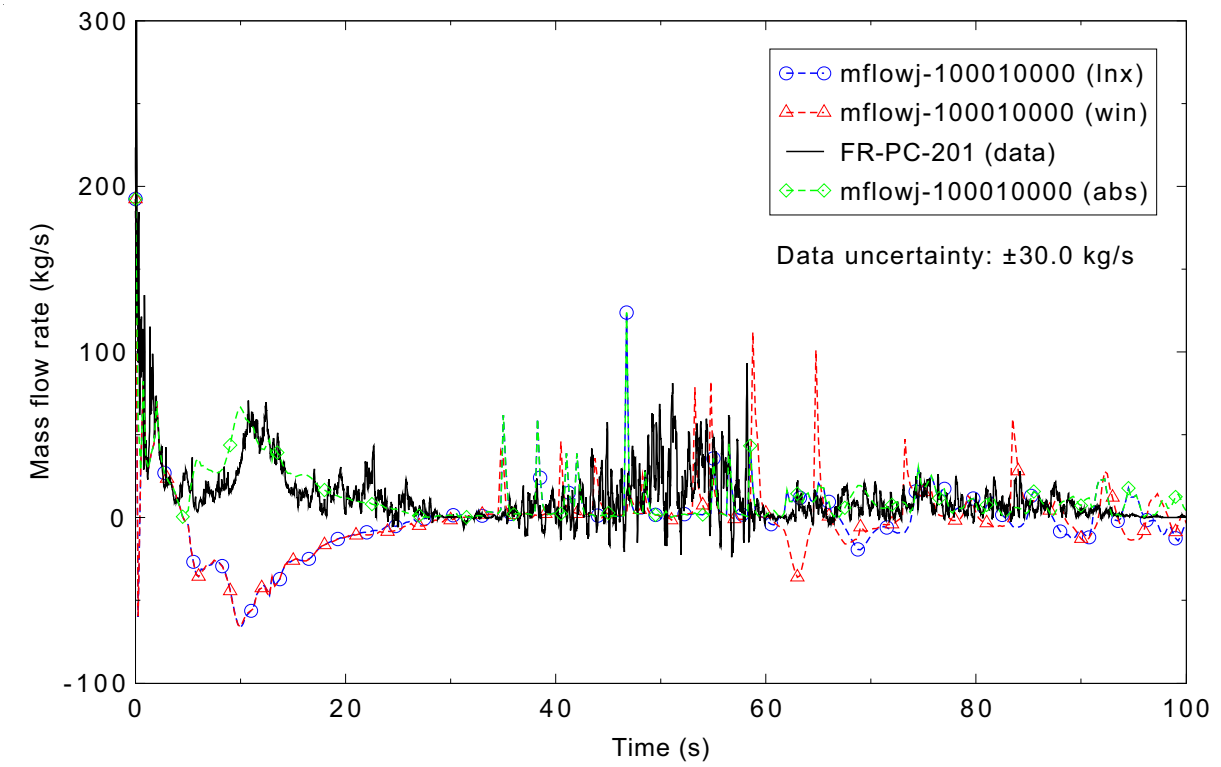

Figure 5.5-8. Measured and calculated mass flow rate in the intact loop hot leg for the LOFT Experiment L2-5 1-D case.

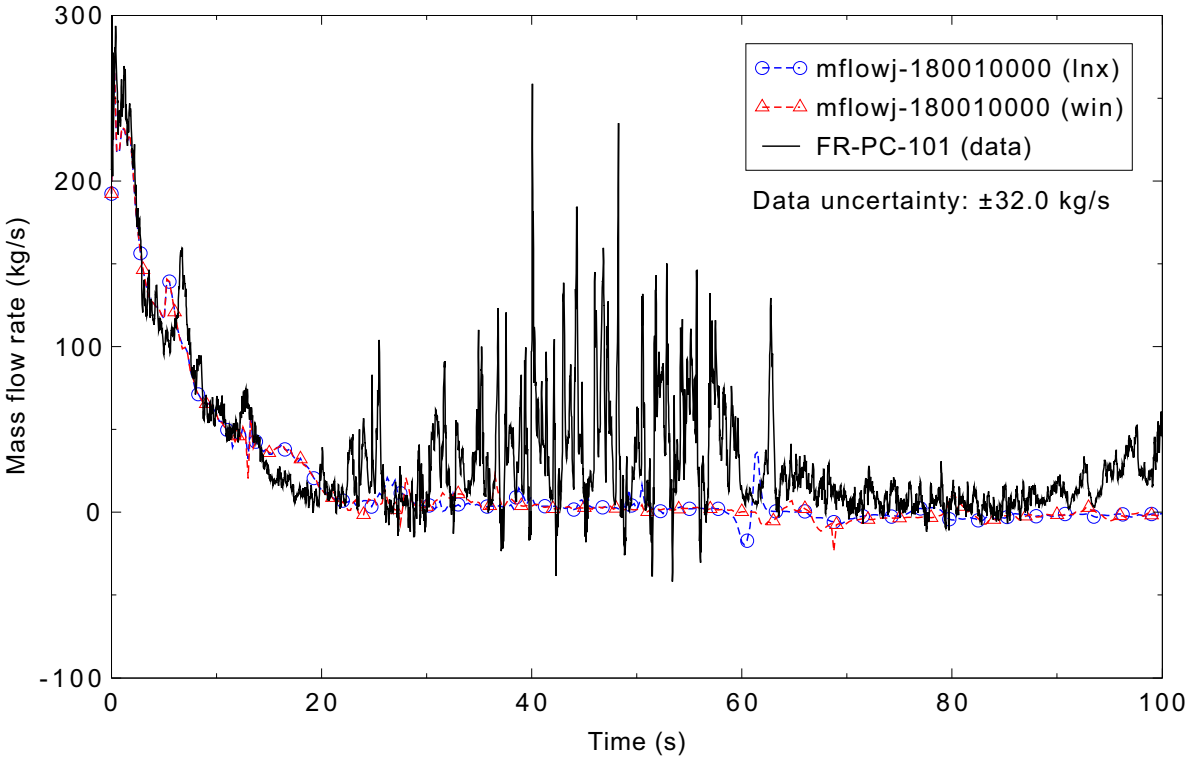

Figure 5.5-9. Measured and calculated mass flow rate in the intact loop cold leg for the LOFT Experiment L2-5 1-D case.

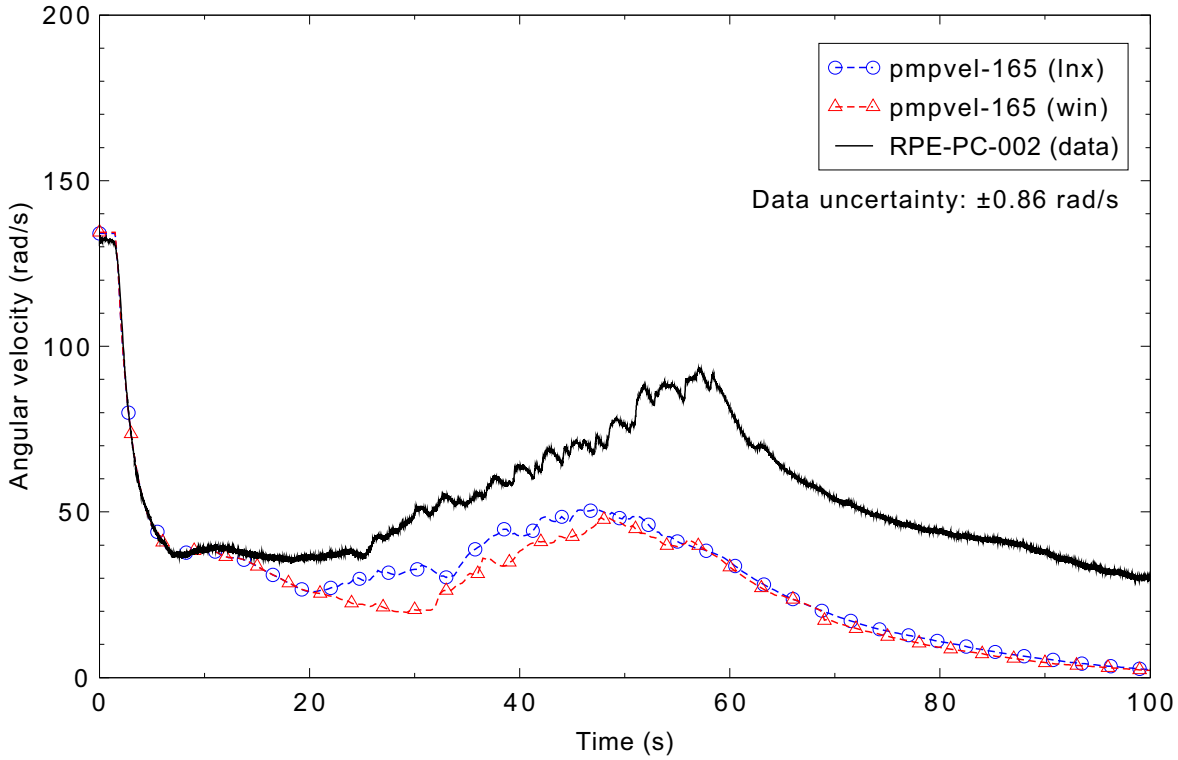

Figure 5.5-10. Measured and calculated speed for primary coolant pump 2 for the LOFT Experiment L2-5 1-D case.

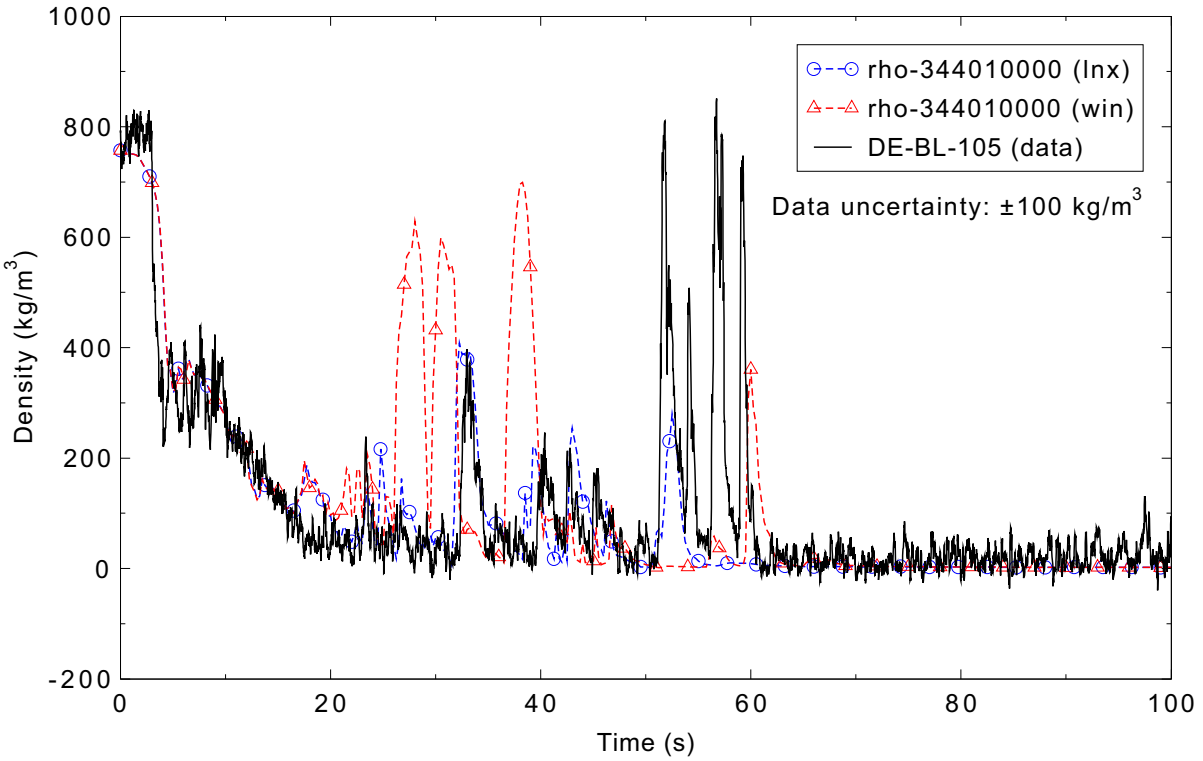

Figure 5.5-11. Measured and calculated density in the broken loop cold leg for the LOFT Experiment L2-5 1-D case.

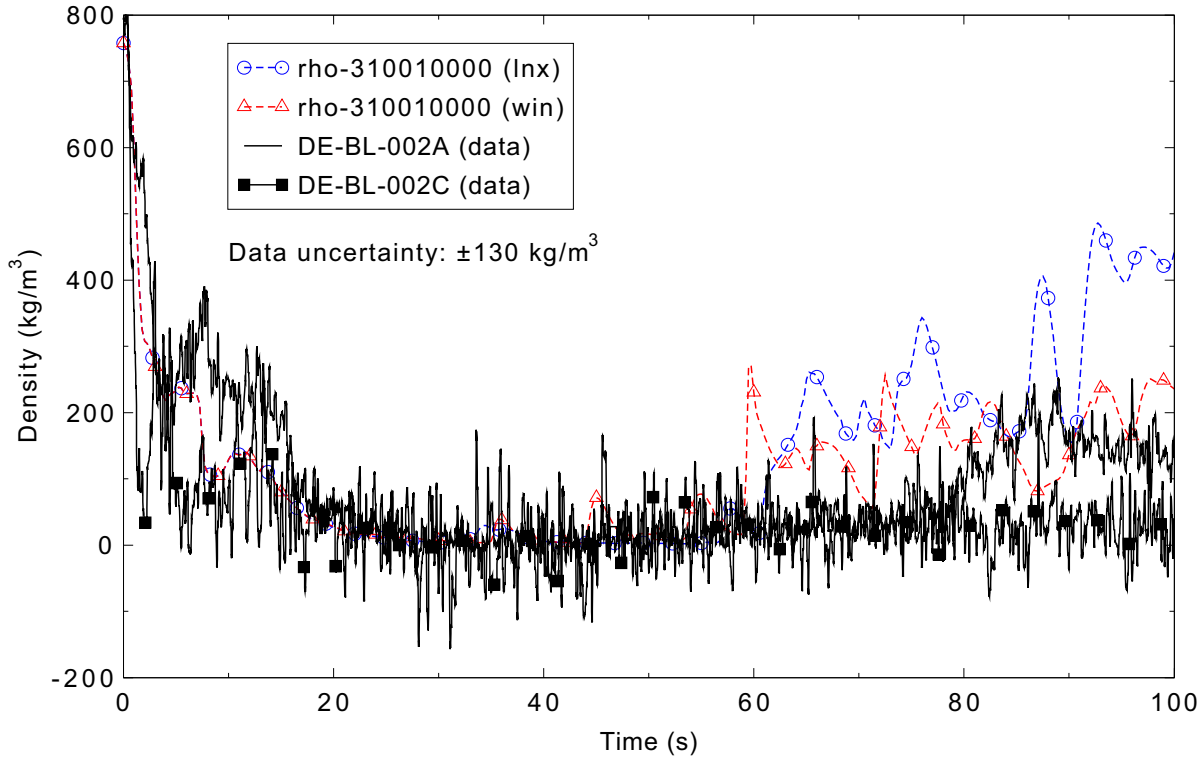

Figure 5.5-12. Measured and calculated density in the broken loop hot leg for the LOFT Experiment L2-5 1-D case.

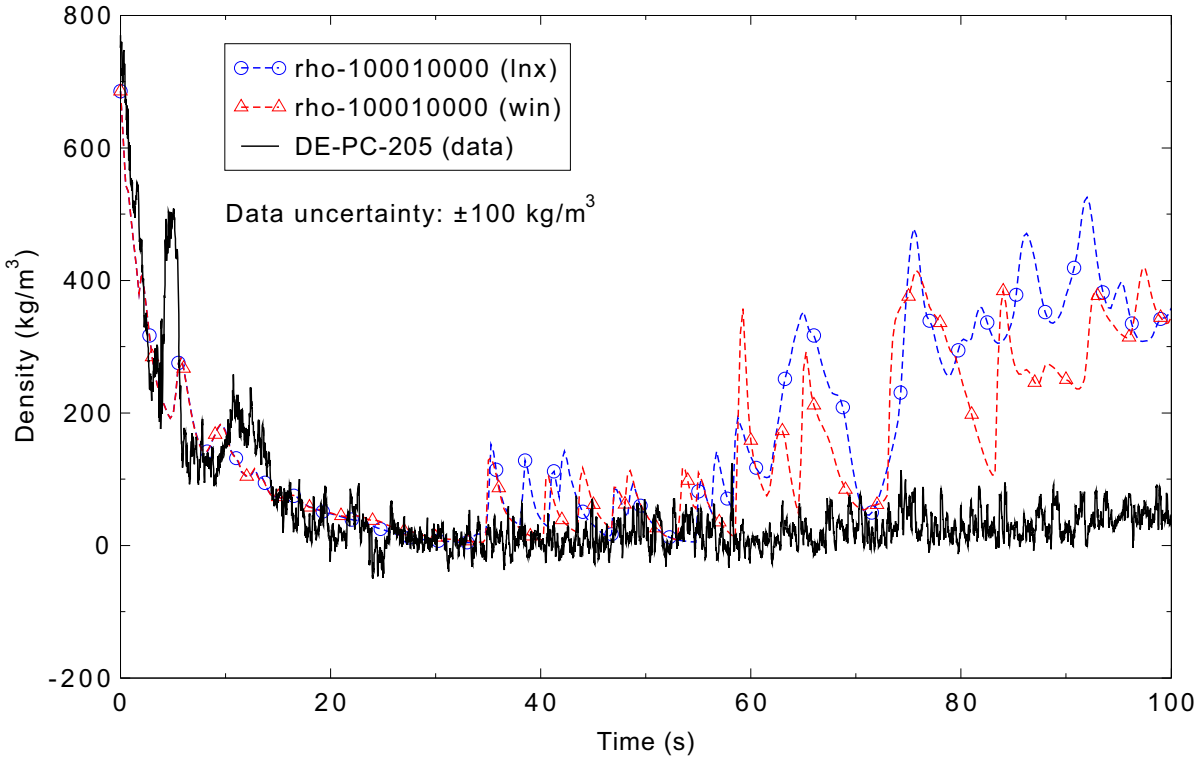

Figure 5.5-13. Measured and calculated density in the intact loop hot leg for the LOFT Experiment L2-5 1-D case.

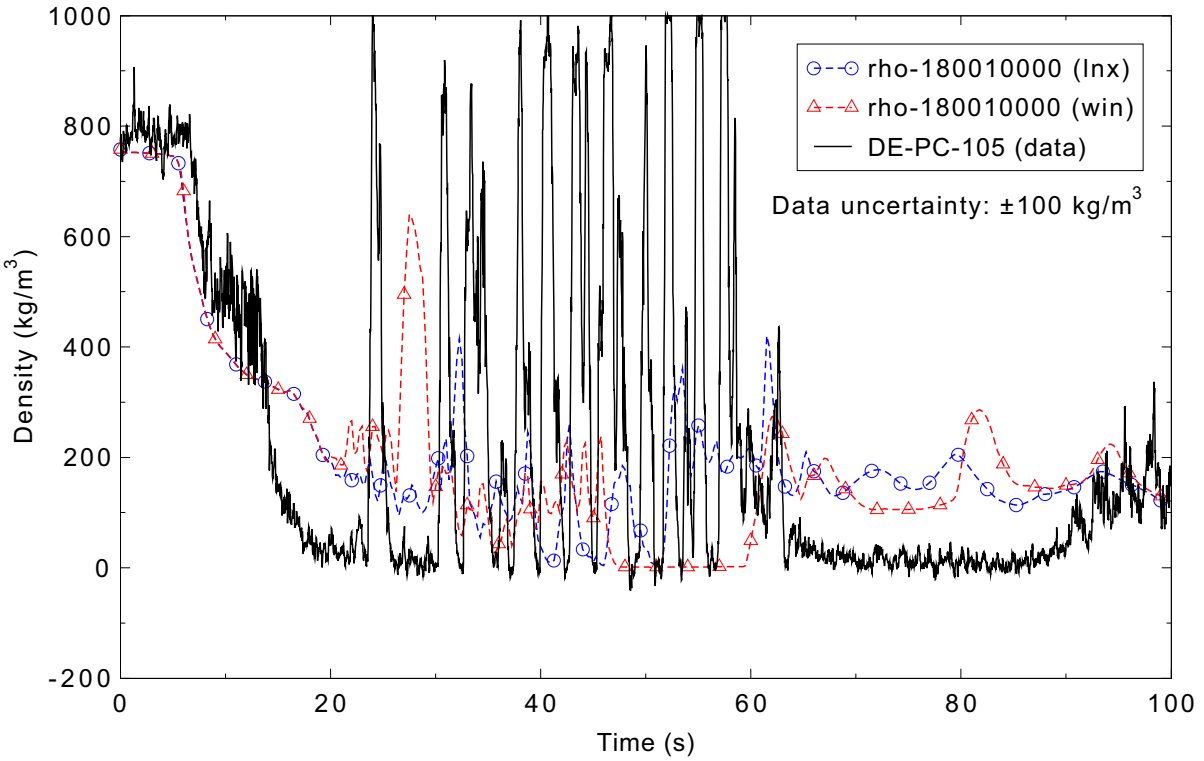

Figure 5.5-14. Measured and calculated density in the intact loop cold leg for the LOFT Experiment L2-5 1-D case.

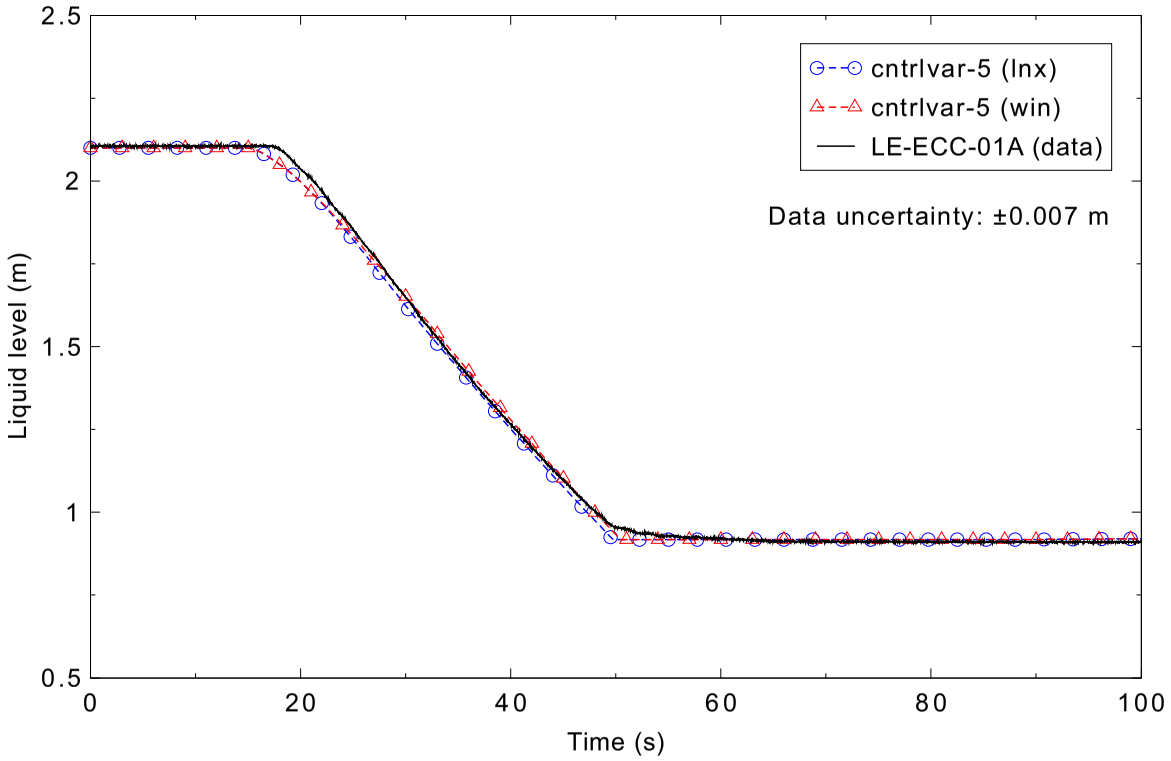

Figure 5.5-15. Measured and calculated accumulator liquid level for the LOFT Experiment L2-5 1-D case.

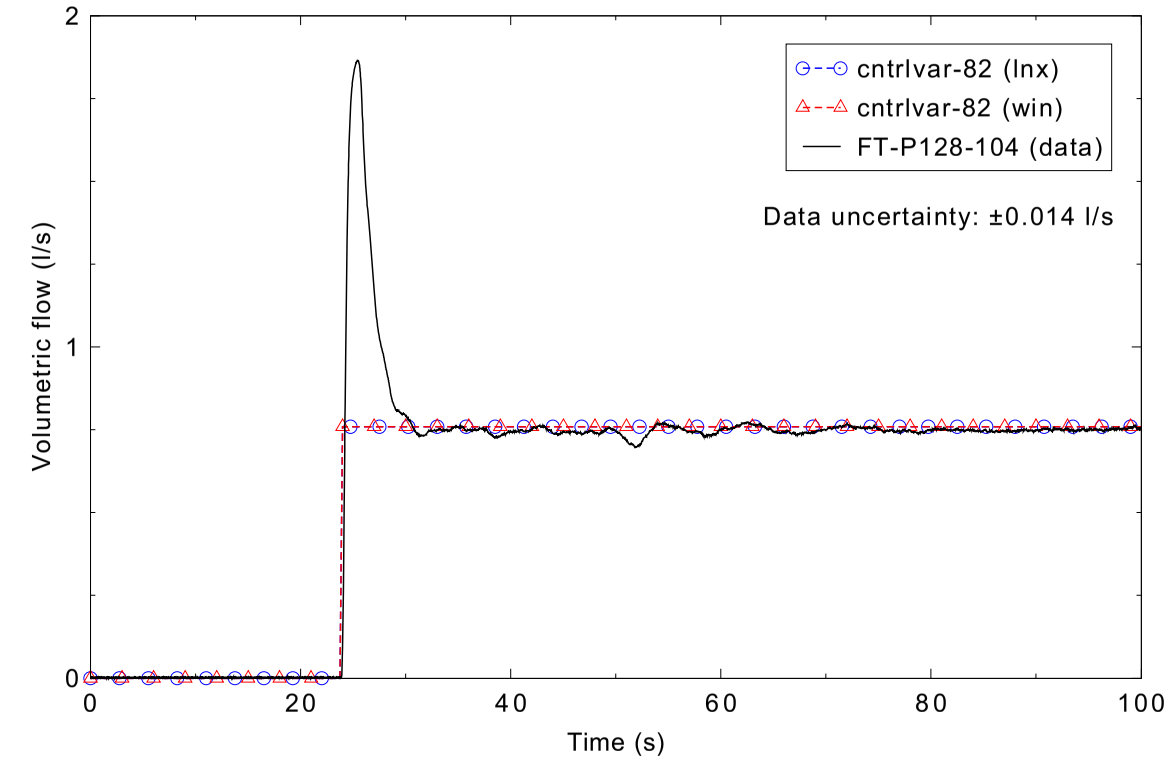

Figure 5.5-16. Measured and calculated HPIS flow for the LOFT Experiment L2-5 1-D case.

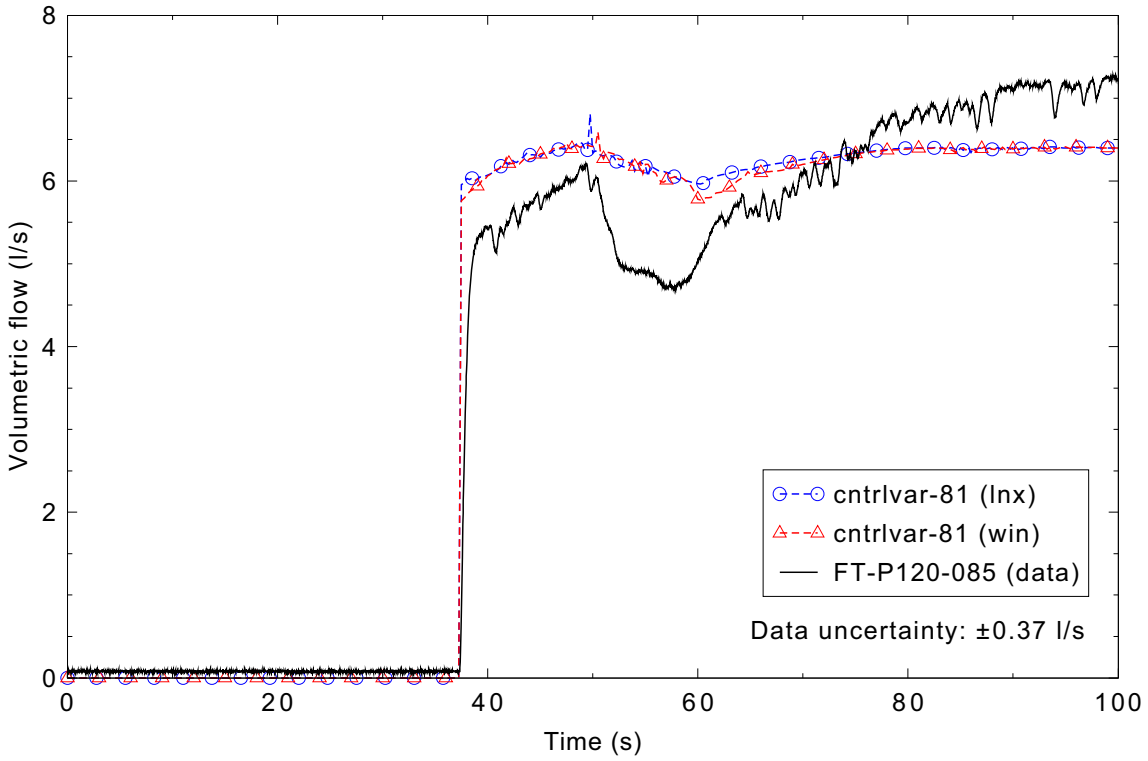

Figure 5.5-17. Measured and calculated LPIS flow for the LOFT Experiment L2-5 1-D case.

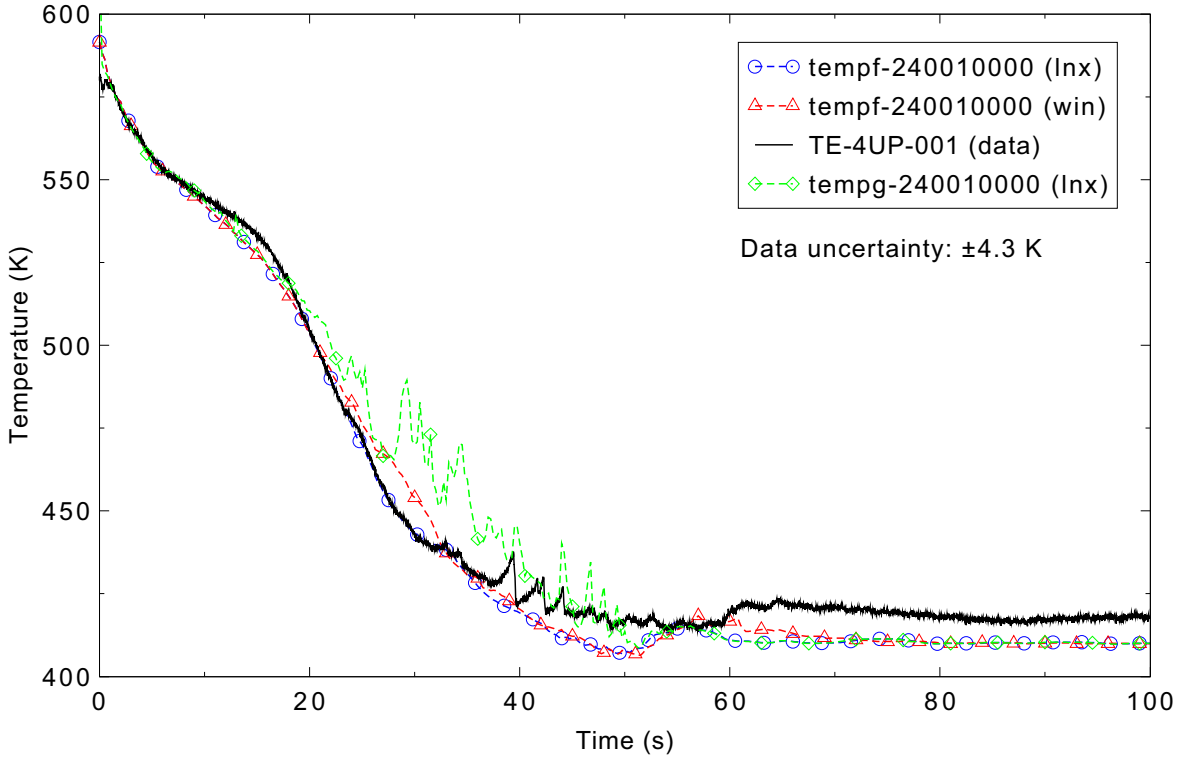

Figure 5.5-18. Measured and calculated reactor vessel upper plenum coolant temperature for the LOFT Experiment L2-5 1-D case.

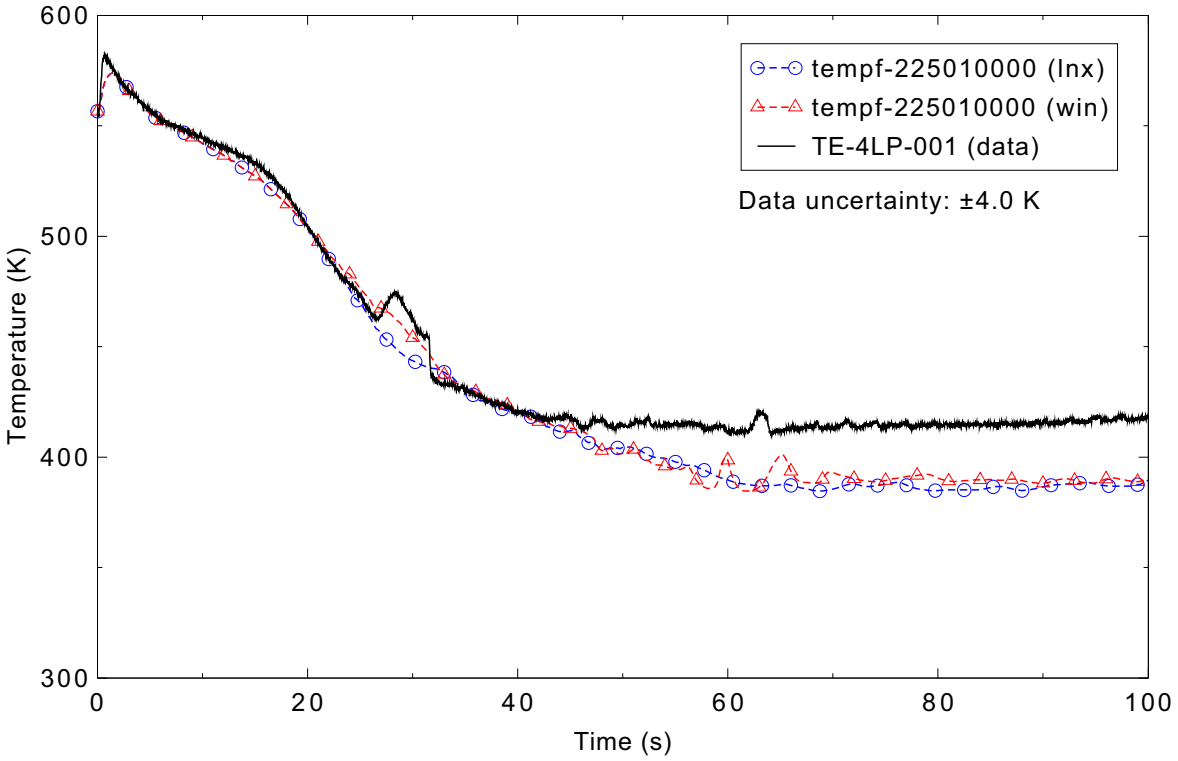

Figure 5.5-19. Measured and calculated reactor vessel lower plenum coolant temperature for the LOFT Experiment L2-5 1-D case.

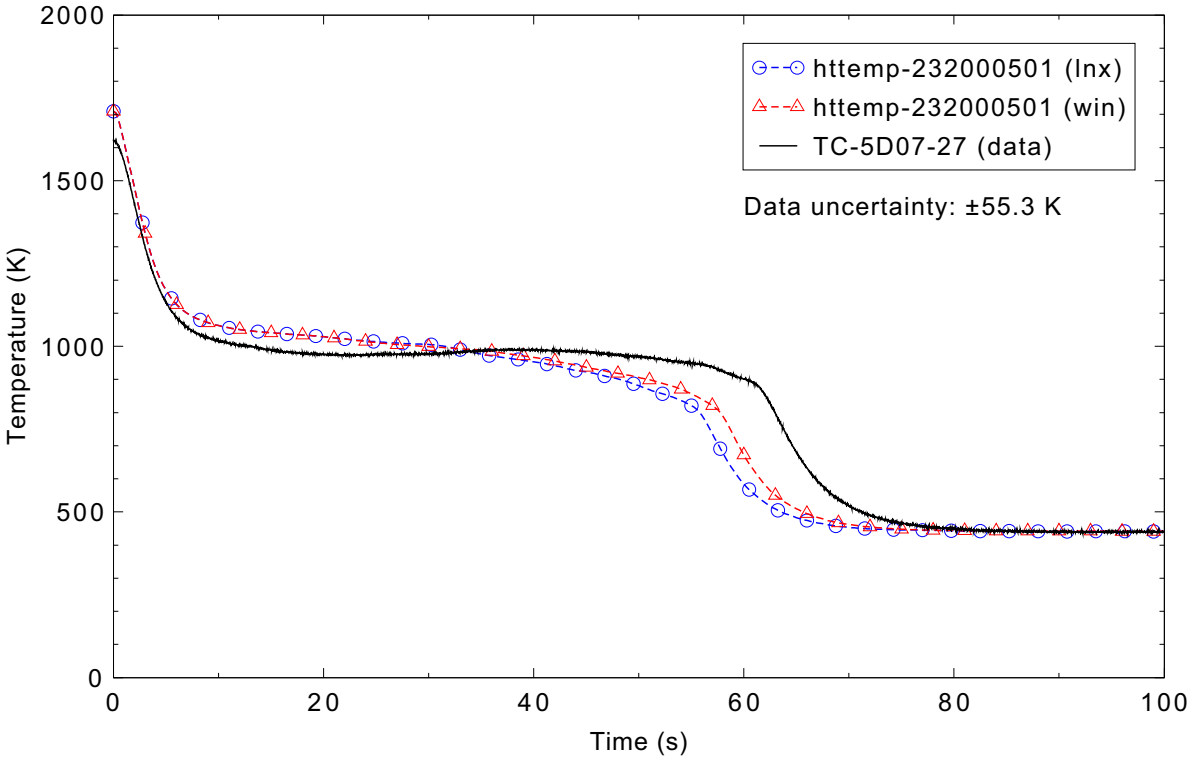

Figure 5.5-20. Measured and calculated fuel centerline temperature 0.69 m above the bottom of the fuel rod for the LOFT Experiment L2-5 1-D case.

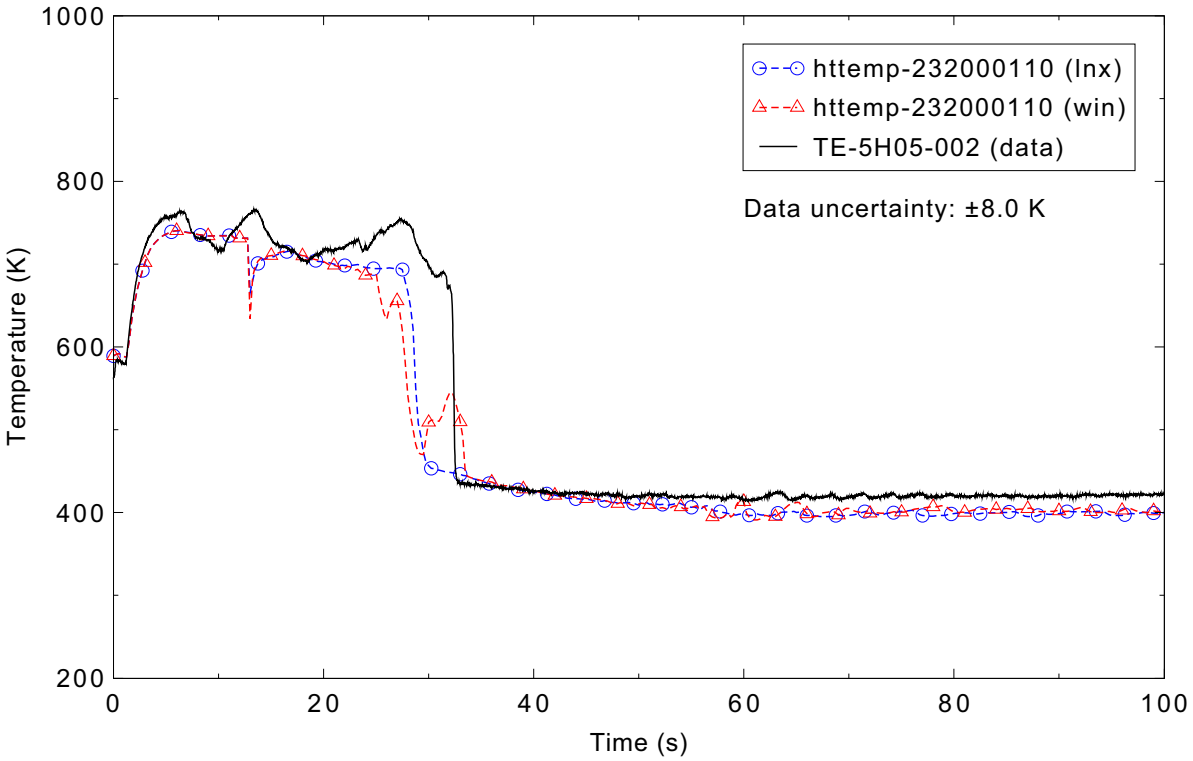

Figure 5.5-21. Measured and calculated fuel cladding surface temperature 0.05 m above the bottom of the fuel rod for the LOFT Experiment L2-5 1-D case.

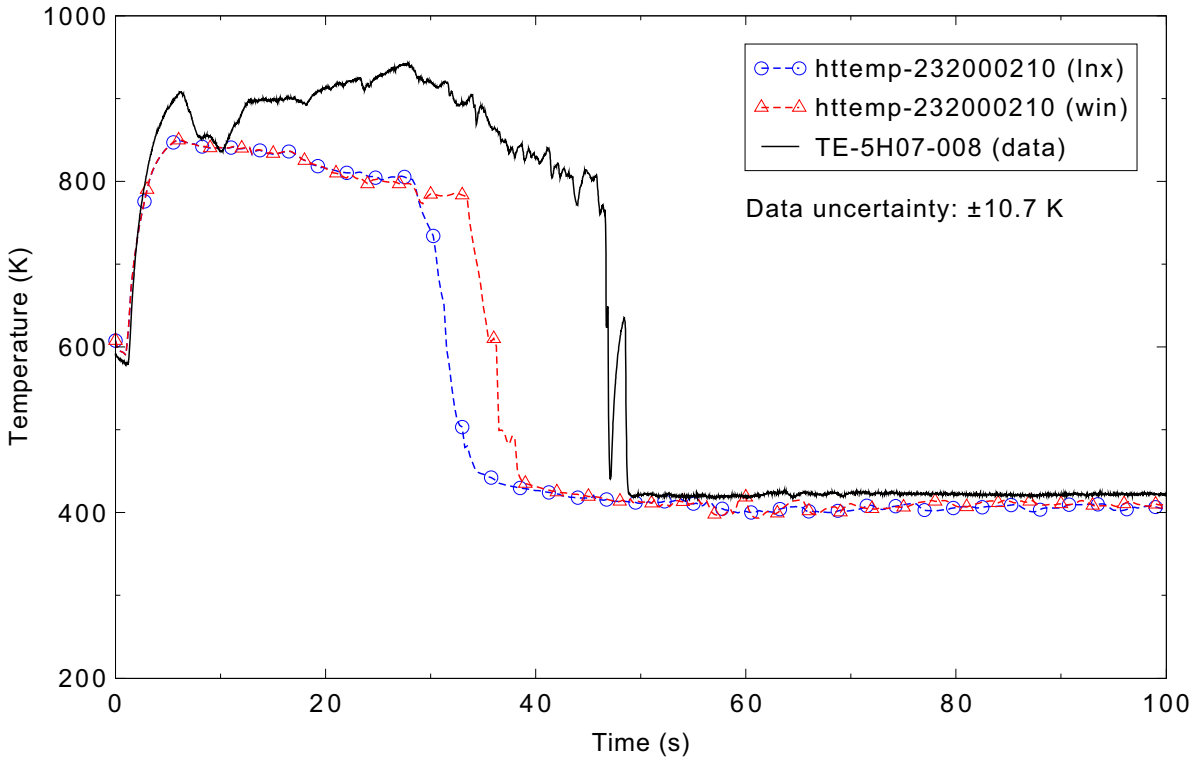

Figure 5.5-22. Measured and calculated fuel cladding surface temperature 0.20 m above the bottom of the fuel rod for the LOFT Experiment L2-5 1-D case.

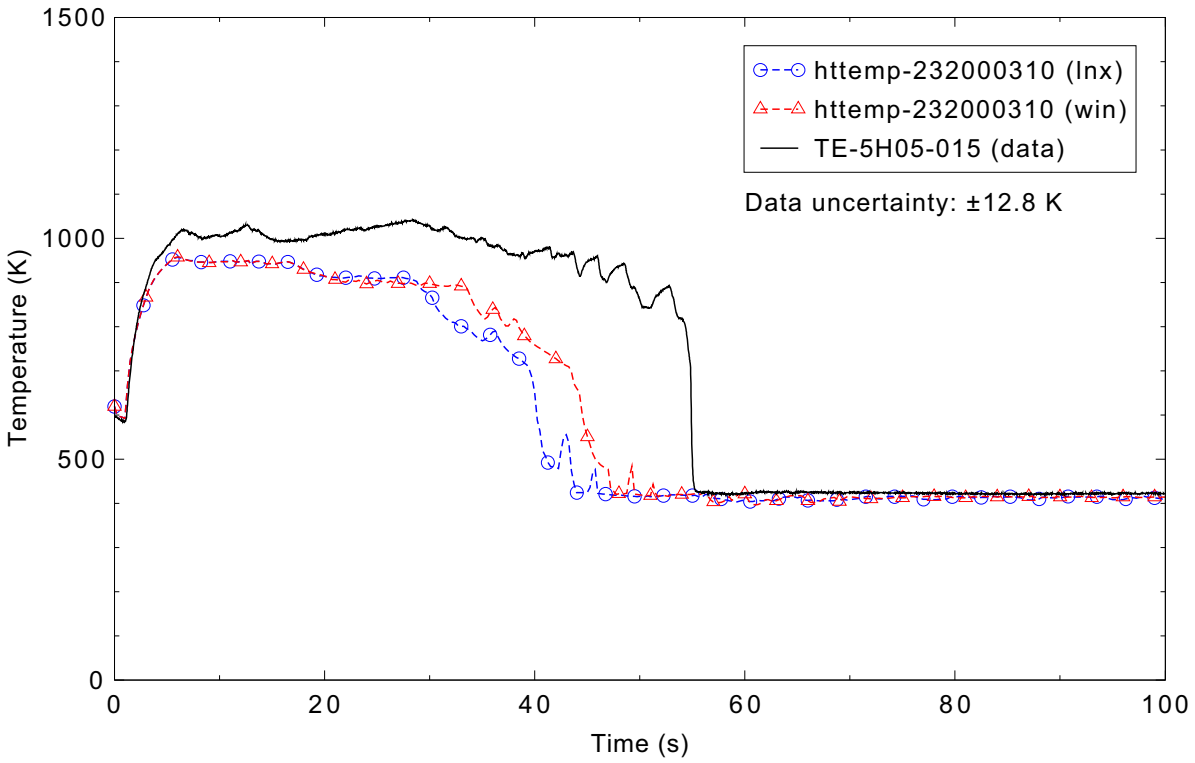

Figure 5.5-23. Measured and calculated fuel cladding surface temperature 0.38 m above the bottom of the fuel rod for the LOFT Experiment L2-5 1-D case.

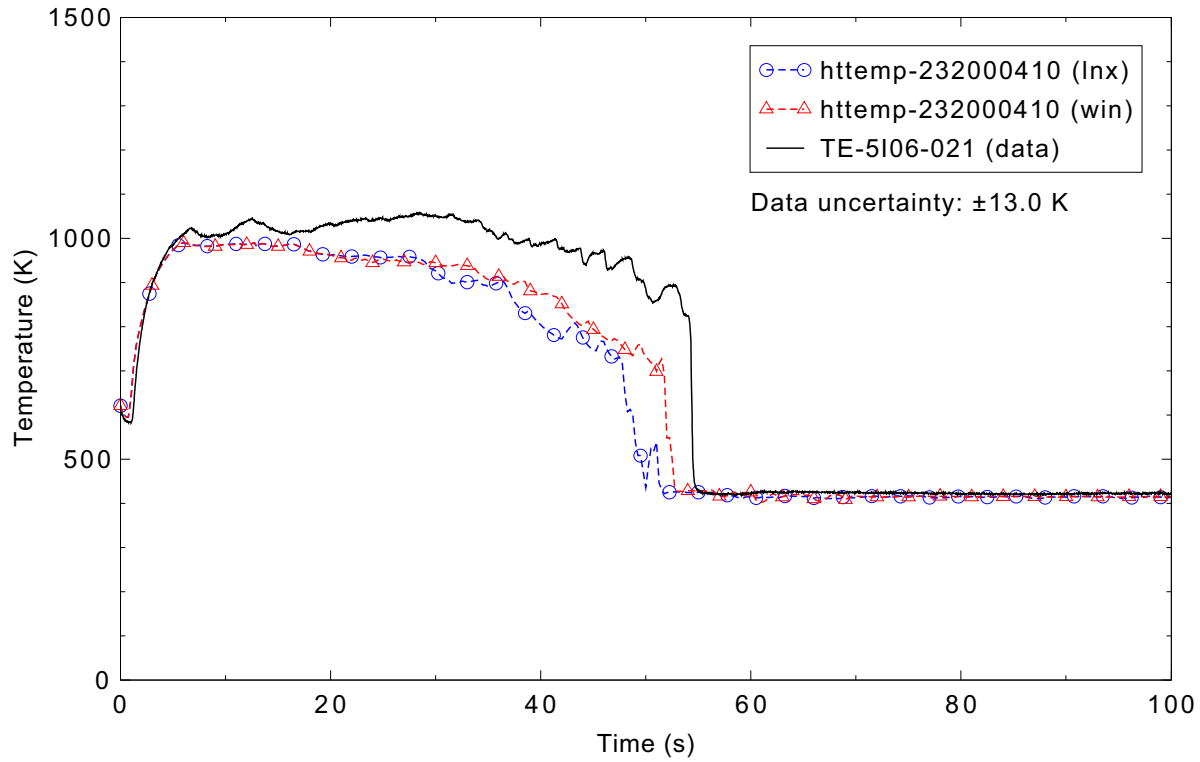

Figure 5.5-24. Measured and calculated fuel cladding surface temperature 0.53 m above the bottom of the fuel rod for the LOFT Experiment L2-5 1-D case.

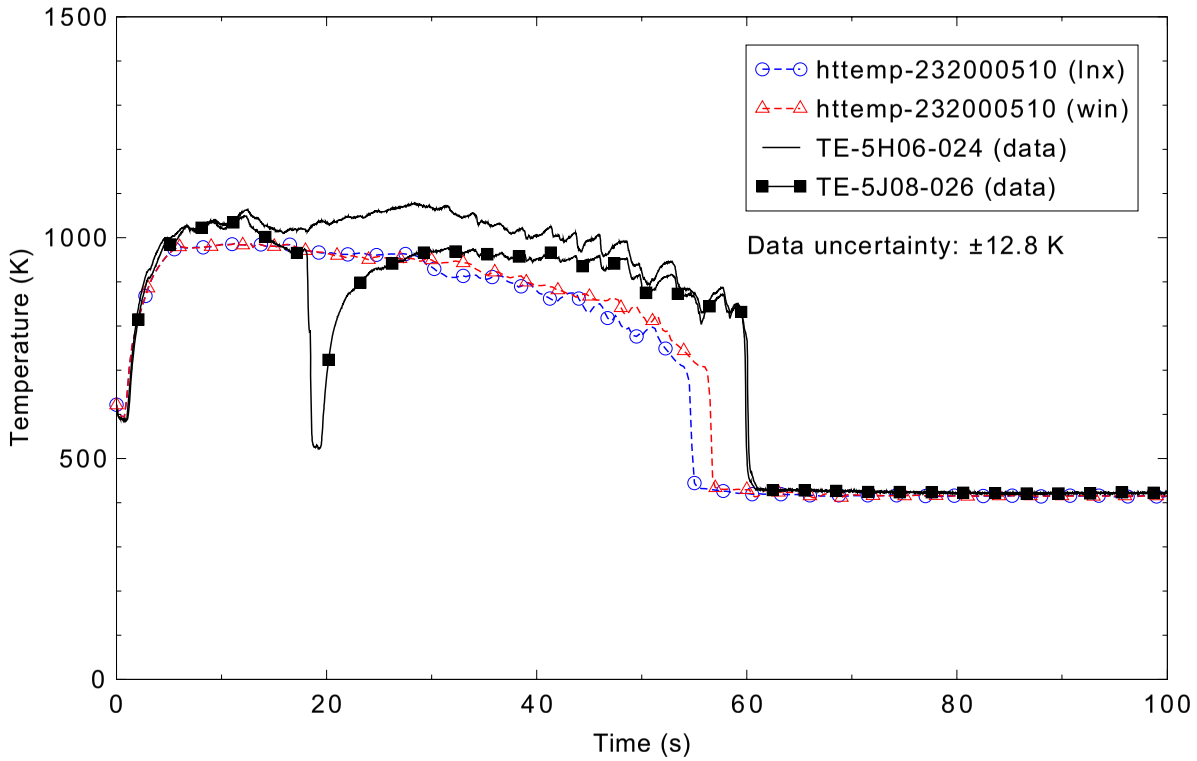

Figure 5.5-25. Measured and calculated fuel cladding surface temperature 0.64 m above the bottom of the fuel rod for the LOFT Experiment L2-5 1-D case.

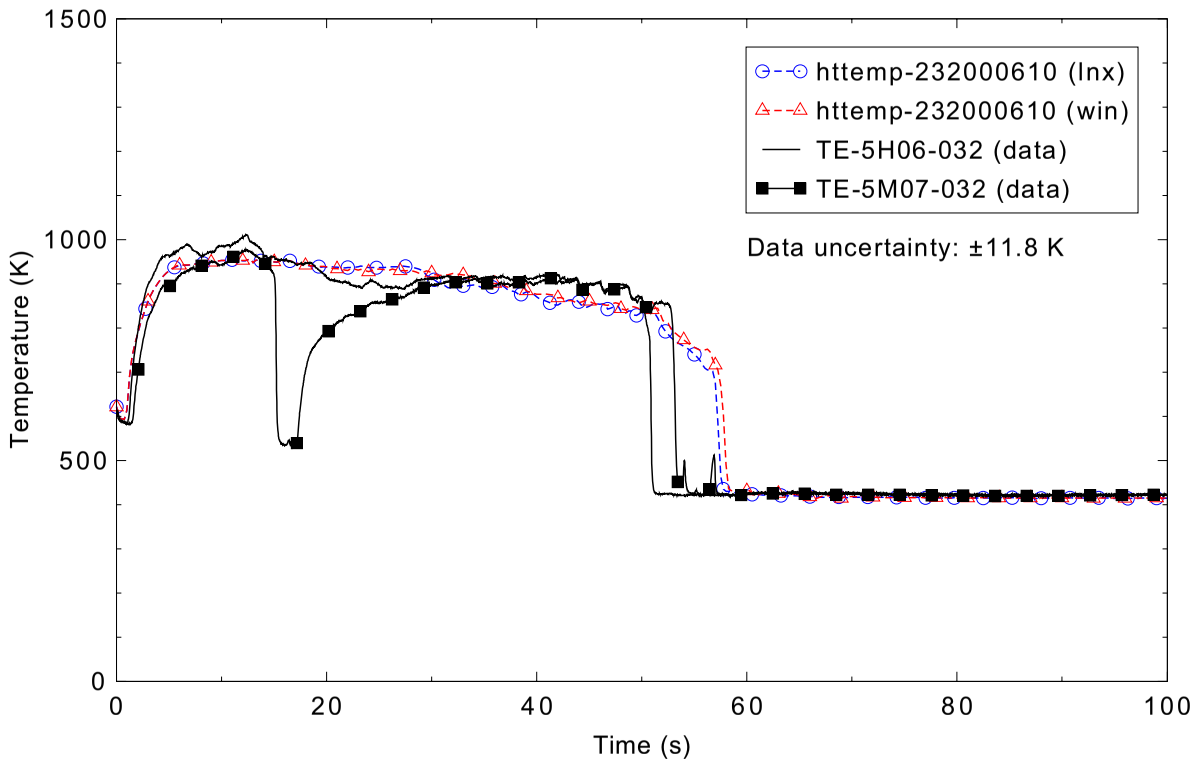

Figure 5.5-26. Measured and calculated fuel cladding surface temperature 0.81 m above the bottom of the fuel rod for the LOFT Experiment L2-5 1-D case.

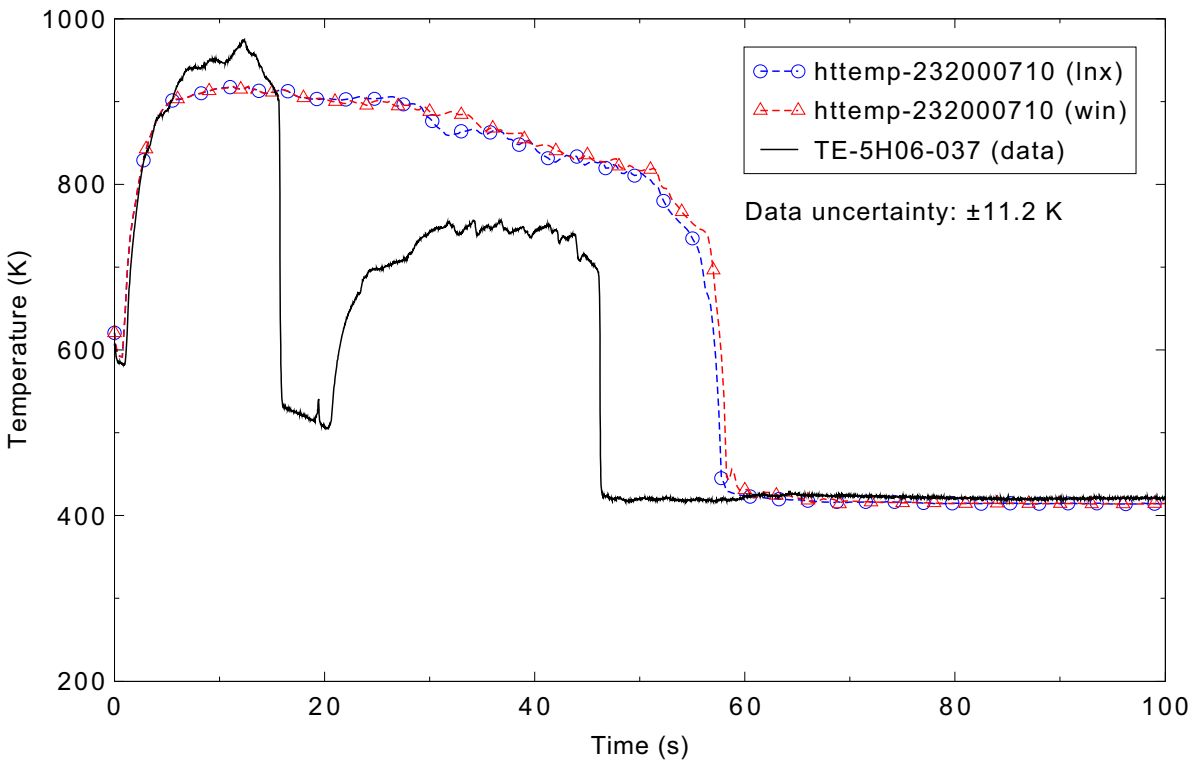

Figure 5.5-27. Measured and calculated fuel cladding surface temperature 0.94 m above the bottom of the fuel rod for the LOFT Experiment L2-5 1-D case.

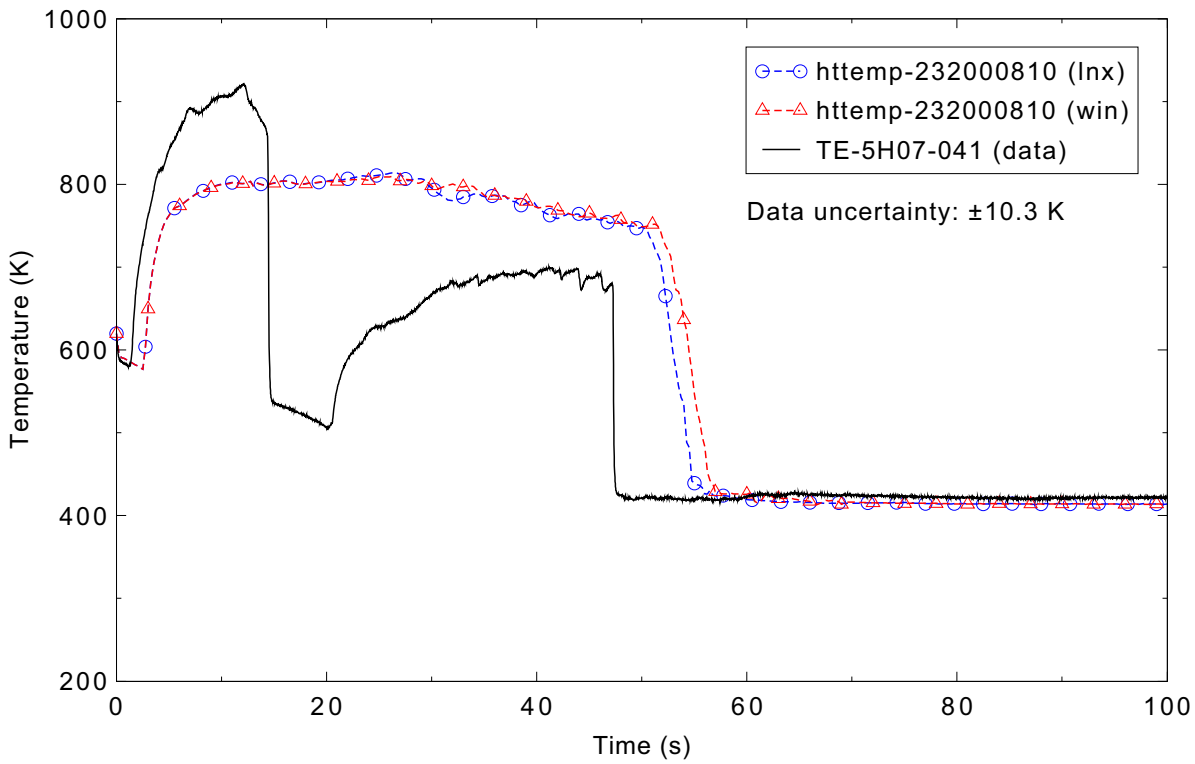

Figure 5.5-28. Measured and calculated fuel cladding surface temperature 1.04 m above the bottom of the fuel rod for the LOFT Experiment L2-5 1-D case.

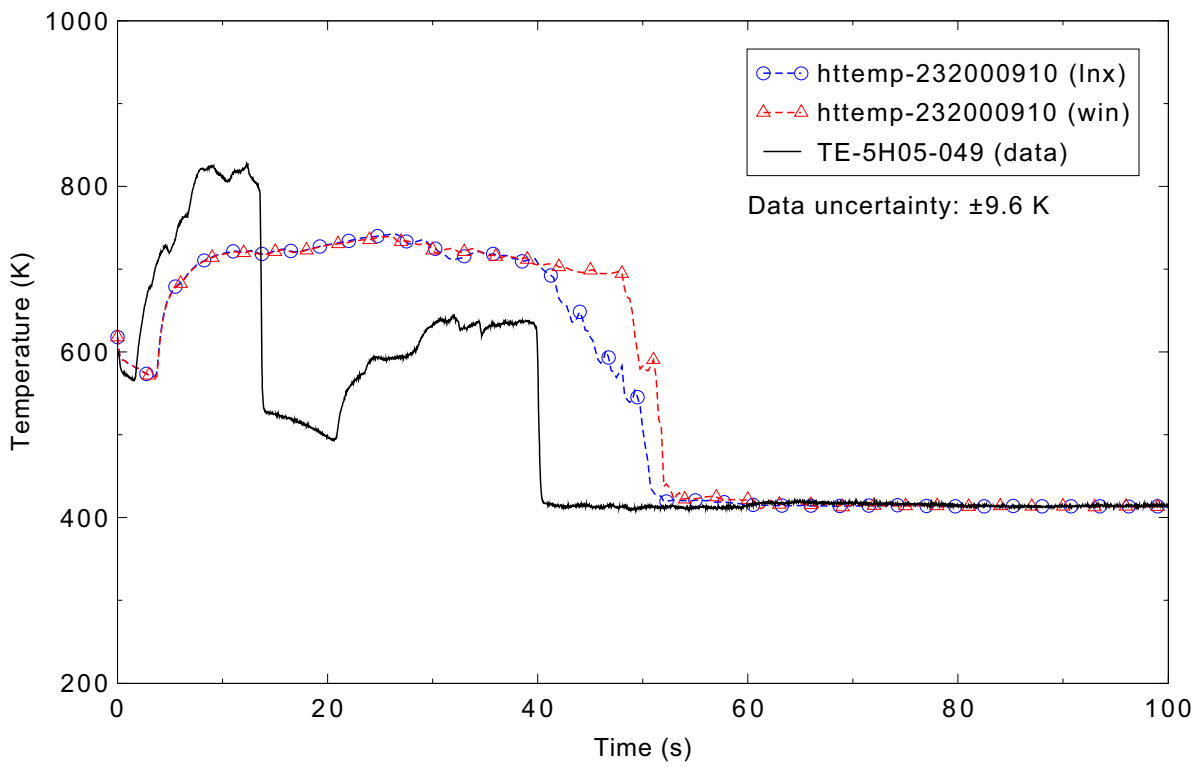

Figure 5.5-29. Measured and calculated fuel cladding surface temperature 1.25 m above the bottom of the fuel rod for the LOFT Experiment L2-5 1-D case.

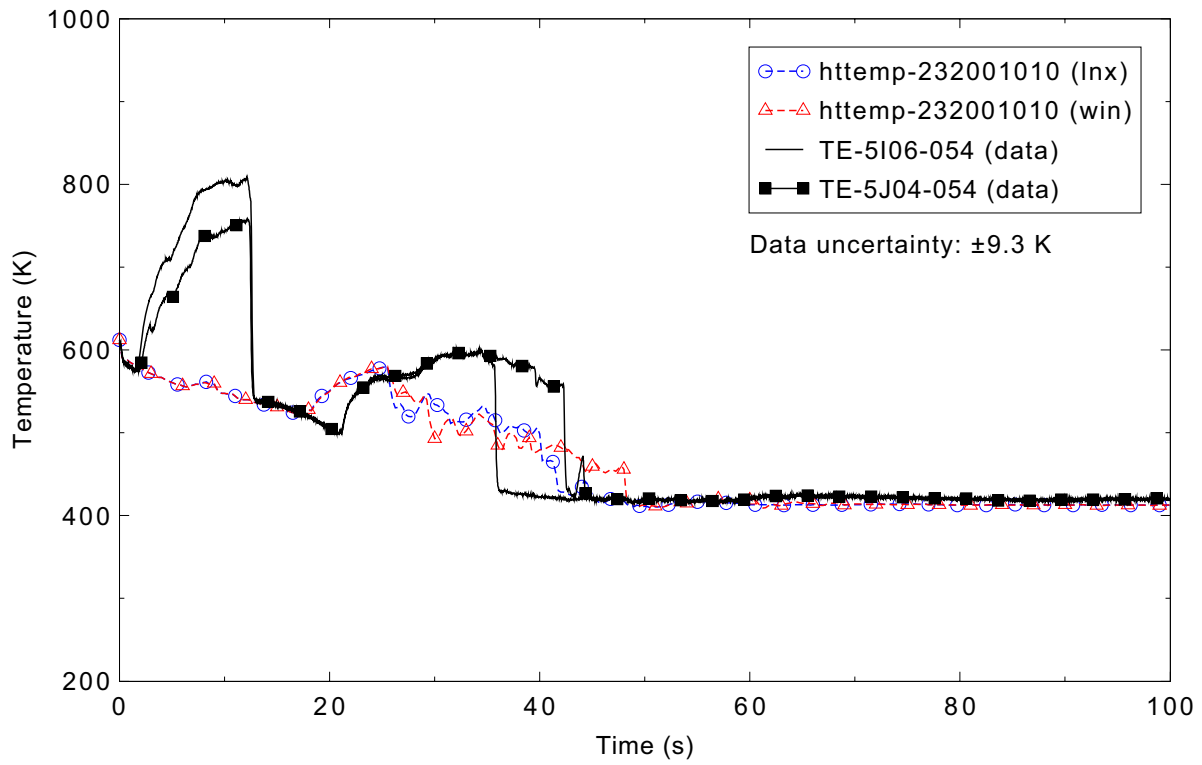

Figure 5.5-30. Measured and calculated fuel cladding surface temperature 1.37 m above the bottom of the fuel rod for the LOFT Experiment L2-5 1-D case.

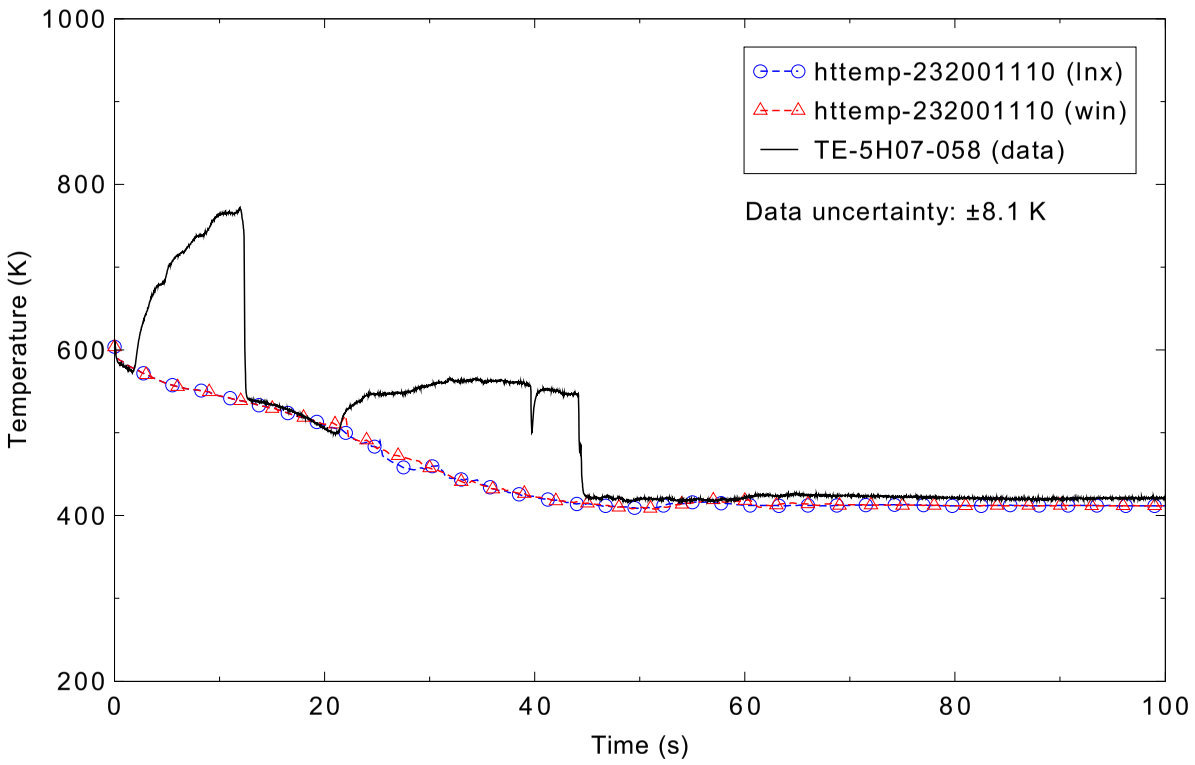

Figure 5.5-31. Measured and calculated fuel cladding surface temperature 1.47 m above the bottom of the fuel rod for the LOFT Experiment L2-5 1-D case.

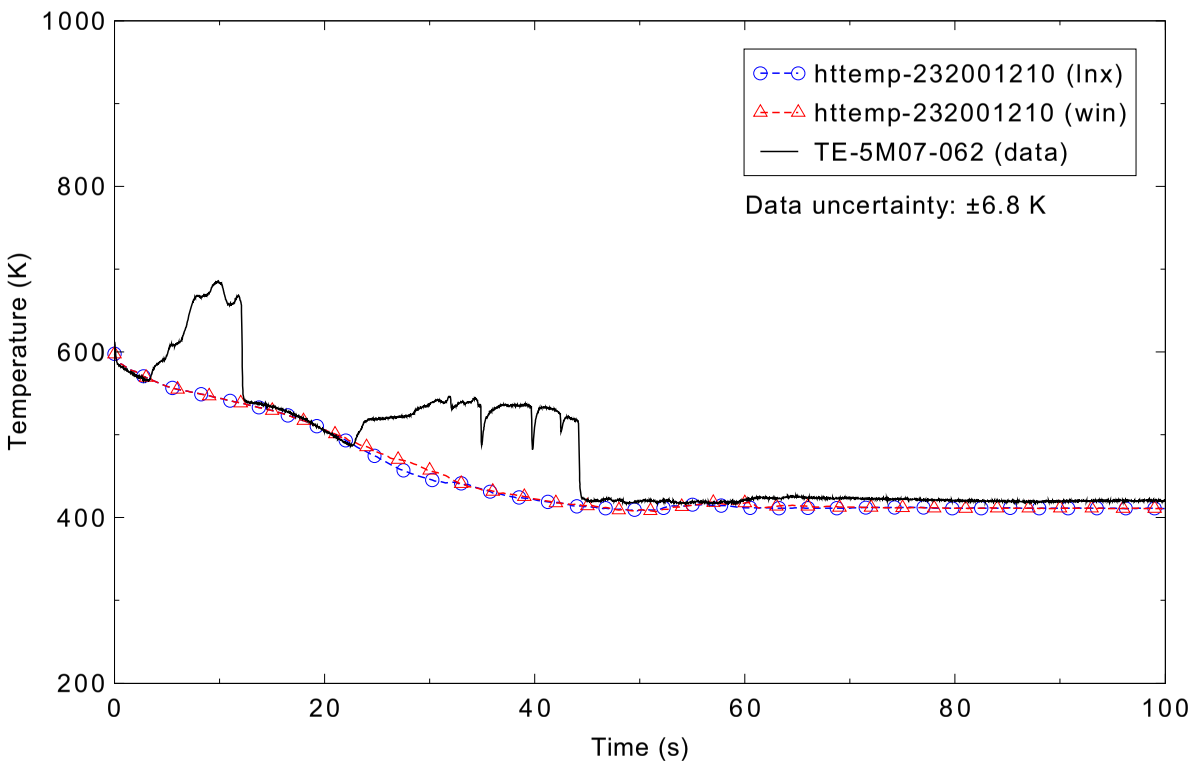

Figure 5.5-32. Measured and calculated fuel cladding surface temperature 1.57 m above the bottom of the fuel rod for the LOFT Experiment L2-5 1-D case.

5.6 LOFT Experiment L2-5 (3-D)

Figures comparing simulations using Linux and Windows code versions are presented. Diagrams are included so that the figure numbering is the same as that in Volume III of the RELAP5-3D code manual. The Windows calculation failed at 54.17 s, so comparisons are made up to the time of the failure. A significant difference was observed in Figure 5.6-33. Noticeable differences were observed in Figures 5.6-6, 8, 9, 10, 11, 12, 13, 14, 15, 16, 19, 20, 21, 22, 23, 24, 25, 26, 27, 28, 29, 30, 31, 32, and 34.

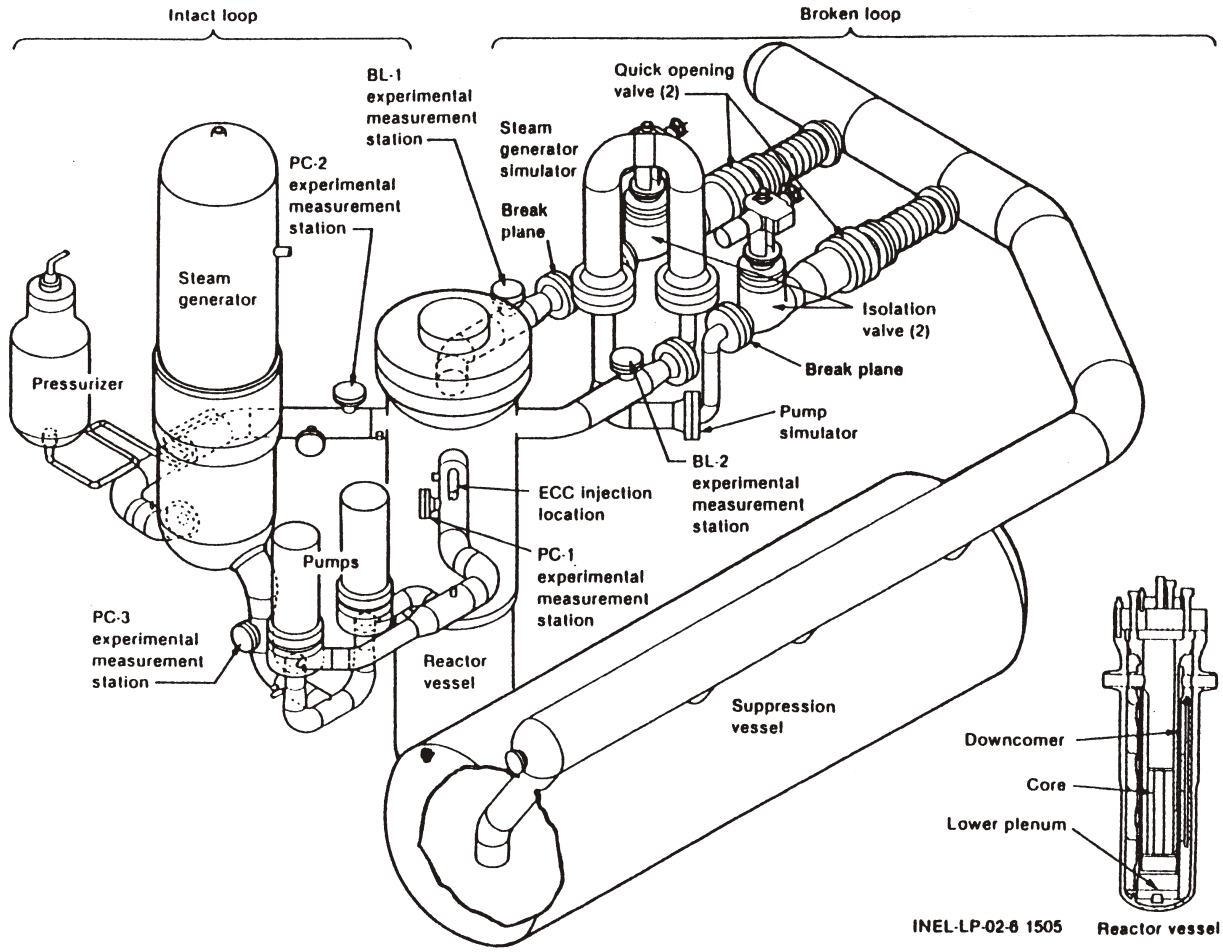

Figure 5.6-1. Schematic of the LOFT facility.

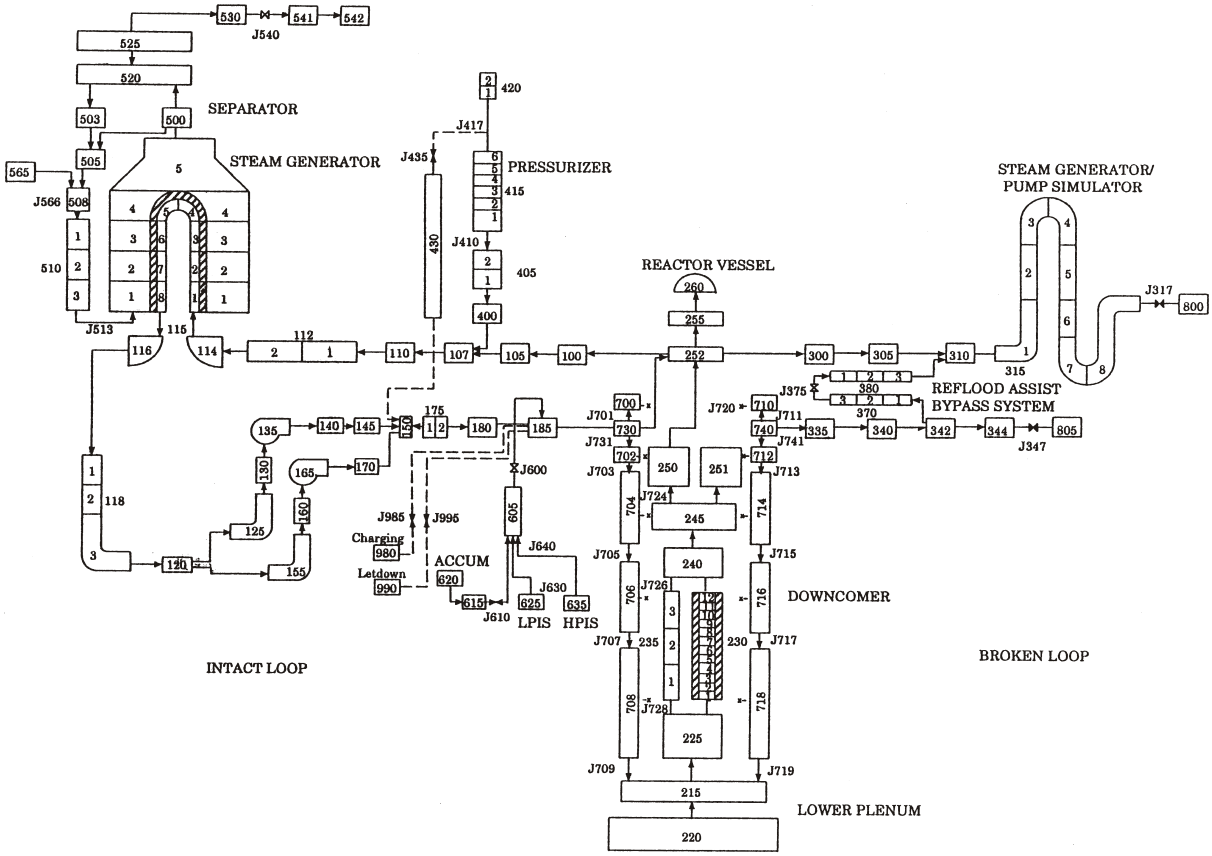

Figure 5.6-2. RELAP5-3D nodalization for the LOFT facility Experiment L2-5 (1-D vessel).

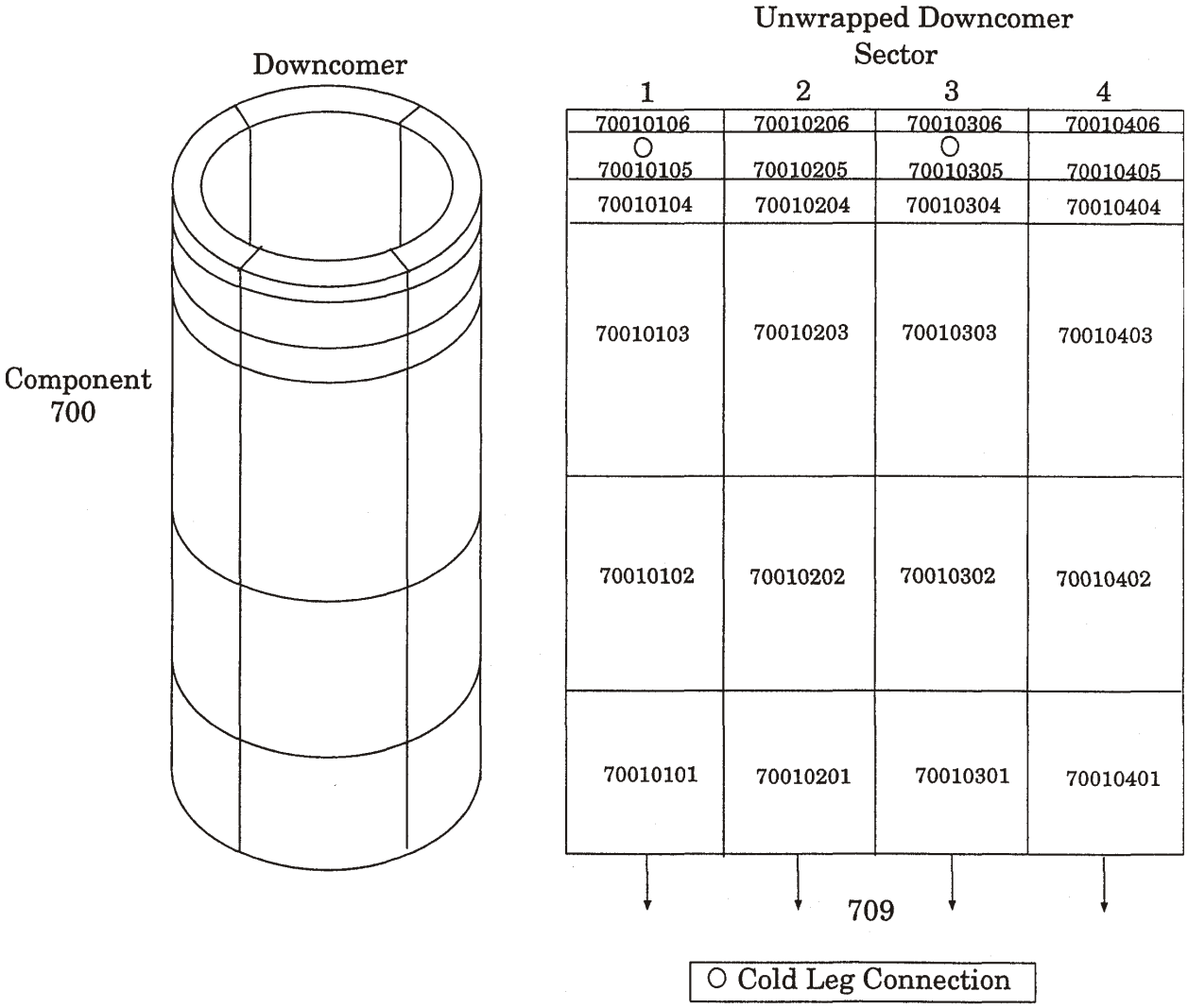

Figure 5.6-3. RELAP-3D nodalization for the LOFT reactor vessel downcomer (3-D vessel).

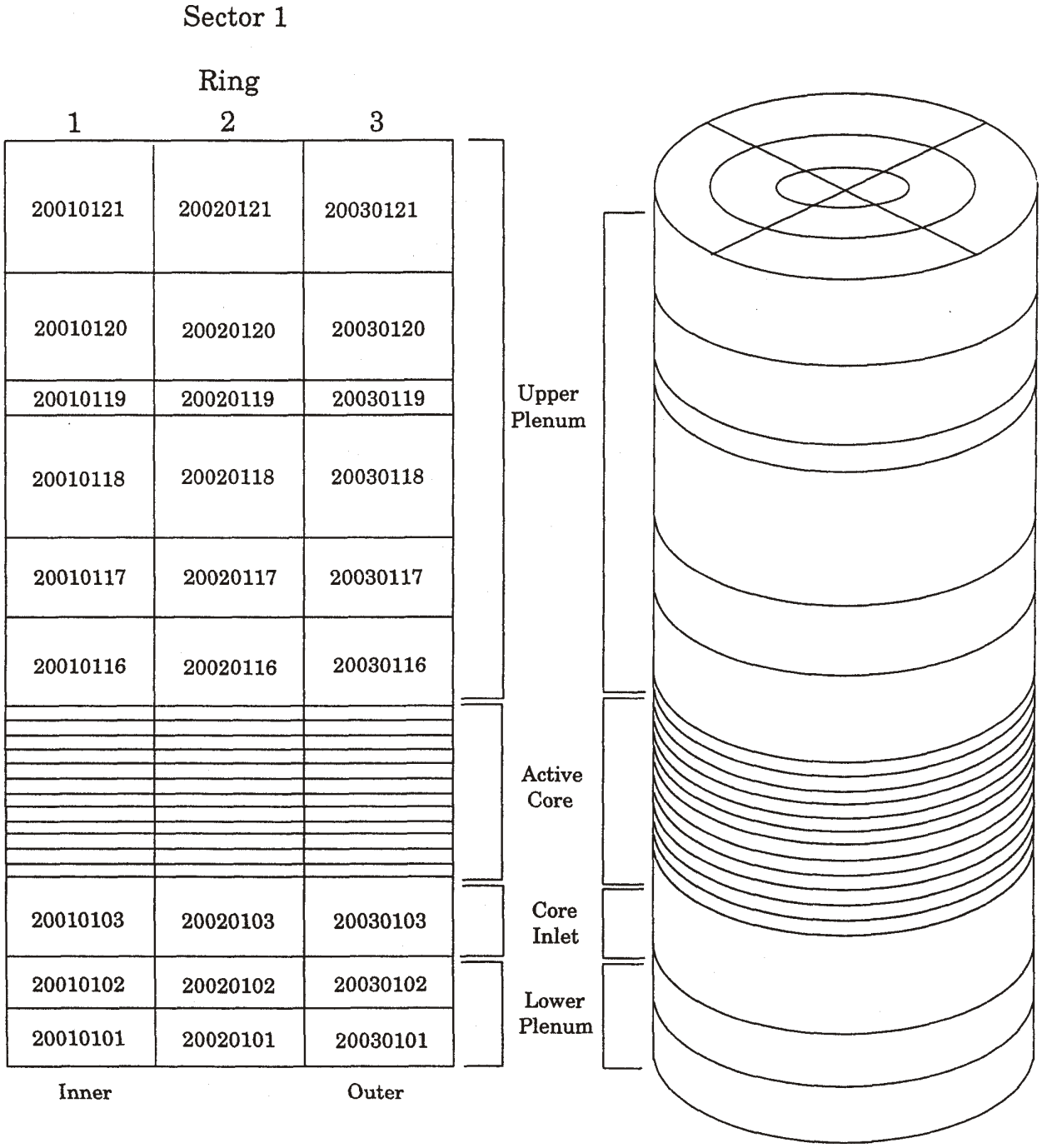

Figure 5.6-4. RELAP5-3D nodalization for the LOFT reactor vessel core region (3-D vessel).

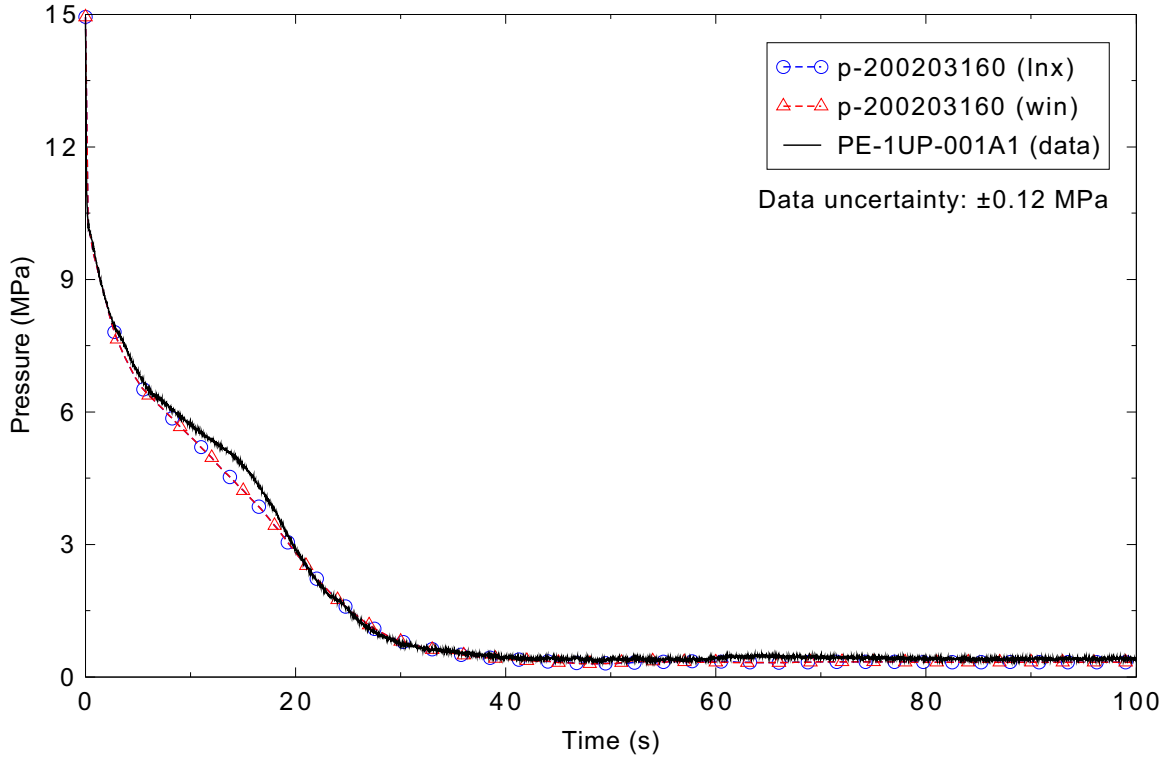

Figure 5.6-5. Measured and calculated reactor vessel upper plenum pressure for the LOFT Experiment L2-5 3-D case.

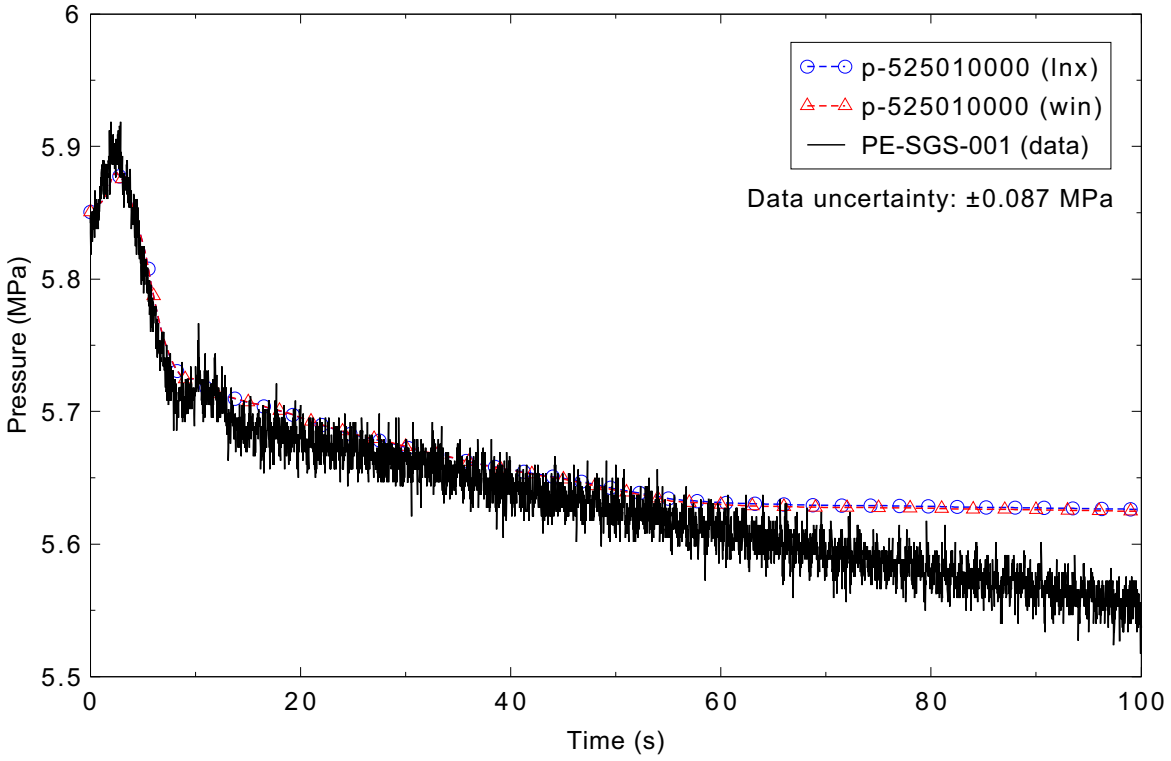

Figure 5.6-6. Measured and calculated steam generator pressure for the LOFT Experiment L2-5 3-D case.

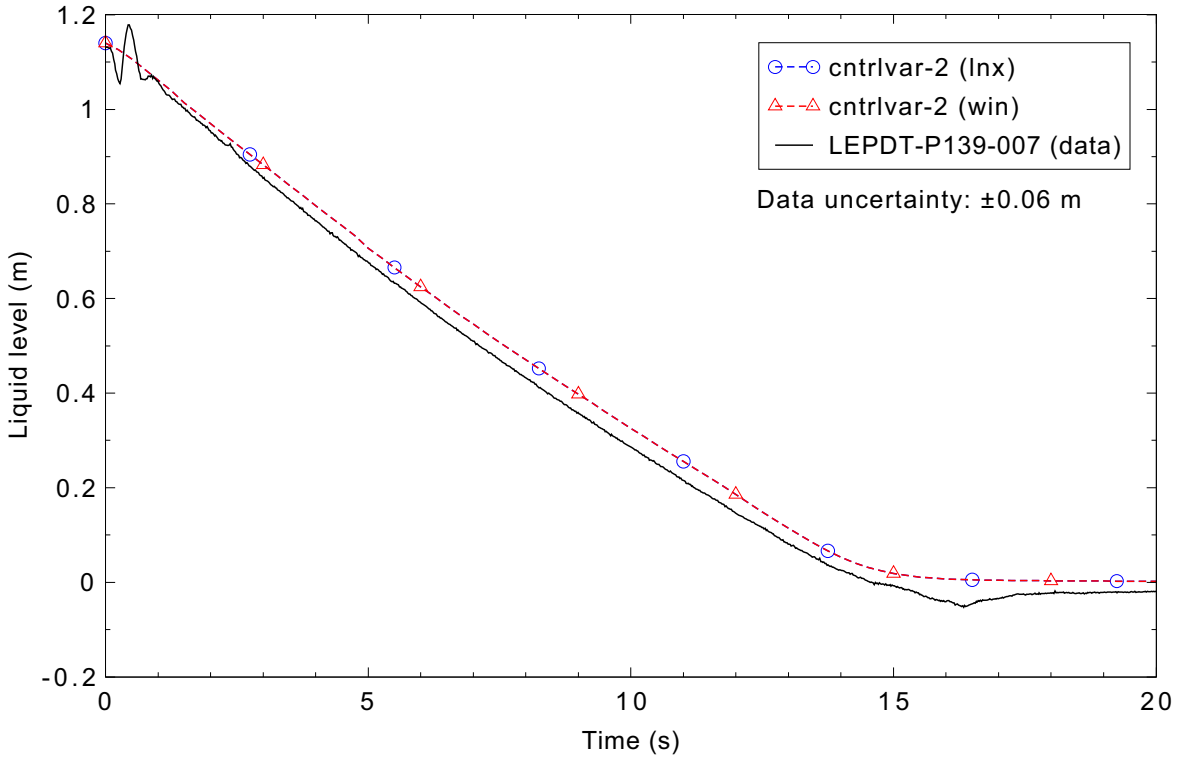

Figure 5.6-7. Measured and calculated pressurizer liquid level for the LOFT Experiment L2-5 3-D case.

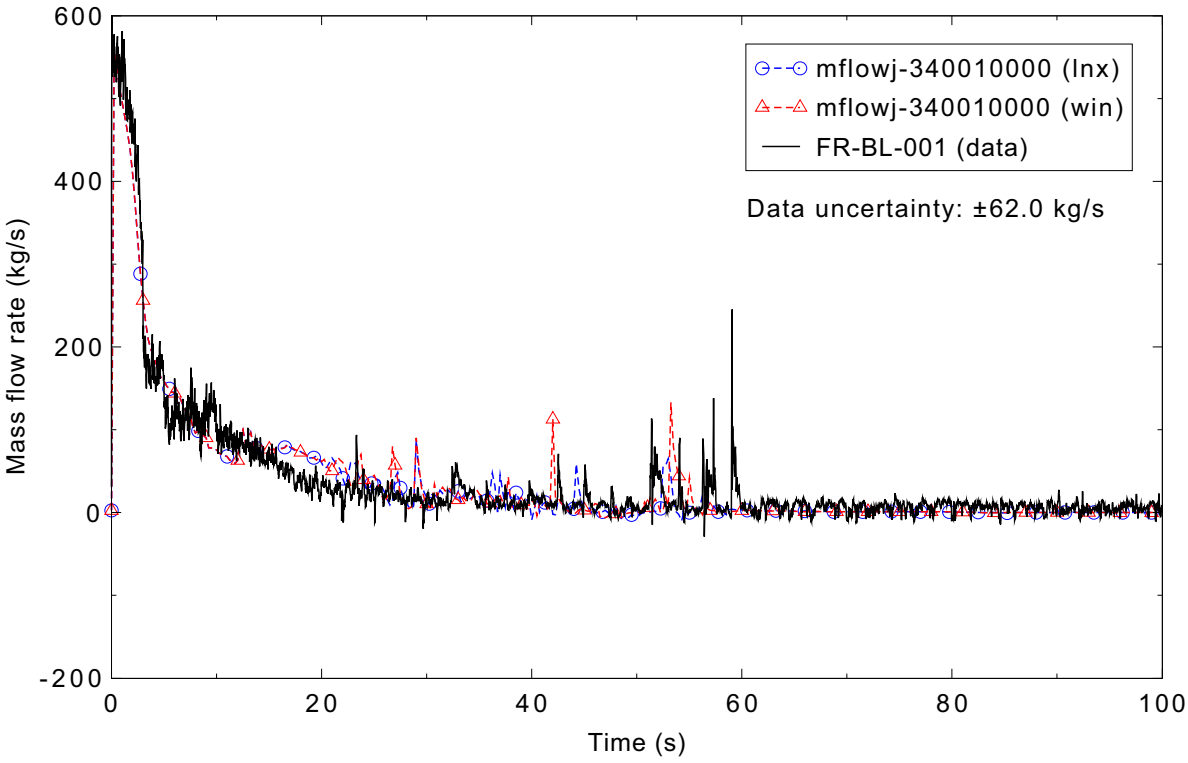

Figure 5.6-8. Measured and calculated mass flow rate in the broken loop cold leg for the LOFT Experiment L2-5 3-D case.

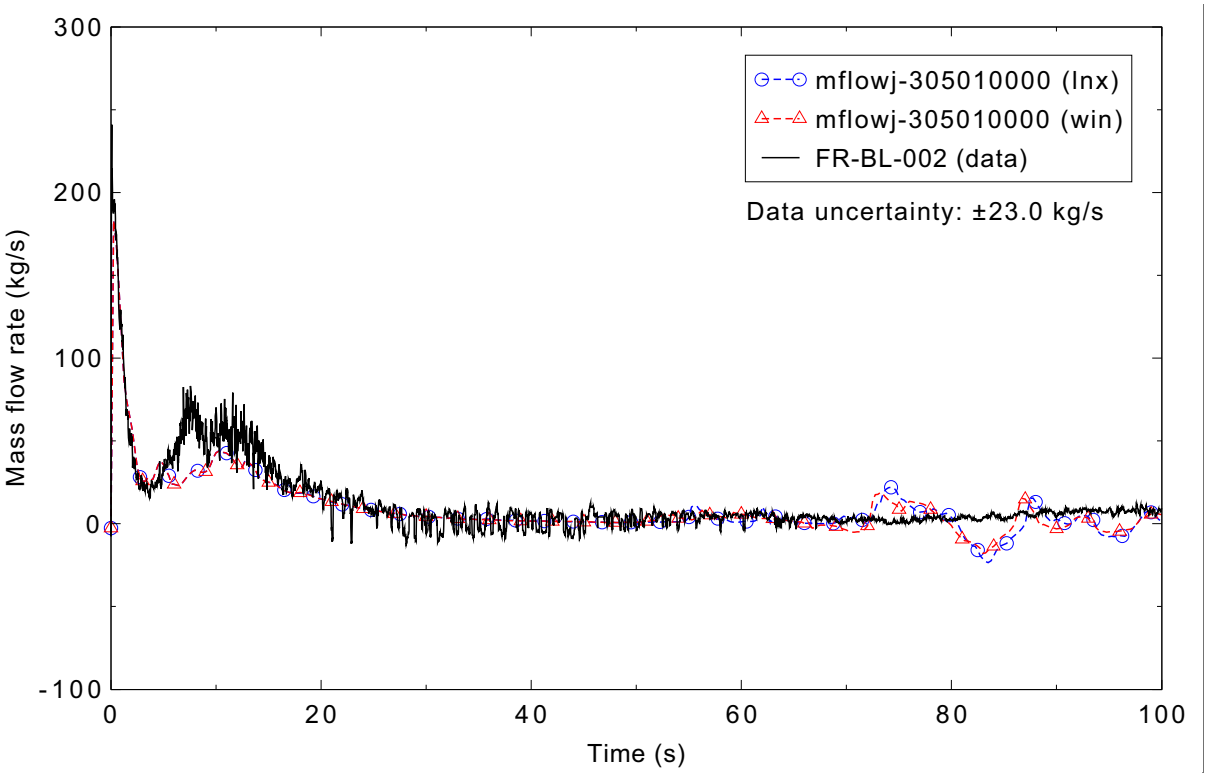

Figure 5.6-9. Measured and calculated mass flow rate in the broken loop hot leg for the LOFT Experiment L2-5 3-D case.

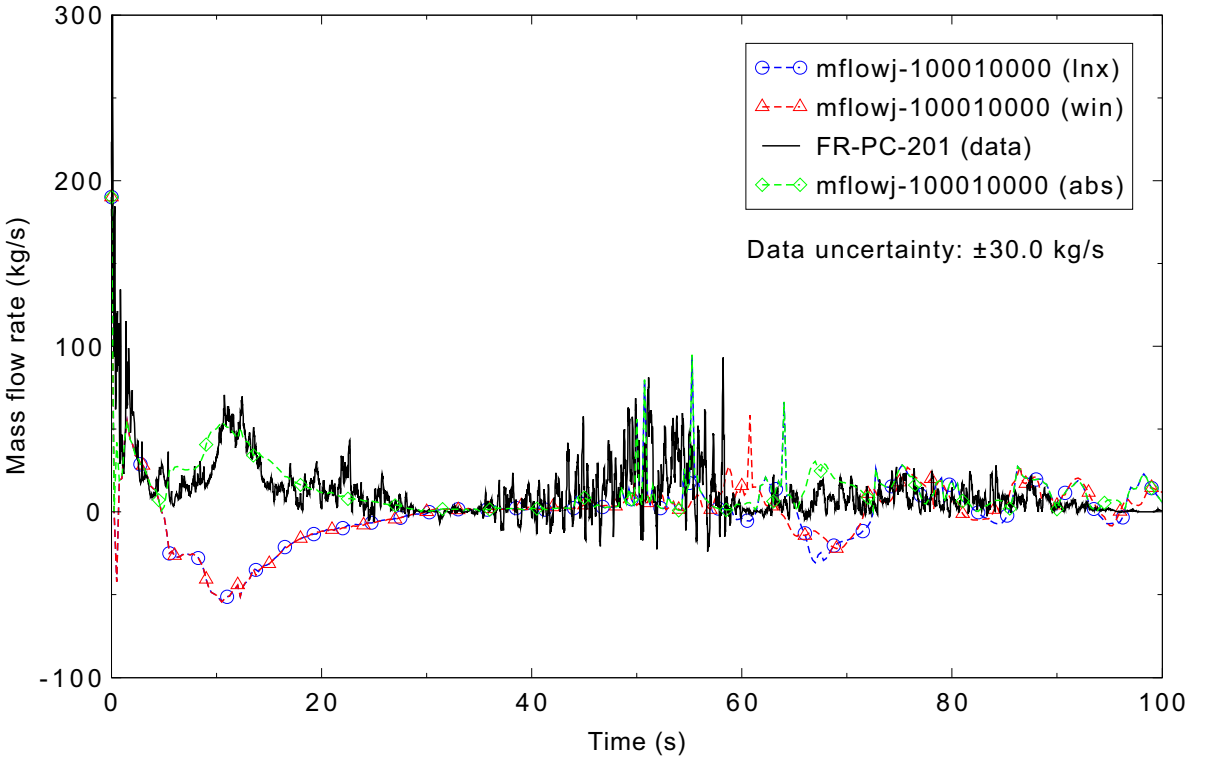

Figure 5.6-10. Measured and calculated mass flow rate in the intact loop hot leg for the LOFT Experiment L2-5 3-D case.

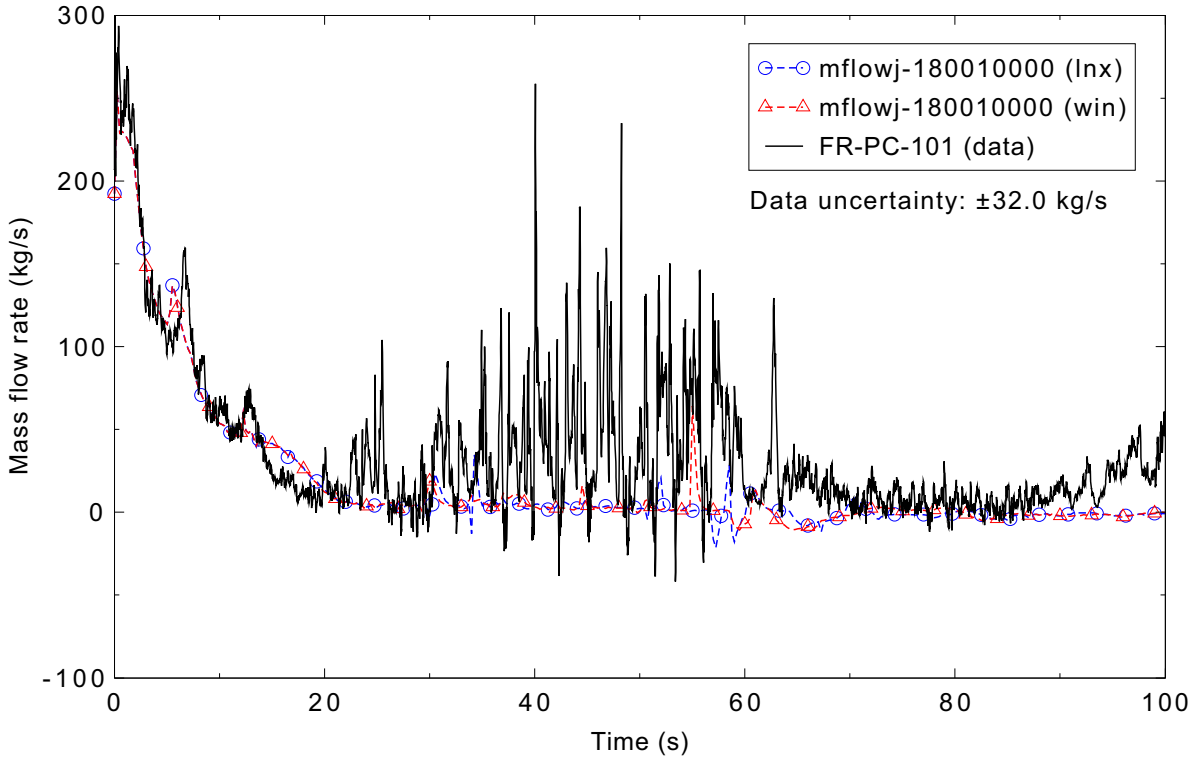

Figure 5.6-11. Measured and calculated mass flow rate in the intact loop cold leg for the LOFT Experiment L2-5 3-D case.

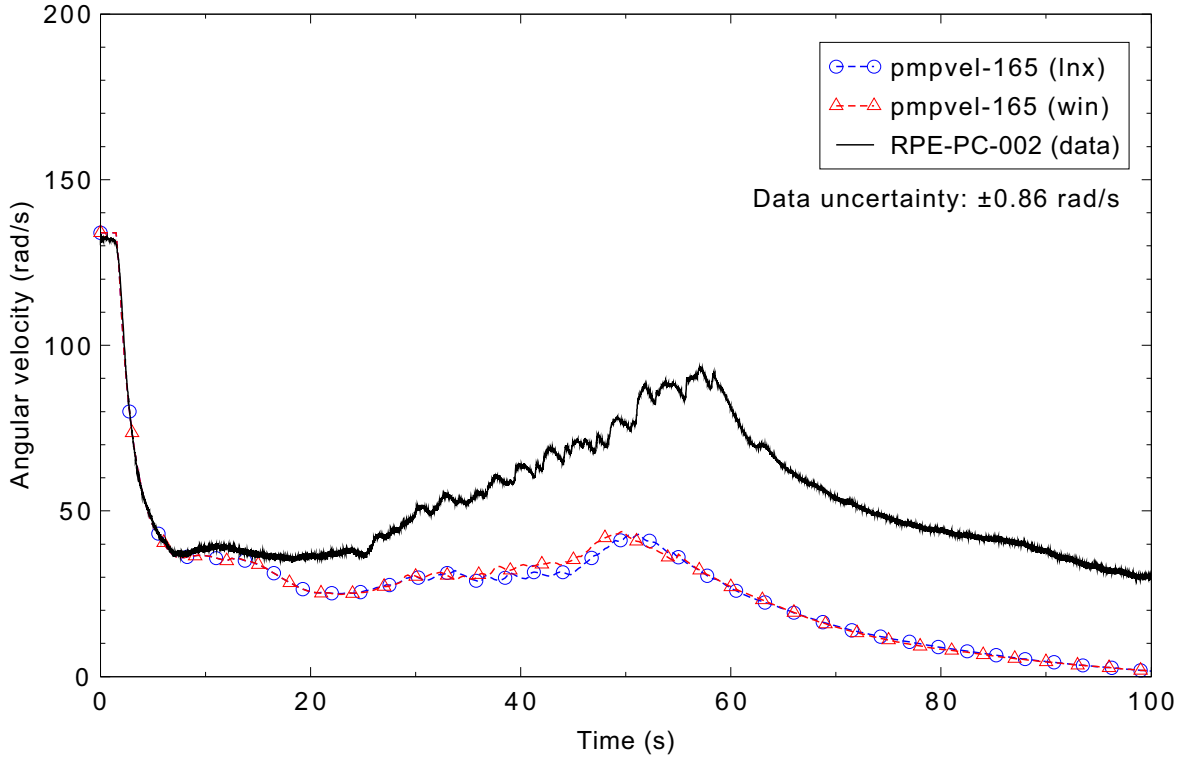

Figure 5.6-12. Measured and calculated speed for primary coolant pump 2 for the LOFT Experiment L2-5 3-D case.

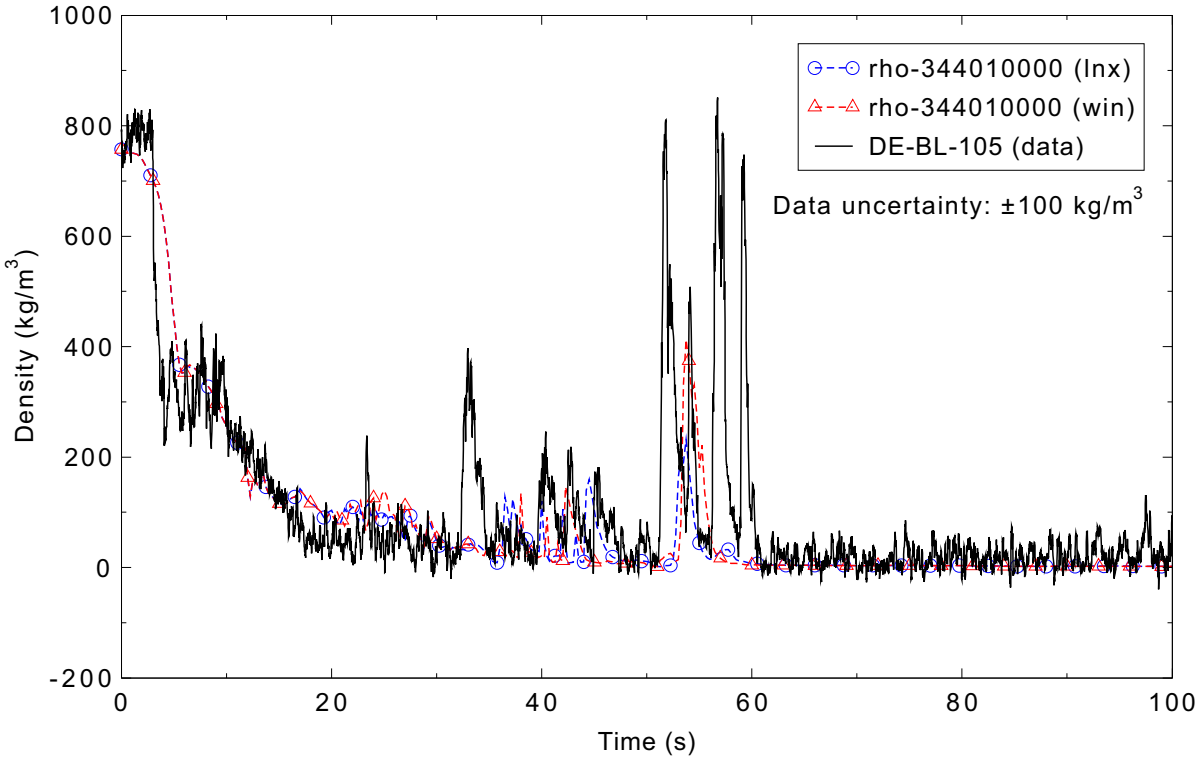

Figure 5.6-13. Measured and calculated density in the broken loop cold leg for the LOFT Experiment L2-5 3-D case.

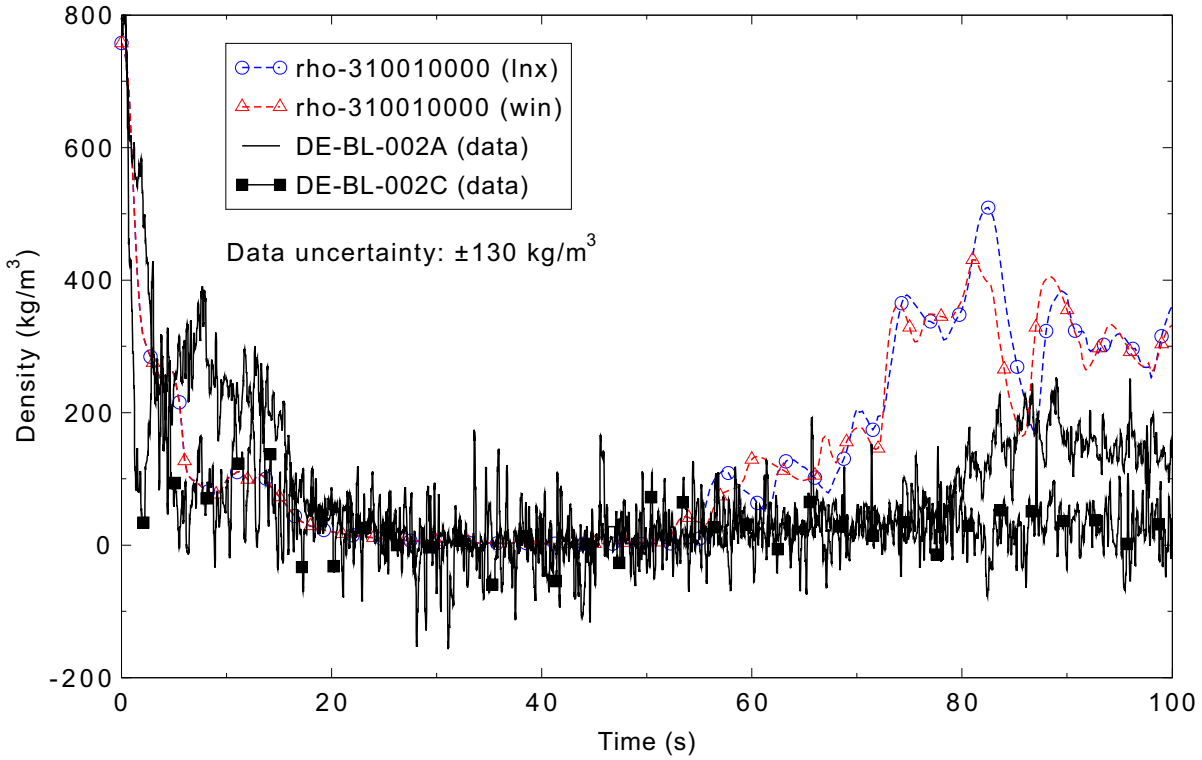

Figure 5.6-14. Measured and calculated density in the broken loop hot leg for the LOFT Experiment L2-5 3-D case.

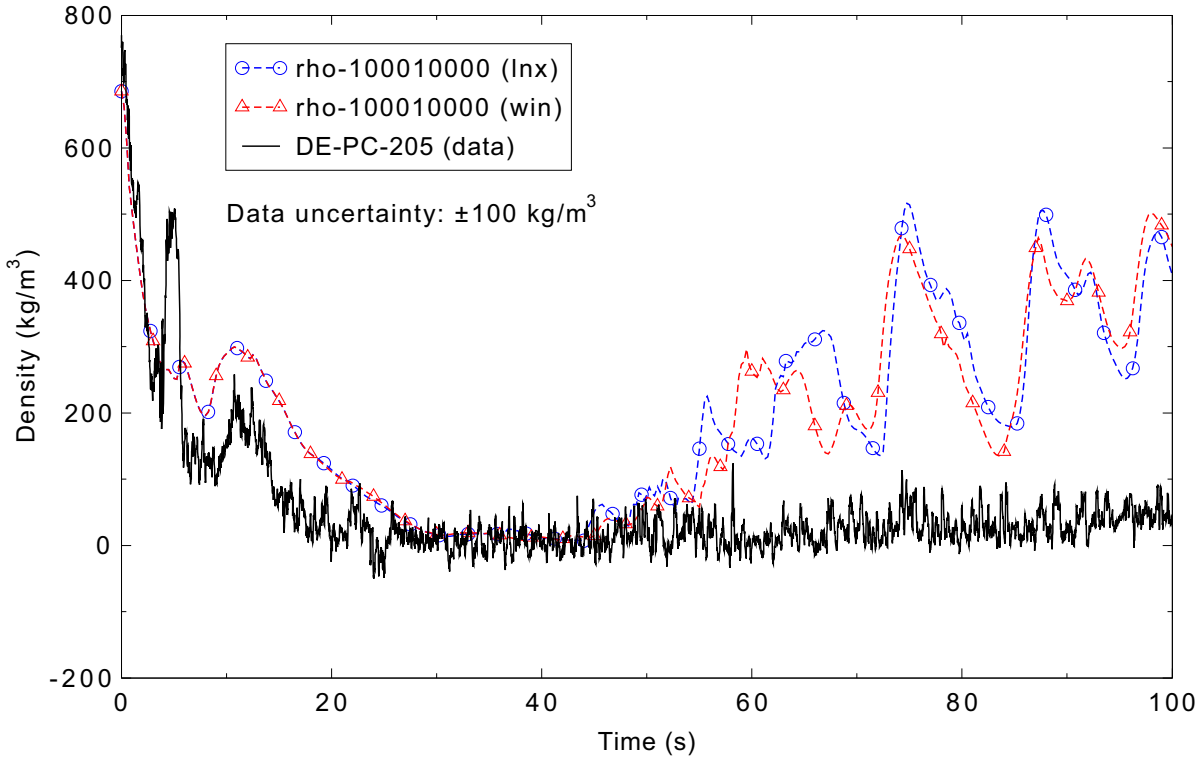

Figure 5.6-15. Measured and calculated density in the intact loop hot leg for the LOFT Experiment L2-5 3-D case.

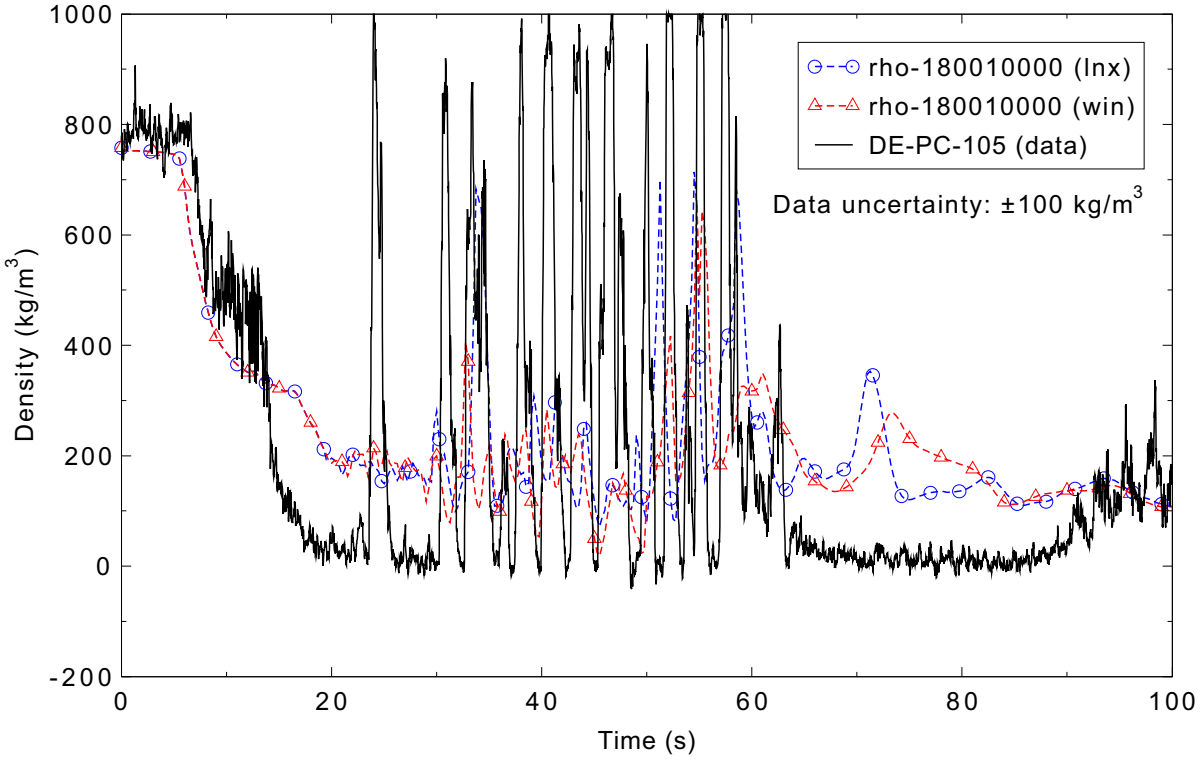

Figure 5.6-16. Measured and calculated density in the intact loop cold leg for the LOFT Experiment L2-5 3-D case.

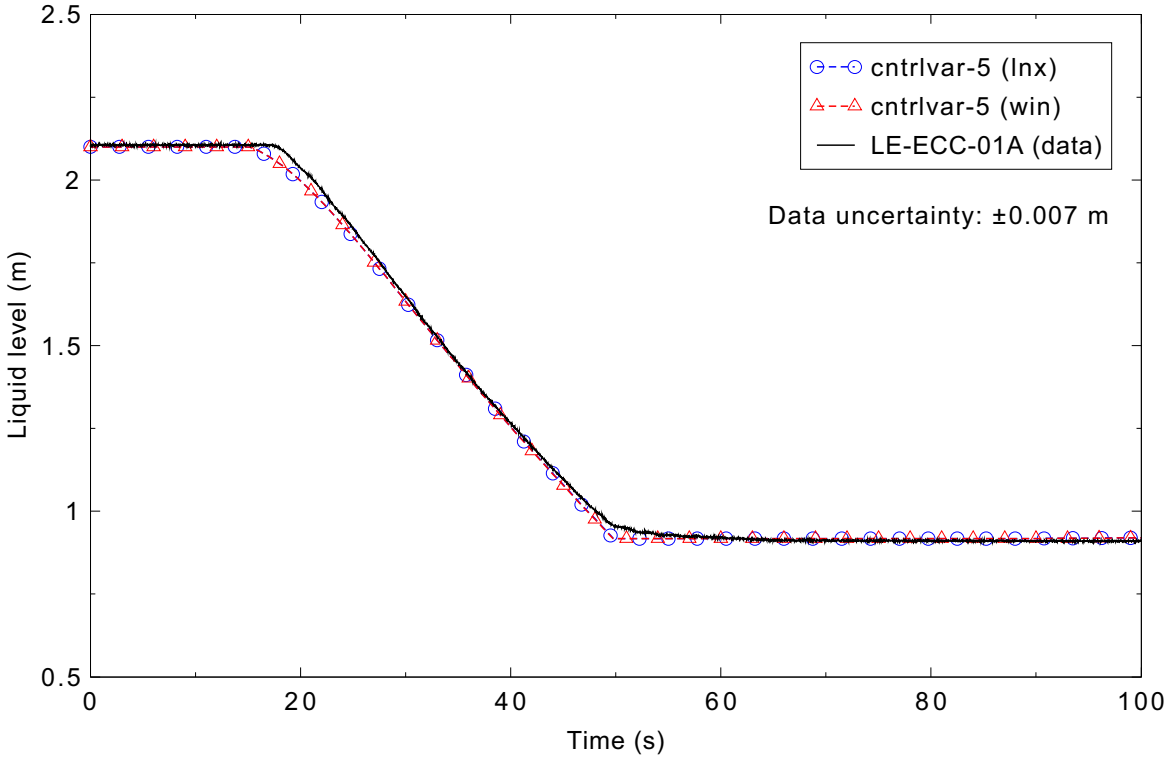

Figure 5.6-17. Measured and calculated accumulator liquid level for the LOFT Experiment L2-5 3-D case.

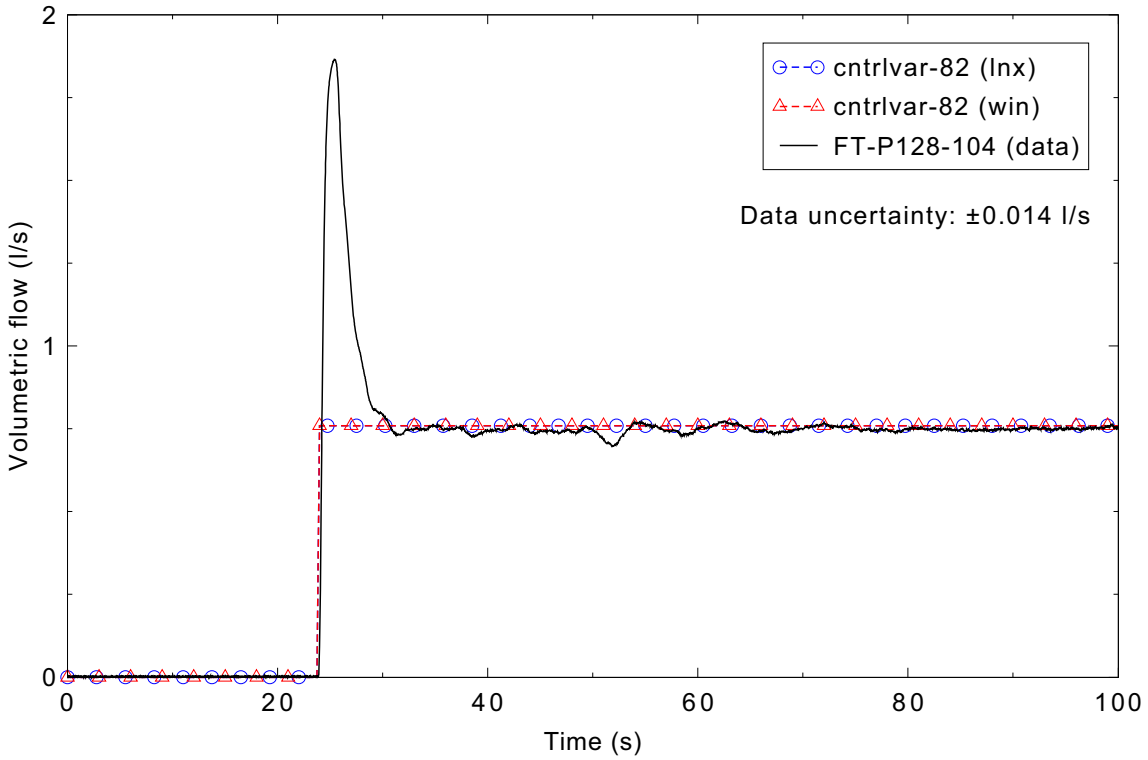

Figure 5.6-18. Measured and calculated HPIS flow for the LOFT Experiment L2-5 3-D case.

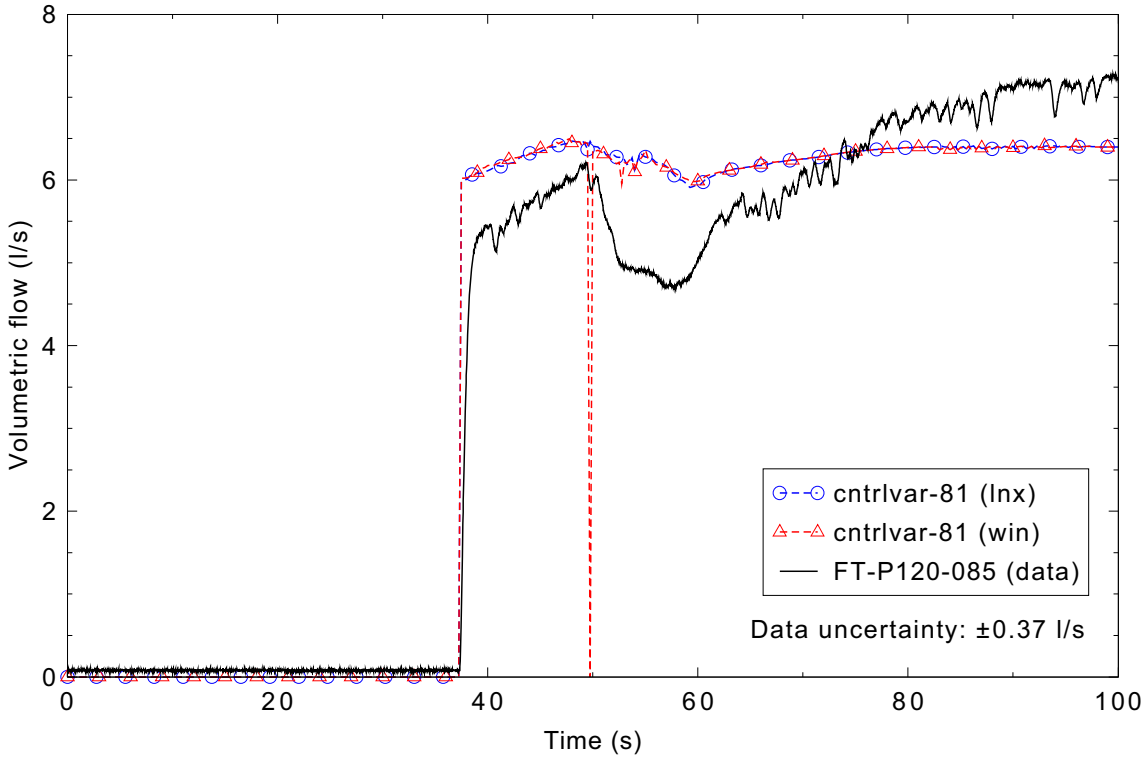

Figure 5.6-19. Measured and calculated LPIS flow for the LOFT Experiment L2-5 3-D case.

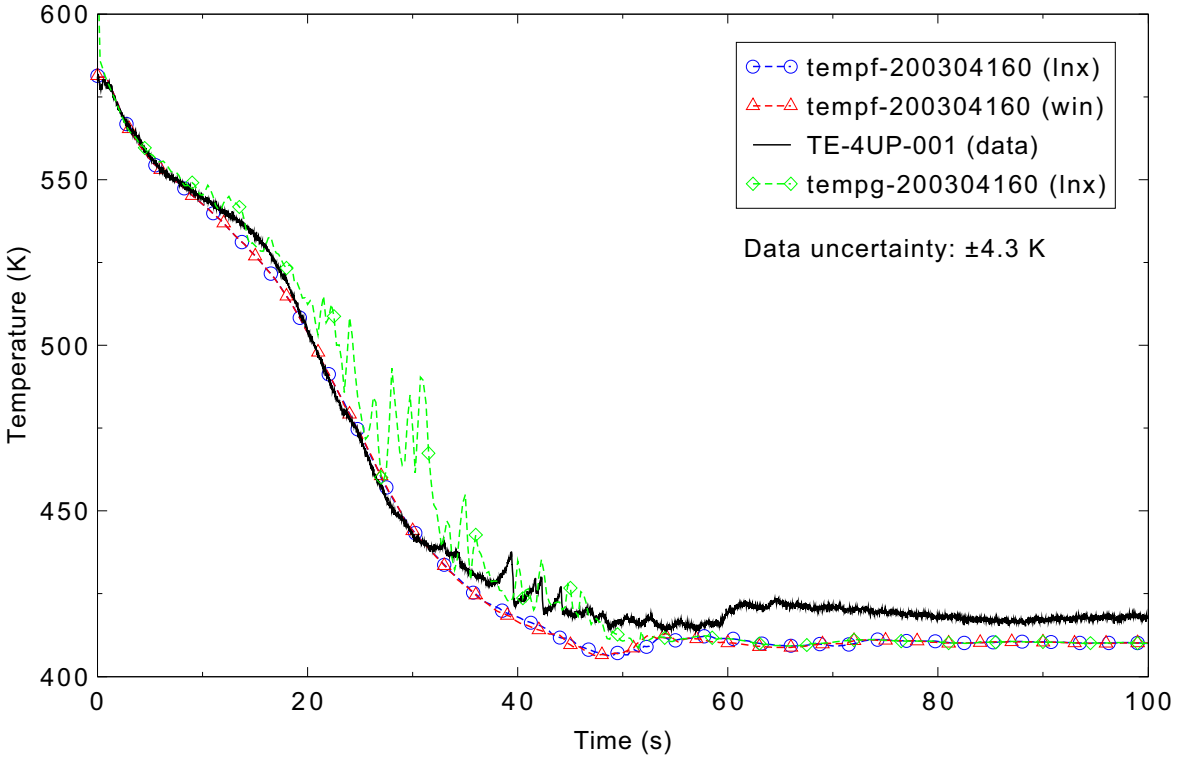

Figure 5.6-20. Measured and calculated reactor vessel upper plenum coolant temperature for the LOFT Experiment L2-5 3-D case.

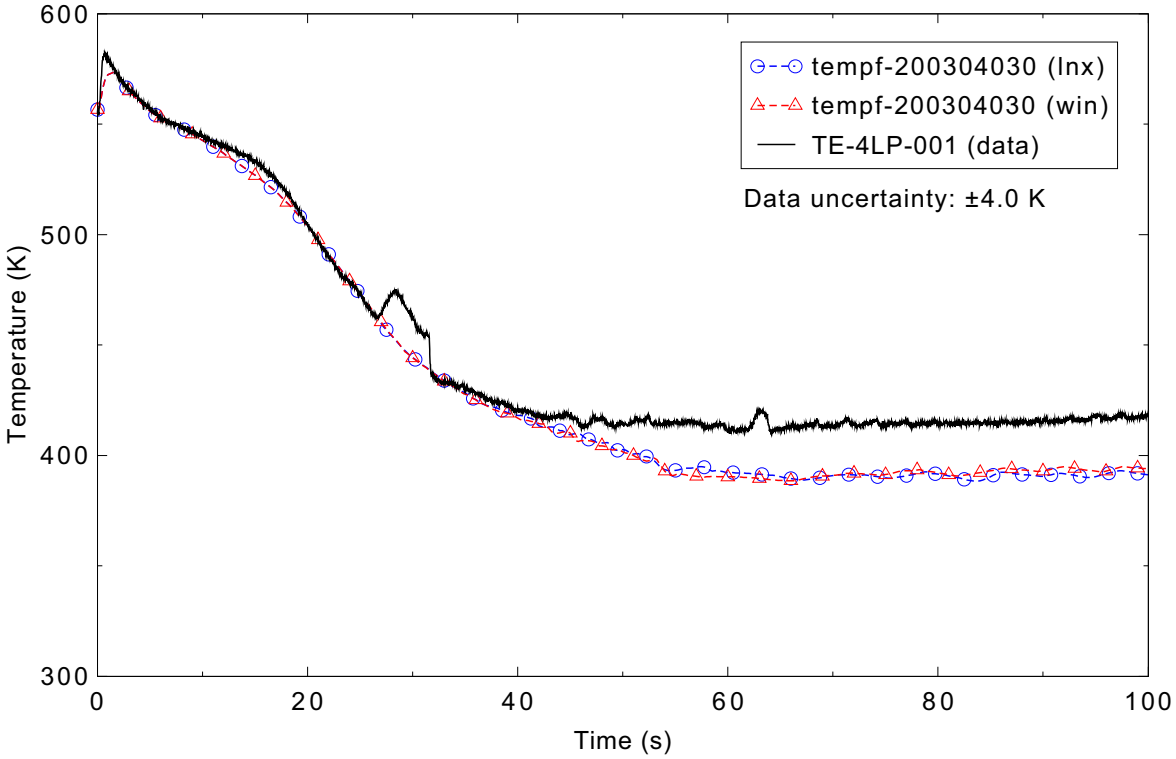

Figure 5.6-21. Measured and calculated reactor vessel lower plenum coolant temperature for the LOFT Experiment L2-5 3-D case.

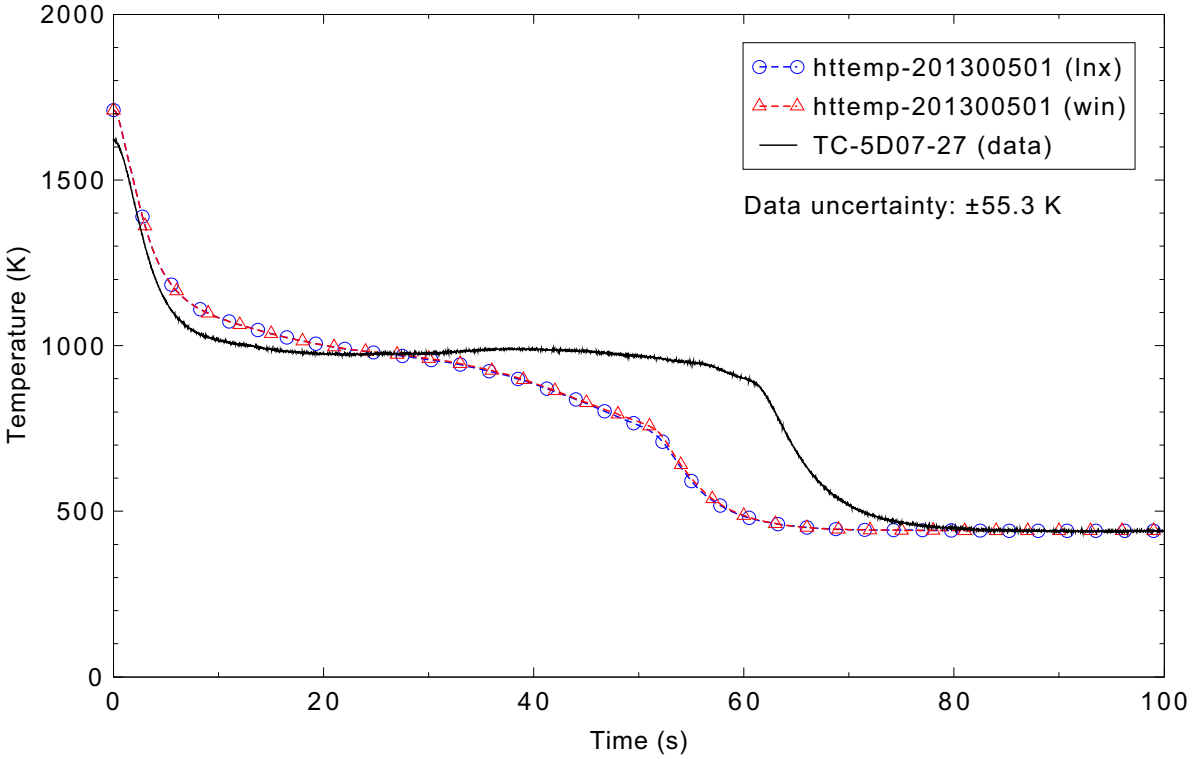

Figure 5.6-22. Measured and calculated fuel centerline temperature in Ring 1, Sector 3, 0.69 m above the bottom of the fuel rod for the LOFT Experiment L2-5 3-D case.

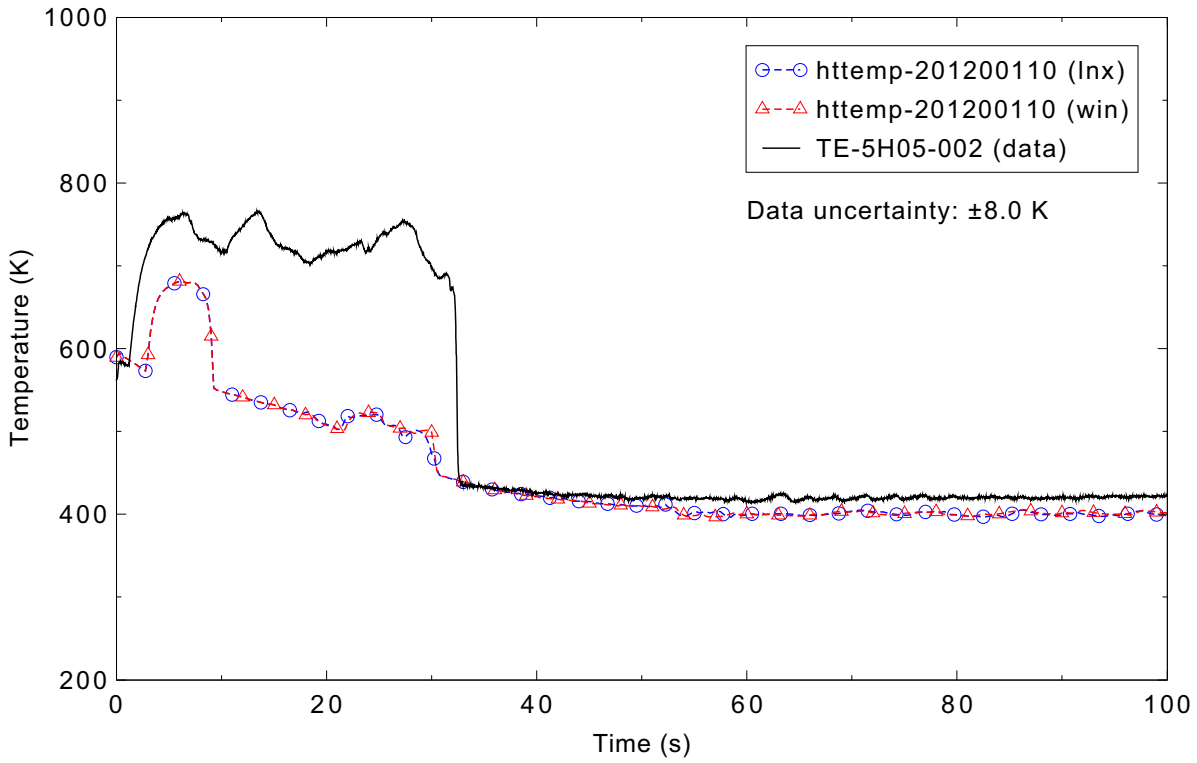

Figure 5.6-23. Measured and calculated fuel cladding surface temperature in Ring 1, Sector 2, 0.05 m above the bottom of the fuel rod for the LOFT Experiment L2-5 3-D case.

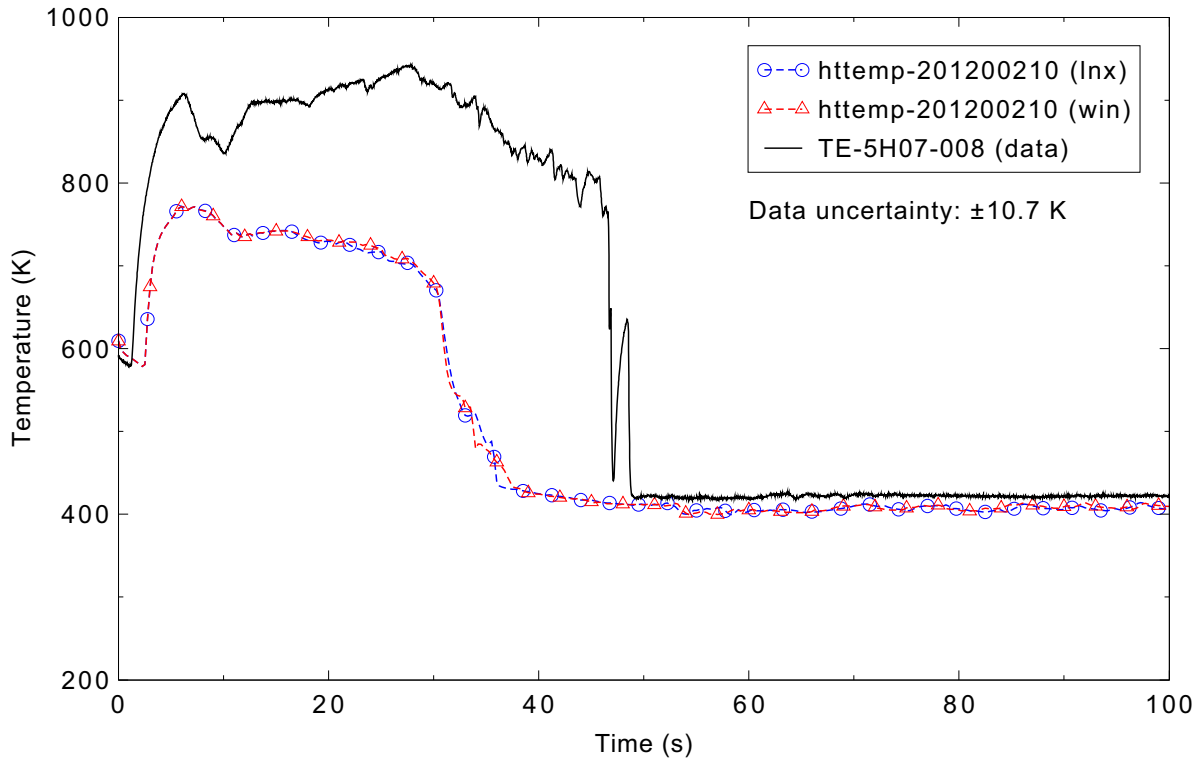

Figure 5.6-24. Measured and calculated fuel cladding surface temperature in Ring 1, Sector 2, 0.20 m above the bottom of the fuel rod for the LOFT Experiment L2-5 3-D case.

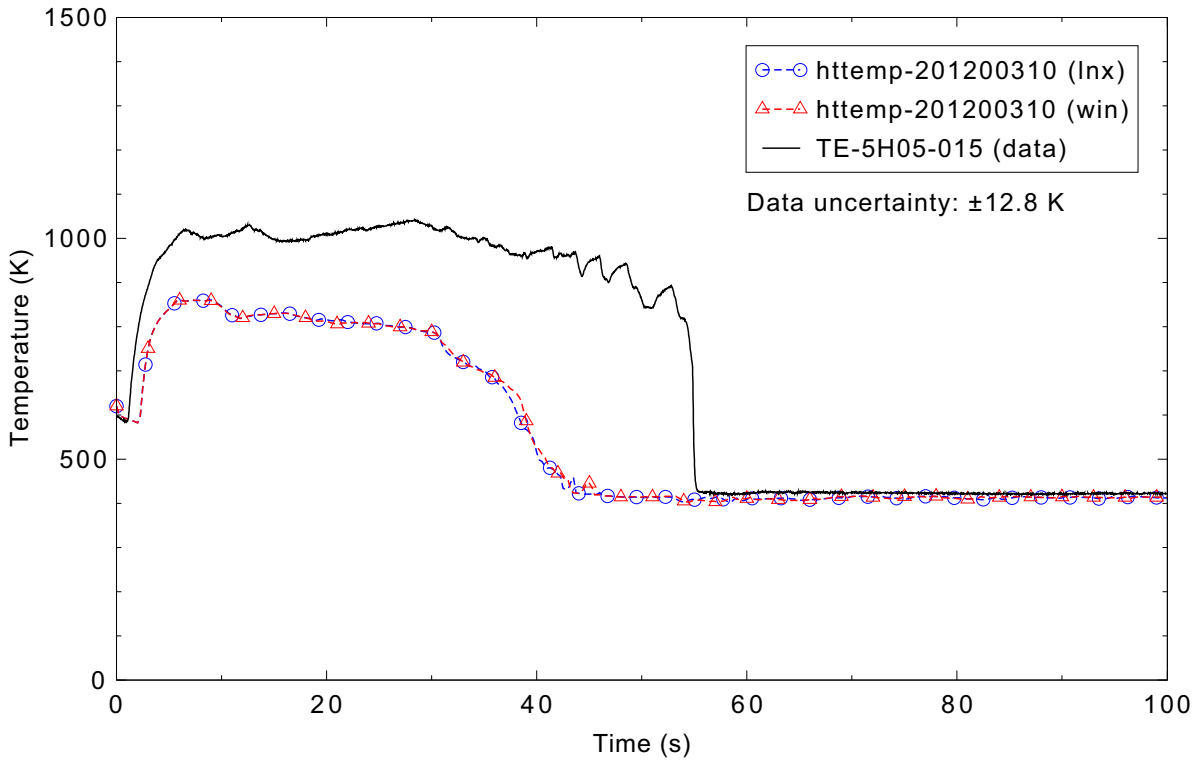

Figure 5.6-25. Measured and calculated fuel cladding surface temperature in Ring 1, Sector 2, 0.38 m above the bottom of the fuel rod for the LOFT Experiment L2-5 3-D case.

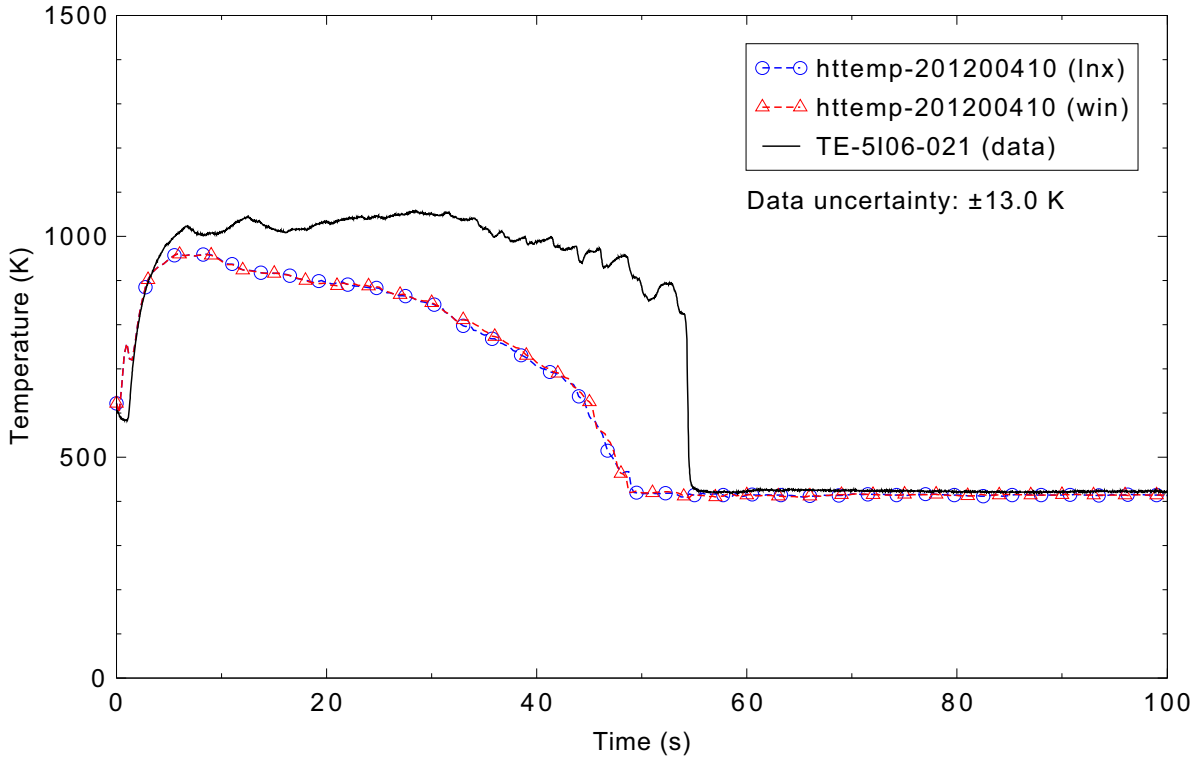

Figure 5.6-26. Measured and calculated fuel cladding surface temperature in Ring 1, Sector 2, 0.53 m above the bottom of the fuel rod for the LOFT Experiment L2-5 3-D case.

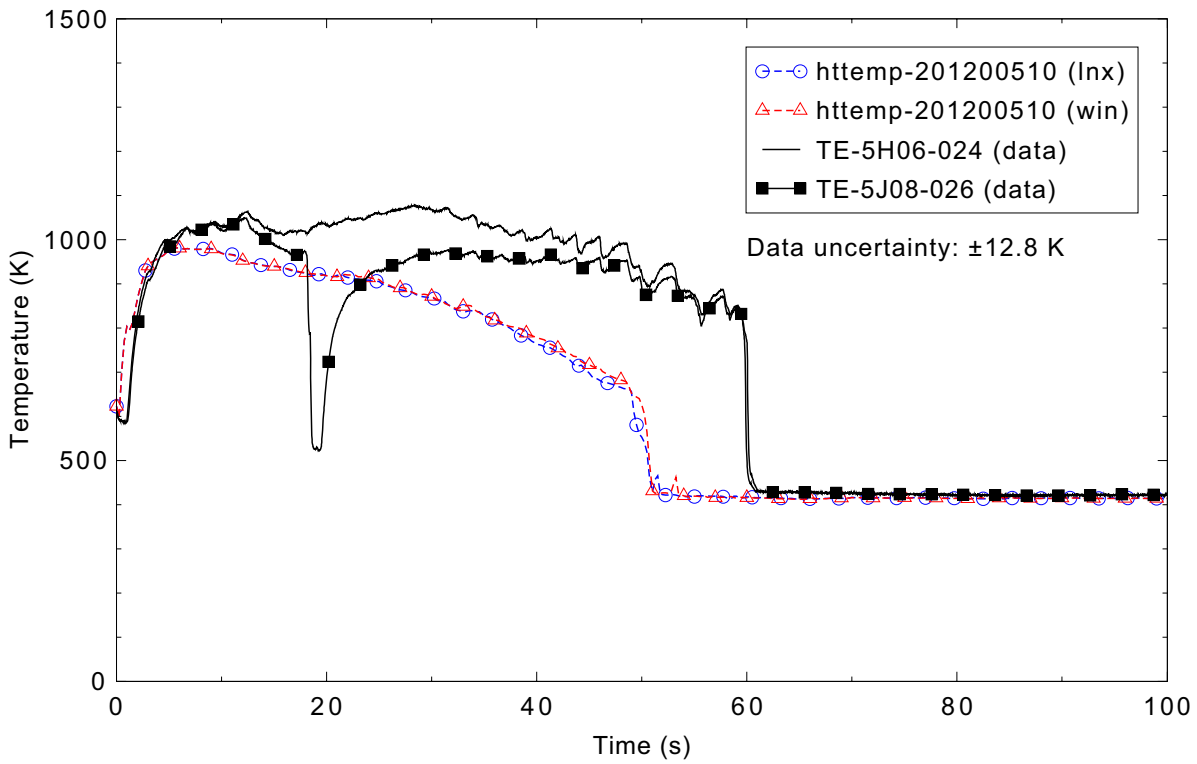

Figure 5.6-27. Measured and calculated fuel cladding surface temperature in Ring 1, Sector 2, 0.64 m above the bottom of the fuel rod for the LOFT Experiment L2-5 3-D case.

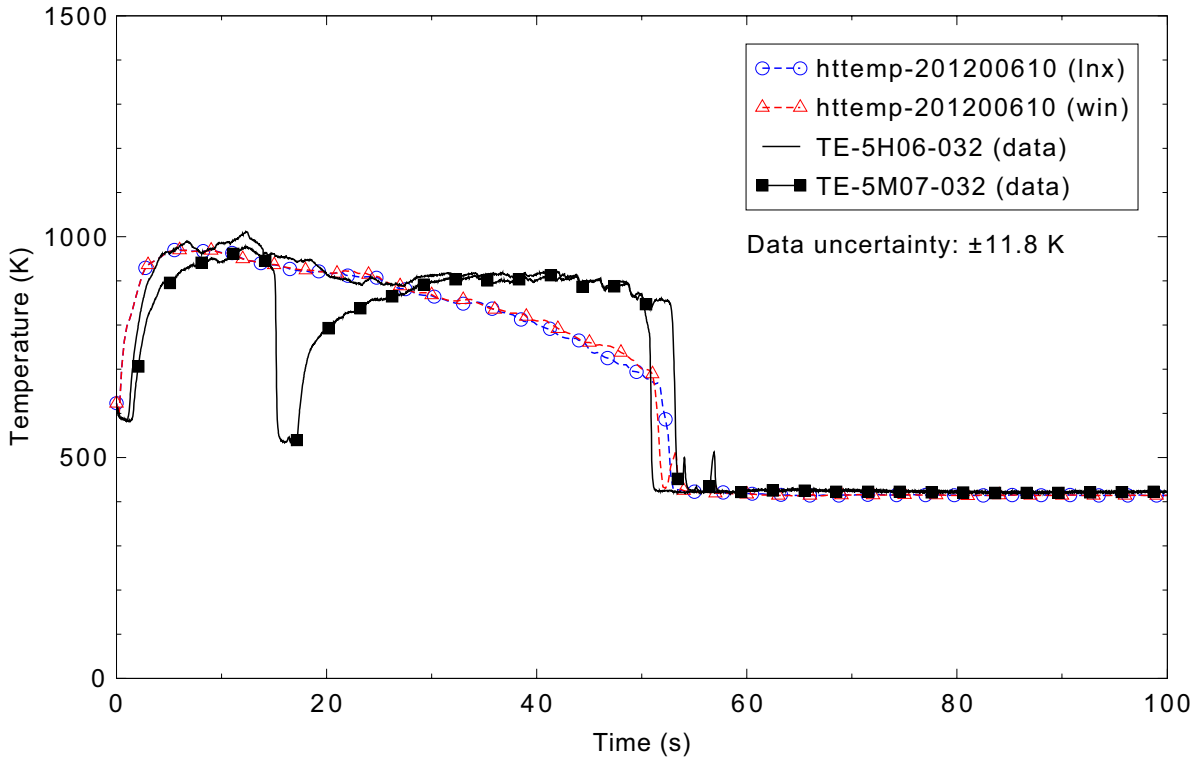

Figure 5.6-28. Measured and calculated fuel cladding surface temperature in Ring 1, Sector 2, 0.81 m above the bottom of the fuel rod for the LOFT Experiment L2-5 3-D case.

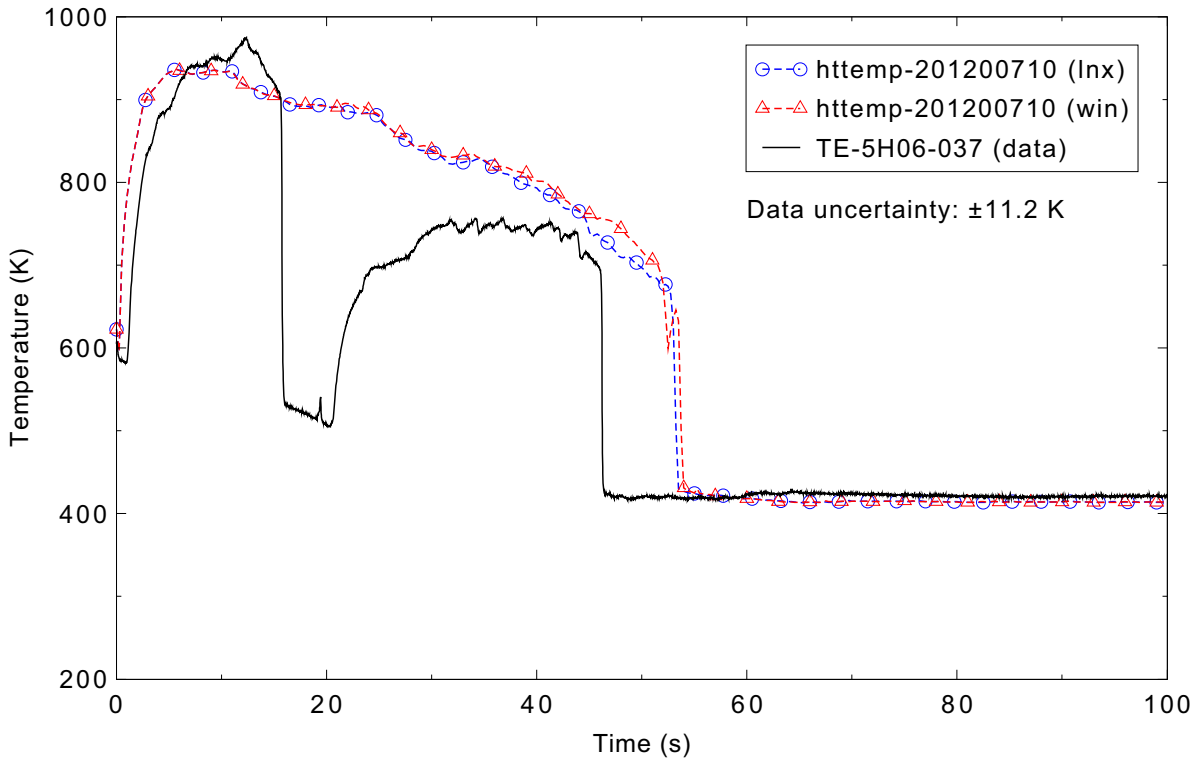

Figure 5.6-29. Measured and calculated fuel cladding surface temperature in Ring 1, Sector 2, 0.94 m above the bottom of the fuel rod for the LOFT Experiment L2-5 3-D case.

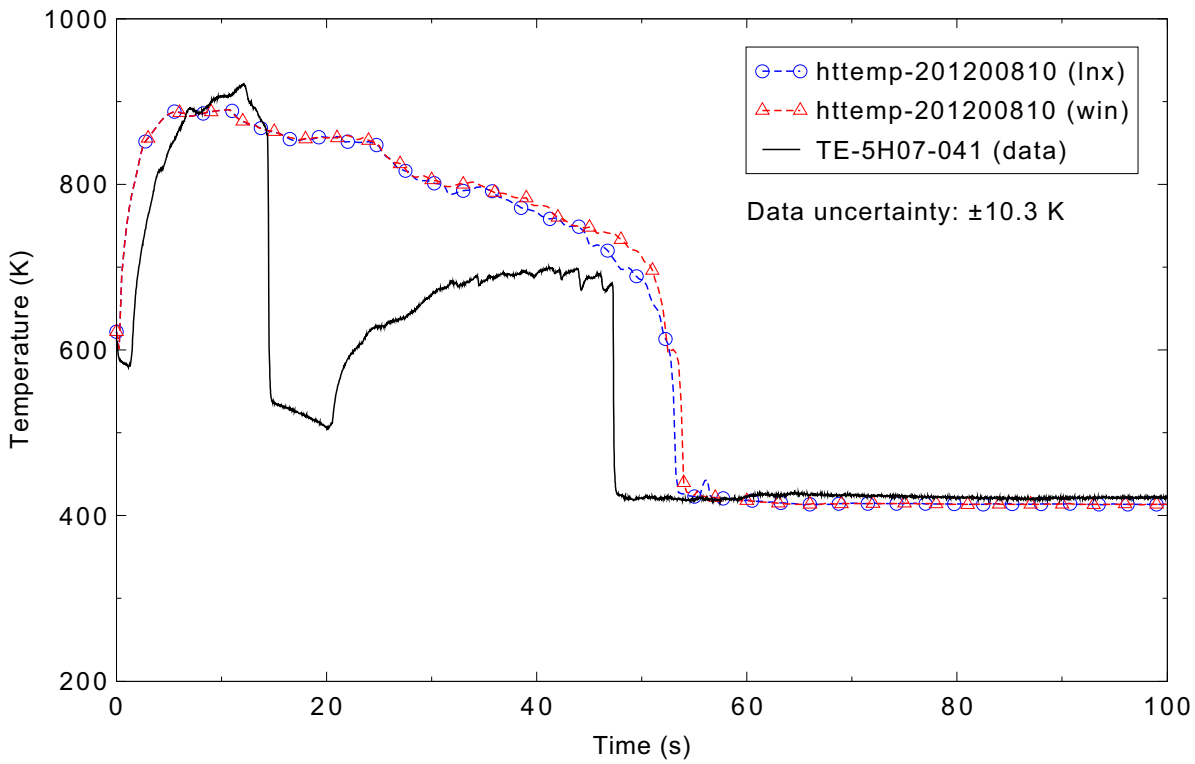

Figure 5.6-30. Measured and calculated fuel cladding surface temperature in Ring 1, Sector 2, 1.04 m above the bottom of the fuel rod for the LOFT Experiment L2-5 3-D case.

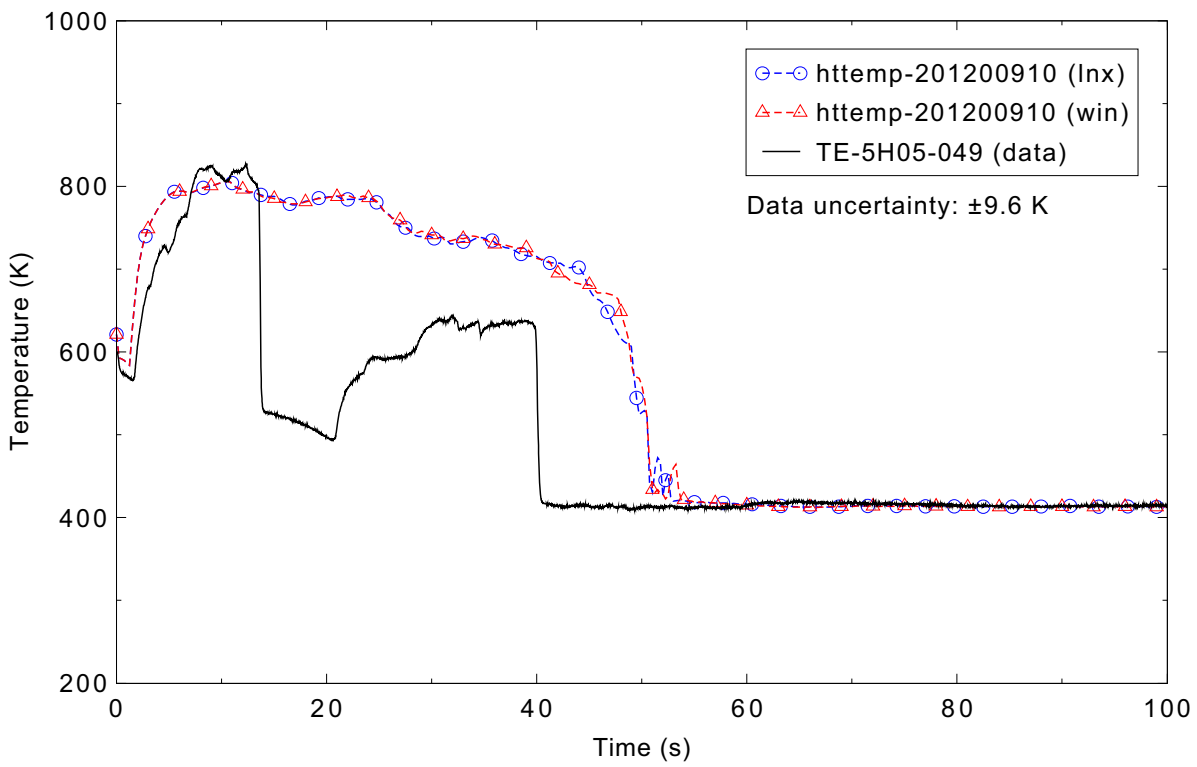

Figure 5.6-31. Measured and calculated fuel cladding surface temperature in Ring 1, Sector 2, 1.25 m above the bottom of the fuel rod for the LOFT Experiment L2-5 3-D case.

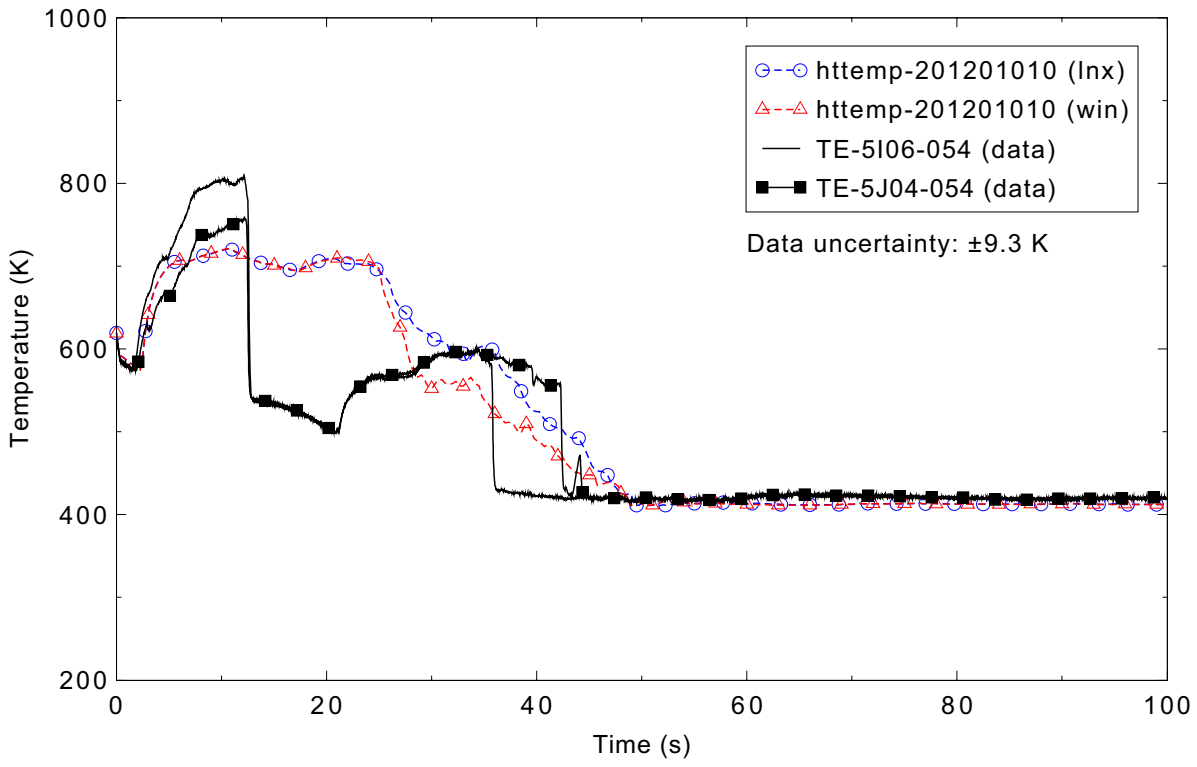

Figure 5.6-32. Measured and calculated fuel cladding surface temperature in Ring 1, Sector 2, 1.37 m above the bottom of the fuel rod for the LOFT Experiment L2-5 3-D case.

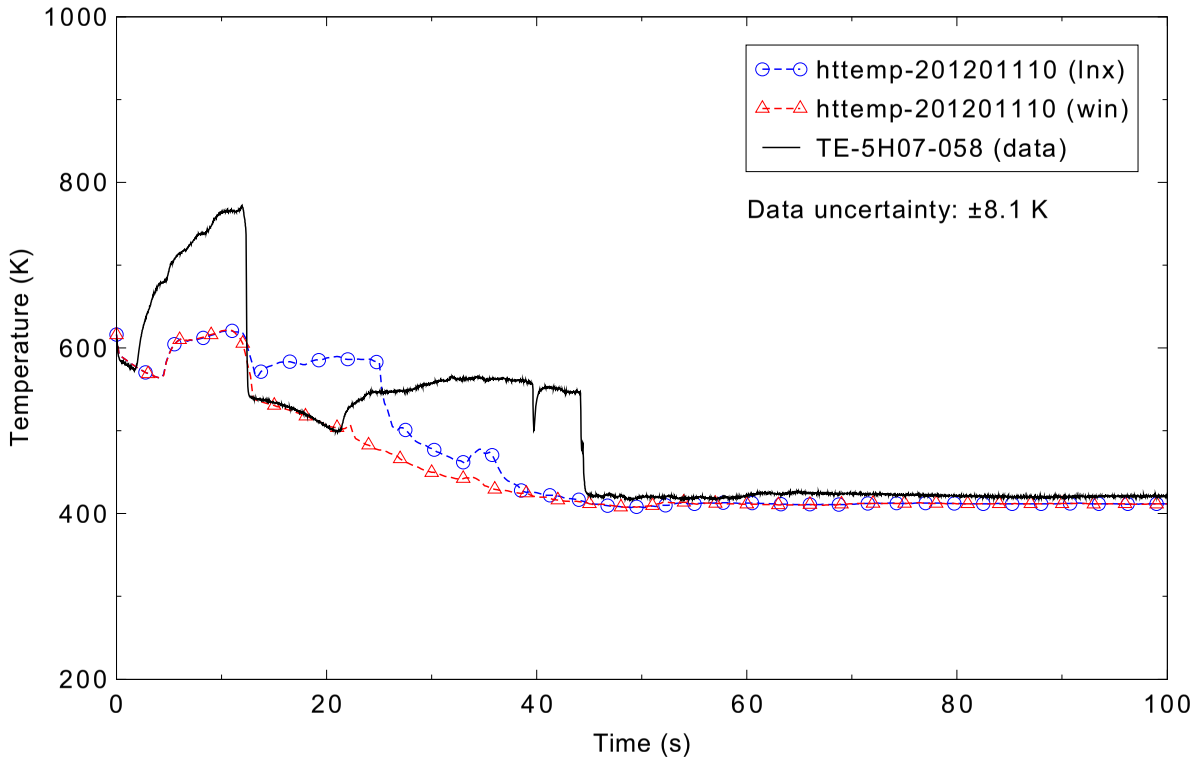

Figure 5.6-33. Measured and calculated fuel cladding surface temperature in Ring 1, Sector 2, 1.47 m above the bottom of the fuel rod for the LOFT Experiment L2-5 3-D case.

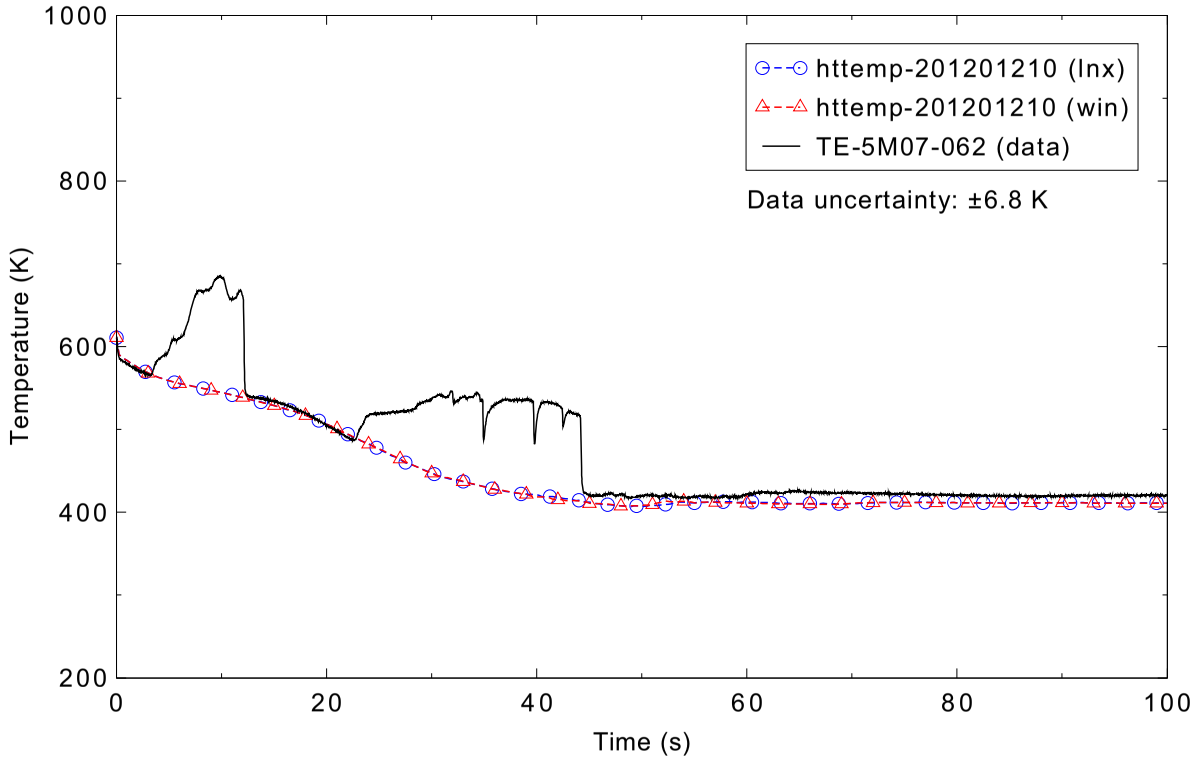

Figure 5.6-34. Measured and calculated fuel cladding surface temperature in Ring 1, Sector 2, 1.57 m above the bottom of the fuel rod for the LOFT Experiment L2-5 3-D case.

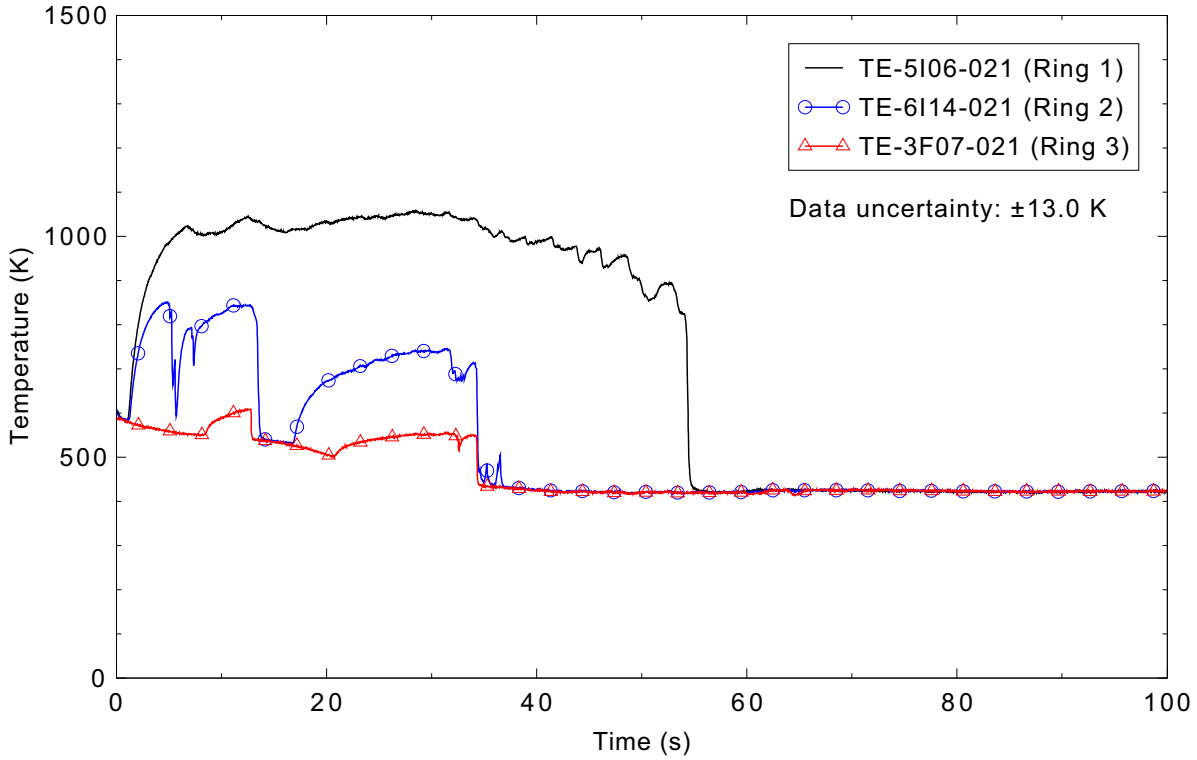

Figure 5.6-35. Measured values showing radial variation in the fuel cladding surface temperature 0.53 m above the bottom of the fuel rod for the LOFT Experiment L2-5 3-D case.

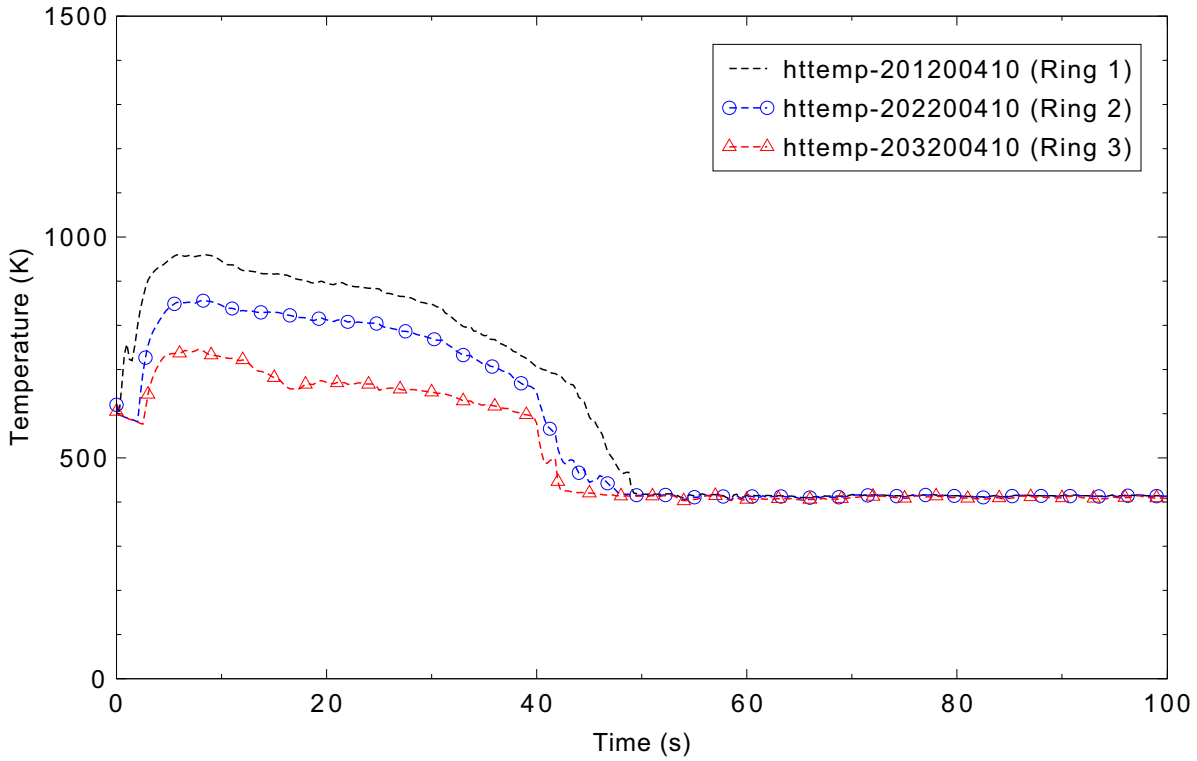

Figure 5.6-36. Calculated values showing radial variation in the fuel cladding surface temperature 0.53 m above the bottom of the fuel rod for the LOFT Experiment L2-5 3-D case.

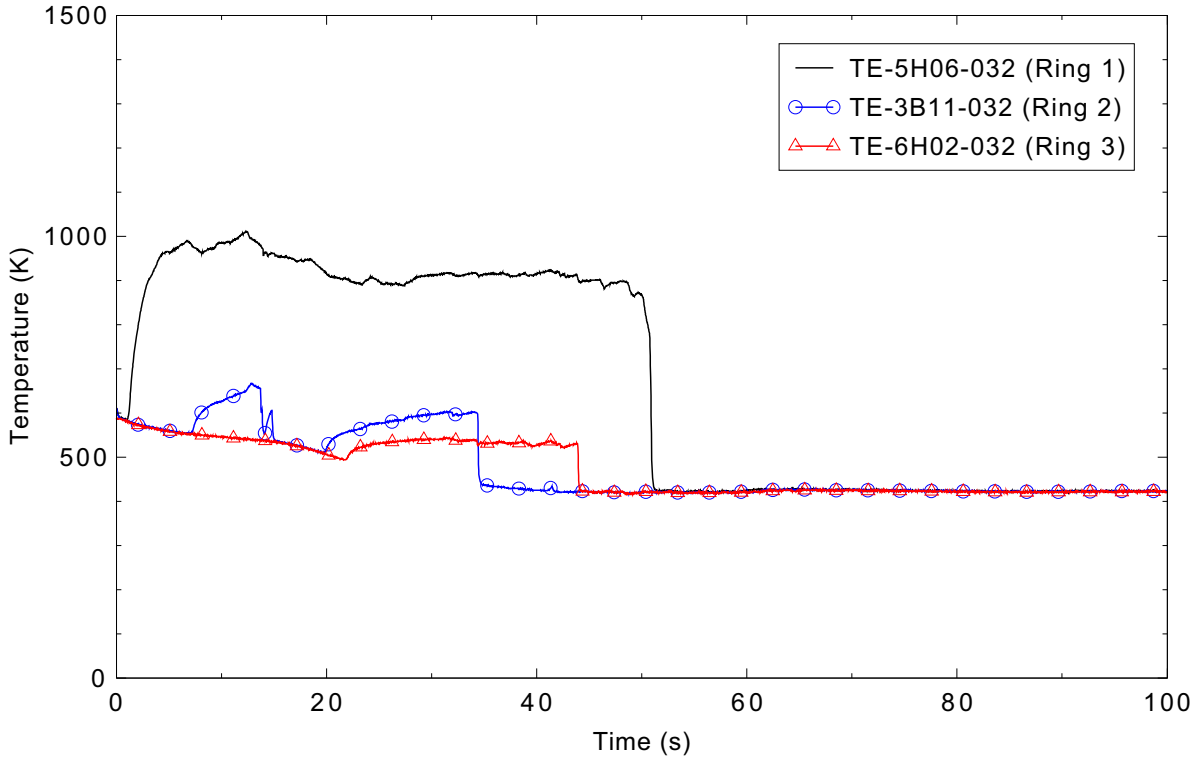

Figure 5.6-37. Measured values showing radial variation in the fuel cladding surface temperature 0.81 m above the bottom of the fuel rod for the LOFT Experiment L2-5 3-D case.

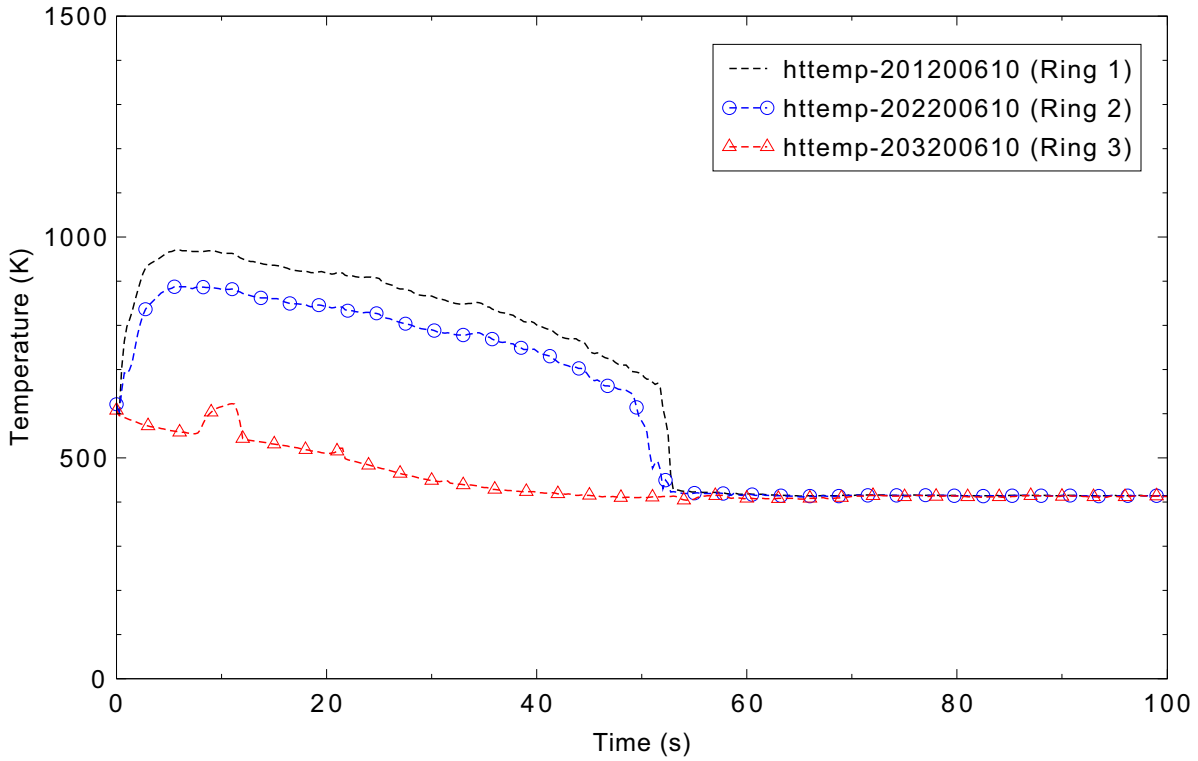

Figure 5.6-38. Calculated values showing radial variation in the fuel cladding surface temperature 0.81 m above the bottom of the fuel rod for the LOFT Experiment L2-5 3-D case.

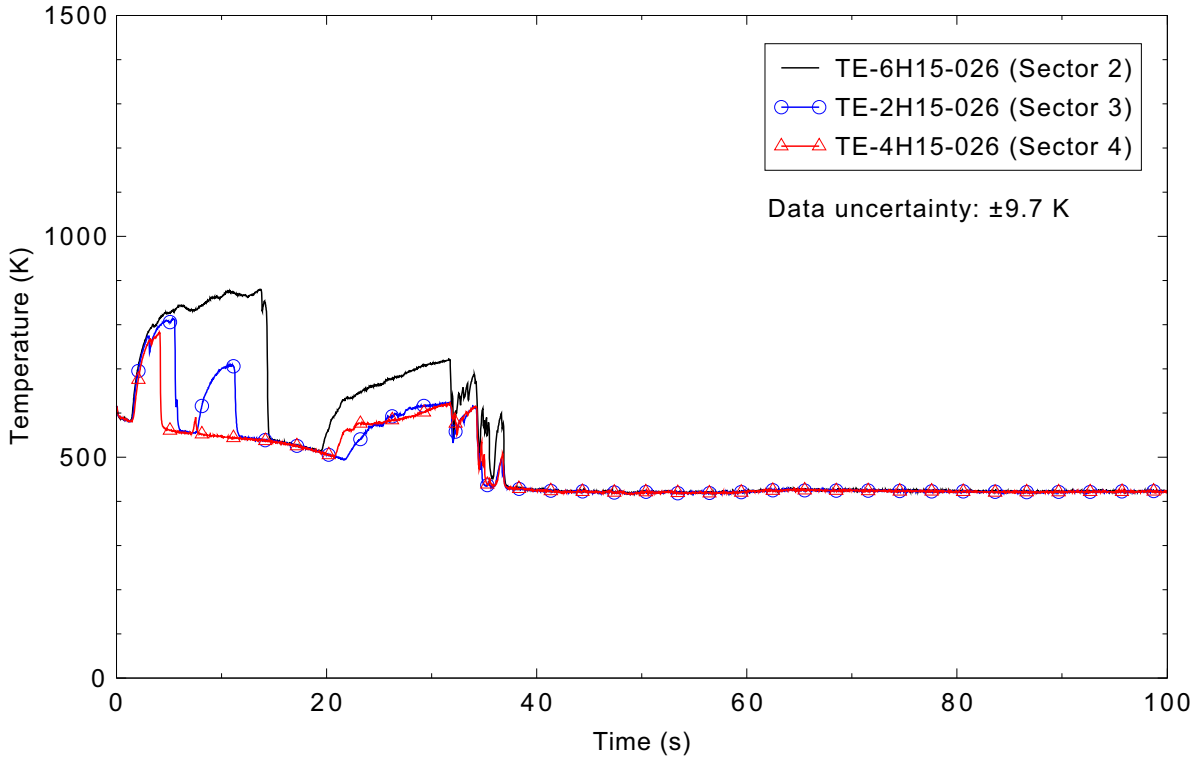

Figure 5.6-39. Measured values showing azimuthal variation in fuel cladding surface temperatures 0.66 m above the bottom of the fuel rod for the LOFT Experiment L2-5 3-D case.

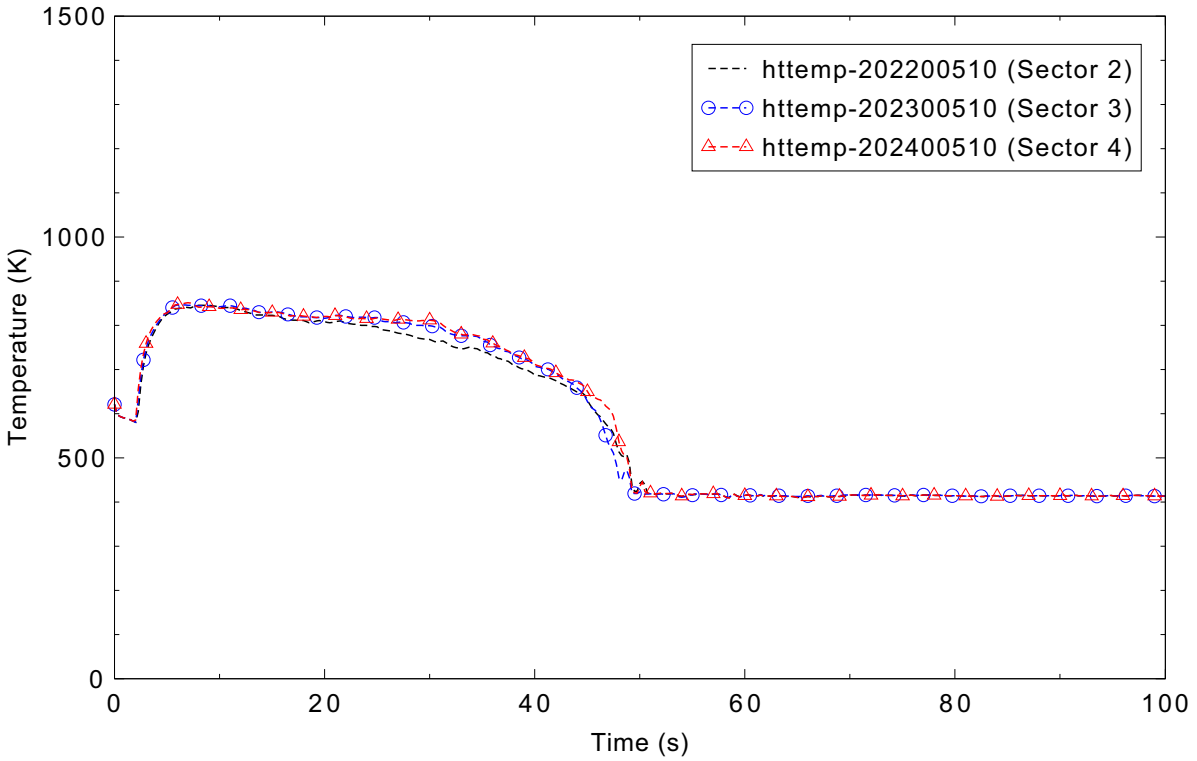

Figure 5.6-40. Calculated values showing azimuthal variation in fuel cladding surface temperatures 0.66 m above the bottom of the fuel rod for the LOFT Experiment L2-5 3-D case.

6. SUMMARY AND CONCLUSIONS

New developmental assessment calculations have been performed for the RELAP5-3D computer code using version 4.3.4i. The results from these calculations run on a Linux platform have been compared to those run on a Windows platform. Comparisons were only made using the semi-implicit solution scheme.

The comparison plots were reviewed, and differences were divided into two categories. Significant differences signify that the assessment judgment may be different. Noticeable differences signify that while the two simulations are different, a difference in the assessment finding is unlikely. No differences were observed in most of the assessment cases; those that had differences are listed below:

- Water over steam (3-D) — three noticeable differences
- Bubbling steam through liquid — three noticeable differences
- FLECHT Test 31504 — six noticeable differences
- FLECHT Test 31701 — ten noticeable differences
- UPTF Test 6 — four noticeable differences
- LOFT Experiment L3-7 — one noticeable difference
- ROSA Test SB-CL-18 — three significant differences, sixteen noticeable differences
- Semiscale natural circulation Tests 1, 2, 3, and 10 — five noticeable differences
- LOBI Test A1-04R — sixteen noticeable differences
- LOFT Experiment L2-5 (1-D) — one significant difference, twenty seven noticeable differences
- LOFT Experiment L2-5 (3-D) — one significant difference, twenty five noticeable differences.

After evaluating these differences, two changes in the assessment judgments would be made. In ROSA-IV, the Windows calculation of the broken loop cold leg density does not show any increase around 600 s, and the assessment judgment would change to minimal from the reasonable agreement in the Linux calculation. The refill of the broken loop hot leg is better predicted in the Windows calculation, but the overall judgment would remain minimal because the amount of liquid is under predicted through most of the transient. The calculated intact loop cold leg density after 600 s in the Windows calculation shows much less liquid than in the data or the Linux calculation, but the overall judgment would still be minimal agreement. In the 1-D LOFT experiment, the broken loop cold leg density prediction is in poorer agreement with the data in the Windows calculation than in the Linux calculation, with a large enough difference that the prediction would be judged to be in minimal agreement. In the LOFT 2-5 3-D case, the

fuel cladding temperature at the 1.47-m elevation does not completely quench from the initial heatup in the Linux calculation, and does not heat up again in the Windows calculation; the assessment judgment of reasonable on the overall core temperature response is unchanged.